Catalytic Activation of Strained C–C Bonds

Dissertation

der Mathematisch-Naturwissenschaftlichen Fakultät

der Eberhard Karls Universität Tübingen

zur Erlangung des Grades eines

Doktors der Naturwissenschaften

(Dr. rer. nat.)

vorgelegt von

M.Sc. Robert Carlo Richter

aus Herrenberg

Tübingen

2025

Gedruckt mit Genehmigung der Mathematisch-Naturwissenschaftlichen Fakultät der Eberhard Karls Universität Tübingen.

Tag der mündlichen Qualifikation:	24.11.2025
Dekan:	Prof. Dr. Thilo Stehle
1. Berichterstatter/-in:	Prof. Dr. Ivana Fleischer
2. Berichterstatter/-in:	Prof. Dr. Florian Beuerle
3. Berichterstatter/-in:	Prof. Dr. Marko Hapke

Preface

This cumulative thesis presents two main projects centered on the activation of strained C–C bonds, with relevance to energy storage and synthesis. The work is structured to include a general introduction, supplemented by dedicated introductory sections for both primary projects. Summaries of both published and unpublished results as well as published scientific articles accompanied by their supporting information have been included.

This work was conducted at the Institute of Organic Chemistry at Eberhard Karls Universität Tübingen, Germany, from October 2022 to August 2025 under the supervision of Prof. Dr. Ivana Fleischer. The Studienstiftung des deutschen Volkes has contributed to funding the doctoral stay.

Acknowledgments

I owe my genuine gratitude to Prof. Dr. Ivana Fleischer, who not only enabled my doctoral research but also supported me throughout this journey. I am deeply thankful for her scientific guidance, inspiring discussions, and for encouraging me to engage with the broader scientific community by attending conferences from the early stages of my PhD. Her integrity and the way she leads by example have shaped my own approach to research and collaboration. I am equally grateful for the trust she placed in me and for fostering an open, welcoming, and collaborative atmosphere within the research group, which made my time here especially enriching.

Within the Fleischer group, I would especially like to thank Ivo Lindenmaier for the many fruitful discussions, his constant willingness to share ideas, and his valuable support with the synthetic work. His insight and helpfulness greatly advanced my research and made our collaboration both productive and enjoyable. I also extend my gratitude to all other current members and alumni of the Fleisher group for their inspiring discussions and for providing such a supportive and enjoyable environment in which to conduct research.

I would like to extend my sincere thanks to Prof. Dr. Holger F. Bettinger, for his valuable scientific advice on my computational work and his contribution to writing my first publication. I am also grateful to the Bettinger group, and in particular to Sonja Biebl and Dr. Ralf Einholz, for providing key molecules for my research and for their continued support and guidance in handling them.

I warmly thank my parents, brother, and friends for their constant support and encouragement throughout my doctoral studies. I am especially grateful to Sonja Biebl for both her personal and scientific support, which made pursuing my doctorate alongside her a truly enjoyable experience.

Last but not least, I would like to thank the Studienstiftung des Deutschen Volkes for their financial support and for encouraging me to broaden my perspectives throughout my PhD.

Abbreviations

AI	Artificial Intelligence
BCB	Benzocyclobutanone
BCF	Tris(pentafluorophenyl)borane
BDE	Bond Dissociation Energy
CuTc	Copper(I) thiophene-2-carboxylate
DHA	Dihydroazulene
DMI	1,3-Dimethyl-2-imidazolidinone
DMPU	*N*,*N*'-Dimethylpropyleneurea
EDC	1-Ethyl-3-(3-dimethylaminopropyl)carbodiimide
EI	Electron Ionization
EOF	Element Organic Framework
FC	Franck Condon
FID	Flame Ionization Detection
FMO	Frontier Molecular Orbital
GC	Gas Chromatography
GP	General Procedure
HAT	Hydrogen Atom Transfer
HDA	Homo-Diels-Alder
HSAB	Hard and Soft Lewis Acids and Bases
IM	Intermediate
IRC	Intrinsic Reaction Coordinate
LA	Lewis Acid
LAG	Liquid Assisted Grinding
LR	Low Resolution
MM	Mixer Mill
MOST	Molecular Solar Thermal
MS	Mass Spectrometry
NBD	Norbornadiene
NICS	Nuclear Independent Chemical Shift
NMP	*N*-Methyl-2-pyrrolidone
NRT	Natural Resonance Theory

OA	Oxidative addition
QC	Quadricyclane
RE	Reductive Elimination
RSE	Resonance Stabilization Energy
rt	Room temperature
sKIE	Secondary Kinetic Isotope Effect
TDAE	Tetrakis(dimethylamino)ethylene
TLC	Thin Layer Chromatography
TM	Transition Metal
TM-TMS_2-DHP	2,3,5,6-Tetramethyl-1,4-bis(trimethylsilyl)-1,4-dihydropyrazine
TS	Transition State
VHF	Vinylheptafulvene
WCA	Weak Coordinating Anion
XEC	Cross Electrophile Coupling
XRD	X-Ray Diffraction

Summary

The activation of C–C bonds is an important and rapidly evolving field in organic chemistry, enabling a range of valuable transformations. Under this common theme, this thesis encompasses two distinct research projects that employ transition metals (TMs) to achieve C–C bond activation.

The first part of this work focused on the catalytic energy release from Dewar isomers of 1,2-dihydro 1,2-azaborinines, a promising scaffold for molecular solar thermal (MOST) energy storage systems. In these systems, light-induced isomerization converts 1,2-dihydro 1,2-azaborinines into high-energy Dewar isomers, storing solar energy through both ring strain and disruption of aromaticity. A key challenge lies in the controlled release of this stored energy on demand. While previous approaches relied on Wilkinson's catalyst, this thesis demonstrated that coinage metal Lewis acids, particularly silver(I) salts with weakly coordinating anions (WCAs) such as $AgSbF_6$ and $Ag[Al(OC(CF_3)_3)_4]$, are highly effective at promoting the cycloreversion under mild conditions.

Mechanistic investigations, including low temperature NMR spectroscopy, single crystal X-ray diffraction, and DFT calculations, revealed that the Lewis acidic silver cation binds to the π-system of the Dewar isomer, stabilizing the transition state and facilitating efficient cycloreversion. Notably, this work provided the first crystal structure of a Dewar 1,2-dihydro 1,2-azaborinine, offering valuable structural insights. These findings broaden the catalyst landscape beyond precious rhodium systems and establish a foundation for rational catalyst design in future MOST applications.

The second major part of this thesis explored nickel catalyzed activation of benzocyclobutanones (BCBs) to construct nortricyclane frameworks through cross-coupling with norbornadienes (NBDs). This transformation exploits the intrinsic ring strain of BCBs to enable oxidative addition to a nickel(0) center, followed by migratory insertion of NBD into the resulting nickelacycle and concluding with reductive elimination to furnish the nortricyclane products.

Optimization studies revealed critical dependencies on concentration and temperature, while demonstrating notable robustness toward different solvents and phosphine ligands. This ligand flexibility also enabled initial investigations into an asymmetric variant of the transformation, which, although achieving only moderate levels of asymmetric induction,

provided valuable proof of concept. Studies on the reaction scope showed broad tolerance for various substitution patterns on both coupling partners, delivering nortricyclane products with good stereoselectivities. To rationalize these stereochemical outcomes, models based on steric interactions were proposed, offering a basis for preliminary mechanistic understanding.

While attempts with other 1,4-dienes were unsuccessful, further investigations extended this system to include the insertion of phenyl isocyanate into BCBs, affording isoquinolinediones. In contrast, a range of other potential insertion partners did not lead to productive transformations.

Together, these studies advance the understanding and practical application of TM mediated C–C bond activation, contributing new strategies for both solar energy storage and the construction of complex, three-dimensional molecular architectures

Zusammenfassung

Die Aktivierung von C–C Bindungen ermöglicht eine Vielzahl für die organische Chemie interessanter Reaktionen und stellt ein wichtiges und wachsendes Forschungsgebiet dar. Unter diesem Leitsatz vereint diese Arbeit zwei thematisch verschiedene Forschungsprojekte, welche Übergangsmetalle nutzen, um C–C Bindungen zu aktivieren.

Der erste Teil dieser Arbeit befasst sich mit der katalytischen Freisetzung von Energie aus Dewar-Isomeren von 1,2-Dihydro 1,2-azaborininen, welche vielversprechende molekulare Energiespeicher darstellen. In diesen Systemen werden 1,2-Dihydro 1,2-azaborinine *per* Photoisomerisierung zu ihrem metastabilen Dewar-Isomer überführt, wodurch Sonnenergie sowohl in Ringspannung als auch durch Dearomatisierung gespeichert wird. Dabei stellt die kontrollierte Freisetzung genau dieser Energie eine zentrale Herausforderung dar. Während bisherige Ansätze auf rhodiumbasierte Katalysatoren angewiesen waren, wurde in dieser Arbeit gezeigt, dass Lewis-saure Münzmetallsalze, insbesondere Silbersalze mit schwach koordinierenden Anionen wie $AgSbF_6$ und $Ag[Al(OC(CF_3)_3)_4]$, die Rückreaktion des Dewar-Isomers katalytisch begünstigen.

Mechanistische Untersuchungen, einschließlich Tieftemperatur-NMR-Spektroskopie, Einkristalldiffraktometrie und quantenmechanischen Rechnungen, zeigten die Koordination von Silberkationen mit dem π-System des Dewar-Isomers. Dabei wird der Überganszustand der thermischen Rückreaktion des Dewar-Isomers stabilisiert, wodurch die Aktivierungsenergie gesenkt wird. Hierbei wurde erstmals die Kristallstruktur eines Dewar-1,2-Dihydro 1,2-azaborinins aufgeklärt, wodurch wertvolle Einblicke in dessen Struktur gewonnen wurde. Diese Ergebnisse erweitern das Spektrum an möglichen Katalysatoren und setzen die Grundlage für die zukünftige rationale Entwicklung anwendungsbezogener Katalysatoren.

Der zweite Teil dieser Arbeit befasst sich mit der nickelkatalysierten Aktivierung von Benzocyclobutanonen, welche in Gegenwart von Norbornadienen Nortricyclan-Strukturen ausbilden. Hierbei ermöglicht die intrinsische Ringspannung von Benzocyclobutanonen die oxidative Addition an ein Nickel(0)-Zentrum. Nach darauffolgender Insertion des Norbornadienes und abschließender reduktiver Eliminierung wird die Nortricyclan-Struktur erhalten.

Die Optimierung des Systems zeigte eine starke Abhängigkeit der Ausbeute von Konzentration und Temperatur, während bemerkenswert viele Lösungsmittel und

Phosphinliganden toleriert wurden. Diese Flexibilität bezüglich der Liganden ermöglichte erste Einblicke in die Entwicklung einer asymmetrischen Variante der Reaktion, die zwar nur moderate Enantioselektivitäten erzielte, jedoch prinzipiell dessen Realisierbarkeit attestierte. Untersuchungen zum Reaktionsspektrum offenbarten eine breite Toleranz gegenüber unterschiedlichen Substitutionsmustern beider Reaktanden und führten zu Produkten mit guten Stereoselektivitäten. Diese wurden mittels postulierter Modelle auf Basis sterischer Wechselwirkungen erklärt, welche einen Ansatzpunkt für mechanistische Studien bieten.

Während die Insertion anderer 1,4-Diene erfolglos blieb, wurde Phenylisocyanat als weiterer Insertionspartner identifiziert. Dagegen wurde mit weiteren ungesättigten Verbindungen unter den entwickelten Bedingungen keine produktive Reaktivität erzielt.

In Summe tragen diese Studien zum besseren Verständnis und zur praktischen Anwendung von Übergangsmetallkatalysierten C–C Bindungsaktivierungen bei und ermöglichen dabei neue Strategien sowohl für die Speicherung von Solarenergie als auch für den Aufbau komplexer, dreidimensionaler molekularer Strukturen.

Publications

A) Publications incorporated into this thesis

1. Facile Energy Release from Substituted Dewar Isomers of 1,2-Dihydro-1,2-Azaborinines Catalyzed by Coinage Metal Lewis Acids.
   R. C. Richter, S. M. Biebl, R. Einholz, J. Walz, C. Maichle-Mössmer, M. Ströbele, H. F. Bettinger*, I. Fleischer*
   Angew. Chem. Int. Ed., **2024**, *63*, e202405818.
   DOI: 10.1002/anie.202405818

2. Cycloaddition of Benzocyclobutanones and Norbornadienes through Nickel Catalyzed C–C Bond Activation.
   R. C. Richter, I. H. Lindenmaier, D. Schray, M. Ströbele, I. Fleischer*
   Org. Lett., **2025**, *27*, 5385-5389.
   DOI: 10.1021/acs.orglett.5c01324

B) Publications with minor contributions

1. Nickel catalyzed C–S cross coupling of sterically hindered substrates enabled by flexible bidentate phosphines.
   I. H. Lindenmaier, R. C. Richter, I. Fleischer*
   Org. Chem. Front., **2024**, *11*, 2485-2493.
   DOI: 10.1039/D4QO00260A

2. High energy density dihydroazaborinine dyads and triad for molecular solar thermal energy storage.
   S. M. Biebl, R. C. Richter, M. Ströbele, I. Fleischer* and H. F. Bettinger*
   Chem. Sci., **2025**.
   DOI: 10.1039/d5sc03159a
3. Nickel Catalyzed C–S Cross Coupling Enhanced by Mechanochemistry
   I. H. Lindenmaier, R. C. Richter, M. Schier, M. Ströbele, I. Fleischer*
   submitted

Personal Contributions

Paper A1

Personal Contribution: 80%

Development of the catalytic system based on previous work from Johannes Walz was carried out by myself. The Synthesis and characterization of the catalysts was conducted by myself, and the 1,2-dihydro 1,2-azaborinines were synthesized and characterized by Sonja Biebl and Dr. Ralf Einholz. Design, execution and interpretation of mechanistic experiments including NMR spectroscopy and kinetic analysis alongside DFT computations were conducted by myself. Crystal structures were measured and resolved by Dr. C. Maichle-Mössmer and Dr. M. Ströbele. HRMS analysis was carried out by the chemistry analytical department of the Eberhard Karls Universität Tübingen. The EDX measurement was conducted by Dr. Ronny Löffler ($LISA^+$). I compiled the results and wrote the manuscript with support from Prof. Dr. Ivana Fleischer and Prof. Dr. Holger F. Bettinger.

Paper A2

Personal Contribution: 80%

Development of the catalytic system, elucidation of the product structure as well as execution and interpretation of the substrate scope was mainly conducted by myself with the aid of David Schray. Synthesis of the staring materials was carried out by myself and Ivo H. Lindenmaier. Mechanistic investigations were carried out by myself. Crystal structures were measured and resolved by Dr. M. Ströbele. HRMS analysis was carried out by the chemistry analytical department of the Eberhard Karls Universität Tübingen. I compiled the results and wrote the manuscript with support from Prof. Dr. Ivana Fleischer.

Paper B1

DFT computations were conducted by myself. Experimental results were obtained by Ivo H. Lindenmaier, who also compiled the results and wrote the manuscript with the support of Prof. Dr. Ivana Fleischer.

Paper B2

Experiments regarding the catalytic cycloreversion were conducted by myself with the support of Prof. Dr. Ivana Fleischer. All other experimental results were obtained by Sonja M. Biebl.

Crystal structures were measured and resolved by Dr. M. Ströbele. HRMS analysis was carried out by the chemistry analytical department of the Eberhard Karls Universität Tübingen. The results were compiled into a manuscript by Sonja M. Biebl with the support of Prof. Dr. Holger F. Bettinger.

Paper B3

Mechanistic experiments were conducted by myself and Ivo H. Lindenmaier. All other results were obtained by mainly by Ivo H. Lindenmaier with the aid of Marius Schier. Crystal structures were measured and resolved by Dr. M. Ströbele. HRMS analysis was carried out by the chemistry analytical department of the Eberhard Karls Universität Tübingen. Ivo H. Lindenmaier compiles the results and wrote the manuscript with the help of Prof. Dr. Ivana Fleischer.

Contents

INTRODUCTION

1 Introduction

1.1 C–C Bonds

Carbon–carbon (C–C) bonds represent a fundamental structural feature of organic molecules.[1] They form the basic framework of molecules across chemical space: from simple hydrocarbons and polymers,[2] to pharmaceuticals,[3] natural products,[4] and biomolecules. Their ubiquity spans major sectors of modern industry: in petrochemistry, the manipulation of C–C bonds underlies fuel and base chemical production,[5] while in the pharmaceutical industry, the controlled formation and transformation of C–C bonds is central to drug development and manufacturing.[6]

Given their pivotal role in both natural and industrial contexts, understanding the reactivity of C–C bonds is of profound importance in modern organic chemistry. Among common covalent bonds, the C–C single bond is notably robust, with an average bond dissociation energy (BDE) of ~83 kcal/mol, rising to ~144 and ~200 kcal/mol for double and triple bonds, respectively.[7] Within carbon-based single bonds (Figure 1.1d), only C–H (~98 kcal/mol) and C–F (~116 kcal/mol) bonds are significantly stronger, while C–O (~85 kcal/mol) bonds are comparable.[8] However, the lower dipole moment of C–C bonds contributes to their chemical inertness relative to more polar bonds like C–O.[9]

This intrinsic stability also stems from their electronic structure. The σ-orbitals of C–C bonds are relatively low in energy, while the corresponding σ*-orbitals lie high, limiting orbital interactions with reactants (Figure 1.1a).[9] In contrast, more reactive bonds such as carbon–halides (C–X) feature lower energy LUMOs (Figure 1.1c). Moreover, the constrained directionality of the C–C bond orbitals along the bond axis restricts orbital overlap with reactants, an essential requirement for many reaction pathways.[9-10] This contrasts with the greater orbital accessibility of C–X and C–H bonds. Although, C–H bonds are thermodynamically more stable and similar in σ*-orbital energy to C–C bonds, their higher reactivity is attributed to the spherical symmetry contribution of hydrogens 1s-orbital to the σ/σ*-bond, which enhances overlap with reaction partners (Figure 1.1b).[11] Additionally, it should be considered, that the BDE describes the thermodynamics of bond homolysis, while in many classic chemical reactions heterolytic bond cleavage is the mode of action. Such reactivity

is usually much more favorable for the activation of C–X and C–H bonds compared to C–C bonds.

These electronic and geometric facets, combined with carbon's diverse ability to bind up to four substituents, render C–C bonds an ideal framework for organic molecules. Consequently, both the formation and strategic cleavage of C–C bonds are central to advancing synthetic methodologies. While bond forming reactions are extensively developed and widely applied, strategies for selective C–C bond cleavage remain comparatively underexplored, despite their considerable synthetic potential.

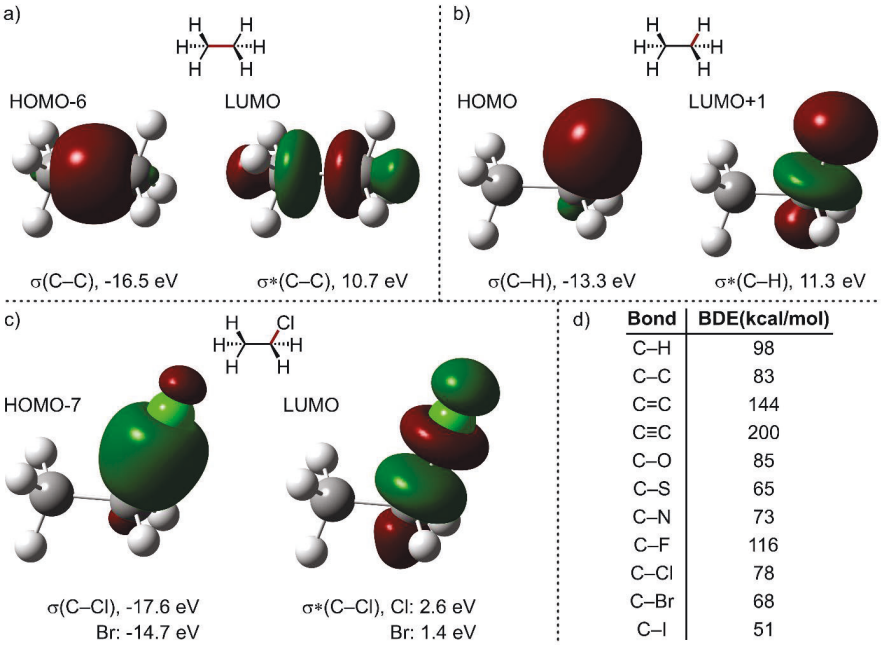

Figure 1.1. Natural bonding orbitals (NBOs, isovalue = 0.08) and corresponding energies of σ- and σ*-orbitals for the [a]C–H, [b]C–C bond in ethane and the [c]C–Cl bond in ethyl chloride, computed at the B3LYP/6-311G* level of theory. Additionally, the σ/σ*-orbital energies, computed at the same level of theory, of C–Br (ethylbromide) are also provided, omitting graphical representation on account of their similar symmetry to ethyl chloride. [d]Average BDE of selected carbon bonds.[8]

1.1.1 Cleavage of C–C bonds

From a thermodynamic perspective, the activation of C–C single bonds poses a challenge, as the resulting products are often less stable than the starting materials. This is illustrated by

comparing the formal hydrolysis of ethylene and ethane. While the 1,2-addition of water to ethylene is energetically favorable, the analogous process involving ethane, requiring scission of the C–C σ-bond, is endergonic.[9]

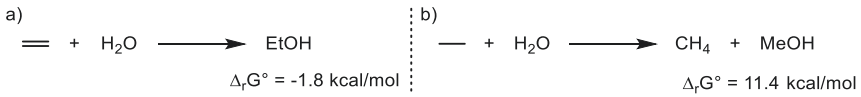

Scheme 1.1. Free energy of the formal hydrolysis of [a]ethylene and [b]ethane calculated from experimental values.[12]

Despite these challenges, C–C bond cleavage reactions are well established in classical organic chemistry, including the *retro*-Aldol reaction (Figure 1.2a),[13] and pericyclic processes (Figure 1.2b) such as the Claisen rearrangement,[14] and *retro*-Diels-Alder reaction.[15] These reactions typically rely on strong driving forces such as ring strain release, reaction cascades, or favorable entropy changes to compensate the thermodynamic challenge of breaking C–C σ-bonds. In pericyclic reactions, the concerted formation and breaking of bonds ensures thermodynamic feasibility, provided that orbital symmetry rules (Woodward-Hoffmann) are satisfied.[16] Furthermore, Lewis-acids (LA) can broaden the reaction scope, either by stabilizing charged intermediates or perturbing orbital symmetry to allow formally forbidden pathways.[17]

Beyond laboratory applications, C–C bond activation plays a vital role in industry. A prominent example is the thermal cracking in petroleum refining (Figure 1.2c),[18] where high temperature and pressure promote homolytic cleavage of C–C σ-bonds. The resulting carbon-centered radicals undergo hydrogen atom transfer (HAT) and *β*-scission, forming smaller, more stable hydrocarbons.[19]

Similar radical pathways are also leveraged in sustainable chemistry. For instance, the upcycling of polystyrene involves benzylic radicals generated *via* light induced processes, which subsequently undergo oxygenation and C–C *β*-scission to initially yield ketones, which under the respective reaction conditions are ultimately converted to benzoic acid (Figure 1.2d).[20] Related mechanisms apply to lignin valorization,[21] potentially providing a renewable feedstock of hydrocarbon building blocks and to photoredox catalyzed transformations driven by strain or the release of small molecules such as CO or CO_2 (Figure 1.2e).[22]

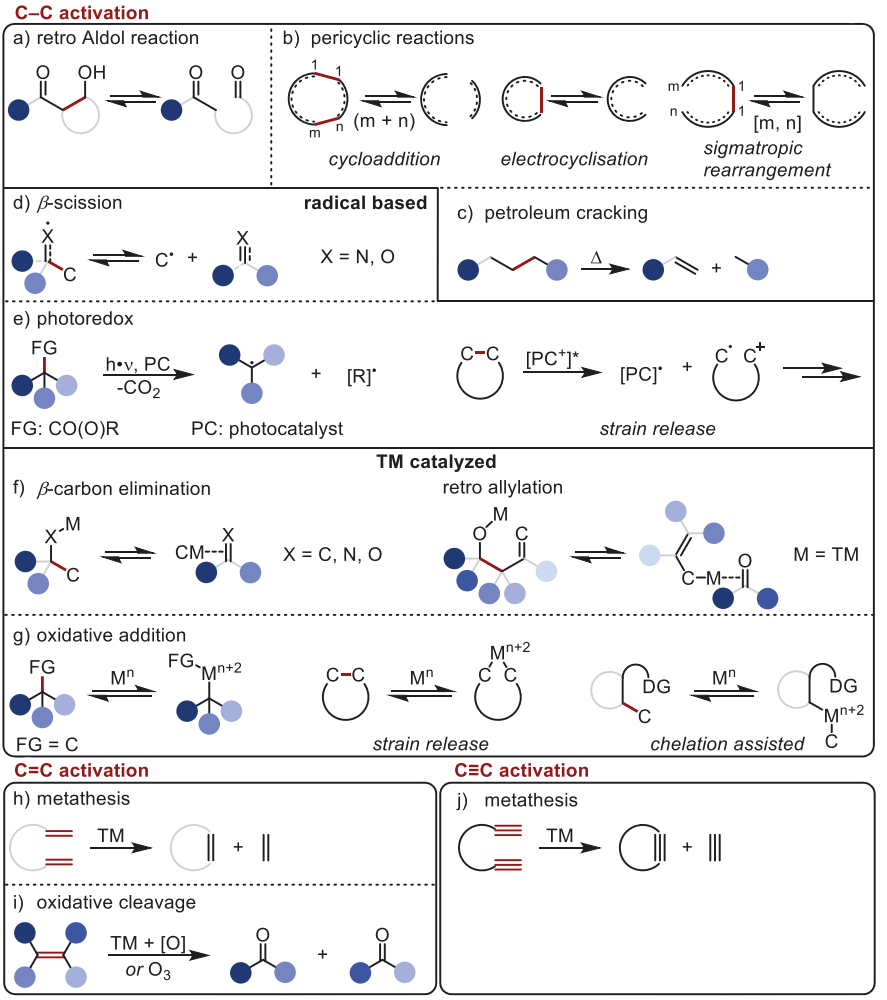

Figure 1.2. Overview of different types of activation of C–C bonds, by classical, radical or TM-catalyzed approaches.

Transition metals (TMs) offer a distinct and versatile platform for C–C bond activation. In *β*-carbon-elimination, the closed shell analogue of *β*-scission, the γ-carbon of TM alkyl, alkoxide, or amide species migrates to the metal, extruding an unsaturated fragment (Figure 1.2f).[23] Similarly, homoallylic TM alkoxides can undergo *retro*-allylation, competing with *β*-carbon-elimination.[24] Another key strategy is the oxidative addition (OA) of a low-valent

TM into a C–C bond (Figure 1.2g). For this step to proceed efficiently, the targeted bond typically requires activation through adjacent functional groups,[25] or embedding in strained rings.[7, 17c, 26] For unactivated bonds, chelation assisted mechanisms have been developed.[27] Notably, even the activation of C=C and C≡C bonds is possible despite their high BDEs (see Figure 1.1d above). Examples include olefin closing metathesis (Figure 1.2h, j),[28] oxidative alkene cleavage,[25] and even classic ozonolysis (Figure 1.2i).[29] In contrast, TM-mediated C≡C bond cleavage remains rare and typically requires multistep cascades.[30]

1.1.2 Oxidative addition in C–C bonds

Among TM-based activation strategies, OA into C–C σ-bonds has gained prominence in recent years. This atom economical route enables the construction of complex carbon frameworks, often bypassing lengthy functional group manipulations common in traditional syntheses.[26a]

Despite its utility, several intrinsic challenges limit its general application. As described earlier, the high BDE of apolar C–C bonds and the modest strength of resulting metal–carbon (M–C) bonds usually render the OA step thermodynamically uphill.[9, 31] Yet, the successful isolation of numerous alkyl and aryl organometallic complexes shows that C–C cleavage is feasible under optimized conditions.[32] For instance, late TMs like rhodium and iridium form strong M–C_{aryl} bonds,[33] sometimes surpassing the strength of the corresponding M–H bonds. This can tip the energy balance in favor of C–C activation over the activation of statistically more abundant C–H bonds. Nonetheless, selectivity remains challenging due to the superior orbital overlap of C–H bonds with TM-orbitals, which provide not only competing pathways but also steric hindrance near the target C–C bond (Figure 1.1a, b). Thus, effective OA into the C–C bond often necessitates the adoption of an eclipsed conformation, enabling an optimal approach trajectory for the TM (Figure 1.3b). Such conformations are energetically disfavored in flexible systems, rendering this alignment transient.[32, 34] In addition, interaction between the TM and the highly localized C–C σ- and σ*-orbitals requires distortion of the bond axis, introducing a significant activation barrier. [9-10] Consequently, elevated temperatures are often required, at the cost of side reactions.

To overcome these constraints, several strategies have been developed that improve both the thermodynamic feasibility and kinetic accessibility of C–C bond cleavage (Figure 1.2g). One effective approach involves the use of strained carbocycles. These small ring systems benefit from the thermodynamic driving force of strain release upon OA (Figure 1.3c).[7, 9-11]

From a kinetic standpoint, such cycles exhibit enhanced orbital accessibility due to electron density extending beyond internuclear axes, as described by the Walsh and Coulson Moffitt models (Figure 1.3a).[10, 34-35] Additionally, substituents on small rings are inherently oriented in eclipsed or near eclipsed conformations, facilitating favorable geometries for TM approach.

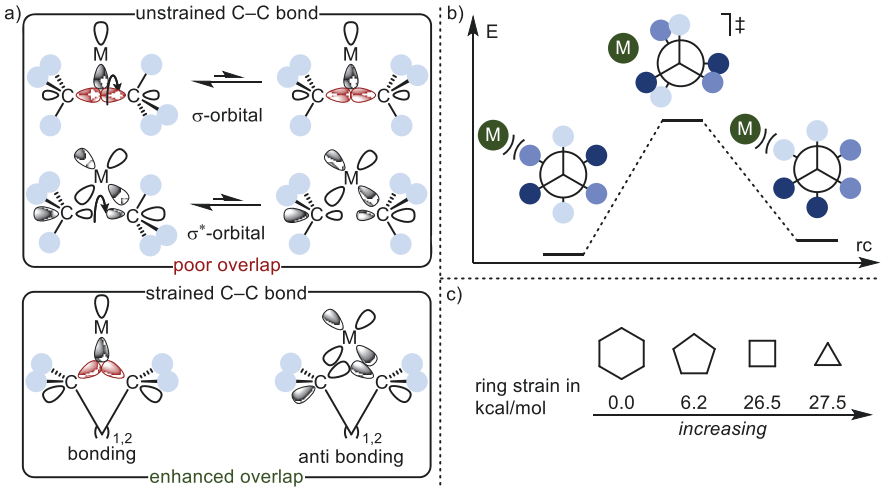

Figure 1.3. [a]Schematic orbital interaction of a TM with an unstrained C–C bond and a strained C–C bond, described according to the Walsh or Coulson Moffitt model. [b]Representation of a conformational transition of a C(sp^3)–C(sp^3) bond indicating steric repulsing with an approaching TM. [c]Ring strain energies of parent three- to six-membered rings.[36]

Another strategy relies on the electronic activation of the C–C bond through adjacent functional groups. These can serve as coordination sites, positioning the TM near the targeted bond. Furthermore, functional groups typically exhibit lower steric demand (sp^2/sp), than standard alkyl substituents (sp^3), thereby alleviating steric hinderance and increasing the likelihood of a productive interaction.[10-11, 25a]

A third approach is chelation assisted activation. In this strategy, a directing group coordinates the TM, guiding it toward the C–C bond and significantly increasing the effective concentration of the metal at the reaction site. This proximity effect enhances the probability of OA, even in cases involving otherwise unreactive C–C bonds.[10-11, 37]

1.2 Molecular Solar Thermal Storage Systems

Strain-induced reactivity, as discussed in the context of C–C bond activation, also plays a key role in Molecular Solar Thermal (MOST) systems designed for energy storage.[38] A prominent example is the norbornadiene/quadricyclane (NBD/QC) system, which stores energy through a light induced [2+2] cycloaddition into a highly strained framework.[39] This transformation exemplifies the core principle behind MOST systems, which utilize reversible photoinduced structural changes to store and release solar energy.[40] The following section will explore this concept in more detail.

1.2.1 Motivation

As global energy consumption continues to rise,[41] reducing reliance on fossil fuels has become essential, both due to their finite availability and their severe environmental impact. The use and storage of solar irradiation is central to the transition towards sustainable energy. Among renewable resources, solar energy is by far the most abundant, delivering approximately 122 Petawatts to Earth's surface,[42] exceeding current global energy demand by several orders of magnitude.[41] Despite its potential, the contribution of solar power falls short of long-term sustainability goals,[41] primarily due to its intermittent nature and geographical variability, which necessitate energy storage solutions. Existing technologies such as photovoltaics coupled with electrochemical batteries offer promising solutions but face challenges related to cost, infrastructure, and efficiency losses.[43] These limitations highlight the need for alternative approaches. One promising direction is the use of photoresponsive molecules that can directly convert and store solar energy in the form of chemical potential.[40b]

1.2.2 Definition

A MOST system is based on a reversible, photoinduced chemical reaction that generates a metastable, high energy state. Upon reversion, the stored energy is released as heat (1).

$$\sum \mu_i x_i \overset{h\cdot\nu}{\rightleftarrows} \sum \nu_j y_j \quad with \quad \sum \nu_j \Delta_f H^\circ{}_j < \sum \mu_i \Delta_f H^\circ{}_i \tag{1}$$

$(\mu, \nu)_i$: stochiometric coefficients; x_i: reactants; ν_j: products

While this process is typically constrained to a single molecular entity, subsequently referred to as a mostophore, energy storage can also be achieved through multi molecular photochemical reactions.

1.2.3 Requirements

While a range of photochemical processes meet the basic definition of a MOST system, several key parameters must be optimized to achieve efficient energy storage and release.

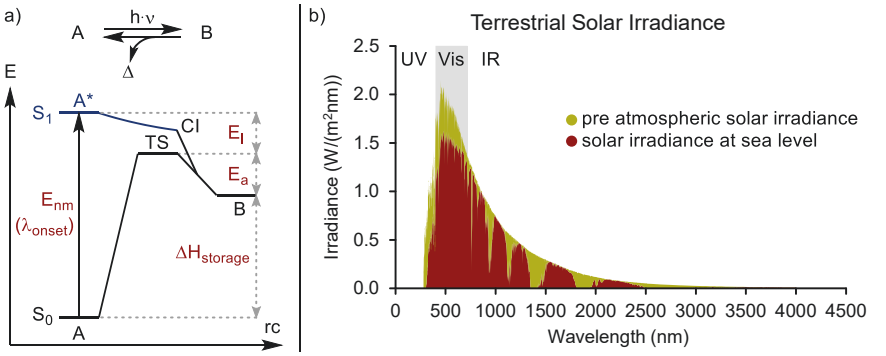

Figure 1.4. [a]Energy diagram (enthalpic space) for a MOST system (A⇄B) displaying the $S_0 \rightarrow S_1$ excitation (E_{nm}), followed by thermal relaxation to the photoisomer *via* a conical intersection (CI) spanning the activation energy (E_a) and the thermal relaxation energy (E_l). The portrayed thermal back reaction over the transition state (TS) subsequently releases the stored energy ($\Delta H_{storage}$). [b]Terrestrail solar irradiance spectrum above earth's atmosphere and at sea level on the 37° tilted surface at AM1.5 conditions. Data from Advancing Standards Transforming Markets (ASTM) international.[44]

The theoretical limiting efficiency (η_{limit}, (2)) is determined by the rate of absorbed photons per area ($\dot{N}$) at a given excitation energy (E_{nm}), multiplied by the stored enthalpy ($\Delta H_{storage}$), and normalized by the total solar irradiance ($E_{AM1.5}$). The latter corresponds to the solar flux at Earth's surface with an air mass of 1.5, implying sunrays passing through 1.5 times the atmosphere compared to a perpendicular path.[40b, 45]

$$\eta_{limit} = \left(\frac{\partial^2 N(E_{nm})}{\partial t \partial A}\right) \frac{E_{nm} - E_a - E_l}{E_{AM1.5}} = \dot{N}(E_{nm}) \frac{\Delta H_{storage}}{E_{AM1.5}} \qquad (2)$$

E_a: activation energy

E_l: thermal relaxation energy

Assuming every photon with $E_{nm} \geq E_{S_0,S_1}$ results in a productive photochemical event, and given a reasonable storage half-life of 24 d (E_a = 28.7 kcal/mol and E_l = 0 kcal/mol), the theoretical maximum efficiency is reached for systems absorbing at approximately 685 nm, yielding η_{limit} = 12.4%, that is 12.4% of the solar irradiation energy can be stored as chemical

potential.[45] In practice, system efficiency ($\tilde{\eta}_{limit}$) must incorporate concentration dependent absorption ($A(c,\lambda)$) and quantum yield (ϕ_{iso}) of photoisomerization.[40b, 46]

$$\tilde{\eta}_{limit} = \int_0^{\lambda_{onset}} \frac{E_{AM1.5}(\lambda)A(c,\lambda)\phi_{iso}}{h\nu \cdot N_A} d\lambda \frac{\Delta H_{storage}}{E_{AM1.5}} \quad (3)$$

Here, $E_{AM1.5}(\lambda)$ represents the spectral solar irradiance (energy current density) under AM1.5 conditions. Resulting $\tilde{\eta}_{limit}$ values are typically in the low single digit percentage range.[40b] Additional losses such as optical inefficiencies, solvent absorption, and thermal back reactions further reduce the measured efficiency ($\eta_{measured}$), often ranging from 0.009% to 1.1%.[40b]

From these theoretical considerations, several practical design criteria emerge. First, the mostophor should absorb in the visible spectrum to overlap with solar irradiance at Earth's surface (Figure 1.4b), while the photoisomer should absorb minimally in this range to avoid competition. For example, excitation of the photoisomer can promote back-conversion resulting in a photostationary state,[47] which depletes efficacy, or enable photodecomposition. Additionally, a high quantum yield of photoisomerization is vital, ensuring that most absorbed photons result in productive switching.[48] While maximizing stored energy is a central design objective, this is constrained by both photophysical and kinetic factors. Specifically, the storable energy is determined by the energy of the absorbed photon minus the activation energy (E_a) needed for back-conversion and the energy lost through thermal relaxation (E_l) between the excited state ($S_{1,\,2...}$) and TS. Since photon energy is largely fixed by the solar spectrum, and E_a must be high enough to support sufficient storage, the only tunable factor is E_l. Minimizing this thermal relaxation loss is therefore key to optimizing net energy storage (Figure 1.4a).[45] Moreover, the molecular weight of the mostophor has to be taken into account, as for practical applications the energy density *per* mass is crucial rather than the molar equivalent.

Another essential criterion is the ability to trigger the back-conversion on demand, whether thermally, electrochemically, photochemically, or *via* catalysis. For practical applications, systems must also be highly cyclable, requiring the mostophor and its photoisomer to be stable towards moisture and oxygen while exhibiting minimal photodegradation. Finally, economic and energetic viability must be considered. The synthesis of the mostophor should be cost effective and energetically favorable, requiring less energy than it can store and release over its lifetime.[48]

1.2.4 Canonical MOST Systems

To better understand how these theoretical principles translate into functional systems, it is instructive to examine representative examples of MOST systems. Several key photoswitches have emerged that store solar energy *via* different underlying mechanisms. NBD/QC pairs rely on the formation of a highly strained cyclic structure. Azobenzenes exploit configurational isomerization around a central double bond, and dihydroazulenes (DHA) store energy through reversible bond cleavage to vinylheptafulvene (VHF). A fourth strategy involves the disruption and reformation of aromaticity, exemplified by the reversible photodimerization of anthracene (Figure 1.5).

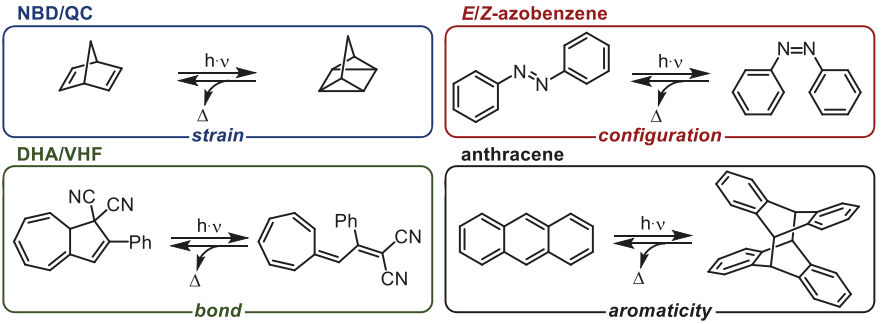

Figure 1.5. Storage of irradiation energy in chemical energy utilizing ring strain, configurational isomerism, covalent bonds and aromaticity exemplified on MOST systems.

Though anthracene-based systems have limited relevance for modern MOST applications, they hold historic significance, with Fritzsche first reporting their reversible photoreaction in 1867.[49] In contrast, modern MOST research has concentrated on a few representative systems, most notably NBD/QC, azobenzenes, and DHA/VHF. These classes of photoswitches differ in key performance parameters such as onset wavelength (λ_{onset}), energy storage density ($\Delta H_{storage}$), quantum yield (ϕ_{iso}), and thermal half-life ($t_{1/2}$), which together are crucial for a MOST system (Figure 1.6).[50]

Among these, NBD/QC systems are the most extensively studied. They combine high energy storage densities, and quantum yields with exceptionally long thermal half-lives. Although the parent compound displays a suboptimal quantum yield, tuning electronic properties through substituents has led to variants with markedly enhanced efficiencies, such as NBD2 (Figure 1.6), which features two cyano groups alongside methyl substituents.[51]

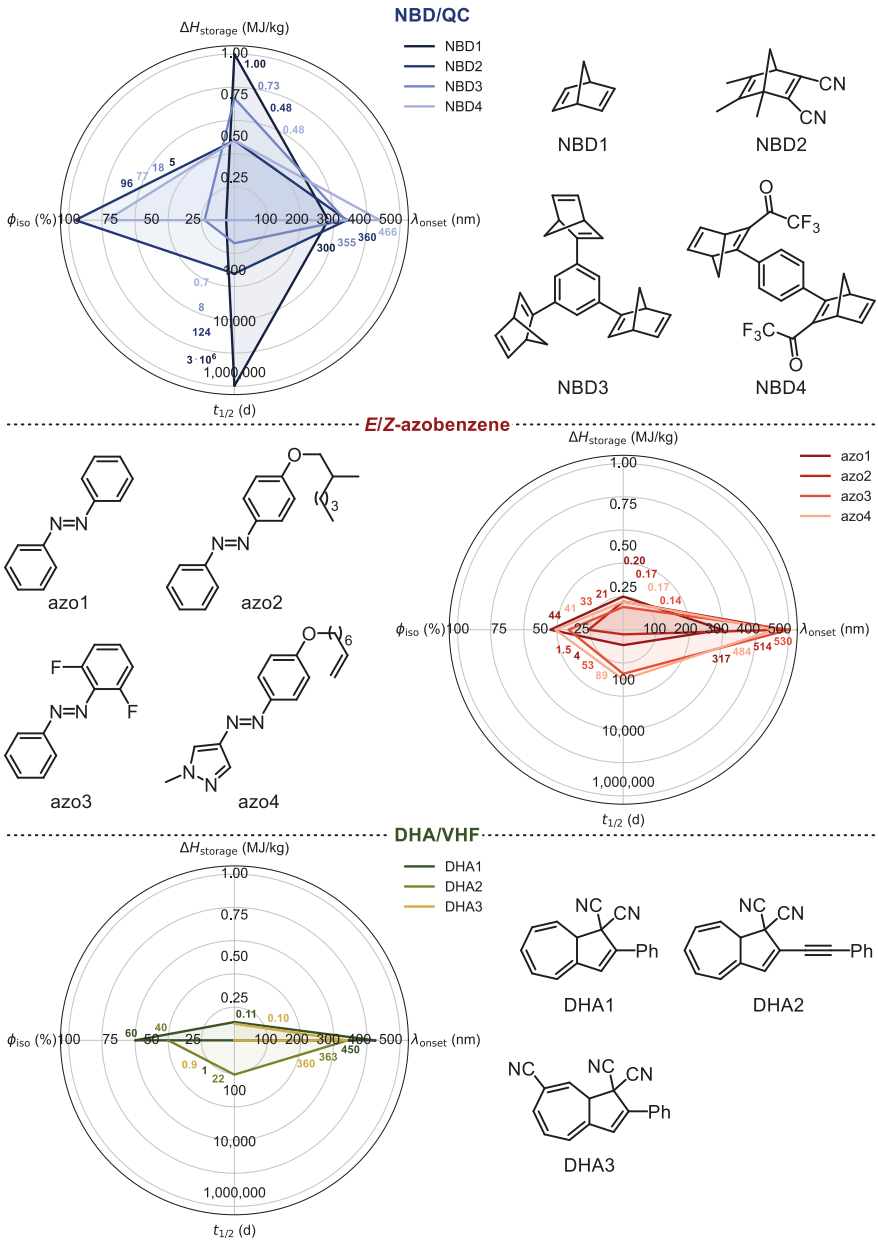

Figure 1.6. Comparison of key MOST properties of selected NBD/QC,[40b, 51-52] azobenzenes,[40b, 50, 53] and DHA/VHF systems.[54] Half-lives are plotted on a $\log_{10}$ scale. Exact property values are given along the axis denoted by their respective color. For the DHA/VHF systems, two datasets are incomplete.

These modifications, however, inevitably reduce the energy density. This drawback can be offset by coupling multiple NBD units *via* molecular linkers, as exemplified by NBD3 and NBD4 (Figure 1.6).[52b] Despite their advantages, many NBD/QC systems still face the limitation of requiring high excitation energies (short wavelength).[55] Nevertheless, decades of research have produced derivatives with substantially bathochromically shifted absorption profiles, partially addressing this challenge. For instance, increasing conjugation and introducing electron-deficient trifluoroacetyl groups into NBD dyads have pushed absorption into the visible region, as demonstrated for NBD4 (Figure 1.6).[51b]

Azobenzenes, by contrast, naturally absorb at longer wavelengths, offering improved spectral overlap with solar irradiance. Additionally, simple substitution enables further bathochromic shifts of their absorption profiles, e.g. azo2 and azo3 (Figure 1.6).[53c, 56] While their quantum yields typically fall below those of optimized NBD/QC systems, they are still considerable. The derivatives highlighted here, especially azo3: a nonsymmetric *ortho*-difluoro azobenzene,[53c] and azo4: a pyrazol-diazobenzene (Figure 1.6),[53d] exhibit unusually long thermal half-lives compared to other azobenzenes. More commonly, thermal reversion occurs rapidly under ambient conditions, posing a persistent challenge.[57] In addition, their relatively low energy storage density remains a limiting factor.[58]

DHA/VHF systems, though less developed, show promising features. They provide decent quantum yields and solar absorption profiles, especially considering their relatively recent emergence in the MOST field.[54a, 59] However, like azobenzenes, they suffer from low energy densities and short half-lives, the latter of which could be combated by inserting an acetylene linker to the phenyl substituent (DHA2, Figure 1.6).[54a]

Another promising and recently developed MOST system involves fluorinated *ortho*-methylacetophenones. Upon irradiation, these compounds can cyclize *via* a Norrish type II reaction, forming the corresponding cyclobutanol (Scheme 1.2).

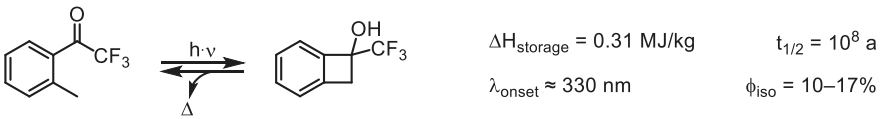

Scheme 1.2. Photoinduced cyclization of fluorinated *ortho*-methylacetophenones to benzocyclobutanols as recently developed MOST system.

Through the imposed strain, this transformation enables a fair energy storage density of 0.31 MJ/kg. In addition, these systems exhibit exceptionally long thermal half-lives. However, they require excitation in the UVA region and show only moderate quantum yields in the range of 10–17%.[60]

Altogether, these systems exemplify the trade-offs intrinsic to MOST design. No single photoswitch currently combines ideal characteristics, underscoring the ongoing challenge for molecular innovation to achieve a balanced and efficient energy storage platform.

1.2.5 Azaborinines

While current MOST systems offer a solid foundation, continued innovation is essential to overcome current limitations. In this context, 1,2-dihydro-1,2-azaborinines have recently emerged as a promising scaffold for solar thermal energy storage.[38b, 61]

Originally reported by Dewar in 1962,[62] the synthesis of 1,2-dihydro-1,2-azaborinines remained challenging for decades. A significant breakthrough was reached with the development of a ring closing metathesis strategy (Scheme 1.3), pioneered by Ashe[63] and later refined by Liu,[64] which enabled efficient access to both the parent compound and a range of derivatives.

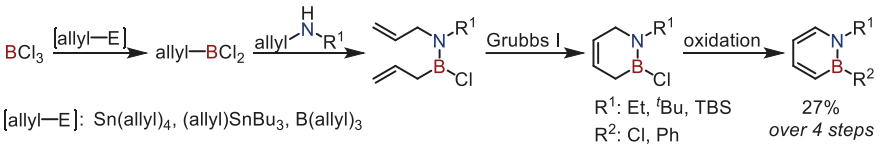

Scheme 1.3. Modern synthesis route toward 1,2-dihydro-1,2-azaborinines *via* ring closing metathesis of a diallyl boramine followed by oxidation.[61, 63-64]

As BN isosteres of benzene, 1,2-dihydro-1,2-azaborinines inherit key properties such as aromaticity, albeit to a lesser extent due to reduced symmetry. This decreased aromaticity is reflected in greater bond localization: Natural Resonance Theory (NRT) computations indicate that the dominant Kekulé structure accounts for 57% of the electronic structure (Figure 1.7a).[65] Nonetheless, the partial delocalization imparts double-bond character to the BN unit.[66]

Aromaticity is further supported by the resonance stabilization energy (RSE), experimentally determined to be 16.6 kcal/mol by comparing the hydration enthalpy discrepancy between 1-(*tert*-butyl)-1,2-dihydro-1,2-azaborinine and its

1,2,3,4-/1,2,5,6-tetrahydro analogues. As a reference, benzene exhibits a substantially higher RSE of 32.4 kcal/mol (Figure 1.7b).[67] Additionally, experimental NMR chemical shifts and Nucleus Independent Chemical Shift (NICS) computations confirm diamagnetic ring currents, consistent with an aromatic character, which is slightly reduced compared to benzene (Figure 1.7a).[65, 68]

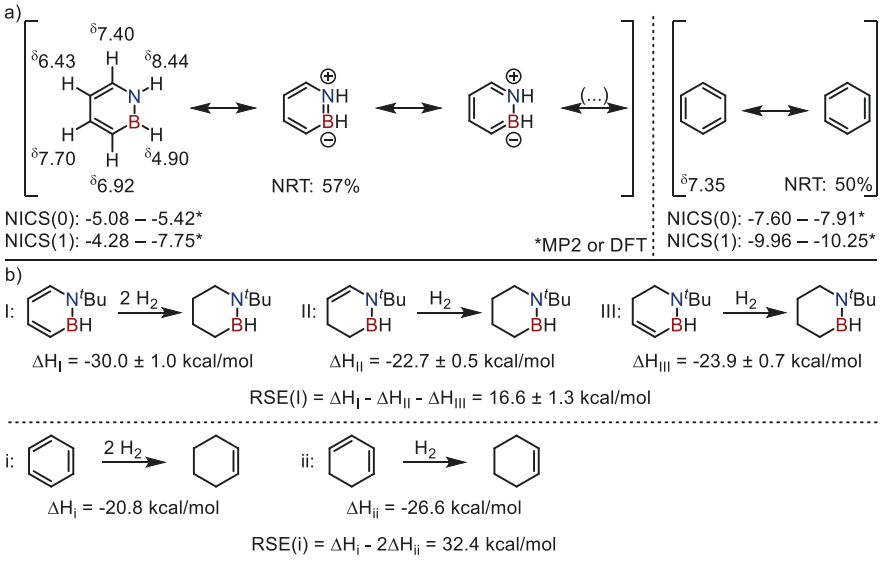

Figure 1.7. [a]Aromaticity comparison between benzene and 1,2-dihydro-1,2-azaborinine using ^{1}H NMR chemical shifts in DCM-d_2,[64a, 69] computed NICS values (MP2/6-311+G(d,p);[65] B3LYP/6-31+G(d,p);[68a] MP2/aug-cc-pVDZ,[68b] or HSE06/def2-QVPPD[68c]), and NRT analysis.[65] [b]Experimentally determined RSEs of 1-(*tert*-butyl)-1,2-dihydro-1,2-azaborinine and benzene-based on hydration enthalpies.[67]

Photochemical Behavior

In contrast to benzene, which upon irradiation yields a plethora of valence isomers,[70] 1,2-dihydro-1,2-azaborinines typically undergo selective photoisomerization to the Dewar isomer (Figure 1.8a).[71] Upon excitation to the S_1 state, the parent compound relaxes thermally towards a CI, funneling the excited state population into a prefulven-like intermediate. From this point, two competing pathways exist: reversion to the 1,2-dihydro-1,2-azaborinine or conversion to the Dewar isomer (Figure 1.8b).[72]

A key distinction from benzene lies in the relative energies of the Franck Condon (FC) region and the CI towards the Dewar isomer. In 1,2-dihydro-1,2-azaborinines, this pathway is

energetically downhill, facilitating efficient isomerization, whereas for benzene it is uphill, limiting conversion.[72b, 73]

Despite the computed photochemical competing pathway back to the 1,2-dihydro-1,2-azaborinine, matrix isolation studies demonstrate complete conversion to the Dewar form under UV irradiation.[74] This selectivity can be ascribed to the higher excitation energy of the Dewar isomer compared to the 1,2-dihydro-1,2-azaborinine, rendering it a photochemical sink to which 1,2-dihydro-1,2-azaborinine is converted under continued irradiation.[72a, 75]

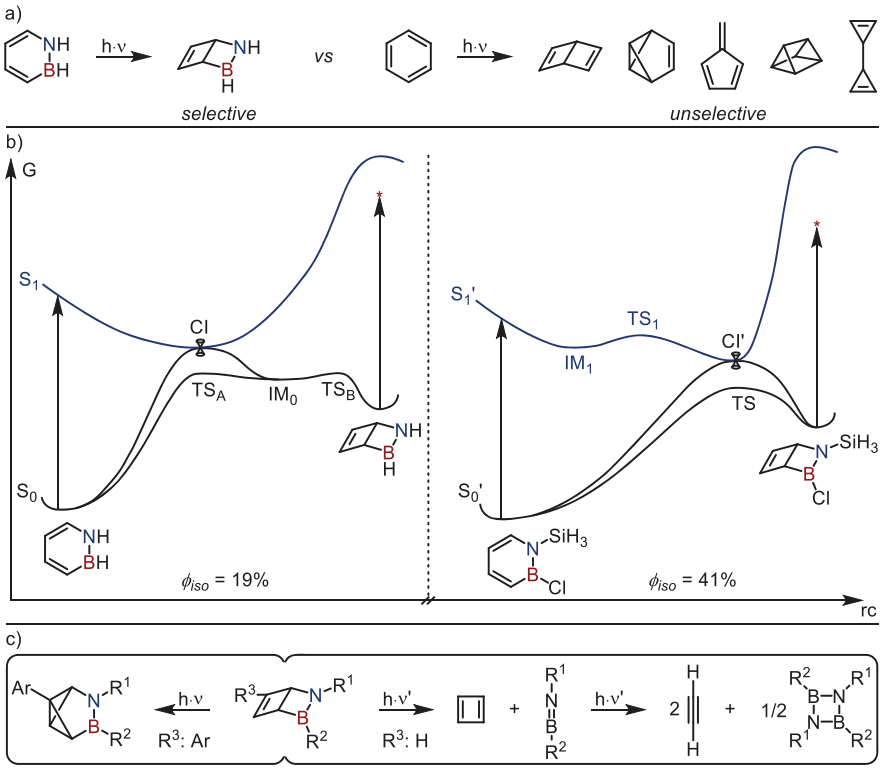

Figure 1.8. Photoisomerization of 1,2-dihydro-1,2-azaborinines. [a]Comparison of the photoisomerization of benzene to its 1,2-BN isostere.[70-71] [b]Schematic representation of the photoisomerization mechanism of the parent and B–Cl, N–SiH_3 substituted 1,2-dihydro-1,2-azaborinine,[72, 75] alongside their quantum yields,[72b] based on computational studies. [c]Photochemistry of Dewar 1,2-dihydro-1,2-azaborinines, showcasing the formation of the benzvalene isomer and a decomposition pathway.[38b, 76]

Substitution at the boron and nitrogen atoms significantly influences both the potential energy surface and consequently the quantum yield. For example, B–Cl/N–SiH_3 substitution

eliminates the presence of an intermediate (IM_0 Figure 1.8b) along the ground state minimum energy path between the Dewar and TS structure. This moves the CI favorably towards Dewar formation boosting the quantum yield from 19% in the parent to 41% in the substituted compound (Figure 1.8b).[72b] Experimental results are in agreement: the B–Mes/N–TBS derivative exhibits an experimental quantum yield of 46%, while portraying no intermediate between the TS and Dewar structure on the calculated energy profile.[38b]

Further photoreactivity is observed for derivatives bearing an aryl substituent in 5-position. In these systems, the Dewar isomers feature a styrene chromophore, lowering excitation energy and enabling benzvalene formation *via* likely a radical mechanism (Figure 1.8c).[76] In contrast, Dewar isomers without extended conjugation undergo photodecomposition if excited at shorter wavelengths, proceeding over an iminoborane intermediate that dimerizes to form a 1,3-diaza-3,4-diboretidine and cyclobutadiene, which decomposes to acetylene (Figure 1.8c).[38b]

1,2-Dihydro-1,2-Azaborinines as MOST Systems

From a MOST perspective, 1,2-dihydro-1,2-azaborinines offer a compelling combination of energy density and quantum efficiency. Photoisomerization of the parent compound stores impressive energy ($\Delta G_{storage}$ = 3.1 MJ/kg),[74] both in the form of ring strain and *via* release of resonance energy upon rearomatization.[38b, 61]

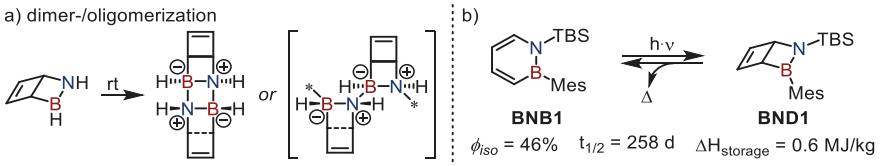

Figure 1.9. [a]Dimer-/oligomerization process observed at temperatures above matrix isolation conditions for the Dewar isomer of 1,2-dihydro-1,2-azaborinine.[74] [b]Steric stabilization of the 1,2-dihydro-1,2-azaborinine furnishing a model suitable as an initial MOST system.[38b]

However, the Dewar isomer of the parent compound is prone to dimerization and oligomerization (Figure 1.9a),[74] Stabilization has been achieved using sterically demanding substituents, yielding isolable Dewar isomers under inert atmosphere at rt (Figure 1.9b). Notably, the B–Mes/N–TBS derivative displays a quantum yield of 46%, an energy density of 0.6 MJ/kg, and a thermal half-life of ~258 d at rt.[38b]

The prolonged half-life aligns with the Woodward-Hoffmann rules: the thermally allowed cycloreversion proceeds *via* a conrotatory mechanism, which is geometrically inaccessible in

the Dewar structure.[16] *Per se*, the alternative disrotatory path is symmetry-forbidden and energetically unfavorable. As a result, the system follows an asymmetric pathway as the lowest-energy route. Specifically, rotation of C^3 towards the nitrogen, boron, C^4, C^5 plane precedes the planarization of C^6, even leading to a stepwise process for certain systems (e.g. parent). These mechanistic features account for the high activation barrier of the cycloreversion and, consequently, the extended thermal stability of the Dewar isomer.[74]

Despite these promising properties, a key challenge remains: the high excitation energy required for isomerization. The parent 1,2-dihydro-1,2-azaborinine absorbs at 279 nm, well outside the optimal solar spectrum window.[38b] Thus, bathochromic shifting strategies are under current investigation.[77]

In summary, the selective isomerization pathway, combined with high energy density, good quantum efficiency, and thermal stability, position 1,2-dihydro-1,2-azaborinines as valuable candidates in the evolving landscape of MOST systems.

1.2.6 Energy Release

The controlled release of stored energy is a defining criterion for the practical implementation of MOST systems. Ideally, this process should be selective, efficient, and tunable, enabling on-demand energy output without compromising the stability or cyclability of the system.

The simplest mode of energy release in MOST systems is thermal back-conversion (Figure 1.10). While straightforward, this process often limits long-term storage. Still, systems with short half-lives suit daily energy cycling, as in polymer coatings that harvest sunlight during the day and release heat at night.[51b] For more stable systems, thermal activation remains viable when the released heat triggers self-propagating conversion.[78]

Another strategy involves photoinduced back-conversion. This approach is particularly common in azobenzene-based systems, which can undergo reversible *E*/*Z* isomerization upon irradiation at different wavelengths (Figure 1.10). While this provides a useful handle for study, it typically leads to photostationary states, which limits energy storage density.[53b, 79]

A photochemically orthogonal approach towards energy release is taken by electrochemistry. By oxidizing or reducing the high energy isomer,[80] the back-conversion can be initiated (Figure 1.10). This strategy has been most prominently demonstrated for NBD/QC

systems, where the $QC^{\bullet+}$ exhibits a substantially reduced half-life and can promote autocatalytic cycloreversion.[81] However, integration in a device remains to be demonstrated.

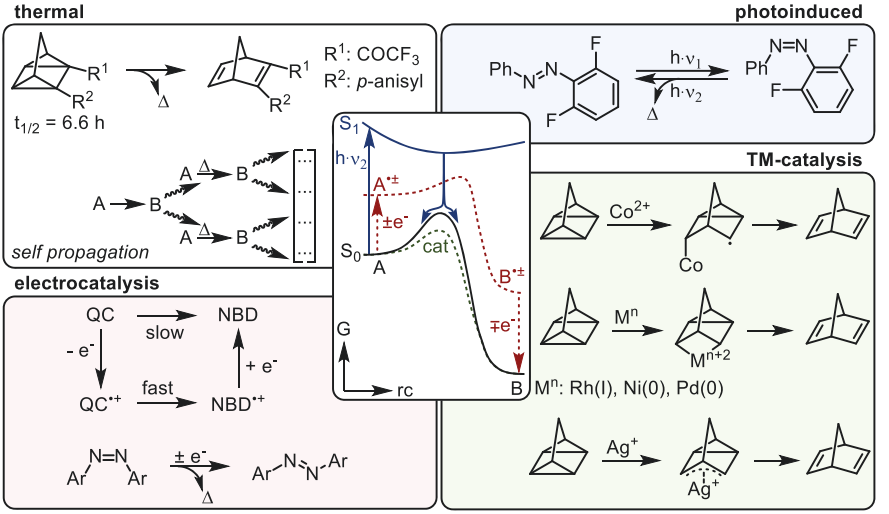

Figure 1.10. Schematic energy diagram based on literature precedents for the energy release in MOST systems: Thermally induced heat release utilizing relatively short half-lives or a self-propagating mechanism.[46, 78] Photoinduced reisomerization of an azobenzene.[53b] Electrocatalytic back-conversion of QC *via* oxidation and *Z*-azobenzene *via* reduction.[80-81] TM-catalyzed energy release exemplified on QC by radical, OA, and LA-based mechanism.[48]

TM-catalysis is the most widely adopted strategy for energy release in MOST systems, particularly for the established NBD/QC pair. TM-catalysts promote back-conversion of QCs, involving the activation of the strained C–C bonds *via* radical mechanisms, OA, or LA coordination (Figure 1.10),[48] paralleling broader C–C bond cleavage strategies discussed earlier. Square planar cobalt complexes, such as cobalt porphyrins, are among the most effective catalysts, enabling radical-mediated ring-opening of QC.[48] Their facile immobilization on solid supports allows for heterogeneous catalysis, rendering them the catalyst of choice in many proof-of-concept devices.[46, 82] Metals and metal oxides have also shown activity, offering alternative heterogeneous platforms.[48, 83] Low-valent TMs such as rhodium(I), nickel(0), and palladium(0) facilitate energy release from QCs through OA followed by reductive extrusion of the TM to generate the respective NBD.[48] This approach extends to strain related scaffolds, such as 1,2-dihydro-1,2-azaborinines, where the Dewar isomer can undergo efficient cycloreversion in the presence of Wilkinson's catalyst.[38b] Similarly, LAs such as silver(I) salts

can mediate the ring-opening of both QC and Dewar 1,2-dihydro-1,2-azaborinines by facilitating an asymmetric cycloreversion pathway.[48, 61] In both systems, this route bypasses the thermal pericyclic inaccessible mechanism.[84] The efficiency of this approach strongly depends on the nature of the counterion.[61] Weakly coordinating anions (WCAs) enhance the reactivity by maximizing Lewis-acidity of silver(I).

Effective WCAs are typically monovalent to reduce Coulombic interactions, feature a delocalized charge distribution to avoid nucleophilic or basic sites, and are chemically robust (e.g. redox persistent). Additionally, they exhibit low polarizability, reducing London dispersion interactions. According to the Hard-Soft Acid-Base (HSAB) principle, the relatively soft silver(I)-cation obtains enhanced reactivity when mismatched with a hard anion that promotes catalytic efficiency.[85] As an example, for the energy release of QCs, $AgClO_4$,[86] $AgCF_3CO_2$,[87] and $AgBF_4$ salts have proven effective,[88] while for the 1,2-dihydro-1,2-azaborinines more modern representatives such as $AgSbF_6$ and $Ag[Al(OC(CF_3)_3)_4]$ achieved proficient activity.[61]

1.3 Benzocyclobutanones

In addition to its role in MOST systems, molecular strain also serves as a powerful driving force in synthetic chemistry. As previously discussed, strained carbocycles can undergo OA with TMs, unlocking valuable pathways for molecular diversification. An initial insight into this reactivity was reported in 1955, when Tipper postulated the formation of a platinacyclobutane complex upon treatment of cyclopropane with $PtCl_2$, laying the foundation for TM-mediated activation of strained rings (Scheme 1.4a).[89]

While cyclopropane and cyclobutane exhibit comparable strain energies, their reactivity can be substantially enhanced through structural modification. Incorporation of a carbonyl group onto cyclobutane yields cyclobutanones, which exhibit slightly increased ring strain and possess a ketone moiety that facilitates interaction with TMs.[90] When fused to an aromatic ring, the resulting benzocyclobutanones (BCBs) display even greater strain due to additional sp^2-hybridized carbons affecting the angle strain.[91] Furthermore, BCBs are planar favoring the approach of a TM. Despite their strain, both cyclobutanones and BCBs are typically bench-stable, rendering them as privileged scaffolds in the development of TM-catalyzed C–C activation strategies.

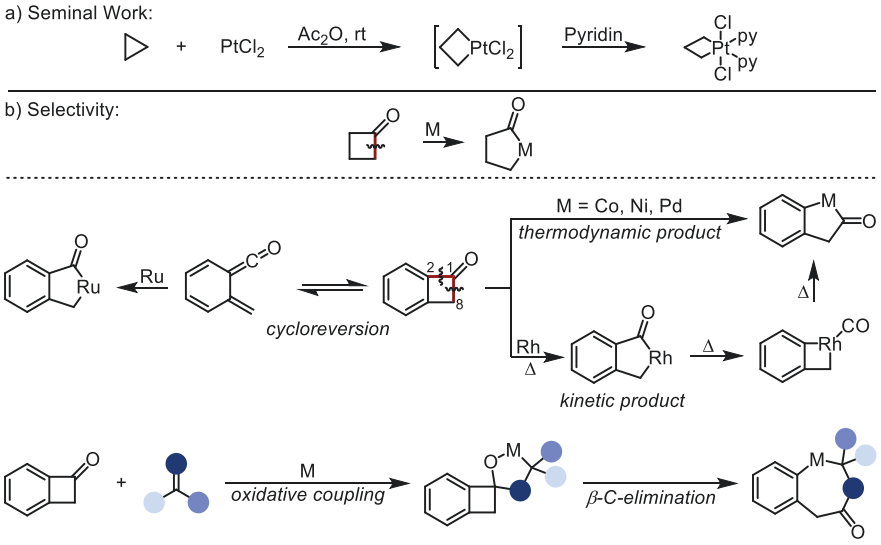

Scheme 1.4. [a]Seminal report by Tipper and co-workers on the OA of $PtCl_2$ into cyclopropane. [b]Comparison of the OA reactivity of cyclobutanone and BCB, highlighting the distinct regioselectivity observed for different TMs in BCB activation.

In contrast to cyclobutanone, which contains a single feasibly cleavable C–C bond adjacent to the carbonyl group, BCB features two distinct C–C bonds that are both susceptible to activation (Scheme 1.4b).[92] In 1992, Liebeskind and co-workers reported that Wilkinson's catalyst selectively engages the less hindered C–C bond of BCB *via* classical OA. Upon thermal treatment, the initially formed complex undergoes decarbonylation followed by CO reinsertion, furnishing the thermodynamically more stable regioisomer (Scheme 1.4b).[93]

A similar regioselectivity has been observed for ruthenium-catalysis, where formation of the kinetic product is proposed to proceed *via* cycloreversion of BCB to the corresponding *ortho*-ketene methide,[94] followed by oxidative cyclization (Scheme 1.4b).[95] In contrast, cobalt, nickel and palladium-catalysts tend to favor concerted OA into the C^1–C^2 bond, directly yielding the thermodynamically preferred product (Scheme 1.4b).[96] This preference is commonly attributed to the formation of a strong aryl–metal bond, which is generally more stable than the corresponding alkyl–metal species (see Section 1.1.1 above).

Regardless of the activation pathway, the resulting metallabenzocyclopentanone intermediate typically engages in the insertion of an unsaturated reaction partner, such as an alkene, alkyne, diene, or strained cyclic compound. This step is followed by reductive elimination (RE), leading to the formation of ring-expanded products, typically five- to eight-membered carbocycles or heterocycles. In some cases, especially for rhodium-based systems, this sequence may be accompanied by decarbonylation, further diversifying the reaction outcome or leading to undesirable side products.[11, 17c, 26, 97]

An alternative mechanism involves initial oxidative coupling at the carbonyl functionality, followed by *β*-carbon-elimination from the resulting metal alkoxide.[98] While less common, this pathway remains a plausible activation mode for BCBs and should not be entirely disregarded (Scheme 1.4b).

1.3.1 Intramolecular reactions

Having outlined the general principles governing the reactivity of BCBs, the following section will focus on their synthetic applications, beginning with intramolecular transformations. Among these, late-stage TM-catalyzed reactions, particularly those involving rhodium complexes, have emerged as the most prominent and versatile class. One notable example is the ring expansion of benzylic substituted BCBs, in which the OA of a rhodium(I)-

catalyst initiates a *β*-hydride-elimination, olefin reinsertion cascade, yielding indanone derivatives (Figure 1.11a).[99]

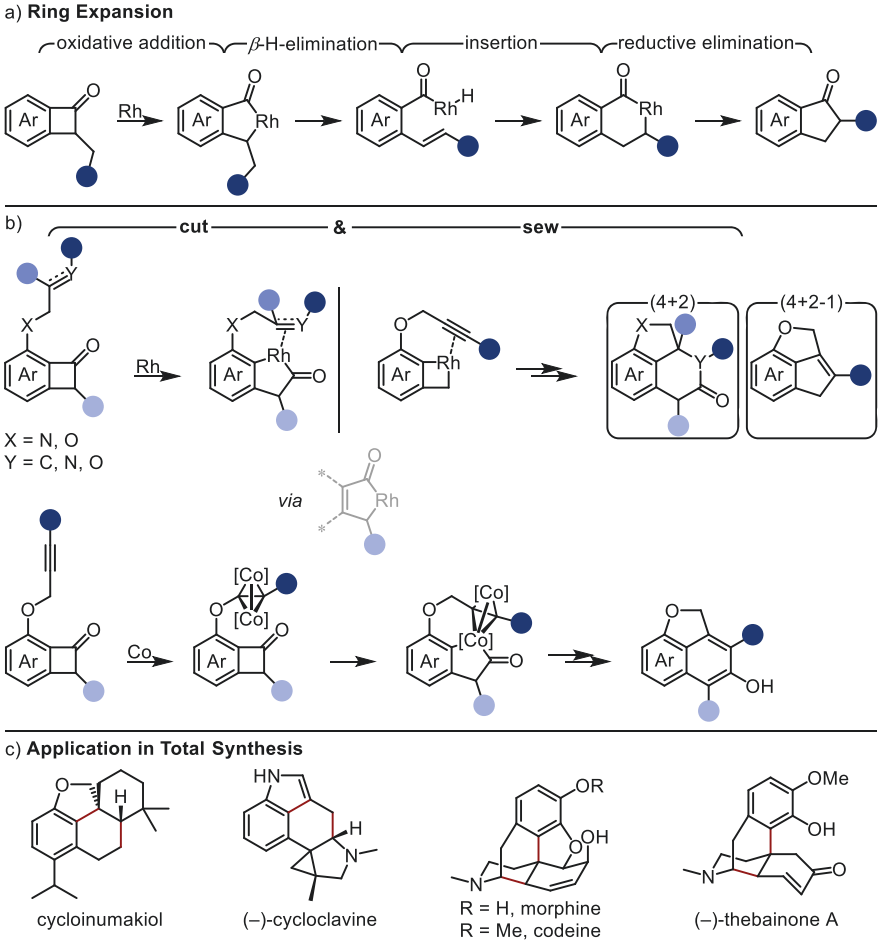

Figure 1.11. Overview of intramolecular rhodium and cobalt-catalyzed transformations of BCBs *via* [a]ring expansion and [b]"cut-and-sew" strategies.[96c, 99] [c]Application of "cut-and-sew" reactions, marked in red, in the total synthesis of selected bioactive compounds.[26a]

Beyond the ring expansion, a broader family of "cut-and-sew" transformations has been developed, wherein BCBs undergo regio- and stereoselective insertion of tethered alkenes, alkynes, ketones or oxime ethers into the strained cycle (Figure 1.11b). Pioneered by Dong and co-workers in 2012,[100] these rhodium-catalyzed reactions offer a highly atom-economical

platform for the construction of polycyclic architectures and can be performed in an enantioselective fashion.[101] Utilizing this strategy, a range of bioactive and structurally complex molecules could be accessed (Figure 1.11c).[26a]

In addition to rhodium, its earth abundant congener cobalt has also been shown to promote intramolecular "cut-and-sew" transformations, enabling the insertion of alkynes into BCBs.[96c] The Pauson-Khand type reaction proceeds *via* initial formation of a tetrahedral dicobalt-alkyne complex from $Co_2(CO)_8$, which, upon ligand exchange with the carbonyl group of the BCB, facilitates C^1–C^2 bond activation. Subsequent migratory insertion and RE deliver the corresponding *β*-naphthol-type polycycles (Figure 1.11b).

1.3.2 Intermolecular reactions

While a wide variety of rhodium-catalyzed intramolecular "cut-and-sew" reactions have been developed, intermolecular examples remain sparse. In this transformation, BCBs are coupled with styrene derivatives in a formal (4+1) cycloaddition (Scheme 1.5).[102]

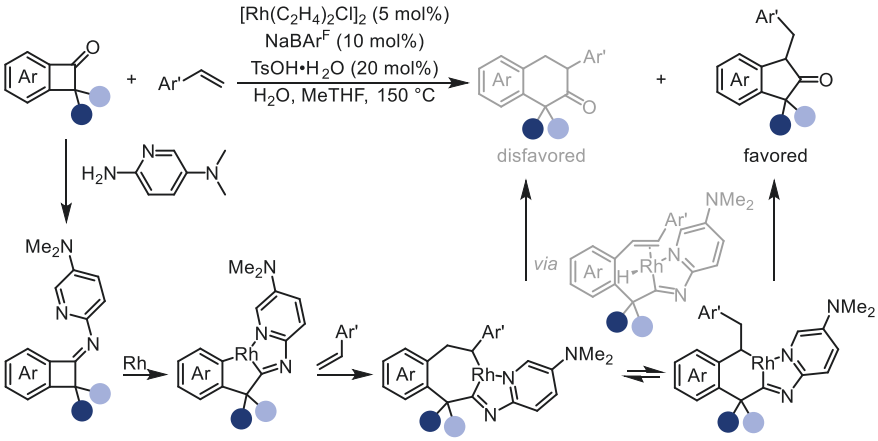

Scheme 1.5. Intermolecular rhodium-catalyzed styrene insertion into BCBs *via* a directing group approach to furnish 2-indanones.

A 2-aminopyridine derivative was employed to form the corresponding imide under Brønsted acid catalysis, which both suppresses decarbonylation and, more importantly, serves as a directing group for C–C activation. The seemingly unusual (4+1) outcome is rationalized by a Curtin–Hammett scenario. Initial OA of rhodium into the BCB ring followed by alkene insertion generates a seven-membered rhodacycle, which is in rapid equilibrium with a six-

membered metallocycle *via* β-H-elimination and reinsertion. As DFT studies showed the RE barrier for the (4+1) product to be lower, this pathway is favored, resulting in high selectivity for the five-membered product.

A second rhodium-catalyzed intermolecular transformation has been reported, involving the coupling of BCBs with indoles. The reaction proceeds *via* directed C–H bond activation, followed by σ-bond metathesis between the resulting Rh–H bond and the C^1–C^8 bond of the BCB. Subsequent decarbonylation and RE yield the biaryl coupling product (Scheme 1.6).[103] Turning to rhodium's neighbor on the periodic table, ruthenium engages in a related intermolecular reaction with indoles. Analogously, the reaction begins with C–H activation, but the subsequent σ-bond metathesis occurs between the Ru–C bond and the C^1–C^8 bond of the BCB. After RE, the resulting aldehyde intermediate cyclizes with the indole and undergoes dehydroaromatization to form benzo[*b*]carbazoles (Scheme 1.6).

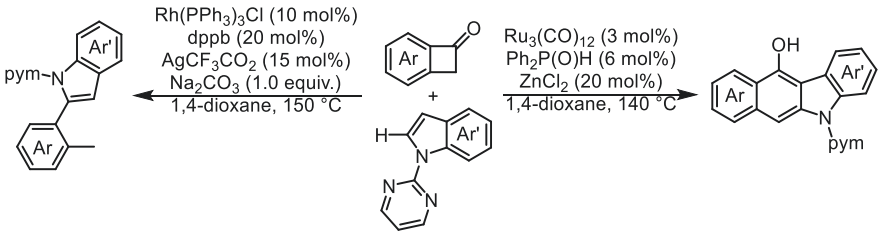

Scheme 1.6. TM-catalyzed intermolecular coupling of BCBs and indoles, enabling the synthesis of different product scaffolds.

Ruthenium has also been employed in intermolecular (4+2) insertion reactions of BCBs. In this context, vicinal diols, ketols or diones serve as coupling partners, affording dihydroxylated α-tetralones through a diastereoconvergent process in excellent yields (Scheme 1.7).[95a] When chiral ligands are employed, the reactions proceed with high levels of enantioselectivity.[95b] Mechanistically, the ruthenium-catalyst first promotes dehydrogenation of the ketol to form the corresponding 1,2-diketone, which then undergoes sequential insertion into the ruthenium BCB OA complex (see Scheme 1.4b above). The resulting ruthenium diolate regenerates ruthenium(0) by dehydrogenating an additional equivalent of ketol, thereby closing the catalytic redox-neutral cycle. When employing a vicinal diol two equivalents of the respective BCB are required, one acting as the coupling partner, the other as the oxidant. Conversely, when using diketones, the reaction requires ^{i}PrOH as a reductant.

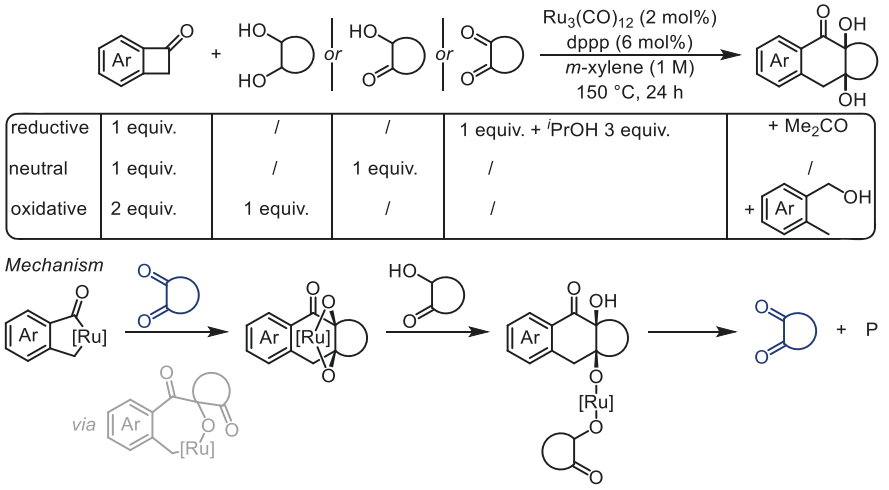

Scheme 1.7. Ruthenium-catalyzed insertion of vicinal diols, ketols or diketones into BCBs *via* oxidative, redox-neutral or reductive conditions respectively.

Palladium has also proven competent in mediating intermolecular insertion reactions with BCBs. Two examples involve the insertion of strained rings, specifically silacyclobutanes and aziridines, *via* a double OA pathway (Scheme 1.8a, b).[96b, 104] These reactions enable access to eight-membered silacycles and benzazepines, the latter being a structural motif frequently encountered in pharmaceuticals and bioactive compounds.[104b] In a more recent development, a palladium-catalyzed intermolecular [4+2] cycloaddition between BCBs and *in situ* generated arynes, from *ortho*-haloaryl boronates, has been reported, further expanding the scope of palladium-mediated insertion reactions (Scheme 1.8c).[105]

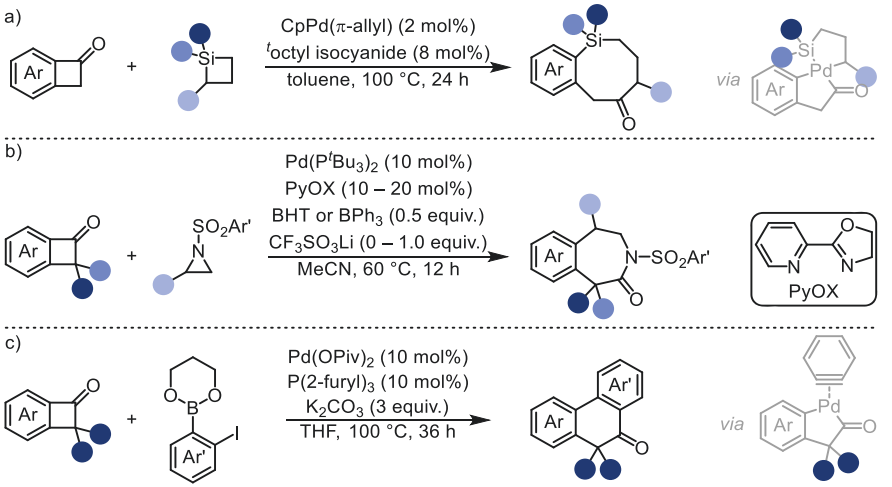

Scheme 1.8. Palladium-catalyzed intermolecular reactions with BCBs, yielding ring expansion products.

While rhodium excels in intramolecular "cut-and-sew" transformations of BCBs, nickel has emerged as a competent choice for the corresponding intermolecular variants. A variety of unsaturated partners, such as 1,3-dienes, NBDs, and alkynes can be inserted into either the C^1–C^2 or C^1–C^8 bond, enabling access to a broad array of polycyclic scaffolds (Scheme 1.9).[98, 106] The observed regioselectivity is primarily governed by steric effects at the C^3 position, with substituents promoting selective activation of the C^1–C^8 bond (Scheme 1.9c), in analogy to rhodium systems.[106a] Although decarbonylation of the OA complex can occur under nickel-catalysis, CO reinsertion, commonly observed in rhodium chemistry, does not take place, offering complementary reactivity. In the absence of an external insertion partner, BCBs can undergo nickel-catalyzed dimerization, leading to two distinct pathways: formation of seven-membered rings through direct coupling of two BCB units of which one is decarbonylated, or a formal [4+2] cycloaddition to yield lactone scaffolds.[107]

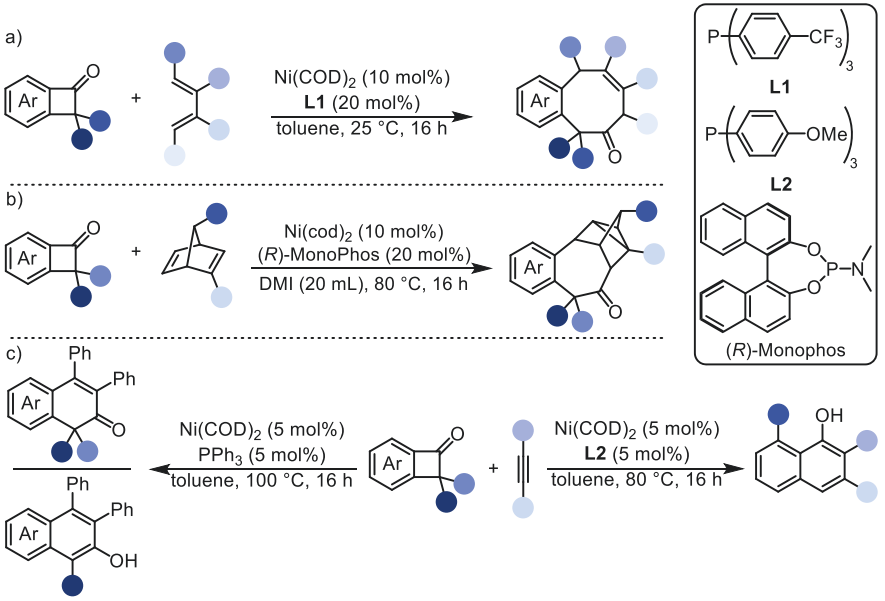

Scheme 1.9. Nickel-catalyzed intermolecular "cut-and-sew"-type reaction with BCBs, furnishing diverse carbon-based scaffolds.

A mechanistically distinct example is the nickel-catalyzed coupling of BCBs with indoles, which deviates from the standard OA, insertion, RE sequence.[103] The reaction proceeds similarly to the previously described ruthenium-catalyzed variant (*cf.* Scheme 1.6), with the difference of an observed decarbonylation, furnishing biaryl methylenes (Scheme 1.10).[108]

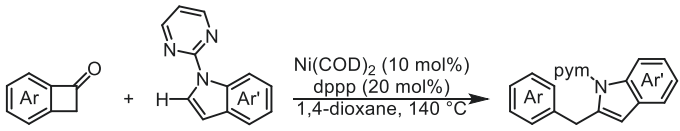

Scheme 1.10. Nickel-catalyzed intermolecular coupling of BCBs and indoles by a sequence of C–H and C–C activation.

1.4 References

[1] E. J. Corey, X.-M. Cheng, *The Logic of Chemical Synthesis*, **1995**.

[2] M. Ishii, I. Takuro, S. Hiroko, I. and Kuwajima, *Sci. Technol. Adv. Mater.* **2024**, *4*, 2354649.

[3] A. Gaulton, L. J. Bellis, A. P. Bento, J. Chambers, M. Davies, A. Hersey, Y. Light, S. McGlinchey, D. Michalovich, B. Al-Lazikani, J. P. Overington, *Nucleic Acids Res.* **2011**, *40*, D1100-D1107.

[4] M. Sorokina, P. Merseburger, K. Rajan, M. A. Yirik, C. Steinbeck, *J. Cheminform.* **2021**, *13*, 2.

[5] P. G. Levi, J. M. Cullen, *Environ. Sci. Technol.* **2018**, *52*, 1725-1734.

[6] a) J. Magano, in *Transition Metal-Catalyzed Couplings in Process Chemistry*, **2003**, pp. 313-355; b) C. J. Borths, S. D. Walker, *Isr. J. Chem.* **2020**, *60*, 340-350.

[7] T. Nanda, M. Fastheem, A. Linda, B. V. Pati, S. K. Banjare, P. Biswal, P. C. Ravikumar, *ACS Catal.* **2022**, 13247-13281.

[8] J. E. Huheey, E. A. Keiter, R. L. Keiter, O. K. Medhi, *Inorganic chemistry: principles of structure and reactivity*, Pearson Education India, **2006**.

[9] M. Murakami, N. Ishida, *J. Am. Chem. Soc.* **2016**, *138*, 13759-13769.

[10] M. Murakami, N. Ishida, in *Cleavage of Carbon-Carbon Single Bonds by Transition Metals*, **2015**, pp. 1-34.

[11] L. Souillart, N. Cramer, *Chem. Rev.* **2015**, *115*, 9410-9464.

[12] a) L. Gurvich, I. Veyts, C. Alcock, *Co., New York* **1989**; b) B. Ruscic, R. E. Pinzon, M. L. Morton, N. K. Srinivasan, M.-C. Su, J. W. Sutherland, J. V. Michael, *J. Phys. Chem. A* **2006**, *110*, 6592-6601; c) E. U. Franck, *Ber. Bunsenges. Phys. Chem.* **1990**, *94*, 93-93.

[13] a) H. Nagata, N. Miyazawa, K. Ogasawara, *Chem. Commun.* **2001**, 1094-1095; b) Y. Zhou, Y.-L. Wei, J. Rodriguez, Y. Coquerel, *Angew. Chem. Int. Ed.* **2019**, *58*, 456-460.

[14] L. Claisen, *Ber. Dtsch. Chem. Ges.* **1912**, *45*, 3157-3166.

[15] O. Diels, K. Alder, *Ber. Dtsch. Chem. Ges.* **1929**, *62*, 2337-2372.

[16] R. B. Woodward, R. Hoffmann, *Angew. Chem., Int. Ed.* **1969**, *8*, 781-853.

[17] a) L. A. Paquette, J. C. Stowell, *J. Am. Chem. Soc.* **1970**, *92*, 2584-2586; b) Z. Chen, L. Wei, J. Zhang, *Org. Lett.* **2011**, *13*, 1170-1173; c) M. Murakami, N. Ishida, *Chem. Rev.* **2021**, *121*, 264-299.

[18] W. M. Burton, in *United States Patent Office* (Ed.: S. O. Company), United States of America, **1912**.

[19] a) Y. Xiao, J. M. Longo, G. B. Hieshima, R. J. Hill, *Ind. Eng. Chem. Res.* **1997**, *36*, 4033-4040; b) L. Du, Y. Han, Y. Zhu, Y. Xu, X. Bai, Y. Ouyang, Y. Luo, X. Shu, *ACS Omega* **2023**, *8*, 7093-7101.

[20] Y. Qin, T. Zhang, H. Y. V. Ching, G. S. Raman, S. Das, *Chem* **2022**, *8*, 2472-2484.

[21] S. Shao, X. Wang, W. Li, Y. Zhang, S. Liu, W. Xiao, Z. Yue, X. Lu, X. Fan, *Catal. Sci. Technol.* **2025**, *15*, 962-987.

[22] C.-Y. Huang, J. Li, C.-J. Li, *Chem. Sci.* **2022**, *13*, 5465-5504.

[23] a) M. Murakami, M. Makino, S. Ashida, T. Matsuda, *Bull. Chem. Soc. Jpn.* **2006**, *79*, 1315-1321; b) M. E. O'Reilly, S. Dutta, A. S. Veige, *Chem. Rev.* **2016**, *116*, 8105-8145.

[24] K. Nogi, H. Yorimitsu, *Chem. Rev.* **2021**, *121*, 345-364.

[25] a) F. Chen, T. Wang, N. Jiao, *Chem. Rev.* **2014**, *114*, 8613-8661; b) Y.-F. Liang, M. Bilal, L.-Y. Tang, T.-Z. Wang, Y.-Q. Guan, Z. Cheng, M. Zhu, J. Wei, N. Jiao, *Chem. Rev.* **2023**, *123*, 12313-12370.

[26] a) Y. Xue, G. Dong, *Acc. Chem. Res.* **2022**, *55*, 2341-2354; b) P.-h. Chen, B. A. Billett, T. Tsukamoto, G. Dong, *ACS Catal.* **2017**, *7*, 1340-1360.
[27] F. Song, B. Wang, Z.-J. Shi, *Acc. Chem. Res.* **2023**, *56*, 2867-2886.
[28] a) D. Villemin, *Tetrahedron Lett.* **1980**, *21*, 1715-1718; b) R. H. Grubbs, *Angew. Chem. Int. Ed.* **2006**, *45*, 3760-3765; c) A. Fürstner, *J. Am. Chem. Soc.* **2021**, *143*, 15538-15555.
[29] C. Harries, *Liebigs Ann.* **1905**, *343*, 311-344.
[30] a) S. Datta, C.-L. Chang, K.-L. Yeh, R.-S. Liu, *J. Am. Chem. Soc.* **2003**, *125*, 9294-9295; b) K. Tanaka, A. Kamisawa, T. Suda, K. Noguchi, M. Hirano, *J. Am. Chem. Soc.* **2007**, *129*, 12078-12079.
[31] J. M. Simoes, J. L. Beauchamp, *Chem. Rev.* **1990**, *90*, 629-688.
[32] B. Rybtchinski, D. Milstein, *Angew. Chem. Int. Ed.* **1999**, *38*, 870-883.
[33] a) R. H. Crabtree, R. P. Dion, *J. Chem. Soc., Chem. Commun.* **1984**, 1260-1261; b) R. H. Crabtree, R. P. Dion, D. J. Gibboni, D. V. McGrath, E. M. Holt, *J. Am. Chem. Soc.* **1986**, *108*, 7222-7227.
[34] P. E. Siegbahn, M. R. Blomberg, *J. Am. Chem. Soc.* **1992**, *114*, 10548-10556.
[35] a) T. M. Sugden, *Nature* **1947**, *160*, 367-368; b) C. A. Coulson, W. E. Moffitt, *Lond. Edinb. Dubl. Phil. Mag. & J. Sci.* **1949**, *40*, 1-35; c) R. Hoffmann, R. B. Davidson, *J. Am. Chem. Soc.* **1971**, *93*, 5699-5705.
[36] K. B. Wiberg, *Angew. Chem. Int. Ed.* **1986**, *25*, 312-322.
[37] C.-H. Jun, *Chem. Soc. Rev.* **2004**, *33*, 610-618.
[38] a) H. Hogeveen, H. Volger, *J. Am. Chem. Soc.* **1967**, *89*, 2486-2487; b) K. Edel, X. Yang, J. S. A. Ishibashi, A. N. Lamm, C. Maichle-Mössmer, Z. X. Giustra, S.-Y. Liu, H. F. Bettinger, *Angew. Chem. Int. Ed.* **2018**, *57*, 5296-5300; c) C. Raju, H. P. Q. Nguyen, G. G. D. Han, *Chem. Sci.* **2024**, *15*, 17273-17283.
[39] G. S. Hammond, N. J. Turro, A. Fischer, *J. Am. Chem. Soc.* **1961**, *83*, 4674-4675.
[40] a) C.-L. Sun, C. Wang, R. Boulatov, *ChemPhotoChem* **2019**, *3*, 268-283; b) Z. Wang, H. Hölzel, K. Moth-Poulsen, *Chem. Soc. Rev.* **2022**, *51*, 7313-7326.
[41] IEA*, Vol. 2025*, Paris, **2024**.
[42] V. Smil, *Energy in Nature and Society: General Energetics of Complex Systems*, MIT Press, **2008**.
[43] Y. Hu, D. Soler Soneira, M. J. Sánchez, *J. Energy Storage* **2021**, *35*, 102262.
[44] ASTM, American Society for Testing & Materials International, West Conshohocken, **2020**.
[45] K. Börjesson, A. Lennartson, K. Moth-Poulsen, *ACS Sustain. Chem. Eng.* **2013**, *1*, 585-590.
[46] Z. Wang, A. Roffey, R. Losantos, A. Lennartson, M. Jevric, A. U. Petersen, M. Quant, A. Dreos, X. Wen, D. Sampedro, K. Börjesson, K. Moth-Poulsen, *Energ. Environ. Sci.* **2019**, *12*, 187-193.
[47] E. Fischer, *J. Am. Chem. Soc.* **1960**, *82*, 3249-3252.
[48] V. A. Bren, A. D. Dubonosov, V. I. Minkin, V. A. Chernoivanov, *Russ. Chem. Rev.* **1991**, *60*, 451-469.
[49] C. J. Fritzsche, *J. prakt. Chem.* **1867**, *101*, 337.
[50] Z. Wang, P. Erhart, T. Li, Z.-Y. Zhang, D. Sampedro, Z. Hu, H. A. Wegner, O. Brummel, J. Libuda, M. B. Nielsen, K. Moth-Poulsen, *Joule* **2021**, *5*, 3116-3136.
[51] a) Z.-i. Yoshida, *J. Photochem.* **1985**, *29*, 27-40; b) A. U. Petersen, A. I. Hofmann, M. Fillols, M. Mansø, M. Jevric, Z. Wang, C. J. Sumby, C. Müller, K. Moth-Poulsen, *Adv. Sci.* **2019**, *6*, 1900367.

[52] a) F. J. Hernández, J. M. Cox, J. Li, R. Crespo-Otero, S. A. Lopez, *J. Org. Chem.* **2023**, *88*, 5311-5320; b) R. Schulte, S. Afflerbach, T. Paululat, H. Ihmels, *Angew. Chem. Int. Ed.* **2023**, *62*, e202309544.

[53] a) Z. Wang, R. Losantos, D. Sampedro, M.-a. Morikawa, K. Börjesson, N. Kimizuka, K. Moth-Poulsen, *J. Mater. Chem. A* **2019**, *7*, 15042-15047; b) D. Schatz, C. Averdunk, R. Fritzius, H. A. Wegner, *Small* **2025**, *n/a*, 2502938; c) C. Knie, M. Utecht, F. Zhao, H. Kulla, S. Kovalenko, A. M. Brouwer, P. Saalfrank, S. Hecht, D. Bléger, *Chem.-Eur. J.* **2014**, *20*, 16492-16501; d) Z.-Y. Zhang, Y. He, Z. Wang, J. Xu, M. Xie, P. Tao, D. Ji, K. Moth-Poulsen, T. Li, *J. Am. Chem. Soc.* **2020**, *142*, 12256-12264.

[54] a) Z. Wang, J. Udmark, K. Börjesson, R. Rodrigues, A. Roffey, M. Abrahamsson, M. B. Nielsen, K. Moth-Poulsen, *ChemSusChem* **2017**, *10*, 3049-3055; b) C. Schøttler, S. K. Vegge, M. Cacciarini, M. B. Nielsen, *ChemPhotoChem* **2022**, *6*, e202200037; c) J. Mogensen, O. Christensen, M. D. Kilde, M. Abildgaard, L. Metz, A. Kadziola, M. Jevric, K. V. Mikkelsen, M. B. Nielsen, *Eur. J. Org. Chem.* **2019**, *2019*, 1986-1993.

[55] A. S. Aslam, L. M. Muhammad, A. Erbs Hillers-Bendtsen, K. V. Mikkelsen, K. Moth-Poulsen, *Chem.-Eur. J.* **2024**, *30*, e202401430.

[56] Z. Wang, A. Roffey, R. Losantos, A. Lennartson, M. Jevric, A. U. Petersen, M. Quant, A. Dreos, X. Wen, D. Sampedro, *Energ. Environ. Sci.* **2019**, *12*, 187-193.

[57] J. Olmsted, J. Lawrence, G. G. Yee, *Sol. Energy* **1983**, *30*, 271-274.

[58] M.-a. Morikawa, Y. Yamanaka, J. K. Ho Hui, N. Kimizuka, *RSC Adv.* **2023**, *13*, 24031-24037.

[59] M. Brøndsted Nielsen, N. Ree, K. V. Mikkelsen, M. Cacciarini, *Russ. Chem. Rev.* **2020**, *89*, 573.

[60] H. Maag, M. Schmitz, A. Sandvoß, D. Mundil, A. Pedada, F. Glaser, C. Kerzig, J. M. Wahl, *J. Am. Chem. Soc.* **2024**, *146*, 32701-32707.

[61] R. C. Richter, S. M. Biebl, R. Einholz, J. Walz, C. Maichle-Mössmer, M. Ströbele, H. F. Bettinger, I. Fleischer, *Angew. Chem. Int. Ed.* **2024**, *63*, e202405818.

[62] M. J. Dewar, P. A. Marr, *J. Am. Chem. Soc.* **1962**, *84*, 3782-3782.

[63] a) A. J. Ashe, Fang, *Org. Lett.* **2000**, *2*, 2089-2091; b) A. J. Ashe, X. Fang, X. Fang, J. W. Kampf, *Organometallics* **2001**, *20*, 5413-5418.

[64] a) A. J. V. Marwitz, M. H. Matus, L. N. Zakharov, D. A. Dixon, S.-Y. Liu, *Angew. Chem. Int. Ed.* **2009**, *48*, 973-977; b) E. R. Abbey, A. N. Lamm, A. W. Baggett, L. N. Zakharov, S.-Y. Liu, *J. Am. Chem. Soc.* **2013**, *135*, 12908-12913.

[65] J. E. Del Bene, M. Yáñez, I. Alkorta, J. Elguero, *J. Chem. Theory Comput.* **2009**, *5*, 2239-2247.

[66] K. Niedenzu, *Angew. Chem., Int. Ed.* **1964**, *3*, 86-92.

[67] P. G. Campbell, E. R. Abbey, D. Neiner, D. J. Grant, D. A. Dixon, S.-Y. Liu, *J. Am. Chem. Soc.* **2010**, *132*, 18048-18050.

[68] a) D. Ghosh, G. Periyasamy, S. K. Pati, *Phys. Chem. Chem. Phys.* **2011**, *13*, 20627-20636; b) A. K. Srivastava, N. Misra, *Chem. Phys. Lett.* **2015**, *625*, 5-9; c) P. A. Brown, C. D. Martin, K. L. Shuford, *Phys. Chem. Chem. Phys.* **2019**, *21*, 18458-18466.

[69] G. R. Fulmer, A. J. M. Miller, N. H. Sherden, H. E. Gottlieb, A. Nudelman, B. M. Stoltz, J. E. Bercaw, K. I. Goldberg, *Organometallics* **2010**, *29*, 2176–2179.

[70] a) J. M. B. D. Bryce-Smith, *Proc. Chem. Soc.* **1957**, 287; b) K. Wilzbach, J. S. Ritscher, L. Kaplan, *J. Am. Chem. Soc.* **1967**, *89*, 1031-1032; c) H. R. Ward, J. S. Wishnok, *J. Am. Chem. Soc.* **1968**, *90*, 5353-5357; d) D. Bryce-Smith, A. Gilbert, D. A. Robinson, *Angew. Chem., Int. Ed.* **1971**, *10*, 745-746; e) W. A. Noyes, Jr., K. E. Al-Ani, *Chem. Rev.* **1974**, *74*, 29-43.

[71] S. A. Brough, A. N. Lamm, S.-Y. Liu, H. F. Bettinger, *Angew. Chem. Int. Ed.* **2012**, *51*, 10880-10883.
[72] a) J. Kim, J. Moon, J. S. Lim, *ChemPhysChem* **2015**, *16*, 1670-1675; b) E. M. Arpa, S. Stafström, B. Durbeej, *Phys. Chem. Chem. Phys.* **2024**, *26*, 11295-11305.
[73] S. Jeong, E. Park, J. Kim, K. H. Kim, *Chem. Phys.* **2025**, *162*.
[74] H. F. Bettinger, O. Hauler, *Beilstein J. Org. Chem.* **2013**, *9*, 761-766.
[75] S. Jeong, E. Park, J. Kim, K. H. Kim, *Phys. Chem. Chem. Phys.* **2023**, *25*, 17230-17237.
[76] T. Ozaki, S. K. Bentley, N. Rybansky, B. Li, S.-Y. Liu, *J. Am. Chem. Soc.* **2024**, *146*, 24748-24753.
[77] A. J. Müller, J. Markhart, H. F. Bettinger, A. Dreuw, *Chem. Commun.* **2025**, *61*, 8351-8354.
[78] S. Chakraborty, H. P. Q. Nguyen, J. Usuba, J. Y. Choi, Z. Sun, C. Raju, G. Sigelmann, Q. Qiu, S. Cho, S. M. Tenney, K. E. Shulenberger, K. Schmidt-Rohr, J. Park, G. G. D. Han, *Chem* **2024**, *10*, 3309-3322.
[79] a) L. Dong, Y. Feng, L. Wang, W. Feng, *Chem. Soc. Rev.* **2018**, *47*, 7339-7368; b) R. J. Salthouse, K. Moth-Poulsen, *J. Mater. Chem. A* **2024**, *12*, 3180-3208.
[80] a) K. Yasufuku, K. Takahashi, C. Kutal, *Tetrahedron Lett.* **1984**, *25*, 4893-4896; b) A. Goulet-Hanssens, M. Utecht, D. Mutruc, E. Titov, J. Schwarz, L. Grubert, D. Bléger, P. Saalfrank, S. Hecht, *J. Am. Chem. Soc.* **2017**, *139*, 335-341.
[81] E. Franz, D. Krappmann, L. Fromm, T. Luchs, A. Görling, A. Hirsch, O. Brummel, J. Libuda, *ChemSusChem* **2022**, *15*, e202201483.
[82] a) S. Miki, Y. Asako, M. Morimoto, T. Ohno, Z.-i. Yoshida, T. Maruyama, M. Fukuoka, T. Takada, *Bull. Chem. Soc. Jpn.* **1988**, *61*, 973-981; b) T. Luchs, P. Lorenz, A. Hirsch, *ChemPhotoChem* **2020**, *4*, 2-2.
[83] a) L. Magson, D. Maggiolo, A. S. Kalagasidis, S. Henninger, G. Munz, M. Knäbbeler-Buß, H. Hölzel, K. Moth-Poulsen, I. Funes-Ardoiz, D. Sampedro, *Adv. Energy Sustainability Res.* **2025**, *6*, 2400230; b) B. Rollins, A. Gimenez-Gomez, A. M. Steele, H. Hölzel, R. J. Salthouse, K. Moreno, K. Moth-Poulsen, I. Funes-Ardoiz, D. Sampedro, *Catal. Sci. Technol.* **2025**, *15*, 3837-3847.
[84] G. F. Koser, P. R. Pappas, S.-M. Yu, *Tetrahedron Lett.* **1973**, *14*, 4943-4946.
[85] I. M. Riddlestone, A. Kraft, J. Schaefer, I. Krossing, *Angew. Chem. Int. Ed.* **2018**, *57*, 13982-14024.
[86] a) K. Maruyama, H. Tamiaki, *J. Org. Chem.* **1987**, *52*, 3967-3970; b) K. Maruyama, H. Tamiaki, *Chem. Lett.* **1987**, *16*, 683-686.
[87] G. F. Koser, J. N. Faircloth, *J. Org. Chem.* **1976**, *41*, 583-585.
[88] S. F. Nelsen, J. P. Gillespie, P. J. Hintz, *Tetrahedron Lett.* **1971**, *12*, 2361-2364.
[89] C. Tipper, *Roy. Soc. Ch.* **1955**, 2045-2046.
[90] a) R. D. Bach, O. Dmitrenko, *J. Am. Chem. Soc.* **2006**, *128*, 4598-4611; b) M. Murakami, H. Amii, Y. Ito, *Nature* **1994**, *370*, 540-541.
[91] S. M. Bachrach, *J. Phys. Chem. A* **2008**, *112*, 7750-7754.
[92] A. Flores-Gaspar, R. Martin, *Synthesis* **2013**, *45*, 563-580.
[93] a) M. A. Huffman, L. S. Liebeskind, W. T. Pennington, *Organometallics* **1992**, *11*, 255-266; b) G. Lu, C. Fang, T. Xu, G. Dong, P. Liu, *J. Am. Chem. Soc.* **2015**, *137*, 8274-8283.
[94] T. Wurm, B. W. H. Turnbull, B. R. Ambler, M. J. Krische, *J. Org. Chem.* **2017**, *82*, 13751-13755.
[95] a) M. Bender, B. W. H. Turnbull, B. R. Ambler, M. J. Krische, *Science* **2017**, *357*, 779-781; b) B. R. Ambler, B. W. H. Turnbull, S. R. Suravarapu, M. M. Uteuliyev, N. O. Huynh, M. J. Krische, *J. Am. Chem. Soc.* **2018**, *140*, 9091-9094.

[96] a) S. Yang, Y. Xu, J. Li, *Org. Lett.* **2016**, *18*, 6244-6247; b) Z.-Y. Xu, S.-Q. Zhang, J.-R. Liu, P.-P. Chen, X. Li, H.-Z. Yu, X. Hong, Y. Fu, *Organometallics* **2018**, *37*, 592-602; c) Z. Zhu, X. Li, S. Chen, P.-h. Chen, B. A. Billett, Z. Huang, G. Dong, *ACS Catal.* **2018**, *8*, 845-849.
[97] G. Fumagalli, S. Stanton, J. F. Bower, *Chem. Rev.* **2017**, *117*, 9404-9432.
[98] F. Juliá-Hernández, A. Ziadi, A. Nishimura, R. Martin, *Angew. Chem. Int. Ed.* **2015**, *54*, 9537-9541.
[99] P.-h. Chen, J. Sieber, C. H. Senanayake, G. Dong, *Chem. Sci.* **2015**, *6*, 5440-5445.
[100] T. Xu, G. Dong, *Angew. Chem. Int. Ed.* **2012**, *51*, 7567-7571.
[101] T. Xu, H. M. Ko, N. A. Savage, G. Dong, *J. Am. Chem. Soc.* **2012**, *134*, 20005-20008.
[102] S. Ochi, Z. Zhang, Y. Xia, G. Dong, *Angew. Chem. Int. Ed.* **2022**, *61*, e202202703.
[103] H. Lu, T.-T. Zhao, J.-H. Bai, D. Ye, P.-F. Xu, H. Wei, *Angew. Chem. Int. Ed.* **2020**, *59*, 23537-23543.
[104] a) S. Okumura, F. Sun, N. Ishida, M. Murakami, *J. Am. Chem. Soc.* **2017**, *139*, 12414-12417; b) R. Li, B. Li, H. Zhang, C.-W. Ju, Y. Qin, X.-S. Xue, D. Zhao, *Nat. Chem.* **2021**, *13*, 1006-1016.
[105] C. J. Wagner, G. Dong, *Angew. Chem. Int. Ed.* **2025**, *64*, e202500148.
[106] a) J.-H. Guo, Y. Liu, X.-C. Lin, T.-M. Tang, B.-Q. Wang, P. Hu, K.-Q. Zhao, F. Song, Z.-J. Shi, *Angew. Chem. Int. Ed.* **2021**, *60*, 19079-19084; b) R. C. Richter, I. H. Lindenmaier, D. Schray, M. Ströbele, I. Fleischer, *Org. Lett.* **2025**, *27*, 5385-5389.
[107] Z. Li, Y. Wang, N. Ma, P. Ma, J. Wang, *Org. Lett.* **2025**, *27*, 3661-3666.
[108] M. Zhang, J. Yang, W. Rong, J. Li, *Org. Chem. Front.* **2023**, *10*, 5216-5230.

2 Objective

The aim of this doctoral research was to investigate transition metal catalyzed C–C bond cleavage in strained carbocycles. Within this overarching framework, two distinct research topics were explored.

The first topic focused on the activation of Dewar 1,2-dihydo 1,2-azaborinines, enabling their cycloreversion to the corresponding non-Dewar isomers. These systems represent promising candidates for molecular solar energy storage. Given the underexplored catalytic ring opening of such compounds, this work aimed to identify suitable catalysts, elucidate their reaction mechanisms, and thereby contribute to the rational design of future generations of catalysts. In addition, preliminary efforts were undertaken toward the development of a heterogeneous catalytic system.

The second topic centered on classical method development involving a nickel-catalyzed system. The goal was to optimize conditions that facilitate the insertion of unsaturated compounds into benzocyclobutanones *via* C–C bond activation. Once optimized, the scope of the reactions was evaluated in respect to generality. Finally, preliminary mechanistic investigations were carried out to gain an initial understanding of the underlying catalytic process. Finally, miscellaneous screening towards additional insertion partners was endeavored.

RESULTS AND DISCUSSION

3 Catalytic Cycloreversion of Dewar 1,2-Dihydro 1,2-Azaborinines

3.1 Summary of Published Results

The goal of this project was to develop an efficient catalytic system for the cycloreversion of 2-(*tert*-butyldimethylsilyl)-3-mesityl-2-aza-3-borabicyclo[2.2.0]hex-5-ene (**BND1**) to its lower-energy valence isomer 1,2-dihydro-1-(*tert*-butyldimethylsilyl)-2-mesityl-1,2-azaborinine (**BNB1**). In addition, gaining mechanistic insight into the catalytic process was a central objective, as such would facilitate rational catalyst design in future studies. The **BNB1**/**BND1** valence isomer pair constitutes a novel molecular solar thermal energy storage (MOST) system, in which UV irradiation drives the photochemical conversion of **BNB1** to the metastable **BND1** isomer, storing energy in chemical form. This energy can then be released *via* cycloreversion, but as the for the formation of *Z*-configured double bonds required disrotatory thermal reisomerization is orbital symmetry-forbidden,[1] elevated temperatures or a catalyst are necessary. An example of such a catalyst was found to be Wilkinson's catalyst, which has previously been shown to promote this transformation.[2] However, its reliance on a precious metal limits its economic viability.

To address this, a series of catalysts were screened, identifying coinage metal salts with weakly coordinating anions (WCAs) as promising candidates. Hereby, the Lewis-acidity of the cation strongly depends on the coordinative ability of the WCA.[3] Among the coinage metals, AgWCA salts were especially effective at low catalyst loading (5 mol%) and rt. Catalytic activity increased with weaker coordination of the anion. Very weakly coordinating anions such as $[SbF_6]^-$ (Table 3.1, entry 1) and $[Al(OC(CF_3)_3)_4]^-$ (Table 3.1, entry 2) exhibited superior activity compared to more coordinating anions like $[BF_4]^-$, $[ClO_4]^-$, and $[NTf_2]^-$ (Table 3.1, entries 3 – 5).[4] In contrast, non-WCA salts such as $AgNO_3$ and AgOPiv showed no observable catalytic activity (Table 3.1, entries 6, 7). These findings aligned with the observed solvent dependence of the reaction. DCM, a polar, non-coordinating solvent was suitable for the cycloreversion, whereas toluene, which can coordinate to silver(I) through its aromatic system, inhibited the transformation.

The formation of elemental silver precipitate was observed upon combining a silver(I) salt with **BND1**. To determine whether silver nanoparticles were catalytically relevant, they were

tested separately and found to be inactive. To confirm that the redox process does not lead to significant decomposition of **BND1**, an upscale experiment was conducted: cycloreversion of **BND1** (500 µmol) using $AgSbF_6$ (5 mol%, rt) resulted in the quantitative isolation of **BNB1**. This demonstrated that the reduction of silver(I) to silver(0) occurs only to a negligible extent under the applied conditions.

Table 3.1. Catalyst screening for the cycloreversion of **BND1** to **BNB1** in DCM-d_2 at rt within 24 h.

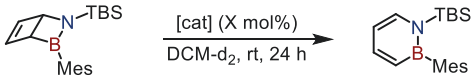

BND1 **BNB1**

Entry	Catalyst	Loading (mol%)	Yield (%)[a]
1	$AgSbF_6$	5	quant.
2	$Ag[Al(OC(CF_3)_3)_4]$	5	quant.
3	$AgBF_4$	5	51
4[b]	$AgClO_4$	5	43
5	$AgNTf_2$	10	38
6	$AgNO_3$	5	/
7	AgOPiv	5	/
8	$[Cu(1,2\text{-}F_2C_6H_4)_{0.6}][Al(OC(CF_3)_3)_4]$	5	quant.

Reaction conditions: BND1 (150 µmol), DCM (0.5 mL), rt ≈ 298 K. [a]Yield determined by ^{1}H NMR. [b]elevated rt ≈ 303 K.

In contrast, the use of stoichiometric AuCl led to substantial decomposition of **BND1**. This behavior is attributed to the higher redox potential of gold(I) reinforced by the coordinative nature of the chloride counterion decreasing the Lewis-acidity of gold(I), thus inhibiting the cycloreversion. Consequently, $[Cu(1,2\text{-}F_2C_6H_4)_{0.6}][Al(OC(CF_3)_3)_4]$, a CuWCA species lacking strongly coordinating ligands and possessing a lower redox potential than silver, was identified as a viable catalyst (Table 3.1, entry 8). It promoted the cycloreversion of **BND1** (5 mol% Cu, rt), and enabled the transformation of the Dewar isomer of 1,2-dihydro-*tert*-butyl-2-mesityl-1,2-azaborinine (**BND2**) (10 mol%, rt), which proved to be challenging for AgWCA catalysts due to the higher thermal stability of **BND2**.

Stoichiometric ^{1}H NMR experiments using $AgSbF_6$ were conducted to understand how AgWCA salts enable the cycloreversion of **BND1** at rt. These revealed coordination of silver(I) to both the azaborinine and its Dewar isomer, as indicated by varied chemical shifts of protons.

Additionally, the stoichiometric NMR experiments showed, that no cycloreversion occurs at low temperatures (-40 °C).

Building on these insights, crystals suitable for X-ray diffraction (XRD) of both **BNB1** and **BND1** coordinated to $AgSbF_6$ could be obtained from DCM (Figure 3.1).

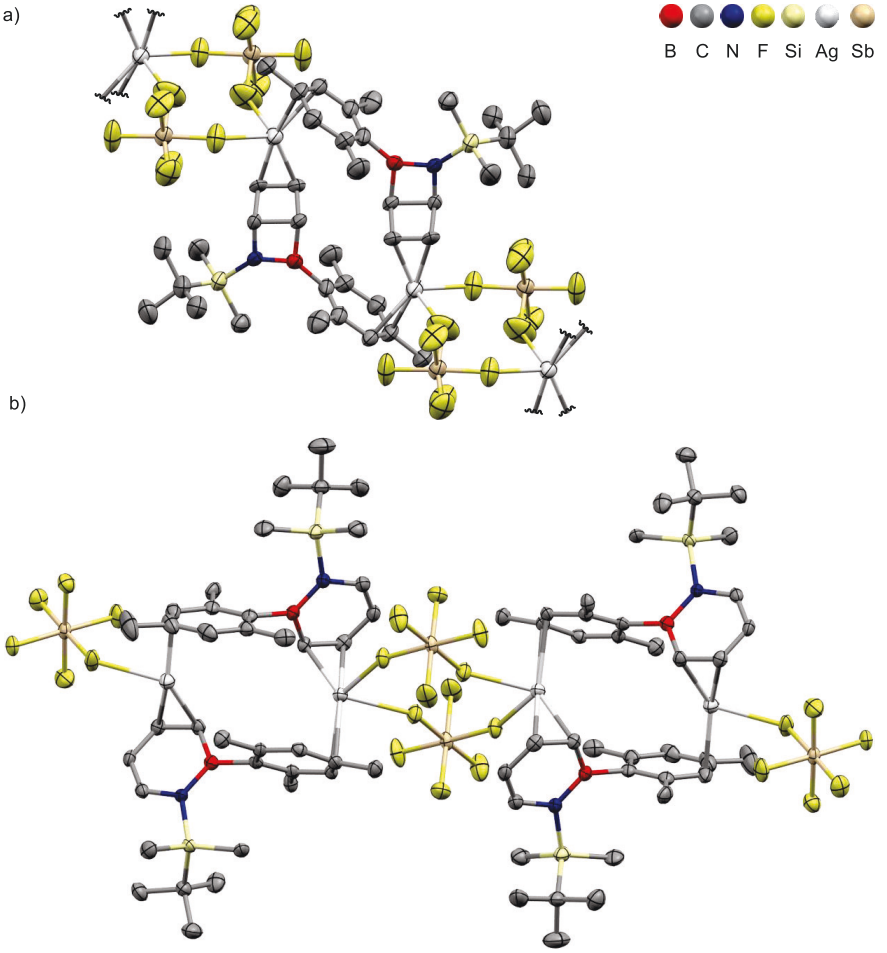

Figure 3.1. ORTEP representation of the [**BND1**•$AgSbF_6$]$_2$ (a) and [**BNB1**•$AgSbF_6$]$_2$ (b) dimers showcasing their packing in the crystal lattice. Hydrogen atoms are omitted for clarity and the thermal ellipsoids are drawn at 50% probability level.

To the best of the authors knowledge,[5] the crystal structure obtained from the highly temperature sensitive crystals of **BND1** represents the first reported crystal structure of a Dewar isomer of a 1,2-dihydro 1,2-azaborinine. In this structure, the silver-cation is coordinated in a η^2 fashion by the C=C double bond of the Dewar and engages in η^2-coordination with the aromatic system of the mesityl substituent from a second Dewar molecule, forming a dimeric species. The remaining coordination sites of the silver(I) ions are saturated by two $[SbF_6]^-$ units, which bridge two silver(I)-centers *via* independent κ^1 coordination. This results in the formation of linear strings of $[\mathbf{BND1}\bullet Ag]_2^{2+}$ units packed in parallel within the crystal lattice. A similar structural motif is observed in the crystal structure of $[\mathbf{BNB1}\bullet AgSbF_6]_2$. Here, the silver(I)-cation is coordinated by the aromatic system of the azaborinine ring and the mesityl substituent of a second **BNB1** molecule, again forming a dimer. Analogously, two $[SbF_6]^-$ anions bridge the silver(I)-cations via κ^1 coordination, giving rise to parallel linear arrays of $[\mathbf{BNB1}\bullet Ag]_2^{2+}$ units.

The crystal structures agree with the observed ^{1}H NMR spectra of **BNB1** and **BND1** in the presence of $AgSbF_6$ in DCM-d_2. As previously noted, both the azaborinine ring and the mesityl substituent protons exhibit chemical shift changes, consistent with the formation of a dimeric complex (Figure 3.2). For **BND1**, all protons of the Dewar structure and mesityl group experience a downfield shift, which can be attributed to deshielding due to electron density donation to the silver(I) center.

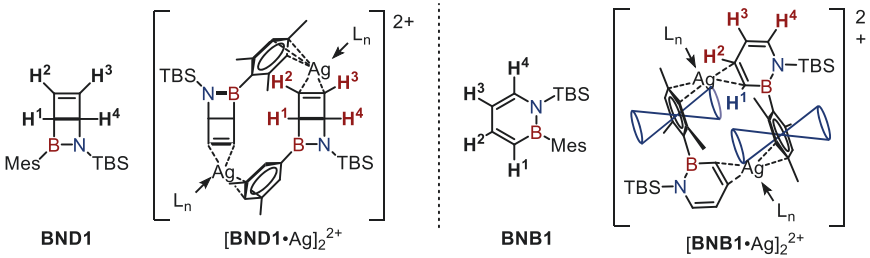

Proton	δ(BND1)	δ([BND1•AgSbF$_6$]$_2$)	δ(BNB1)	δ([BNB1•AgSbF$_6$]$_2$)
H^1	2.98	3.17	6.55	6.27
H^2	6.54	7.06	7.56	7.95
H^3	6.35	6.64	6.39	6.61
H^4	4.76	4.99	7.47	7.76

Figure 3.2. ^{1}H NMR chemical shifts (in ppm) of the 1,2-dihydro 1,2-azaborinine in **BND1**, $[\mathbf{BND1}\bullet AgSbF_6]_2$ at 240 K and **BNB1**, $[\mathbf{BNB1}\bullet AgSbF_6]_2$ at 298 K in DCM-d_2. For $[\mathbf{BNB1}\bullet AgSbF_6]_2$ shielding cones from the mesityl substituent are illustrated. Signals that shift downfield in presence of $AgSbF_6$ are highlighted red; an upfield shift is shown blue.

In the case of **BNB1**, all proton signals of the mesityl substituent and the majority of the azaborinine ring protons, are also shifted downfield. However, one signal from the azaborinine ring shifts upfield. This can be rationalized by the proximity of the proton to the shielding cone of the mesityl ring from the adjacent **BNB1** molecule in the dimeric species (Figure 3.2).[6] This interaction is not possible in a monomeric complex due to geometric constraints, further supporting the formation of a dimeric assembly in solution.

To quantify the effect of AgWCA salts on the cycloreversion of **BND1**, kinetic experiments were conducted to determine activation parameters *via* an Eyring plot. The results are summarized in Table 3.2, and they include enthalpy ($\Delta H^{\ddagger}$) and entropy ($\Delta S^{\ddagger}$) of activation, as well as the half-lives and free energies of activation ($\Delta G_{298\,K}^{\ddagger}$) extrapolated to 298 K. For comparison, kinetic data for the thermal reisomerization of **BND1** in the absence of a catalyst was taken from literature.[2]

Table 3.2. Enthalpy and entropy of activation determined by an Eyring plot. Half-life and free energy of activation extrapolated from kinetic data at 298 K.

	BND1*	**[BND1•AgSbF$_6$]$_2$**	**[BND1•Ag[Al(OC(CF$_3$)$_3$)$_4$]]$_x$**
$t_{1/2,\,298\,K}$ (min)	$2.3 \cdot 10^5$	6.4	1.2
$\Delta H^{\ddagger}$ (kcal mol^{-1} K^{-1})	26.3 ± 0.3	23.0 ± 0.7	24.3 ± 0.5
$\Delta S^{\ddagger}$ (kcal mol^{-1} K^{-1})	-3.7 ± 0.9	6.1 ± 2.4	14.0 ± 1.9
$\Delta G_{298\,K}^{\ddagger}$ (kcal mol^{-1})	27.4 ± 0.4	21.2 ± 1.0	20.2 ± 0.8

* Kinetic data for **BND1** was extracted from literature.[2]

The kinetic data demonstrates that AgWCA salts substantially lower the reaction barrier for the cycloreversion of **BND1** compared to the uncatalyzed process. This is most notably reflected in the drastic reduction of the half-life at 298 K, from approximately 159 days to just a few minutes. Among the two AgWCA salts, Ag[Al(OC(CF$_3$)$_3$)$_4$] exhibited superior performance, lowering the free energy of activation by 1 kcal mol^{-1} compared to AgSbF$_6$. This observation underlines that the weaker coordination of the aluminate WCA is beneficial for the reaction outcome.

To elucidate the rate determining step of the silver-mediated cycloreversion of **BND1**, a secondary kinetic isotope effect (sKIE) experiment was conducted. This was enabled through selective deuteration of **BNB1** at the C^3 position (**BNB1d1**), achieved *via* bromination of **BNB1** at the 3-position,[7] followed by lithiation and quenching with D_2O. The reaction rates of the

cycloreversion of the corresponding Dewar isomers (**BND1** and **BND1d1**) were then compared under identical conditions in DCM at 288 K, mediated by equimolar amounts of $AgSbF_6$. The observed sKIE, calculated as the ratio of rate constants k_{obs}(**BND1**)/k_{obs}(**BND1d1**), was determined to be 1.10 ± 0.02, indicating that the rate determining step involves rehybridization from sp^3 to sp^2 at the labeled carbon center during the rate-determining step. As such, the data suggests that the rehybridization involved in the valence isomerization of **BND1** constitutes the rate determining state, rather than pre-equilibria such as dimer dissociation.

To gain further insight into the mechanism of the cycloreversion of **BND1**, DFT computations were conducted at the M06-2X(PCM:DCM)/def2-QZVPP// M06-2X(PCM:DCM)/def2-SVP level of theory.[8] Three systems were modeled: the dimeric [**BND1**•$AgSbF_6$]$_2$ complex (Figure 3.3), the monomeric [**BND1**Ag]$^+$ species, and neat **BND1** as a reference. Conformational analyses were conducted to ensure identification of the respective global minima for each structure. In addition, intrinsic reaction coordinate (IRC) computations were carried out for each transition state (TS) to confirm the continuity of the free energy profile along the reaction coordinate. Importantly, the cycloreversion for each system was found to proceed in a concerted fashion, consistent with the conclusion from the sKIE experiment, that the cycloreversion itself constitutes the rate-determining step. Gratifyingly, the activation energies for the silver-mediated cycloreversions of **BND1** were found to be favorable compared to that of the thermal isomerization of neat **BND1** ($\Delta G^{\ddagger}$(298 K) = 28.6 kcal/mol). As expected, the lowest barrier was computed for the monomeric [**BND1**•Ag]$^+$ species ($\Delta G^{\ddagger}$(298 K) = 22.9 kcal/mol), where the silver(I)-cation is not coordinated by any counterion or additional ligand, thereby exhibiting maximal Lewis-acidity. In contrast, in the dimeric [**BND1**•$AgSbF_6$]$_2$ complex, silver(I) is coordinated both by the $[SbF_6]^-$ anion and the aromatic system of the adjacent mesityl substituent, leading to a slightly higher activation barrier ($\Delta G^{\ddagger}$(298 K) = 26.6 kcal/mol). For the dimeric system, a second TS corresponding to the cycloreversion of the [**BND1**•$AgSbF_6$][**BNB1**•$AgSbF_6$] intermediate was identified, exhibiting a lower reaction barrier ($\Delta G^{\ddagger}$(298 K) = 23.9 kcal/mol) and thus not being rate-limiting. Although the calculated activation barrier for the first TS of the dimer (26.6 kcal/mol) exceeds the experimentally determined barrier (21.2 ± 1.0 kcal/mol, Table 3.2), the overall trend of a reduced reaction barrier in the presence of silver(I) is in good agreement with experimental observations.

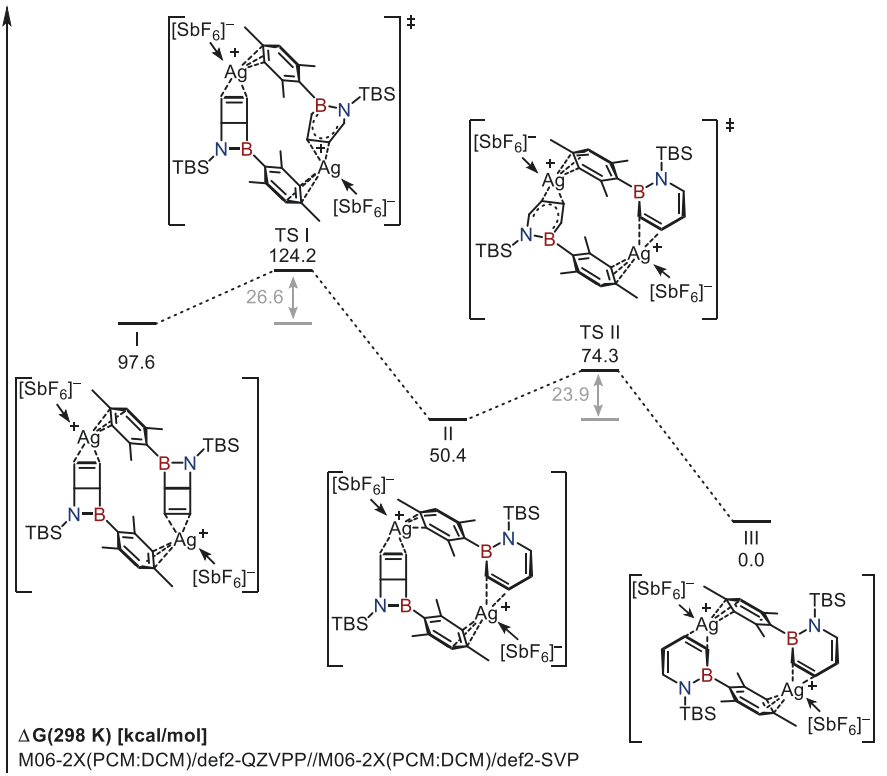

Figure 3.3. Schematic free energy profile of the $AgSbF_6$-mediated stepwise cycloreversion of the [**BND1**•$AgSbF_6$]$_2$ dimer computed at the M06-2X(PCM:DCM)/def2-QZVPP//M06-2X(PCM:DCM)/def2-SVP level of theory.

In an effort to elucidate the beneficial reaction outcome in the presence of silver(I)-cations, the electrostatic potential was mapped for the thermal cycloreversion of **BND1**. It was observed that the TS exhibits a significantly higher affinity toward a positive test charge on the 1,2-dihydro 1,2-azaborinine motif compared to either **BND1** or **BNB1**, indicating that interaction with a Lewis-acid (LA) is particularly favorable in the TS. Consequently, the presence of a silver(I)-cation stabilizes the TS and lowers the reaction barrier.

On the backdrop of these results, the following mechanism was proposed for the cycloreversion of **BND1** in the presence of a AgWCA salt (Scheme 3.1). Initially, a dimeric species is formed containing two **BND1** as described above. Computations indicated that dissociation into monomeric species is unfavorable compared to direct cycloreversion.

Therefore, a direct valence isomerization of one of the two **BND1** units within the dimer is proposed, followed by cycloreversion of the second unit. Each cycloreversion proceeds *via* a concerted mechanism. Additionally, equilibria between different dimeric species ([**BND1**•Ag]$_2^{2+}$, [**BND1**•Ag][**BNB1**•Ag]$^{2+}$, [**BNB1**•Ag]$_2^{2+}$) likely exist and shift as the reaction progresses.

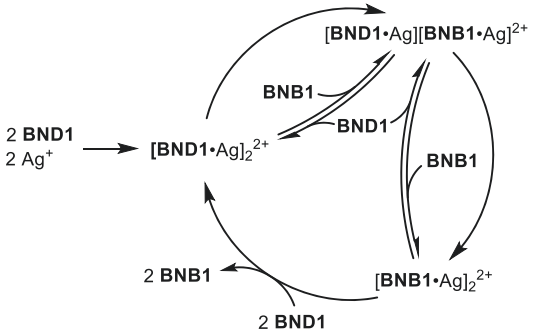

Scheme 3.1. Proposed mechanism for the silver(I)-catalyzed cycloreversion of **BND1** in DCM.

In conclusion, a coinage metal LA-based catalytic system for the cycloreversion of the Dewar isomer of a 1,2-dihydro 1,2-azaborinine MOST energy storage system was developed. $AgSbF_6$ and $Ag[Al(OC(CF_3)_3)_4]$ were identified as particularly effective catalysts, with $[Cu(1,2\text{-}F_2C_6H_4)_n][Al(OC(CF_3)_3)_4]$ providing a valuable alternative, especially in promoting the cycloreversion of a more challenging Dewar isomer. Mechanistic studies furnished the first crystal structure of a Dewar isomer of a 1,2-dihydro 1,2-azaborinine unit, while NMR spectroscopy provided insights into the solution-phase speciation. Kinetic analysis, in conjunction with DFT computations, further elucidated the catalytic role of the catalyst, offering fundamental insights that may guide future rational catalyst design.

3.2 Unpublished results

3.2.1 Lewis-Acids

In light of recent findings on the catalytic cycloreversion of 1,2-dihydro 1,2-azaborinines,[5] LAs were hypothesized to be a promising class of catalysts. To further explore this, a selection of common LAs was evaluated in preliminary studies.

Among these, tris(pentafluorophenyl)borane (BCF), a strongly Lewis-acidic organoborane, was investigated as a neutral, metal-free alternative to the previously studied coinage metal salts bearing weakly coordinating anions (WCA´s). Despite its distinct properties, BCF is classified as a υ-type LA implying a high affinity for π-systems, similar to silver AgWCA salts.[9] Delightfully, BCF was found to catalyze the cycloreversion of **BND1** in DCM-d_2 at rt (Table 3.3, entry 1). However, it showed no appreciable activity toward the more thermally stable **BND2** (Table 3.3, entry 2). Nonetheless, this result demonstrates that LA-catalysts are not limited to coinage metal systems, thereby expanding the scope of viable catalyst classes for the cycloreversion of 1,2-dihydro 1,2-azaborinines.

Inspired by these results, a LA containing the higher homolog of boron, $AlCl_3$, was employed as a readily accessible compound. A stoichiometric experiment showed that $AlCl_3$ could mediate the cycloreversion of both **BND1** and **BND2** in DCM-d_2 at rt, though the process was accompanied by significant decomposition (Table 3.3, entries 3, 4).

Table 3.3. Catalyst screening for the cycloreversion of **BND1** and **BND2** with LAs of the triel group.

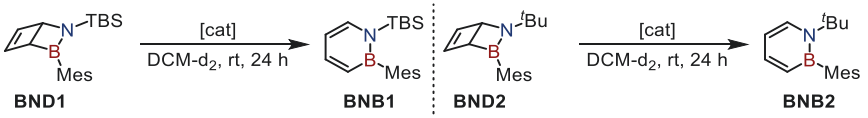

BND1 **BNB1** **BND2** **BNB2**

Entry	Catalyst	Compound	Outcome*
1	BCF (20 mol%)	**BND1**	quant. conversion
2	BCF (20 mol%)	**BND2**	no reaction
3	$AlCl_3$ (1.0 equiv.)	**BND1**	conversion and decomposition
4	$AlCl_3$ (1.0 equiv.)	**BND2**	conversion and decomposition

* Determined by ^{1}H and ^{11}B NMR.

Finally, a variation of a Kaminsky-type catalyst was tested, typically formed by addition of methyl aluminoxane to Cp_2MCl_2 (M = Ti, Zr, Hf), which induces transmetalation and

abstraction of a ligand, leading to a cationic species with a vacant coordination site.[10] These Lewis-acidic catalysts are utilized in the polymerization of alkenes demonstrating their affinity towards π-systems and suggesting potential in promoting the cycloreversion of 1,2-dihydro 1,2-azaborinines.

In the conducted experiment, Cp_2ZrCl_2 was activated by $Ag[Al(OC(CF_3)_3)_4]$ in DCM-d_2 at rt *via* chloride abstraction, monitored by precipitation of AgCl. Subsequent addition of **BND1** resulted in a slow, quantitative cycloreversion (Scheme 3.2), but also in the formation of silver(0), indicating the presence of remnant silver(I). Therefore, the assignment of catalytic activity to the Zr species is ambiguous, as $Ag[Al(OC(CF_3)_3)_4]$ is known to be an efficient catalyst for the cycloreversion of **BND1**.[5]

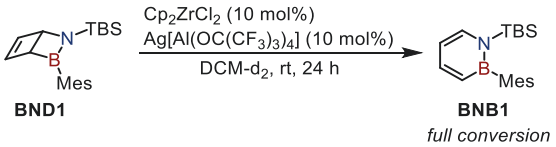

Scheme 3.2. Cycloreversion of **BND1** is presence of Cp_2ZrCl_2 (10 mol%) activated by $Ag[Al(OC(CF_3)_3)_4]$ (10 mol%) in DCM-d_2 at rt.

3.2.2 Mechanistic Investigations on Wilkinson's Catalyst

In addition to LAs, Wilkinson's complex was identified as a suitable catalyst for the cycloreversion of **BND1** by Bettinger and co-workers in 2018.[2] However, a detailed mechanistic understanding remained elusive, prompting investigations into the reaction pathway.

To probe the cycloreversion of **BND1** in the presence of Wilkinson's catalyst, low temperature NMR studies were conducted. No conversion was observed at -40 °C or -20 °C using 20 mol% $Rh(PPh_3)_3Cl$. At 0 °C, a slow reaction was detected at the same catalyst loading. Upon raising the temperature to 25 °C, the reaction rate increased substantially, even with a reduced catalyst loading of 5 mol% (Figure 3.4a). Notably, Wilkinson's catalyst also proved effective for the more thermally stable and thus more challenging isomer **BND2**, enabling efficient reisomerization to **BNB2** (Figure 3.4b).

Despite the stability of **BND1** in presence of Wilkinson's catalyst at low temperatures, no Rh-**BND1** intermediates or coordination complexes could be detected by either ^1H or ^{31}P NMR, suggesting that the catalytically active species is likely short-lived.

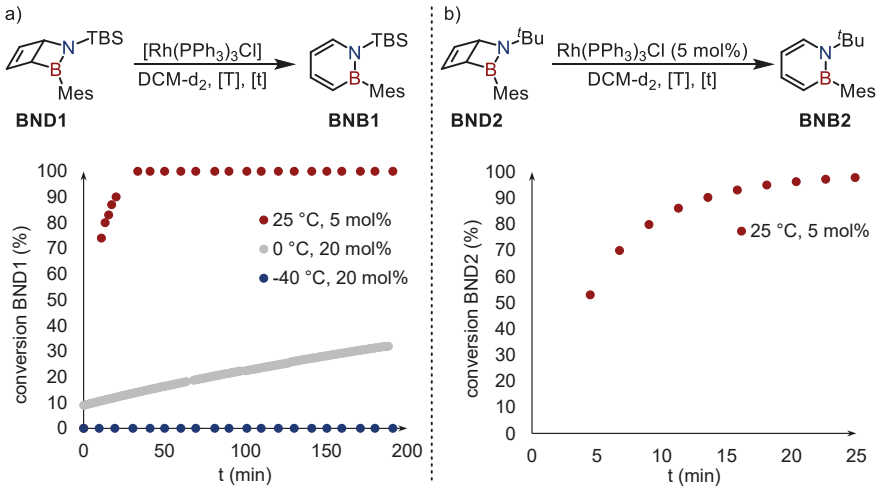

Figure 3.4: Kinetic analysis of the cycloreversion of **BND1** and **BND2** catalyzed by Wilkinson's catalyst at different temperatures and catalyst loadings in DCM-d_2. Conversion determined by ^{1}H NMR, assuming absence of ^{1}H NMR silent decomposition.

To gain further mechanistic insight, kinetic analysis was performed using an artificial intelligence (AI) model developed by J. Burés and I. Larrosa.[11] This model analyzes reactions of the general form A $\overset{\text{cat.}}{\longrightarrow}$ B and predicts one or more plausible mechanisms from a library of 20 mechanistic scenarios. The required input data were obtained from ^{1}H NMR spectroscopy by measuring reaction kinetics at three different catalyst loadings, as well as in one experiment where product (**BNB1**) was added at the beginning of the reaction (Figure 3.5a).

Since acquiring data at t = 0 min is not feasible in NMR experiments, the time axis was corrected by fitting the kinetic data to a linear combination of up to three exponential decay functions (4):

$$f(t) = \sum_{i=1}^{n\leq 3} A_i e^{-k_i t} + y_0 \qquad (4)$$

Assuming that the course of the reaction to the past can be modeled by the same function (i.e., no induction period is present), the time axis was shifted by ε until: $\sum_{i=1}^{n\leq 3} A_i + y_0 = c_{0,i}$ with $c_{0,j} = 1$ for j ≠ excess **BNB1** and $c_{0,\text{excess BNB1}} = 0.47$. With the corrected time values ($t_i^{corr} = t_i + \varepsilon$, Figure 3.5a), the resulting dataset was evaluated using the AI model.

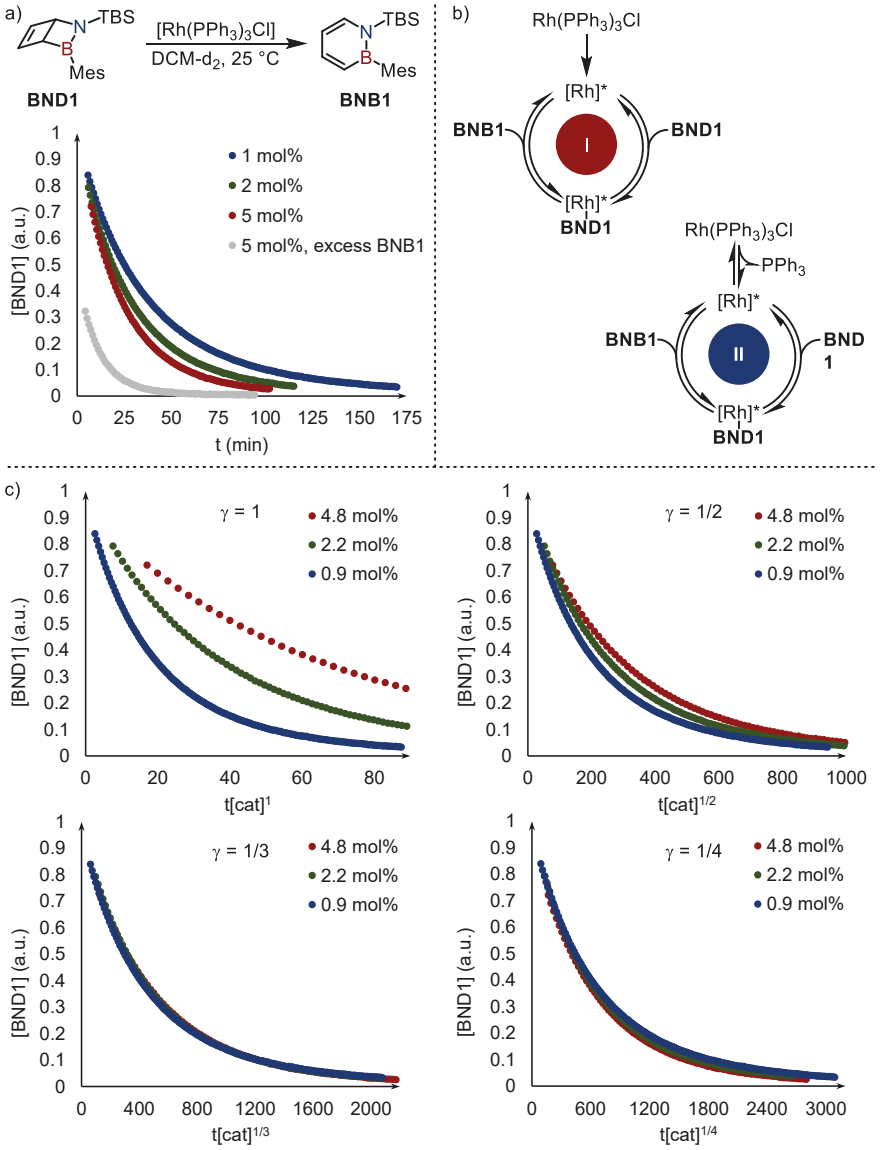

Figure 3.5. [a]Time adjusted kinetic data of the cycloreversion of **BND1** catalyzed by $Rh(PPh_3)_3Cl$ in DCM-d_2 at 25 °C for three different catalyst loadings and one experiment with excess **BNB1** added at the beginning of the reaction (5 mol% $Rh(PPh_3)_3Cl$). Conversion determined by ^1H NMR, assuming absence of ^1H NMR silent decomposition. [b]Proposed mechansims by an AI model-based on the kinetic data from a.[11] [c]Determination of the order in catalyst *via* visual kinetic analysis by plotting $t[cat]^{\gamma}$ (γ = 1, ½, ⅓, and ¼) against the concentration of **BND1** utilizing adjusted catalyst loading values provided by the AI model.[12]

Among the 20 candidate mechanisms, two were identified as plausible, both falling into the "catalyst activation" category (Figure 3.5b). Based on chemical reasoning, the mechanism involving catalyst activation *via* ligand dissociation (Figure 3.5b, II) appeared most compelling, as Wilkinson's catalyst likely requires a vacant coordination site to interact with BND1.

Based on the kinetic data, the order in catalyst was further assessed. A plot of time multiplied by the catalyst loading raised to the power of γ against the **BND1** concentration revealed a fractional order of ⅓ by visual kinetic analysis (Figure 3.5, c).[12] This may correspond to an inactive predominant trimeric catalyst species present in solution, which dissociates to its active monomeric form enabling catalysis:

$$[Rh_3] \overset{K_1}{\rightleftharpoons} [Rh_2] + [Rh] \overset{K_2}{\rightleftharpoons} 3[Rh] \quad K := K_1 K_2 = \frac{[Rh]^3}{[Rh_3]} \tag{5}$$

$$[Rh]_{total} = 3[Rh_3] + 2[Rh_2] + [Rh], \quad if\ [Rh_3] \gg [Rh_2], [Rh] \Rightarrow [Rh]_{total} \approx 3[Rh_3] \tag{6}$$

$$K \approx \frac{3[Rh]^3}{[Rh]_{total}} \Rightarrow [Rh] \approx \left(\frac{K[Rh]_{total}}{3}\right)^{\frac{1}{3}} with: [Rh] \Rightarrow \tag{7}$$

A dimeric form of Wilkinson's catalyst has already been reported in the original literature of Wilkinson,[13] lending support to this hypothesis. These results therefore suggest that the activation process is more complex than a simple ligand dissociation.

While these findings provide valuable insight into the cycloreversion mechanism of **BND1** catalyzed by Wilkinson's catalyst, further studies are required to fully elucidate the nature of the activation process.

A possible mode of action for Wilkinson's catalyst in enabling the catalytic reisomerization of **BND1** was hypothesized to involve oxidative addition (OA) into the strained bridge bond of **BND1**,[14] followed by elimination of the catalyst to yield **BNB1** (Scheme 3.3, a). To test this hypothesis, $[Rh(CO)_2Cl]_2$, a rhodium complex containing CO ligands known to mediate the cycloreversion of **BND1** in DCM-d_2 at rt was employed.[5] It was anticipated that if OA occurred, CO insertion might follow, as observed for quadricyclane,[15] indirectly supporting the proposed mechanism through formation of a CO inserted byproduct (Scheme 3.3, b).

The reaction of **BND1** with equimolar $[Rh(CO)_2Cl]_2$ in DCM-d_2 at rt resulted mainly in **BNB1**, which was isolated *via* column chromatography. However, additional unidentified side products were observed, and the crude mixture displayed paramagnetic behavior in the ^{1}H NMR

spectrum (see Experimental Section for details). Unfortunately, the anticipated CO insertion complex could not be identified.

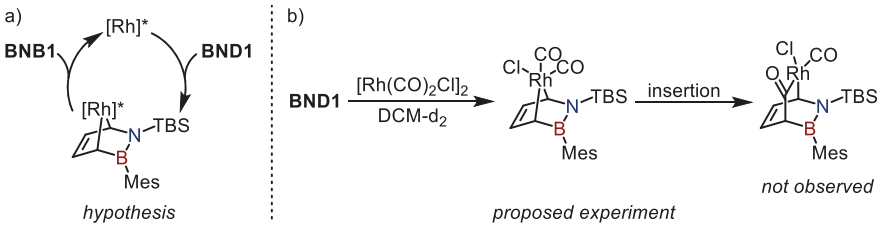

Scheme 3.3. [a]Proposed mechanism for the Wilkinson's catalyst-mediated cycloreversion of **BND1** *via* OA and elimination of the catalyst. [b]Cycloreversion of **BND1**-mediated by $[Rh(CO)_2Cl]_2$ to probe the formation of a CO insertion complex as mechanistic evidence.

An alternative strategy to indirectly verify OA was explored by adding reactive unsaturated compounds that could potentially undergo insertion after OA.[16] For this purpose, an electron deficient alkyne (methyl but-2-ynoate) and an allene (ethyl allenecarboxylate) were added to the Wilkinson's catalyst-mediated cycloreversion of **BND1** in DCM-d_2 (Scheme 3.4).

In the presence of the alkyne, no cycloreversion occurred at rt. This inhibition is most likely due to coordination of the alkyne to the rhodium center, as suggested by shifts of the PPh_3 ligand signals in the ^{1}H NMR spectrum. Upon heating the mixture to 40 – 70 °C, cycloreversion was observed. However, no insertion product could be detected. Similarly, in the case of the allene, coordination to rhodium was evident from shifts in the PPh_3 signal (^{1}H NMR), suppressing the cycloreversion even at 70 °C. Consequently, no insertion products were formed under either set of conditions.

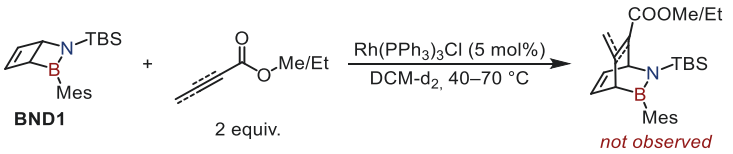

Scheme 3.4. Rhodium-catalyzed cycloreversion of **BND1** in presence of unsaturated potential insertion partners (methyl but-2-ynoate or ethyl allenecarboxylate).

3.2.3 Heterogeneous Catalysts

For the development of a proof-of-concept MOST device based on the 1,2-dihydro 1,2-azaborinine system, homogeneous catalysts such as Wilkinson's catalyst constitute inherent

practical limitations. Their solubility necessitates separation from the photoswitchable species prior to irradiation and reintroduction for energy release, complicating the overall process. In contrast, heterogeneous catalysts offer a promising solution by alleviating this separation challenge.[17] This approach not only simplifies device operation but also minimizes chemical waste, enhancing both the economic and environmental sustainability of the system.[18] The advantages of heterogeneous catalysis for reversible photoswitching have already been demonstrated in related systems, such as the NBD/QC pair,[19] underscoring its potential for practical application in MOST technologies.

Given the high efficiency of Wilkinson's catalyst in homogeneous systems, its immobilization was envisioned. In general, immobilization strategies include adsorption,[20] as well as more robust ionic binding or covalent attachment through linker molecules to a solid support.[21] A wide variety of support materials are available, ranging from polymers and alumina to carbon-based materials.[22] Nonetheless, silica remains a commonly used support due to its high surface area, tunable porosity, and ease of functionalization.[23]

Two different strategies, to immobilize rhodium-catalysts on silica were pursued, employing two distinct phosphine-based linkers (Scheme 3.5). The first approach involved anchoring a $RPPh_2$-type ligand to the silica surface, followed by coordination of Wilkinson's catalyst to the functionalized support. In the second approach, a rhodium precatalyst was synthesized and envisioned to be immobilized on silica.

In a first attempt, Wilkinson's catalyst was to be immobilized *via* an alkyl-diphenylphosphine linker to silica (**linker I**, Scheme 3.5a).[24] **Linker I** was synthesized by nucleophilic substitution of lithiated chlorodiphenylphosphine with 3-chloropropyltriethoxysilane. The resulting compound was then subjected to a condensation reaction with SiO_2, after which the modified silica was treated with Wilkinson's catalyst *via* ligand exchange. However, solid state ^{31}P-MAS-NMR revealed that the condensation step had failed, resulting in only physisorption of Wilkinson's catalyst on the silica surface. Consequently, major catalyst leaching was observed, rendering the material (**1@SiO$_2$**) unsuitable for heterogeneous catalysis.

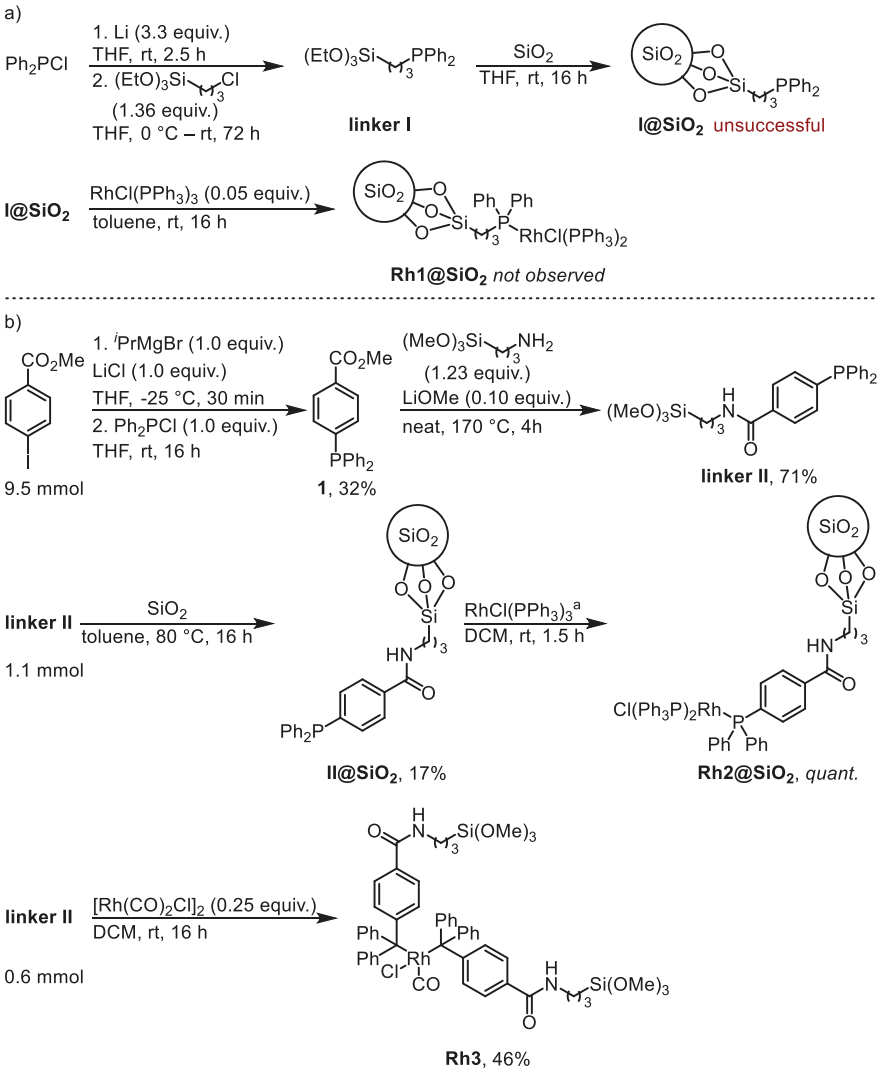

Scheme 3.5. Attempts to immobilize rhodium-centered catalysts onto silica *via* two different linkers and two different approaches. [a]50 mmol $RhCl(PPh_3)_3$ per 1.0 g of $II@SiO_2$.

In a second attempt, a triphenylphosphine derived linker was employed (**linker II**, Scheme 3.5b).[25] Methyl 4-(diphenylphosphino)benzoate (**1**) was reacted with 3-(trimethoxysilyl)propylamine to form the respective amide (**linker II**), which was then

condensed onto activated silica. Wilkinson's catalyst was subsequently coordinated to the modified surface, yielding the supported catalyst **2@SiO$_2$**. Soxhlet extraction was performed to remove any physisorbed or unbound species.

Catalytic testing of **2@SiO$_2$** with **BND1** in DCM-d_2 at rt showed no observable cycloreversion. Upon heating to 70 °C, a slow conversion to **BNB1** was detected, but the reaction proceeded at a rate comparable to the uncatalyzed thermal reaction, indicating that **2@SiO$_2$** was not catalytically active.

In a third attempt a precatalyst containing **linker II** was synthesized by reacting **linker II** with $[Rh(CO)_2Cl]_2$ yielding complex **Rh3**. However, **Rh3** exhibited no catalytic activity regarding the cycloreversion of **BND1** under homogeneous conditions. As a result, further immobilization of this complex was not pursued. This finding aligns with separate screenings of $Rh(CO)Cl(PPh_3)_2$, which also lacked catalytic activity, even upon activation with $AgBF_4$ in DCM-d_2. These results suggest that rhodium complexes bearing a halide, one CO ligand, and two triphenylphosphine derived ligands are not catalytically competent in this transformation.

An alternative strategy for immobilizing Wilkinson's catalyst involved the use of commercially available diphenylphosphine functionalized polystyrene. The polymer support was treated with a THF solution of Wilkinson's catalyst, and the resulting material (**Rh@PS**) was evaluated for catalytic activity regarding the cycloreversion of **BND1**.[22a] While catalytic conversion was observed in toluene-d_8, both the toluene-d_8 and DCM-d_2 filtrates of the catalyst also displayed catalytic activity. This indicated major leaching of the rhodium complex into solution, rendering the material unsuitable for practical use. Furthermore, a commercially available version of Wilkinson's catalyst immobilized on diphenylphosphine modified polystyrene showed no detectable catalytic activity under the tested conditions.

In a final attempt to immobilize Wilkinson's catalyst, an element organic framework (**EOF**) incorporating PPh_3 units was synthesized (Scheme 3.6).[26] This was achieved *via* dlithiation of 4,4′-dibromobiphenyl followed by reaction with phosphorus trichloride. The resulting colorless solid was then treated with a chloroform solution of Wilkinson's catalyst, and the material was evaluated for its catalytic activity regarding the cycloreversion of **BND1**.

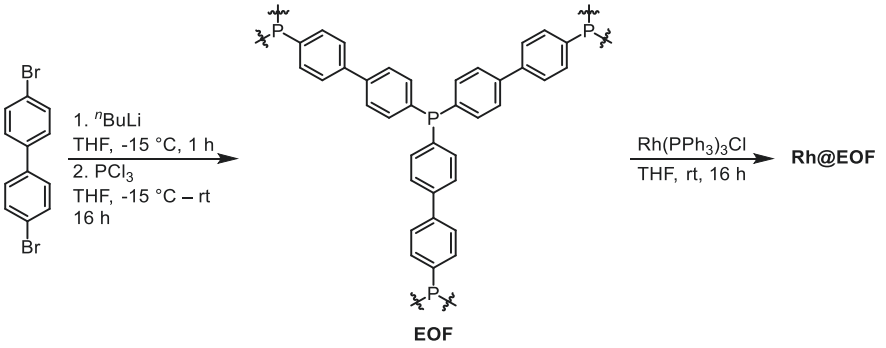

Scheme 3.6: Synthesis of an **EOF** consisting of PPh3 units and subsequent immobilization of Wilkinson's catalyst.

At rt, no conversion was observed. However, upon heating the reaction mixture to 70 °C, an appreciable reaction rate was noted, exceeding that of the thermal reisomerization even at 77 °C (Figure 3.6). Importantly, hot filtration confirmed that no catalyst leaching occurred at the operated 70 °C. These results demonstrate that Wilkinson's catalyst can be effectively immobilized while retaining catalytic activity towards the cycloreversion of **BND1**. Nevertheless, further optimization is necessary to improve catalytic efficiency, ideally enabling the reaction to proceed at rt.

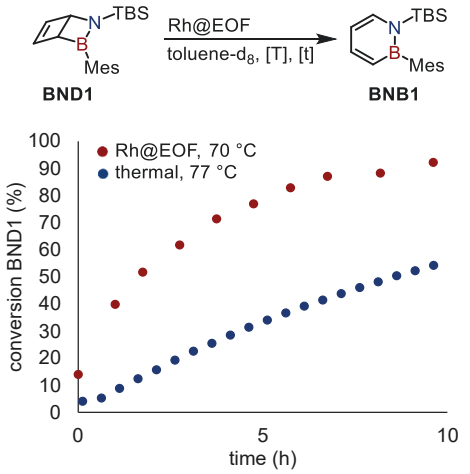

Figure 3.6. Kinetic profile of the cycloreversion of **BND1** catalyzed by **Rh@EOF** at 70 °C and the thermal back-conversion at 77 °C in toluene-d_8. Conversion determined by ^{1}H NMR, assuming absence of ^{1}H NMR silent decomposition.

In summary, Wilkinson's catalyst was immobilized on three different support materials resulting in poor to no reactivity in respect to the cycloreversion of **BND1** (Figure 3.7). Nonetheless, further attempts to synthesize a heterogeneous catalyst should be carried out, as such could promote the development of proof-of-concept MOST devices utilizing 1,2-dihydro 1,2-azaborinins.

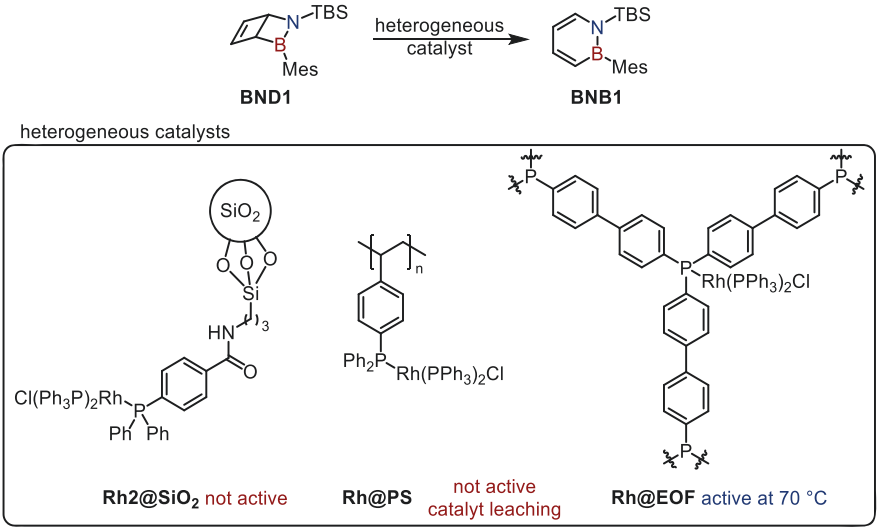

Figure 3.7. Overview of synthesized heterogeneous catalysts and their activity towards the cycloreversion of **BND1**.

3.2.4 Experimental Details

Chemicals and General Techniques

All reactions, unless denoted otherwise were carried out under argon employing standard Schlenk technique or a glovebox (GS MEGA E-Line, Glovebox Systemtechnik, <0.1 ppm O_2, <0.1 ppm H_2O) with pre-dried glassware. Solvents were either dried via a commercially available solvent purification system (MB SPS-5) or distilled and stored over 3 Å molecular sieves from abcr (activated *in vacuo* at 280 °C for 30 min). In addition, solvents were degassed by freeze-pump-thaw or by purging with argon with a cannula. Unless otherwise stated, all chemicals were used with the quality specified by the supplier. Solvents employed during chromatography were HPLC grade or distilled prior to use. Flash chromatography was carried out using the Interchim Puriflash XS420 system with FlashPure EcoFlex Silica 25 g columns (50 µm, irregular). Low reaction temperatures were achieved employing the Julabo FT902 Cryostat. Irradiation was carried out employing a 500 W high pressure mercury lamp in an Oriel housing with quartz optics and a dichromic mirror (280 nm – 400 nm).

Analytical Techniques

NMR spectra were recorded using the Bruker Avance III HDX 700, Bruker Avance III HDX 600, Bruker Avance 400 or Bruker Avance III HD 300 NanoBay spectrometers. ^{11}B-, ^{13}C, ^{31}P NMR were ^{1}H-broadband decoupled (not denoted explicitly). MAS-NMR-spectra were measured on a Bruker Avance III HD 300 XWB. Chemical shifts are reported in parts per million relative to tetramethyl silane using the residual NMR solvent signals[27] (chloroform-d: ^{1}H δ = 7.26, and ^{13}C δ = 77.16; dichloromethane-d_2: ^{1}H δ = 5.32 and ^{13}C δ = 53.85; toluene-d_8: ^{1}H δ = 2.08, 6.97, 7.01, 7.09, and ^{13}C δ = 20.43, 125.13, 127.96, 128.87, 137.48) and the J coupling constants are given in Hertz with the usual designations for splitting patterns (s = singlet, d = doublet, t = triplet, q = quartet, m = multiplet).

GC-LR-MS (EI) analysis was carried out with an Agilent 7820A/5977B GC-system/MSD employing an Agilent 190915-433UI column (30 m × 250 µm × 0.25 µm). Program: 50 °C – 280 °C over 15 minutes.

FT-IR spectra were measured by a Cary 630 FTIR by applying the neat sample on a diamond ATR sampler.

Crude products were monitored by thin layer chromatography (TLC), performed on aluminum plates coated with 0.20 mm silica gel 60 with fluorescence indicator UV_{254} from Macherey-Nagel and compounds were detected under UV light (254 nm).

Attempted CO insertion into BND1 with $[Rh(CO)_2Cl]_2$

In a J. Young NMR tube, $[Rh(CO)_2Cl]_2$ (50 µmol, 1.0 equiv.) was added to a solution of **BND1** (50 µmol, 1.0 equiv.) in DCM-d_2 (0.4 mL) at rt. ^{1}H NMR spectra were measured at their respective time. Subsequent flash chromatography (23 g SiO2, gradient from 100:0 to 90:10 *n*-hexane/DCM over 10 CV) furnished **BNB1** (6.7 mg, 22 µmol, 43%).

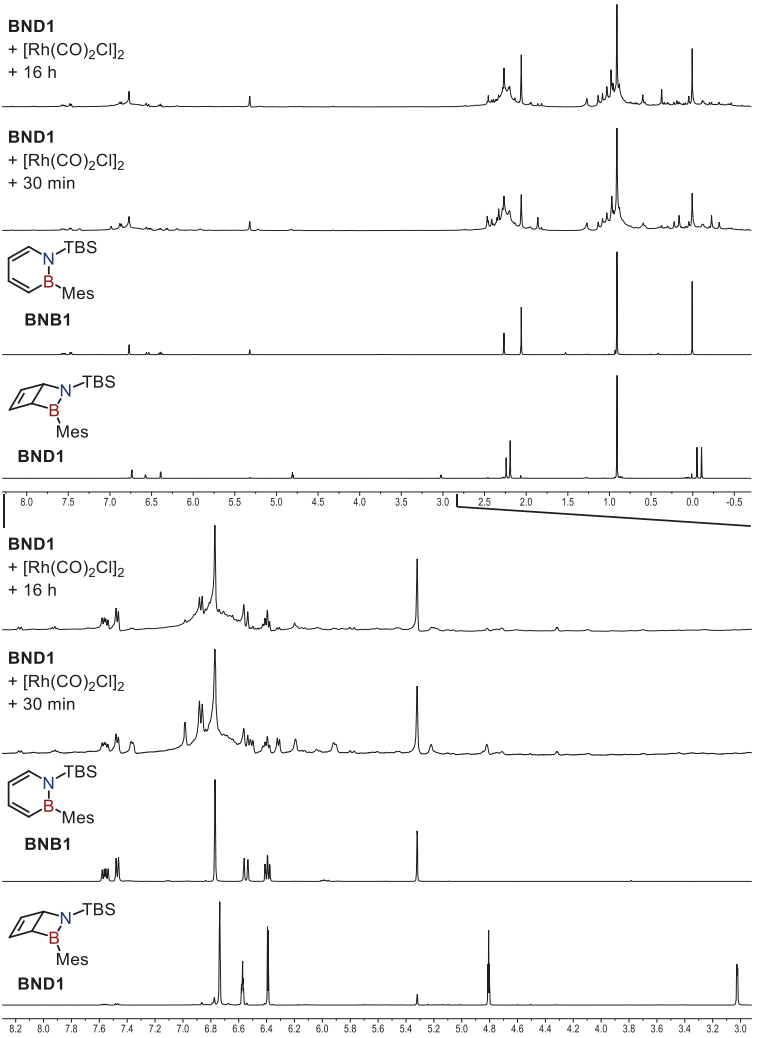

Figure 3.8. Stack plot of the ^{1}H NMR spectra of **BND1**, **BNB1** and **BND1** + $[Rh(CO)_2Cl]_2$ (1 equiv.) after 30 min and 16 h at rt in DCM-d_2.

Attempted alkyne or allene insertion into BND1 in presence of Wilkinson's catalyst

In a J. Young NMR tube, first either methyl but-2-ynoate (Figure 3.9) or ethyl allenecarboxylate (Figure 3.10) (2 equiv.) and then **BND1** (50 µmol, 1.0 equiv.) was added to a solution of $Rh(PPh_3)_3Cl$ (5 mol%) in DCM-d_2 (0.4 mL). The reaction was measured by 1H NMR after 30 min and 13 h, after which the NMR tube was initially heated to 40 °C for 1 h and then to 70 °C for 1 h.

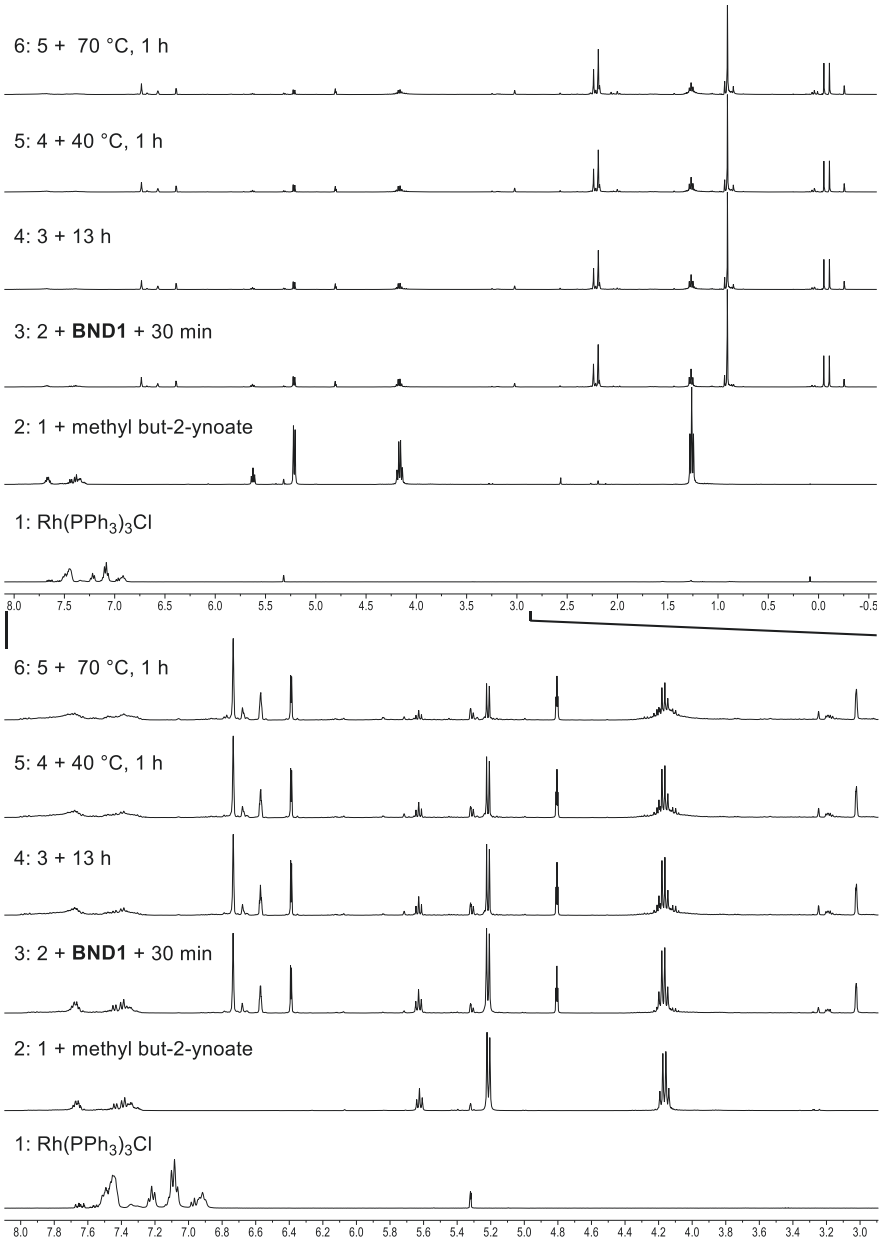

Figure 3.9. ^{1}H-NMR spectra in DCM-d_2 of Wilkinson's catalyst (5 mol%) (1), with added methyl but-2-ynoate (2 equiv.) (2), and **BND1** (50 µmol, 1 equiv.) after 30 min at rt (3), after 13 h at rt (4), after an additional 1 h at 40 °C (5), and after an additional 1 h at 70 °C (6).

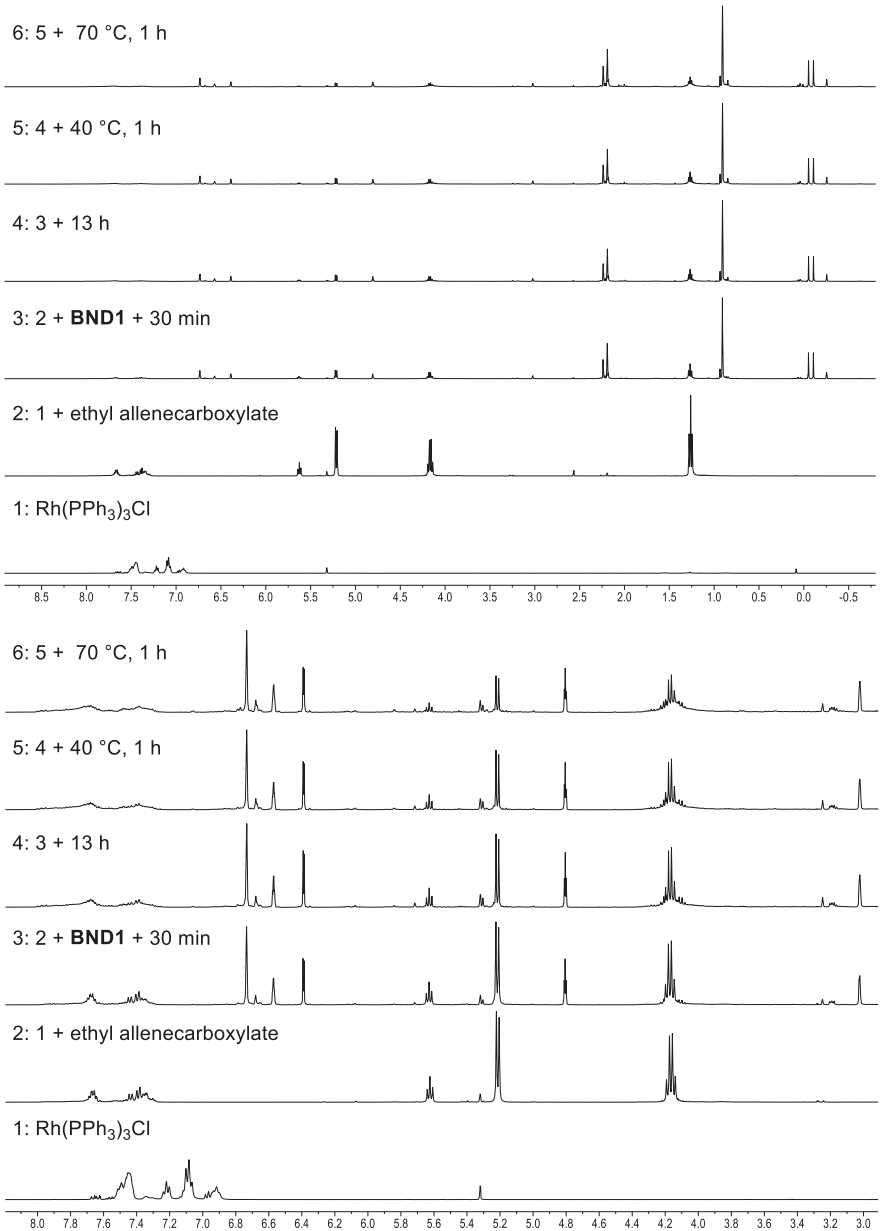

Figure 3.10. ^{1}H-NMR spectra in DCM-d_2 of Wilkinson's catalyst (5 mol%) (1), with added ethyl allenecarboxylate (2 equiv.) (2), and **BND1** (50 µmol, 1 equiv.) after 30 min at rt (3), after 13 h at rt (4), after an additional 1 h at 40 °C (5), and after an additional 1 h at 70 °C (6).

Kinetic studies

In a glovebox, **BND1**, the studied catalyst and the respective deuterated solvent (DCM-d_2 or toluene-d_8, 0.4 mL) were added to a J. Young NMR tube. Directly after solvent addition, the reaction mixtures were monitored over time by ^{1}H-NMR spectroscopy to assess catalytic performance. For catalysts exhibiting activity, spectra were recorded at sensible intervals until substantial conversion of the starting material was achieved. Since no decomposition products were detected (unless denoted explicitly), the conversion was quantified by comparing the integral values of reactant and product signals.

Methyl-4-(diphenylphosphino)benzoate (1)

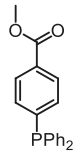

1

1 was synthesized following literature with slight modifications.[28] Before use, ^{i}PrMgBr in THF was titrated against I_2 in a 0.5 M LiCl/THF solution.[29]

In a 100 mL Schlenk flask, lithium chloride (574 mg, 9.50 mmol, 1.00 equiv.) was flame-dried *in vacuo*. Once cooled, methyl 4-iodobenzoate (2.49 g, 9.50 mmol, 1.00 equiv.) was added, and the reactants were suspended in THF (20 mL). The suspension was cooled to -25 °C, and ^{i}PrMgBr in THF (0.60 M, 15.8 mL, 9.50 mmol, 1.0 equiv.) was added dropwise. The reaction mixture was stirred for 30 min at -25 °C. Subsequently, solution was transferred *via* cannula into a stirred solution of chlorodiphenylphosphine (1.71 mL, 9.50 mmol, 1.00 equiv.) in THF (10 mL) at rt. The mixture, was allowed to stir for 16 h, after which the reaction was then quenched by the slow addition of water (25 mL). The aqueous phase was extracted with THF (2 × 20 mL), and the combined organic layers were washed with 1 M HCl (2 × 20 mL) and brine (2 × 20 mL). The organic phase was dried over $MgSO_4$, filtered, and concentrated under reduced pressure. The crude product was purified by flash chromatography (23 g SiO_2, 95:5 PE(60/90)/EA over 15 CV), affording compound **1** as a colorless oil (0.96 g, 3.00 mmol, 32%). Spectral data matched previously reported values.[30]

$C_{20}H_{17}O_2P$ (320.33 $\frac{g}{mol}$)

R$_f$: 0.40 (PE(60/90)/EA = 90:10) [UV]

^{1}H-NMR(400 MHz, $CDCl_3$): δ = 7.97 (m, 2H, H4), 7.34 (m, 12H), 3.91 (s, 3H, H1).

^{13}C-NMR(101 MHz, $CDCl_3$): δ = 134.1 (d, ^{2}J = 19.8 Hz), 133.3 (d, ^{2}J = 18.4 Hz), 129.4 (d, ^{3}J = 6.5 Hz), 129.3 (C10), 128.8 (d, ^{3}J = 7.4 Hz), 52.3 (C1).

^{31}P-NMR(162 MHz, $CDCl_3$): δ = -5.0.

GC-MS(EI): t_r = 11.81 min, $\frac{m}{z}$($I_{base\ peak}$ %) = 320 ($M^{\bullet+}$, 32), 183 (23), 154 (18), 78 (100), 77 ($M^{\bullet+}$ - $C_{14}H_{12}O_2P^{\bullet}$, 32), 51 (24).

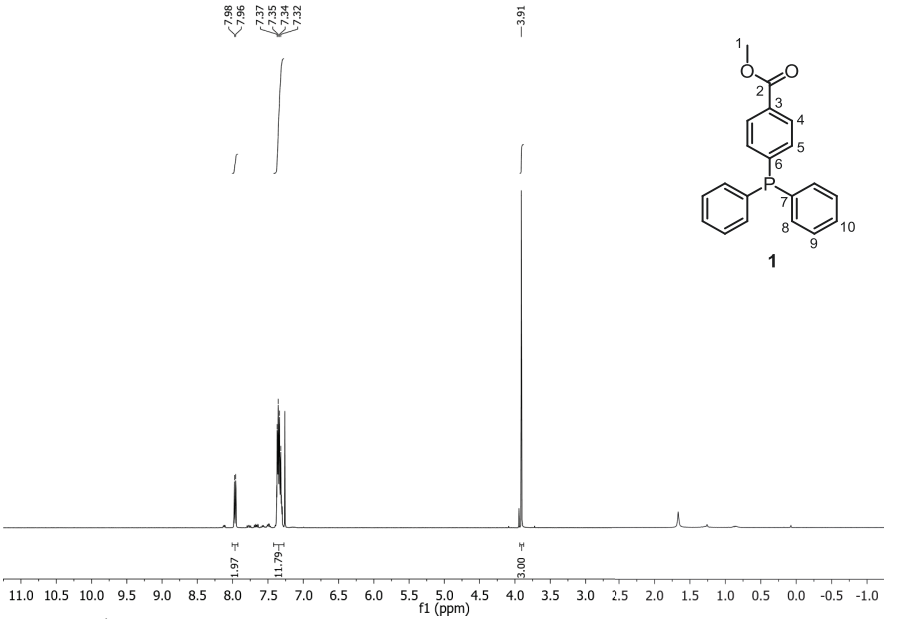

Figure 3.11. ^{1}H NMR spectrum of **1** in $CDCl_3$, measured at 400.16 MHz.

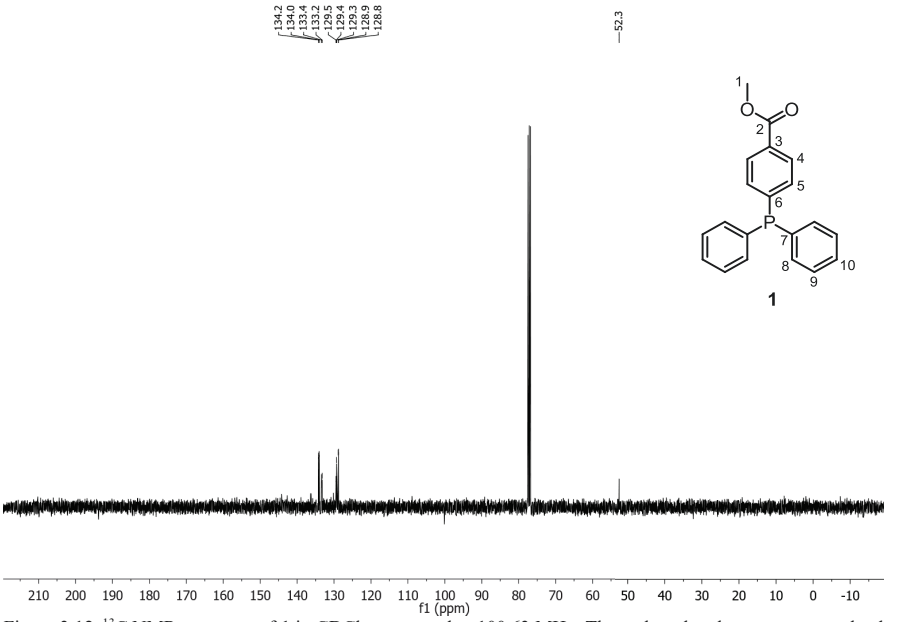

Figure 3.12. ^{13}C NMR spectrum of **1** in $CDCl_3$, measured at 100.63 MHz. The carbonyl carbon was not resolved due to the low intensity.

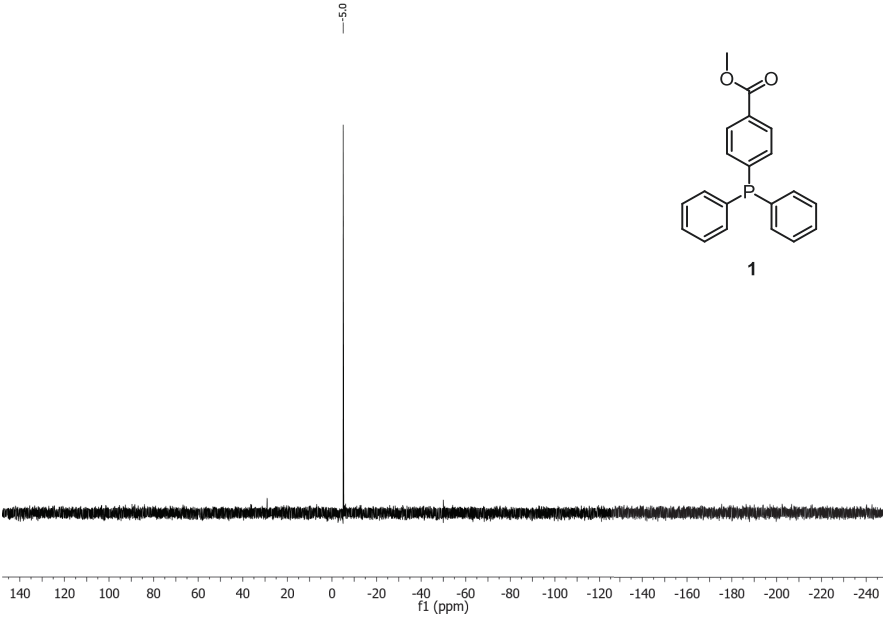

Figure 3.13. ^{31}P NMR spectrum of **1** in $CDCl_3$, measured at 161.98 MHz.

Diphenylphosphinylbenzenecarboxylicacid-4-*N*-(3-trimethoxy-silylpropyl)amide (linker II)

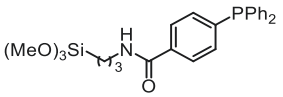

linker II

Linker II was prepared following a literature protocol with minor adjustments.[25] 1 (0.96 g, 3.00 mmol, 1.0 equiv.), LiOMe (11.4 mg, 0.30 mmol, 0.10 equiv.), and 3-trimethoxysilylpropylamine (0.65 mL, 3.70 mmol, 1.23 equiv.) was placed in a pressure tube, heated to 170 °C, and stirred for 4 h. Subsequently, volatiles were removed *in vacuo* at 100 °C. The remnant was dissolved in DCM, filtered and then concentrated under reduced pressure furnishing the product as a yellow oil (0.99 g, 2.14 mmol, 71%). Spectroscopic data were consistent with previously reported values.[31]

Note: The product was stored under an inert atmosphere.

$C_{25}H_{30}NO_4PSi$ (467.58 $\frac{g}{mol}$)

^{1}H-NMR(400 MHz, $CDCl_3$): δ = 7.71 (m, 2H, H8), 7.34 (m, 12H), 6,44 (bs, 1H, H5), 3.56 (s, 9H, H1), 3.47 (m, 2H, H4), 1.75 (q, ^3J = 7.7 Hz, 2H, H3), 0.72 (t, ^3J = 8.0 Hz, 2H, H2).

^{13}C-NMR(176 MHz, $CDCl_3$): δ = 167.3 (s, C6), 141.9 (d, ^1J = 13.3 Hz, C10), 136.5 (d, ^1J = 10.4 Hz, C11), 135.0 (s, C7), 134.0 (d, ^2J = 19.8 Hz, C12), 133.7 (d, ^2J = 18.9 Hz, C9), 129.2 (s, C14), 128.8 (d, ^3J = 7.3 Hz, C13), 126.9 (d, ^3J = 6.6 Hz, C8), 50.8 (s, C1), 42.4 (s, C4), 22.8 (s, C3), 6.7 (s, C2).

^{31}P-NMR(162 MHz, $CDCl_3$): δ = -5.5.

IR(ATR, $\tilde{\nu}$ [cm^{-1}]): 3051 (w), 2935 (w), 2838 (w), 1634 (m, CO), 1597 (w), 1536 (s), 1481 (m), 1433 (m), 1302 (m), 1190 (m), 1075 (vs), 810 (s), 740 (s), 692 (vs).

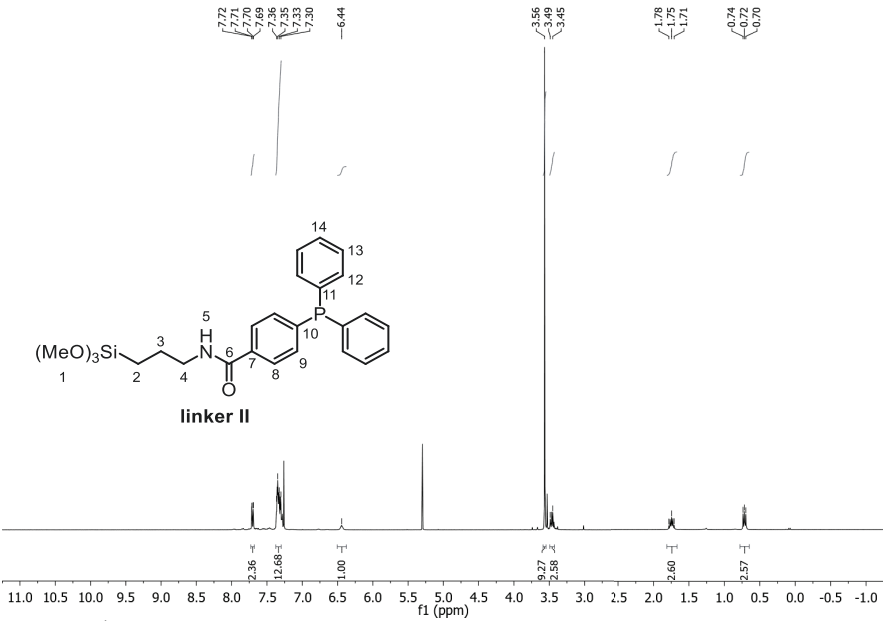

Figure 3.14. ^{1}H NMR spectrum of **linker II** in $CDCl_3$, measured at 400.16 MHz.

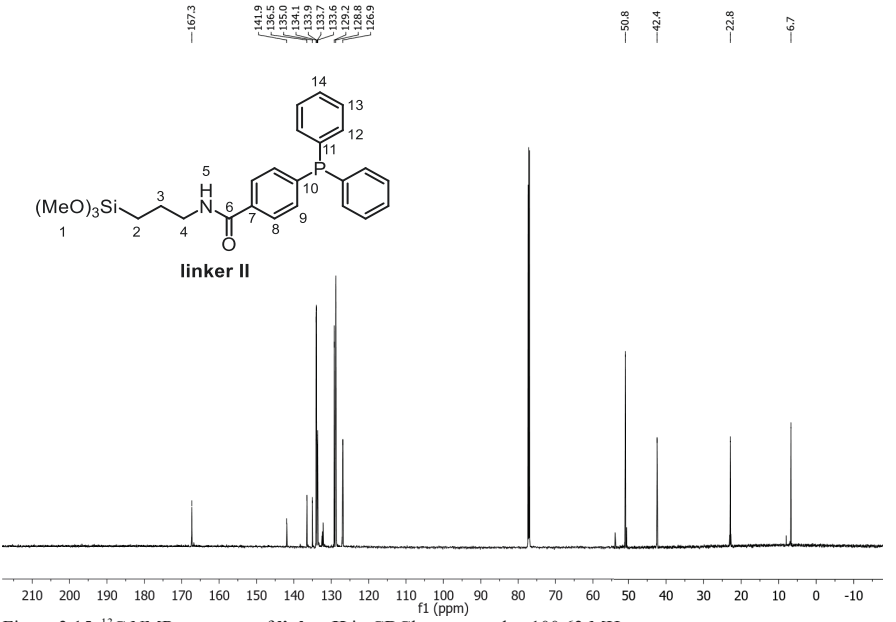

Figure 3.15. ^{13}C NMR spectrum of **linker II** in $CDCl_3$, measured at 100.63 MHz.

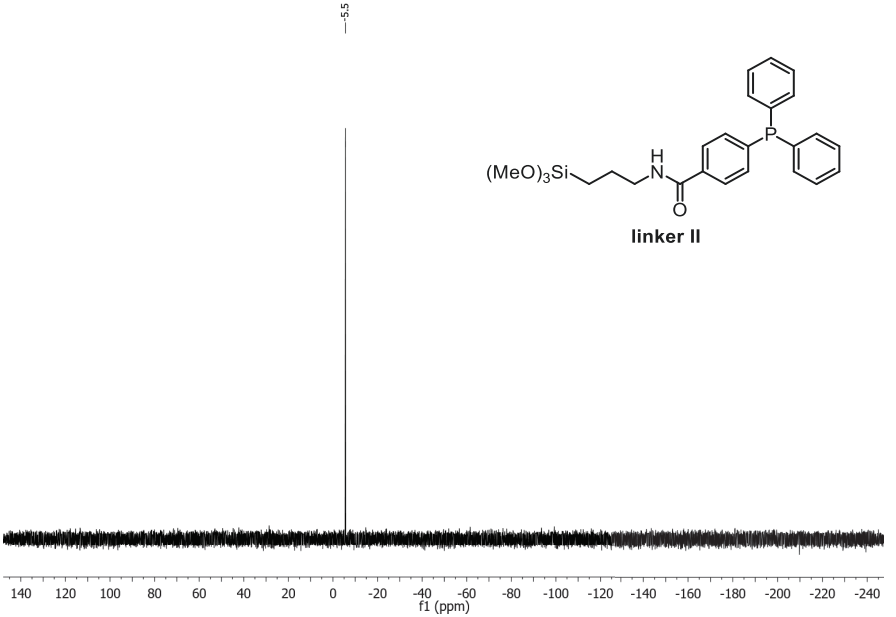

Figure 3.16. ^{31}P NMR spectrum of **linker II** in $CDCl_3$, measured at 161.98 MHz.

4-Diphenylphosphinylbenzenecarboxylicacid-4-*N*-(3-trimethoxy-silylpropyl)amide on silica (II@SiO2)

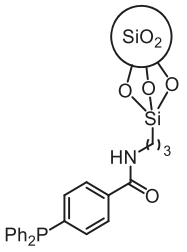

II@SiO2

The synthesis of **II@SiO2** followed reported procedures with modifications.[24-25] Silica gel (249 mg, particle size 40–60 µm) was activated *in vacuo* at 250 °C for 2.5 h. Once cooled, **linker II** (1.05 mmol, 1.0 equiv.) in DCM (0.7 M) was added and the solvent volume was reduced *in vacuo* to approximately 5 mL. Subsequently, toluene (25 mL) was added, and the mixture was stirred at 80 °C for 20 h. After the reaction, the solvent was removed under reduced pressure, and the residue was suspended in DCM. The suspension was filtered through a medium porosity frit (P3, 16–40 µm) under ambient atmosphere and washed thoroughly with degassed DCM. The final product was obtained as a pale yellow powder after drying *in vacuo* (107 mg, 17%).

^{31}P-MAS-NMR(121 MHz): δ = -5.2

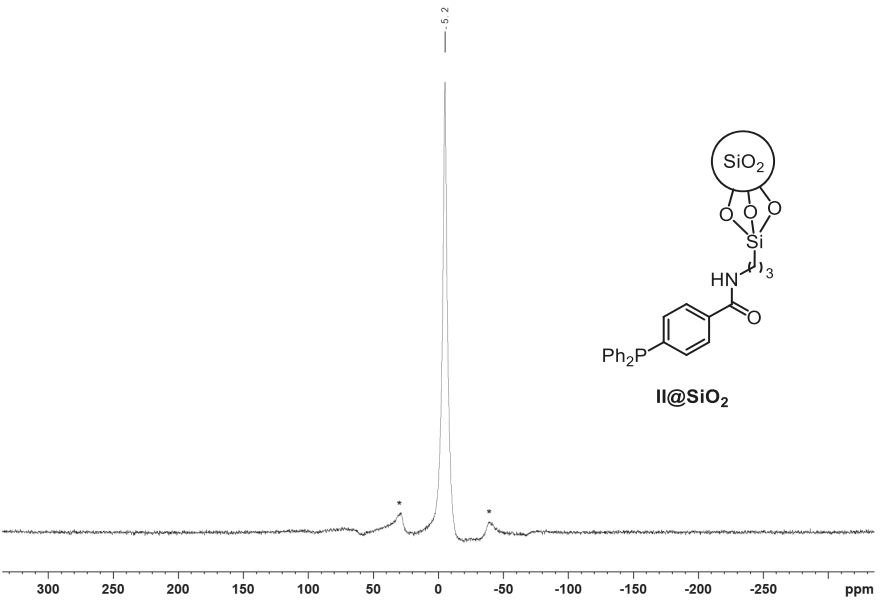

Figure 3.17. ^{31}P MAS NMR of **II@SiO$_2$**, measured at 121.49 MHz. * Denotes spinning sidebands.

Rh2@SiO$_2$

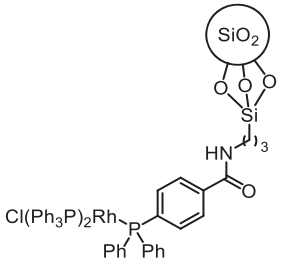

Rh2@SiO$_2$

II@SiO$_2$ (107 mg) and RhCl(PPh$_3$)$_3$ (50.0 mg, 54.0 µmol) were suspended in DCM (5 mL) and stirred at rt for 1.5 h. After the reaction, the mixture was filtered, and the solid residue was washed with DCM (2 × 5 mL). To ensure thorough removal of any physisorbed species, the solid was subjected to Soxhlet extraction (DCM) for 96 h. Subsequent drying under reduced pressure afforded the final product as a rusty brown powder (164 mg, 113%).

^{1}H-MAS-NMR(300 MHz): δ = 6.70, 3.37.

^{13}C-MAS-NMR(75 MHz): δ = 238.0, 166.9 (C1), 131.6, 127.3, 49.8, 41.8, 22.0, 8.2.

^{31}P-MAS-NMR(121 MHz): δ = -5.0.

IR(ATR, $\tilde{\nu}$ [cm^{-1}]): 1042 (m), 792 (w), 744 (w), 692 (w).

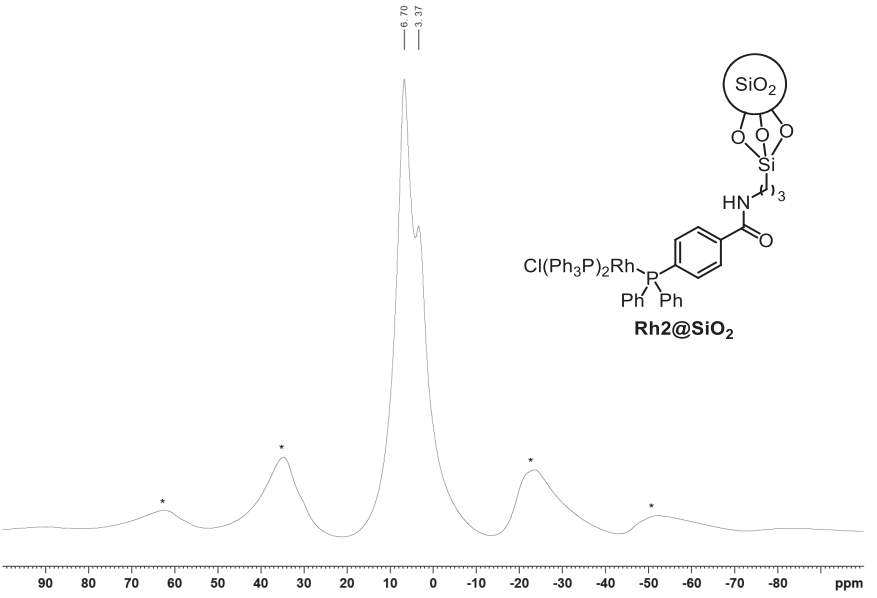

Figure 3.18. ^{1}H MAS NMR of **Rh2@SiO$_2$**, measured at 300.13 MHz. * Denotes spinning sidebands.

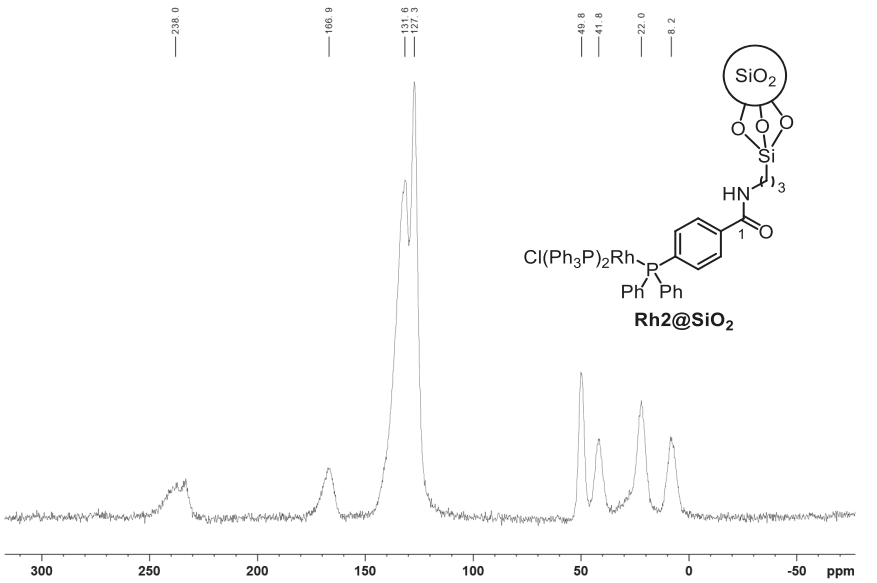

Figure 3.19. ^{13}C MAS NMR of **Rh2@SiO$_2$**, measured at 75.48 MHz.

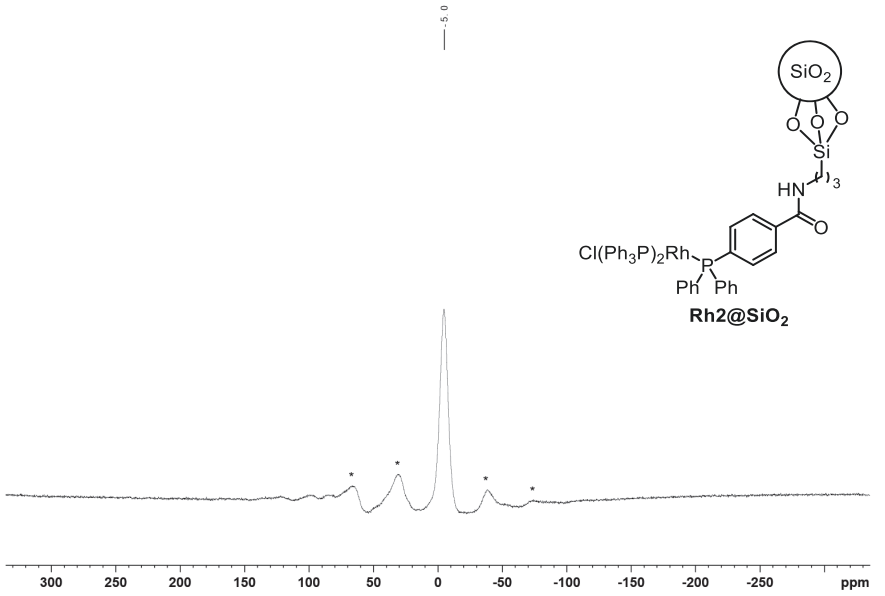

Figure 3.20. ^{31}P MAS NMR of **Rh2@SiO$_2$**, measured at 121.49 MHz. * Denotes spinning sidebands.

Carbonylchloridobis[(4-diphenylphosphinylbenzenecarboxylicacid-4-*N*-(3-trimethoxysilylpropyl)amide]rhodium(I) (Rh3)

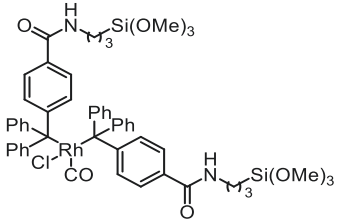

Rh3

Following a literature procedure with slight modifications,[25] $[Rh(CO)_2Cl]_2$ (56.2 mg, 145 µmol, 0.25 equiv.) was dissolved in DCM (8 mL) and a solution of **linker II** (578 µmol, 1.0 equiv.) in DCM (0.7 M) was added. The reaction mixture was stirred at rt for 16 h. After completion, all volatiles were removed *in vacuo*. This resinous residue was treated with Et_2O (10 mL) and sonicated for 45 min. The resulting solid was isolated by decanting the solvent, followed by washing with Et_2O (3 × 8 mL). Subsequently, the product was dried *in vacuo* to afford **2** as a yellow solid (291 mg, 264 µmol, 46%). The spectroscopic data obtained matched previously reported values.[25]

$C_{51}H_{60}ClN_2O_9P_2RhSi_2$ (1101.52 $\frac{g}{mol}$)

^{1}H-NMR(400 MHz, $CDCl_3$): δ = 7.65 (m, 16H), 7.39 (m, 12H), 6.48 (bs, 2H, H1), 3.55 (m, 18H, H5), 3.45 (m, 4H, H2), 1.74 (m, 4H, H3), 0.71 (m, 4H, H4).

^{13}C-NMR(101 MHz, $CDCl_3$): δ = 134.6 , 130.3, 128.6, 126.7, 50.8 (C5), 42.4 (C2), 22.8 (C3), 6.7 (C4).

IR(ATR, $\tilde{\nu}$ [cm^{-1}]): 2935 (w), 2835 (w), 1970 (w), 1634 (w), 1536 (w), 1481 (w), 1433 (w), 1303 (w), 1187 (w), 1077 (m), 808 (w), 747 (w), 691 (m).

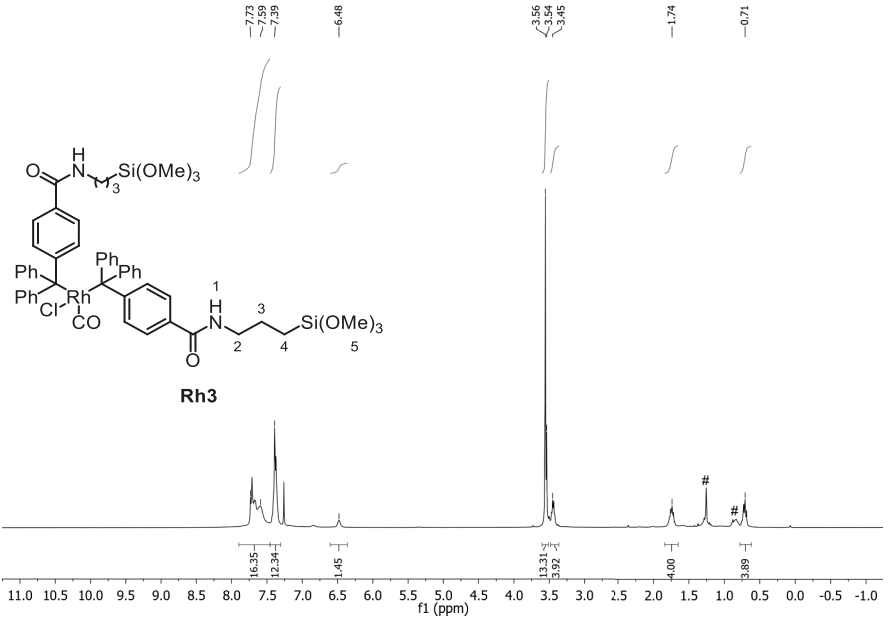

Figure 3.21. ^{1}H NMR spectrum of **Rh3** in $CDCl_3$, measured at 400.16 MHz. # Denotes unknown impurities.

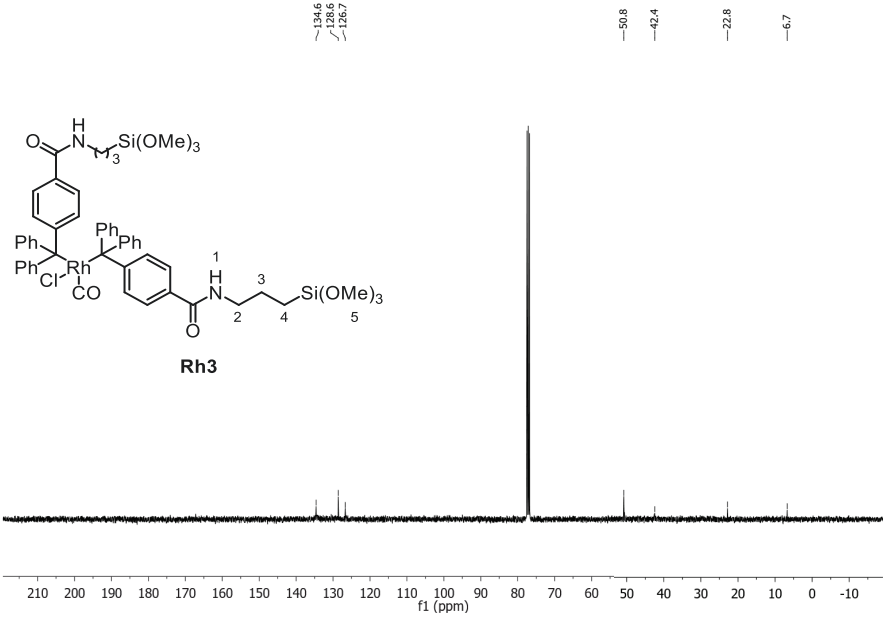

Figure 3.22. ^{13}C NMR spectrum of **Rh3** in $CDCl_3$, measured at 100.63 MHz. The carbonyl carbon was not resolved due to the low intensity.

Rh@diphenylphosphine polystyrene (Rh@PS)

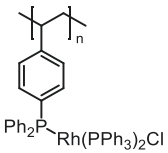

Rh@PS

Rh@PS was synthesized according to literature.[32] In a glovebox, diphenylphosphine polystyrene (1.6 mmol/g loading, 59.0 mg, 95.3 μmol, 1.0 equiv.) and $RhCl(PPh_3)_3$ (176 mg, 191 μmol, 2.0 equiv.) were suspended THF (2 mL) and stirred for 3 weeks. After the reaction period, the mixture was filtered through a P4 frit, and the remaining solid was washed thoroughly with toluene until the filtrate appeared colorless. The solid was then dried under reduced pressure to afford the product as a dark red solid (34.1 mg, 39%). The material was used directly in subsequent experiments without additional purification.

Element Organic Framework (EOF)

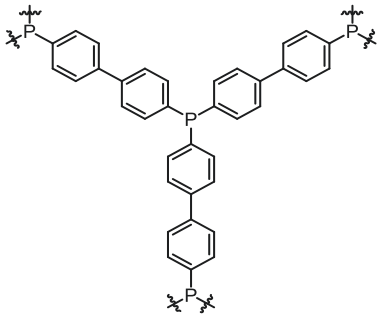

EOF

Step 1: Preparation of 4,4′-Dilithiumbiphenyl:

The organolithium intermediate was prepared according to literature with slight modificatins.[26] The concentration of *n*-BuLi (*n*-hexane) was determined by titration against *N*-benzylbenzamide in THF at -20 °C.[33] *n*-BuLi (3.65 M, 6.85 mL, 25.0 mmol, 2.0 equiv.) was added dropwise to a cooled (-15 °C) THF (250 mL) solution of 4,4′-dibromobiphenyl (3.90 g, 12.5 mmol, 1.0 equiv.). After complete addition, the mixture was stirred at -15 °C for 10 min and used directly in the next step without further purification.

Step 2: Synthesis of Element Organic Framework:

Phosphorus trichloride was freshly distilled at 76 °C under atmospheric pressure prior to use.

PCl_3 (0.72 mL, 8.25 mmol, 0.66 equiv.) was added to a cooled (-15 °C) THF (250 mL) solution of 4,4′-dilithiumbiphenyl (2.08 g, 12.5 mmol, 1.0 equiv.). Subsequently, the mixture was stirred at rt for 16 h.

After completion, the majority of solvent was decanted, and the residue was transferred to an inert falcon tube and centrifuged (9000 rpm, 5 min). The supernatant was decanted, and the residue was washed sequentially with THF (2 × 45 mL) and degassed H_2O (30 mL). The resulting solid was extracted with EtOH in a Soxhlet apparatus for 72 h. After drying under vacuum, **EOF** was isolated as a colorless powder (0.75 g, 35%). The spectroscopic data matched the literature values.[26]

^{1}H-MAS-NMR(300 MHz): δ = 6.78.

^{13}C-MAS-NMR(75 MHz): δ = 139.8, 131.5, 126.4.

^{31}P-MAS-NMR(121 MHz): δ = -6.8.

IR(ATR, $\tilde{\nu}$ [cm^{-1}]): 3021 (w), 2965 (w), 1594 (w), 1478 (w), 1381 (w), 1187 (w), 1094 (m), 1046 (m), 1001 (m), 807 (s), 695 (m).

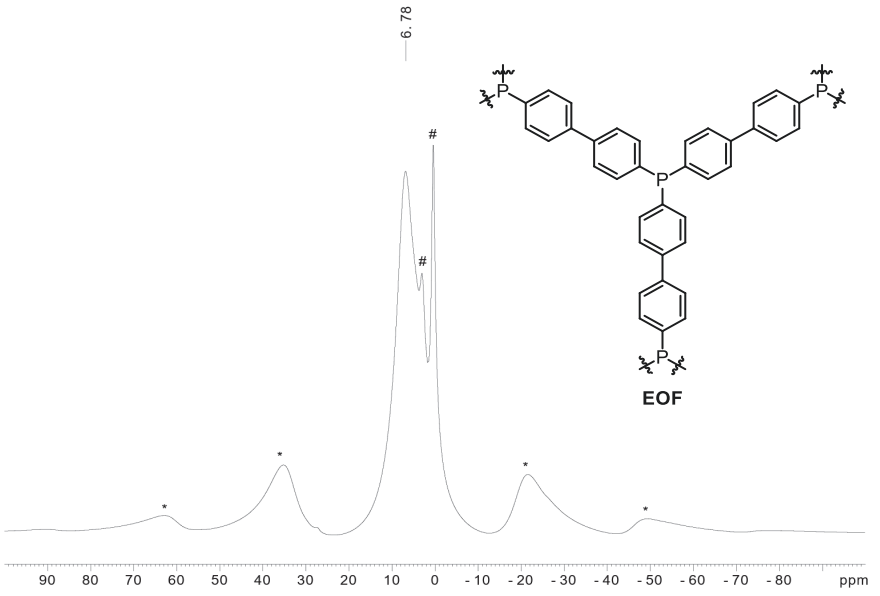

Figure 3.23. ^{1}H MAS NMR of **EOF**, measured at 300.13 MHz. * Denotes spinning sidebands. # Denotes unknown impurities.

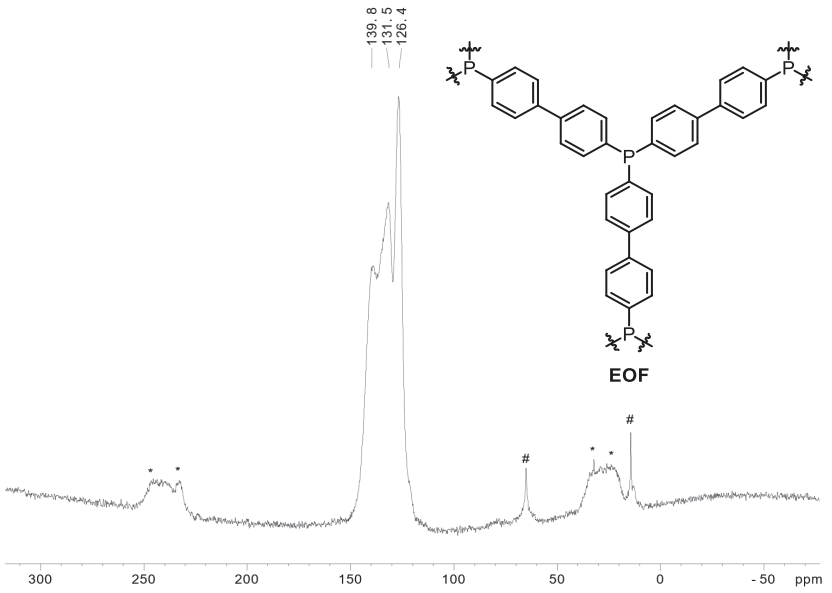

Figure 3.24. ^{13}C MAS NMR of **EOF**, measured at 75.48 MHz. * Denotes spinning sidebands. # Denotes unknown impurities.

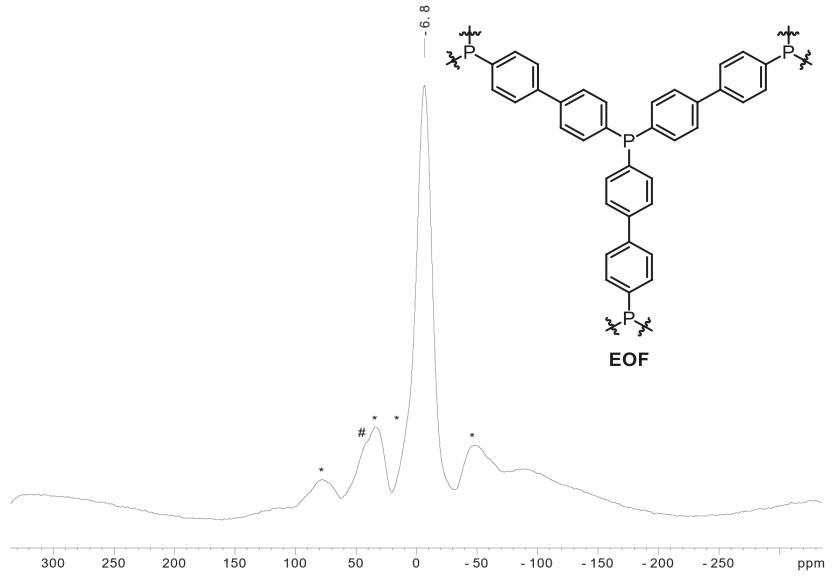

Figure 3.25. ^{31}P MAS NMR of **EOF**, measured at 121.49 MHz. * Denotes spinning sidebands. # Denotes unknown impurities.

Rh@EOF

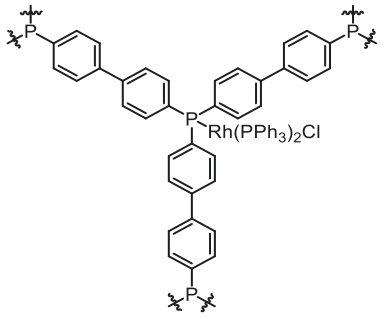

Rh@EOF

Rh@EOF was synthesized according to literature.[26] $RhCl(PPh_3)_3$ (20.9 mg, 22.6 µmol) and **EOF** (200 mg) were suspended in $CHCl_3$ (20 mL) and stirred at rt for 16 h. After the reaction period, the mixture was filtered through a P4 frit (10 –16 µm) and the residue was washed thoroughly with Et_2O (3 × 10 mL). The resulting solid was dried *in vacuo* to give **Rh@EOF** as a pale orange powder. The obtained spectroscopic data was consistent with literature.[26]

^{1}H-MAS-NMR(300 MHz): δ = 6.87.

^{13}C-MAS-NMR(75 MHz): δ = 139.1, 131.3, 126.6.

^{31}P-MAS-NMR(121 MHz): δ = -5.5.

IR(ATR, $\tilde{\nu}$ [cm^{-1}]): 2965 (w), 1739 (w), 1594 (w), 1478 (w), 1381 (w), 1195 (w), 1113 (w), 1001 (w), 844 (w), 807 (m), 758 (w), 696 (m).

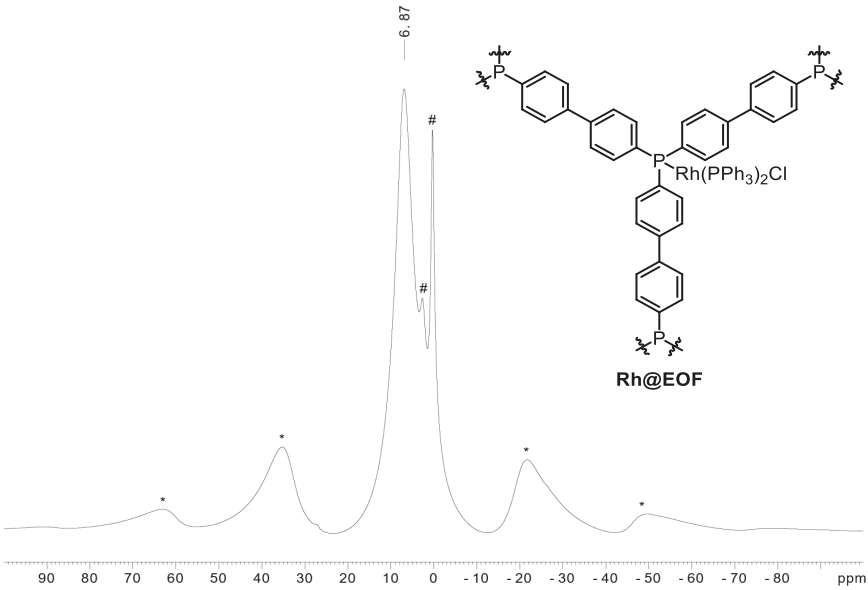

Figure 3.26. ^{1}H MAS NMR of **Rh@EOF**, measured at 300.13 MHz. * Denotes spinning sidebands. # Denotes unknown impurities.

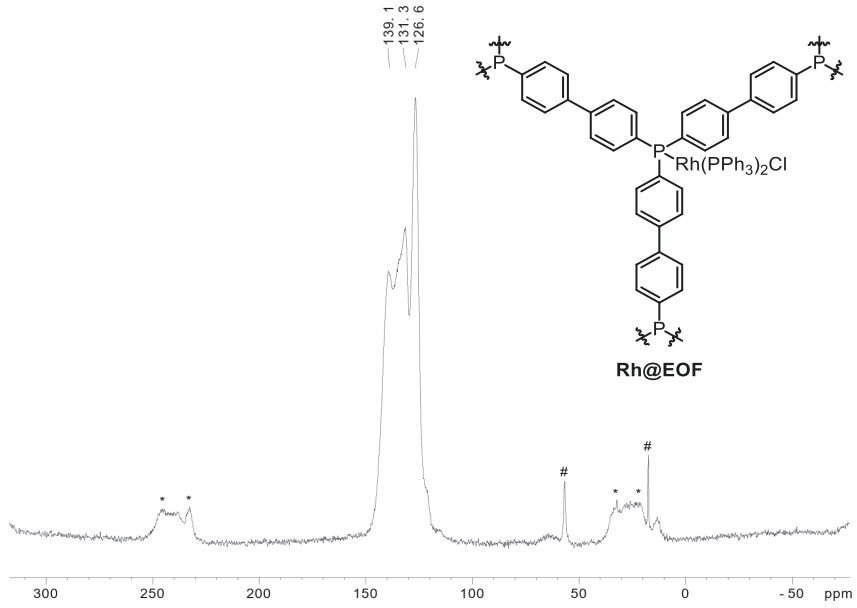

Figure 3.27. ^{13}C MAS NMR of **Rh@EOF**, measured at 75.48 MHz. * Denotes spinning sidebands. # Denotes unknown impurities.

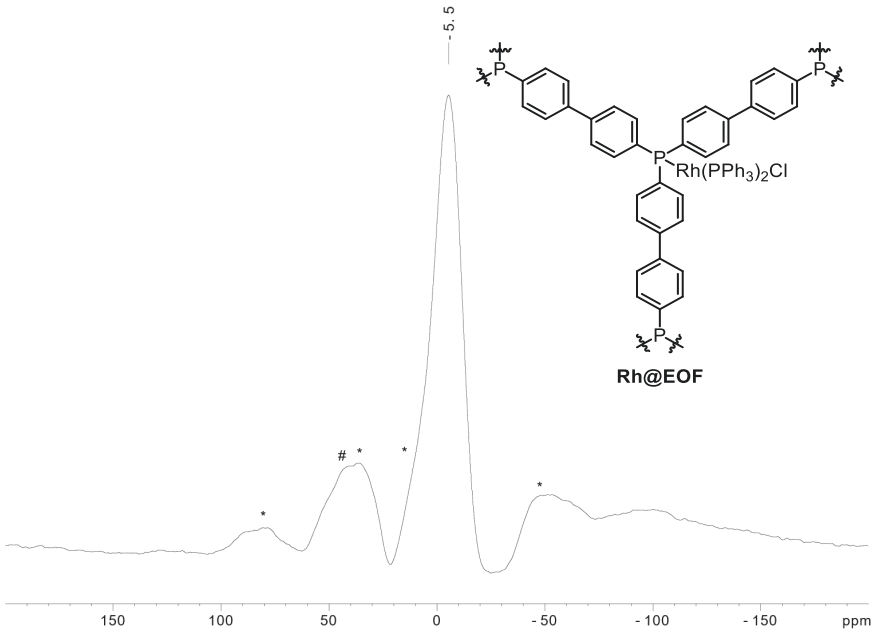

Figure 3.28. ^{31}P MAS NMR of **Rh@EOF**, measured at 121.49 MHz. * Denotes spinning sidebands. # Denotes unknown impurities.

3.3 References

[1] R. B. Woodward, R. Hoffmann, *Angew. Chem., Int. Ed.* **1969**, *8*, 781-853.
[2] K. Edel, X. Yang, J. S. A. Ishibashi, A. N. Lamm, C. Maichle-Mössmer, Z. X. Giustra, S.-Y. Liu, H. F. Bettinger, *Angew. Chem. Int. Ed.* **2018**, *57*, 5296-5300.
[3] I. M. Riddlestone, A. Kraft, J. Schaefer, I. Krossing, *Angew. Chem. Int. Ed.* **2018**, *57*, 13982-14024.
[4] I. Krossing, *Chem.-Eur. J.* **2001**, *7*, 490-502.
[5] R. C. Richter, S. M. Biebl, R. Einholz, J. Walz, C. Maichle-Mössmer, M. Ströbele, H. F. Bettinger, I. Fleischer, *Angew. Chem. Int. Ed.* **2024**, *63*, e202405818.
[6] a) L. Pauling, *Chem. Phys.* **1936**, *4*, 673-677; b) K. Baskaran, C. W. Wilburn, J. R. Wedell, L. M. I. Koharudin, E. L. Ulrich, A. D. Schuyler, H. R. Eghbalnia, A. M. Gronenborn, J. C. Hoch, *Magn. Reson.* **2021**, *2*, 765-775.
[7] A. W. Baggett, M. Vasiliu, B. Li, D. A. Dixon, S.-Y. Liu, *J. Am. Chem. Soc.* **2015**, *137*, 5536-5541.
[8] a) Y. Zhao, D. G. Truhlar, *Theor. Chem. Acc.* **2008**, *120*, 215-241; b) F. Weigend, R. Ahlrichs, *Phys. Chem. Chem. Phys.* **2005**, *7*, 3297-3305; c) G. W. T. M. J. Frisch, H. B. Schlegel, G. E. Scuseria, M. A. Robb, J. R. Cheeseman, G. Scalmani, V. Barone, G. A. Petersson, H. Nakatsuji, X. Li, M. Caricato, A. V. Marenich, J. Bloino, B. G. Janesko, R. Gomperts, B. Mennucci, H. P. Hratchian, J. V. Ortiz, A. F. Izmaylov, J. L. Sonnenberg, D. Williams-Young, F. Ding, F. Lipparini, F. Egidi, J. Goings, B. Peng, A. Petrone, T. Henderson, D. Ranasinghe, V. G. Zakrzewski, J. Gao, N. Rega, G. Zheng, W. Liang, M. Hada, M. Ehara, K. Toyota, R. Fukuda, J. Hasegawa, M. Ishida, T. Nakajima, Y. Honda, O. Kitao, H. Nakai, T. Vreven, K. Throssell, J. A. Montgomery, Jr., J. E. Peralta, F. Ogliaro, M. J. Bearpark, J. J. Heyd, E. N. Brothers, K. N. Kudin, V. N. Staroverov, T. A. Keith, R. Kobayashi, J. Normand, K. Raghavachari, A. P. Rendell, J. C. Burant, S. S. Iyengar, J. Tomasi, M. Cossi, J. M. Millam, M. Klene, C. Adamo, R. Cammi, J. W. Ochterski, R. L. Martin, K. Morokuma, O. Farkas, J. B. Foresman, and D. J. Fox, Revision g16.C.01 ed., Inc., Wallingford CT, **2016**; d) S. Miertuš, E. Scrocco, J. Tomasi, *Chem. Phys.* **1981**, *55*, 117-129.
[9] L. Greb, *Chem.-Eur. J.* **2018**, *24*, 17881-17896.
[10] H. Sinn, W. Kaminsky, H.-J. Vollmer, R. Woldt, *Angew. Chem. Int. Ed.* **1980**, *19*, 390-392.
[11] J. Burés, I. Larrosa, *Nature* **2023**, *613*, 689-695.
[12] C. D. T. Nielsen, J. Burés, *Chem. Sci.* **2019**, *10*, 348-353.
[13] J. A. Osborn, F. H. Jardine, J. F. Young, G. Wilkinson, *J. Chem. Soc. A. Inorg. phys. theor.* **1966**, 1711-1732.
[14] J. Halpern, *Acc. Chem. Res.* **1970**, *3*, 386-392.
[15] L. Cassar, J. Halpern, *J. Chem. Soc. D* **1970**, 1082-1083.
[16] R. Noyori, I. Umeda, H. Kawauchi, H. Takaya, *J. Am. Chem. Soc.* **1975**, *97*, 812-820.
[17] V. A. Bren, A. D. Dubonosov, V. I. Minkin, V. A. Chernoivanov, *Russ. Chem. Rev.* **1991**, *60*, 451-469.
[18] A. Corma, H. Garcia, *Adv. Synth. Catal.* **2006**, *348*, 1391-1412.
[19] a) S. Miki, T. Maruyama, T. Ohno, T. Tohma, S.-i. Toyama, Z.-i. Yoshida, *Chem. Lett.* **1988**, *17*, 861-864; b) L. Magson, D. Maggiolo, A. S. Kalagasidis, S. Henninger, G. Munz, M. Knäbbeler-Buß, H. Hölzel, K. Moth-Poulsen, I. Funes-Ardoiz, D. Sampedro, *Adv. Energy Sustainability Res.* **2025**, *6*, 2400230.
[20] P. McMorn, G. J. Hutchings, *Chem. Soc. Rev.* **2004**, *33*, 108-122.

[21] R. L. Augustine, S. K. Tanielyan, N. Mahata, Y. Gao, A. Zsigmond, H. Yang, *Appl. Catal. A Gen.* **2003**, *256*, 69-76.
[22] a) R. H. Grubbs, L. C. Kroll, *J. Am. Chem. Soc.* **1971**, *93*, 3062-3063; b) P. Li, W. Thitsartarn, S. Kawi, *Ind. Eng. Chem. Res.* **2009**, *48*, 1824-1830.
[23] a) R. Sayah, E. Framery, V. Dufaud, *Green Chemistry* **2009**, *11*, 1694-1702; b) M. Srour, S. Hadjiali, G. Sauer, K. Brunnengräber, H. Breitzke, Y. Xu, H. Weidler, H.-H. Limbach, T. Gutmann, G. Buntkowsky, *ChemCatChem* **2016**, *8*, 3409-3416.
[24] K. Bogár, P. Krumlinde, Z. Bacsik, N. Hedin, J.-E. Bäckvall, *Eur. J. Org. Chem.* **2011**, *2011*, 4409–4414.
[25] L. Wang, M. Jia, S. Shylesh, T. Philippi, A. Seifert, S. Ernst, A. P. Singh, W. R. Thiel, *ChemCatChem* **2010**, *2*, 1477–1482.
[26] J. Fritsch, F. Drache, G. Nickerl, W. Böhlmann, S. Kaskel, *Microporous Mesoporous Mater.* **2013**, *172*, 167-173.
[27] M. J. O'Neil, 14th ed., The Merck index : an encyclopedia of chemicals, drugs, and biologicals, Merck Whitehouse Station, N.J., **2006**.
[28] Y. Oonishi, T. Yokoe, A. Hosotani, Y. Sato, *Angew. Chem. Int. Ed. Engl.* **2014**, *53*, 1135–1139.
[29] A. Krasovskiy, P. Knochel, *Synthesis* **2006**, *5*, 0890–0891.
[30] Y. Li, L. Q. Lu, S. Das, S. Pisiewicz, K. Junge, M. Beller, *J. Am. Chem. Soc.* **2012**, *134*, 18325–18329.
[31] L. Wang, A. Reis, A. Seifert, T. Philippi, S. Ernst, M. Jia, W. R. Thiel, *Dalton Trans.* **2009**, 3315–3320.
[32] R. H. Grubbs, L. C. Kroll, *J. Am. Chem. Soc.* **1971**, *93*, 3062–3063.
[33] A. F. Burchat, J. M. Chong, N. Nielsen, *J. Organomet. Chem.* **1997**, *542*, 281–283.

4 Nickel Catalyzed Activation of Benzocyclobutanones

4.1 Summary of Published Results

The objective of this study was to develop a catalytic system capable of promoting the intermolecular insertion of norbornadienes (NBDs) into benzocyclobutanones (BCBs) *via* C–C bond activation, thereby generating the three-dimensional nortricyclane scaffold. This motif is traditionally obtained from NBDs through a [2+2+2] homo-Diels-Alder (HDA) reaction (Figure 4.1a),[1] which formally can also be facilitated catalytically (Figure 4.1b),[2] enabling the asymmetric formation of four stereocenters.[3]

For the activation of BCBs, a nickel-based catalytic system was selected, as the 3d transition metal (TM) has previously enabled intermolecular insertion of 1,3-dienes and alkynes into BCBs.[4] In contrast, the more commonly used rhodium-catalysts, typically favor intramolecular transformations.[5]

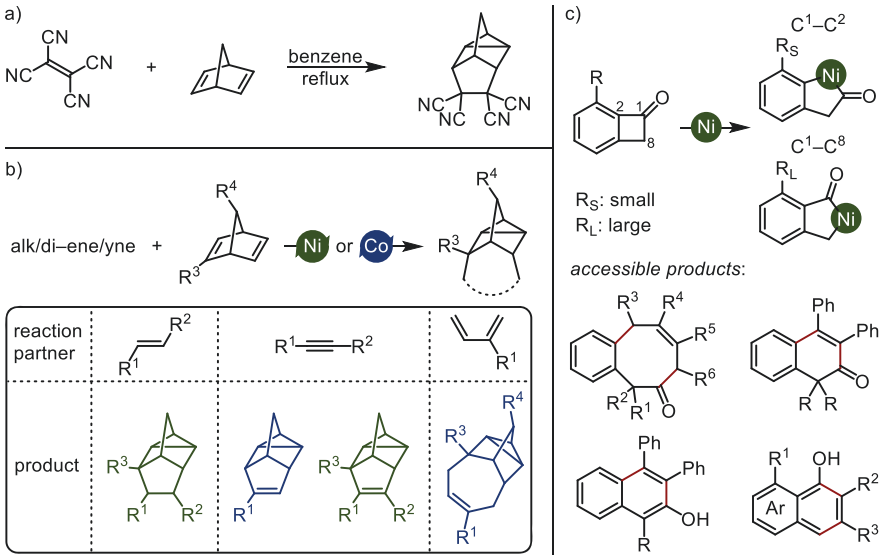

Figure 4.1. Literature overview on the HDA reaction of NBD and nickel-catalyzed intermolecular insertion reactions. [a]Classical HDA reaction of NBD with tetracyanoethylene, furnishing a nortricyclan framework.[1] [b]Nickel and cobalt-catalyzed [2+2+2/4] cycloaddition involving NBD.[2-3] [c]Nickel-catalyzed C^1–C^2 vs. C^1–C^8 bond activation of BCBs, leading to distinct product classes.[4, 6]

A notable feature of the nickel-catalyzed system is its tunable regioselectivity, which enables selective activation of either the C^1–C^2 or C^1–C^8 bond of BCBs. This selectivity can be modulated through steric effects at the pseudo-*ortho* position relative to the ketone functionality (Figure 4.1c).[6] This property was also envisioned to broaden the scope of accessible products in the developed system.

The study commenced with the optimization of the nickel-catalyzed insertion of NBD into BCB. $Ni(COD)_2$ was selected as a convenient and widely used source of nickel(0) with toluene as a solvent-based on literature precedents.[4, 6] Under these preliminary conditions, phosphine-based ligands were evaluated, including both monodentate and bidentate types. The system proved tolerant of both classes, with MonoPhos, TyrannoPhos, and dppb performing best in their respective categories (Table 4.1, entries 1–6). Notably, elevated temperatures generally improved performance (Table 4.1, entries 1–6). Surprisingly, electron poor **L4** and electron rich **L5**, which had been found to be optimal in related nickel-catalyzed insertion reactions,[4, 6] performed poorly despite **L5** showing quantitative conversion of BCB (Table 4.1, entries 7, 8). Generally, high conversions were observed, even for reactions with low yields, indicating, that BCB decomposes under the reaction conditions.

Table 4.1. Initial optimization of the nickel-catalyzed insertion of NBD into BCB.

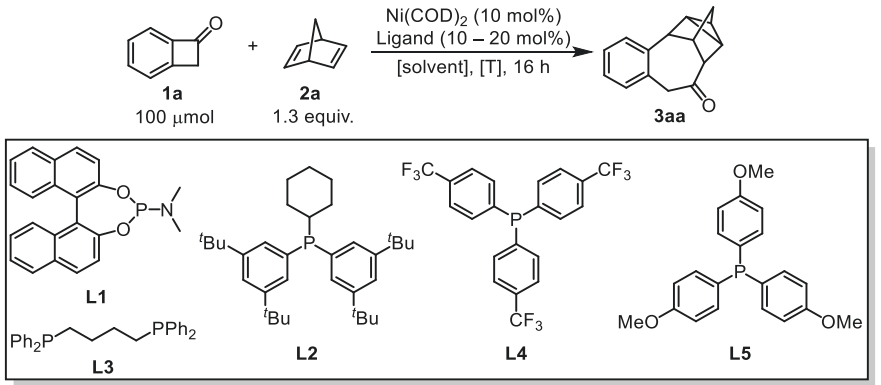

Entry	Ligand	Solvent	T (°C)	Yield (%)[a]	Conversion (%)[a]
1	MonoPhos (**L1**)	toluene	50	30	70
2	MonoPhos (**L1**)	toluene	80	61	100
3	TyrannoPhos (**L2**)	toluene	50	30	81

4	TyrannoPhos (**L2**)	toluene	80	51	100
5	dppb (**L3**)	toluene	50	44	83
6	dppb (**L3**)	toluene	80	55	100
7	P(*p*-$CF_3C_6H_4$)$_3$ (**L4**)	toluene	50	11	56
8	P(*p*-$OMeC_6H_4$)$_3$ (**L5**)	toluene	50	33	100
9	MonoPhos (**L1**)	*n*-octane	80	80	100
10	MonoPhos (**L1**)	dioxane	80	70	100
11	MonoPhos (**L1**)	DMF	80	78	100
12	MonoPhos (**L1**)	DMI	80	85	n.d.
13	MonoPhos (**L1**)	EtOH	80	49	100

Reaction conditions: **1a** (100 µmol, 1.0 equiv.), NBD (1.3 equiv.), $Ni(COD)_2$ (10 mol%), monodentate ligand (20 mol%) / bidentate ligand (10 mol%), solvent (2 mL). [a]Determined by GC-FID using *n*-pentadecane as an internal standard.

Among the top performing ligands, **L1** was selected for further development, as its phosphoramidite framework is highly modular, and available in enantiopure form. This offers a valuable platform for the development of asymmetric catalysis, supported by a literature precedent in which phosphoramidite ligands enabled nickel-catalyzed intramolecular asymmetric insertions of alkenes into cyclobutanones.[7]

A subsequent solvent screening demonstrated that the transformation could proceed in a wide range of solvents, including aliphatic hydrocarbons (*n*-octane), ethers (1,4-dioxane), amides (DMF, 1,3-dimethyl 2-imidazolidinone: DMI), and even polar protic solvents (EtOH) (Table 4.1, entries 9–13). Among these, DMI gave the best results, delivering the highest yields with consistent reproducibility. In contrast, other solvents often showed inconsistent performance, likely due to limited solubility.

Table 4.2. Final optimization of the nickel-catalyzed insertion of NBD into BCB.

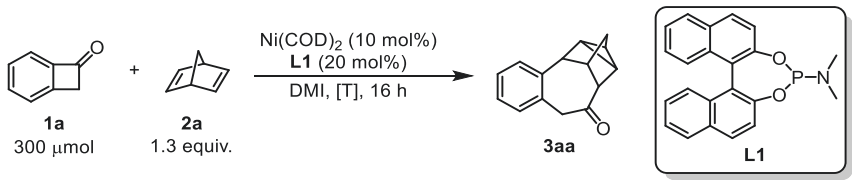

Entry	$Ni(COD)_2$ (mol%)	DMI (mL)	T [°C]	Yield (%)[a]
1[b]	5	6	80	86

2[c]	10	6	50	96
3	10	6	80	91
4	10	6	80	74
5[d]	10	2	80	63

Reaction conditions: **1a** (300 µmol, 1.0 equiv.), NBD (1.3 equiv.), $Ni(COD)_2$ (10 mol%), MonoPhos (20 mol%), DMI (2 – 6 mL), 16 h. [a]Determined by GC-FID using *n*-pentadecane as an internal standard. [b]5 mol% $Ni(COD)_2$, 10 mol% **L1** [c]24 h. [d] 12 mol% **L1**.

In the final phase of optimization, it was found that both the catalyst loading and reaction temperature could be lowered to 5 mol% (86%, Table 4.2, entry 1) and 50 °C (96%, Table 4.2, entry 2) respectively in DMI without substantially altering the yield (91%, Table 4.2, entry 3). Nevertheless, higher catalyst loading and temperature ($Ni(COD)_2$ 10 mol%, 80 °C) were retained for subsequent substrate scope studies, to ensure robustness across a broad range of reactants. It was also observed that increasing the overall reaction concentration (74%, Table 4.2, entry 4) or reducing the ligand loading (63%, Table 4.2, entry 5) led to diminished yields.

Under the optimized conditions, the model reaction afforded **3aa** in an isolated yield of 90%, and the reaction could be successfully scaled up to 10 mmol, giving a slightly reduced yield of 83% (Figure 4.2).

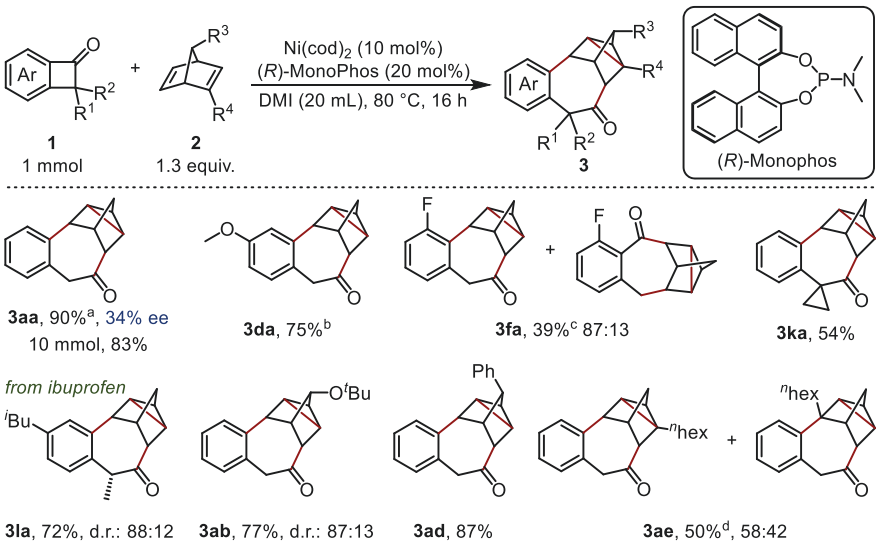

Figure 4.2. Selected examples from the substrate scope of the nickel-catalyzed insertion of NBDs into BCBs. [a]50 °C for 24 h. [b]150 °C. [c]100 °C. [d]PhCN (2 equiv.) as additive. *ee* Values were determined by GC-MS on a chiral stationary phase.

Subsequently, the scope of the reaction was investigated. Elevated reaction temperatures proved crucial for the transformation of both electron-poor and -rich BCBs. Electron-rich **3da** was isolated in 75% yield, whereas an electron-poor BCB proved more challenging, affording **3fa** in only 39% yield as a mixture of C^1–C^2 and C^1–C^8 regioisomers. This was likely due to steric strain introduced by the pseudo-*ortho* substituent. BCBs bearing benzylic substituents, both mono- and disubstituted, were tolerated, providing the corresponding products in fair to good yields (Figure 4.2, **3ka**: 54%; **3la**: 72%). Notably, insertion into a BCB derivative of ibuprofen proceeded in good diastereoselectivity, a trend generally observed for BCBs mono-substituted in benzylic position. This selectivity can be rationalized utilizing mechanistic insights of similar systems gained from experimental and computational data.[6, 8] These propose that the oxidative addition (OA) of nickel(0) into BCB requires two ligands forming a distorted tetrahedral complex. The ligand *syn*- to the benzylic substituent is sterically more hindered and dissociates, creating a vacant site on the same side of the benzylic substituent for NBD coordination. This leads to preferential formation of the *syn*- diastereomer relatively to the nortricyclane scaffold.

Substitution on the NBD core also provided valuable insights. When NBDs substituted in 7-position were employed, the reactions proceeded in good to excellent yields and displayed distinct diastereoselectivities (Figure 4.2, **3ab**: 77%; **3ad**: 87%). A bulky substituent favored formation of the *syn*-product relatively to the ketone, while an aromatic substituent led to the *anti*-isomer. This can be explained with the insertion step following OA. The sterically demanding substituent tends to orient away from the ligand sphere, while the aromatic substituent may engage in favorable π-interactions with the nickel catalyst. Consequently, insertion is proposed to occur at the Ni–C^2 bond, as insertion at Ni–C^1 would result in the opposite diastereoselectivity.

For 2-hexyl substituted NBD (**2e**), the reaction afforded two constitutional isomers in 50% yield, differing in connectivity across a pseudo C_2-axis of the nortricyclane framework (Figure 4.2). This selectivity can be tentatively explained by preferential coordination of the unsubstituted double bond of **2e** to the nickel center, with the *n*-hexyl substituent oriented away from the sterically more demanding benzylic group of the BCB. Subsequent clockwise or counterclockwise rotation of **2e**, enables insertion, and yields the observed isomers.

Although the enantiopure (*R*)-MonoPhos ligand was employed throughout the substrate scope, the enantiomeric excess was only determined for a few products. The measured *ee* of **3aa** was only moderate 34% (Figure 4.2). Selectivity could be enhanced by utilizing a sterically

more demanding phosphoramidite ligand, accompanied by changing the solvent to *n*-hexane reaching good 71% *ee* (Scheme 4.1) considering the relatively high temperature (70 °C). However, this improvement came at the cost of yield (42%). Despite this trade off, the result highlights the feasibility of developing an enantioselective variant of this catalytic transformation.

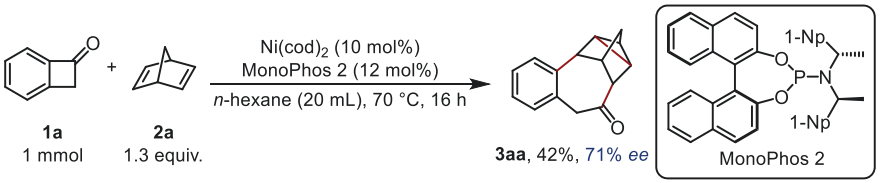

Scheme 4.1. Nickel-catalyzed insertion of **2a** into **1a** using a modified catalytic system to enhance the enantiomeric excess of **3aa**. *ee* Value was determined by GC-MS on a chiral stationary phase.

To gain a deeper insight into the effect of pseudo-*ortho* substituent on regioselectivity, two BCBs bearing such substituents, a methyl (**1m**) and a methoxy group (**1n**), were examined. While the previously optimized conditions could be applied to **1m** (Scheme 4.2a), **1n** required re-optimization, revealing PCy_3 as the optimal ligand and toluene as the solvent (Scheme 4.2b). As anticipated, both substrates predominantly afforded the C^1–C^8 bond insertion products in good yields (Scheme 4.2, **3ma**: 74%; **3na**: 66%). Interestingly, while the main side product from **3ma** resulted from C^1–C^2 activation, the side product observed in the case of **3na** was unexpectedly the formal [2+2] cycloaddition product.

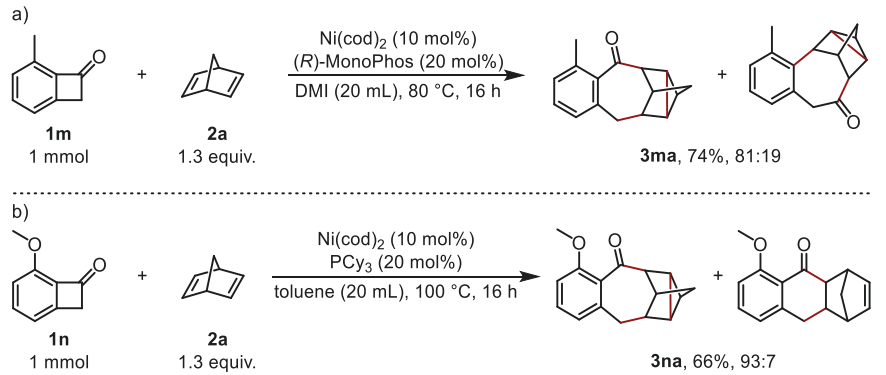

Scheme 4.2. Nickel-catalyzed insertion of NBD into pseudo-*ortho* substituted BCBs.

Following the investigation of the reaction scope, the synthetic utility of the product scaffold was explored using **3aa** as a representative example (Figure 4.3). As expected, the ketone functionality exhibited classical reactivity, with nucleophilic additions occurring diastereoselectively from the same face as the three-membered ring of the nortricyclane motif (Figure 4.3a).

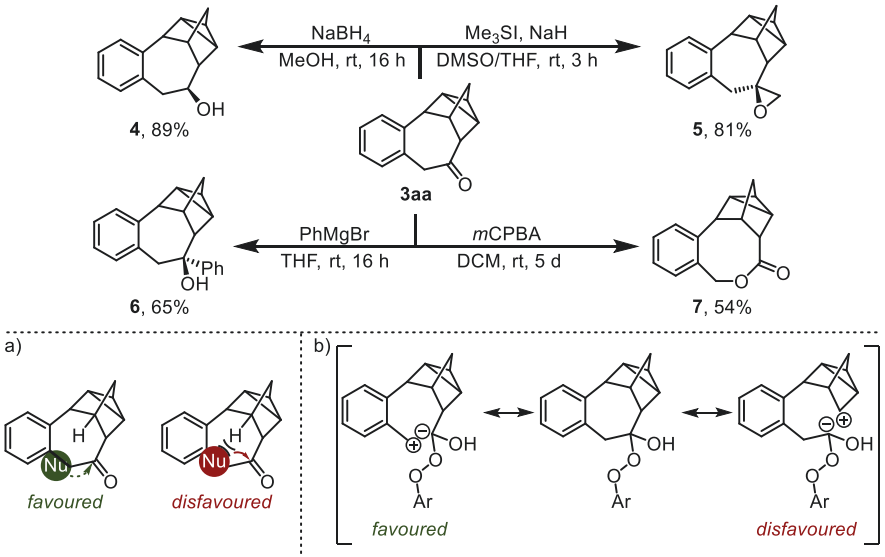

Figure 4.3. Functionalization of **3aa** and proposed models explaining the observed selectivities for the respective derivatization. [a]Nucleophilic attack. [b]Bayer-Villinger oxidation.

For instance, reduction with $NaBH_4$ afforded the corresponding alcohol (**4**, Figure 4.3) in 89% yield selectively, while the Johnson-Corey-Chaykovsky reaction with trimethylsulfonium iodide gave the epoxide derivative in 81% yield (**5**, Figure 4.3). Additionally, 1,2-addition of PhMgBr led to the respective secondary alcohol (**6**, Figure 4.3). Notably, Bayer-Villinger oxidation with *m*CPBA resulted in formal oxygen insertion at the benzylic position (**7**, Figure 4.3), likely due to the greater stabilization of the developing positive charge in the Criegee intermediate at this site (Figure 4.3b), providing the lactone in 54% yield.[9]

Finally, initial mechanistic insights were obtained through *in situ* ^{31}P NMR spectroscopy. Preligating $Ni(COD)_2$ with MonoPhos (2 equiv.) in DMI led to the formation of two distinct phosphorus containing species (Figure 4.4a), likely corresponding to $Ni(COD)_x(MonoPhos)_m$ and $Ni(MonoPhos)_n$ (with $n > m$), potentially involving ancillary DMI as a ligand. Upon

addition of NBD, COD displacement was observed, and Ni(MonoPhos)$_n$ was consumed, forming Ni(NBD)$_x$(MonoPhos)$_m$, which was identified as the resting state of the catalytic cycle (Figure 4.4b). Upon addition of BCB, NBD was gradually consumed, leading to the reappearance of Ni(MonoPhos)$_n$, accompanied by the emergence of a new signal. This was assigned to a nickel carbonyl complex, presumably formed *via* decarbonylation of the OA complex (Figure 4.4c). The formation of this species suggests a possible catalyst deactivation pathway, as the nickel carbonyl is likely catalytically inactive and may contribute to catalyst poisoning.

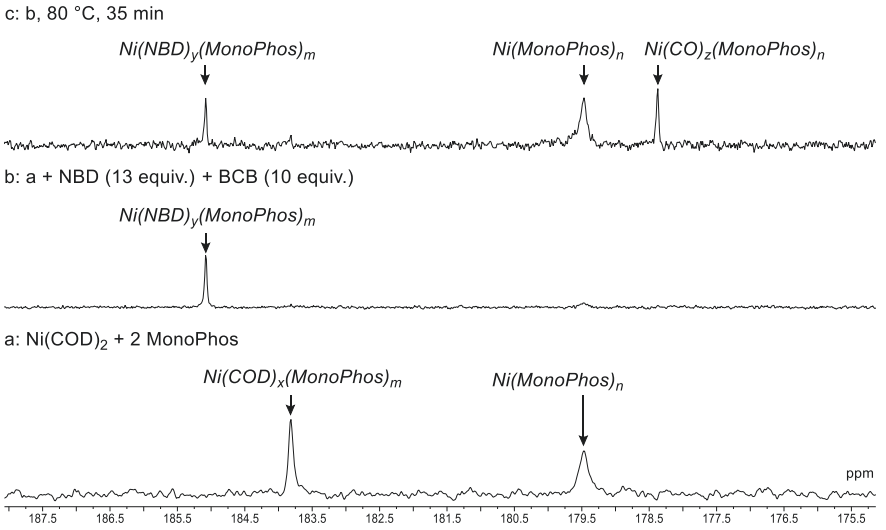

Figure 4.4. Mechanistic *in situ* ^{31}P NMR study of the nickel-catalyzed insertion of NBD into BCB in DMI. ^{31}P NMR spectra were measured without locking or shimming.

4.2 Unpublished Results

4.2.1 Alternative 1,4-Dienes

Building on the successful nickel-catalyzed insertion of NBD into BCBs, the aim was to extend the scope of the reaction utilizing alternative 1,4-dienes. However, deviations from the NBD framework were not tolerated under the optimized conditions. Attempts to elongate the NBD bridge by one carbon using bicyclo[2.2.2]octa-2,5-diene, or to replace a bridgehead carbon with oxygen, as in 7-oxa-NBD, failed to yield any product. Likewise, simplification of the bicyclic system, such as employing 1,4-cyclohexadiene, resulted in no reaction. A NBD derivative bearing an electron-withdrawing substituent in the 2-position, obtained *via* Diels-Alder reaction of cyclopentadiene and ethyl propiolate, also proved unreactive (Figure 4.5).

Further variations of the diene core, including structurally related frameworks such as barbaralone, also proved unreactive (Figure 4.5). These results highlight the sensitivity of the transformation to the precise geometry and electronic properties of the diene component, emphasizing the unique reactivity of NBD in this catalytic system.

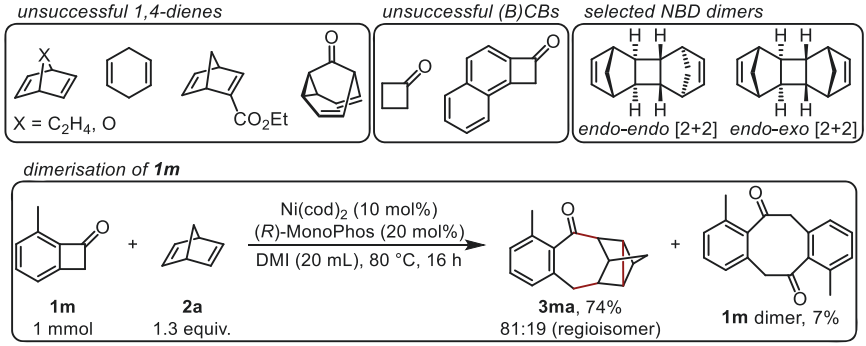

Figure 4.5. Unsuccessful substrates screened for the nickel-catalyzed NBD insertion into BCBs alongside commonly observed side products. Depicted are the two NBD dimers most commonly formed from NBD in presence of $Ni(COD)_2$.[10]

When unsuitable 1,4-dienes were employed, substantial consumption of BCB was observed despite the absence of desired product formation. However, most resulting side products remained unidentified. In one instance, a side product was identified by GC-MS, isolated, and characterized as the dimer of **1m** (Figure 4.5). Additionally, molecular weights corresponding

to dimeric species of other BCBs were observed by GC-MS throughout the substrate scope of the nickel-catalyzed NBD insertion into BCB.

Similarly, when challenging or incompatible substrates regarding the C–C activation were employed, the predominant byproducts were dimers of NBD (Figure 4.5).[10] Notable examples of ineffective C–C activation partners include cyclobutanone and cyclobuta[*a*]naphthalen-2(1*H*)-one. The low reactivity of cyclobutanone is likely attributable to its reduced ring strain relative to BCB, owing to the absence of the annulated aromatic system. In contrast, the lack of reactivity with cyclobuta[*a*]naphthalen-2(1*H*)-one is presumably a result of steric hindrance in the expected NBD insertion product, imposed by the hydrogen atom at the 8-position (Figure 4.5).

The scope in respect to BCBs was further constrained by the challenging syntheses of particularly electron deficient BCBs, which proved difficult to access and decomposed under ambient conditions (Scheme 4.3). In general, BCBs bearing electron withdrawing groups are scarcely reported in the literature. Available synthetic strategies, such as palladium-catalyzed intramolecular acylation of aryl bromides *via* C–H activation,[11] or the photochemical cyclization of *o*-toluoylchlorides using a phosphonate auxiliary,[12] are limited by low scalability, the requirement for complex reagents, or restricted to disubstituted benzylic precursors. Consequently, further research is required to develop more robust and versatile methods for the synthesis of electron poor BCBs.

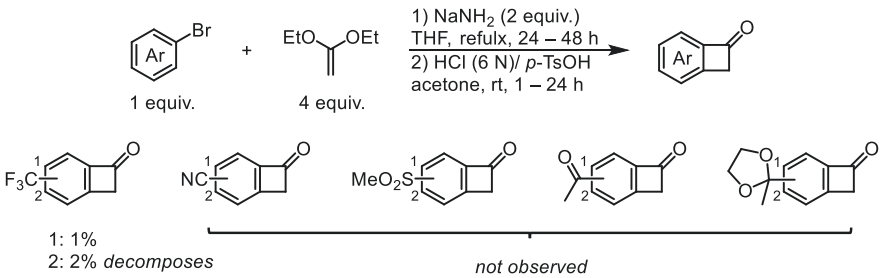

Scheme 4.3. Unsuccessful syntheses of BCBs *via* [2+2] cycloaddition of arynes with ketene acetals.

4.2.2 Screening of Insertion Partners

1,3-Dienes:

The nickel-catalyzed insertion of 1,3-dienes into BCBs to form eight-membered rings is a known transformation in literature.[4] As a side reaction the insertion of only one double bond from the 1,3-diene has occasionally been observed during ligand optimization. However, in cases where a relatively high ratio of the [4+2] to [4+4] product was observed, the overall yield remained low. A separate literature precedent describes the intramolecular insertion of an alkene into cyclobutanone using a phosphoramidite-type ligand.[7]

To explore the possibility of favoring mono alkene insertion, reaction conditions inspired by the second study were applied to the reactants from the first study (Scheme 4.4). Although the desired alkene insertion product was not observed, minor amounts of the [4+4] 1,3-diene insertion product were detected. Despite the low yield, this outcome may be interesting for future studies, as phosphoramidite ligands could provide a pathway toward asymmetric catalysis under further optimized conditions.

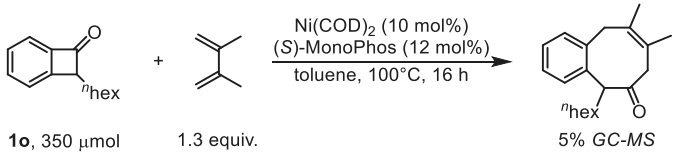

Scheme 4.4. Nickel-catalyzed insertion of 2,3-dimethyl 1,3-butadiene into **1o** utilising (*S*)-MonoPhos as a chiral ligand.

Alkenes:

During investigations on the nickel-catalyzed insertion of NBD into pseudo-*ortho* OMe-substituted BCB (**1n**), the insertion of a single NBD double bond was observed as a side product. This prompted the evaluation of norbornene as a similar reaction partner for the intermolecular insertion into BCB under nickel-catalysis.

Optimization began with a ligand screening involving seven phosphine-based mono- and bidentate ligands (Scheme 4.5). Unfortunately, none of the tested ligands led to formation of the desired insertion product. Instead, unreacted **1o** and a decarbonylated byproduct, probably corresponding to a styrene derivative, were detected by GC-MS. To probe this further, the reaction with PPh_3 was repeated at 150 °C, which resulted in increased formation of the

decarbonylated species, while not forming the desired insertion product. Subsequently, $Ni(PPh_3)_2(CO)_2$ was employed as the catalyst at both 100 °C and 150 °C in toluene in an effort to suppress decarbonylation. However, at 100 °C, only decarbonylated **1o** was observed, while the reaction at 150 °C afforded only trace amounts of the desired insertion product.

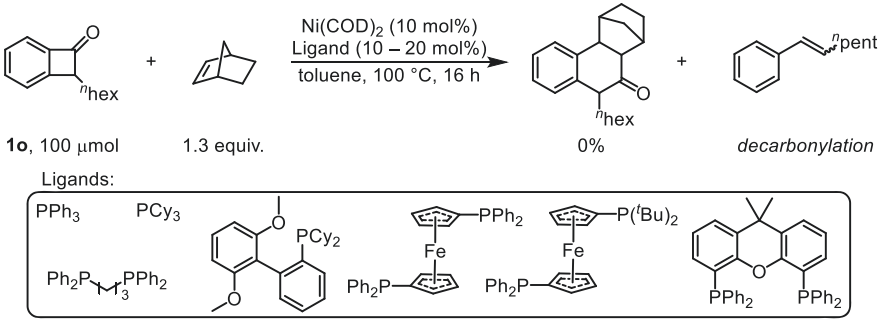

Scheme 4.5. Ligand screening for the nickel-catalyzed insertion of norbornene into **1o**. Monodentate ligands (20 mol%), bidentate ligands (10 mol%).

As varying the ligand was unsuccessful, a solvent screening was conducted using PPh_3 as the ligand. The most notable result was obtained with the polar protic EtOH, which furnished a product, likely corresponding to the decarbonylated insertion product of norbornene and **1o** in minor amounts (entry 1, Table 4.3). All other solvents, except $CHCl_3$, primarily resulted in observation of **1o** and its decarbonylated byproduct (entries 2–5, Table 4.3). In the case of $CHCl_3$, no conversion of **1o** was observed (entry 6, Table 4.3). These results suggest that solvent polarity and protic nature may modestly influence the reaction pathway, though no clear trend emerged.

Table 4.3. Solvent screening for the nickel-catalyzed insertion of norbornene in **1o**.

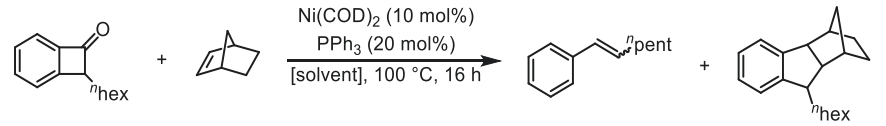

Entry	solvent	conversion[a]	4[a]	5[a]
1	EtOH	fair	fair	minor
2	MeCN	minor	minor	/

3	THF	fair	fair	trace
4	DMA	minor	minor	/
5	DMF	minor	minor	/
6	$CHCl_3$	/	/	/

[a] estimated by GC-MS.

Finally, two attempts were conducted to assess, whether the insertion of NBD into **1a** could be achieved with alternative activation methods. However, neither UV irradiation (Scheme 4.6a) nor mechanochemical activation using a mixer mill (Scheme 4.6b) in presence of the $Ni(COD)_2/PCy_3$ system led to product formation.

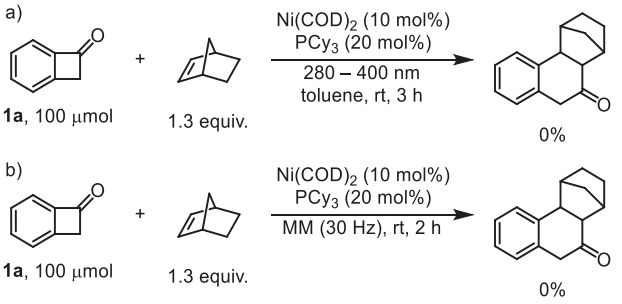

Scheme 4.6. Attempted insertion of norbornene into **1a** using nickel-catalysis under [a]UV irradiation or [b]mechanochemical conditions.

Given the limited success with norbornene, styrene was next evaluated as an alternative alkene for the nickel-catalyzed insertion into BCB (Scheme 4.7a). A similar transformation has previously been reported under rhodium-catalysis, where styrene participates formally as a carbenoid in a (4+1) cycloaddition.[13] In addition, a vinyl cyclopropane was selected as another interesting insertion partner, as successful insertion could be accompanied by the ring-opening of the strained three-membered ring, furnishing a structurally intriguing product (Scheme 4.7b).

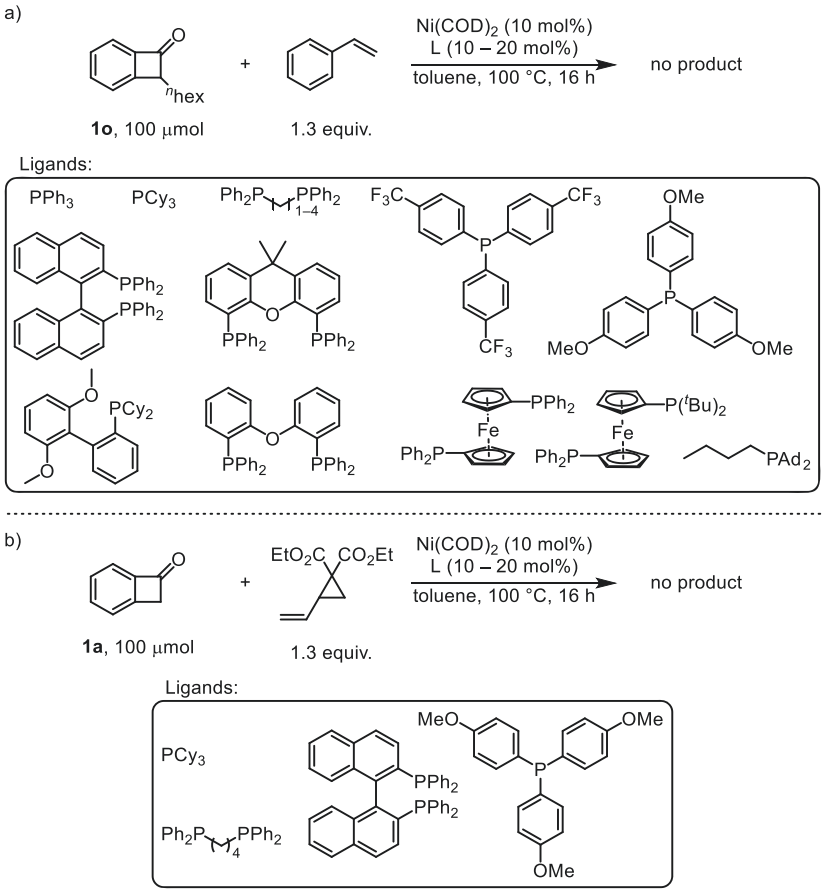

Scheme 4.7. Ligand screening for the nickel-catalyzed insertion of [a]styrene into **1o** and [b]diethyl 2-vinylcyclopropane 1,1-dicarboxylate into **1a**.

To this end, a ligand screening was performed, evaluating 15 ligands for the insertion of styrene in **1o** (Scheme 4.7a) and four ligands for the insertion of a vinyl cyclopropane into **1a** (Scheme 4.7a). In the case of styrene, only decarbonylation of **1o** and unreacted starting material were observed, mirroring the behaviour previously seen with norbornene. Similarly, no desired insertion product was detected in any of the reactions involving the vinyl cyclopropane.

High Throughput Screening

Based on previous results and literature precedents,[4, 6, 14] common features of both successful and unsuccessful insertion partners were assessed. While alkenes were found to be unreactive in the nickel-catalyzed insertion into BCBs, 1,3-dienes proved productive in such transformations.[4] A comparison of the frontier molecular orbitals (FMOs) between alkenes and 1,3-dienes shows an inverse parity. Meanwhile, the FMO symmetries of NBD align with those of 1,3-dienes, providing a rationale for their reactivity under nickel-catalysis (Figure 4.6).

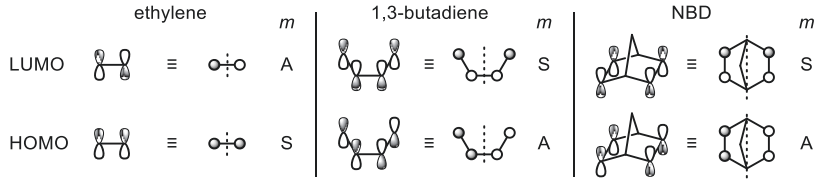

Figure 4.6. Comparison of the FMOs of ethylene, 1,3-butadiene and NBD, depicted from the front and top including the mirror plane *m* and the symmetry of each orbital towards this element (S = symmetric, A = antisymmetric).

This observation led to the hypothesis that alkene insertion is symmetry-forbidden due to FMO mismatch with the OA complex of the BCB nickel system. This raises the question of why alkyne insertion, which was also reported in the literature is feasible.[4, 6] A computational study investigating this transformation suggests that, the HOMO of the nickel OA complex interacts with the LUMO of the alkyne (PhCCPh), which possesses orthogonal π-systems that confer partial symmetry characteristics akin to those of a 1,3-diene.[8]

Although existing studies do not provide a fully conclusive mechanistic picture, they inspired the design of a high throughput screening (HTS) experiment. Specifically, insertion partners exhibiting orbital symmetry features similar to those of 1,3-dienes and alkynes were selected for evaluation (Figure 4.7).

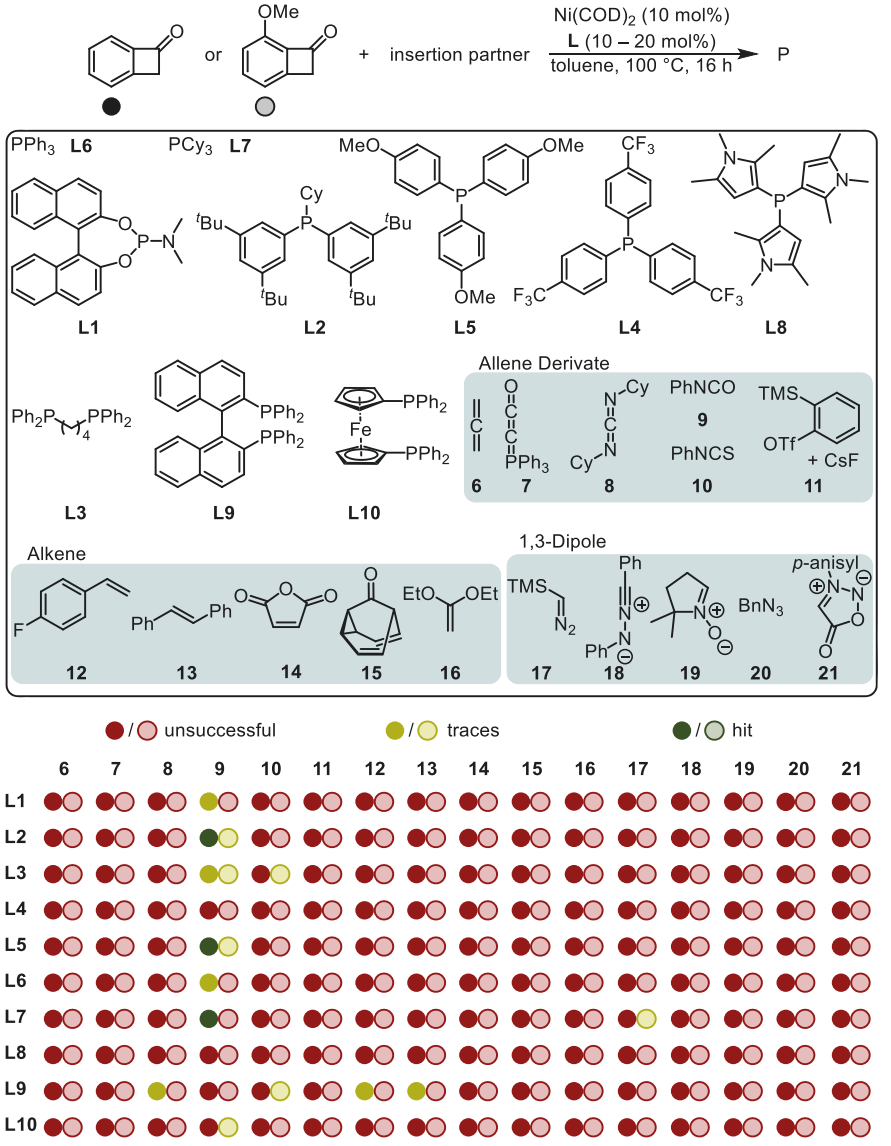

Figure 4.7. High throughput ligand screening for the nickel-catalyzed activation of **1a** or **1n** in presence of insertion partners. Reactions were evaluated by GC-MS and qualitatively categorized into unsuccessful and successful reactions, which were parted into detection of traces and hits corresponding to yields > 5%.

A total of 10 ligands, identified from literature as promising candidates,[4, 6, 14] were paired with 16 insertion partners for this study. These reactants were evaluated for the insertion into two different BCB substrates, **1a** and **1n**, chosen for their distinct regioselectivity in respect to nickel-catalyzed activation. In particular, OA occurs at the C^1–C^2 bond of **1a**, and at the C^1–C^8 bond of **1n**, resulting in differing electronic environments for the intermediate nickel complexes. This distinction had previously been shown to influence the regioselectivity of the NBD insertion into BCB.[14]

The investigated insertion partners could be sorted into three categories: (i) Allene-type reactants, selected for their unique orbital geometry partially mimicking that of alkynes.[15] (ii) Activated or strongly coordinating alkenes, included to revise their challenging insertion. (iii) 1,3-Dipoles, which exhibit orbital symmetry resembling 1,3-dienes. (iv) Miscellaneous reaction conditions, were selected to align with those reported in successful literature protocols.[4, 6]

Among the screened tranformations, only the reaction of **1a** with phenyl isocyanate (**9**) yielded a notable amount of product, as determined by GC-MS. Hereby, **L2**, **L5** and **L7** delivered the most promising results, prompting successful isolation of the corresponding isoquinolinedione in 27% yield (Scheme 4.8).

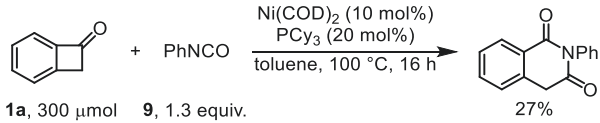

Scheme 4.8. Isolation of the *N*-phenyl isoquinolinedione, resulting from the nickel-catalyzed insertion of **9** into **1a**.

Intriguingly, the insertion of **9** into **1n**, *via* nickel-catalysis proved substantially less effective. Only trace amounts of product were observed in the presence of ligands **L2**, **L3**, **L5** and **L10**, and these were insufficient for isolation. This discrepancy highlights the distinct reactivity profiles of the nickel OA complexes formed with **1a** and **1n**. In contrast, when the higher homologue phenyl isothiocyanate (**10**) was employed, only trace amounts of product were detected *via* GC-MS with **L3** and **L9** in reactions with **1n**. No product formation was observed with **1a**. Similarly, **L9** gave trace product formation only with **1n** for the carbodiimide (**8**), concluding all found product structures *via* GC-MS within the allene-type derivates.

Attempts to insert an aryne, generated *in situ* from a Kobayashi precursor, an approach previously reported under palladium-catalysis,[16] were unsuccessful under the investigated conditions.

Within the alkene and 1,3-dipole categories, only a sparce number of reactions led to trace product formation. Ligand **L9** enabled trace insertion of both 4-fluorostyrene (**12**) and *trans*-stilbene (**13**) into **1a**. However, no desired products were observed from the electron deficient maleic anhydride (**14**) or the electron rich ketene diethylacetal (**16**). Additionally, barbaralone (**15**), a representative of 1,4-dienes known to form coordination complexes with nickel,[17] failed to undergo insertion.

Among the 1,3-dipoles, only trimethylsilyl diazomethane (**17**) afforded trace product formation in the presence of **L7** and **1n**. Reactions involving nitril imide (**18**), nitrone (**19**), azide (**20**), and sydnone (**21**) showed no formation of the desired insertion products.

In most cases, GC-MS data indicated nearly complete conversion of the BCB substrates, while the insertion partners remained often largely unreacted. This suggests that OA of nickel in **1a** or **1n** occurred efficiently. However, the subsequent insertion step failed, likely leading to decarbonylation and formation of unidentified side products.

As isoquinolinediones, such as those formed by the insertion of isocyanates into BCBs (Scheme 4.8), can be easily accessed *via* condensation of an amine with readily available homophthalic acid,[18] further development of this catalytic system was deemed less valuable. Consequently, the focus shifted to the insertion of disubstituted ketenes, which exhibit similar orbital symmetry to isocyanates and hold potential for generating a distinct and synthetically valuable product class.

Therefore, the same reaction conditions previously utilized for the insertion of **9** into **1a** were applied to the reaction of diphenyl ketene with **1a**. Gratifyingly, the expected dihydro naphthalenedione product was detected in minor amounts by GC-MS analysis (Scheme 4.9).

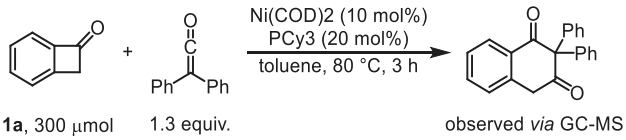

Scheme 4.9. Nickel-catalyzed insertion of diphenyl ketene into **1a** furnishing a naphtalenedione.

However, given the limited availability of ketenes and the low yield observed in the initial experiment, further optimization of this catalytic transformation was not pursued.

4.2.3 Alternative Synthesis of *o*-Iodo Weinreb Amides

o-Iodo benzylic Weinreb amides serve as valuable precursors for the synthesis of BCBs, offering a synthetic link between benzylic acids, a broadly available compound class that includes pharmaceuticals such as ibuprofen and naproxen, and their corresponding BCB derivatives. Generally, these benzylic acids can be iodinated at the *ortho* position *via* palladium-catalyzed C–H activation,[19] followed by conversion to the Weinreb amide (Scheme 4.10a).[20] However, this approach was met with substantial challenges for certain substrates, often requiring prolonged reaction times and high loadings of the expensive palladium-catalyst. To address these limitations, an alternative literature-reported sequence was evaluated.[21] In this approach, phenylacetic acids are first converted to their respective Weinreb amides, followed by ortho iodination *via* palladium-catalyzed C–H activation *via* an isodesmic reaction (Scheme 4.10b). Notably, this method allows the incorporation of a chiral ligand, opening the door to the synthesis of chiral *o*-iodo benzylic Weinreb amides.

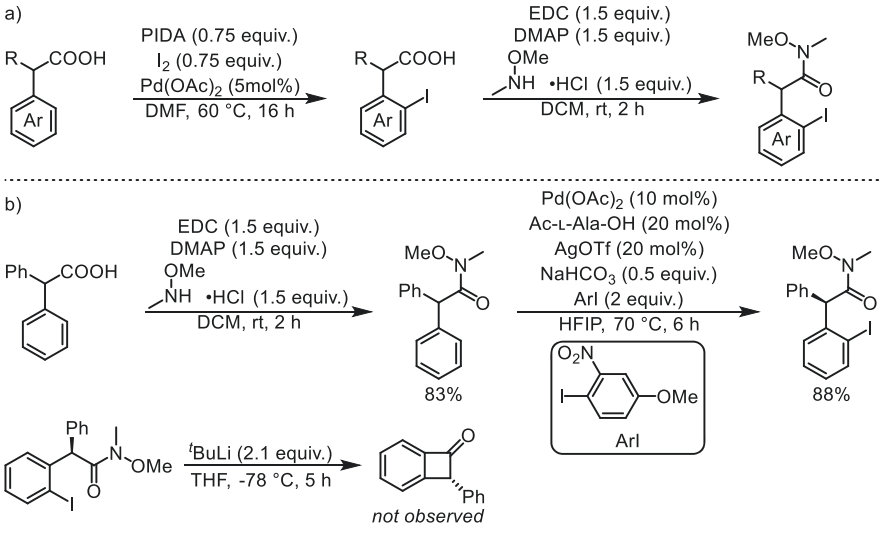

Scheme 4.10. Synthesis of *o*-iodo benzylic Weinreb amides *via* [a]palladium-catalyzed C–H activation,[19] followed by Weinreb amide formation,[20] or [b]initial Weinreb amide formation followed by asymmetric palladium-catalyzed *ortho* iodination.[21]

Although both the formation of the Weinreb amide and the subsequent *ortho* iodination proceeded in good yields, the final conversion to the corresponding BCB failed to yield product (Scheme 4.10b). This lack of reactivity is most likely due to the increased acidity of the benzylic proton, resulting from the presence of a second phenyl substituent. This favours the thermodynamic deprotonation, which most likely outcompetes the kinetic halogen metal exchange. Given that the literature reports only moderate yields when the aromatic substituent is changed, this synthetic route to chiral benzylic substituted BCBs appears to be of limited applicability.

4.2.4 Experimental Details

Chemicals and General Techniques

Reactions requiring inert conditions were conducted under an argon atmosphere using either standard Schlenk technique or a glovebox (GS MEGA E-Line, Glovebox Systemtechnik, <5 ppm O_2, <0.1 ppm H_2O) with pre-dried glassware. Solvents (except DMI) were dried by a commercial solvent purification system (MB SPS-5). DMI was dried over activated neutral Al_2O_3. For nickel-catalyzed reactions, further degassed by sparging with argon and stored over activated 3 Å MS (abcr, flame dried *in vacuo*). Chromatography solvents were either HPLC grade or freshly distilled before use. Column chromatography was carried out on silica (35 – 70 µm, 60A, Thermo Fischer), and flash chromatography was performed on an Interchim Puriflash XS420 system with FlashPure EcoFlex Silica 25 g columns (50 µm, irregular, Büchi). Eluent gradients are reported as binary solvent mixtures X:Y (Y is the more polar solvent) with X + Y = 100. All reagents were purchased from abcr, BLDpharm, fluorochem, Sigma-Aldrich, Thermo Fischer, Acros or TCI and were used without further purification. Low temperatures reactions were carried out using a Julabo FT902 Cryostat or a liquid nitrogen acetone cooling bath. Irradiation was carried out employing a 500 W high pressure mercury lamp in an Oriel housing with quartz optics and a dichromic mirror (280 nm – 400 nm). Mechanochemical reactions were carried out in the Mixer Mill MM 400 (Retsch) in a stainless steel jar (10 mL) with two stainless steel balls (⌀ = 10 mm, m = 4 g).

Analytical Techniques

NMR spectra were recorded on Bruker Avance III HDX 600 or Bruker Avance 400 spectrometers. All ^{13}C NMR spectra were measured with broadband proton decoupled (not explicitly denoted). Chemical shifts are reported in parts per million (ppm) relative to tetramethyl silane using solvent peaks as internal standards (chloroform-d: ^{1}H δ = 7.26 and ^{13}C δ = 77.16, benzene-d_6 ^{1}H δ = 7.16 and ^{13}C δ = 128.06)[22] Coupling constants (*J*) are given in Hertz, and splitting patterns are designated as follows: s = singlet, d = doublet, dm = doublet of multiplet, t = triplet, m = multiplet.

GC-LR-MS (EI) analysis was carried out with an Agilent 7820A/5977B GC-system/MSD employing an Agilent 190915-433UI column (30 m × 250 µm × 0.25 µm). Program: 50 °C – 280 °C over 15 minutes.

GC-FID analysis was performed on an Agilent 7820A system with an Agilent 19091J-431 column (30 m × 320 µm × 0.25 µm), utilizing H_2 as the carrier gas. The program used heated from 50 °C to 280 °C within 15 min.

Thin layer chromatography (TLC) was performed on aluminum plates coated with 0.20 mm silica gel 60 with fluorescence indicator UV_{254} from Macherey-Nagel and compounds were either detected under UV light (254 nm) or using an anisaldehyde stain (4 mL anisaldehyde, 3 mL glacial acetic acid, 10 mL H_2SO_4 (96%), 200 mL EtOH).

Reaction Screening for the Nickel Catalyzed NBD Insertion into BCB

In a glovebox, $Ni(COD)_2$ (10 mol%) and the respective ligand (monodentate: 20 mol%, bidentate: 10 mol%, *unless denoted otherwise*) were added to a dried Schlenk tube. The respective solvent (0.05 M) was added and the reaction was stirred for 5 min at rt. Subsequently, first the respective insertion partner (1.3 equiv.) and then the respective BCB (1.0 equiv.) were added, after which the reaction was transferred to a preheated (100 °C, *unless denoted otherwise*) metal block and stirred for 16 h (*unless denoted otherwise*). *n*-pentadecane (30 µL) was added, the reaction was diluted with EA (2 mL) and quenched with $HCl_{(aq.)}$ (1 M, 2 mL). The organic phase was separated and filtered through Celite, Al_2O_3 and $MgSO_4$, before being analyzed by GC-MS/FID.

Irradiation: For photochemical reactions, a quartz Schlenk tube was utilized, which was irradiated at rt.

Mechanochemical: In a glovebox all reactants were added into the ball mill jar alongside two steel balls. The reaction was milled for 2 h (30 Hz).

High Throughput Screening

In a glovebox, an equal volume of a $Ni(COD)_2$ (25 mM in toluene) solution was added to a solution/suspension of the respective ligand (monodentate: 50 mM, bidentate: 25 mM in toluene) and stirred for 10 min. PhCN (100 µL, 1.3 equiv., 0.33 M in toluene), **1a** (100 µL, 1.0 equiv., 0.25 M in toluene) and the respective insertion partner (100 µL, 1.3 equiv., 0.33 M in toluene) were added to GC-vials, equipped with stirring bars and arranged analogous to a well plate, utilizing a multichannel Eppendorf pipette. Subsequently, the respective $Ni(COD)_2$ ligand mixture (200 µL, 10 mol%) was added to each corresponding vial, after which they were stirred at 100 °C for 16 h. Upon cooled, *n*-pentadecane (10 µL) was added to each reaction, which were filtered through Celite, Al_2O_3 and $MgSO_4$, before being analyzed by GC-MS/FID.

General procedure A (GP-A): Synthesis of phenylsulfonyl acetylenes:

Phenylsulfonyl acetylenes were synthesized according to literature.[23] In a Schlenk RBF, benzenesulfonyl chloride (1.2 equiv.) was added to $AlCl_3$ (1.2 equiv.) in DCM (50 mL). The solution was stirred for 30 min at rt, after which it was slowly transferred by cannula (30 min) to an ice-cooled solution of 1,2-bis(trimethylsilyl)ethyne (58 mmol, 1.0 equiv.) in DCM (50 mL). This mixture was stirred at rt for 24 h and then added to an ice (50 g)/HCl (50 mL,

1 M) mixture. The organic layer was separated, washed with water (2 × 50 mL) and dried over Na_2SO_4. The solvent was removed *in vacuo* and the unreacted benzenesulfonyl chloride was removed under 130 °C *via* distillation furnishing a brown oil residue.

2-(2-Iodophenyl)octanoic acid

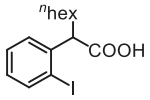

2-(2-Iodophenyl)octanoic acid was synthesized according to literature.[20] A THF (12 mL) solution of 2-(2-iodophenyl)acetic acid (3.1 g, 12 mmol, 1.0 equiv.) was added dropwise into freshly prepared LDA (26 mmol, 2.2 equiv., in 36 mL THF) at 0 °C. The mixture was stirred for 1 h at 0 °C before 1-iodohexane (8.8 mL, 60 mmol, 5.0 equiv.) was slowly added. The reaction was allowed to warm to rt and was stirred for 2 h. Subsequently, the reaction was quenched with 0.5 M $NH_4OAc_{(aq.)}$ (15 mL). Afterwards, 6 M $HCl_{(aq.)}$ (7.5 mL) was added and the aqueous phase was extracted wit EA (3 × 30 mL). The combined organic phases were washed with sat. $Na_2S_2O_{3(aq.)}$ (45 mL), brine (45 mL) and dried over $NaSO_4$. The solvent was removed *in vacuo* and the product was purified *via* column chromatography (4:3 = *n*-hexane/EA). The product was obtained as a yellow oil (3.90 g, 11.2 mmol, 94%).

$C_{14}H_{19}IO_2$ (346.21 $\frac{g}{mol}$)

R_f = (0.44 *n*hex/EA:4/1) [UV]

^{1}H-NMR(400 MHz, $CDCl_3$): δ = 11.57 (s, 1H, H-1), 7.87 (dd, ^3J = 8.0 Hz, ^4J = 1.1 Hz, 1H), 7.36 (m, 1H), 7.33 (m, 1H), 6.95 (m, 1H), 4.10 (t, ^3J = 7.5 Hz, 1H, H-2), 2.03 (m, 1H, H-3a), 1.77 (m, 1H, H-3b), 1.30 (m, 8H, H-4–7), 0.87 (t, 3H, ^3J = 6.7 Hz, H-8).

^{13}C-NMR(101 MHz, $CDCl_3$): δ = 179.9 (C-1), 141.7, 139.9, 129.1, 128.8, 128.1, 102.1, 55.0 (C-2), 33.4 (C-3), 31.7, 29.2, 27.3, 22.7, 14.2 (s, C-8).

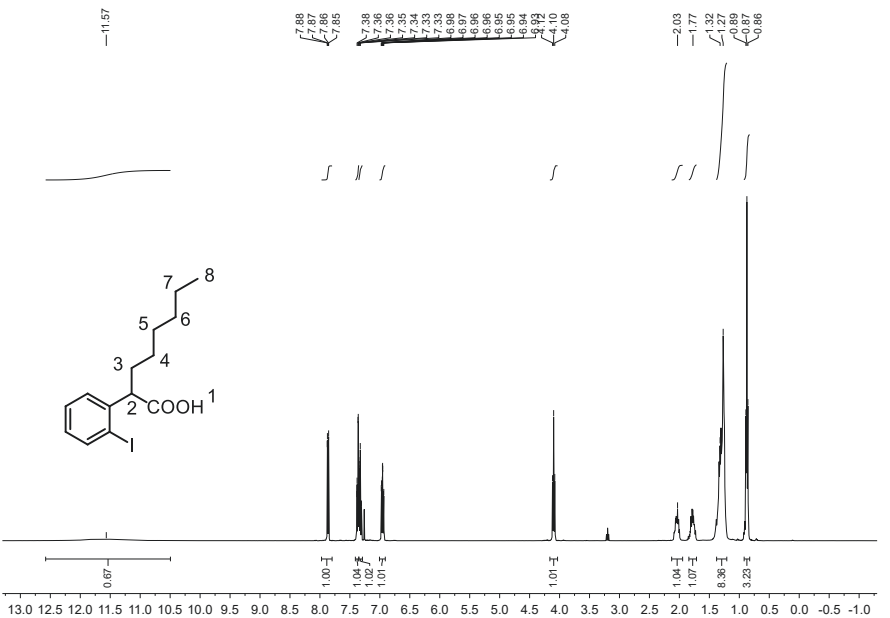

Figure 4.8. ^{1}H NMR spectrum of 2-(2-iodophenyl)octanoic acid in $CDCl_3$, measured at 400.16 MHz.

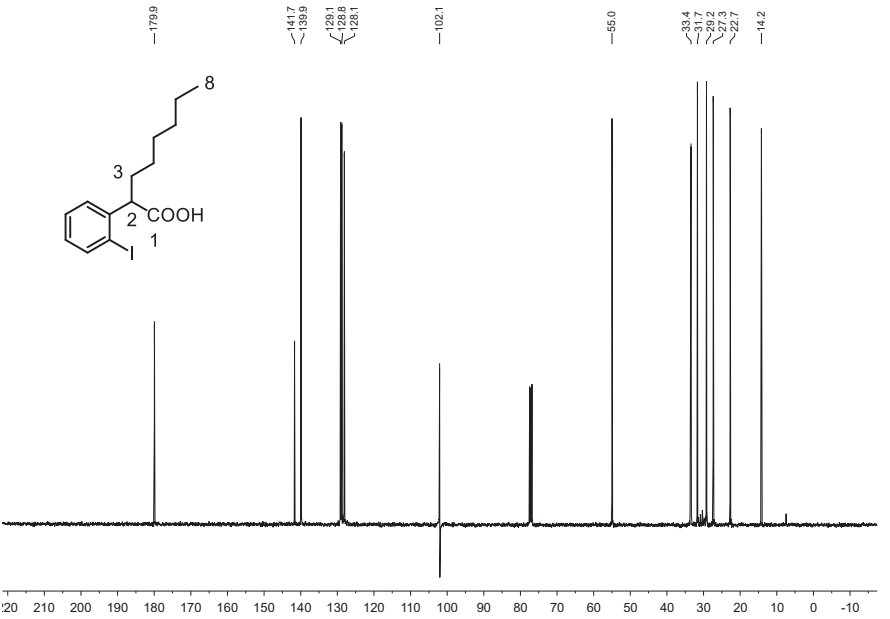

Figure 4.9: ^{13}C NMR spectrum of 2-(2-iodophenyl)octanoic acid in $CDCl_3$, measured at 100.63 MHz.

2-(2-Iodophenyl)-*N*-methoxy-*N*-methyloctanamide

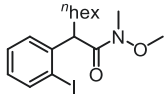

2-(2-Iodophenyl)-*N*-methoxy-*N*-methyloctanamide was synthesized according to literature.[24] 2-(2-iodophenyl)octanoic (3.5 g, 10 mmol, 1.0 equiv.) and *N*,*O*-dimethylhydroxylamine hydrochloride (1.5 g, 15 mmol, 1.5 equiv.) were dissolved in DCM (25 mL) in a RBF. Subsequently, DMAP (1.85 g, 15 mmol, 1.5 equiv.) and EDC (2.34 g, 15 mmol, 1.5 equiv.) were added and the reaction was stirred for 3 h at rt. Afterwards, the mixture was diluted with H_2O (25 mL) and the aqueous phase was extracted with DCM (3 × 20 mL). The combined organic phases were washed with sat. $NaHCO_{3(aq.)}$ (20 mL), 1 M $HCl_{(aq.)}$ (20 mL) and brine (20 mL) and dried over Na_2SO_4. The filtrate was concentrated *in vacuo* and purified *via* column chromatography (4:3 = *n*-hexane/EA). The product was obtained as a yellow oil (3.29 g, 8.4 mmol, 84%).

$C_{16}H_{24}INO_2$ (389.28 $\frac{g}{mol}$)

R_f = (0.64 *n*hex/EA:4/1) [UV]

^{1}H-NMR(400 MHz, $CDCl_3$): δ = 7.84 (dd, ^3J = 8.0 Hz, ^4J = 1.2 Hz, 1H), 7.36 (dd, ^3J = 7.8 Hz, ^4J = 1.7 Hz, 1H), 7.27 (m, 1H), 6.90 (m, 1H), 4.31 (s, 1H, H-3), 3.48 (s, 3H, H-1), 3.15 (s, 3H, H-2), 1.98 (m, 1H, H-4a), 1.57 (m, 1H, H-4b), 1.27 (m, 8H, H-5–8), 0.86 (t, ^3J = 6.6 Hz, 3H, H-9).

^{13}C-NMR(101 MHz, $CDCl_3$): δ = 174.3 (C-3), 143.6, 139.7, 128.8, 128.5, 128.0, 101.9, 61.6 (C-1), 51.8 (C-4), 34.3 (C-5), 32.5 (C-2), 31.8, 29.5, 27.9, 22.8, 14.2 (C-9).

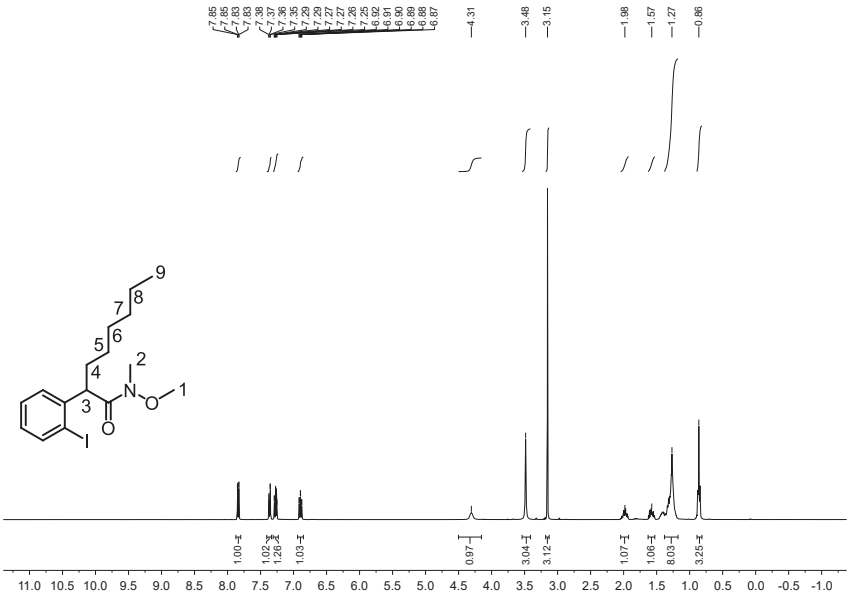

Figure 4.10: ^{1}H NMR spectrum of 2-(2-iodophenyl)-*N*-methoxy-*N*-methyloctanamide in $CDCl_3$, measured at 400.16 MHz.

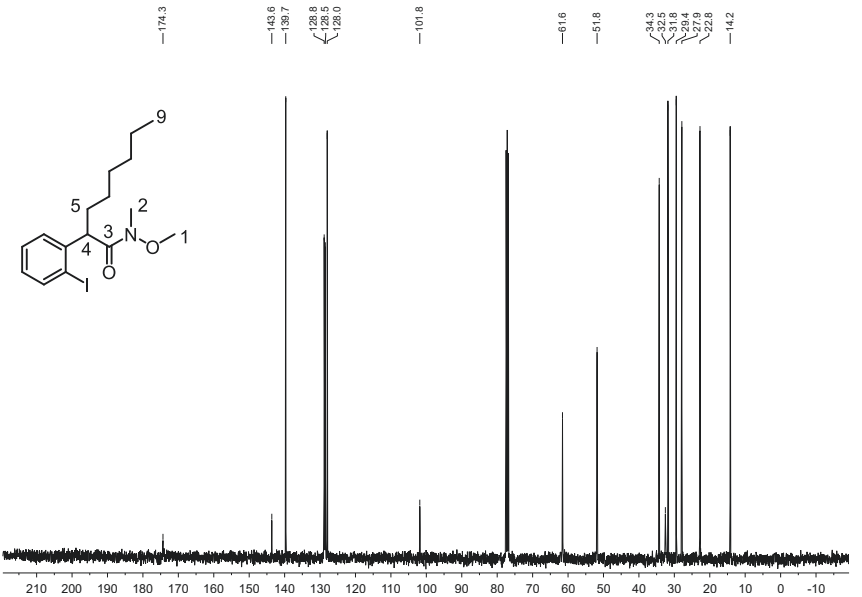

Figure 4.11: ^{13}C NMR spectrum of 2-(2-iodophenyl)-*N*-methoxy-*N*-methyloctanamide in $CDCl_3$, measured at 100.63 MHz.

8-Hexylbicyclo[4.2.0]octa-1,3,5-trien-7-one

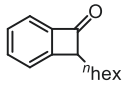

1o

1o was synthesized according to literature with slight modifications.[24] In a flame dried Schlenk RBF, 2-(2-iodophenyl)-*N*-methoxy-*N*-methyloctanamide (3.2 g, 8.3 mmol, 1.0 equiv.) was dissolved in THF (25 mL) and cooled to -78 °C. *t*BuLi (9.7 mL, 16.5 mmol, 2.0 equiv, 1.7 M in *n*-pentane) was added dropwise over 10 min and the mixture was stirred for 4 h at -78 °C. Afterwards, saturated $NH_4Cl_{(aq.)}$ (12 mL) was added to quench the reaction and the aqueous phase was extracted with Et_2O (3 × 20 mL). The combined organic phases were washed with brine (25 mL) and dried over Na_2SO_4. The filtrate was concentrated *in vacuo* and the product was obtained as a yellow oil without further purification (1.65 g, 8.1 mmol, 99%). The analytical data was in accordance with literature.[4]

$C_{14}H_{18}O$ (202.30 $\frac{g}{mol}$)

R_f = (0.87 *n*hex/EA:4/1) [UV]

^{1}H-NMR(400 MHz, $CDCl_3$): δ = 7.51 (m, 2H), 7.40 (m, 1H, H-4), 7.26 (m, 1H, H-1), 4.23 (m, 1H, H-5), 1.90 (m, 1H, H-6a), 1.76 (m, 1H, H-6b), 1.47 (m, 2H, H-7), 1.29 (m, 6H, H-8–10), 0.88 (t, ^3J = 6.9 Hz, 3H, H-11).

^{13}C-NMR(101 MHz, $CDCl_3$): δ = 193.3 (C-1), 156.9, 146.9, 135.1, 129.1 (s, C-2), 123.5, 120.9 (s, C-3), 65.2 (s, C-4), 31.8, 30.5 (s, C-5), 29.3, 27.5 (s, C-6), 22.7, 14.2 (s, C-7).

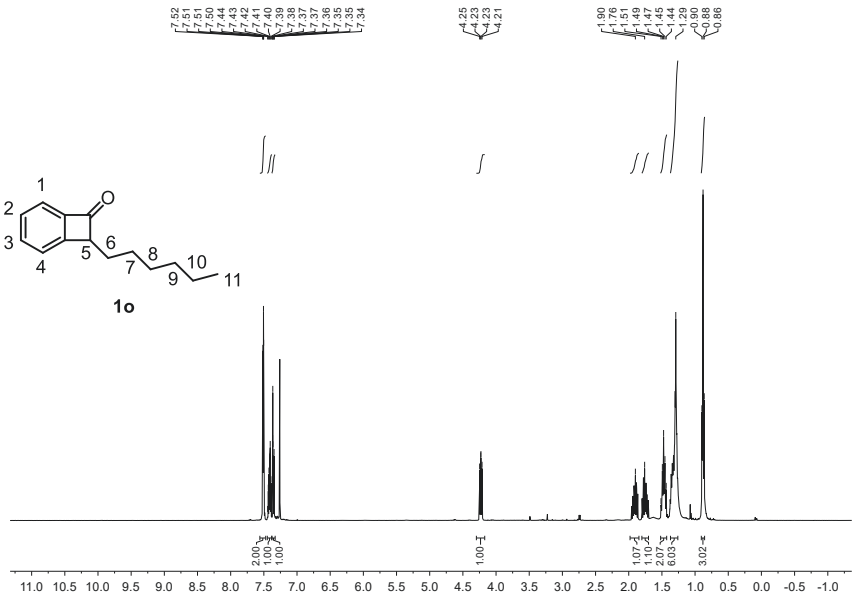

Figure 4.12: ^{1}H NMR spectrum of 8-hexylbicyclo[4.2.0]octa-1,3,5-trien-7-one in $CDCl_3$, measured at 400.16 MHz.

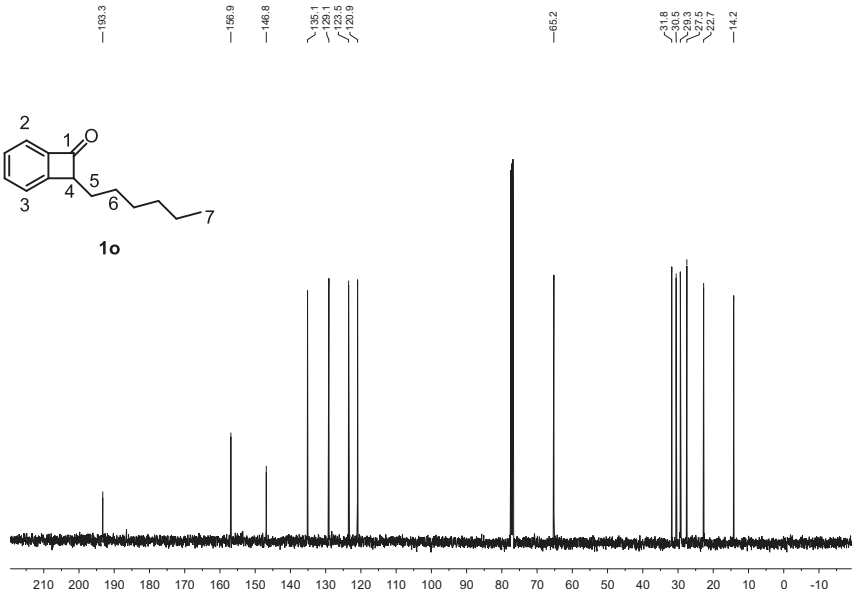

Figure 4.13: ^{13}C NMR spectrum of 8-hexylbicyclo[4.2.0]octa-1,3,5-trien-7-one in $CDCl_3$, measured at 100.63 MHz.

2-(2-Iodonaphthalen-1-yl)-N-methoxy-N-methylacetamide

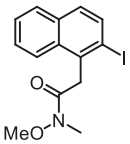

2-(2-Iodonaphthalen-1-yl)-N-methoxy-N-methylacetamide was synthesized according to literature.[14]

In a 50 mL RBF, 1-naphthaleneacetic acid (1.86 g, 10.0 mmol, 1.0 equiv.), $Pd(OAc)_2$ (112 mg, 0.5 mmol, 5 mol%), (Diacetoxyiodo)benzene (2.42 g, 7.5 mmol, 0.75 equiv.), I_2 (1.90 g, 7.5 mmol, 0.75 equiv.) were dissolved in anhydrous DMF (60 mL) under air. The reaction was stirred at 70 °C for 16 h under light exclusion. After reaction control by ^{1}H NMR spectroscopy showed only partial conversion, (Diacetoxyiodo)benzene (2.42 g, 7.5 mmol, 0.75 equiv.), and I_2 (1.90 g, 7.5 mmol, 0.75 equiv.) were added once again and the reaction was stirred at 70 °C for further 16 h under light exclusion. Afterwards, the mixture was quenched with Na_2SO_3, and the aqueous phase was extracted with EA (3 × 15 mL), concentrated *in vacuo* and the crude product was directly transformed to the respective Weinreb amide without further purification.

The crude intermediate and *N*,*O*-dimethylhydroxylamine hydrochloride (1.46 g, 15.0 mmol, 1.5 equiv.) were dissolved in DCM (25 mL) in a RBF. Subsequently, DMAP (1.83 g, 15.0 mmol, 1.5 equiv.) and EDC (2.33 g, 15.0 mmol, 1.5 equiv.) were added and the reaction was stirred for 3 h at rt. Afterwards, the mixture was diluted with 1 M $HCl_{(aq.)}$ (25 mL) and the aqueous phase was extracted with DCM (3 × 20 mL). The combined organic phases were washed with 1 M $HCl_{(aq.)}$ (20 mL), $NaHCO_{3(aq.)}$ (20 mL), and brine (20 mL) and dried over Na_2SO_4. The filtrate was concentrated *in vacuo* and purified *via* flash column chromatography (23 g SiO_2, 80:20 *n*-hexane/EA over 10 CV) affording 2-(2-iodonaphthalen-1-yl)-*N*-methoxy-*N*-methylacetamide (201 mg, 0.57 mmol, 6%) as a viscous yellow oil.

$C_{14}H_{14}INO_2$ (355.18 $\frac{g}{mol}$)

^{1}H-NMR(400 MHz, $CDCl_3$): δ = 7.90 (m, 2H), 7.81 (m, 1H), 7.49 (m, 3H), 4.53 (s, 2H, H-1), 3.82 (s, 3H), 3.26 (s, 3H).

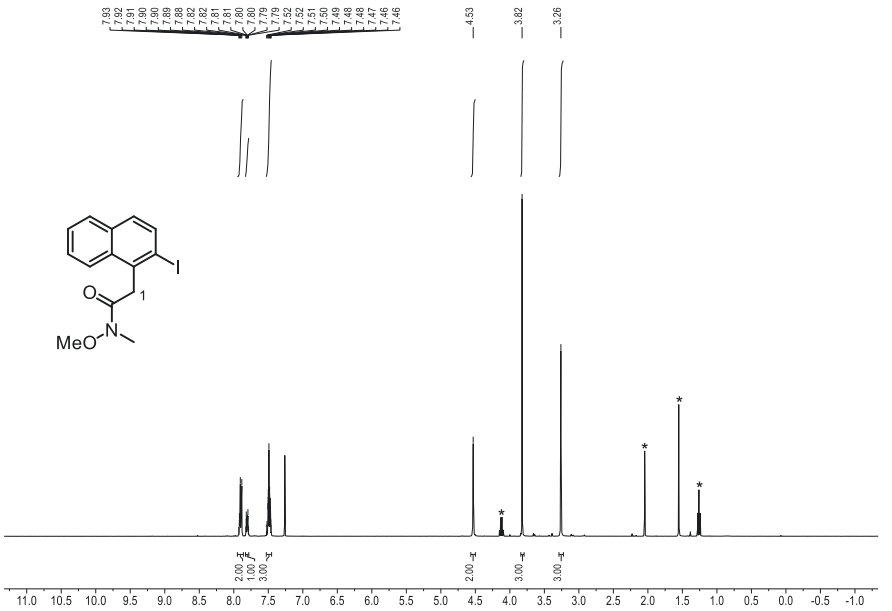

Figure 4.14. ^{1}H NMR spectrum of 2-(2-iodonaphthalen-1-yl)-*N*-methoxy-*N*-methylacetamide in $CDCl_3$, measured at 400.16 MHz. * Denotes residual EA and H_2O.

Cyclobuta[*a*]naphthalen-2(1*H*)-one

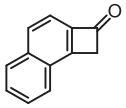

Cyclobuta[*a*]naphthalen-2(1*H*)-one was synthesized according to literature.[24] In a flame-dried Schlenk RBF, 2-(2-iodonaphthalen-1-yl)-*N*-methoxy-*N*-methylacetamide (190 mg, 0.53 mmol, 1.0 equiv.) was dissolved in THF (3 mL) and cooled to -78 °C. ^{t}BuLi (0.63 mL, 1.07 mmol, 2.0 equiv, 1.7 M in *n*-pentane) was added dropwise over 10 min and the mixture was stirred for 4 h at -78 °C. Afterwards, saturated $NH_4Cl_{(aq.)}$ (2 mL) was added to quench the reaction and the aqueous phase was extracted with Et_2O (3 × 5 mL). The combined organic phases were washed with brine (5 mL) and dried over Na_2SO_4. The filtrate was concentrated *in vacuo* and the product was purified by flash column chromatography (23 g SiO_2, 100:0 to 85:15 *n*-hexane/EA over 15 CV). Cyclobuta[*a*]naphthalen-2(1*H*)-one (71 mg, 0.42 mmol, 79%) was obtained as a yellow solid. Analytical data is in accordance with literature.[24]

$C_{12}H_{18}O$ ($168.20\ \frac{g}{mol}$)

^{1}H-NMR(400 MHz, $CDCl_3$): δ = 7.96 (m, 1H), 7.91 (m, 1H), 7.84 (m, 1H), 7.68 (m, 2H), 7.36 (m, 1H), 4.16 (s, 2H, H-1).

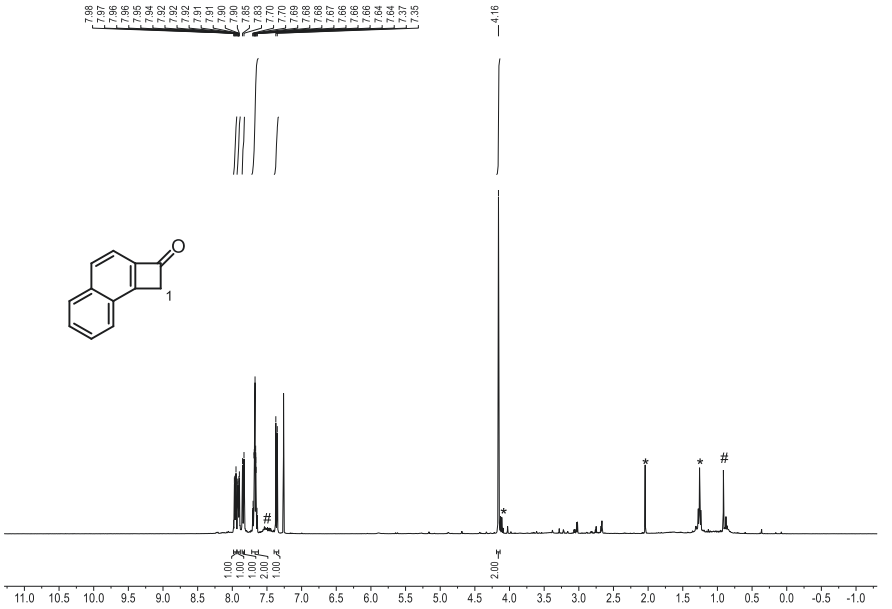

Figure 4.15. ^{1}H NMR spectrum of cyclobuta[*a*]naphthalen-2(1*H*)-one in $CDCl_3$, measured at 400.16 MHz. * Denotes residual EA. # Denotes unknown impurities.

Trimethyl((phenylsulfonyl)ethynyl)silane

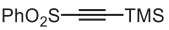

Trimethyl((phenylsulfonyl)ethynyl)silane was synthesized according to GP-A,[23a] employing benzenesulfonyl chloride (11.48 g, 65.0 mmol, 1.2 equiv.), $AlCl_3$ (8.67 g, 65 mmol, 1.2 equiv.) and 1,2-bis(trimethylsilyl)ethyne (9.88 g, 58 mmol, 1.0 equiv.). The crude product was recrystallized from *n*-pentane yielding colorless crystals of trimethyl((phenylsulfonyl)ethynyl)silane (4.89 g, 20.5 mmol, 32%). The analytical data was in accordance with literature.[25]

$C_{11}H_{14}O_2SSi$ (238,38 $\frac{g}{mol}$)

^{1}H-NMR (400 MHz, $CDCl_3$): δ = 8.02 (m, 2H, H-1), 7.69 (m, 1H), 7.59 (m, 1H), 0.22 (s, 9H, H-2).

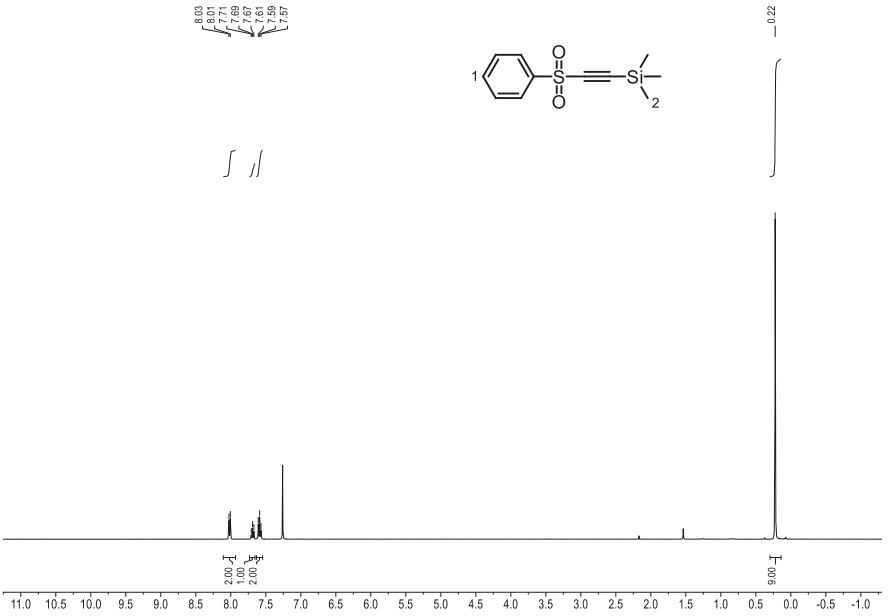

Figure 4.16. ^{1}H NMR spectrum of trimethyl((phenylsulfonyl)ethynyl)silane in $CDCl_3$, measured at 400.16 MHz.

Trimethyl(3-(phenylsulfonyl)bicyclo[2.2.2]octa-2,5-dien-2-yl)silane

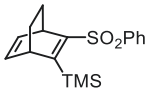

Trimethyl(3-(phenylsulfonyl)bicyclo[2.2.2]octa-2,5-dien-2-yl)silane was synthesized according to literature.[26] Trimethyl((phenylsulfonyl)ethynyl)silane (1.36 g, 5.71 mmol, 1.0 equiv.) and cyclohexa 1,4-diene (1.08 mL, 11.4 mmol, 2.0 equiv.) were dissolved in benzene (50 mL) and stirred at 60 °C for 5 d. The solution was quenched with $NaHCO_3$ (20 mL) and the aqueous layer was extracted with EA (3 × 20 mL). The combined organic layers were washed with brine (10 mL), dried over $MgSO_4$ and the volatiles were removed *in vacuo*, furnishing trimethyl(3-(phenylsulfonyl)bicyclo[2.2.2]octa-2,5-dien-2-yl)silane in 87% purity as a colorless oil (1.63 g, 5.13 mmol, 90%)

$C_{17}H_{22}O_2SSi$ (318.51 $\frac{g}{mol}$)

^{1}H-NMR (400 MHz, $CDCl_3$): δ = 7.80 (m, 2H), 7.58 (m, 1H, H-1), 7.52 (m, 2H), 6.22 (m, 1H), 6.13 (m, 1H), 4.14 (m, 1H), 3.80 (m, 1H), 1.35 (m, 1H), 1.19 (m, 3H), 0.37 (s, 9H, H-2).

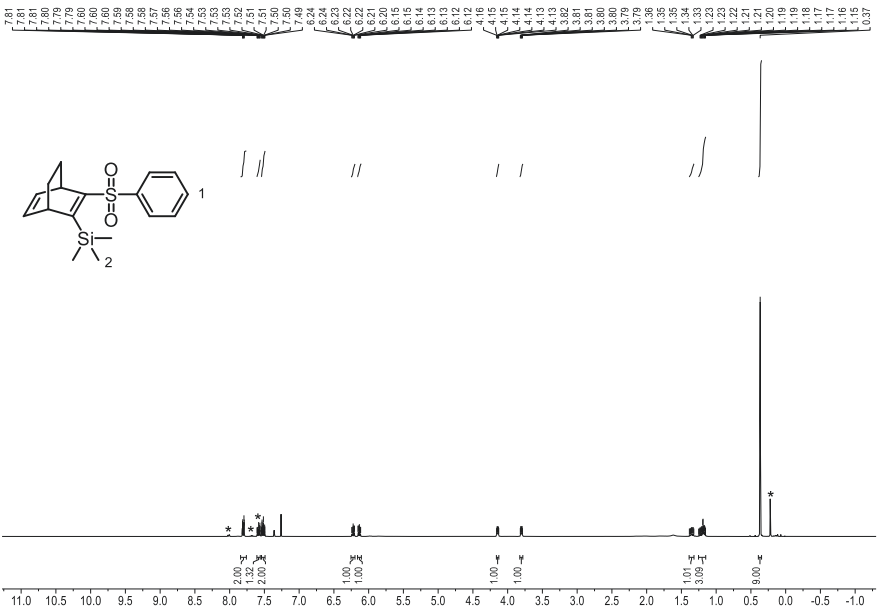

Figure 4.17. ^{1}H NMR spectrum of trimethyl(3-(phenylsulfonyl)bicyclo[2.2.2]octa-2,5-dien-2-yl)silane in $CDCl_3$, measured at 400.16 MHz. * Denotes residual trimethyl((phenylsulfonyl)ethynyl)silane.

Trimethyl(3-(phenylsulfonyl)bicyclo[2.2.2]oct-5-en-2-yl)silane

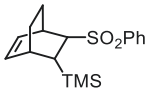

Trimethyl(3-(phenylsulfonyl)bicyclo[2.2.2]oct-5-en-2-yl)silane was synthesized according to literature.[26] In a glovebox, a Schlenk RBF was charged with trimethyl(3-(phenylsulfonyl)bicyclo[2.2.2]octa-2,5-dien-2-yl)silane (3.19 g, 10.0 mmol, 1.0 equiv.) and THF (10 mL). $LiAlH_4$ (380 mg, 10.0 mmol, 1.0 equiv.) was added in portions, after which the reaction was heated to 65 °C for 4 h. Subsequently, the reaction was quenched with sat. $NH_4Cl_{(aq.)}$ (10 mL), the aqueous phase was extracted with EA (3 × 10 mL). The combined organic phases were washed with brine (20 mL) and dried over $MgSO_4$ and the volatiles were removed *in vacuo*, furnishing trimethyl(3-(phenylsulfonyl)bicyclo[2.2.2]oct-5-en-2-yl)silane in 66% purity as a colorless oil (2.47 g, 7.72 mmol, 77%).

$C_{17}H_{24}O_2SSi$ (320.52 $\frac{g}{mol}$)

^{1}H-NMR (400 MHz, $CDCl_3$): δ = 7.85 (m, 2H), 7.63 (m, 1H, H-1), 7.55 (m, 2H), 6.33 (m, 1H), 5.92 (m, 1H), 3.29 (dd, ^3J = 7.3 Hz, ^3J = 1.7 Hz, 1H), 2.78 (m, 1H), 2.66 (m, 1H), 1.31 (m, 5H), 0.16 (s, 9H, H-2).

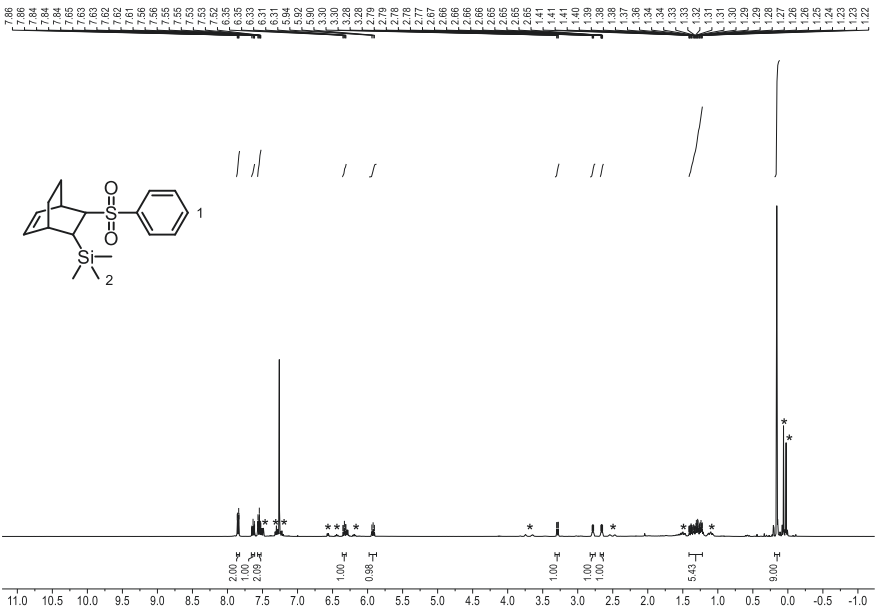

Figure 4.18. ^{1}H NMR spectrum of trimethyl(3-(phenylsulfonyl)bicyclo[2.2.2]oct-5-en-2-yl)silane in $CDCl_3$, measured at 400.16 MHz. * Denotes unknown impurities.

Bicyclo[2.2.2]octadiene

Bicyclo[2.2.2]octadiene was synthesized according to literature.[26] In a Schlenk tube, trimethyl(3-(phenylsulfonyl)bicyclo[2.2.2]oct-5-en-2-yl)silane (2.47 g, 7.70 mmol, 1.0 equiv.) was dissolved in a Bu_4NF solution (23.11 mL, 23.1 mmol, 3.0 equiv., 1 M in THF) and refluxed for 8 h. Subsequently, the reaction was quenched with $NH_4Cl_{(aq.)}$ (10 mL), the aqeous phase was extracted with *n*-pentane (3 × 10 mL). The combined organic phases were washed with brine (20 mL) and dried over $MgSO_4$ and the volatiles were removed *in vacuo*. Subsequently, the crude product was purified by column chromatography (*n*-pentane) and distilled (126 °C, oil bath) furnishing bicyclo[2.2.2]octadiene in 50% purity as a colorless oil (16.4 mg, 0.15 mmol, 2%). The analytical data is in accordance with literature.[27]

Note: As bicyclo[2.2.2]octadiene is volatile the solvent must be carefully removed in vacuo.

C_8H_{10} ($106.17\ \frac{g}{mol}$)

^{1}H-NMR (400 MHz, $CDCl_3$): δ = 6.31 (m, 4H, H-1), 3.62 (m, 2H, H-2), 1.26 (m, 4H, H-3).

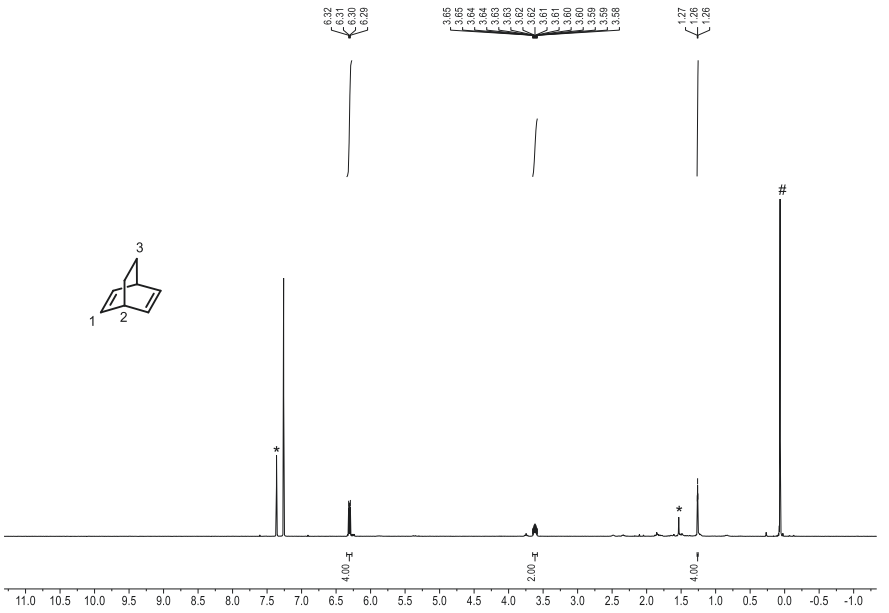

Figure 4.19. ^{1}H NMR spectrum of bicyclo[2.2.2]octadiene in $CDCl_3$, measured at 400.16 MHz. # Denotes residual grease. * Denotes unknown impurities.

(Ethynylsulfonyl)benzene

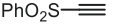

(Ethynylsulfonyl)benzene was synthesized according to GP-A,[23b] employing benzenesulfonyl chloride (11.48 g, 65.0 mmol, 1.2 equiv.), $AlCl_3$ (8.67 g, 65 mmol, 1.2 equiv.) and 1,2-bis(trimethylsilyl)ethyne (9.88 g, 58 mmol, 1.0 equiv.). The crude product was purified by column chromatography (70:30 ″hex/EA) furnishing (ethynylsulfonyl)benzene as a brown oil (7.63 g, 42.3 mmol, 65%). The analytical data was in accordance with literature.[23b]

$C_8H_6O_2S$ (166.19 $\frac{g}{mol}$)

^{1}H-NMR (400 MHz, $CDCl_3$): δ = 8.02 (m, 2H), 7.71 (m, 1H, H-1), 7.61 (m, 2H), 3.48 (s, 1H, H-2).

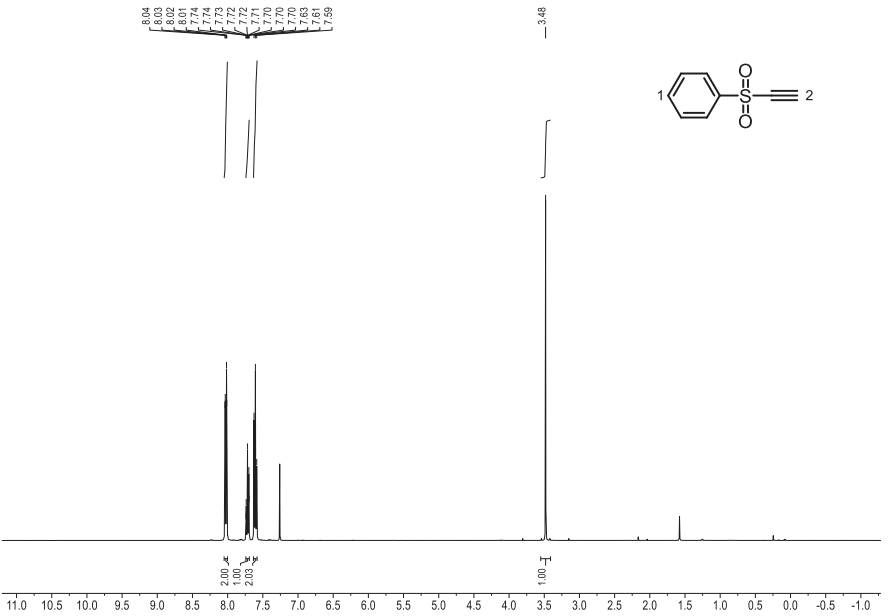

Figure 4.20. ^{1}H NMR spectrum (ethynylsulfonyl)benzene in $CDCl_3$, measured at 400.16 MHz.

2-(Phenylsulfonyl)-7-oxabicyclo[2.2.1]hepta-2,5-diene

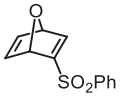

2-(Phenylsulfonyl)-7-oxabicyclo[2.2.1]hepta-2,5-diene was synthesized according to literature.[28] To a stirred DCM (10 mL) solution of (ethynylsulfonyl)benzene (3.34 g, 20.1 mmol, 1.0 equiv.) furane (29.2 mL, 402 mmol, 20 equiv.) was added in portions over 6 d. Subsequently, volatiles were removed *in vacuo* and the crude product was purified by column chromatography (gradient from 80:20 to 50:50 *n*-hex/EA) furnishing 2-(phenylsulfonyl)-7-oxabicyclo[2.2.1]hepta-2,5-diene as a colorless solid (1.40 g, 5.97 mmol, 30%).

$C_{12}H_{10}O_3S$ (234.27 $\frac{g}{mol}$)

^{1}H-NMR (400 MHz, $CDCl_3$): δ = 7.87 (m, 2H), 7.66 (m, 1H, H-2), 7.66 (d, ^3J = 1.9 Hz, 1H, H-1), 7.57 (m, 2H), 7.05 (m, 1H), 6.98 (m, 1H), 5.64 (m, 1H), 5.39 (m, 1H).

^{13}C-NMR(101 MHz, $CDCl_3$): δ = 159.7, 152.9, 143.9, 142.3, 138.7, 134.0, 129.6, 128.0, 84.3, 82.6.

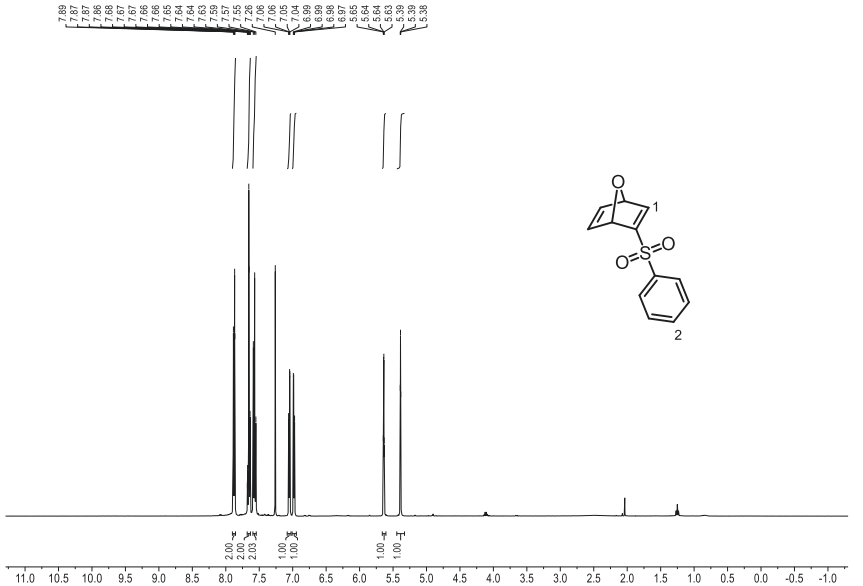

Figure 4.21. ^{1}H NMR spectrum of 2-(phenylsulfonyl)-7-oxabicyclo[2.2.1]hepta-2,5-diene in $CDCl_3$, measured at 400.16 MHz.

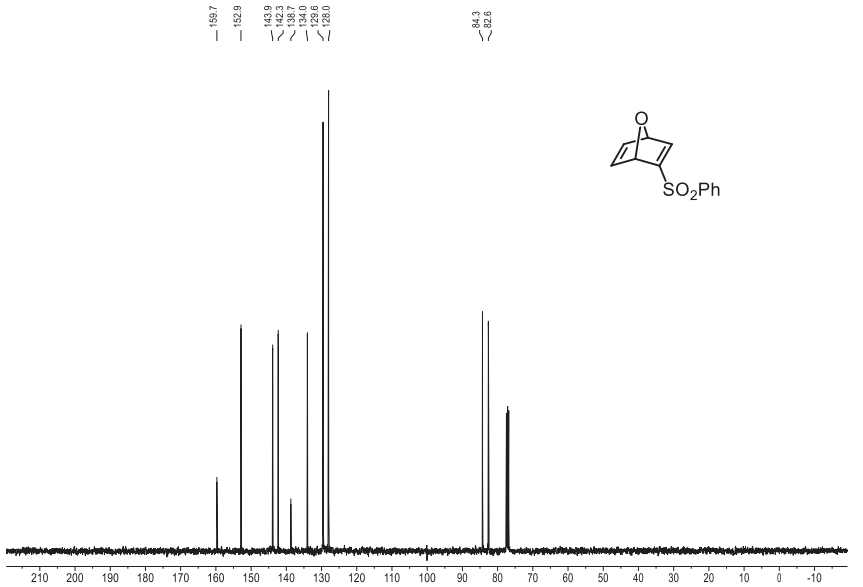

Figure 4.22. ^{13}C NMR spectrum of 2-(phenylsulfonyl)-7-oxabicyclo[2.2.1]hepta-2,5-diene in $CDCl_3$, measured at 101.63 MHz.

7-Oxa-norbornadiene

7-Oxa-norbornadiene was synthesized derived from literature.[29] In a Schlenk tube, 2-(phenylsulfonyl)-7-oxabicyclo[2.2.1]hepta-2,5-diene (1.19 g, 5.08 mmol, 1.0 equiv.) and $NaH_2PO_4(H_2O)$ (2.80 g, 20.3 mmol, 4.0 equiv.) were dissolved in MeOH (50 mL). Sodium amalgam (2.34 g, 20.3 mmol, 4.0 equiv., 20 wt% Na) was added and the mixture was stirred under reflux for 2 h. Afterwards, the reaction was quenched with H_2O (10 mL) and the aqueous phase was extracted with EA (3 × 5 mL). The combined organic extracts were concentrated *in vacuo* and purified by flash column chromatography (23 g SiO_2, 100:0 to 50:50 *n*-pentane/DCM over 20 CV) affording 7-oxa-norbornadiene as a colorless DCM solution (~50% purity, 0.10 mmol, 2%). The analytical data was in accordance with literature.[30]

Note: As 7-oxa-norbornadiene is volatile the solvent must be carefully removed in vacuo.

C_6H_6O (94.11 $\frac{g}{mol}$)

^{1}H-NMR (400 MHz, $CDCl_3$): δ = 7.08 (m, 4H, H-1), 5.46 (m, 2H, H-2).

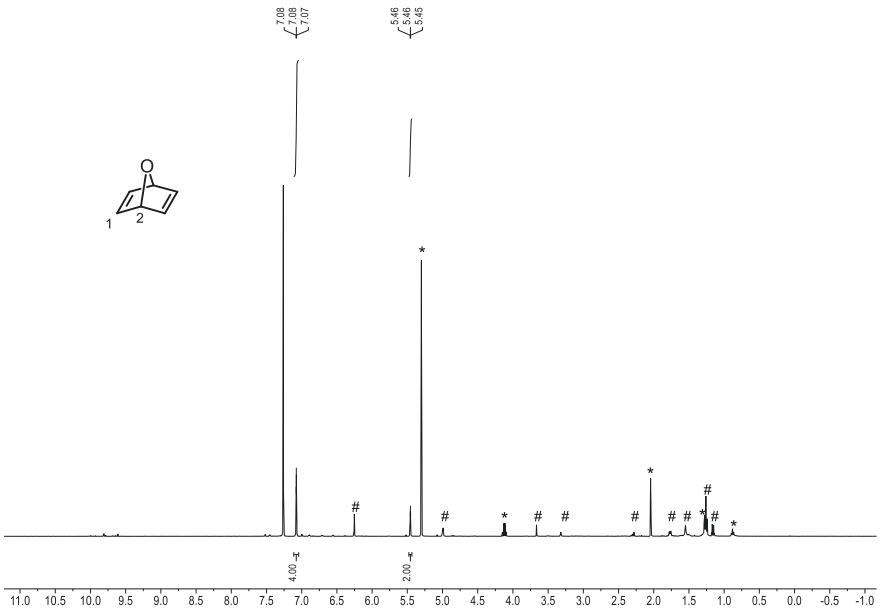

Figure 4.23. ^{1}H NMR spectrum of 7-oxa-norbornadiene in $CDCl_3$, measured at 400.16 MHz. * Denotes residual solvent: DCM, EA, *n*-pentane. # Denotes unknown impurities.

7-Ethinylcyclohepta-1,3,5-triene

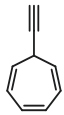

7-Ethinylcyclohepta-1,3,5-triene was synthesized according to literature with slight modifications.[31] $LiCl(H_2O)$ (817 mg, 13.5 mmol, 2.4 equiv.) was added to a Schlenk RBF and dried with a propane torch *in vacuo*. Ethynylmagnesium bromide (51.5 mL, 12.4 mmol, 2.2 equiv., 0.24 M in THF) was then added at rt. Subsequently, the reaction was cooled to -78 °C and tropylium tetrafluoroborate (1.00 g, 5.62 mmol, 1.0 equiv.) was added to the reaction mixture. The reaction was allowed to warm to rt while stirring for 16 h. The reaction was quenched by the addition of sat. $NH_4Cl_{(aq.)}$ (20 mL). The aqueous phase was extracted with Et_2O (3 × 30 mL). The combined organic layers were dried over $MgSO_4$, filtered, and concentrated *in vacuo*. The resulting crude residue was purified by flash column chromatography (23 g SiO_2, *n*-pentane), affording 7-ethinylcyclohepta-1,3,5-triene as a colorless oil (603 mg, 5.19 mmol, 92%). The analytical data was in accordance with literature.[31]

Note: As 7-ethinylcyclohepta-1,3,5-triene is volatile one must care when removing the solvent in vacuo.

C_9H_8 ($116.16\ \frac{g}{mol}$)

^{1}H-NMR (400 MHz, $CDCl_3$): δ = 6.66 (m, 2H), 6.19 (m, 2H), 5.35 (dd, ^3J = 8.8 Hz, ^3J = 5.6 Hz, 2H, H-3), 2.53 (tdt, ^3J = 5.6 Hz, ^3J = 2.6 Hz, ^4J = 1.4 Hz, 1H, H-2), 2.17 (d, ^3J = 2.6 Hz, 1H, H-1).

^{13}C-NMR(101 MHz, $CDCl_3$): δ = 131.0, 125.0, 122.8, 85.6 (C-2), 68.4 (C-1), 31.4 (C-3).

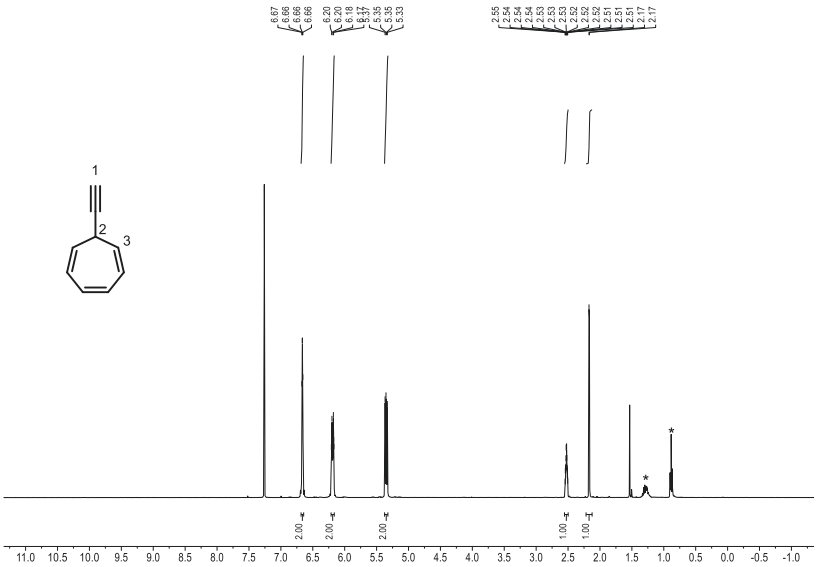

Figure 4.24. ^{1}H NMR spectrum of 7-ethinylcyclohepta-1,3,5-triene in $CDCl_3$, measured at 400.16 MHz. * Denotes residual *n*-pentane.

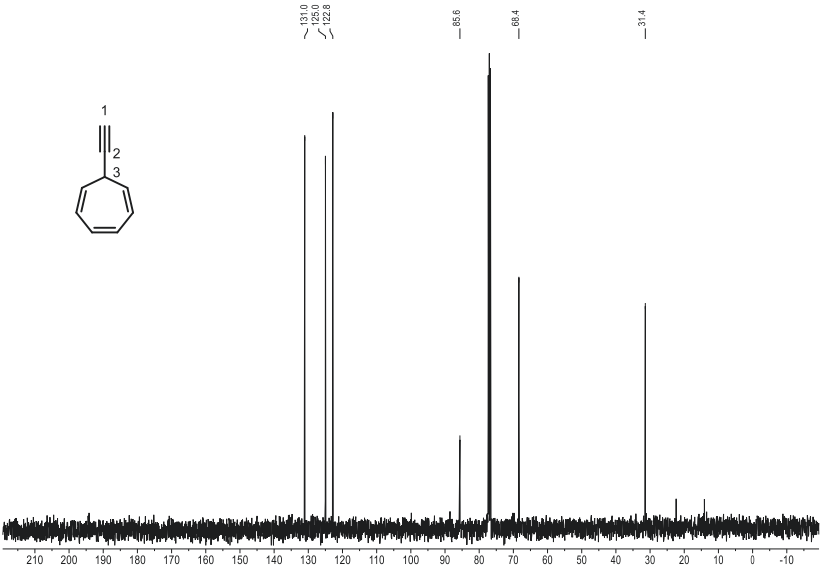

Figure 4.25. ^{13}C NMR spectrum of 7-ethinylcyclohepta-1,3,5-triene in $CDCl_3$, measured at 101.63 MHz.

Tricyclo[3.3.1.02,8]nona-3,6-dien-9-one (Barbaralone)

Barbaralone was synthesized according to literature.[31] In a RBF, 7-ethinylcyclohepta-1,3,5-triene was dissolved (600 mg, 5.17 mmol, 1.0 equiv.) and diphenyl sulphoxide (2.09 g, 10.3 mmol, 2.0 equiv) were dissolved in anhydrous DCM (9 mL). (Acetonitrile)[1,3-bis(2,6-diisopropylphenyl)-imidazol-2-ylidene]gold(I) tetrafluoroborate (111 mg, 0.15 mmol, 3 mol%) was added and the reaction was stirred for 16 h at rt. The reaction was quenched with 6 drops of Et3N and the solvent was removed *in vacuo*. The crude product was purified by flash column chromatography (23 g SiO_2, from 100:0 to 80:20 *n*hex/EA over 15 CV) affording Barbaralone as an off-white solid (544 mg, 4.12 mmol, 80%). The analytical data was in accordance with literature.[31]

C_9H_8O (132.16 $\frac{g}{mol}$)

^{1}H-NMR (400 MHz, $CDCl_3$): δ = 5.72 (t, ^3J = 5.8 Hz, 2H, H-1, H-5), 4.31 (m, 4H, HH-2, H-4), 2.72 (t, ^3J = 6.0 Hz, 2H, H-3).

^{13}C-NMR(101 MHz, $CDCl_3$): δ = 210.8 (C-6), 121.4 (C-2, C-3, C-4), 38.0 (C-1, C-5).

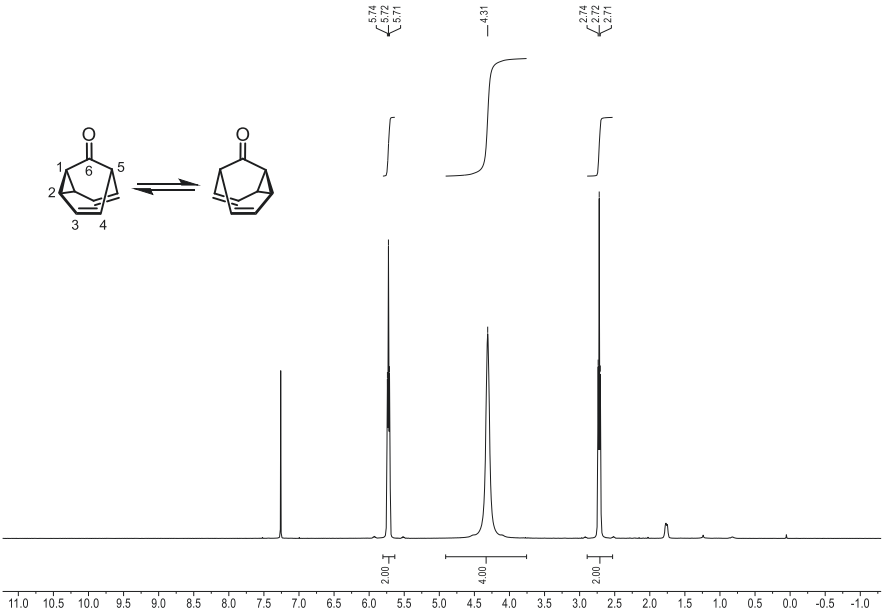

Figure 4.26. ^{1}H NMR spectrum of Barbaralone in $CDCl_3$, measured at 400.16 MHz.

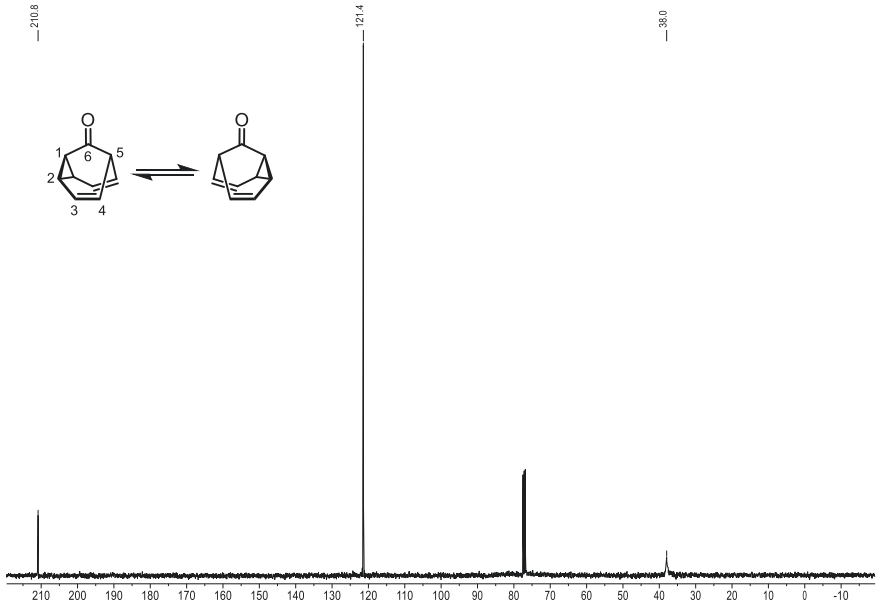

Figure 4.27. ^{13}C NMR spectrum of Barbaralone in $CDCl_3$, measured at 101.63 MHz.

Diphenylketene

Diphenylketene was synthesized according to literature.[32] In a Schlenk RBF, Et_3N (3.61 mL, 26.0 mmol, 1.2 equiv.) was added to 2,2-diphenylacetyl chloride (5.0 g, 21.7 mmol, 1.0 equiv.) in Et2O (30 mL) at 0 °C over 30 min. The mixture was stirred at -20 °C for 16 h. After warming to rt, the suspension was filtered in a glovebox and the filtrate was concentrated *in vacuo*. Vacuum distillation ($3.4\ 10^{-1}$ mbar, 35 °C, 130 °C oil bath) afforded diphenylketene as an orange oil (694 mg, 3.58 mmol, 16%). Analytical data was in accordance with literature.[32]

Note: Diphenylketene decomposes with time.[32]

$C_{14}H_{10}O$ ($194.23\ \frac{g}{mol}$)

b.p.: 35 °C ($3.4\ 10^{-1}$ mbar, 130 °C oil bath)

^{1}H-NMR (400 MHz, C_6D_6): δ = 7.15 (m, 7H), 7.06 (m, 3H).

^{13}C-NMR(101 MHz, C_6D_6): δ = 201.8 (C-1), 131.1 (C-3), 129.5, 128.0, 126.4 (C-6), 47.3 (C-2).

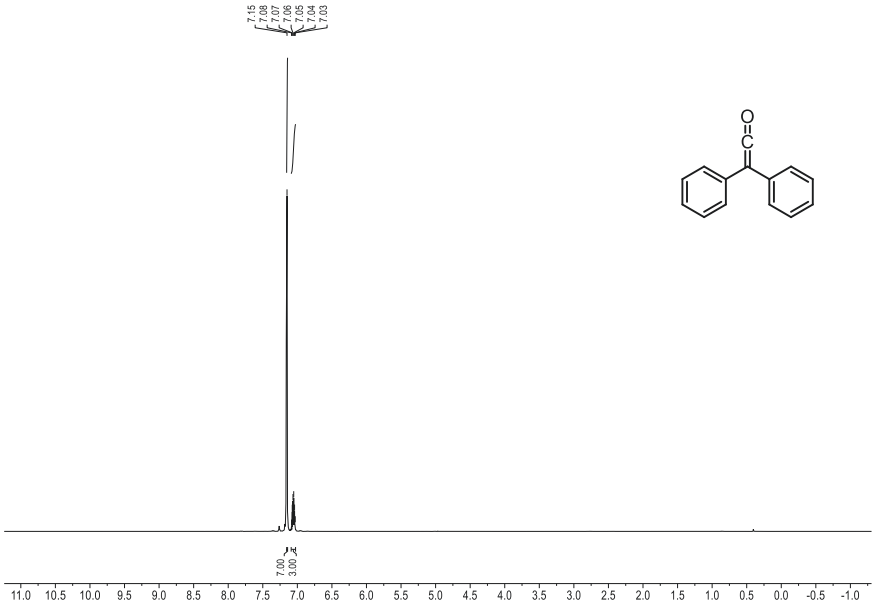

Figure 4.28. ^{1}H NMR spectrum of diphenylketene in C_6D_6, measured at 400.16 MHz.

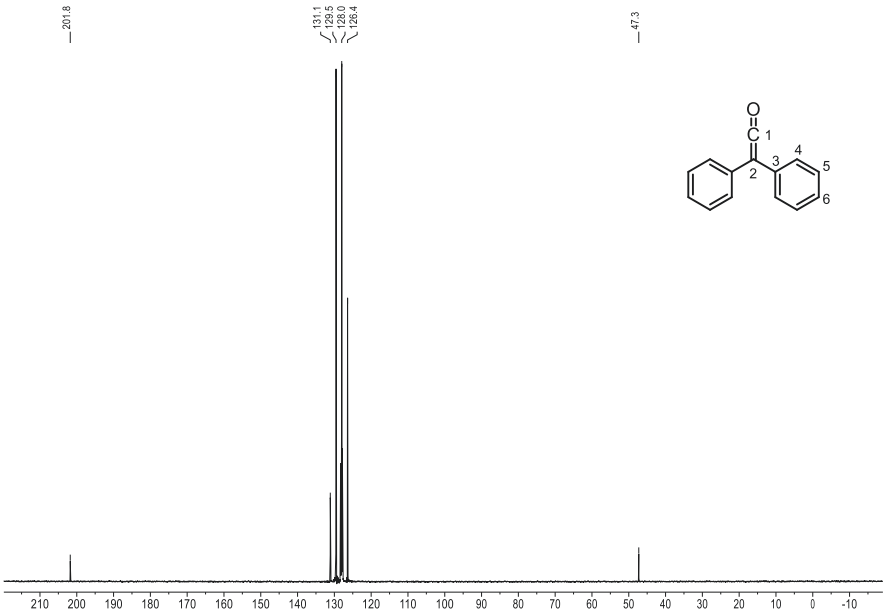

Figure 4.29. ^{13}C NMR spectrum of diphenylketene in C_6D_6, measured at 101.63 MHz.

4,10-Dimethyldibenzo[*a*,*e*][8]annulene-5,11(6*H*,12*H*)-dione

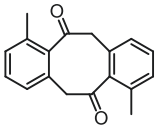

4,10-Dimethyldibenzo[*a*,*e*][8]annulene-5,11(6*H*,12*H*)-dione was obtained as a side product during the nickel-catalyzed insertion of **2a** in **1m**. In a glove box, $Ni(COD)_2$ (27.5 mg, 0.1 mmol, 10 mol%) and (*R*)-(+)-(3,5-dioxa-4-phosphacyclohepta[2,1-*a*;3,4-*a*']dinaphthalen-4-yl)dimethylamine (71.9 mg, 0.2 mmol, 20 mol%) were added to a dried 50 mL Schlenk RBF. DMI (20 mL) was added and the reaction was stirred for 5 min at rt. Subsequently, **2a** (132 µL, 1.3 mmol, 1.3 equiv.) and **1m** (132 mg, 1.0 mmol, 1.0 equiv.) were added, after which the reaction was transferred to a preheated (80 °C) oil bath and stirred for 16 h. The reaction was diluted with EA (20 mL) and washed once with $HCl_{(aq.)}$ (1M, 50 mL). The aqueous phase was extracted with EA (3 × 20 mL) and the combined organic phases were washed with brine (1 × 50 mL), dried over $MgSO_4$ and filtered. The solvent was removed *in vacuo* and the crude product was purified by flash column chromatography (23 g SiO_2, gradient from 100:0 to 85:15 *n*-hexane/EA over 15 CV) affording 4,10-dimethyldibenzo[*a*,*e*][8]annulene-5,11(6*H*,12*H*)-dione (9.1 mg, 0.03 mmol, 7%) as a side product (colorless solid).

$C_{18}H_{16}O_2$ (264.32 $\frac{g}{mol}$)

^{1}H-NMR (600 MHz, C_6D_6): δ = 7.08 (m, 2H, H-4), 6.99 (d, ^3J = 7.6 Hz, 2H), 6.87 (d, ^3J = 7.5 Hz, 2H), 3.98 (s, 4H, H-9), 2.22 (s, 6H, H-1).

^{13}C-NMR(151 MHz, C_6D_6): δ = 205.5 (C-8), 138.8, 136.0, 131.2, 130.6, 130.2, 127.2, 51.4 (C-9), 20.0 (C-1).

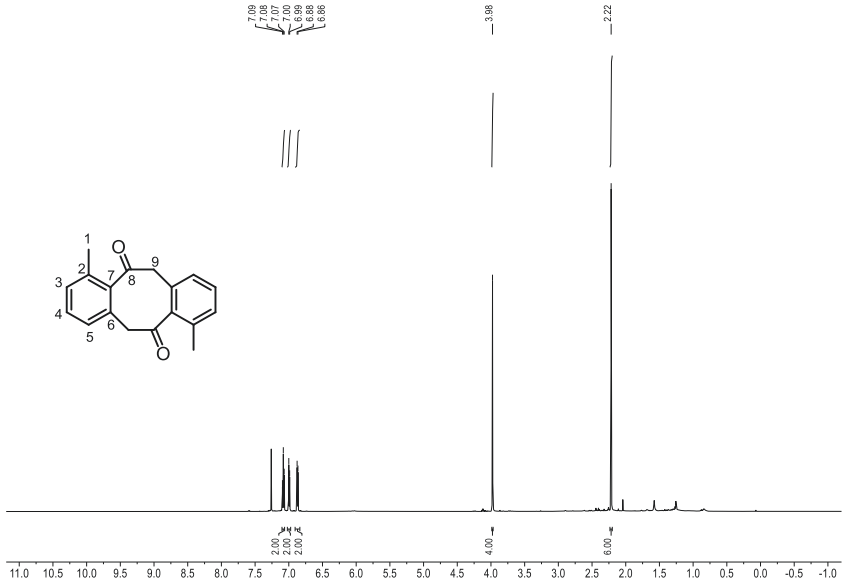

Figure 4.30. ^{1}H NMR spectrum of 4,10-dimethyldibenzo[*a*,*e*][8]annulene-5,11(6*H*,12*H*)-dione in $CDCl_3$, measured at 600.13 MHz.

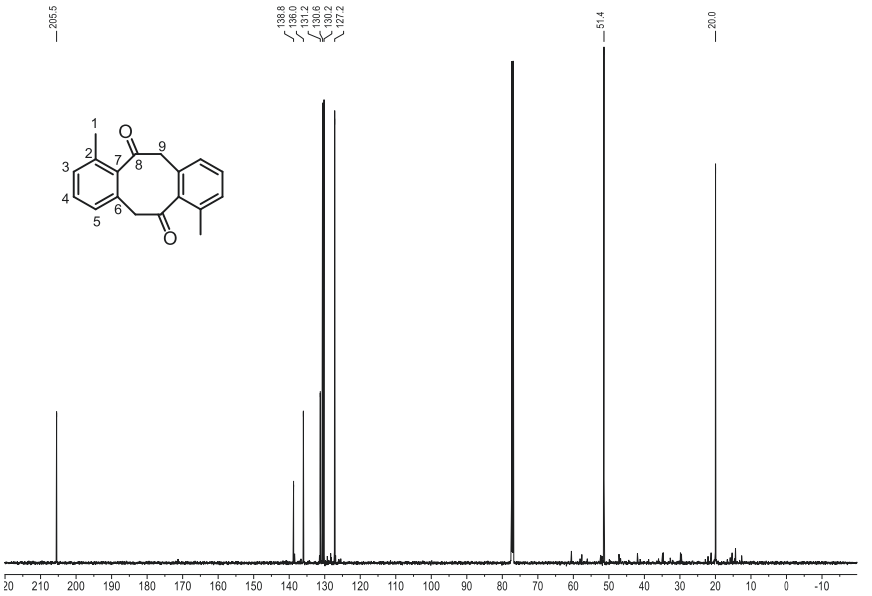

Figure 4.31. ^{13}C NMR spectrum of 4,10-dimethyldibenzo[*a*,*e*][8]annulene-5,11(6*H*,12*H*)-dione in $CDCl_3$, measured at 150.92 MHz.

Homophthalimide

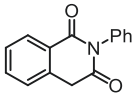

In a glovebox, $Ni(COD)_2$ (8.3 mg, 30 µmol, 10 mol%) and PCy_3 (16.8 mg, 60 µmol, 20 mol%) were dissolved in toluene (6 mL) in a dried Schlenk tube. The mixture was stirred for 5 min at rt. Subsequently, PhNCO (43 µL, 0.39 mmol, 1.3 equiv.) and **1a** (35.4 mg, 0.30 mmol, 1.0 equiv.) were added, after which the reaction was transferred to a preheated (100 °C) metal block and stirred for 16 h. The reaction was diluted with EA (5 mL) and washed once with $HCl_{(aq.)}$ (1 M, 10 mL). The aqueous phase was extracted with EA (3 × 50 mL) and the combined organic phases were washed with brine (1 × 10 mL), dried over $MgSO_4$ and filtered. The solvent was removed *in vacuo* and the crude product was purified by flash column chromatography (23 g SiO_2, gradient from 100:0 to 50:50 *n*-hexane/EA over 15 CV) affording homophthalimide (19.5 mg, 82 µmol, 27%) as a colorless solid. Analytical data was in accordance with literature.[33]

$C_{15}H_{11}NO_2$ (237.26 $\frac{g}{mol}$)

^{1}H-NMR (400 MHz, $CDCl_3$): δ = 8.25 (m, 1H), 7.65 (m, 1H), 7.49 (m, 4H), 7.35 (m, 1H), 7.21 (m, 2H), 4.23 (s, 2H, H-1).

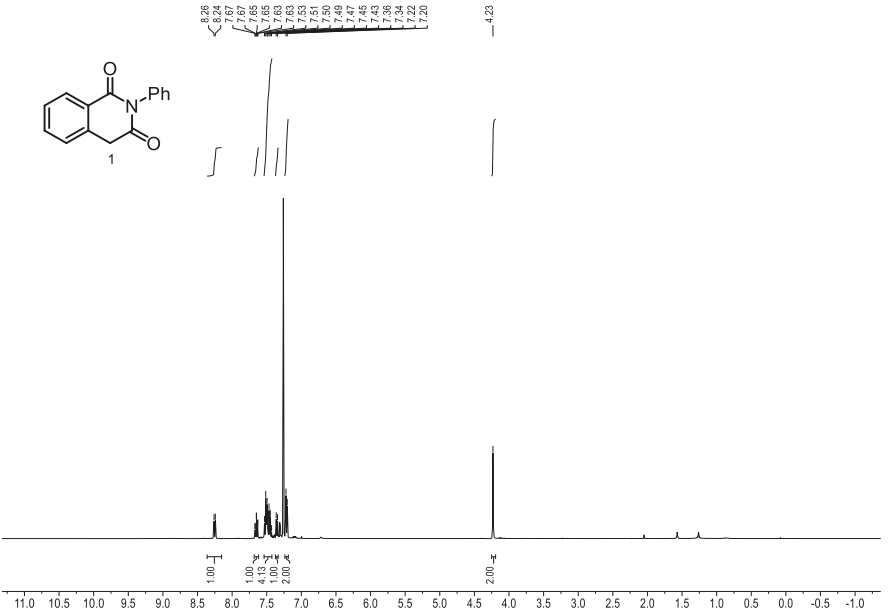

Figure 4.32. ^{1}H NMR spectrum of Homophthalimide in $CDCl_3$, measured at 400.16 MHz.

_N_-methoxy-_N_-methyl-2,2-diphenylacetamide

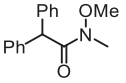

_N_-Methoxy-_N_-methyl-2,2-diphenylacetamide was synthesized according to literature.[20] Diphenylacetic acid (2.12 g, 10.0 mmol, 1.0 equiv.) and _N_,_O_-dimethylhydroxylamine hydrochloride (1.46 g, 15.0 mmol, 1.5 equiv.) were dissolved in DCM (25 mL) in a RBF. Subsequently, DMAP (1.83 g, 15.0 mmol, 1.5 equiv.) and EDC (2.33 g, 15.0 mmol, 1.5 equiv.) were added and the reaction was stirred for 3 h at rt. Afterwards, the mixture was diluted with 1 M $HCl_{(aq.)}$ (25 mL) and the aqueous phase was extracted with DCM (3 × 20 mL). The combined organic phases were washed with 1 M $HCl_{(aq.)}$ (20 mL), $NaHCO_{3(aq.)}$ (20 mL), and brine (20 mL) and dried over Na_2SO_4. The filtrate was concentrated _in vacuo_ and purified _via_ column chromatography (90:10 _n_-hexane/EA) affording _N_-methoxy-_N_-methyl-2,2-diphenylacetamide (2.11 g, 8.27 mmol 83%) as a yellow oil. Analytical data is in accordance with literature.[21]

$C_{16}H_{17}NO_2$ (255.32 $\frac{g}{mol}$)

^{1}H-NMR (400 MHz, $CDCl_3$): δ = 7.32 (m, 8H), 7.24 (m, 2H), 5.55 (s, 1H, H-5), 3.50 (s, 3H, H-7), 3.24 (s, 3H, H-8).

^{13}C-NMR(101 MHz, C_6D_6): δ = 173.2 (C-6), 139.6 (C-4), 129.1, 128.6, 127.1 (C-1), 61.6 (C-7), 53.0 (C-5), 32.6 (C-8).

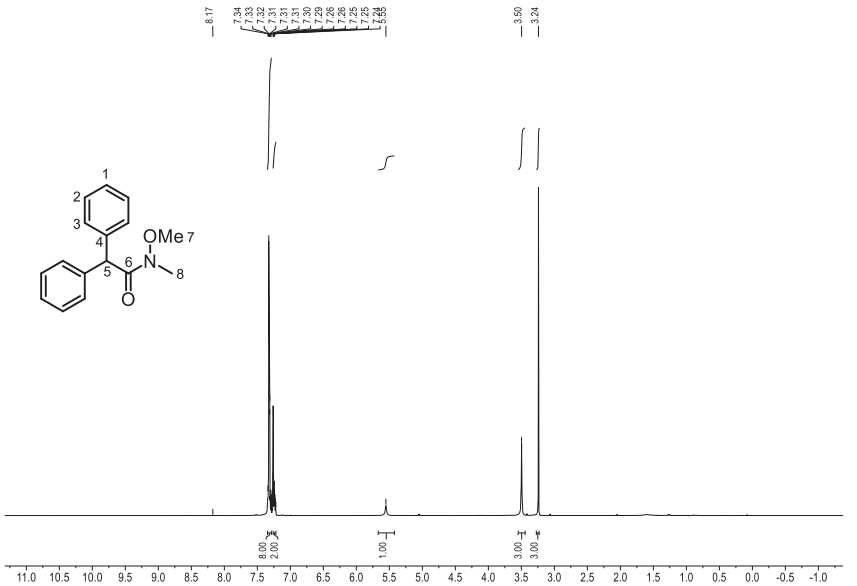

Figure 4.33. ^{1}H NMR spectrum of *N*-methoxy-*N*-methyl-2,2-diphenylacetamide in $CDCl_3$, measured at 400.16 MHz.

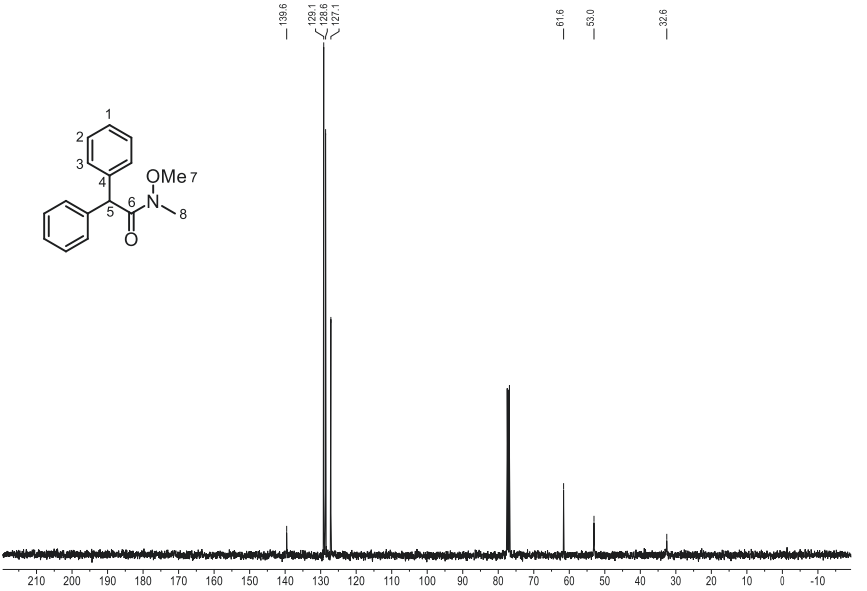

Figure 4.34. ^{13}C NMR spectrum of *N*-methoxy-*N*-methyl-2,2-diphenylacetamide in $CDCl_3$, measured at 400.16 MHz.

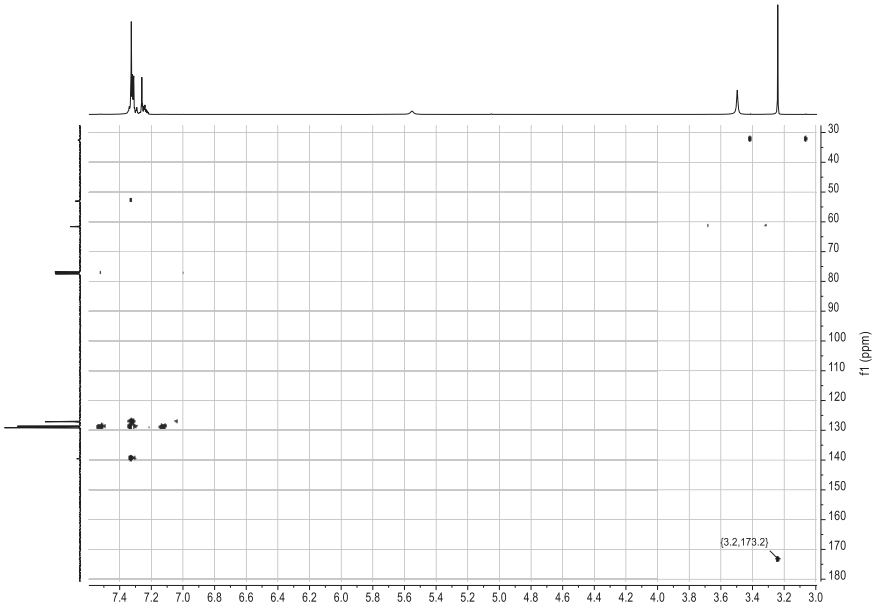

Figure 4.35. $^{1}H,^{13}C$ HMBC NMR spectrum of *N*-methoxy-*N*-methyl-2,2-diphenylacetamide in $CDCl_3$, measured at 400.16 MHz.

(*R*)-2-(2-Iodophenyl)-*N*-methoxy-*N*-methyl-2-phenylacetamide

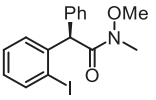

(*R*)-2-(2-Iodophenyl)-*N*-methoxy-*N*-methyl-2-phenylacetamide was synthesized according to literature.[21] In a flame dried Schlenk RBF, *N*-methoxy-*N*-methyl-2,2-diphenylacetamide (511 mg, 2.0 mmol, 1.0 equiv.), 4-iodo 3-nitroanisole (1.12 g, 4.0 mmol, 2.0 equiv.), $Pd(OAc)_2$ (44,9 mg, 0.2 mmol, 10 mol%), Ac-L-Ala-OH (52.5 mg, 0.4 mmol, 20 mol%), AgOTf (103 mg, 0.4 mmol, 0.2 equiv.) and $NaHCO_3$ (84.0 mg, 1.0 mmol, 0.5 equiv.) were suspended in HFIP (30 mL). The reaction was placed in a preheated oil bath (70 °C) and stirred for 6 h. After cooling to rt, the mixture was diluted with EA (50 mL), filtered through Celite and rinsed with EA (100 mL). The filtrate was concentrated *in vacuo* and the crude product was purified by column chromatography (90:10 *n*-hexane/EA) affording (*R*)-2-(2-iodophenyl)-*N*-methoxy-*N*-methyl-2-phenylacetamide (672 mg, 1.76 mmol, 88%). Analytica data is in accordance with literature.[21]

$C_{16}H_{17}INO_2$ (381.21 $\frac{g}{mol}$)

^{1}H-NMR (400 MHz, $CDCl_3$): δ = 7.86 (dm, ^3J = 7.9 Hz, 1H), 7.31 (m, 7H), 6.94 (m, 1H), 5.85 (m, 1H, H-1), 3.50 (s, 3H, H-2), 3.24 (s, 3H, H-3).

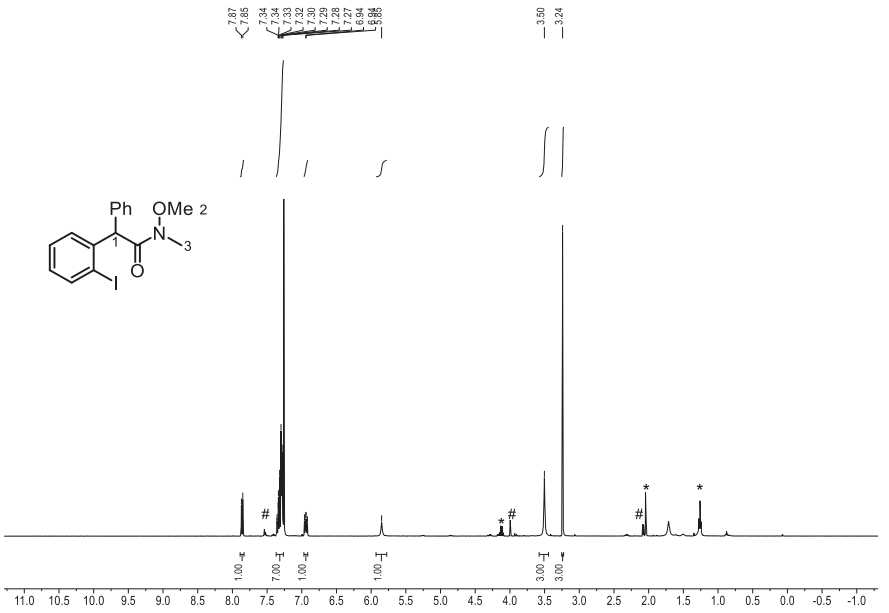

Figure 4.36. ^{1}H NMR spectrum of 2-(2-iodophenyl)-*N*-methoxy-*N*-methyl-2,2-diphenylacetamide in $CDCl_3$, measured at 400.16 MHz. * Denotes residual EA. # Denotes unknown impurities.

4.3 References

[1] A. T. Blomquist, Y. C. Meinwald, *J. Am. Chem. Soc.* **1959**, *81*, 667-672.
[2] a) M. Lautens, L. G. Edwards, W. Tam, A. J. Lough, *J. Am. Chem. Soc.* **1995**, *117*, 10276-10291; b) Y. Chen, J. K. Snyder, *J. Org. Chem.* **1998**, *63*, 2060-2061.
[3] a) H. Brunner, F. Prester, *J. Organomet. Chem.* **1991**, *414*, 401-409; b) O. Pardigon, A. Tenaglia, G. Buono, *J. Org. Chem.* **1995**, *60*, 1868-1871.
[4] F. Juliá-Hernández, A. Ziadi, A. Nishimura, R. Martin, *Angew. Chem. Int. Ed.* **2015**, *54*, 9537-9541.
[5] Y. Xue, G. Dong, *Acc. Chem. Res.* **2022**, *55*, 2341-2354.
[6] J.-H. Guo, Y. Liu, X.-C. Lin, T.-M. Tang, B.-Q. Wang, P. Hu, K.-Q. Zhao, F. Song, Z.-J. Shi, *Angew. Chem. Int. Ed.* **2021**, *60*, 19079-19084.
[7] L. Liu, N. Ishida, M. Murakami, *Angew. Chem. Int. Ed.* **2012**, *51*, 2485-2488.
[8] M. Zhang, J. Yang, W. Rong, J. Li, *Org. Chem. Front.* **2023**, *10*, 5216-5230.
[9] M. F. Hawthorne, W. D. Emmons, K. S. McCallum, *J. Am. Chem. Soc.* **1958**, *80*, 6393-6398.
[10] V. R. Flid, M. L. Gringolts, R. S. Shamsiev, E. S. Finkelshtein, *Russ. Chem. Rev.* **2018**, *87*, 1169-1205.
[11] P. Álvarez-Bercedo, A. Flores-Gaspar, A. Correa, R. Martin, *J. Am. Chem. Soc.* **2010**, *132*, 466-467.
[12] T. Yano, T. Kawasaki, T. Yuhki, N. Ishida, M. Murakami, *Org. Lett.* **2018**, *20*, 1224-1227.
[13] S. Ochi, Z. Zhang, Y. Xia, G. Dong, *Angew. Chem. Int. Ed.* **2022**, *61*, e202202703.
[14] R. C. Richter, I. H. Lindenmaier, D. Schray, M. Ströbele, I. Fleischer, *Org. Lett.* **2025**.
[15] J. Clayden, N. Greeves, S. G. Warren, *Organische Chemie, Vol. 2*, Springer, **2013**.
[16] C. J. Wagner, G. Dong, *Angew. Chem. Int. Ed.*, *n/a*, e202500148.
[17] A. N. Bismillah, T. G. Johnson, B. A. Hussein, A. T. Turley, P. K. Saha, H. C. Wong, J. A. Aguilar, D. S. Yufit, P. R. McGonigal, *Nat. Chem.* **2023**, *15*, 615-624.
[18] A. R. K. Murthy, J. M. Chapman, S. D. Wyrick, I. H. Hall, *Pharm. Res.* **1986**, *3*, 286-289.
[19] T.-S. Mei, D.-H. Wang, J.-Q. Yu, *Org. Lett.* **2010**, *12*, 3140-3143.
[20] P.-h. Chen, J. Sieber, C. H. Senanayake, G. Dong, *Chem. Sci.* **2015**, *6*, 5440-5445.
[21] H. Wang, C. Zhou, Z. Gao, S. Li, G. Li, *Angew. Chem. Int. Ed.* **2023**, *62*, e202300905.
[22] M. J. O'Neil, 14th ed., The Merck index : an encyclopedia of chemicals, drugs, and biologicals, Merck Whitehouse Station, N.J., **2006**.
[23] a) J. J. Eisch, M. Behrooz, S. K. Dua, *J. Organomet. Chem.* **1985**, *285*, 121-136; b) Z. Chen, M. L. and Trudell, *Synth. Commun.* **1994**, *24*, 3149-3155.
[24] R. Li, B. Li, H. Zhang, C.-W. Ju, Y. Qin, X.-S. Xue, D. Zhao, *Nat. Chem.* **2021**, *13*, 1006-1016.
[25] J. L. García Ruano, J. Alemán, C. G. Paredes, *Org. Lett.* **2006**, *8*, 2683-2686.
[26] R. V. Williams, K. Chauhan, V. R. Gadgil, *J. Chem. Soc., Chem. Commun.* **1994**, 1739-1740.
[27] M. Olbrich, P. Mayer, D. Trauner, *Org. Biomol. Chem.* **2014**, *12*, 108-112.
[28] O. Arjona, F. Iradier, R. Medel, J. Plumet, *Heterocycles* **1999**, *50*, 653-656.
[29] S. Mirsadeghi, B. Rickborn, *J. Org. Chem.* **1985**, *50*, 4340-4345.
[30] H. Prinzbach, H. Bingmann, J. Markert, G. Fischer, L. Knothe, W. Eberbach, J. Brokatzky-Geiger, *Chem. Ber.* **1986**, *119*, 589-615.
[31] S. Ferrer, A. M. Echavarren, *Angew. Chem. Int. Ed.* **2016**, *55*, 11178-11182.
[32] A. Viceriat, I. Marchand, S. Carret, J.-F. Poisson, *Org. Lett.* **2021**, *23*, 2449-2454.

[33] S. H. Kennedy, M. N. Schaeff, D. A. Klumpp, *J. Org. Chem.* **2019**, *84*, 14133-14140.

5 Nickel Catalyzed XEC of Alkyl Halides with Thioesters Mediated by Mechanochemistry

5.1 Introduction

Nucleophilic substitution reactions are fundamental in chemistry, involving the replacement of a leaving group by a nucleophile (Figure 5.1a). Classic mechanisms like S_N1 and S_N2 are widely taught and used, but their utility is often limited, especially when applied to complex molecules, due to the need for strong bases or organometallic reagents and elevated temperatures. To address these challenges, transition metal catalysis has opened new possibilities, enabling previously challenging or inaccessible transformations (Figure 5.1a). A particularly exciting development is cross-electrophile coupling (XEC), expanding the set of feasibly reactions by combining two electrophiles, despite their inherent polarity, under reductive conditions (Figure 5.1a).[1]

XECs are powerful because they tolerate a wide range of functional groups that are typically reactive under classical conditions. For instance, ketones, which are ubiquitous in pharmaceuticals, natural products, and bioactive molecules,[2] can be accessed *via* XEC, as first demonstrated by Mukaiyama in 1981 through the nickel-catalyzed coupling of pyridyl esters and alkyl iodides under reductive conditions.[3] Expanding on this, in 2012 the Weix and Gong groups introduced bidentate nitrogen ligands, enabling efficient XEC of acyl chlorides with a wider scope of alkyl iodides (Figure 5.1b).[4]

Despite these advances, XEC reactions continue to face challenges, such as achieving high selectivity, prolonged reaction times at elevated temperatures, and the heterogeneous nature of metal reductants can compromise reproducibility. Mechanochemistry addresses several of these issues by offering solvent-minimized, rapid transformations under ambient conditions, without the need for heating or an inert atmosphere.[5] Moreover, the vigorous mixing inherent to mechanochemical methods ensures, optimal conditions for heterogeneous reductants employed in XECs, thus improving reproducibility.[6]

Although mechanochemistry is gaining traction in the field of XEC research, it remains largely underexplored, with only a single report describing the mechanochemical coupling of twisted amides with an alkyl bromides to furnish ketones (Figure 5.1c).[7]

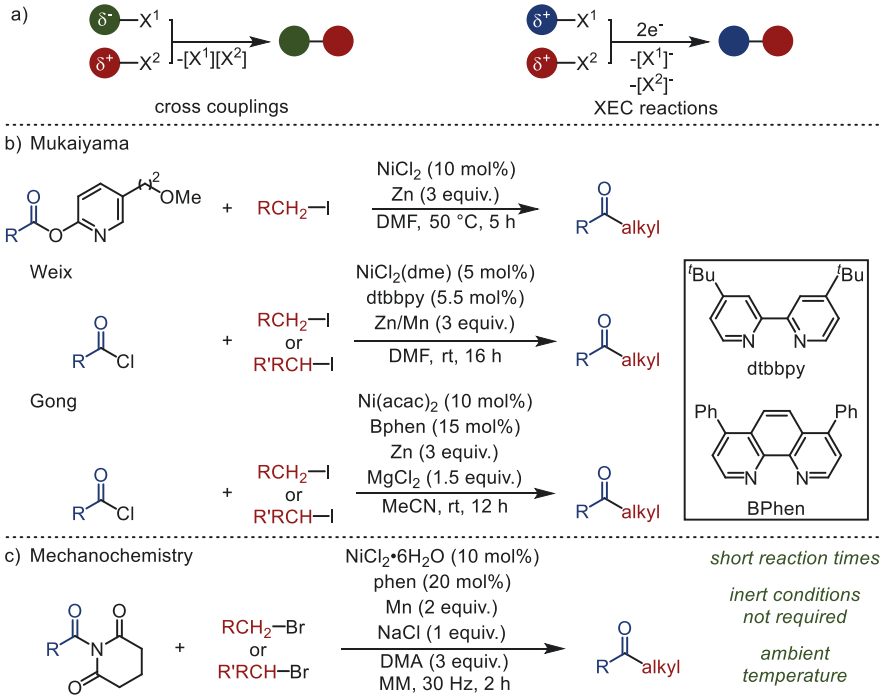

Figure 5.1. [a]General comparison of redox-neutral nucleophile–electrophile couplings versus reductive XEC. [b]Seminal work on nickel-catalyzed acyl–alkyl XECs to access ketones.[3-4] [c]Mechanochemical XEC of a twisted amide with an alkyl bromide.[7]

In this context, and as part of a collaborative project with Ivo Lindenmaier, we aimed to expand mechanochemical C(sp^2)–C(sp^3) XECs by exploring thioesters, specifically as readily available and bench-stable acyl donors, in couplings with alkyl bromides.

5.2 Concept

Thioesters, particularly *S*-pyridyl thioesters, are well-established acylating agents in conventional XECs.[4a, 8] However, we sought to investigate the more common but less reactive and explored variants, such as *S*-alkyl and *S*-phenyl thioesters,[9] for use in mechanochemically mediated XECs with alkyl halides.

Preliminary experiments revealed that *S*-phenyl thioesters were competent coupling partners under mechanochemical conditions, delivering the desired ketone products. Encouraged by

these results, we initiated a bachelor thesis project focused on the systematic optimization of this transformation.

The following section summarizes the optimization studies carried out by Pascal Faßnacht, conducted under my supervision as part of his bachelor thesis.[10]

5.3 Optimization

5.3.1 Ligand Screening

The optimization of the reaction was initiated with a ligand screening, evaluating a total of 16 nitrogen-based, two phosphine, and one *N*-heterocyclic carbene (NHC) ligands under mechanochemical conditions. Among the ligands tested, the bidentate nitrogen ligands dtbbpy (**L12**) and phen (**L7**) provided the highest yields, affording the desired ketone in 54% and 44% yield, respectively (Table 5.1, entries 1 and 2).

Several other bidentate ligands from the phenanthroline and bipyridine families (**L8**, **L11** and **L13**–**L15**) gave low to moderate yields (20–34%) despite achieving high conversions of the thioester **8** (Table 5.1, entries 3–5, 7, 8). In contrast, sterically demanding phen-type ligands such as bathocuproine (**L10**) and neocuprine (**L9**) led to severely diminished yields (Table 5.1, entries 15 and 16), suggesting that increased bulk hinders catalyst performance. Related bidentate nitrogen ligands such as BOX (**L16**) and PyOX (**L17**) delivered comparable but limited yields (22% and 20%, respectively; Table 5.1, entries 6 and 9). Tridentate ligands, including terpyridine (**L20**), along with PyBOX derivatives (**L18**, **L19**), showed uniformly poor reactivity, affording less than 20% yield (Table 5.1, entries 10–12, 14). Furthermore, **L21** furnished no observable product (Table 5.1, entry 20). Similarly, the monodentate pyridine (**L6**) failed to efficiently promote the transformation, resulting in a mere 4% yield (Table 5.1, entry 13).

Phosphine-based ligands, including PPh_3 (**L23**) and dppf (**L24**), as well as the NHC ligand (**L22**), were ineffective under the reaction conditions, delivering only trace amounts of the desired product (<2%, Table 5.1, entries 17–19).

Table 5.1. Ligand screening for the nickel catalyzed XEC of an alkyl bromide with a *S*-phenyl thioester mediated by mechanochemistry.

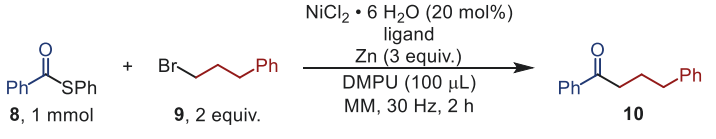

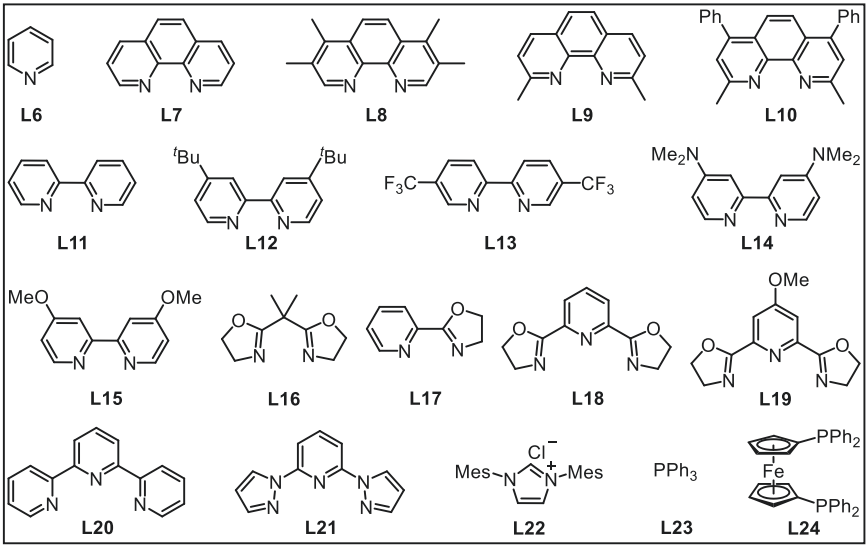

Entry	Ligand / Loading (mol%)		Yield (%)[a]	Conversion 8 / 9 (%)[a]	
1	dtbbpy (**L12**)	40	54	quant.	63
2	phen (**L7**)	40	44	55	36
3	$^{3,4,7,8\text{-Me}}$phen (**L8**)	40	34	43	36
4	$^{5,5'\text{-CF3}}$bpy (**L13**)	40	29	quant.	6
5	bpy (**L11**)	40	24	86	46
6	BOX (**L16**)	40	22	62	19
7	$^{4,4'\text{-NMe2}}$bpy (**L14**)	40	21	38	38
8	$^{4,4'\text{-OMe}}$bpy (**L15**)	40	20	25	21
9	PyOX (**L17**)	40	20	25	32
10	Terpy (**L20**)	40	19	52	81
11	Terpy (**L20**)	20	17	48	69
12	$^{4\text{-OMe}}$PyBOX (**L19**)	40	9	31	27

13	Pyridine (**L6**)	80	4	25	53
14	PyBOX (**L18**)	40	4	86	28
15	Neocuprine (**L9**)	40	2	59	31
16	Bathocuproine (**L10**)	40	1	53	23
17	IMes•HCl[b] (**L22**)	20	1	30	62
18	PPh_3 (**L23**)	40	1	33	40
19	dppf (**L24**)	20	1	34	36
20	bpp (**L21**)	40	0	31	19

Reaction conditions: **8** (1 mmol, 1.0 equiv.), **9** (2.0 equiv.), $NiCl_2(H_2O)_6$ (20 mol%), ligand (20 – 80 mol%), Zn (3 equiv.), DMPU (100 µL), MM (30 Hz, 2 h). [a]Determined by GC-FID using *n*-pentadecane as an internal standard. [b]Cs_2CO_3 (40 mol%).

5.3.2 LAG Additive Screening

Following the identification of **L7** and **L12** as the most effective ligands, a screening of liquid-assisted grinding (LAG) additives was conducted to assess their impact on reaction efficiency (Table 5.2). Amide- and urea-derived solvents proved most effective for both ligands, with DMPU delivering the highest yields (24–54%; Table 5.2, entries 1, 3, 6, 17).

MeOH also performed well: 31% with **L7** and 47% with **L12** (Table 5.2, entries 4 and 23), prompting further investigations into alcoholic solvents. An inverse correlation between steric bulk and reactivity was observed. More hindered alcohols such as ^{i}PrOH and ^{t}BuOH resulted in lower yields (Table 5.2, entries 8 and 10), while EtOH gave moderate results (27%; Table 5.2, entry 5). Among other solvents, MeCN showed fair activity (22%; Table 5.2, entry 7), whereas THF, toluene, H_2O, HFIP, and PhCN all led to poor yields (9–15%; Table 5.2, entries 9, 11–14).

In solvent mixtures, a 1:1 ratio of DMA/MeOH with **L7** slightly improved the yield (49%; Table 5.2, entry 15). However, all tested mixtures using **L12**, including MeOH/DMA, DMPU/MeOH, and DMA/EtOAc, led to marginally reduced yields compared to neat DMPU (Table 5.2, entries 24–26).

Table 5.2. LAG additive screening for the nickel catalyzed XEC of an alkyl bromide with a *S*-phenyl thioester mediated by mechanochemistry.

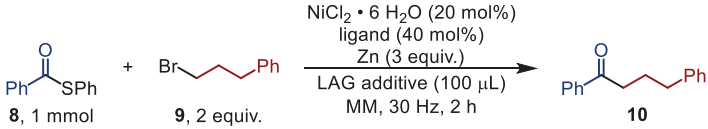

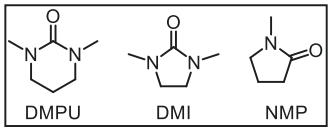

Entry	LAG	Ligand	Yield (%)[a]	Conversion 8 / 9 (%)[a]	
1	DMPU	**L7**	44	55	36
2	NMP	**L7**	32	54	37
3	DMF	**L7**	32	67	35
4	MeOH	**L7**	31	62	25
5	EtOH	**L7**	27	54	26
6	DMI	**L7**	24	48	26
7	MeCN	**L7**	22	61	13
8	^{i}PrOH	**L7**	20	35	24
9	THF	**L7**	15	41	9
10	^{t}BuOH	**L7**	14	33	18
11	toluene	**L7**	11	29	9
12	H_2O	**L7**	9	27	9
13	HFIP	**L7**	9	19	23
14	PhCN	**L7**	9	39	8
15	DMA/MeOH (1:1)	**L7**	49	quant.	44
16	/	**L7**	8	23	/
17	DMPU	**L12**	54	quant.	63
18	DMA	**L12**	51	quant.	51
19[b]	DMA	**L12**	35	85	24
20[c]	DMA	**L12**	51	90	50
21[d]	DMA	**L12**	43	75	39
22[e]	DMA	**L12**	39	71	40

23	MeOH	**L12**	47	95	34
24	DMA/MeOH (1:1)	**L12**	45	quant.	44
25	DMPU/MeOH (1:1)	**L12**	43	85	44
26	DMA/EA (1:1)	**L12**	41	92	28

Reaction conditions: **8** (1 mmol, 1.0 equiv.), **9** (2.0 equiv.), $NiCl_2(H_2O)_6$ (20 mol%), ligand (40 mol%), Zn (3 equiv.), LAG additive (100 µL), MM (30 Hz, 2 h). [a]Determined by GC-FID using *n*-pentadecane as an internal standard. [b]DMA (50 µL). [c]DMA (200 µL). [d]**L12** (21 mol%). [e]**L12** (10 mol%).

5.3.3 Nickel-Source Screening

As **L12** consistently outperformed **L7**, subsequent screening of nickel(II) salts was conducted exclusively with **L12** (Table 5.3). A marked decrease in yield was observed when deviating from $NiCl_2(H_2O)_6$, which remained the optimal Ni(II) source (Table 5.3, entries 1–7). Notably, even the use of a pre-formed Ni(**L12**) complex, generated from $NiCl_2(H_2O)_6$, resulted in reduced yields. This loss in activity could only be partially recovered by the addition of extra **L12** (Table 5.3, entries 8 and 9).

Table 5.3. Nickel-source screening for the nickel catalyzed XEC of an alkyl bromide with a *S*-phenyl thioester mediated by mechanochemistry.

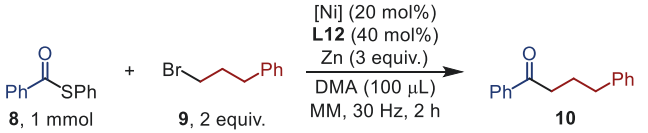

Entry	Ni Source	Ni loading	Yield (%)[a]	Conversion 8 / 9 (%)[a]	
1	$NiCl_2(H_2O)_6$	20	51	quant.	51
2	$NiBr_2$(diglyme)	20	29	84	36
3	$Ni(acac)_2$	20	18	63	51
4	$NiCl_2$(DME)	20	18	63	47
5	$NiCl_2$	20	17	70	61
6	$Ni(OTf)_2$	20	17	73	17
7	$Ni(OAc)_2(H_2O)_4$	20	13	quant.	59
8[b]	Ni(**L12**)$Cl_2(H_2O)_4$	40	12	96	16
9[c]	Ni(**L12**)$Cl_2(H_2O)_4$	40	23	quant.	32

Reaction conditions: **8** (1 mmol, 1.0 equiv.), **9** (2.0 equiv.), Ni source (20–40 mol%), **L12** (40 mol%), Zn (3 equiv.), DMA (100 µL), MM (30 Hz, 2 h). [a]Determined by GC-FID using *n*-pentadecane as an internal standard. [b]Without ligand. [c]Additional **L12** (20 mol%).

5.3.4 Reductant Screening

Substitution of zinc powder with alternative reductants led to reduced yields overall (Table 5.4). Among the tested reductants, TDAE and manganese showed moderate performance (Table 5.4, entries 2 and 3), whereas all other reductants resulted in poor outcomes.

Table 5.4. Reductant screening for the nickel catalyzed XEC of an alkyl bromide with a *S*-phenyl thioester mediated by mechanochemistry.

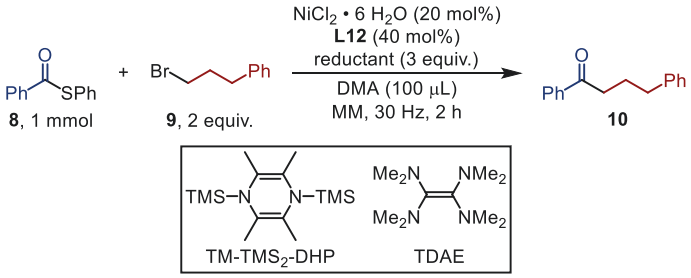

Entry	reductant	Yield (%)[a]	Conversion 8 / 9 (%)[a]	
1	Zn	51	quant.	51
2	TDAE	27	39	15
3	Mn	21	63	30
4	Mg	2	quant.	quant.
5	TM-TMS$_2$-DHP	0	43	20

Reaction conditions: **8** (1 mmol, 1.0 equiv.), **9** (2.0 equiv.), $NiCl_2(H_2O)_6$ (20 mol%), **L12** (40 mol%), reductant (3 equiv.), DMA (100 µL), MM (30 Hz, 2 h). [a]Determined by GC-FID using *n*-pentadecane as an internal standard.

5.3.5 Additive Screening

To further improve the reaction yield, a variety of additives were screened (Table 5.5). Among them, pyridine and Ph_3PO provided the most promising results, each moderately increasing the yield of the desired ketone (Table 5.5, entries 2 and 3). Both Lewis bases may act by coordinating *in situ* generated Lewis acidic zinc(II)-salts,[11] which appear to inhibit catalysis (Table 5.5, entry 13).

Encouraged by the effect of pyridine, derivatives, including picoline, 2,4,6-collidine, and DMAP were evaluated. However, all led to diminished yields, likely due to steric or electronic mismatches (Table 5.5, entries 4, 8, 9).

Given that Ph_3PO could potentially be reduced to PPh_3 under the reaction conditions, the latter was tested independently, clarifying which species was responsible for the observed effect. The sharp decrease in yield upon PPh_3 addition (Table 5.5, entry 11) confirmed that Ph_3PO, and not its reduced form, was the active additive.

To assess whether water present in hydrated nickel salts played a beneficial role, excess H_2O was added to the reaction. As the yield remained largely unchanged, it was concluded that while water is not beneficial, the reaction is neither moisture sensitive (Table 5.5, entry 5).

In an effort to scavenge liberated thiol byproducts, copper(I)-salts, namely CuCl and CuTc were tested (Table 5.5, entries 6 and 14).[12] Both negatively affected the yield, likely due to their inherent Lewis acidity as thiol scavengers. Similarly, additives such as $Fe(acac)_3$ and $MgCl_2(H_2O)_6$ also reduced the reaction efficiency (Table 5.5, entries 7, 12), reinforcing the conclusion that Lewis acidic metal salt are generally unfavorable additives.

Finally, inspired by the work of the MacMillan group, phthalimide was evaluated as an additive but showed no beneficial effect in this system (Table 5.5, entry 10).[13]

Table 5.5. Additive screening for the nickel catalyzed XEC of an alkyl bromide with a *S*-phenyl thioester mediated by mechanochemistry.

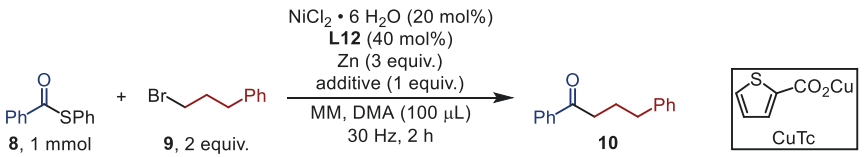

Entry	Additive	Yield (%)[a]	Conversion 8 (%)[a]	Conversion 9 (%)[a]
1	/	51	quant.	51
2	PyH	64	quant.	90
3	Ph_3PO	60	97	68
4	Picoline	53	94	79
5[b]	H_2O	47	quant.	43
6	CuCl	43	82	42
7	$Fe(acac)_3$	43	42	78
8	2,4,6-Collidine	41	88	50
9	DMAP	32	94	78
10	Phthalimide	28	89	29

11	PPh_3	19	58	54
12	$MgCl_2(H_2O)_6$	16	59	13
13	$ZnBr_2$	6	30	7
14	CuTc	4	38	85
15	LiI	2	11	38

Reaction conditions: **8** (1 mmol, 1.0 equiv.), **9** (2.0 equiv.), $NiCl_2(H_2O)_6$ (20 mol%), **L12** (40 mol%), Zn (3 equiv.), additive (1 equiv.), DMA (100 µL), MM (30 Hz, 2 h). [a]Determined by GC-FID using *n*-pentadecane as an internal standard. [b]H_2O (1.4 equiv.)

Building on the beneficial effect of Ph_3PO, further screening was carried out to evaluate its influence under modified reaction conditions (Table 5.6). Increasing the amount of Ph_3PO proved advantageous, affording 71% of **10**, even at a reduced catalyst loading (Table 5.6, entry 2).

In contrast, lowering the amount of zinc consistently reduced the yield, regardless of catalyst or alkyl halide loading (Table 5.6, entries 3–5). Although MeOH had shown promise during the LAG additive screening, its usage under these conditions led to a reduction in yield (Table 5.6, entry 6).

Table 5.6. Ph_3PO additive screening for the nickel catalyzed XEC of an alkyl bromide with a *S*-phenyl thioester mediated by mechanochemistry.

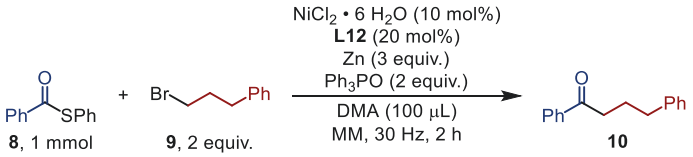

8, 1 mmol + **9**, 2 equiv. → **10**

Entry	Deviation from Conditions Above	Yield (%)[a]	Conversion 8 / 9 (%)[a]	
1[b]	[Ni] (20 mol%), Ph_3PO (3.0 equiv.)	60	97	68
2	None	71	88	69
3	Zn (2.0 equiv.)	52	66	50
4[c]	[Ni] (5 mol%), Zn (2.0 equiv.)	46	56	42
5	**9** (1.3 equiv.), Zn (2.0 equiv.)	43	56	71
6	MeOH as LAG additive	47	77	44

Reaction conditions: **8** (1 mmol, 1.0 equiv.), **9** (2.0 equiv.), Ni source (10 mol%), **L12** (20 mol%), Zn (3 equiv.), Ph_3PO (2.0 equiv.), DMA (100 µL), MM (30 Hz, 2 h). [a]Determined by GC-FID using *n*-pentadecane as an internal standard. [b]**L12** (40 mol%). [c]**L12** (10 mol%).

Analogous to the screening with Ph_3PO, reaction conditions incorporating pyridine as an additive were further optimized (Table 5.7). The reaction tolerated a reduction in zinc (Table 5.7, entry 2) and catalyst loading (Table 5.7, entry 3) without significant loss in yield. However, reducing the amount of alkyl halide or pyridine led to diminished performance (Table 5.7, entries 4 and 5). In contrast, increasing the pyridine amount enhanced the yield (Table 5.7, entry 6), and at elevated pyridine concentrations, lower ligand loadings became tolerable (Table 5.7, entry 7). Under these conditions, reduction of zinc equivalents was also feasible without compromising efficiency (Table 5.7, entry 8). A decrease in catalyst loading to 5 mol% was accompanied by a slight drop in yield (Table 5.7, entry 9), and therefore 10 mol% was selected for subsequent studies. The observed tolerance to ligand reduction (Table 5.7, entry 7) was specific to high catalyst loadings. At 10 mol% catalyst, reducing the ligand loading was accompanied by a decrease in yield (Table 5.7, entry 10). Additionally, use of a preformed $Ni(phen)Cl_2$ complex resulted in slightly lower yields (entry 11).

Replacing DMA with MeOH led to comparable results (Table 5.7, entry 12), but again, lowering the alkyl halide equivalents negatively impacted the outcome (Table 5.7, entry 13). In this system, a 5 mol% catalyst loading remained effective (Table 5.7, entry 14), and although further increasing pyridine did not improve the yield, it reduced alkyl halide consumption, thereby minimizing byproduct formation (Table 5.7, entry 15).

A key finding was that pyridine could function as the LAG additive itself, eliminating the need for additional solvents, while even slightly improving the yield (Table 5.7, entry 16). This discovery enabled further exploration of minimal conditions: reductions in ligand, catalyst, zinc, and halide equivalents were all tolerated (Table 5.7, entries 17–20), though such minimization was avoided in the final protocol to retain operational freedom during scope investigations. Similarly, while lower pyridine loading was feasible (Table 5.7, entry 21), the higher concentration was maintained to ensure robustness, given the prior observed sensitivity. Attempts to simultaneously minimize multiple variables led to decreased yields and reproducibility issues (Table 5.7, entry 22), underscoring the optimization limits of the developed system. Finally, the addition of NaCl proved beneficial, delivering an improved yield and defining the optimized conditions used in subsequent scope studies (Table 5.7, entry 23).[7]

Table 5.7. Pyridine additive screening for the nickel catalyzed XEC of an alkyl bromide with a *S*-phenyl thioester mediated by mechanochemistry.

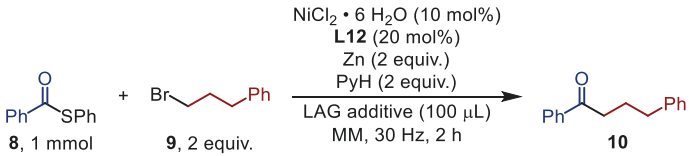

Entry	LAG	Deviation from Conditions Above	Yield (%)[a]
1[b]	DMA	[Ni] (20 mol%), Zn (3 equiv.), PyH (1 equiv.)	64
2[b]	DMA	[Ni] (20 mol%), PyH (1 equiv.)	61
3	DMA	Zn (3equiv.), PyH (1 equiv.)	60
4[b]	DMA	[Ni] (20 mol%), **9** (1.3 equiv.), Zn (3 equiv.), PyH (1 equiv.)	48
5[b]	DMA	[Ni] (20 mol%), Zn (3equiv.), PyH (0.25 equiv.)	51
6[b]	DMA	[Ni] (20 mol%), Zn (3 equiv.)	76
7	DMA	[Ni] (20 mol%), **L12** (20 mol%)	75
8	DMA	None	72
9[c]	DMA	[Ni] (5 mol%)	51
10	DMA	**L12** (11 mol%)	62
11	DMA	$Ni(phen)Cl_2$ (10 mol%) instead of $NiCl_2(H_2O)_6$ and **L12**	63
12	MeOH	None	77
13	MeOH	**9** (1.5 equiv.)	69
14[c]	MeOH	[Ni] (5 mol%)	81
15	MeOH	[Ni] (5 mol%), PyH (3 equiv.)	80
16	PyH[d]	None, PyH (2 equiv.)	87
17	PyH[d]	**L12** (11 mol%)	89
18	PyH[d]	**9** (1.5 equiv.)	92
19	PyH[d]	Zn (1.5 equiv.)	86
20[c]	PyH[d]	[Ni] (5 mol%)	80
21	PyH	None	89
22[e]	PyH	**9** (1.5 equiv.), **L12** (11 mol%)	70
23	PyH[d]	NaCl (2 equiv.) as additive	quant.
24	PyH[d]	Without $NiCl_2(H_2O)_6$	2

Reaction conditions: **8** (1 mmol, 1.0 equiv.), **9** (2.0 equiv.), Ni source (10 mol%), **L12** (20 mol%), Zn (2 equiv.), Pyridine (2.0 equiv.), DMA (100 µL), MM (30 Hz, 2 h). [a]Determined by GC-FID using *n*-pentadecane as an internal standard. [b]**L12** (40 mol%). [c]**L12** (10 mol%). [d]Pyridine (2 equiv.). [e]1 h.

5.3.6 Reaction Time Screening

A key advantage of mechanochemical XECs is their significantly reduced reaction time compared to conventional methods. Thus, the optimal reaction time for the model system was assessed. Notably, full conversion of the alkyl bromide was achieved within 30 min (Table 5.8). However, to accommodate potentially more challenging substrates during scope studies, a 1 h reaction time was selected as the standard.

Table 5.8. Reaction time screening for the nickel catalyzed XEC of an alkyl bromide with a *S*-phenyl thioester mediated by mechanochemistry.

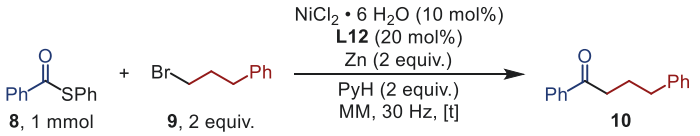

Entry	Time (h)	Yield (%)[a]	Conversion 8 / 9 (%)[a]	
1	2	87	quant.	quant.
2	1	94	quant.	81
3	0.5	92	quant.	61
4	0.25	78	84	44

Reaction conditions: **8** (1 mmol, 1.0 equiv.), **9** (2.0 equiv.), $NiCl_2(H_2O)_6$ (10 mol%), **L12** (20 mol%), reductant (2 equiv.), Pyridine (2 equiv.), MM (30 Hz). [a]Determined by GC-FID using *n*-pentadecane as an internal standard.

Following optimization, the model substrate was isolated under the standard conditions, affording the desired product in 85% yield (Scheme 5.1). This result establishes the foundation for the ongoing work on the substrate scope.

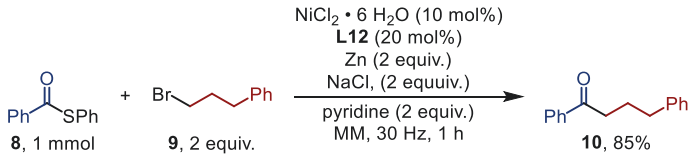

Scheme 5.1. Isolated yield of the model ketone obtained from the standard conditions for the nickel catalyzed XEC of an alkyl bromide with a S–Ph thioester mediated by mechanochemistry.

5.3.7 Experimental Details

Chemicals and General Techniques

Mechanochemical reactions were set up without taking special precautions towards reaction atmosphere utilizing the Mixer Mill MM 400 (Retsch) in a stainless steel jar (10 mL) with two stainless steel balls (⌀ = 10 mm, m = 4 g). Chemicals were purchased from abcr, BLDpharm, fluorochem, Sigma-Aldrich, Thermo Fischer, Acros or TCI and were used without further purification.

Analytical Techniques

GC-LR-MS (EI) analysis was carried out with an Agilent 7820A/5977B GC-system/MSD employing an Agilent 190915-433UI column (30 m × 250 µm × 0.25 µm). Program: 50 °C – 280 °C over 15 minutes.

GC-FID analysis was performed on an Agilent 7820A system with an Agilent 19091J-431 column (30 m × 320 µm × 0.25 µm), utilizing H_2 as the carrier gas. The program used heated from 50 °C to 280 °C within 55 min.

Reaction Screening

A 10 mL stainless steel milling jar was charged with the respective nickel source (5–20 mol%), ligand (10–80 mol%), *S*-phenyl benzothioate (1.0 mmol, 1.0 equiv.), reductant (1.5–3.0 equiv., if solid), potential additive (1.0–2.0 equiv., if solid) and two stainless steel balls (⌀ = 10 mm, m = 4 g). Subsequently, all liquid components: hydrocinnamyl bromide (1.3–2.0 equiv.), LAG additive (100 µL), reductant (3.0 equiv., if liquid) and potential additive (0.3–3.0 equiv., if liquid) were added. The milling jar was closed, placed in a MM 400 and shaken at 30 Hz for the respective time (0.25–2 h). After the reaction, the jar was opened and *n*-pentadecane and EtOAc were added. An aliquot was taken and filtered through Celite, Al_2O_3 and $MgSO_4$, before being analyzed by GC-MS/FID.

5.4 References

[1] L. E. Ehehalt, O. M. Beleh, I. C. Priest, J. M. Mouat, A. K. Olszewski, B. N. Ahern, A. R. Cruz, B. K. Chi, A. J. Castro, K. Kang, J. Wang, D. J. Weix, *Chem. Rev.* **2024**, *124*, 13397-13569.

[2] P. Ertl, T. Schuhmann, *J. Nat. Prod.* **2019**, *82*, 1258-1263.

[3] M. Onaka, Y. Matsuoka, T. Mukaiyama, *Chem. Lett.* **1981**, *10*, 531-534.

[4] a) A. C. Wotal, D. J. Weix, *Org. Lett.* **2012**, *14*, 1476-1479; b) F. Wu, W. Lu, Q. Qian, Q. Ren, H. Gong, *Org. Lett.* **2012**, *14*, 3044-3047.

[5] a) A. C. Jones, W. I. Nicholson, J. A. Leitch, D. L. Browne, *Org. Lett.* **2021**, *23*, 6337-6341; b) S. Wu, W. Shi, G. Zou, *New J. Chem.* **2021**, *45*, 11269-11274; c) M. T. J. Williams, L. C. Morrill, D. L. Browne, *Adv. Synth. Catal.* **2023**, *365*, 1477-1484.

[6] a) Q. Cao, J. L. Howard, E. Wheatley, D. L. Browne, *Angew. Chem. Int. Ed.* **2018**, *57*, 11339-11343; b) Q. Cao, R. T. Stark, I. A. Fallis, D. L. Browne, *ChemSusChem* **2019**, *12*, 2554-2557; c) J. Yin, R. T. Stark, I. A. Fallis, D. L. Browne, *J. Org. Chem.* **2020**, *85*, 2347-2354.

[7] A. C. Jones, M. T. J. Williams, L. C. Morrill, D. L. Browne, *ACS Catal.* **2022**, *12*, 13681-13689.

[8] a) Y. Ai, N. Ye, Q. Wang, K. Yahata, Y. Kishi, *Angew. Chem. Int. Ed.* **2017**, *56*, 10791-10795; b) J. Wang, B. P. Cary, P. D. Beyer, S. H. Gellman, D. J. Weix, *Angew. Chem. Int. Ed.* **2019**, *58*, 12081-12085; c) A. Umehara, Y. Kishi, *Chem. Lett.* **2019**, *48*, 947-950.

[9] A. Haupt, I. Fleischer, *ChemCatChem* **2025**, *17*, e202500221.

[10] P. Faßnacht, Eberhard Karls Universität Tübingen **2025**.

[11] D. C. Batesky, M. J. Goldfogel, D. J. Weix, *J. Org. Chem.* **2017**, *82*, 9931-9936.

[12] L. S. Liebeskind, J. Srogl, *J. Am. Chem. Soc.* **2000**, *122*, 11260-11261.

[13] C. N. Prieto Kullmer, J. A. Kautzky, S. W. Krska, T. Nowak, S. D. Dreher, D. W. C. MacMillan, *Science* **2022**, *376*, 532-539.

PUBLICATIONS

6 Publications

Publication A1: Reprinted *via* „free reuse" policy from *Angew. Chem. Int. Ed.* **2024**, *63*, e202405818.

Publication A2: Reprinted with permission from *Org. Lett*. **2025**, *27*, 21, 5385–5389. Copyright 2025 American Chemical Society.

How to cite: *Angew. Chem. Int. Ed.* **2024**, *63*, e202405818
doi.org/10.1002/anie.202405818

Photoisomerization **Hot Paper**

Facile Energy Release from Substituted Dewar Isomers of 1,2-Dihydro-1,2-Azaborinines Catalyzed by Coinage Metal Lewis Acids

Robert C. Richter, Sonja M. Biebl, Ralf Einholz, Johannes Walz, Cäcilia Maichle-Mössmer, Markus Ströbele, Holger F. Bettinger, and Ivana Fleischer**

Dedicated to Professor Lars Wesemann on the occasion of his 60th birthday.

Abstract: Molecular solar thermal systems (MOST) represent an auspicious solution for the storage of solar energy. We report silver salts as a unique class of catalysts, capable of releasing the stored energy from the promising 1,2-dihydro-1,2-azaborinine based MOST system. Mechanistic investigations provided insights into the silver catalyzed thermal backreaction, concurrently unveiling the first crystal structure of a 2-aza-3-borabicyclo[2.2.0]hex-5-ene, the Dewar isomer of 1,2-dihydro-1,2-azaborinine. Quantification of activation energies by kinetic experiments has elucidated the advantageous energy change associated with Lewis acid catalysts, a phenomenon corroborated through computational analysis. By means of low temperature NMR spectroscopy, mechanistic insights into the coordination of Ag^+ to the 1,2-dihydro-1,2-azaborinine were gained.

Introduction

The use and storage of solar energy constitute essential tools for the shift towards sustainable energy production. Presently, solar energy is predominantly utilized via photovoltaic technology, which can be coupled to batteries to store the captured energy. However, the efficacy of these technologies is contingent upon variables like spatial and temporal constraints. To overcome these fluctuations, simple solutions for the storage of solar energy are a crucial facet of ongoing research.

Molecular concepts, such as molecular solar thermal energy storage (MOST) systems could complement established technologies on a small scale.[1] A photo isomer pair is considered a MOST system when irradiation of the low energy molecular entity leads reversibly to a metastable isomer. The stored energy can be released as heat upon demand, e.g. via the action of a catalyst. The most thoroughly studied system is the valence isomer pair norbornadiene/quadricyclane (Scheme 1a), which was already deployed in proof-of-concept devices.[2] Nonetheless, numerous alternative MOST systems such as the E/Z diazobenzene (Scheme 1a),[3] dihydroazulene/vinylheptafulvene[4] or the fulvalene diruthenium system[5] each offer distinct benefits and merit further studies, since no molecular pair fulfils all requirements of the ideal MOST system.

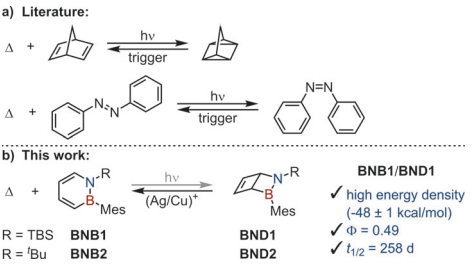

Scheme 1. Examples of MOST systems investigated in current literature (a), and our contribution (b).TBS = *tert*-butyldimethylsilyl, Mes = mesityl.

[*] R. C. Richter, S. M. Biebl, Dr. R. Einholz, J. Walz, Prof. H. F. Bettinger, Prof. I. Fleischer
Institute of Organic Chemistry, Faculty of Science, Eberhard Karls Universität Tübingen, Auf der Morgenstelle 18, 72076 Tübingen, Germany
E-mail: holger.bettinger@uni-tuebingen.de
ivana.fleischer@uni-tuebingen.de
Dr. C. Maichle-Mössmer, Dr. M. Ströbele
Institute of Inorganic Chemistry, Faculty of Science, Eberhard Karls Universität Tübingen, Auf der Morgenstelle 18, 72076 Tübingen, Germany
Prof. H. F. Bettinger
Center for Light-Matter Interaction, Sensors & Analytics (LISA+) at the University of Tübingen, Auf der Morgenstelle 18, 72076 Tübingen, Germany
J. Walz
Current address: Institute of Organic Chemistry, Albert-Ludwigs-University Freiburg, Albertstr. 21, 79104 Freiburg, Germany

The 1,2 BN isostere of benzene, 1,2-dihydro-1,2-azaborinine, was introduced as a novel MOST system by Liu, Bettinger and co-workers in 2018,[6] following the observation of the selective valence isomerization via electrocyclization upon UV irradiation under matrix isolation conditions.[7] Its derivative 1,2-dihydro-1-*tert*-butyldimethylsilyl-2-mesityl-1,2-azaborinine (**BNB1**) carrying bulky groups on the boron and nitrogen atoms underwent selective valence isomerization to its isolable Dewar isomer (**BND1**) upon irradiation in solution at ambient temperature (Scheme 1b).[6] The **BNB1**-**BND1** isomer pair has promising properties compared to other MOST systems: a high energy density (-48 ± 1 kcal/mol) along with a high quantum yield for photoisomerization and a long half-life of the metastable isomer (Scheme 1b).[6]

The Dewar isomers of 1,2-dihydro-1,2-azaborinines were employed by Liu and co-workers for the synthesis of aminoborylated cyclobutanes,[8] while Liu, Jäkle and co-workers achieved polymers containing the 1,2-azaboretidine ring from these monomers.[9] Yet, the efficient and controlled energy release, a decisive characteristic of a successful MOST system, has received limited attention. The only catalyst able to trigger the cycloreversion of **BND1** was reported to be Wilkinson's catalyst.[6] Although this Rh-based complex showed good performance in transforming **BND1** to **BNB1** at 3 mol% in less than 1 h, its economic viability is limited due to the use of the precious metal. Hence, endeavours towards alternative catalysts are important for development of MOST systems. For instance, Ag^+ salts have been employed in the NBD/QC system,[2d,10] and are known to facilitate electrocyclic reactions in strained ring systems, such as cubane[11] and tricyclooctadiene.[12]

Herein, we show that Ag^+ and Cu^+ are efficient catalysts for the electrocyclic ring opening of Dewar isomers of 1,2-dihydro-1,2-azaborinine derivatives. By combination of NMR spectroscopy, single crystal X-ray crystallography, kinetic measurements, and computational methods the mechanism for the catalyzed isomerization could be substantiated for **BND1** and for the new derivative 2-*tert*-butyl-3-mesityl-2-aza-3-borabicyclo[2.2.0]hex-5-ene (**BND2**) leading to the respective valence isomers **BNB1** and 1,2-dihydro-1-*tert*-butyl-2-mesityl-1,2-azaborinine (**BNB2**).

Results and Discussion

Known for its weakly coordinating anion, $AgSbF_6$ is frequently employed for the activation of other catalysts in C–C bond cleavage reactions.[13] Indeed, we identified the commercially available $AgSbF_6$ as a potent catalyst enabling the quantitative cycloreversion of **BND1** within 24 h at ambient temperature in DCM (Table 1, entry 1). The weakly coordinating character of SbF_6^- proved to be a crucial facet of an efficient Ag^+ catalyst during optimization. Coordinating anions found in compounds like $AgNO_3$ led to complete suppression of the cycloreversion of **BND1** (Table 1, entries 2–4). This limitation partially results from their poor solubility in organic solvents, but primarily from their relatively low Lewis acidity. In contrast, Ag^+ salts with relatively weakly coordinating anions (WCA) (Table 1, entries 5–7), such as $AgClO_4$, displayed elevated catalytic activity despite their low solubility, albeit not reaching full conversion. Nonetheless, slight increase of the temperature facilitated the quantitative cycloreversion (Table 1, entry 8). Interestingly, $AgPF_6$ deviated from the expected behavior; while the PF_6^- anion was anticipated to behave similarly to its higher homologue SbF_6^-, it lacked discernible catalytic activity (Table 1, entry 9).

Table 1: Screening of the silver and copper based catalysts for the cycloreversion of the Dewar valence isomer of **BNB1**.[a]

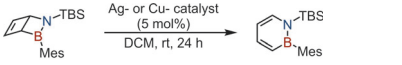

BND1 **BNB1**

Entry	Catalyst	Yield (%)[b]
1	$AgSbF_6$	quant.
2	$AgNO_3$	0
3	$AgCF_3CO_2$	0
4	$AgCF_3SO_3$	traces
5[c]	$AgClO_4$	43
6	$AgBF_4$	51
7	$AgNTf_2$	38
8[c]	$AgNTf_2$	quant.
9	$AgPF_6$	0
10	$Ag[Al(OC(CF_3)_3)_4]$[d]	quant. (99[e])
11	Ag nanoparticles	0
12	$[Cu][Al(OC(CF_3)_3)_4]$[f]	quant.
13	CuI	0

[a] Reaction conditions: **BND1** (150 µmol), Ag source (5 mol%), DCM (0.5 mL), rt ≈ 298 K, 24 h. [b] GC-FID-yields using *n*-pentadecane as a standard. [c] rt ≈ 303 K. [d] Reaction conditions: **BND1** (500 µmol), $Ag[Al(OC(CF_3)_3)_4]$ (5 mol%), DCM-d_2 (1.5 mL), rt (298 K), 5 h. [e] Isolated yield. [f] $[Cu(1,2\text{-}F_2C_6H_4)_n][Al(OC(CF_3)_3)_4]$.

In view of the high catalytic activity attributed to Ag^+ salts bearing weakly coordinating anions we set out to investigate further Ag^+ salts featuring exceedingly weakly coordinating anions such as $[BArF_{24}]^-$ ($[(3,5\text{-}(CF_3)_2C_6H_3)_4B]^-$) and $[BArF_{20}]^-$ ($[B(C_6F_5)_4]^-$). $Ag[BArF_{20}](C_6H_6)_n$ could only slowly cyclorevert **BND1**, while $Ag[BArF_{24}]$ lacked any perceptible catalytic activity, likely due to the coordination of residual solvent. Unfortunately, these Ag salts have not been reported solvent adduct free in the literature.[14] Consequently, $Ag[Al(OC(CF_3)_3)_4]$, which was developed by Krossing and co-workers in 2001,[15] was employed as a strongly Lewis acidic silver salt devoid of residual solvents. Leveraging its increased reactivity, this compound enabled the quantitative cycloreversion of **BND1** within 5 h (298 K, 5 mol%), and **BNB1** could also be isolated by column chromatography in high yield (Table 1, entry 10).

Whilst employing any silver salt in the presence of **BND1** dissolved in DCM or toluene, the formation of Ag(0) precipitate was observed, likely resulting from the oxidation of **BND1**. In order to examine whether Ag(0) is catalytically active, surfactant free silver nanoparticles were tested. Unfortunately, they exhibited no activity, diminishing the possibility of heterogeneous catalysis (Table 1, entry 11).

Employing AuCl in a stoichiometric fashion proved to mediate the cycloreversion of **BND1**. However, due to its elevated redox potential combined with reduced Lewis acidity due to the chloride anion, AuCl was deemed unsuitable for further investigation. Thus, we decided to examine a smaller and more redox neutral Cu(I) based catalyst and chose $[Cu(1,2\text{-}F_2C_6H_4)_n][Al(OC(CF_3)_3)_4]$, which could catalyze the cycloreversion of **BND1** effectively (Table 1, entry 12).[16] Analogously to Ag^+, Cu^+ catalysts require a WCA to exhibit catalytic activity (Table 1, entry 13).

In order to investigate the reaction in more detail, we employed stoichiometric amounts of $AgSbF_6$. We grew crystals of [**BND1**$AgSbF_6]_2$ and [**BNB1**$AgSbF_6]_2$ suitable for single-crystal X-ray analysis from DCM at −40 °C (Figure 1) to analyse the interaction of the Ag^+ with the BN heterocycles. The structure of $[\mathbf{BND1}Ag]_2^{2+}$ (Figure 1a) provides the first structural proof of the Dewar arrangement. The coordination of the Ag^+ ion turned out to be beneficial for crystallization, as previous attempts to crystallize **BND1** have not met with success.[6] This discovery concurrently expands the sparse collection of hetero Dewar benzene crystal structures.[17]

The [**BND1**$AgSbF_6]_2$ assembly manifests a dimeric structure, wherein the **BND1** unit is coordinated η^2 via the C=C double bond of the BN-Dewar moiety and the mesityl substituent to two distinct Ag^+ cations (Figure 1a). The Ag^+/C=C double bond length measures 221.4 pm and is thus shorter than the mesityl/Ag^+ distance of 240.9 pm. Each Ag^+ ion is further coordinated κ^1 by two SbF_6^- anions via fluorine atoms (not depicted in Figure 1 for clarity reasons). This arrangement bridges the $[\mathbf{BND1}Ag]_2^{2+}$-dimers forming one dimensional parallel strings. Hereby, the Ag–F distances measure 244.5 pm and 247.0 pm respectively, which is similar to the values reported for $AgSbF_6$ (250.5 pm).[18]

Comparing the BN-Dewar substructure to an all-carbon Dewar benzene crystal structure,[19] the lower overall symmetry was evident in the molecular geometry. Nonetheless, the small dihedral angle of each fused four membered ring in **BND1** is in agreement with that of the all-carbon Dewar benzene. The short boron-nitrogen bond length (141.4 pm) of **BND1** is indicative of double bond character, and is similar to that computed (139.7 pm) for parent 2-aza-3-borabiyclo[2.2.0]hex-2-ene at the very high CCSD(T) level of theory,[7] and that reported for the respective Dewar borazine ($d(B{=}N)_{avg.} = 137.4$ pm, d(B–N) = 155.5–175.2 pm).[17a] The CB distance (158.9 pm) is longer than the NC distance (146.7 pm) in agreement with structural data of 1,2-azaboretidines.[20] Furthermore, the BN and the C–C bond lengths of the bridgehead carbons of **BND1** (156.6 pm) were found to closely align to the corresponding C–C distance of the 1,2-azaboretidine motif.[20]

A slightly elongated BN-distance was observed for [**BNB1**$AgSbF_6]_2$ (144.6 pm) signifying the aromatic character. Generally, the crystal structure of [**BNB1**$AgSbF_6]_2$ shows resemblance to [**BND1**$AgSbF_6]_2$, with Ag^+ similarly η^2 coordinated to the C=C double bond proximal to the boron atom, and to the mesityl substituent, resulting in a comparable dimeric structure. The average Ag^+/C=C double bond length was found to be 228.4 pm, while the shortest mesityl/Ag^+ ion distance measures 233.2 pm, indicating a stronger coordination of Ag^+ to the C=C bond. Comparable to [**BND1**$AgSbF_6]_2$, the Ag^+ is additionally coordinated by two SbF_6^- units (d(Ag–F) = 251.8 pm, 253.0 pm respectively), which link the $[\mathbf{BNB1}Ag]_2^{2+}$ dimers into linear strings parallel to one another. The structural parameters of the 1,2-dihydro-1,2-azaborinine unit in [**BNB1**$AgSbF_6]_2$

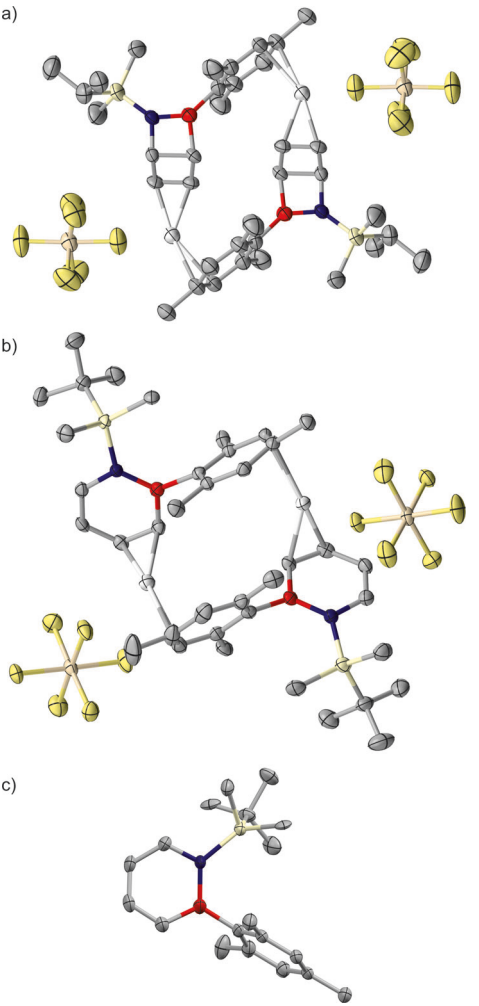

Figure 1. Molecular structures of [**BND1**$AgSbF_6]_2$ (a, CCDC: 2337845), [**BNB1**$AgSbF_6]_2$ (b, CCDC: 2337844), and **BNB1** (c, CCDC: 2298028) in the solid state. Hydrogen atoms were omitted for clarity and the thermal ellipsoids were drawn at 50% probability level.

closely resemble that of free **BNB1** (Figure 1c), with the TBS substituent arranged in the same direction relative to the 1,2-dihydro-1,2-azaborinine plane. Bond lengths of **BNB1** with and without $AgSbF_6$ are similar, with the greatest deviation observed for the C–B bond (**BNB1**: 150.7 pm, [**BNB1**$AgSbF_6$]$_2$: 153.0 pm) and its consecutive C–C bond (**BNB1**: 136.0 pm, [**BNB1**$AgSbF_6$]$_2$: 138.5 pm). Generally, all bonds in the 1,2-dihydro-1,2-azaborinine backbone of the dimer were slightly elongated compared to uncoordinated **BNB1**, and the structural paramters of **BNB1** are similar to those of other 1,2-dihydro-1,2-azaborinines.[21]

Utilizing variable temperature ^{1}H NMR spectroscopy allowed us to observe Ag^+ coordination to **BND1** and **BNB1**. At low temperature (240 K) **BND1** in the presence of Ag^+ experienced a downfield shift of signals of the bicyclic unit. This can be attributed to the transfer of electron density from the BN-Dewar benzene moiety to the silver ion (Figure 2a). Notably, also the aromatic protons of the mesityl moiety were shifted downfield (Figure 2), indicating direct coordination of Ag^+ to the aromatic system of the mesityl substituent. Considering the addition of only 1 equiv. $AgSbF_6$, a dimeric arrangement as in the solid state is proposed based on the geometrical restraints imposed by the morphology of singular **BND1**. At 240 K, the cycloreversion of **BND1** in presence of $AgSbF_6$ was imperceptible for several hours. Upon increasing the temperature to 270 K, a gradual cycloreversion of **BND1** became apparent. The reaction rate further increased appreciably with temperature, thus facilitating the efficient transformation at room temperature.

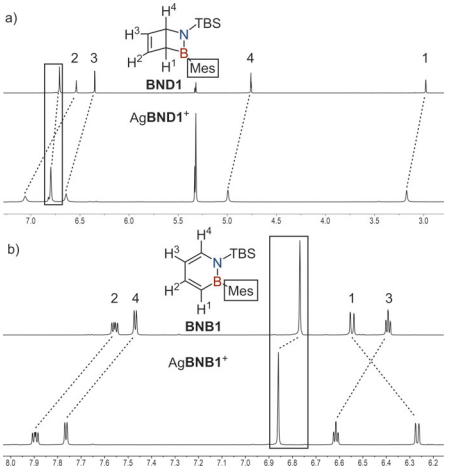

Figure 2. Selected regions of the ^{1}H NMR spectra of **BND1** (a) and **BNB1** (b) in DCM-d_2 compared to **BND1** (a)/**BNB1** (b) with 1 equiv. of $AgSbF_6$ in DCM-d_2. Spectra of **BND1** were measured at 240 K and spectra of **BNB1** at 298 K.

Analogously to **BND1**, the coordination of Ag^+ to **BNB1** is evident from the observed shifts in the ^{1}H NMR in DCM-d_2 (Figure 2b). Once again, the aromatic mesityl protons are also shifted downfield, indicating Ag^+ coordination and hence a dimeric structure consistent with the crystal structure (Figure 1a). Moreover, the chemical shifts of the 1,2-dihydro-1,2-azaborinine backbone further support a dimeric species. Protons H^2, H^3 and H^4 experienced a downfield shift, while proton H^1 is shifted upfield compared to neat **BNB1** in DCM-d_2 (Figure 2b). The upfield shift of H^1 necessitates the intermolecular interaction with the shielding cone of an aromatic group, providing further evidence for a dimeric structure akin to that of the solid state (Figure 3, Figure 1).

As illustrated in Figure 3, the proximity between H^1 and the mesityl substituent coupled with the almost orthogonal orientation of the mesityl group in relation to the plane defined by the 1,2-dihydro-1,2-azaborinine result in projection of a deshielding cone towards H^1, ultimately leading to the observed upfield shift in the ^{1}H NMR spectrum (Figure 3). Such shielding effects are documented in the literature and frequently used for the three-dimensional characterization of nucleotides.[22] Based on these observations, the likelihood that the downfield shift of the aromatic mesityl protons originates from a dynamic process unresolved within the NMR timescale can reasonably be discounted. Moreover, the postulated dimeric structures of **BNB1** and **BND1** with $AgSbF_6$ in solution align with the observed crystal structures (Figure 1).

The measured NMR spectra of **BND1** and **BNB1** with $Ag[Al(OC(CF_3)_3)_4]$ closely resemble those measured with $AgSbF_6$. Therefore, their interpretation is analogous and the spectra, alongside additional details are available in the Supporting Information.

As mentioned above, the solvent substantially impacts the reaction. Even solvents with relatively weakly coordinating aromatic systems, such as toluene-d_8, proved to dampen the reactivity drastically, with benzene completely inhibiting the reaction. This phenomenon occurs due to the tendency of Ag^+ cations to efficiently coordinate to π-systems.[23] Hence, the excess of solvent favors its coordination to Ag^+, obstructing the interaction between the silver catalyst and **BND1** (see Supporting Information for further information), and thus leading to a long reaction time (Scheme 2).

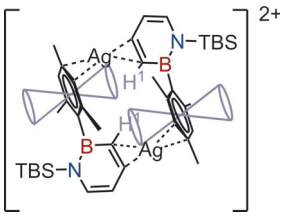

Figure 3. Schematic drawing of a possible [**BNB1**Ag]$_2^{2+}$ dimer in solution, with indicated magnetic shielding of the H^1 proton (blue) induced by the diatropic ring current of the mesityl substituent.

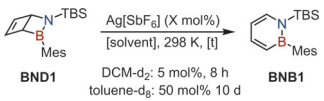

Scheme 2. Solvent effect on the $AgSbF_6$ catalyzed cycloreversion of **BND1**.

Kinetic NMR experiments were conducted to explore the first-order cycloreversion of **BND1** in the presence of 1 equiv. of $AgSbF_6$ or $Ag[Al(OC(CF_3)_3)_4]$ at different temperatures in DCM-d_2. At 288 K, a half-life of approximately 25 minutes was observed for [**BND1**$AgSbF_6]_2$, while neat **BND1** has a similar half-life only at a temperature higher by 85 K (373 K).[6] [**BND1**$Ag[Al(OC(CF_3)_3)_4]]_x$ showed an even lower half-life of around 5 min at 288 K, likely owing to the weaker coordination of the $[Al(OC(CF_3)_3)_4]^-$ anion. Upon analyzing the data via an Eyring plot, the activation energy (E_a) of [**BND1**$AgSbF_6]_2$ was determined to be 23.6 ± 0.7 kcal/mol, while E_a of [**BND1**$Ag[Al(OC(CF_3)_3)_4]]_x$ amounted to 24.9 ± 0.5 kcal/mol (Figure 4).[24] This result was initially surprising, as

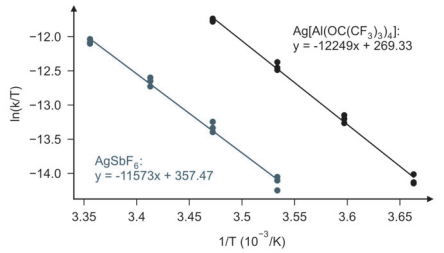

	BND1*	[**BND1**$AgSbF_6]_2$	[**BND1**$Ag[Al(OC(CF_3)_3)_4]]_x$
E_a (kcal mol^{-1})	27.0 ± 1.2	23.6 ± 0.7	24.9 ± 0.5
lnA	12.5 ± 0.7	33.5 ± 1.2	37.4 ± 1.0
$\Delta H^{\ddagger}$ (kcal mol^{-1} K^{-1})	26.3 ± 0.3	23.0 ± 0.7	24.3 ± 0.5
$\Delta S^{\ddagger}$ (cal mol^{-1} K^{-1})	-3.7 ± 0.9	6.1 ± 2.4	14.0 ± 1.9

Figure 4. Eyring plot for the cycloreversion of **BND1** in DCM-d_2 in presence of 1 equiv. $AgSbF_6$ or $Ag[Al(OC(CF_3)_3)_4]$ respectively. Triplets at four different temperatures were measured for each AgWCA salt between 298 K and 278 K in 5 K intervals. Summary of determined and literature (*) values.[6]

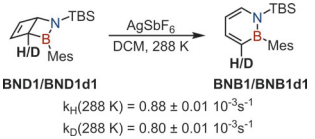

Scheme 3. Cycloreversion of **BND1**/**BND1d1** in presence of $AgSbF_6$ (1 equiv.) in DCM at 288 K.

[**BND1**$AgSbF_6]_2$ ($k_{283K} = 0.21 \cdot 10^{-3}\ s^{-1}$) exhibited a lower reaction rate than [**BND1**$Ag[Al(OC(CF_3)_3)_4]]_x$ ($k_{283K} = 1.12 \cdot 10^{-3}\ s^{-1}$), but can be explained by considering the preexponential factor A ($\ln(A) = 33.5 \pm 1.2$ for [**BND1**$AgSbF_6]_2$ and $\ln(A) = 37.4 \pm 1.0$ for [**BND1**$Ag[Al(OC(CF_3)_3)_4]]_x$). For comparison, the uncatalyzed reaction of **BND1** has activation parameters of $E_a = 27.0 \pm 1.2$ kcal/mol and $\ln A = 12.5 \pm 0.7$.[6]

To gain insight into the rate determining step of the cycloreversion of **BND1**, the secondary kinetic isotope effect (sKIE) was investigated (Scheme 3). Kinetic data were acquired for both **BND1** and **BND1d1** via ^{11}B NMR-spectroscopy in the presence of equimolar amounts of $AgSbF_6$ in DCM at 288 K (^{11}B NMR spin lattice relaxation time: T_1(**BNB1**) = 1.35 ms, T_1(**BND1**) = 1.33 ms). From these measurements, a sKIE of 1.10 ± 0.02 was determined, concluding that the rate-determining step involves the rehybridization of the bridge head carbon from C-sp^3 to C-sp^2. This result dismisses the dissociation of the dimeric [**BND1**$AgSbF_6]_2$ species to be rate determining.

To further substantiate this conclusion, DFT computations of the catalyzed cycloreversion mechanism were carried out. All structures were optimized with the M06-2X hybrid functional[25] employing the def2-SVP basis set in Gaussian 16.[26] The effect of DCM solvent was considered using the polarizable continuum model (PCM).[27] In addition, the electronic energies were refined by computing M06-2X(PCM:DCM) single point energies with the large def2-QZVPP basis set. Two different Ag^+ based systems are depicted in Figure 5, with (a) showcasing the dimeric [**BND1**$AgSbF6]_2$, and (b) illustrating the influence of bare Ag^+ on the thermal ring opening of **BND1**. For the dimeric system, conformational analysis for both transition states (TSI, TSII), the starting material (I), intermediate (II) and product (III) yielded various optimized minima, ensuring well founded energy differences.

The computations demonstrated a decrease in activation energy compared to the thermal isomerisation of neat **BND1** ($\Delta G^{\ddagger}(298\ K) = 28.6$ kcal/mol, M06-2X(PCM:DCM)/def2-QVPP//M06-2X(PCM:DCM)/def2-SVP). As expected, the monomeric cationic system lacking a WCA or an additional **BND1** providing secondary electron density to Ag^+ (Figure 5b), resulted in the most favorable activation energy of $\Delta G^{\ddagger}(298\ K) = 22.9$ kcal/mol benefiting the thermal ring opening by 5.7 kcal/mol compared to neat **BND1**. Concurrently, the dimeric system (Figure 5a) showed a more modest effect, with $\Delta G^{\ddagger}(298\ K) = 26.6$ kcal/mol, corresponding to a 2.0 kcal/mol decrease in activation energy. It is important to note that the computations slightly overestimate the activation energies, as the experimental data for the cycloreversion of neat **BND1** is $\Delta G^{\ddagger}(298\ K) = 25.2 \pm 0.4$ kcal/mol.[6] Nonetheless, the computational outcome clearly indicates the advantageous role of a Lewis acid in facilitating the thermal ring opening.

All Ag^+ mediated cycloreversions of **BND1** occur in a concerted fashion, in agreement with computations of the neat **BND1**,[6] while the parent system showed an additional minimum along the intrinsic reaction coordinate.[28] Whilst a second minimum was not identified within the studied

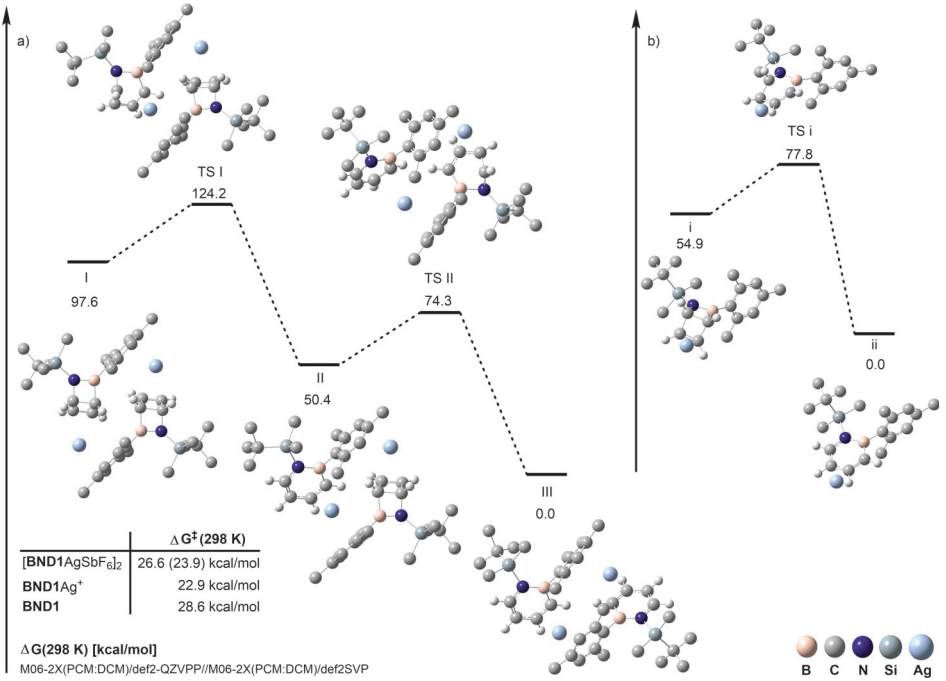

Figure 5. Free energy profile of the $AgSbF_6$ catalyzed cycloreversion of **BND1** at the M06-2X(PCM:DCM)/def2-QVPP//M06-2X(PCM:DCM)/def2-SVP level of theory. Displayed is the stepwise ring opening of the dimeric [**BND1**$AgSbF_6$]$_2$ (a) and the thermal isomerisation of a cationic **BND1**Ag^+-species (b). Gibbs free energies of activation are given for the [**BND1**$AgSbF_6$]$_2$ (first and second ring opening), **BND1**Ag^+, and **BND1** systems. For clarity, all fluorine, antimony, and hydrogen atoms except those bound directly to Dewar isomers or 1,2-dihydro-azaborinine are omitted.

system, characteristically flat potential energy surfaces, reminiscent to those of the parent system,[28] were observed along the intrinsic reaction coordinates of several transition states (see SI). Additionally, the concerted mechanism is in accordance with the observations of the sKIE, as the bridgehead C3 atoms feature near planar geometry in the transition states. To elucidate the interaction of an Ag^+ ion with **BND1**, the molecular electrostatic potentials of **BND1**, **BNB1** and the corresponding transition state were visualized (Figure 6, red = attractive/blue = repulsive interaction with a positive test charge). The transition state has a relatively higher cation affinity at the 1,2-dihydro-1,2-azaborinine ring compared to both **BND1** and **BNB1**. Additionally, a partial negative charge can be observed at the aromatic system of the mesityl substituent for all three structures, which explains its interaction with Ag^+ in the dimers. From these results, it can be concluded that electrostatic interaction with a cation, such as Ag^+, decreases the energy difference between **BNB1**, **BND1** and their transition state, thereby favoring the thermal ring opening. A second argument can be made by comparing each HOMO of the dimers. These exhibit a σ type interaction of the $d_{z^2}(Ag^+)$ orbital with the 1,2-dihydro-1,2-azaborinine (Figure 6d) solely in the transition state, indicative of a covalent contribution to the bonding interaction.

The computational analysis of the dimeric system delineates the cycloreversion of each individual **BND1** unit in the dimers, with the second step having a slightly lower activation energy of $\Delta G^{\ddagger}(298\ K) = 23.9$ kcal/mol. The computed difference in free energy between [**BND1**$AgSbF_6$]$_2$ and **BND1**$AgSbF_6$ is 13.5 kcal/mol, representing the lower limit for the activation energy for dissociation. Assuming that the minimal activation energy for the silver catalyzed thermal ring opening corresponds to that of **BND1**Ag^+ (Figure 5b), a lower limit for the activation energy starting from the monomeric **BND1**$AgSbF_6$ with prior dissociation can be estimated to 36.4 kcal/mol. This value notably is larger than the activation energy for the thermal ring opening of the dimeric species depicted in Figure 5a. Thus, the cycloreversion of **BND1** is likely initiated from its dimer [**BND1**$AgSbF_6$]$_2$, with subsequent reaction of the second **BND1** unit.

According to these findings, we propose the catalytic cycle outlined in Scheme 4 for the Ag^+ catalyzed cyclo-

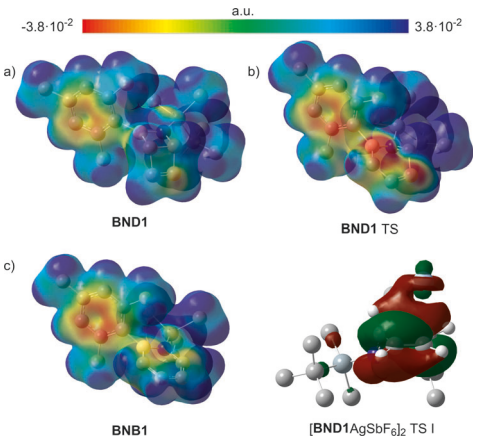

Figure 6. Electrostatic potential maps (isoval = 0.01) of neat **BND1**, **BNB1** and the respective transition state (all hydrogen atoms are omitted for clarity) as well as the HOMO of [**BND1**$AgSbF_6$]$_2$ (TS I, Figure 5) at the ring opening **BND1** unit. The second **BND1**Ag^+ unit, the two $[SbF_6]^-$ anions, and their orbital contribution to the HOMO are omitted for clarity. Hydrogen atoms except those bound directly to 1,2-dihydro-azaborinine are omitted for clarity.

reversion of **BND1** to **BNB1**. Initially, the silver salt is coordinated by the Dewar isomer via its mesityl substituent and the C=C double bond forming a dimeric structure **1** (Scheme 4). Subsequently, the cycloreversion of each 1,2-dihydro-1,2-azaborinine unit proceeds thermally, transitioning from **1** via **2** to **3**. Additionally, scrambling between **1**, **2**, and **3** is likely, with their respective equilibrium shifting, as the reaction advances and the concentration ratio of **BND1** and **BNB1** alters.

To elucidate the boundaries of the developed catalytic system, the Ag^+ catalyzed cycloreversion of the strongly stabilized *tert*-butyl-2-mesityl-1,2-azaborinine (**BND2**) was attempted (Scheme 5). This is the most stable Dewar valence isomer known ($E_a = 28.3 \pm 1.4$ kcal/mol, $\ln A = 28.5 \pm 1.8$; $\Delta H^{\ddagger} = 27.6 \pm 1.4$ kcal/mol, $\Delta S^{\ddagger} = -4.4 \pm 3.7$ cal/(mol·K)), and therefore it constitutes a demanding challenge for catalytic isomerization. AgWCA salts such as $AgSbF_6$ or $Ag[Al(OC(CF_3)_3)_4]$ were unsuccessful in catalyzing the cycloreversion of **BND2**, but the weakly coordinated Cu salt, $[Cu(1,2\text{-}F_2C_6H_4)_n][Al(OC(CF_3)_3)_4]$ exhibited catalytic activity. Quantitative conversion of **BND2** could be achieved at rt with 10 mol % catalyst loading in DCM-d_2 within 48 h. This demonstrates that by optimizing the Lewis acidic character even the very challenging thermal ring opening of this MOST system can be catalyzed.

Conclusions

We developed a silver based catalytic system for the energy release from the high energy Dewar valence isomer of the promising 1,2-dihydro-1,2-azaborinine MOST system. $AgSbF_6$ and $Ag[Al(OC(CF_3)_3)_4]$ were identified as efficient catalysts for the cycloreversion of the Dewar isomer. Comprehensive mechanistic inquiries shed light onto the

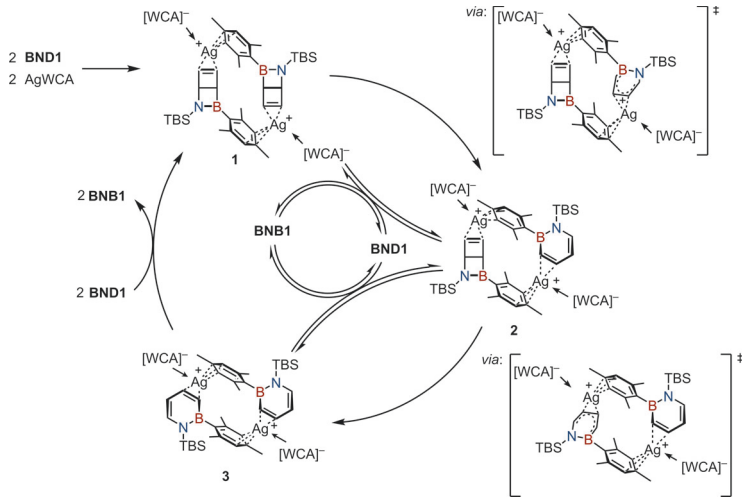

Scheme 4. Postulated mechanism of the Ag^+ catalyzed cycloreversion of **BND1**, relying on experimental and computational results. WCA = weakly coordinating anion.

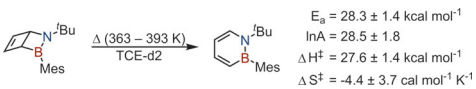

Scheme 5. Kinetic data obtained from the thermal cycloreversion of **BND2** in TCE-d_2.

novel Lewis acid driven catalysis, thereby enhancing the fundamental understanding of the thermal ring opening of Dewar isomers of 1,2-dihydro-1,2-azaborinines. The identification of a dimeric structure by NMR and X-ray were pivotal in uncovering a key motif within the catalytic cycle. Kinetic experiments not only elucidated the rate-determining step but also quantified the activation energy, which was further supported by computational studies. These broadened the understanding of elements required to develop catalysts suitable for proof-of-concept devices, which is currently under investigation.

Supporting Information

The authors have cited additional references within the Supporting Information (Ref. [29–56]).

Acknowledgements

We thank the analytic facilities of the Institute of Organic Chemistry at the University of Tübingen, as well as Dr. Ronny Löffler (LISA$^+$, University of Tübingen) for the EDX measurement. Additionally, we would like to express our gratitude to Prof. Ingo Krossing and Julie Willrett for assistance with synthesizing the CuWCA. We are grateful for financial support of this work by the German Research Foundation (DFG) within the Research Unit FOR 5499 "Molecular Solar Energy Management – Chemistry of MOST Systems" (project 496207555), Dr. K. H. Eberle Stiftung, Studienstiftung des Deutschen Volkes (scholarship R.C.R), and Fonds der Chemischen Industrie (scholarship S.M.B). The computations were performed on the BwForCluster JUSTUS2. The authors acknowledge support from the state of Baden-Württemberg through bwHPC and the German Research Foundation (DFG) through grant no INST 40/575-1 FUGG. Open Access funding enabled and organized by Projekt DEAL.

Conflict of Interest

The authors declare no conflict of interest.

Data Availability Statement

The data that support the findings of this study are available in the supplementary material of this article.

Keywords: Azaborinine · Dewar isomer · photoisomerization · Lewis acids · silver

[1] a) A. Lennartson, K. Moth-Poulsen, in *Molecular Devices for Solar Energy Conversion and Storage* (Eds.: H. Tian, G. Boschloo, A. Hagfeldt), Springer Singapore, Singapore, **2018**, pp. 327–352; b) C.-L. Sun, C. Wang, R. Boulatov, *ChemPhotoChem* **2019**, *3*, 268–283; c) Z. Wang, H. Hölzel, K. Moth-Poulsen, *Chem. Soc. Rev.* **2022**, *51*, 7313–7326; d) A. Gimenez-Gomez, L. Magson, B. Peñin, N. Sanosa, J. Soilán, R. Losantos, D. Sampedro, *Photochem* **2022**, *2*, 694–716.

[2] a) Z. Wang, A. Roffey, R. Losantos, A. Lennartson, M. Jevric, A. U. Petersen, M. Quant, A. Dreos, X. Wen, D. Sampedro, *Energy Environ. Sci.* **2019**, *12*, 187–193; b) A. U. Petersen, A. I. Hofmann, M. Fillols, M. Mansø, M. Jevric, Z. Wang, C. J. Sumby, C. Müller, K. Moth-Poulsen, *Adv. Sci.* **2019**, *6*, 1900367; c) S. Miki, T. Maruyama, T. Ohno, T. Tohma, S.-i. Toyama, Z.-i. Yoshida, *Chem. Lett.* **1988**, *17*, 861–864; d) Z.-i. Yoshida, *J. Photochem.* **1985**, *29*, 27–40.

[3] a) L. Dong, Y. Feng, L. Wang, W. Feng, *Chem. Soc. Rev.* **2018**, *47*, 7339–7368; b) G. S. Hartley, *Nature* **1937**, *140*, 281–281.

[4] a) M. Brøndsted Nielsen, N. Ree, K. V. Mikkelsen, M. Cacciarini, *Russ. Chem. Rev.* **2020**, *89*, 573; b) J. Daub, T. Knöchel, A. Mannschreck, *Angew. Chem. Int. Ed.* **1984**, *23*, 960–961.

[5] a) K. Moth-Poulsen, D. Ćoso, K. Börjesson, N. Vinokurov, S. K. Meier, A. Majumdar, K. P. C. Vollhardt, R. A. Segalman, *Energy Environ. Sci.* **2012**, *5*, 8534–8537; b) R. Boese, J. K. Cammack, A. J. Matzger, K. Pflug, W. B. Tolman, K. P. C. Vollhardt, T. W. Weidman, *J. Am. Chem. Soc.* **1997**, *119*, 6757–6773.

[6] K. Edel, X. Yang, J. S. A. Ishibashi, A. N. Lamm, C. Maichle-Mössmer, Z. X. Giustra, S.-Y. Liu, H. F. Bettinger, *Angew. Chem. Int. Ed.* **2018**, *57*, 5296–5300.

[7] S. A. Brough, A. N. Lamm, S.-Y. Liu, H. F. Bettinger, *Angew. Chem. Int. Ed.* **2012**, *51*, 10880–10883.

[8] Z. X. Giustra, X. Yang, M. Chen, H. F. Bettinger, S.-Y. Liu, *Angew. Chem. Int. Ed.* **2019**, *58*, 18918–18922.

[9] H. Lin, X. Yang, S.-Y. Liu, F. Jäkle, *ACS Macro Lett.* **2024**, *13*, 21–27.

[10] K. Maruyama, H. Tamiaki, *J. Org. Chem.* **1987**, *52*, 3967–3970.

[11] L. A. Paquette, J. C. Stowell, *J. Am. Chem. Soc.* **1970**, *92*, 2584–2586.

[12] W. Merk, R. Pettit, *J. Am. Chem. Soc.* **1967**, *89*, 4788–4789.

[13] L. Deng, Y. Fu, S. Y. Lee, C. Wang, P. Liu, G. Dong, *J. Am. Chem. Soc.* **2019**, *141*, 16260–16265.

[14] I. M. Riddlestone, A. Kraft, J. Schaefer, I. Krossing, *Angew. Chem. Int. Ed.* **2018**, *57*, 13982–14024.

[15] I. Krossing, *Chem. Eur. J.* **2001**, *7*, 490–502.

[16] G. Santiso-Quiñones, A. Higelin, J. Schaefer, R. Brückner, C. Knapp, I. Krossing, *Chem. Eur. J.* **2009**, *15*, 6663–6677.

[17] a) P. Paetzold, C. v. Plotho, G. Schmid, R. Boese, *Z. Naturforsch. B* **1984**, *39*, 1069–1075; b) J. Fink, M. Regitz, *Chem. Informationsdienst* **1986**, *17*; c) J. Fink, W. Rösch, U.-J. Vogelbacher, M. Regitz, *Angew. Chem. Int. Ed.* **1986**, *25*, 280–282; d) Y. Kobayashi, A. Ohsawa, Y. Iitaka, *Tetrahedron Lett.* **1973**, *14*, 2643–2646.

[18] a) K. Matsumoto, R. Hagiwara, Y. Ito, O. Tamada, *J. Fluorine Chem.* **2001**, *110*, 117–122; b) H. Bode, *Z. Anorg. Allg. Chem.* **1952**, *267*, 62–64.

[19] a) Y. Inagaki, M. Nakamoto, A. Sekiguchi, *Nat. Commun.* **2014**, *5*, 3018; b) E. Rivera, I. Paul, J. Fajardo, M. A. Garcia-Garibay, *Chem. Sci.* **2023**, *14*, 5802–5810; c) T. Hanamoto, Y. Koga, T. Kawanami, H. Furuno, J. Inanaga, *Angew. Chem. Int. Ed.* **2004**, *43*, 3582–3584.

[20] M. Suginome, T. Fukuda, Y. Ito, *J. Organomet. Chem.* **2002**, *643–644*, 508–511.

[21] a) M. Heß, T. E. Stennett, F. Fantuzzi, R. Bertermann, M. Schock, M. Schäfer, T. Thiess, H. Braunschweig, *Chem. Sci.* **2020**, *11*, 9134–9140; b) E. R. Abbey, L. N. Zakharov, S.-Y. Liu, *J. Am. Chem. Soc.* **2008**, *130*, 7250–7252; c) A. N. Brown, B. Li, S.-Y. Liu, *Tetrahedron* **2019**, *75*, 580–583; d) E. R. Abbey, A. N. Lamm, A. W. Baggett, L. N. Zakharov, S.-Y. Liu, *J. Am. Chem. Soc.* **2013**, *135*, 12908–12913; e) G. E. Rudebusch, L. N. Zakharov, S.-Y. Liu, *Angew. Chem. Int. Ed.* **2013**, *52*, 9316–9319.

[22] a) P. O. P. Ts'o, N. S. Kondo, M. P. Schweizer, *Biochemistry* **1969**, *8*, 997–1029; b) K. H. Scheller, H. Sigel, *J. Am. Chem. Soc.* **1983**, *105*, 5891–5900; c) R. B. Westkaemper, *Biochem. Biophys. Res. Commun.* **1987**, *144*, 922–929; d) N. Stern, D. T. Major, H. E. Gottlieb, D. Weizman, A. H. Sayer, E. Blum, B. Fischer, *J. Biol. Inorg. Chem.* **2012**, *17*, 861–879.

[23] A. E. Hill, *J. Am. Chem. Soc.* **1921**, *43*, 254–268.

[24] S. Arrhenius, *Z. Phys. Chem.* **1889**, *4U*, 226–248.

[25] Y. Zhao, D. G. Truhlar, *Theor. Chem. Acc.* **2008**, *120*, 215–241.

[26] a) F. Weigend, R. Ahlrichs, *Phys. Chem. Chem. Phys.* **2005**, *7*, 3297–3305; b) M. J. Frisch, G. W. Trucks, H. B. Schlegel, G. E. Scuseria, M. A. Robb, J. R. Cheeseman, G. Scalmani, V. Barone, G. A. Petersson, H. Nakatsuji, X. Li, M. Caricato, A. V. Marenich, J. Bloino, B. G. Janesko, R. Gomperts, B. Mennucci, H. P. Hratchian, J. V. Ortiz, A. F. Izmaylov, J. L. Sonnenberg, Williams, F. Ding, F. Lipparini, F. Egidi, J. Goings, B. Peng, A. Petrone, T. Henderson, D. Ranasinghe, V. G. Zakrzewski, J. Gao, N. Rega, G. Zheng, W. Liang, M. Hada, M. Ehara, K. Toyota, R. Fukuda, J. Hasegawa, M. Ishida, T. Nakajima, Y. Honda, O. Kitao, H. Nakai, T. Vreven, K. Throssell, J. A. Montgomery Jr., J. E. Peralta, F. Ogliaro, M. J. Bearpark, J. J. Heyd, E. N. Brothers, K. N. Kudin, V. N. Staroverov, T. A. Keith, R. Kobayashi, J. Normand, K. Raghavachari, A. P. Rendell, J. C. Burant, S. S. Iyengar, J. Tomasi, M. Cossi, J. M. Millam, M. Klene, C. Adamo, R. Cammi, J. W. Ochterski, R. L. Martin, K. Morokuma, O. Farkas, J. B. Foresman, D. J. Fox, *Wallingford, CT* **2016**.

[27] S. Miertuš, E. Scrocco, J. Tomasi, *Chem. Phys.* **1981**, *55*, 117–129.

[28] H. F. Bettinger, O. Hauler, *Beilstein J. Org. Chem.* **2013**, *9*, 761–766.

[29] M. J. O'Neil, *The Merck index : an encyclopedia of chemicals, drugs, and biologicals*, *14th ed.,* Merck Whitehouse Station, N. J. **2006**.

[30] B. Thiedemann, P. J. Gliese, J. Hoffmann, P. G. Lawrence, F. D. Sönnichsen, A. Staubitz, *Chem. Commun.* **2017**, *53*, 7258–7261.

[31] A. J. V. Marwitz, M. H. Matus, L. N. Zakharov, D. A. Dixon, S.-Y. Liu, *Angew. Chem. Int. Ed.* **2009**, *48*, 973–977.

[32] a) A. W. Baggett, M. Vasiliu, B. Li, D. A. Dixon, S.-Y. Liu, *J. Am. Chem. Soc.* **2015**, *137*, 5536–5541; b) J. E. Borger, M. S. Bakker, A. W. Ehlers, M. Lutz, J. Chris Slootweg, K. Lammertsma, *Chem. Commun.* **2016**, *52*, 3284–3287.

[33] H. Doi, T. Sakai, K.-i. Yamada, K. Tomioka, *Chem. Commun.* **2004**, 1850–1851.

[34] A. W. Baggett, F. Guo, B. Li, S.-Y. Liu, F. Jäkle, *Angew. Chem. Int. Ed.* **2015**, *54*, 11191–11195.

[35] M. Schäfer, J. Schäfer, R. D. Dewhurst, W. C. Ewing, M. Krahfuß, M. W. Kuntze-Fechner, M. Wehner, C. Lambert, H. Braunschweig, *Chem. Eur. J.* **2016**, *22*, 8603–8609.

[36] A. N. Lamm, S.-Y. Liu, *Mol. BioSyst.* **2009**, *5*, 1303–1305.

[37] Y. Naruta, Y. Nishigaichi, K. Maruyama, *Chem. Lett.* **2006**, *15*, 1857–1860.

[38] K. S. Dunne, S. E. Lee, V. Gouverneur, *J. Organomet. Chem.* **2006**, *691*, 5246–5259.

[39] P. J. Malinowski, T. Jaroń, M. Domańska, J. M. Slattery, M. Schmitt, I. Krossing, *Dalton Trans.* **2020**, *49*, 7766–7773.

[40] P. J. Malinowski, D. Himmel, I. Krossing, *Angew. Chem. Int. Ed.* **2016**, *55*, 9259–9261.

[41] M. Kuprat, M. Lehmann, A. Schulz, A. Villinger, *Organometallics* **2010**, *29*, 1421–1427.

[42] A. Decken, C. Knapp, G. B. Nikiforov, J. Passmore, J. M. Rautiainen, X. Wang, X. Zeng, *Chem. Eur. J.* **2009**, *15*, 6504–6517.

[43] SAINT, v. 8.38 A; Bruker AXS Inc., Madison, WI 2017.

[44] APEX 3, v. 2016.2015–2010; Bruker AXS Inc., Madison, WI 2017.

[45] L. Krause, R. Herbst-Irmer, G. M. Sheldrick, D. Stalke, *J. Appl. Crystallogr.* **2015**, *48*, 3–10.

[46] G. Sheldrick, *Acta Crystallogr. Sect. C* **2015**, *71*, 3–8.

[47] C. B. Hübschle, G. M. Sheldrick, B. Dittrich, *J. Appl. Crystallogr.* **2011**, *44*, 1281–1284.

[48] G. M. Sheldrick, *Acta Crystallogr. Sect. A* **2008**, *64*, 112–122.

[49] O. V. Dolomanov, L. J. Bourhis, R. J. Gildea, J. A. K. Howard, H. Puschmann, *J. Appl. Crystallogr.* **2009**, *42*, 339–341.

[50] C. F. Macrae, I. Sovago, S. J. Cottrell, P. T. A. Galek, P. McCabe, E. Pidcock, M. Platings, G. P. Shields, J. S. Stevens, M. Towler, P. A. Wood, *J. Appl. Crystallogr.* **2020**, *53*, 226–235.

[51] H. H. Ku, *J. Res. Nbs. C Eng. Inst.* **1966**, *70C*, 263.

[52] M. M. Schwab, D. Himmel, S. Kacprzak, D. Kratzert, V. Radtke, P. Weis, K. Ray, E.-W. Scheidt, W. Scherer, B. de Bruin, S. Weber, I. Krossing, *Angew. Chem. Int. Ed.* **2015**, *54*, 14706–14709.

[53] J. Tomasi, B. Mennucci, R. Cammi, *Chem. Rev.* **2005**, *105*, 2999–3094.

[54] M. Page, C. Doubleday, J. W. McIver, Jr., *Chem. Phys.* **1990**, *93*, 5634–5642.

[55] D. A. McQuarrie, J. D. Simon, *Molecular Thermodynamics*, University Science Books, **1999**.

[56] F. Weigend, *Phys. Chem. Chem. Phys.* **2006**, *8*, 1057–1065.

[57] Deposition Numbers 2337845 (for **BND1AgSbF$_6$**), 2337844 (for **BNB1AgSbF$_6$**), 2298028 (for **BNB1**) contain the supplementary crystallographic data for this paper. These data are provided free of charge by the joint Cambridge Crystallographic Data Center and Fachinformationszentrum Karlsruhe Access Structures service.

Manuscript received: March 26, 2024
Accepted manuscript online: April 25, 2024
Version of record online: June 21, 2024

Angewandte Chemie
Eine Zeitschrift der Gesellschaft Deutscher Chemiker

Supporting Information

Facile Energy Release from Substituted Dewar Isomers of 1,2-Dihydro-1,2-Azaborinines Catalyzed by Coinage Metal Lewis Acids

R. C. Richter, S. M. Biebl, R. Einholz, J. Walz, C. Maichle-Mössmer, M. Ströbele, H. F. Bettinger, I. Fleischer**

SUPPORTING INFORMATION

Contents

1 General information

1.1 Chemicals and general techniques

All reactions were carried out under argon employing standard Schlenk technique or a glovebox (GS MEGA E-Line, Glovebox Systemtechnik, <1 ppm O_2, <0.1 ppm H_2O; mBraun UNIlab with LMF, <30 ppm O_2, <0.1 ppm H_2O) with pre-dried glassware unless denoted otherwise. Solvents for the synthesis were dried via a commercially available solvent purification system (MB SPS-800). Solvents for the catalytic cycloreversion were degassed *via* freeze pump thaw or by passing through argon and were dried over 3 Å MS from abcr (activated *in vacuo* at 280 °C for 30 min) prior to use. Solvents employed during chromatography were HPLC grade or distilled prior to use. Flash chromatography was carried out using the Interchim Puriflash 430 and XS420 systems with PF-30SIHP-F0025/40/80 columns (30 µm). For separations, the gradients are given as a binary eluent combination X:Y (Y is the more polar solvent) with X + Y = 100. Thin layer chromatography (TLC) was performed on aluminum plates coated with 0.20 mm silica gel 60 with fluorescence indicator UV_{254} from Macherey-Nagel and compounds were detected under UV light (254 nm). Chemicals were purchased from abcr, Apollo Scientific (TBSCl), BLDpharm (Grubbs I), Merck, Sigma-Aldrich (Pd/C, BF_3•Et_2O), Thermo Fischer Acros (BCl_3, allyl bromide, cyclohexene) or TCI and were used without further purification. Low reaction temperatures were achieved employing the Julabo FT902 Cryostat or a liquid nitrogen acetone cooling bath.

1.2 Analytical techniques

NMR spectra were recorded using the Bruker Avance III HDX 700, Bruker Avance III HDX 600, Bruker Avance 400 and the Bruker Avance III HD 300 NanoBay spectrometers, ^{11}B NMR, ^{13}C NMR and ^{19}F NMR experiments were proton-decoupled (not denoted explicitly). Chemical shifts are reported in parts per million relative to tetramethyl silane using the residual NMR solvent signals[1] (dichloromethane: ^{1}H δ = 5.32 and ^{13}C δ = 53.84; cyclohexane: ^{1}H δ = 1.38 and ^{13}C δ = 26.43, tetrahydrofuran: ^{1}H δ = 3.58, 1.73 and ^{13}C δ = 67.57, 25.37, benzene: ^{1}H δ = 7.16 and ^{13}C δ = 128.39) and the J coupling constants are given in Hertz with the usual designations for splitting patterns (s = singlet, d = doublet, t = triplet, q = quartet, m = multiplet, br = broad).

Information on the crystal structures are found in section 5.

HR-MS (APCI) measurements were carried out by the mass spectrometry department of the Institute of Organic Chemistry, University of Tübingen. Measurements were carried out using maXis 4G from Bruker (APCI). The molecular ion $[M+H]^+$ is given in m/z units.

GC-LR-MS (EI) analysis was carried out with an Agilent 7820A/5977B GC-system/MSD employing an Agilent 190915-433UI column (30 m × 250 µm × 0.25 µm). Program: 50 °C – 280 °C over 15 minutes.

GC-FID analysis was carried on an Agilent 7820A system with an Agilent 19091J-431 column (30 m × 320 µm × 0.25 µm), utilizing H_2 as the carrier gas. The program used heated from 50 °C to 280 °C within 15 min.

PXRD patterns were obtained from finely ground powders using a StadiP diffractometer (Stoe, Darmstadt) equipped with Ge-monochromated Cu−Kα1 radiation and a Mythen1 Detector.

EDX measurements were conducted on a JEOL JSM-6500F with an Oxford INCA energy 200 EDX system carrying a type 300 crystal. Several points and one area were scanned to acquire an equitable mean.

FT-IR spectra were measured by a Cary 630 FTIR by applying the neat sample on a diamond ATR sampler.

Irradiation was carried out employing a 500 W high pressure mercury lamp in an Oriel housing with quartz optics and a dichromic mirror (280 nm – 400 nm).

Melting points were determined either by visual detection employing a Büchi B-540 (heating rate 5 °C/min) or on a Netzsch DSC 300 Caliris in a sealed aluminum crucible.

2 General procedures

General procedure A (GP-A) – Irradiation of 1,2-dihydro-1,2-azaborinines:

Quartz J. Young tube

A 0.01 – 0.3 M solution (0.4 mL) of 1,2-dihydro-1,2-azaborinine in C_6D_{12} was irradiated (280 nm – 400 nm) in a quartz J. Young tube for 10 min – 1 h (depending on the concentration) until full conversion of the respective 1,2-dihydro-1,2-azaborinine to its Dewar isomer was reached. Reaction progress was monitored *via* $^1H/^{11}B$ NMR (when utilizing ^{11}B NMR without locking the solvent, reaction progress could be monitored in non-deuterated *n*-hexane, enabling

irradiation in non-deuterated solvents). Subsequently, the solvent was removed with a gentle Ar stream (removal of solvent was necessairy, as the employed catalyst were poorly soluble in aliphatic solvents).

Flow reactor

A 0.1 M solution (10 mL, *n*-hexane) of a 1,2-dihydro-1,2-azaborinine was irradiated (280 nm – 400 nm) in a flow reactor (V = 420 µL, FEP tubing, ID = 0.75 mm, OD = 1.6 mm, tube attached by G28 type flat bottom fittings) (Figure S1, Figure S2) with a flow rate of 1.2 mL/h (*via* syringe pump).

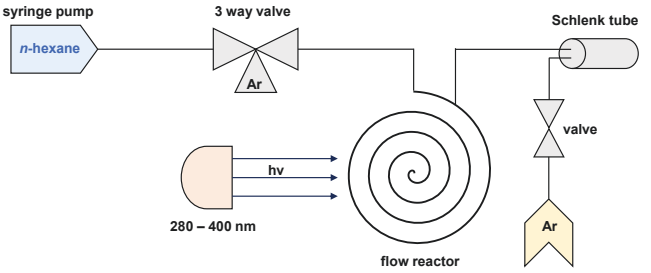

Figure S1. Flow reactor setup for the irradiation of 1,2-dihydro-azaborinines.

The solvent was directly removed utilizing a gentle Ar stream during irradiation. Subsequent exposition of the Dewar isomer to vacuum ensured removal of residual solvent (removal of solvent was necessairy, as the employed catalyst were poorly soluble in aliphatic solvents).

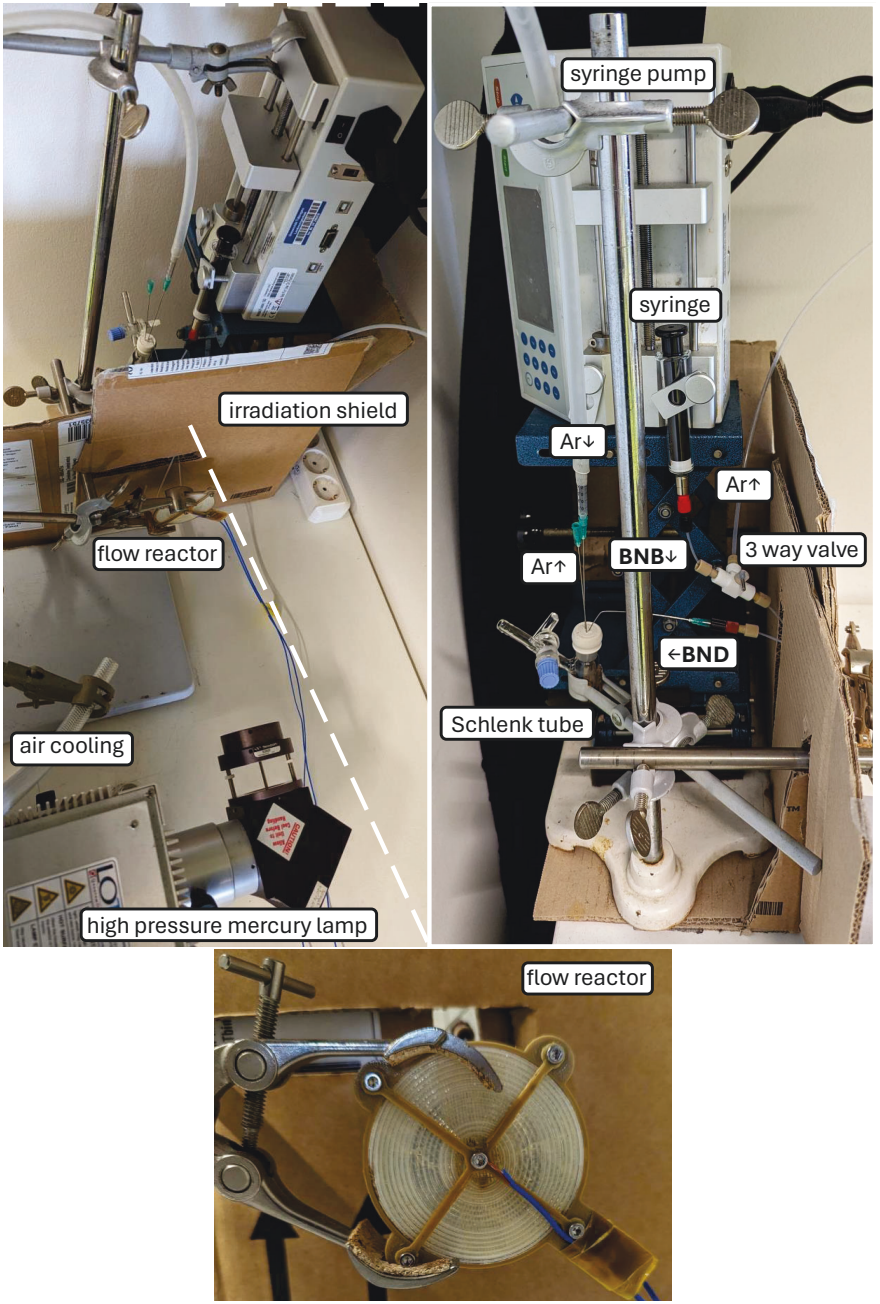

Figure S2. Picture of the flow reactor setup for the irradiation of 1,2-dihydro-azaborinines.

General procedure B (GP-B) – preparation of silver complexes of 2-(*tert*-butyldimethylsilyl)-3-mesityl-2-aza-3-borabicyclo[2.2.0]hex-5-ene (AgWCA•BND1, WCA = SbF_6^-, $[Al(=C(CF_3)_3)_4]^-$):

Glovebox

In a glovebox, 2-(*tert*-butyldimethylsilyl)-3-mesityl-2-aza-3-borabicyclo[2.2.0]hex-5-ene (**BND1**,1.0 equiv.) was dissolved in DCM-d_2 (5–10 mM) in a screw cap vial and cooled to 245 K. AgWCA (1.0 equiv.) was added and the mixture was stirred at 245 K until complete dissolution of AgWCA. To precooled (245 K) J. Young NMR tubes 0.4 mL of the prepared stock solution was added and the NMR-tube was swiftly transported to an acetone cooling bath (178 K) outside of the glovebox.

Schlenk technique

BND1 (1.0 equiv.) was dissolved in DCM-d_2 (5–10 mM) in a Schlenk tube and cooled to 178 K in an acetone cooling bath. In a second Schlenk tube, the respective AgWCA (1.0 equiv.) was added and cooled to 178 K in an acetone cooling bath. Subsequently, the **BND1** solution was added to the AgWCA *via* a two-pointed cannula and the mixture was stirred until complete dissolution of AgWCA. To a precooled (178 K) J. Young NMR tube placed inside a Schlenk vessel, 0.4 mL of the stock solution was added, and the NMR tube was placed in an acetone cooling bath at 178 K.

General procedure C (GP-C)–re-isolation of BNB1/2 after the catalytic cycloreversion of the Dewar isomers:

BNB1/**2** were re-isolated after removal of solvent by flash column chromatography (23 g SiO_2, gradient from 100:0 = *n*-hexane/DCM to 95:5 = *n*-hexane/DCM over 10 CV) utilizing a dry load (celite).

3 Synthesis

3.1 Synthesis of N-TBS substituted Azaborinine (BNB1) and its Dewar isomer

In analogy to Liu and co-workers in situ generated allylboron dichloride is reacted with *tert*-butyldimethylsilylamine to obtain boramine **2**.[2] As the precursor for the allylboron dichloride triallylborane is employed instead of the allyltriphenylstannane originally used by Liu and co-workers The absence of the tin species allows for a direct subsequent reaction of the higly reactive and sensitive boramine **2** in the following ring-closing metathesis without prior distillation.[3] This improves the overall yield of the two steps to about 60%. All following steps are conducted without alteration from the original publications.[3-4]

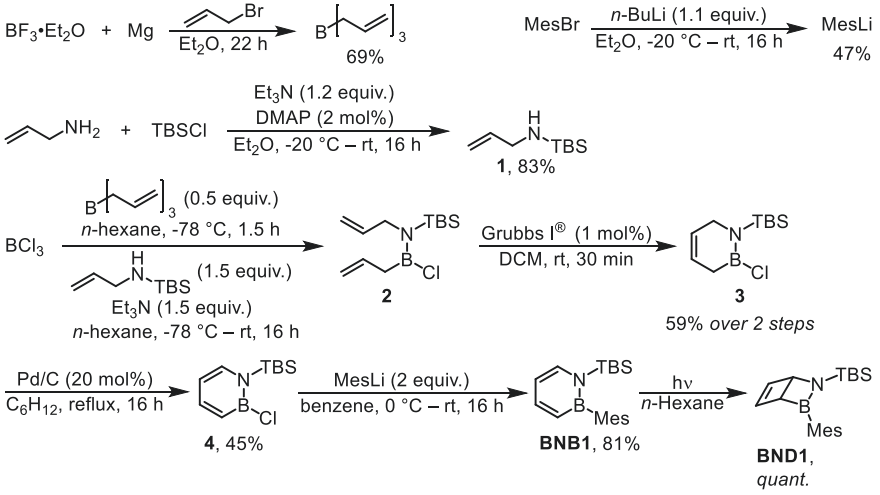

Scheme S1. Synthesis route of **BNB1** and its subsequent irradiation to **BND1**.

Triallyl borane

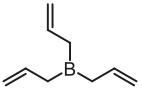

Triallyl borane was synthesized according to the literature.[2] In an inert dried five necked round bottom flask equipped with a reflux condenser, mechanical stirrer and septum, magnesium turnings (19.4 g, 4 equiv.) were stirred for 24 h. Et_2O (850 mL) and BF_3•Et_2O (25 mL, 200 mmol, 1 equiv.) were added, followed by addition of allyl bromide (50 mL, 600 mmol, 3 equiv.) portion wise (0.5 mL) until the reaction started. The remaining allyl bromide was added with a syringe pump over the course of 6 h, ensuring a gentle reflux. The mixture was stirred for 16 h (a highly viscous precipitate formed) and the solution was filtered with PTFE tubing. The remaining precipitate was washed with Et_2O (2 × 250 mL), and solvent was removed *in vacuo* (under inert conditions). Triallyl borane was obtained as a colorless oil *via* vacuum distillation (10 mbar, 32–34 °C, 18.5, 69%). The analytical data is in accordance with literature.[2]

C_9BH_{15} (134.03 $\frac{g}{mol}$)

b. p.: 32–34 °C (10 mbar)

^{1}H NMR(400.16 MHz, C_6D_6): 5.81 (m, 1H, H-2), 4.94 (br m, 2H, H-1), 2.03 (br m, 2H, H-3).

^{11}B NMR(128.39 MHz, C_6D_6): δ = 81.0.

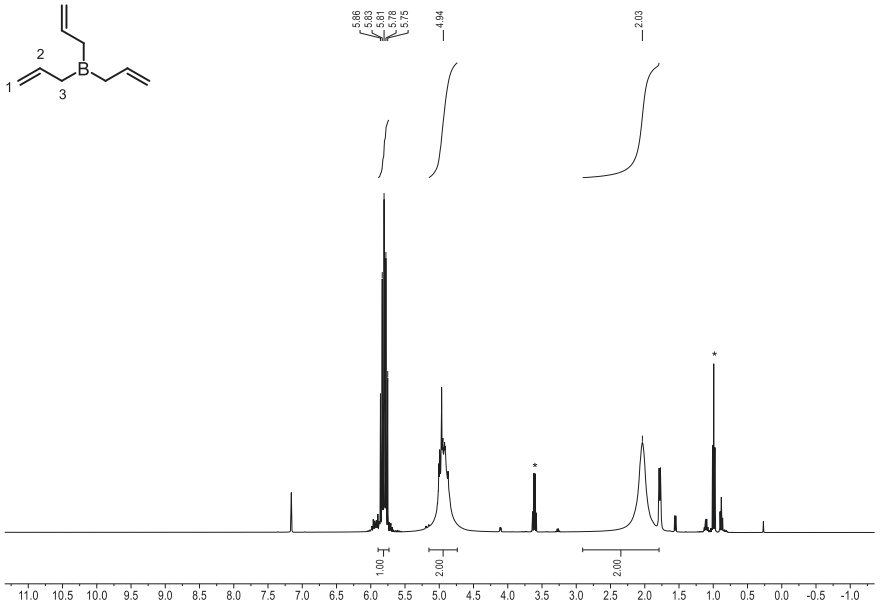

Figure S3. ^{1}H NMR of triallyl borane in C_6D_6 (* denotes residual Et_2O).

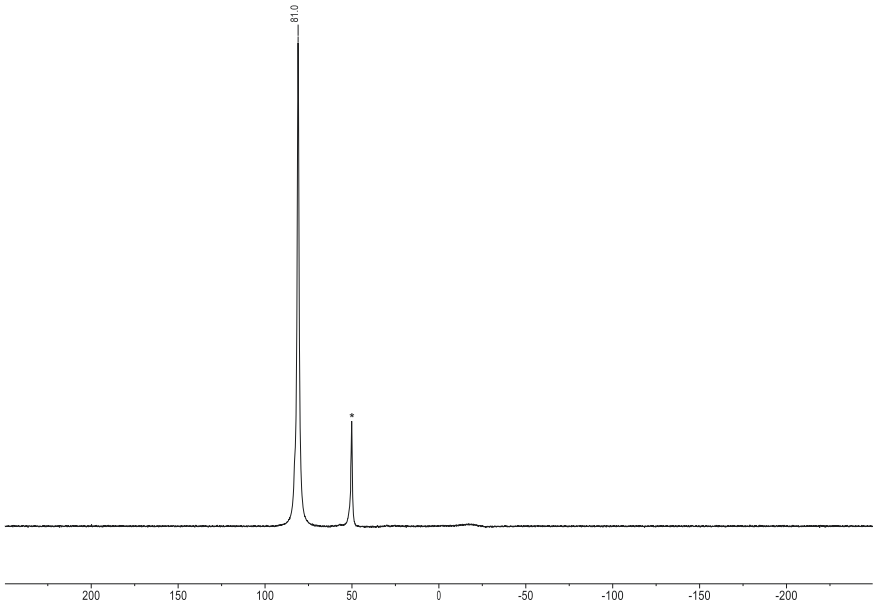

Figure S4. ^{11}B NMR of triallyl borane in C_6D_6 (* denotes hydrolysed species).

N-allyl-1-(*tert*-butyl)-1,1-dimethylsilanamine (1)

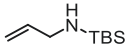

1

1 was synthesized according to the literature.[5] In a dried Schlenk round bottom flask allylamine (34 mL, 0.46 mol, 1.0 equiv.) was dissolved in Et_2O (150 mL). Whilst stirring, Et_3N (75 mL, 0.54 mol, 1.2 equiv.) and DMAP (1 g, 9 mmol, 2 mol%) dissolved in Et_2O (15 mL) were added dropwise, after which the solution was cooled to -20 °C and *tert*-butyldimethylchlorosilane (69 g, 0.46 mol, 1.0 equiv., in 150 mL Et_2O) was added slowly. The resulting suspension was stirred at rt for 16 h and subsequently filtered. The solvent of the filtrate was removed *in vacuo* and *n*-hexane (50 mL) was added. The suspension was filtered with a P4 frit and the solvent was removed *in vacuo*. **1** was obtained *via* vacuum distillation (15 mbar, 50–53 °C) as a colorless oil (65.4 g, 83%). The analytical data is in accordance with the literature.[5]

$C_9H_{21}NSi$ ($171.36\ \frac{g}{mol}$)

b. p.: 50–53 °C (15 mbar)

^{1}H NMR(400.16 MHz, CD_2Cl_2): 5.92 (m, 1H, H-3), 5.14 (ddt, ^2J = 1.9, ^3J = 17.0, ^4J = 1.9, 1H, H-2), 4.97 (ddt, ^2J = 1.9, ^3J = 10.2, ^4J = 1.7, 1H, H-1), 3.38 (ddt, ^3J = 7.9, ^3J = 5.1, ^4J = 1.7, 2H, H-4), 0.89 (s, 9H, H-7), 0.01 (s, 6H, H-6).

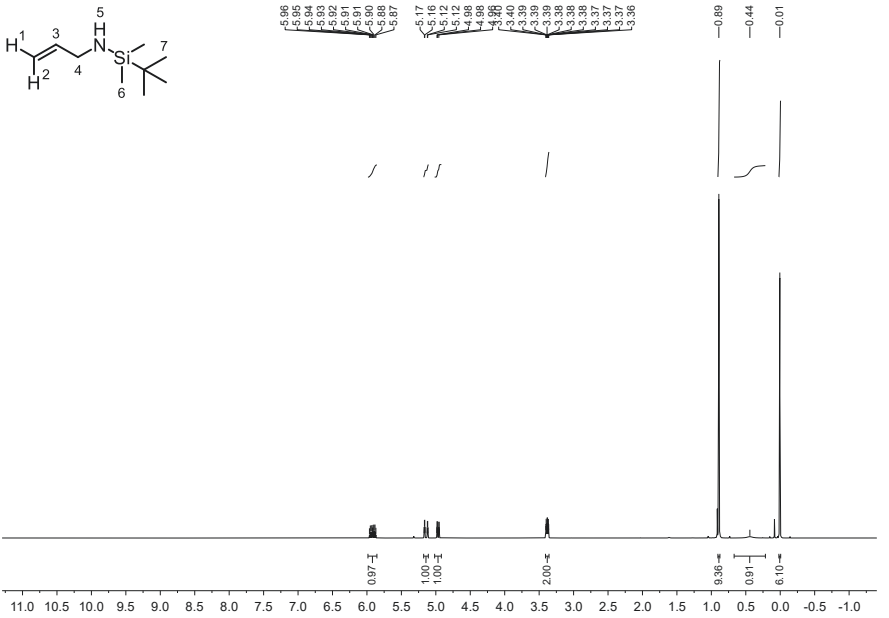

Figure S5. ^{1}H NMR of **1** in CD_2Cl_2.

N-allyl-N-(allylchloroboraneyl)-1-(*tert*-butyl)-1,1-dimethylsilanamine (2)

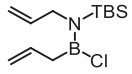

2

2 was synthesized based on a literature procedure with modifications.[2] A dried three necked flask (1 L), equipped with a mechanical stirrer, dropping funnel (250 mL), and septum was dried and cycled thrice with Ar. *n*-hexane (50 mL) was added and cooled to -78 °C. BCl_3 (230 mL, 230 mmol, 1 equiv., 1 M in *n*-hexane) was added in one portion, after which triallyl borane (15.5 g, 115 mmol, 0.5 equiv.) was added portion wise via PTFE tubing over the course of 5 min. The mixture was stirred for 1.5 h at -78 °C (note: shorter orlonger stirring time decreased the yield). Afterwards, **1** (74 mL, 350 mmol, 1.5 equiv.) and triethylamine (54 ml, 350 mmol, 1.5 equiv.) dissolved in *n*-hexane (50 mL) were added dropwise over 1.5 h (note: the mixture became very viscous towards the end of addition of **1**). The mixture was allowed to warm to rt and was stirred for 16 h (Note: a large amount of white precipitate formed, which required a mechanical stirrer for adequate mixing). Subsequently, the suspension was filtered, and the remnants were washed thoroughly with *n*-hexane. The solvent was removed *in vacuo* and the product was purified by vacuum distillation ($3.9 \cdot 10^{-3}$ mbar, 60 °C) yielding **2** as a colorless oil (138 mmol, 60%). The analytical data is in accordance with the literature.[3]

Note: Vacuum distillation is not necessary for the subsequent metathesis reaction. Proceeding the synthesis with the crude product results in an increased overall yield (59% over both steps).

$C_{12}H_{25}BNSiCl$ (257.68 $\frac{g}{mol}$)

b. p.: 60 °C ($3.9 \cdot 10^{-3}$ mbar)

^{1}H NMR(400.16 MHz, $CDCl_3$): 5.92 (br m, 1H, H-2/2'), 5.84 (br m, 1H, H-2'/2), 5.07 (br m, 2H, H-1/1'), 4.97 (br m, 2H, H-1'/1), 3.93 (br s, 1H), 3.80 (br s, 1H), 2.08 (br s, 1H), 2.00 (br s, 1H), 0.94 (s, 9H, H-4), 0.30 (s, 6H, H-3).

^{11}B NMR(128.39 MHz, $CDCl_3$): δ = 43.2.

*The broadening of signals in the proton spectrum is caused by hindered rotation along the B–N bond and the resulting occurrence of multiple rotamers.

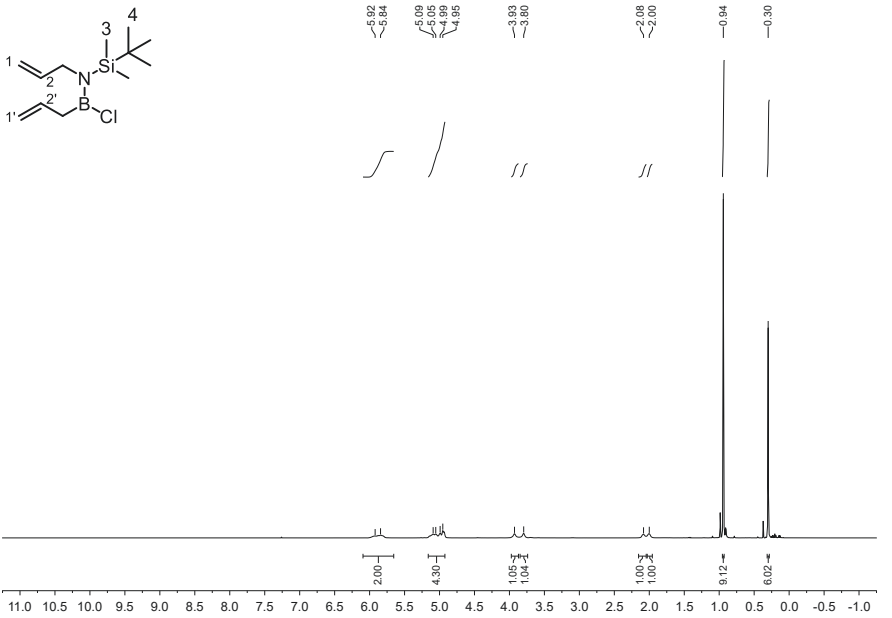

Figure S6. ^{1}H NMR of **2** in $CDCl_3$.

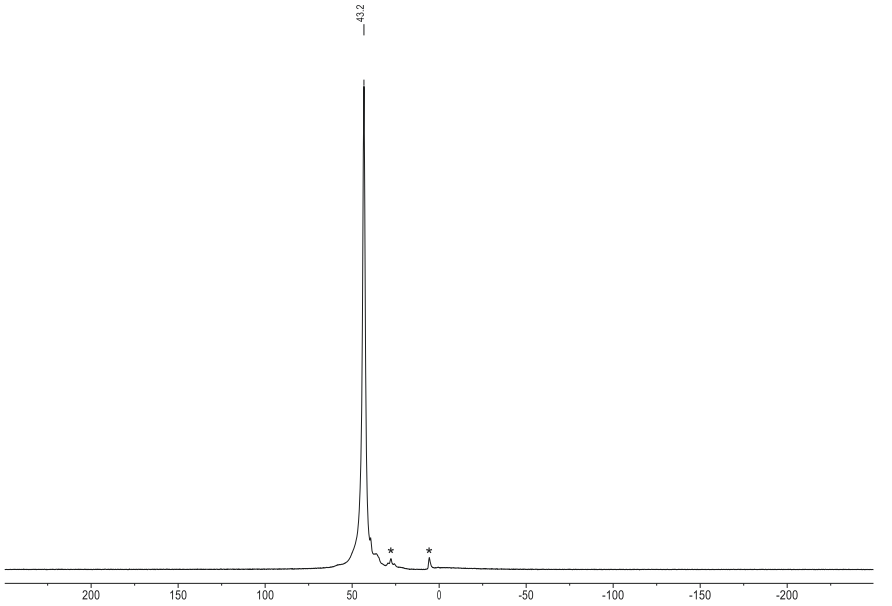

Figure S7. ^{11}B NMR of **2** in $CDCl_3$ (* unidentified impurities).

1-(*tert*-butyldimethylsilyl)-2-chloro-1,2,3,6-tetrahydro-1,2-azaborinine (3)

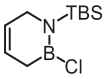

3

3 was synthesized according to the literature.[3] In a dried Schlenk round bottom flask, **2** (13.5 g, 52.0 mmol, 1 equiv.) was dissolved in DCM (200 mL). Subsequently, benzylidene-bis(tricyclohexylphosphine)dichlororuthenium (Grubbs I, 0.43 g, 0.5 mmol, 1 mol%) was added and the solution was stirred at rt. The reaction progress was monitored via a bubble counter. Upon completion (~30 min), the solvent was removed in vacuo and the product was distilled under vacuum ($6.8 \cdot 10^{-2}$ mbar, 50–58 °C). **3** was isolated as a colorless liquid (46 mmol, 75%). The analytical data is in accordance to literature.[3]

$C_{10}H_{21}BNSiCl$ (229.63 $\frac{g}{mol}$)

b. p.: 50–58 °C ($6.8 \cdot 10^{-2}$ mbar)

^{1}H NMR(400.16 MHz, CD_2Cl_2): δ = 5.76 (br m, 1H), H-3, 5.61 (m, 1H, H), 3.75 (m, 2H, H-1), 1.71 (m, 2H, H-4), 0.97 (s, 9H-6), 0.34 (s, 6H, H-5).

^{11}B NMR(128.39 MHz, CD_2Cl_2): δ = 42.4.

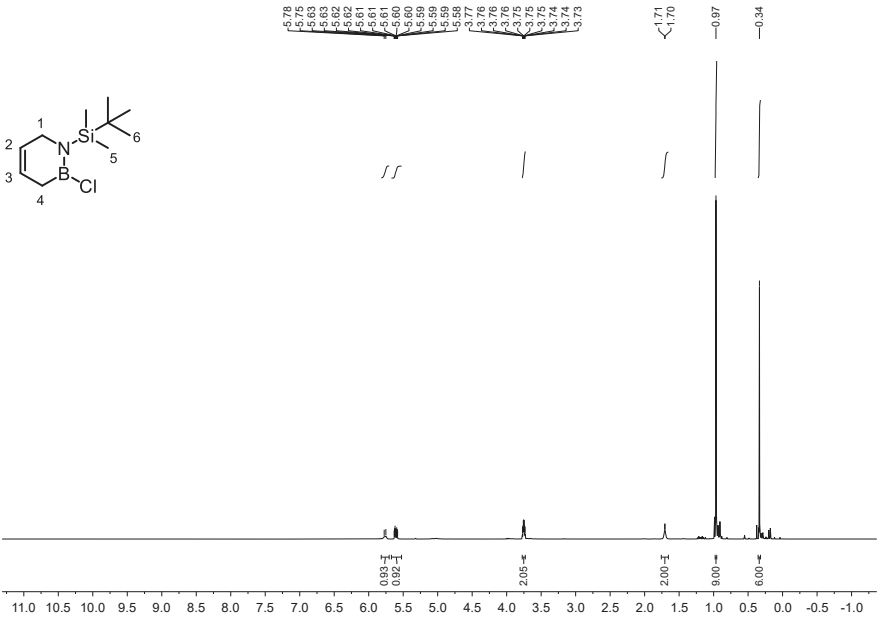

Figure S8. ^{1}H NMR of **3** in CD_2Cl_2.

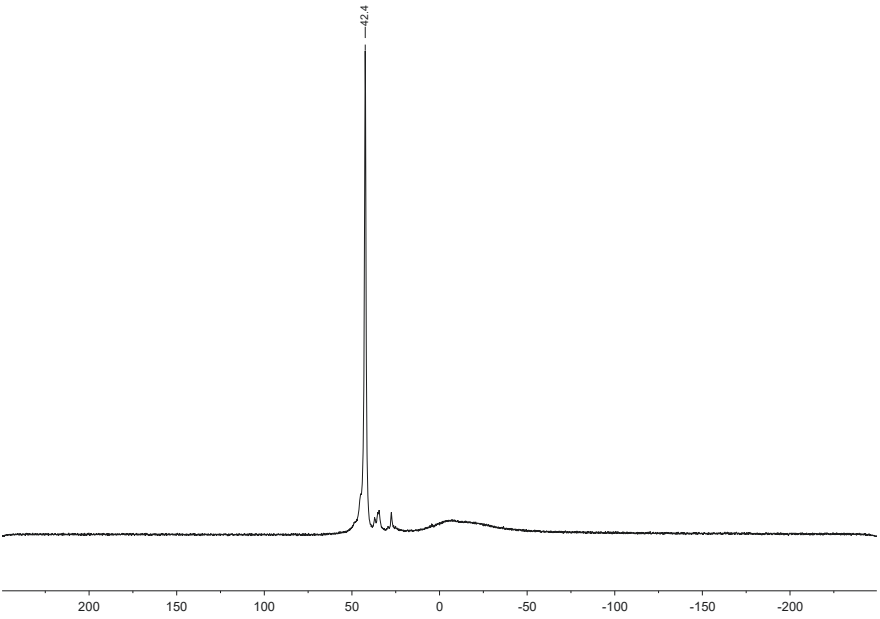

Figure S9. ^{11}B NMR of **3** in CD_2Cl_2.

1-(*tert*-butyldimethylsilyl)-2-chloro-1,2-dihydro-1,2-azaborinine (4)

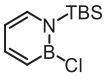

4

4 was synthesized according to the literature with minor modifications.[3] In a dried Schlenk round bottom flask equipped with a reflux condenser, palladium on activated charcoal (7.40 g, 7.00 mmol, 0.2 equiv.) was dried thoroughly for 30 min with a heat gun *in vacuo*. Subsequently, cyclohexene (100 mL) was added whilst cooling with an ice bath (Note: strongly exothermic reaction). Subsequently, **3** (9.40 g, 41. 0 mmol, 1 equiv.) was added and the stirred mixture was heated to reflux (100 °C) for 16 h. The resulting suspension was cooled to room temperature, filtered and the solvent was removed *in vacuo*. Afterwards the product was purified *via* vacuum distillation ($3.1 \cdot 10^{-3}$ mbar, 50–55 °C). **4** was obtained as a colorless oil (18 mmol, 45%). The analytical data is in accordance with the literature.[3]

$C_{10}H_{19}BNSiCl$ (227.61 $\frac{g}{mol}$)

b. p.: 50–55 °C ($3.1 \cdot 10^{-3}$ mbar)

^{1}H NMR(400.16 MHz, CD_2Cl_2): 7.55 (m, 1H, H-3), 7.28 (d, ^{3}J = 6.6 Hz, 1H, H-1), 6.60 (ddd, ^{3}J = 11.1, ^{4}J = 1.4, ^{5}J = 0.6 Hz, 1H, H-4), 6.33 (m, 1.4 Hz, 1H, H-2), 0.95 (s, 9H, H-6), 0.55 (s, 6H, H-6).

^{11}B NMR(128.39 MHz, CD_2Cl_2): δ = 35.3.

^{13}C NMR(100.62 MHz, CD_2Cl_2): δ = 145.7 (s, C-3), 139.1 (s, C-1), 128.5 (br, C-4), 111.8 (s, C-2), 26.8 (s, C-7), 19.6 (s, C-6), -1.6 (s, C-5).

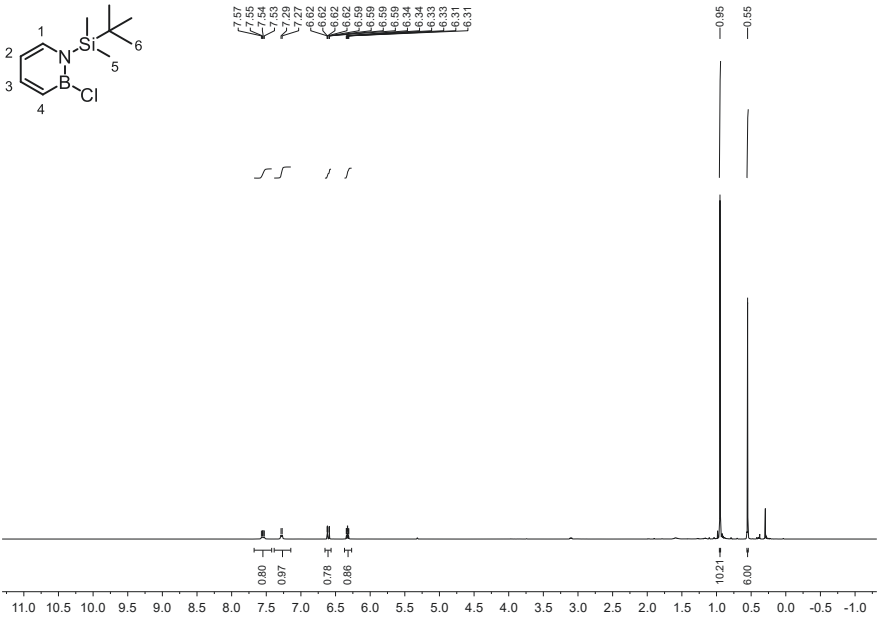

Figure S10. ^{1}H NMR of **4** in CD_2Cl_2.

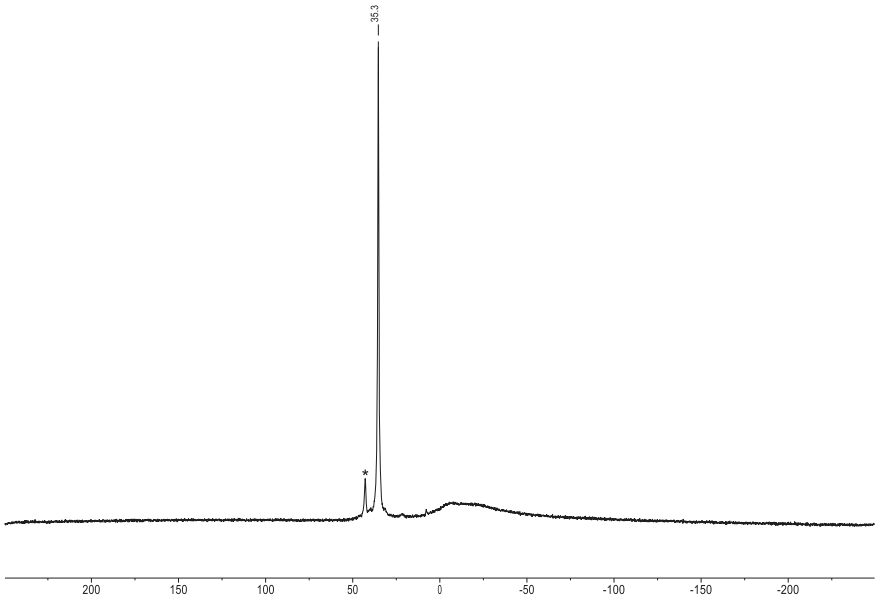

Figure S11. ^{11}B NMR of **4** in CD_2Cl_2. The signal denoted by * originates from the fully hydrogenated species.

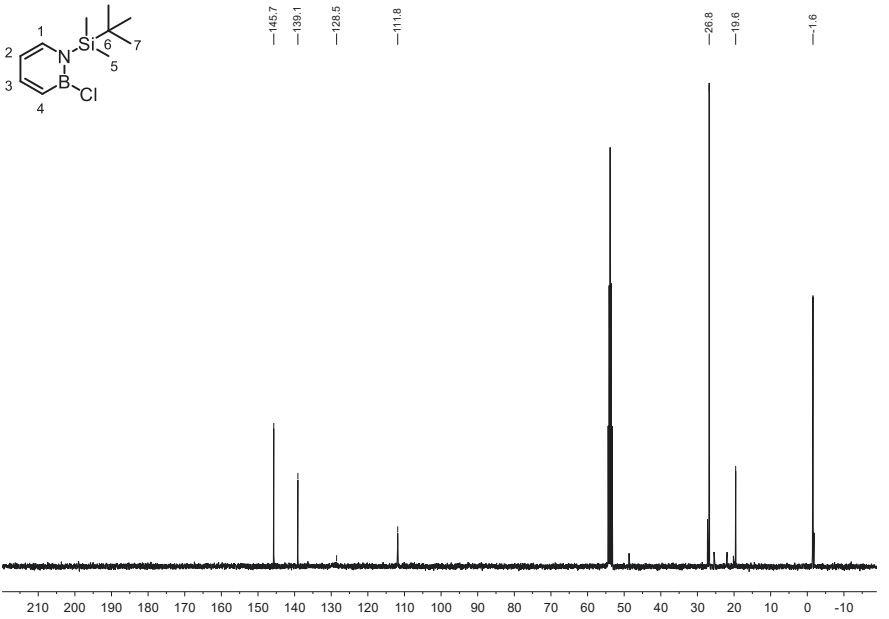

Figure S12: ^{13}C NMR of **4** in CD_2Cl_2.

Mesityl lithium

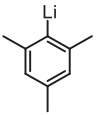

Mesityl lithium was synthesized according to the literature.[4b] In a dried Schlenk round bottom flask, mesityl bromide (15.0 mL, 100 mmol, 1.0 equiv.) dissolved in Et_2O (150 mL) was cooled to -20 °C. *n*-BuLi (44 mL, 1.1 equiv., 2.5 M in *n*-hexane) was added dropwise over the course of 30 min. The reaction mixture was stirred for 1 h at -20 °C, after which it was stirred for 16 h at rt. The white precipitate was filtered with a Schlenk frit, washed with Et_2O (2 × 15 mL) and dried *in vacuo*. Mesityl lithium was obtained as a white powder (9.2 g, 47%). The analytical data is in accordance with the literature.[4b]

$C_9H_{11}Li$ (126.13 $\frac{g}{mol}$)

^{1}H NMR(600.13 MHz, THF-d_8): δ = 6.49 (s, 2H), 2.42 (s, 6H), 2.10 (s, 3H).

^{7}Li NMR(233.23 MHz, THF-d_8): δ = 2.23.

^{13}C NMR(150.92 MHz, THF-d_8): δ = 179.6 (C-1), 149.6 (C-3), 132.0 (C-5), 123.3 (C-4), 28.7 (C-2), 21.4 (C-6).

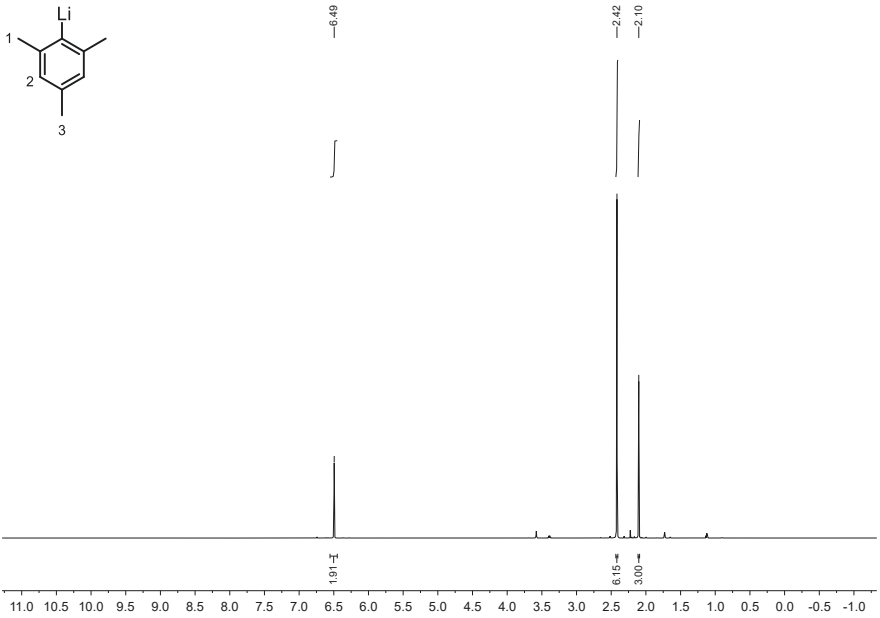

Figure S13. ^{1}H NMR of mesityl lithium in THF-d_8.

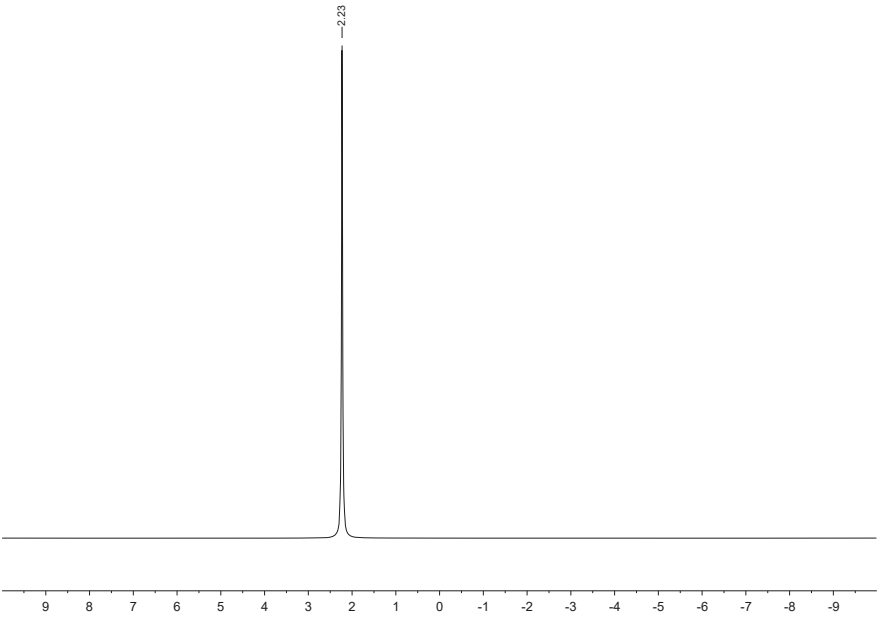

Figure S14. ^{7}Li NMR of mesityl lithium in THF-d_8.

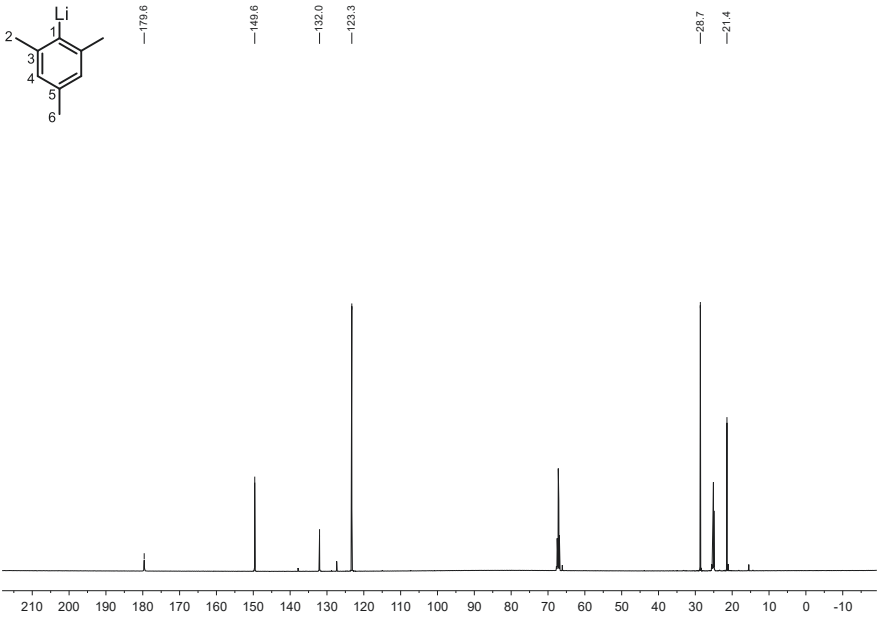

Figure S15: ^{13}C NMR of mesityl lithium in THF-d_8.

1-(*tert*-butyldimethylsilyl)-2-mesityl-1,2-dihydro-1,2-azaborinine (BNB1)

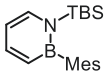

BNB1

BNB1 was synthesized according to literature with minor modifications.[4a] In a dried Schlenk round bottom flask mesityllithium (1.01 g, 6.00 mmol, 2 equiv.) was dissolved in benzene and cooled with an ice bath. Subsequently, **4** (0.95 g, 4.0 mmol, 1 equiv.) was added whilst stirring. The mixture was allowed to warm to rt and stirred for 16 h. Distilled water (6 mL) was added and the aqueous phase was extracted with *n*-pentane (3 × 10 mL). The combined organic phases were washed with sat. $NaCl_{(aq.)}$ (2 × 40 mL) and dried over $MgSO_4$. The crude product was purified by flash column chromatography (80 g SiO_2, gradient from 100:0 = *n*-hexane/DCM to 95:5 = *n*-hexane/DCM over 10 CV). **BNB1** was obtained as a colorless crystalline solid (3.3 mmol, 81%). The analytical data is in accordance with the literature.[4a]

$C_{19}H_{29}DBNSi$ (311.36 $\frac{g}{mol}$)

M_p: 56.9 °C

R_f: 0.27 (*n*-hexane/$CHCl_3$ = 20:1) [UV]

^{1}H NMR(700.29 MHz, CD_2Cl_2): δ = 7.56 (m, 1H, H-2), 7.47 (d, ^3J = 6.8 Hz, 1H, H-4), 6.77 (s, 2H, H-8), 6.55 (d, ^3J = 10.8 Hz, 1H, H-1), 6.39 (m, 1H, H-3), 2.27 (s, 3H, H-9), 2.06 (s, 6H, H-7), 0.91 (s, 9H, H-6), 0.00 (s, 6H, H-5).

^{11}B NMR(128.39 MHz, C_6D_{12}): δ = 40.2.

^{13}C NMR(100.62 MHz, C_6D_{12}): δ = 143.0 (s, C-2), 142.5 (br, C-8), 138.9 (s, C-13), 138.2 (s, C-4), 136.5 (s, C-12), 133.2 (br, C-1), 127.6 (s, C-10), 112.2 (s, C-3), 27.9 (s, C-7), 23.7 (s, C-9), 21.4 (s, C-11), 19.8 (s, C-6), -3.0 (s, C-5).

GC-MS(EI): t_r = 9.14 min, $\frac{m}{z}$($I_{base\ peak}$ %) = 311.2 ($M^{\bullet+}$, 9), 254.1 ($M^{\bullet+}$ - ^{t}Bu$^\bullet$, 100), 238.1 (11), 224.1 (15), 120 (5), 105 (8), 73 (8), 57 (^{t}Bu$^+$, 13).

IR (ATR, $\tilde{\nu}$): 3062 (w), 3017 (w), 2957 (w), 2931 (m), 2857 (w), 1605 (m), 1504 (m), 1456 (m), 1385 (s), 1265 (s), 1232 (w), 1176 (w), 1150 (w), 1090 (m), 1001 (m), 963 (m), 930 (m), 814 (vs), 781 (s), 740 (s), 710 (s), 677 (m).

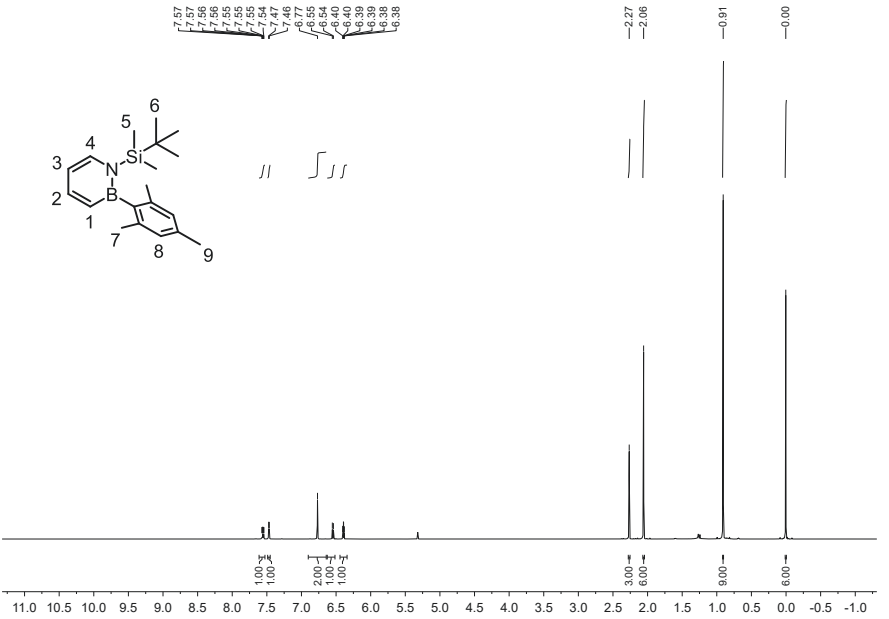

Figure S16. ^{1}H NMR of **BNB1** in CD_2Cl_2.

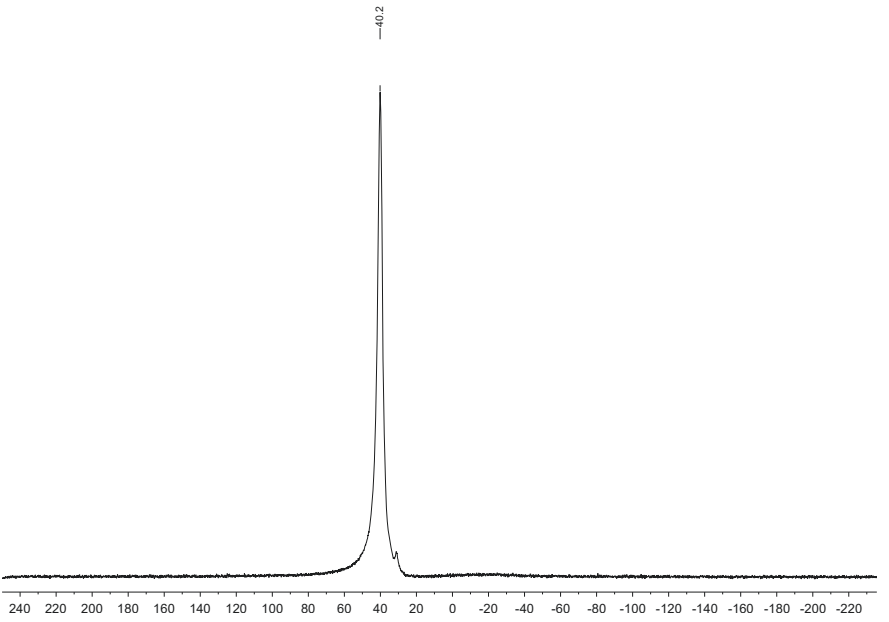

Figure S17. ^{11}B NMR of **BNB1** in C_6D_{12}.

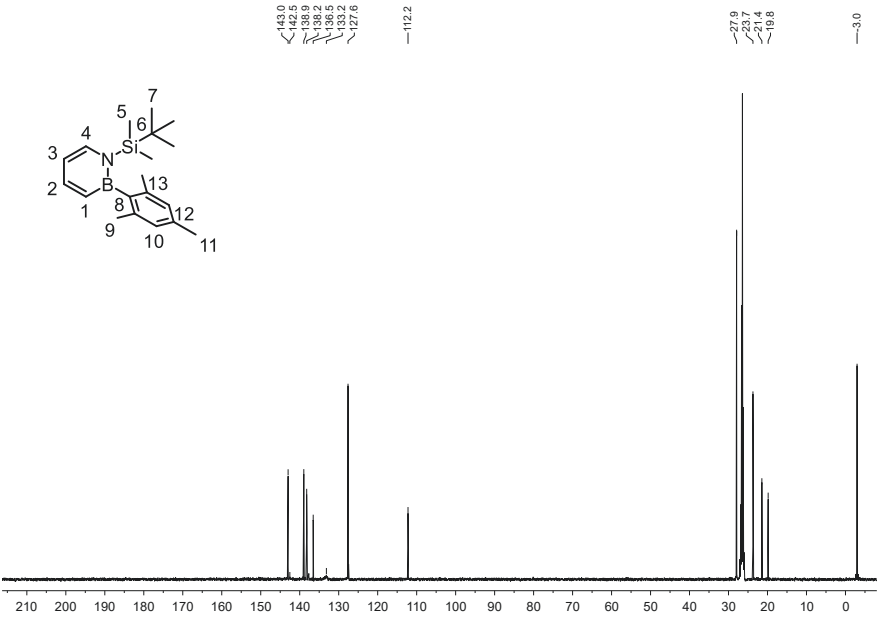

Figure S18: ^{13}C NMR of **BNB1** in C_6D_{12}.

2-(*tert*-butyldimethylsilyl)-3-mesityl-2-aza-3-borabicyclo[2.2.0]hex-5-ene (BND1)

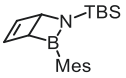

BND1

BNB1 was dissolved in C_6D_{12} and irradiated (280 nm – 400 nm) according to GP-A in a dried quartz J. Young tube or in the flow reactor. After removal of the solvent **BND1** was quantitatively obtained as a pale-yellow oil. The analytical data are in agreement with the data reported previously.REF

$C_{19}H_{29}DBNSi$ (311.36 $\frac{g}{mol}$)

^{1}H NMR(400.16 MHz, C_6D_{12}): δ = 6.63 (m, 2H, H-8), 6.49 (m, 1H, H-2), 6.32 (m, 1H, H-3), 4.75 (m, 1H, H-4), 3.00 (m, 1H, H-1), 2.18 (s, 3H, H-9), 2.16 (s, 6H, H-7), 0.90 (s, 9H, H-6), -0.07 (s, 3H, H-5/5'), -0.12 (s, 3H, H-5'/5).

^{11}B NMR(128.39 MHz, C_6D_{12}): δ = 52.9.

^{13}C NMR(100.62 MHz, C_6D_{12}): δ = 143.9 (s, C-2), 139.6 (s, C-3), 138.3 (s, C-13), 138.0 (br, C-8), 137.1 (s, C-12), 127.4 (s, C-10), 64.2 (s, C-4), 44.4 (br, C-1), 26.8 (s, C-7), 22.6 (s, C-9), 21.4 (s, C-11), 18.8 (s, C-6), -5.3 (s, C-5/5'), -5.5 (s, C-5'/5).

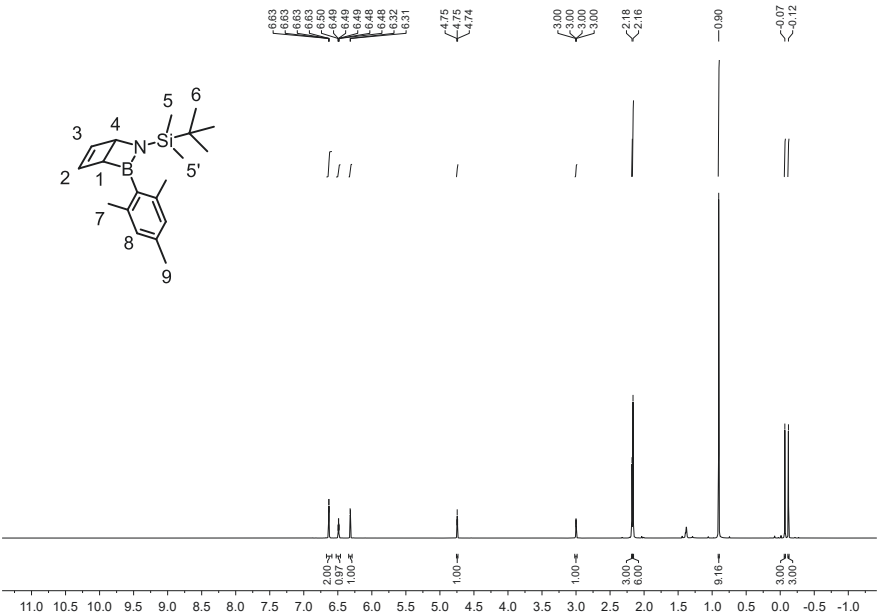

Figure S19. ^{1}H NMR of **BND1** in C_6D_{12}.

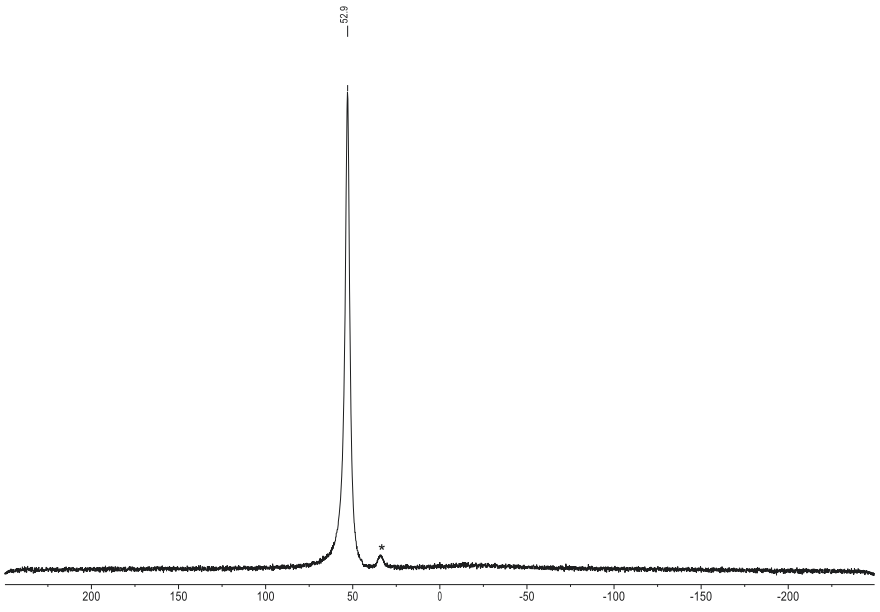

Figure S20. ^{11}B NMR of **BND1** in C_6D_{12}. * Denotes residual **BNB1**.

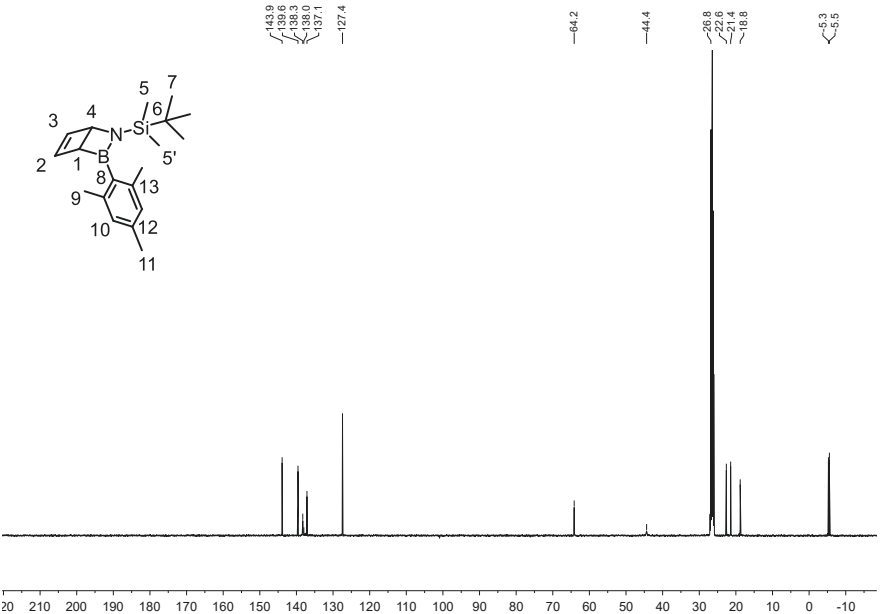

Figure S21: ^{13}C NMR of **BND1** in C_6D_{12}.

3.2 Synthesis of deuterated BNB1 (BNB1d1) and its Dewar isomer

BNB1Br was first synthesized in 2015 by Liu and co-workers.[6] While Liu and co-workers. brominated 1,2-dihydro-1,2-azaborinine **4**, followed by distillation and subsequent nucleophilic attack at the boron position, we opted for an inverse execution of these steps. This enables the synthesis to be carried out on a smaller scale, as column chromatography can be utilized. In contrast, for the distillation of the brominated azaborinine **4** described by Liu and co-workers we encountered losses in yield (<20%) in all our attempts when using smaller reaction scales. Upon obtaining **BNB1Br**, lithiation and subsequent hydrolysis with D_2O lead to the desired deuterated product.

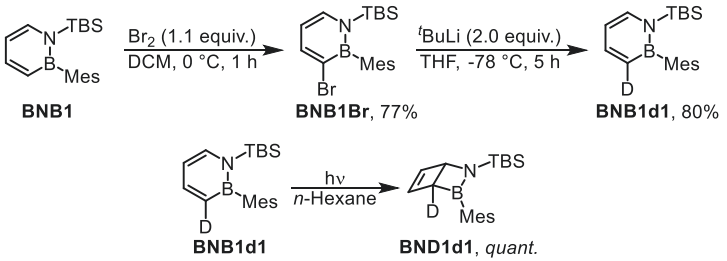

Scheme S2. Synthesis route for **BNB1d1** and its subsequent irradiation to **BND1d1**.

3-bromo-1-(*tert*-butyldimethylsilyl)-2-mesityl-1,2-dihydro-1,2-azaborinine (BNB1Br)

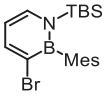

BNB1Br

In a dried Schlenk round bottom flask Br_2 (5.5 mL, 0.12 M in DCM, 1.1 equiv.) was added dropwise to **BNB1** (0.19 g, 0.60 mmol, 1.0 equiv.) dissolved in DCM (2 mL) at 0 °C over 1 h. Afterwards, the reaction was quenched with an aqueous sodium thiosulfate solution and the aqueous phase was extracted with *n*-hexane (3 × 10 mL). The combined organic phases were washed with brine, dried over $MgSO_4$, filtered, and the solvent was removed *in vacuo*. **BNB1Br** was purified by column chromatography (*n*-hexane/DCM, 99/1) yielding a colorless solid (0.23 g, 80%). The analytical data is in accordance with the literature.[6]

$C_{19}H_{29}BNSiBr$ (390.25 $\frac{g}{mol}$)

M_p: 85.0 °C

R_f: 0.86 (*n*-hexane/EA = 98:2) [UV]

^{1}H NMR(600.13 MHz, C_6D_{12}): δ = 7.78 (dd, ^3J = 7.1 Hz, ^4J = 0.8 Hz, 1H, H-1), 7.36 (dd, ^3J = 6.8 Hz, ^4J = 0.7 Hz, 1H, H-3), 6.72 (s, 2H, H-7), 6.15 (m, 1H, H-2), 2.23 (s, 3H, H-8), 2.04 (s, 6H, H-6), 0.92 (s, 9H, H-5), -0.03 (s, 6H, H-4).

^{11}B NMR(192.55 MHz, C_6D_{12}): δ = 39.8.

^{13}C NMR(150.90 MHz, C_6D_{12}): δ = 144.6 (C-2), 140.1 (br, C-8), 139.3 (C-13), 137.6 (C-4), 137.3 (C-12), 133.7 (br, C-1), 127.6 (C-10), 112.0 (C-3), 27.9 (C-7), 23.1 (C-9), 21.5 (C-11), 19.9 (C-6), -2.8 (C-5).

GC-MS(EI): t_r = 10.36 min, $\frac{m}{z}$ ($I_{base\ peak}$ %) = 391.1 ($M^{\bullet+}$, 13), 389.2 ($M^{\bullet+}$, 13), 334.1 ($M^{\bullet+}$ - ^{t}Bu$^\bullet$, 96), 332.1 ($M^{\bullet+}$ - ^{t}Bu$^\bullet$, 100), 317.0 (5), 311.3 ($M^{\bullet+}$ - Br$^\bullet$, 6), 304.1 (13), 302.0 (12), 254.2 ($M^{\bullet+}$ - ^{t}Bu$^\bullet$, Br$^\bullet$, 89), 253.2 (90), 252.2 (62), 238.2 (74), 224.1 (26), 210.1 (21), 194.1 (21), 73.0 (50), 59.0 (23), 57.1 (25, ^{t}Bu$^+$).

IR (ATR, $\tilde{\nu}$): 3017 (w), 2958 (w), 2928 (w), 2857 (w), 1601 (m), 1553 (w), 1463 (m), 1441 (m), 1403 (w), 1329 (s), 1261 (s), 1236 (m), 1159 (w), 1105 (m), 1057 (w), 983 (s), 934 (m), 814 (vs), 777 (vs), 743 (m), 702 (vs).

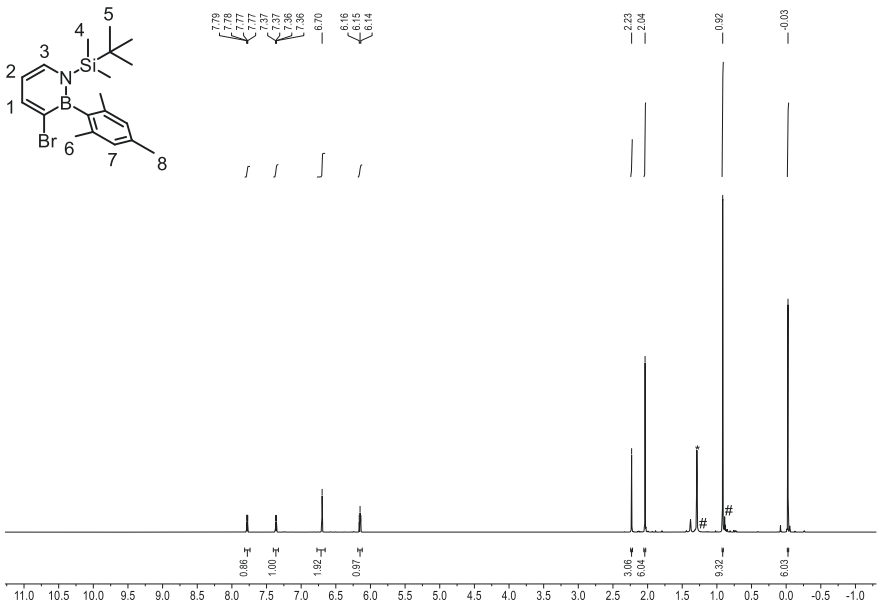

Figure S22. ^{1}H NMR of **BNB1Br** in C_6D_{12} (* denotes grease and # residual *n*-hexane).

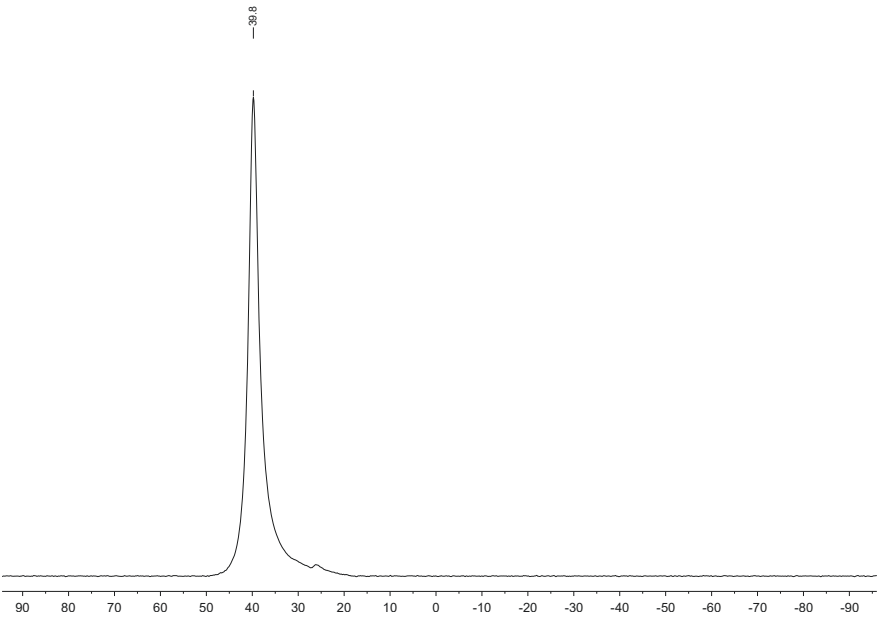

Figure S23: ^{11}B NMR of **BNB1Br** in C_6D_{12}.

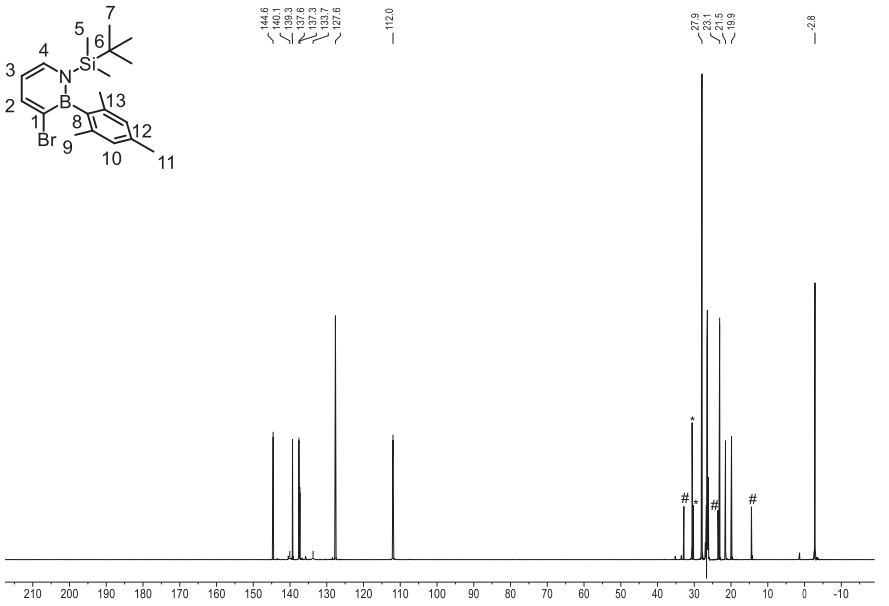

Figure S24: ^{13}C NMR of **BNB1Br** in C_6D_{12} (* denotes grease and # residual *n*-hexane).

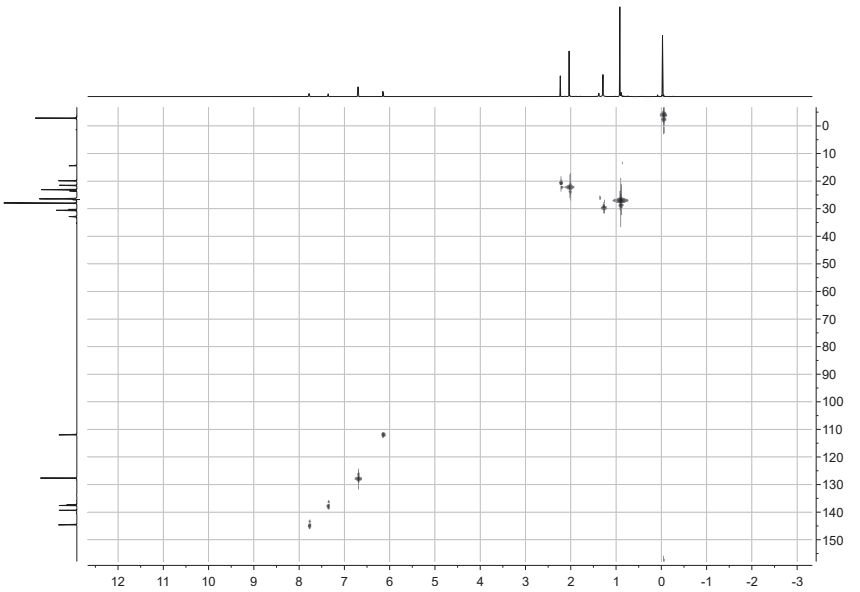

Figure S25. ^{1}H,^{13}C HSQC-NMR of **BNB1Br** in C_6D_{12}.

1-(*tert*-butyldimethylsilyl)-2-mesityl-1,2-dihydro-1,2-azaborinine-3-d (BNB1d1)

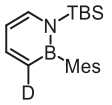

BNB1d1

BNB1Br (88.2 mg, 226 µmol, 1 equiv.) was dissolved in THF (2 mL) in a flame dried Schlenk tube and cooled to -78 °C before ^{t}BuLi (0.27 mL, 1.7 M in *n*-pentane, 2 equiv.) was added dropwise. The solution was stirred for 5 h, before being quenched with D_2O (1 mL) and allowed to warm to rt. The aqueous phase was extracted with DCM (3 × 5 mL) and the combined organic phases were dried over Na_2SO_4. The filtrate was reduced *in vacuo* and purified via flash column chromatography (100:0 to 95:5, *n*-hexane/DCM over 10 CV) and the product was obtained as a colorless oil (54.4 mg, 174 µmol, 77 %).

$C_{19}H_{29}DBNSi$ (312.36 $\frac{g}{mol}$)

R$_f$: 0.27 (n-hexane/$CHCl_3$ = 20:1) [UV]

^{1}H NMR(600.13 MHz, C_6D_{12}): δ = 7.44 (d, ^3J = 5.9 Hz, 1H, H-1), 7.37 (d, ^3J = 6.6 Hz, 1H, H-3), 6.68 (s, 2H, H-7), 6.27 (m, 1H, H-2), 2.21 (s, 3H, H-8), 2.04 (s, 6H, H-6), 0.91 (s, 9H, H-5), -0.01 (s, 6H, H-4).

^{2}H NMR(107.49 MHz, *n*-hexane): δ = 6.64.

^{11}B NMR(192.55 MHz, C_6D_{12}): δ = 40.2.

^{13}C NMR(150.90 MHz, C_6D_{12}): δ = 142.9 (s, C-2), 142.6 (br, C-8), 139.0 (s, C-13), 138.2 (s, C-4), 136.5 (s, C-12), 132.8 (br, C-1), 127.6 (s, C-10), 112.2 (s, C-3), 27.9 (s, C-7), 23.7 (s, C-9), 21.4 (s, C-11), 19.8 (s, C-6), -3.0 (s, C-5).

HR-MS (APCI): m/z calc. For $[M+H]^+$ 313.23741, 313.23798 found.

IR (ATR, ṽ): 3062 (w), 2957 (w), 2928 (m), 2857 (w), 1605 (m), 1500 (s), 1466 (m), 1448 (m), 1392 (w), 1351 (m), 1262 (s), 1228 (w), 1160 (w), 1098 (m), 1068 (w), 997 (w), 960 (m), 930 (w), 840 (s), 811 (s), 781 (s), 736 (m), 710 (s), 680 (m).

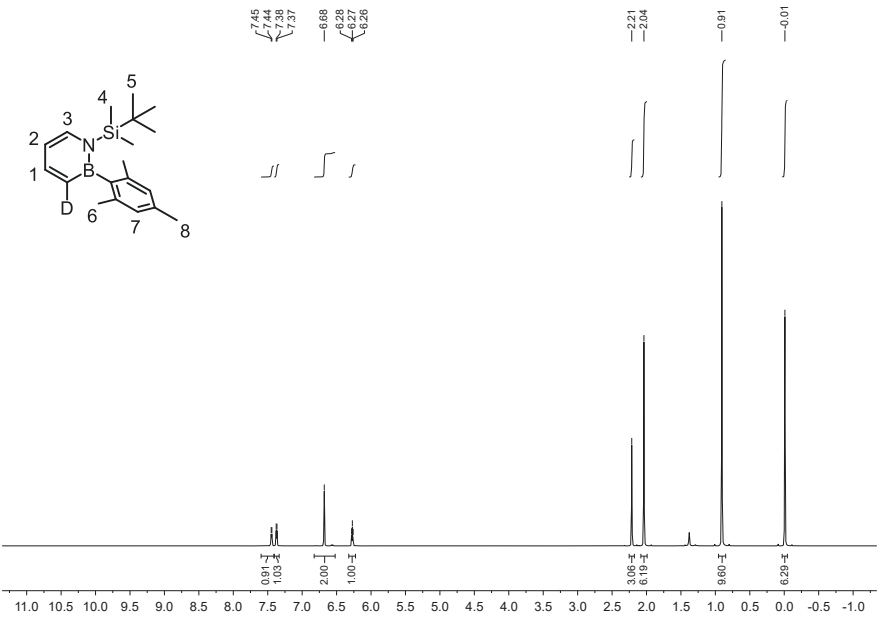

Figure S26. ^{1}H NMR of **BNB1d1** in C_6D_{12}.

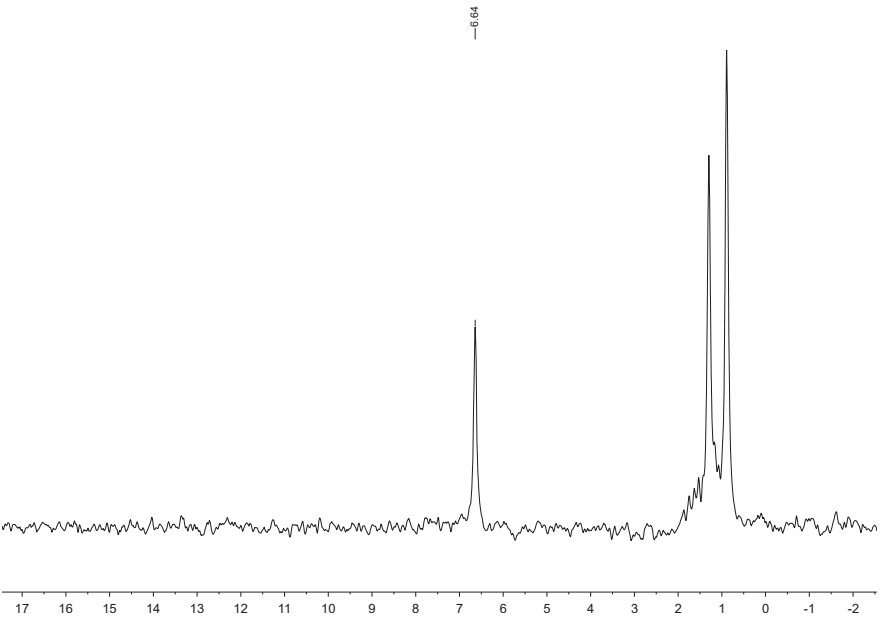

Figure S27. ^{2}H NMR of **BNB1d1** in *n*-hexane. The remaining signals originate from partially deuterated *n*-hexane.

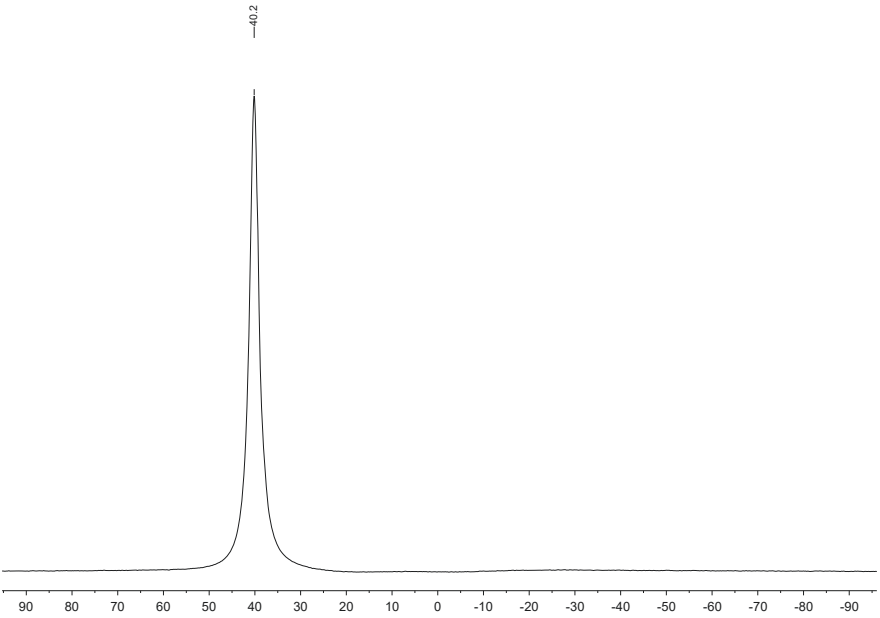

Figure S28: ^{11}B NMR of **BNB1d1** in C_6D_{12}.

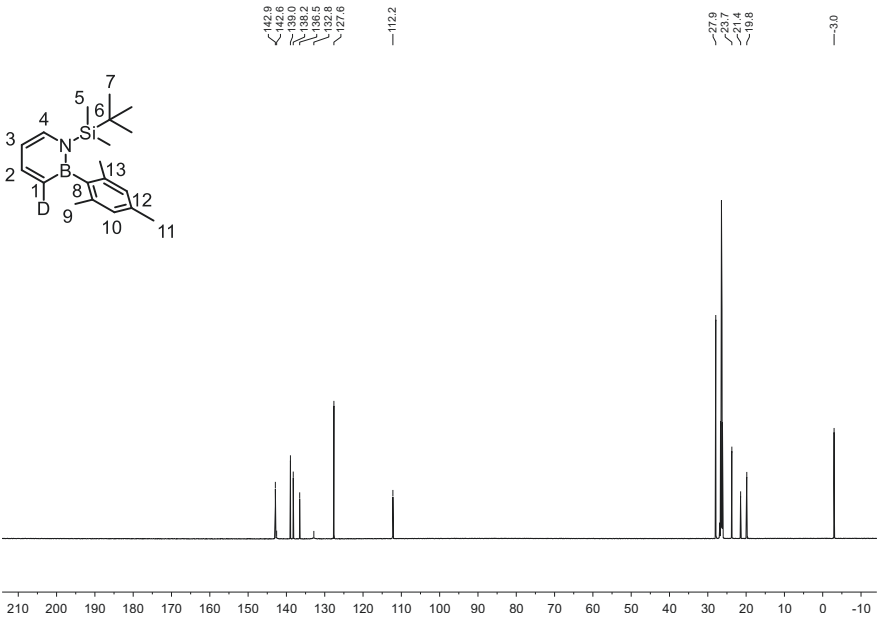

Figure S29: ^{13}C NMR of **BNB1d1** in C_6D_{12}.

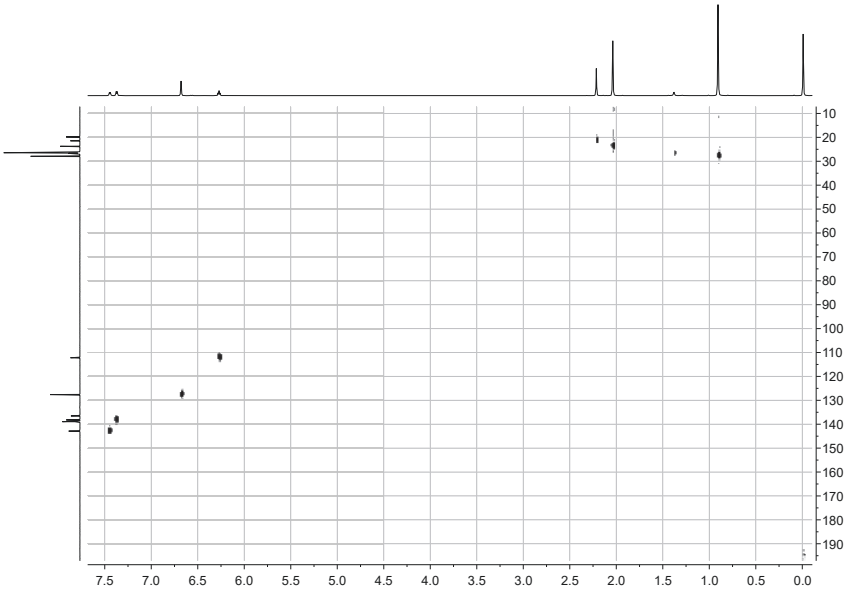

Figure S30. $^{1}H,^{13}C$ HSQC-NMR of **BNB1d1** in C_6D_{12}.

2-(*tert*-butyldimethylsilyl)-3-mesityl-2-aza-3-borabicyclo[2.2.0]hex-5-ene-4-d (BND1d1)

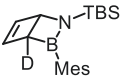

BND1d1

BNB1d1 (30 mg, 96 µmol) was dissolved in C_6D_{12} (0.4 mL) in a dried quartz J. Young tube and irradiated according to GP-A (280 nm – 400 nm) until full conversion of **BNB1d1** to **BND1d1** was reached. Subsequently, the solvent was removed *in vacuo* yielding a pale-yellow oil. (30 mg, 96 µmol, quant.).

$C_{19}H_{29}DBNSi$ (312.36 $\frac{g}{mol}$)

^{1}H NMR(600.13 MHz, C_6D_{12}): δ = 6.63 (s, 2H, H-7), 6.49 (m, 1H, H-1), 6.32 (m, 1H, H-2), 4.74 (m, 1H, H-3), 2.18 (s, 3H, H-8), 2.16 (s, 6H, H-6), 0.90 (s, 9H, H-5), -0.07 (s, 3H, H-4/4'), -0.12 (s, 3H, H-4'/4).

^{2}H NMR(107.49 MHz, *n*-hexane): δ = 3.04.

^{11}B NMR(192.55 MHz, C_6D_{12}): δ = 52.8.

^{13}C NMR(150.90 MHz, C_6D_{12}): δ = 143.8 (s, C-2), 139.6 (s, C-3), 138.2 (s, C-13), 137.8 (br, C-8), 137.1 (s, C-12), 127.4 (s, C-10), 64.0 (s, C-4), 44.1 (br, C-1), 26.8 (s, C-7), 22.6 (s, C-9), 21.4 (s, C-11), 18.8 (s, C-6), -5.3 (s, C-5/5'), -5.6 (s, C-5'/5).

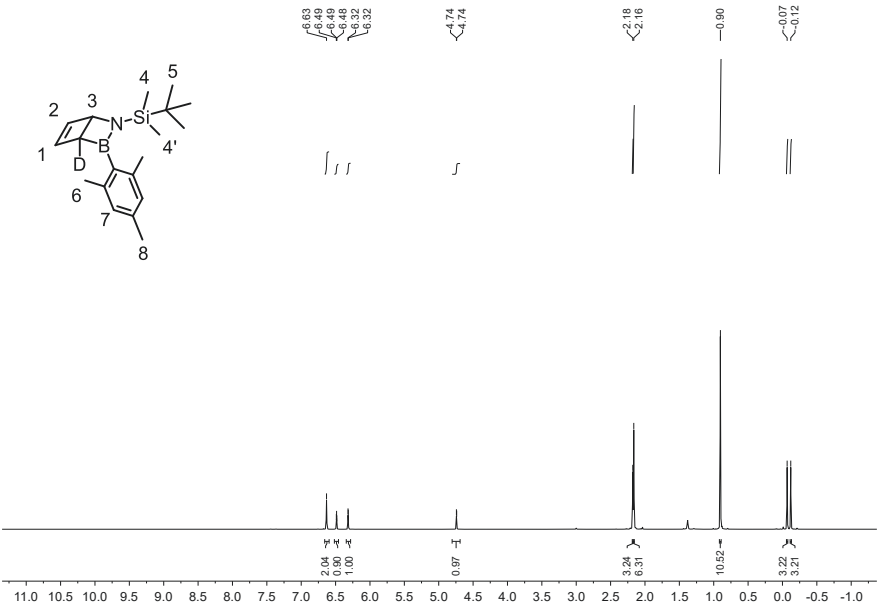

Figure S31. ^{1}H NMR of **BND1d1** in C_6D_{12}.

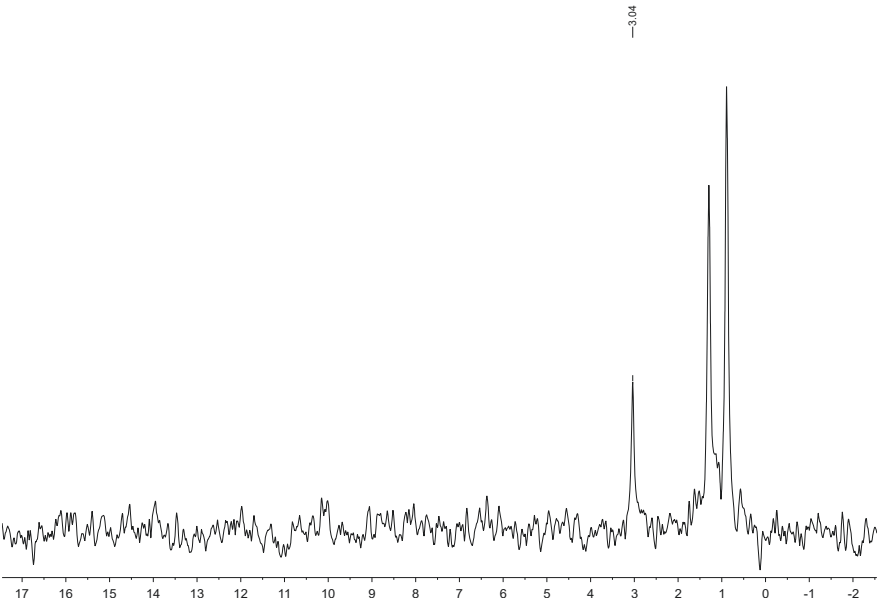

Figure S32. ^{2}H NMR of **BND1d1** in *n*-hexane. The remaining signals originate from partially deuterated *n*-hexane.

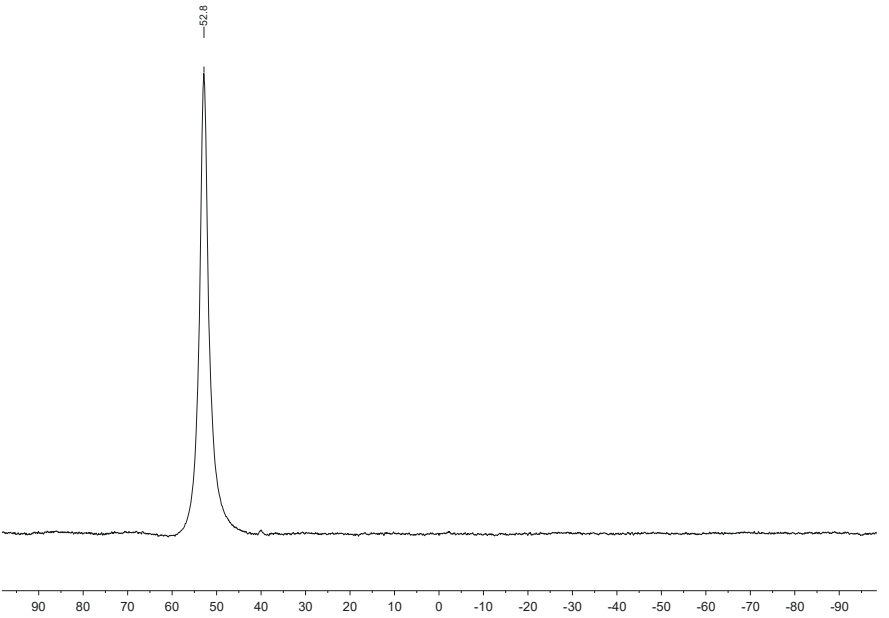

Figure S33: ^{11}B NMR of **BND1d1** in C_6D_{12}.

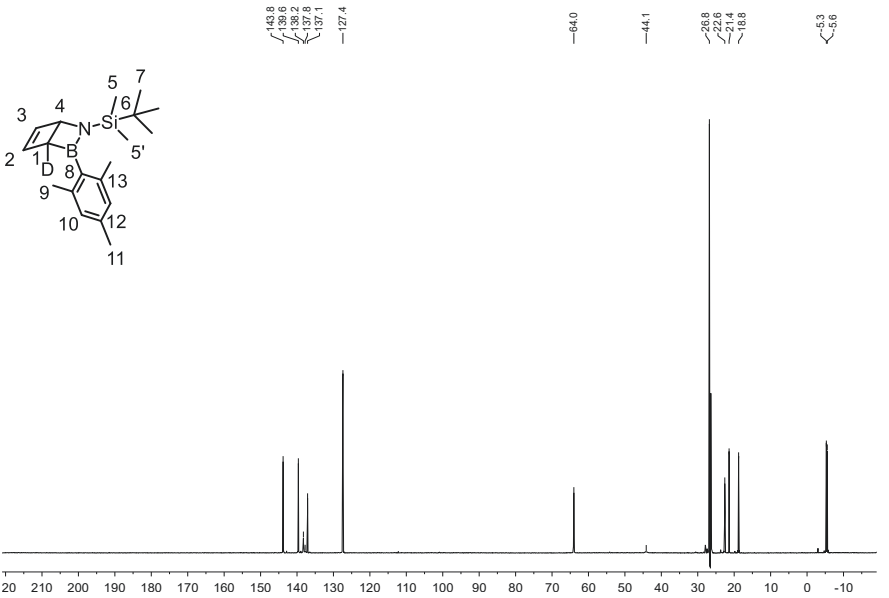

Figure S34: ^{13}C NMR of **BND1d1** in C_6D_{12}.

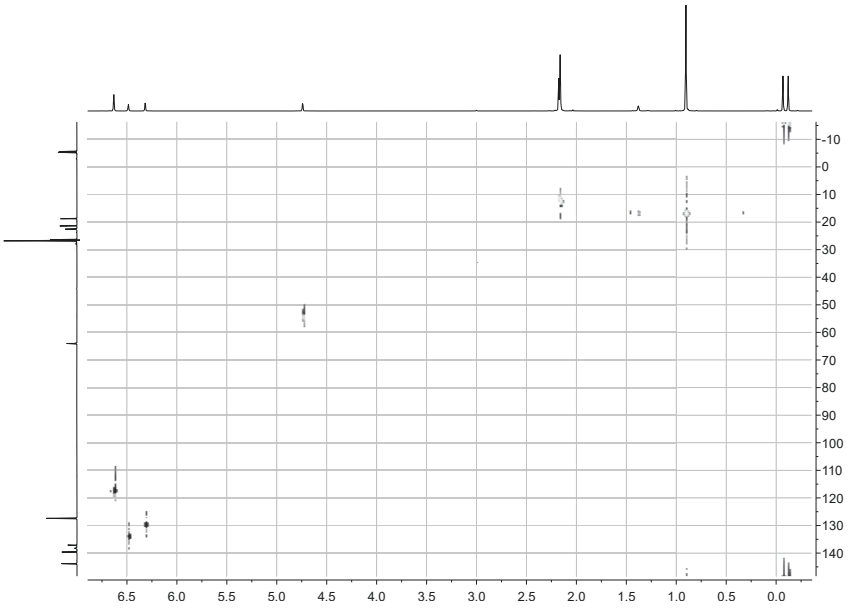

Figure S35. $^{1}H,^{13}C$ HSQC-NMR of **BND1d1** in C_6D_{12}.

3.3 Synthesis of N-^{t}Bu substituted 1,2-dihydro-1,2-azaborinine BNB2 and its Dewar isomer

BNB2 was first synthesized by Braunschweig and co-workers from the corresponding iminoborane and acetylene using Rh catalysis.[7] We instead opted for a synthetic strategy through the 1,2-dihydro-1,2-azaborinine derivative **7**, which was reported by Lamm and Liu.[8] In analogy to Liu and co-workers in situ generated allylboron dichloride is reacted with allyl tin species to obtain boramine **5**.[9] Hereby, tetraallyl tin is employed instead of the allyltriphenyl tin originally used by Liu and co-workers for atom efficiency reasons. Tetraallyl tin was synthesized by transmtalation of $SnCl_4$ with comercially available allylmagnesium chloride.[10] The subsequent ring closing metathesis and dehydrogenation were carried out following the estabilshed protocolls by Liu and co-workers.[8-9] **7** was used in the next step without seperation from the fully hydrated side product. Based on the synthesis of **BNB1**, the reaction of **7** with MesLi yielded the air stable **BNB2**, which upon irradiation lead to **BND2**.[4c]

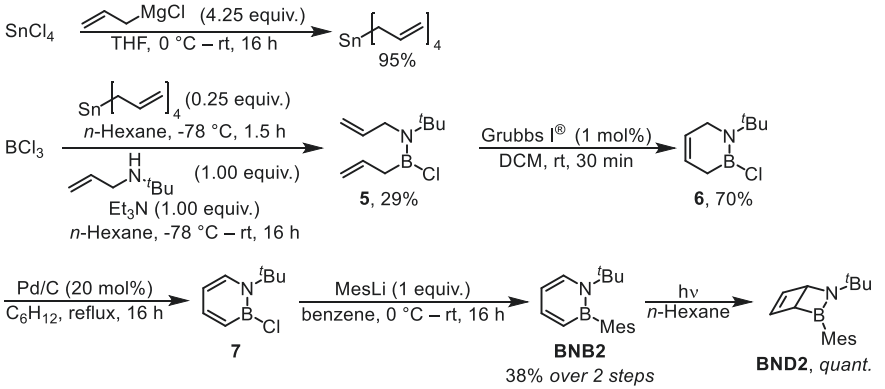

Scheme S3. Synthesis route of **BNB2** and its subsequent irradiation to **BND2**.

Tetraallyl tin

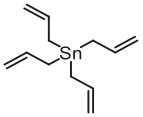

Tetraallyl tin was synthesized according to literature with slight modifications.[10] In a dry, cooled (ice bath) three-necked flask containing 100 mL of dry *n*-hexane tin(IV)chloride (100 mmol, 12 mL) was added quickly. Then 100 mL of THF was added carefully. This led to the formation of tin-THF complexes precipitating as a colorless solid. After the addition of 200 mL diethyl ether, allyl magnesium chloride (425 mmol, 250 mL of 1.7 M solution in THF) was added dropwise over one hour. The reaction mixture was brought to room temperature slowly and the reaction mixture was stirred overnight. Remnant allyl magnesium chloride was quenched with saturated $NH_4Cl_{(aq.)}$. The organic phase was separated and washed with water, brine, and dried over $MgSO_4$. The solvents were removed in vacuo to give tetraallyl tin (95 mmol, 27.8 g, 95 %) as a colorless oil. The analytical data is in accordance with literature.[11]

$C_{10}H_{19}BNCl$ (283.00 $\frac{g}{mol}$)

^{1}H NMR (300.13 MHz, C_6D_6): δ = 5.89 (m, 4H, H-2), 4.87 (m, 4H, H-3‘), 4.78 (m, 4H, H-3), 1.80 (m, 8H, H-1).

^{13}C NMR (75.48 MHz, C_6D_6): δ = 136.8, 111.3, 16.3 (C1).

^{119}Sn NMR (111.89 MHz, C_6D_6): δ = -48.1.

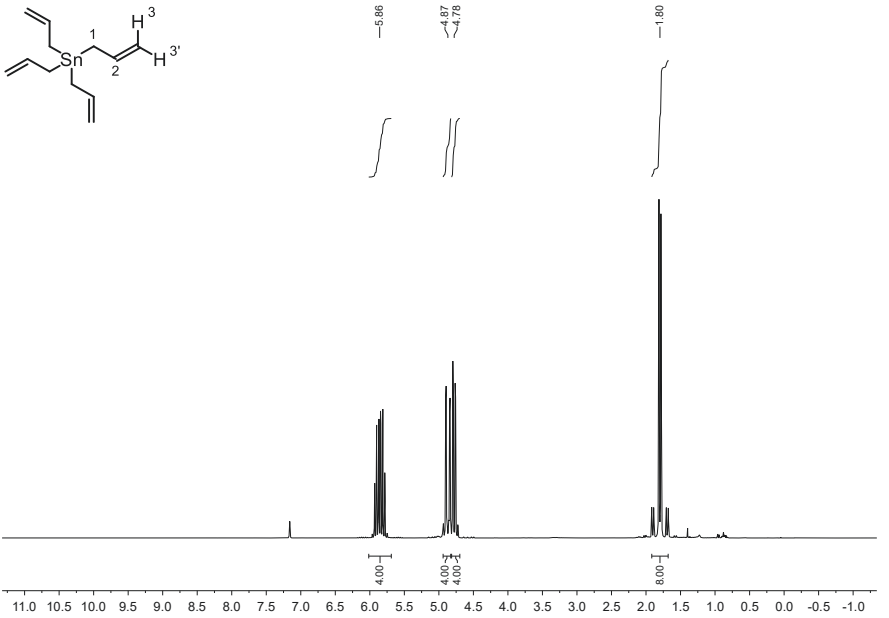

Figure S36. ^{1}H NMR of tetraallyl tin in C_6D_6.

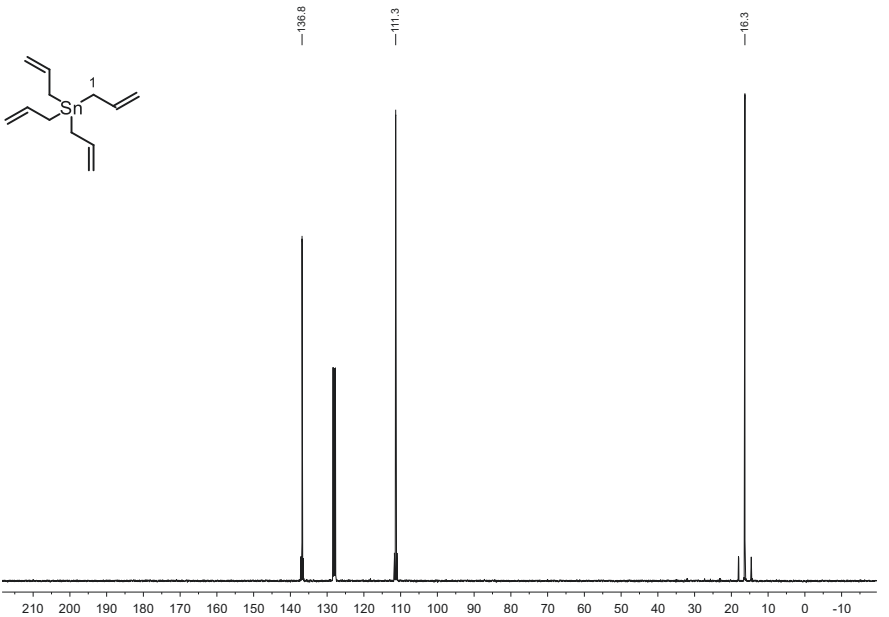

Figure S37: ^{13}C NMR of tetraallyl tin in C_6D_6.

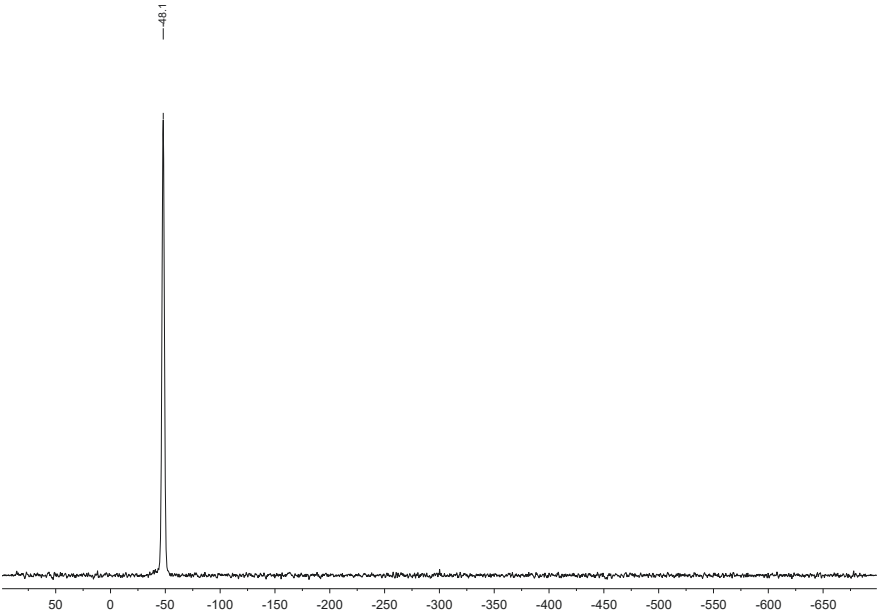

Figure S38: ^{119}Sn-NMR of tetraallyl tin in C_6D_6.

N,1-diallyl-N-(*tert*-butyl)-1-chloroboranamine (5)

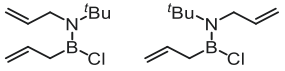

5

5 was synthesized according to literature with slight modifications.[9] To a mixture of 100 mL DCM and 100 mL hexane in a dried Schlenk round bottom flask, cooled to -78 °C, BCl_3 (100 mmol, 1 M solution in DCM, 100 mL) was added. Tetraallyl tin (7.07 g, 25.0 mmol) was dissolved in 50 mL hexane and added dropwise to the rection mixture. After 3 h of stirring at -78°C, N-(*tert*-butyl)prop-2-en-1-amine (100 mmol dissolved in 50 mL hexane) was added dropwise. After complete addition, the reaction mixture was stirred for 20 minutes. Then dry triethylamine (110 mmol in 50 mL hexanes) was added. The reaction mixture was brought to room temperature overnight. The dichloromethane was removed *in vacuo* and the resulting mixture was filtered. The filtrate was concentrated under reduced pressure. The crude product was subjected to vacuum distillation resulting in 11.5 g (29%) **5** (b. p. 34-38 °C, 60 µbar) still containing impurities and hydrolyzed product. As the ^{1}H and ^{11}B NMR spectral data was in good accordance with literature the product was used as obtained.[9]

$C_{10}H_{19}BNCl$ (399.06 $\frac{g}{mol}$)

b. p.: 34–38 °C (60 µbar)

^{1}H NMR (400.16 MHz, C_6D_6): δ = 6.09 (m, 2H, H-2, H-2', rotamer 1), 5.70 (m, 1H, H-2/2', rotamer 2), 5.55 (m, 1H, H-2'/2, rotamer 2), 5.01 (m, 8H, H-1, H-1', rotamer 1 + 2), 3.91 (s, 2H), 3.54 (s, 2H), 2.26 (s, 2H), 1.98 (s, 2H), 1.31 (s, 9H, H-3), 1.10 (s, 9H, H-3).

^{11}B NMR (128.39 MHz, C_6D_6): 39.9 (rotamer 1), 39.1 (rotamer 2), 31.8 (hydrolyzed product, 15 %), 26.1 (unknown impurity 3 %).

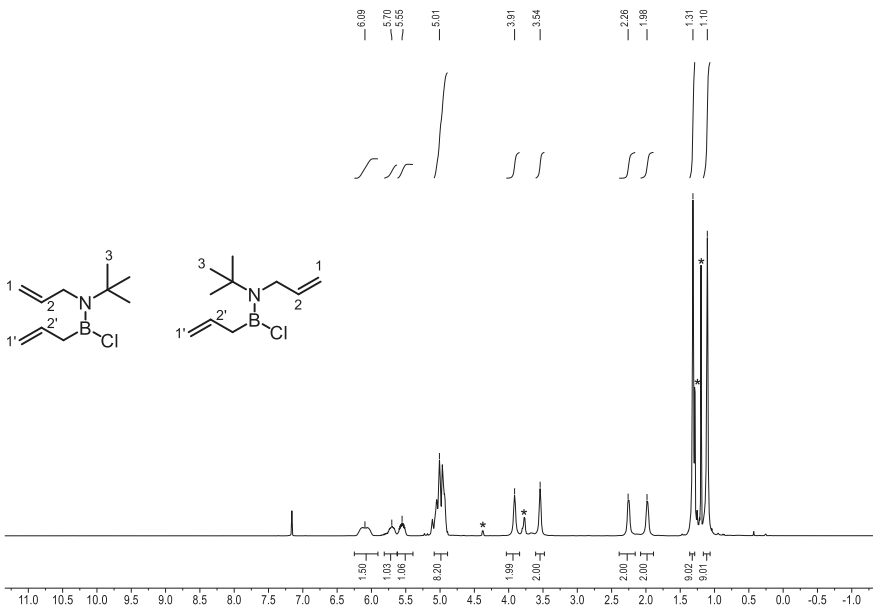

Figure S39. ^{1}H NMR of **5** in C_6D_6. Both rotamers are present. *Denotes signals of the hydrolysed species and unknown impurities.

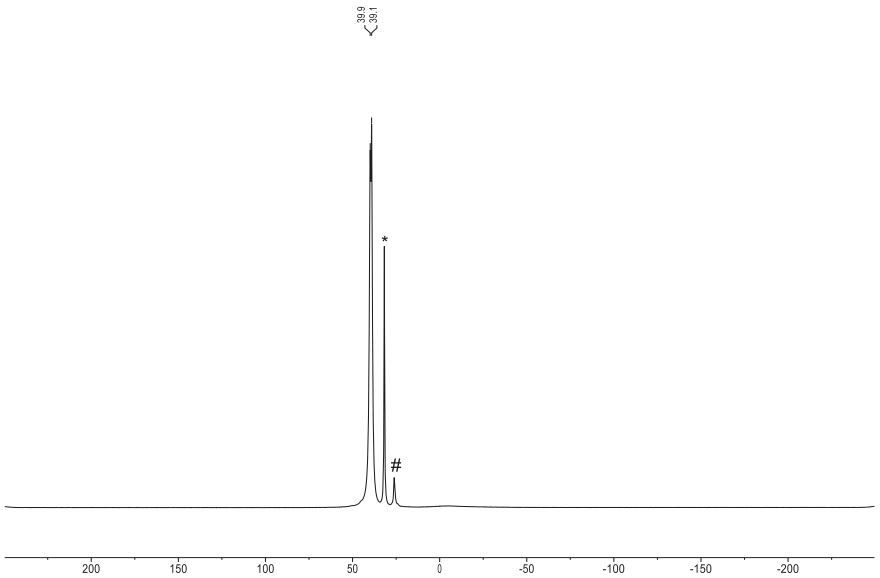

Figure S40. ^{1}H NMR of **5** in C_6D_6. Both rotamers are present. * Denotes the hydrolysed species. # Denotes an unknown side product.

1-(*tert*-butyl)-2-chloro-1,2,3,6-tetrahydro-1,2-azaborinine (6)

6

6 was synthesized according to literature.[9] In a glove box, a solution of Grubbs 1st generation catalyst (0.45 mg, 0.55 mmol in 20 mL dichloromethane) was prepared and added to a stirring solution of **5** (11.5g, 67 mmol in 200 mL dichloromethane). The solution was stirred at rt for 30 min until no further gas development was observed. The solvent was removed. Then *n*-hexane (200 mL) was added, and the mixture was filtered. The solvent was removed again under reduced pressure. The crude product was distilled *in vacuo* (b. p. 30–34 °C, 66 µbar) yielding **6** (8.15 g, 47.6 mmol, 70%) as a clear colorless oil. The ^{1}H and ^{11}B NMR spectroscopic data are in good accordance with reported literature and the product was used as received.[9]

$C_8H_{15}BNCl$ (171.48 $\frac{g}{mol}$)

b. p.: 30–34 °C (66 µbar)

^{1}H NMR (400.16 MHz, C_6D_6): δ = 5.55 (s, 1H), 5.26 (m, 1H), 3.39 (m, 2H), 1.82 (m, 2H), 1.27 (s, 9H).

^{11}B NMR (128.39 MHz, C_6D_6): δ = 38.2 (product 89 %), 31.8 (hydrolyzed product 9 %), 26.0 (unknown impurity 2 %).

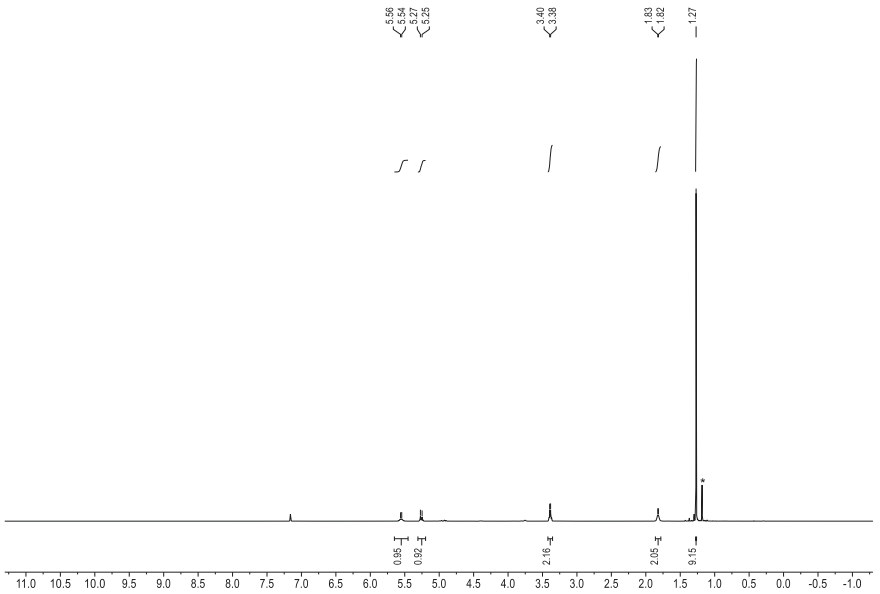

Figure S41. ^{1}H NMR of **6** in C_6D_6. *Denotes the ^{t}Bu-signal of the hydrolysed species.

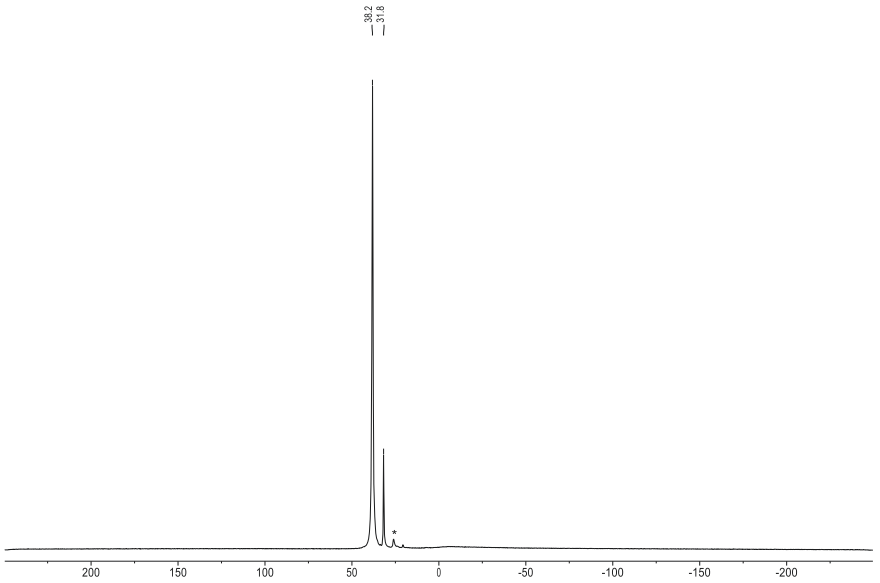

Figure S42. ^{11}B NMR of **6** in C_6D_6. The signal at 31.8 ppm corresponds to the hydrolysed species.*Denotes an unknown impurity.

1-(*tert*-butyl)-2-chloro-1,2-dihydro-1,2-azaborinine (7)

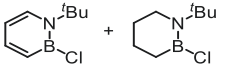

product **7** sideproduct

7 was synthesized following a procedure of Lamm *et al*. with minor modifications.[8] To a dried Schlenk round bottom flask containing a suspension of Pd/C (2.22 g, Pd 10%wt) in 40 mL freshly distilled cyclohexene, **6** (1.80 g) was added under argon. The flask was sealed and heated to 75 °C for 18 h. After cooling down, the suspension was passed through a glass fiber filter to remove the charcoal. The solvents were removed in vacuum and NMR spectra were recorded. ^{11}B and ^{13}C NMR spectra indicated that the resulting product mixture consists of dehydrogenated product (~80%) and the hydrogenated side product (~20%),[8] which was used in further steps as obtained. The side product did not affect the progress of the following reaction and could be removed in the next step by column chromatography easily.

$C_8H_{13}BNCl$ (169.46 $\frac{g}{mol}$)

^{1}H NMR (400.16 MHz, CD_2Cl_2): δ = 7.59 (m, 1H), 7.50 (m, 1H), 6.60 (m, 1H), 6.26 (m, 1H), 1.71 (s, 2H).

^{11}B NMR (128.39 MHz, CD_2Cl_2): δ = 33.3 (product), 38.4 (fully hydrogenated side product).

^{13}C NMR (100.62 MHz, CD_2Cl_2): δ = product: 144.1, 135.7, 131.2 (br.), 110.2, 61.3, 30.9, fully hydrogenated side product: 57.2, 47.2, 32.2, 30.6, 29.3, 21.8.

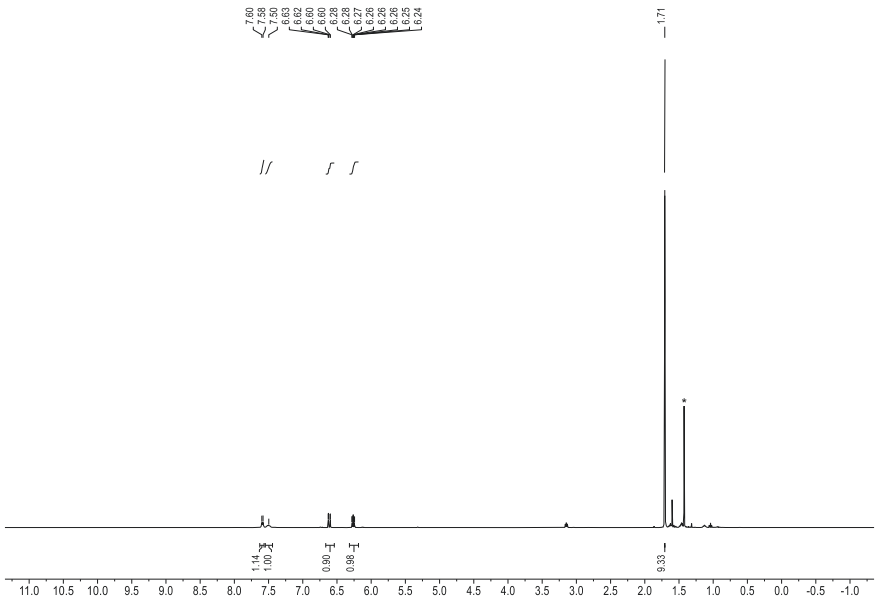

Figure S43. ^{1}H NMR of **7** in CD_2Cl_2. *Denotes the ^{t}Bu-signal of the fully hydrogenated species.

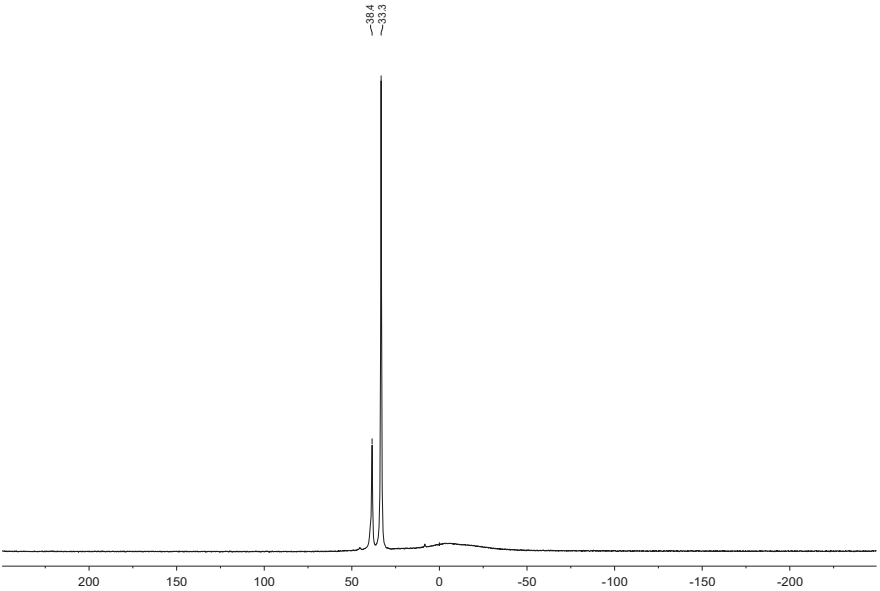

Figure S44. ^{11}B NMR of **7** in CD_2Cl_2. The signal 38.4 ppm corresponds to the fully hydrogenated species.

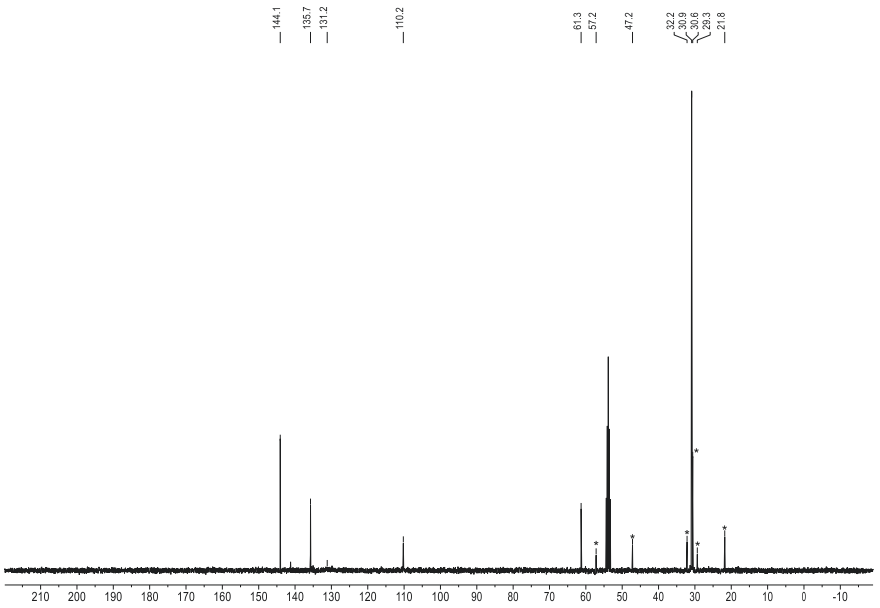

Figure S45. ^{1}H NMR of **7** in CD_2Cl_2. *Denotes signals corresponding to the fully hydrogenated species.

1-(*tert*-butyl)-2-mesityl-1,2-dihydro-1,2-azaborinine (BNB2)

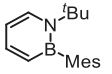

BNB2

In a dried Schlenk tube mesityllithium (630 mg, 5 mmol, 1.0 equiv.) was suspended in benzene. Subsequently **7** (845 mg, 5.00 mmol, 1 equiv.) was added. The tube was sealed and heated for 24 h to 75 °C. After cooling to room temperature distilled water (5 mL) was added. The aqueous phase was separated and washed with *n*-pentane. The combined organic phases were washed with brine and dried over $MgSO_4$. After removal of the solvents the crude mixture was subjected to flash column chromatography (SiO_2 80 g, *n*-hexane/DCM gradient from 100:0 to 95:0 over 15 CV). The product was obtained as crystalline white solid (480 mg, 1.9 mmol, 38%). The analytical data is in good agreement with that of Schäfer *et al.*.[7]

$C_{17}H_{24}BN$ ($253.20\ \frac{g}{mol}$)

M_p: 107.8 °C

R_f: 0.58 (*n*-hexane/EA = 98:2) [UV]

^{1}H NMR(600.13 MHz, CD_2Cl_2): δ = 7.63 (d, ^3J = 7.3 Hz, 1H, H-4), 7.46 (dd, ^3J = 10.7, 6.1 Hz, 1H, H-2), 6.79 (s, 2H, H-7), 6.40 (dd, ^3J = 10.7 Hz, ^4J = 1.7 Hz, 1H, H-1), 6.37 (ddd, ^3J = 7.3, 6.1 Hz ^4J = 1.7 Hz, 1H, H-3), 2.28 (s, 3H, H-8), 2.08 (s, 6H, H-6), 1.40 (s, 9H, H-5).

^{11}B NMR(128.39 MHz, C_6D_{12}): δ = 36.7.

^{13}C NMR(150.92 MHz, CD_2Cl_2): δ = 145.2 (br, C-7), 141.3 (s, C-2), 138.0 (s, C-12), 136.8 (s, C-4), 136.0 (s, C-11), 133.3 (br, C-1), 127.2 (s, C-9), 111.2 (s, C-3), 61.0 (s, C-6), 32.3 (s, C-5), 23.8 (C-8), 21.3 (C-10).

HR-MS (APCI): m/z calc. For $[M+H]^+$ 254.20776, found 254.20730.

GC-MS(EI): t_r = 8.15 min, $\frac{m}{z}$($I_{base\ peak}$ %) = 253.1 ($M^{\bullet+}$, 67), 197.1 ($MH^{\bullet+}$ - ^{t}Bu$^\bullet$, 100), 182.1 (74), 166.0 (13), 155.0 (9), 119.0 (Mes^+, 14), 105.1 (30), 91.0 (17), 78.0 (20), 57 (^{t}Bu$^+$, 68).

IR (ATR, ṽ): 2973 (w), 2910 (w), 2853 (w), 1605 (m), 1556 (w), 1512 (m), 1466 (m), 1385 (m), 1291 (m), 1195 (s), 1102 (m), 1031 (w), 971 (m), 934 (w), 882 (w), 848 (m), 747 (s), 703 (m).

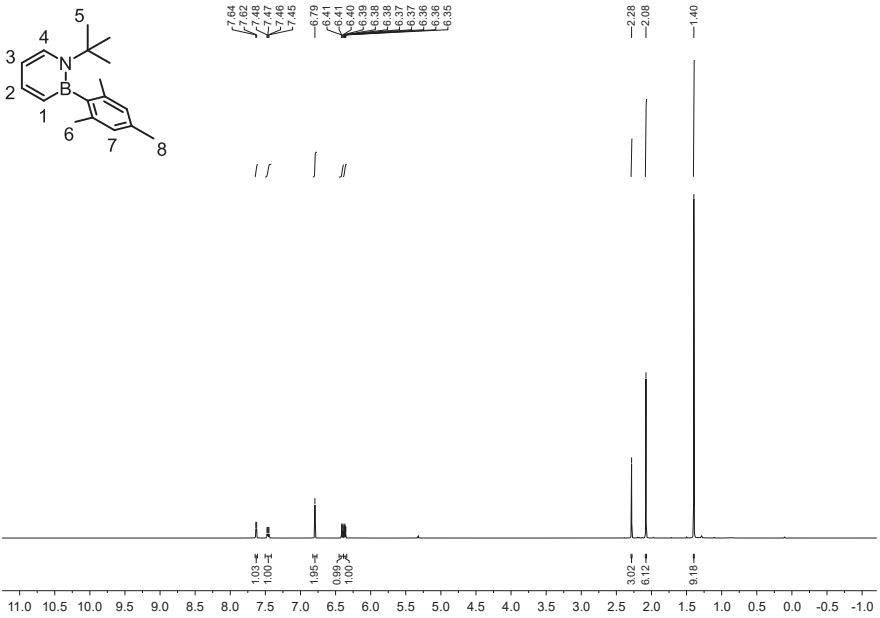

Figure S46. ^{1}H NMR of **BNB2** in CD_2Cl_2.

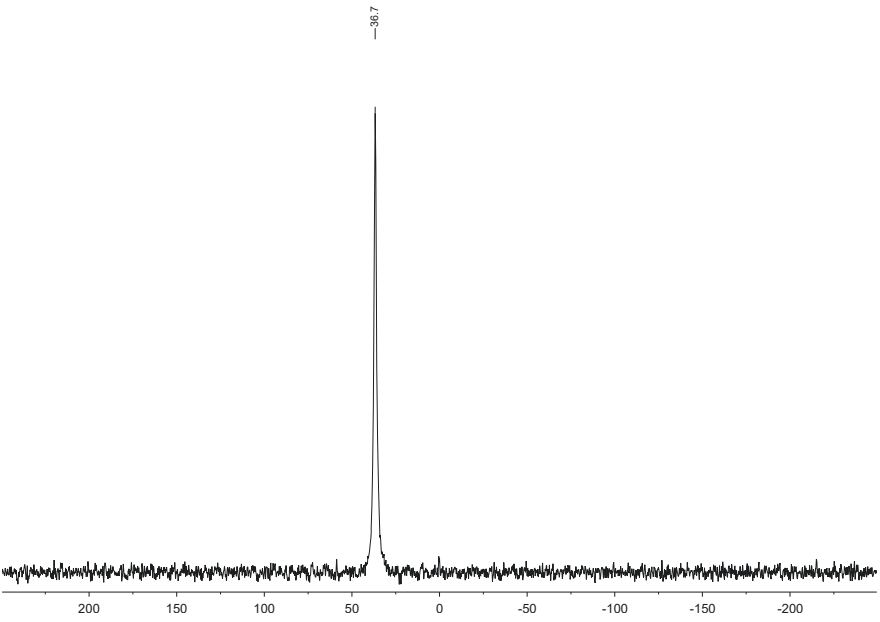

Figure S47: ^{11}B NMR of **BNB2** in CD_2Cl_2.

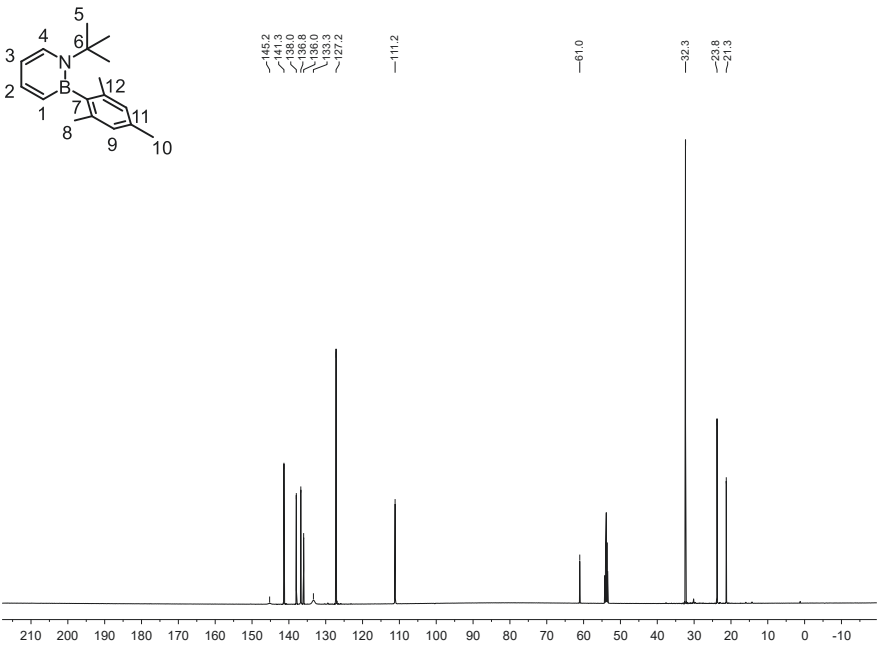

Figure S48: ^{13}C NMR of **BNB2** in CD_2Cl_2.

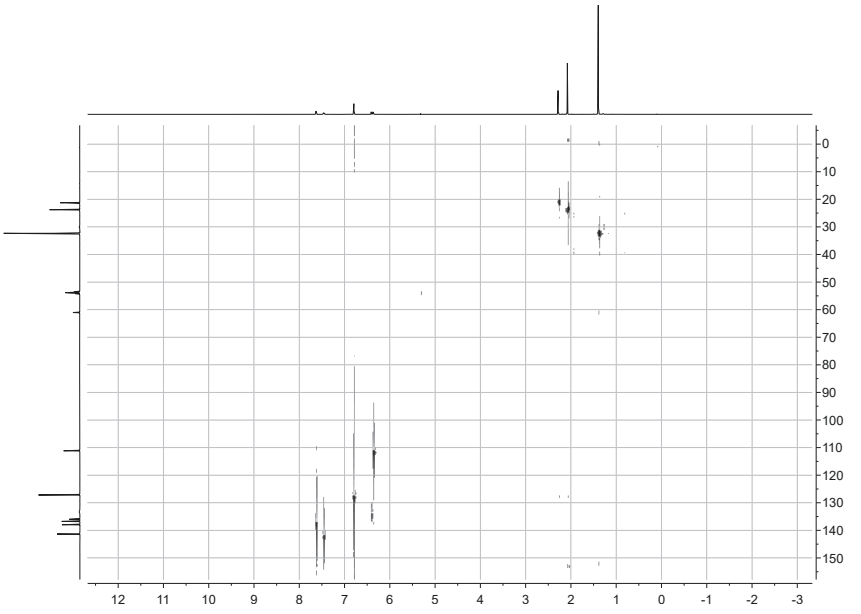

Figure S49. $^{1}H,^{13}C$ HSQC-NMR of **BNB2** in CD_2Cl_2.

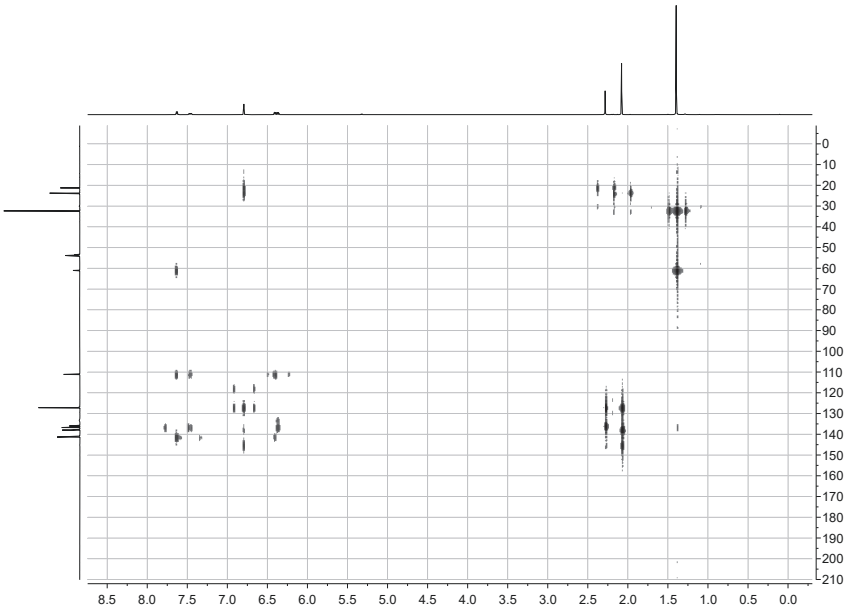

Figure S50. $^{1}H,^{13}C$ HMBC-NMR of **BNB2** in CD_2Cl_2.

2-(*tert*-butyl)-3-mesityl-2-aza-3-borabicyclo[2.2.0]hex-5-ene (BND2)

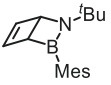

BND2

BNB2 (10 mg, 39 µmol) was dissolved in C_6D_{12} (0.4 mL) in a dried quartz J. Young tube and irradiated according to GP-A (280 nm – 400 nm) until full conversion of **BNB2** to **BND2** was reached. Subsequently, the solvent was removed *in vacuo* yielding a pale-yellow oil. (10 mg, 39 µmol, quant.).

$C_{17}H_{24}BN$ (253.20 $\frac{g}{mol}$)

M_p: 37.3 °C

^{1}H NMR(400.16 MHz, CD_2Cl_2): δ = 6.74 (s, 1H, H-8/8'), 6.73 (s, 1H, H-8/8'), 6.55 (m, 1H, H-2), 6.42 (d, ^3J = 2.3 Hz, 1H, H-3), 4.56 (t, ^3J = 2.2 Hz, 1H, H-4), 2.84 (dd, ^3J = 2.2 Hz, ^2J = 0.9 Hz, 1H, H-1), 2.23 (s, 3H, H-7/7'), 2.22 (s, 3H, H-7/7'), 2.15 (s, 3H, H-9), 1.10 (s, 9H, H-5).

^{11}B NMR(128.39 MHz, CD_2Cl_2): δ = 43.8.

^{13}C NMR(150.92 MHz, CD_2Cl_2): δ = 144.3 (s, C-2), 139.7 (s, C-3), 139.1 (s, C-12), 138.5 (s, C-9/9'), 137.5 (br, C-7), 137.0 (s, C-9/9'), 127.0 (s, C-10/10'), 126.9 (s, C-10/10'), 61.1 (s, C-4), 52.9 (s, C-5), 39.3 (br, C-1), 28.8 (s, C-6), 22.6 (s, C-8/8'), 22.3 (s, C-11), 21.3 (s, C-8/8').

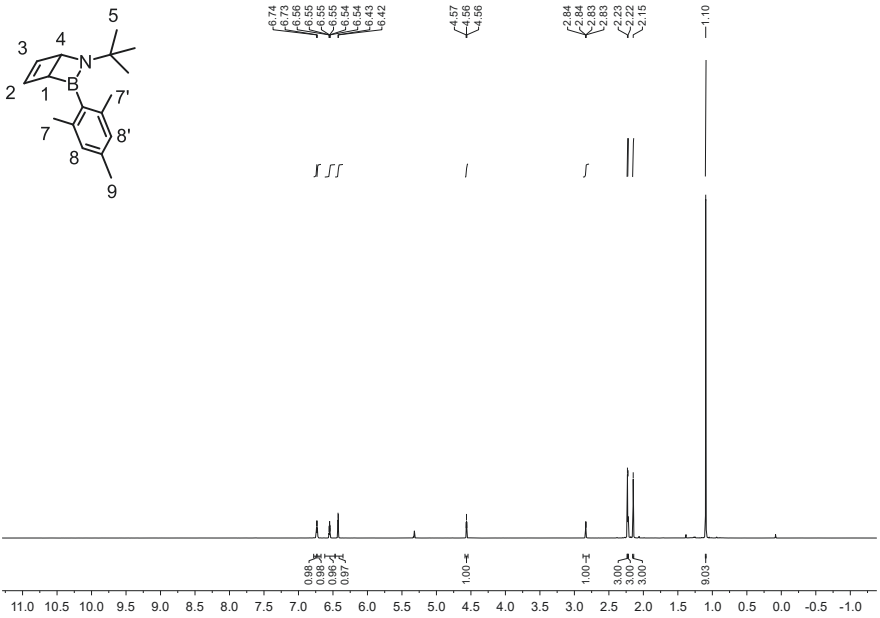

Figure S51. ^{1}H NMR of **BND2** in CD_2Cl_2.

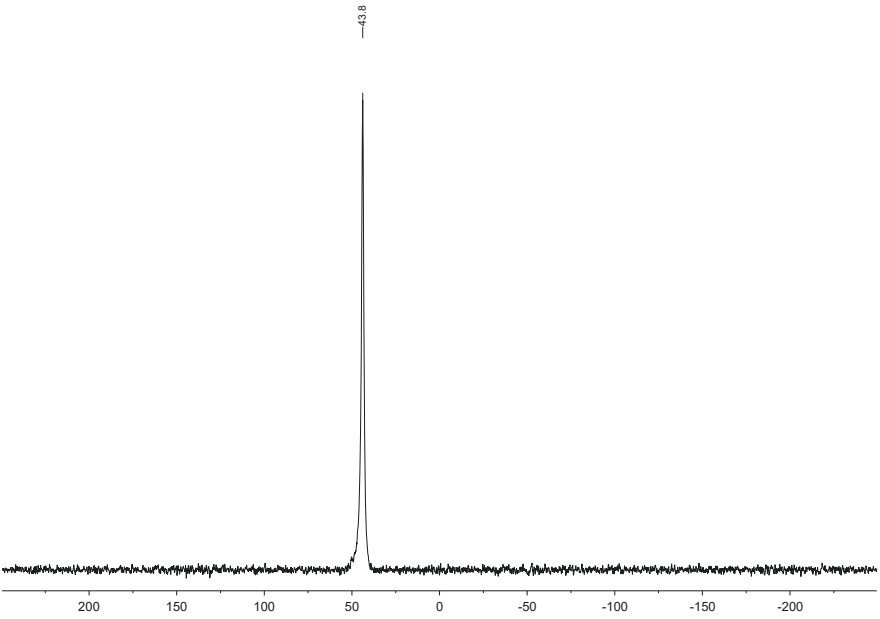

Figure S52. ^{11}B NMR of **BND2** in CD_2Cl_2.

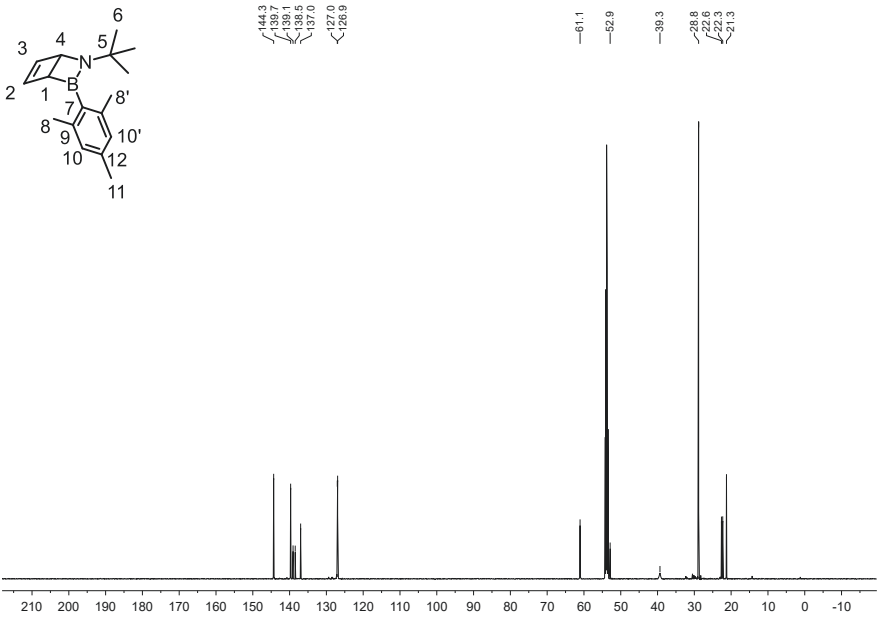

Figure S53: ^{13}C NMR of **BND2** in CD_2Cl_2. The aromatic carbon atom directly bound to boron was determined to be 137.5 ppm by LR-HSQCMBC optimized for ${}^{n}J_{CH}$ = 2 Hz.

3.4 Synthesis of Ag(I) and Cu(I) salts

$Li[Al(OC(CF_3)_3)_4]$ was synthesized by protonolysis of $LiAlH_4$ with perfluoro-*tert*-butanol and subsequent extraction of the product utilizing perfluoro hexanes according to the improved protocol by Krossing and coworkers.[12] $Ag[Al(OC(CF_3)_3)_4]$ was synthesized by salt metathesis of AgF with $Li[Al(OC(CF_3)_3)_4]$ in perfluoro hexanes. The product was subsequently extracted with $SO_{2(l)}$.[13] $[Cu(1,2\text{-difluorobenzene})_{0.6}][Al(OC(CF_3)_3)_4]$ was synthesized according to literature with slight modification *via* a cascade reaction from $Ag[Al(OC(CF_3)_3)_4]$ and CuI in 1,2-difluorobenzene.[14]

$Ag[B(C_6F_5)_4]\bullet(toluene)_2$ was synthesized over two steps from $Li[B(C_6F_5)_4]\bullet(Et_2O)_{2.5}$ by salt metathesis with $AgNO_3$ and subsequent crystallization from toluene.[15]

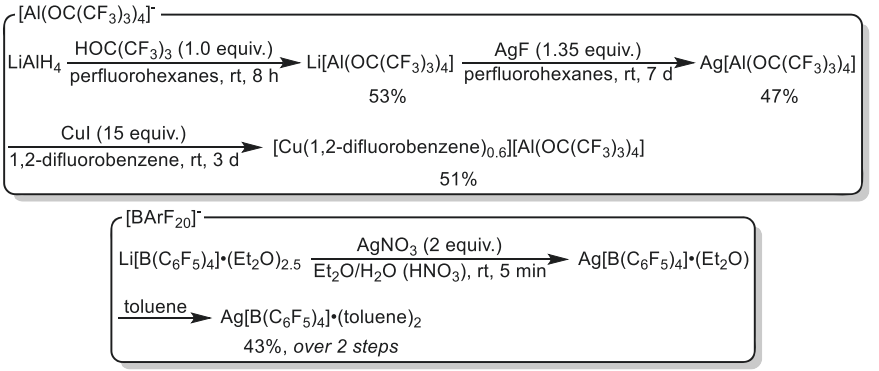

Scheme S4. Synthesis of $Ag[Al(OC(CF_3)_3)_4]$ and $[Cu(1,2\text{-difluorobenzene})_{0.6}][Al(OC(CF_3)_3)_4]$ as well as the synthesis of $Ag[B(C_6F_5)_4]\bullet(toluene)_2$.

$Li[Al(OC(CF_3)_3)_4]$

$Li[Al(OC(CF_3)_3)_4]$ was synthesized according to literature.[12] $LiAlH_4$ (7.03 g, 185 mmol, 2.33 equiv.) was placed on a flame dried P4 frit equipped with a pressure equalizing tube, connected with a Claisen adapter to a reflux condenser and a Schlenk round bottom flask at the bottom. perfluoro hexanes (10 mL) were added and the Schlenk round bottom flask was heated to 75 °C, whilst cooling the condenser to 0 °C, *via* a cryostat and an external pump (isopropanol). Upon reaching system equilibrium, perfluoro-*tert*-butanol (11.1 mL, 79.5 mmol, 1 equiv.) was added dropwise to the $LiAlH_4$ *via* a syringe pump over the course of 8 h (note instability of $LiAlH_4$ above 120 °C). After complete addition, the system was left another 1 h at equilibrium to completely extract the $Li[Al(OC(CF_3)_3)_4]$. Subsequently, residual solvent was removed *in vacuo* and the product was obtained as a white solid (53% yield).[16]

$LiC_{16}O_4F_{36}Al$ (974.04 $\frac{g}{mol}$)

^{7}Li NMR(150.90 MHz, C_6D_{12}): δ = -1.1 (s).

^{13}C NMR(150.90 MHz, C_6D_{12}): δ = 121.3 (q, ^{1}J = 292.3 Hz), 79.0.

^{19}F NMR(150.90 MHz, C_6D_{12}): δ = -75.3 (s).

^{27}Al NMR(150.90 MHz, C_6D_{12}): δ = 37.7 (s).

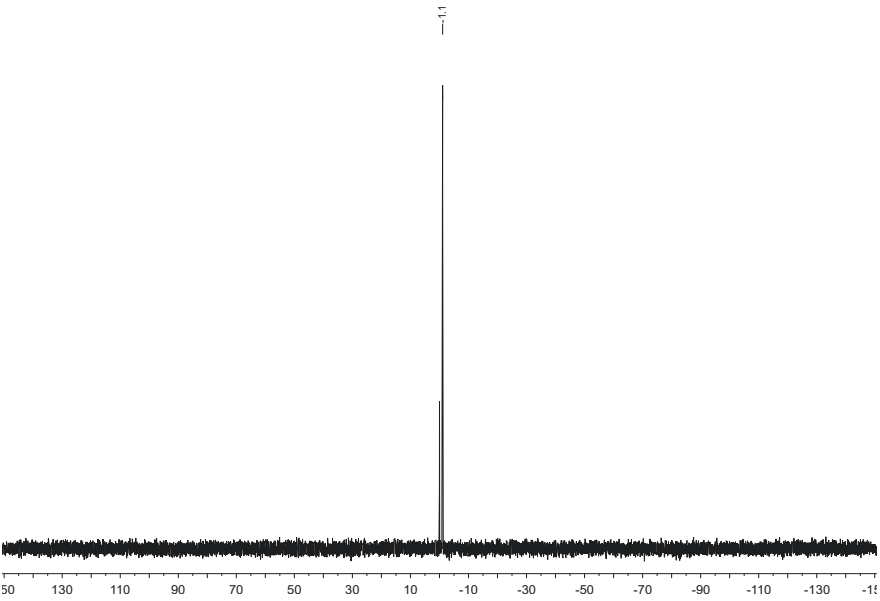

Figure S54. ^{7}Li NMR of Li[Al(OC(CF$_3$)$_3$)$_4$] in DCM-d$_2$. The signal at 0.0 ppm is an unknown impurity.

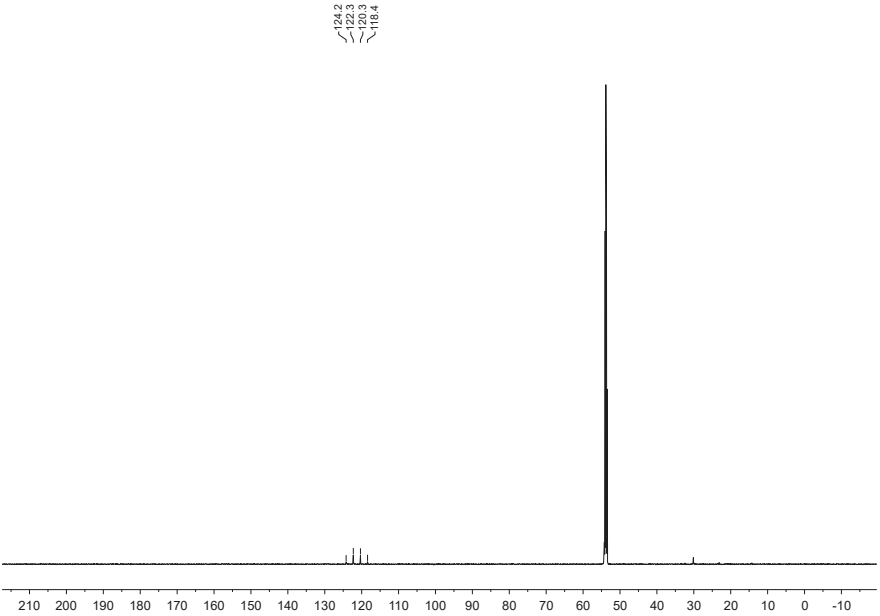

Figure S55. ^{13}C NMR of Li[Al(OC(CF$_3$)$_3$)$_4$] in DCM-d$_2$. The carbon bound directly to oxygen could only be observed via $\{^{19}F\}$ ^{13}C NMR (79.0 ppm).

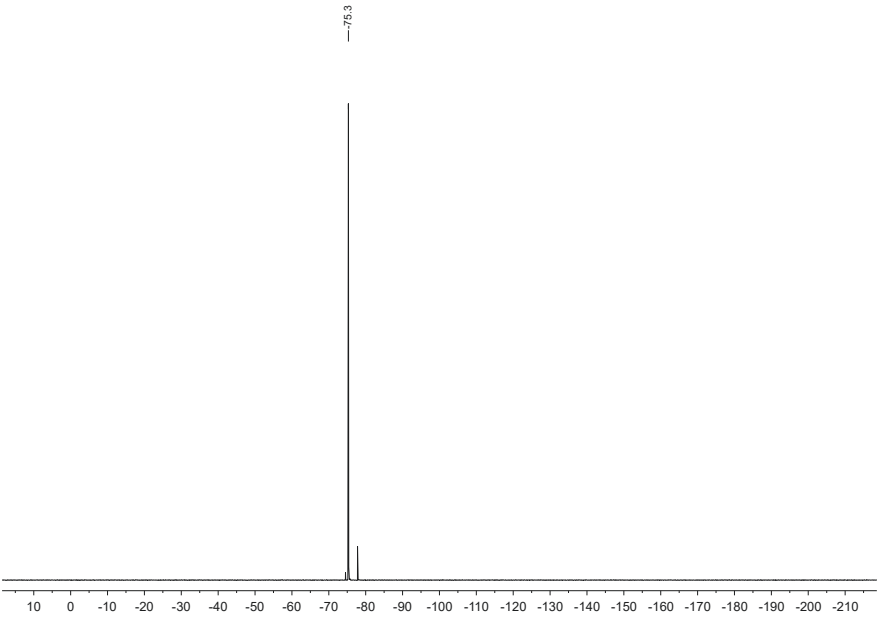

Figure S56: ^{19}F NMR of $Li[Al(OC(CF_3)_3)_4]$ in DCM-d_2.

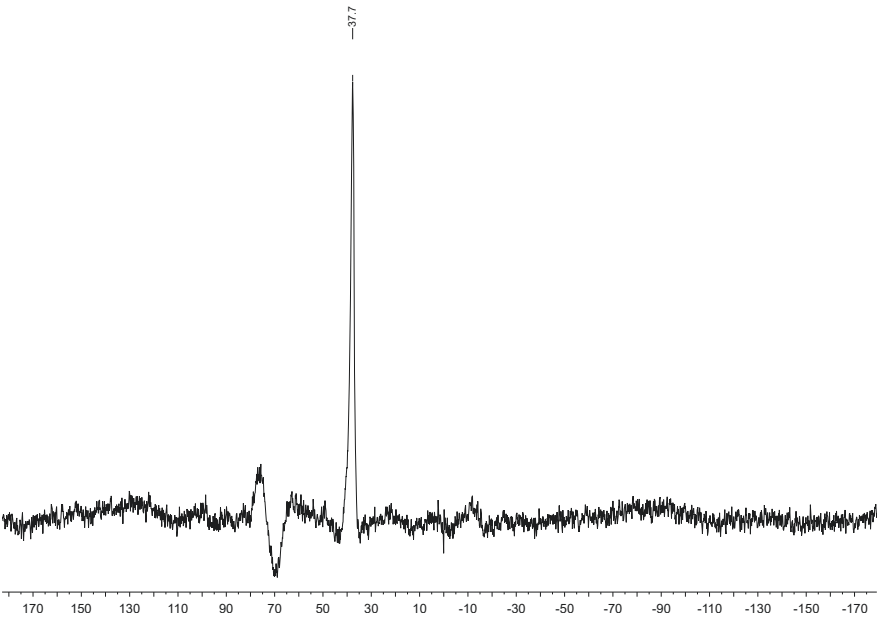

Figure S57: ^{27}Al NMR of $Li[Al(OC(CF_3)_3)_4]$ in DCM-d_2.

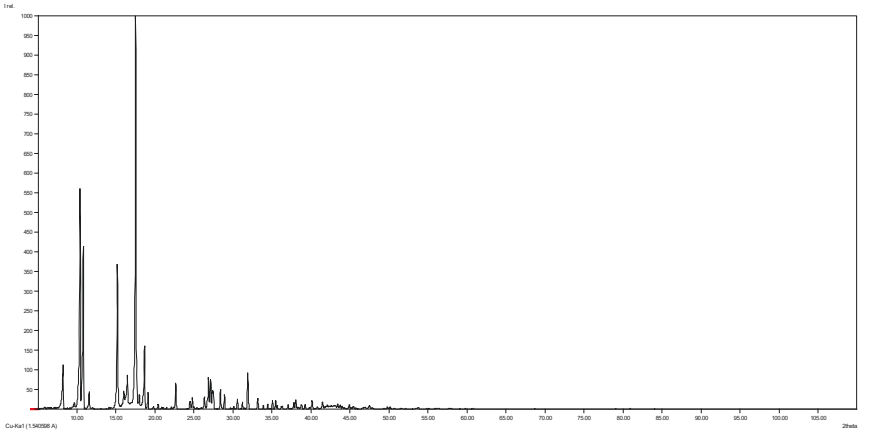

Figure S58. Powder X-ray diffraction pattern of $Li[Al(OC(CF_3)_3)_4]$.

$Ag[Al(OC(CF_3)_3)_4]$

$SO_{2(l)}$ was obtained by slow addition of $Na_2SO_{3(s)}$ (43 g) to 200 mL of conc. H_2SO_4 *via* a dropping funnel. The generated $SO_{2(g)}$ was collected in a cooling trap at -75 °C and was recondensed through a gas washing bottle containing $CaCl_2$ into a cooled pressure tube before use.

$Ag[Al(OC(CF_3)_3)_4]$ was synthesized according to literature.[13] $Li[Al(OC(CF_3)_3)_4]$ (5.69 g, 5.58 mmol, 1 equiv.) and AgF (1.00 g, 7.88 mmol, 1.35 equiv.) were stirred in a flame dried Schlenk round bottom flask with perfluoro hexanes (30 mL) as a solvent for seven days. Reaction progress was monitored *via* ^{7}Li NMR spectroscopy. After full conversion, the perfluoro hexanes were removed *in vacuo*. Subsequently, $SO_{2(l)}$ (20 mL) was condensed onto the remaining solid and the suspension was filtered through a frit (P4). The $SO_{2(l)}$ was recondensed onto the other side, resuspending the remnants and the suspension was filtered through a frit (P4) once more. Thereafter the $SO_{2(l)}$ was removed *in vacuo*, and the product was dried for 2 h under dynamic vacuum. The product was obtained as a colorless solid (46% yield). NMR spectra were recorded with $SO_{2(l)}$ in an insert surrounded by DCM-d_2 at 253 K. The data is in accordance with the literature.[17]

$AgC_{16}O_4F_{36}Al$ ($1074.96\ \frac{g}{mol}$)

^{13}C NMR(150.90 MHz, $SO_{2(l)}$/DCM-d_2): 122.6 (q, ^1J = 291.9 Hz, C-2), 80.1 (s, C-1).

^{19}F NMR(564.68 MHz, $SO_{2(l)}$/DCM-d_2): -74.1.

^{27}Al NMR(156.38 MHz, $SO_{2(l)}$/DCM-d_2): 37.1.

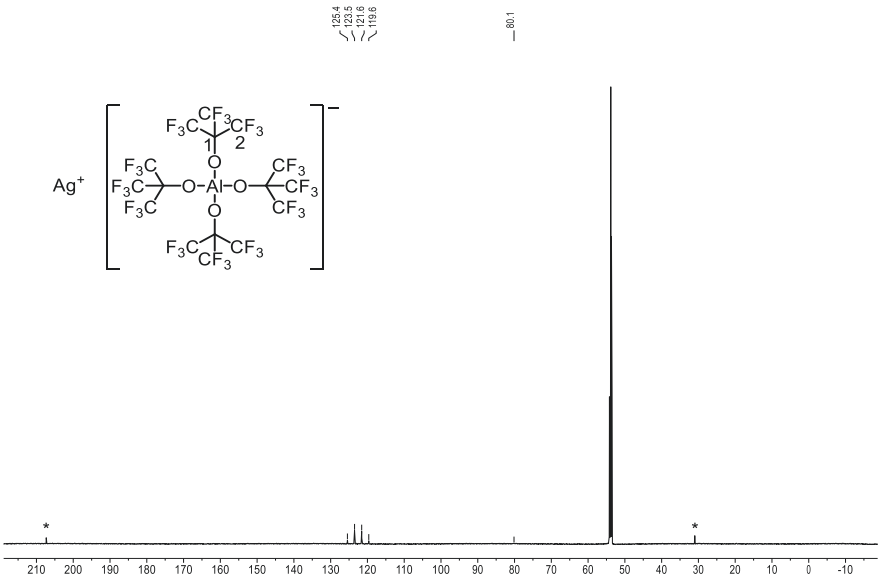

Figure S59: ^{13}C NMR spectrum of $Ag[Al(OC(CF_3)_3)_4]$ in $SO_{2(l)}$/DCM-d_2 at 253 K. * Denotes residual acetone present in the DCM-d_2.

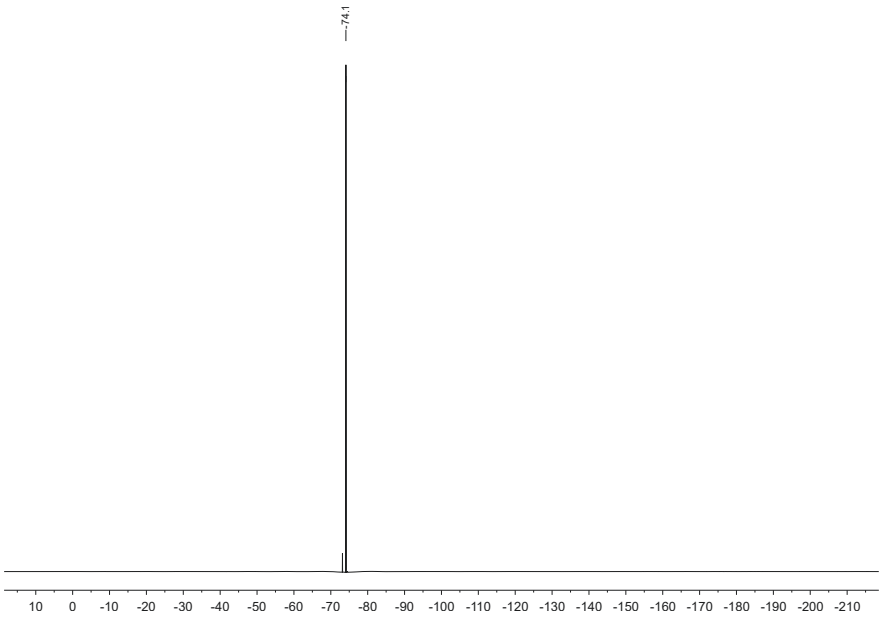

Figure S60: ^{19}F NMR spectrum of $Ag[Al(OC(CF_3)_3)_4]$ in $SO_{2(l)}$/DCM-d_2 at 253 K.

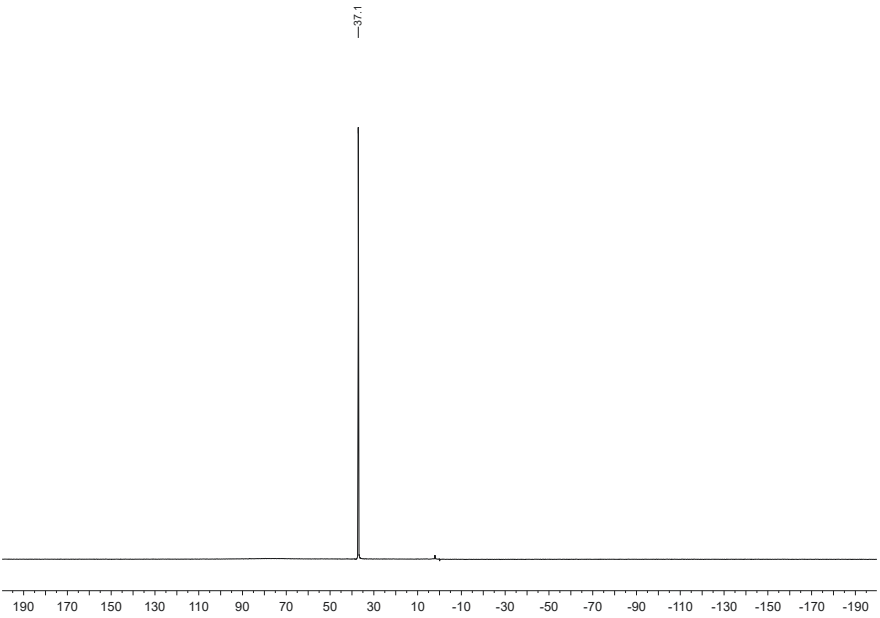

Figure S61: ^{27}Al NMR spectrum of $Ag[Al(OC(CF_3)_3)_4]$ in $SO_{2(l)}$/DCM-d_2 at 253 K.

[Cu(1,2-difluorobenzene)$_{0.6}$][Al(OC(CF$_3$)$_3$)$_4$]

[Cu(1,2-difluorobenzene)$_{0.6}$][Al(OC(CF$_3$)$_3$)$_4$] was synthesized according to literature with slight modifications.[14] To a screw cap vessel, Ag[Al(OC(CF$_3$)$_3$)$_4$] (101.8 mg, 94.7 µmol, 1.0 equiv.) and CuI (90.2 mg, 473.5 µmol, 5 equiv.) and 2 mL of 1,2-difluorobenzene were added in a glove box. The mixture was stirred at rt under light exclusion for 24 h, after which the solids were filtered and washed with 2 mL of 1,2-difluorobenzene. Subsequently, CuI (90.2 mg, 474 µmol, 5 equiv.) was added to the solution and the mixture was stirred at rt under light exclusion for 24 h. This process was repeated once more. After removing the solid residue, *n*-hexane was added until an off-white precipitate formed, which was filtered and washed thrice with 2 mL *n*-hexane. The solid was dried in vacuo yielding an off-white solid (51 % yield). The spectral data is in agreement with the literature.[14]

$CuC_{19.6}H_{2.4}O_4F_{37.2}Al$ (1099.09 $\frac{g}{mol}$)

^{1}H NMR(300.13 MHz, DCM-d$_2$): 7.15 (m, 2H).

^{13}C NMR(176.07 MHz, DCM-d$_2$): 150.9 (m, C-5), 125.0 (m, C-4), 121.7 (q, ^1J = 291.3 Hz, C-2), 117.7 (m, C-3), 79.6 (s, C-1).

^{19}F NMR(282.40 MHz, DCM-d$_2$): -75.7 (s, 36F), -139.3 (m, 1.26F).

^{27}Al NMR(78.20 MHz, DCM-d$_2$): 34.6.

EDX: $\frac{m(Cu)}{m(Ag)}$ = 24.5.

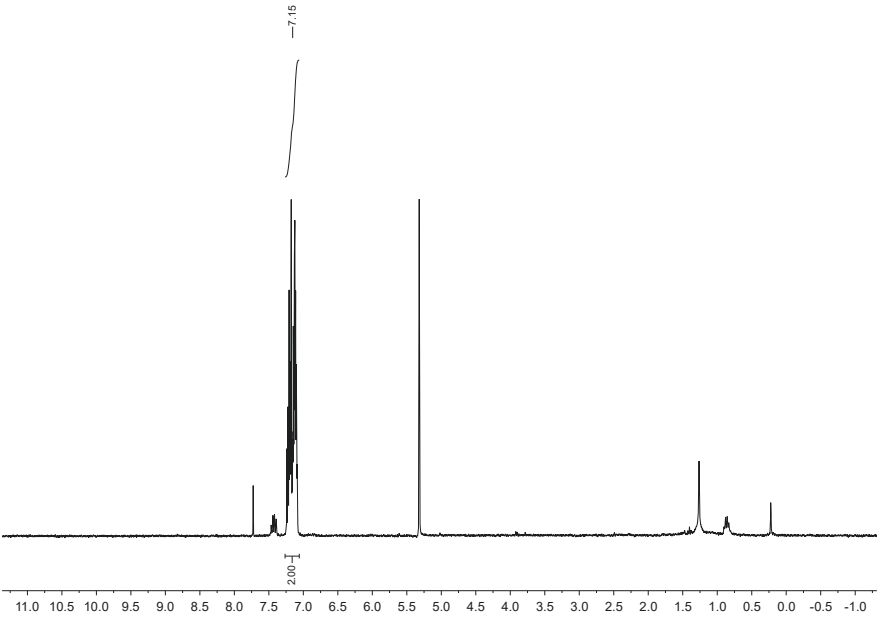

Figure S62. ^{1}H NMR of [Cu(1,2-difluorobenzene)$_{0.6}$][Al(OC(CF$_3$)$_3$)$_4$] in DCM-d$_2$.

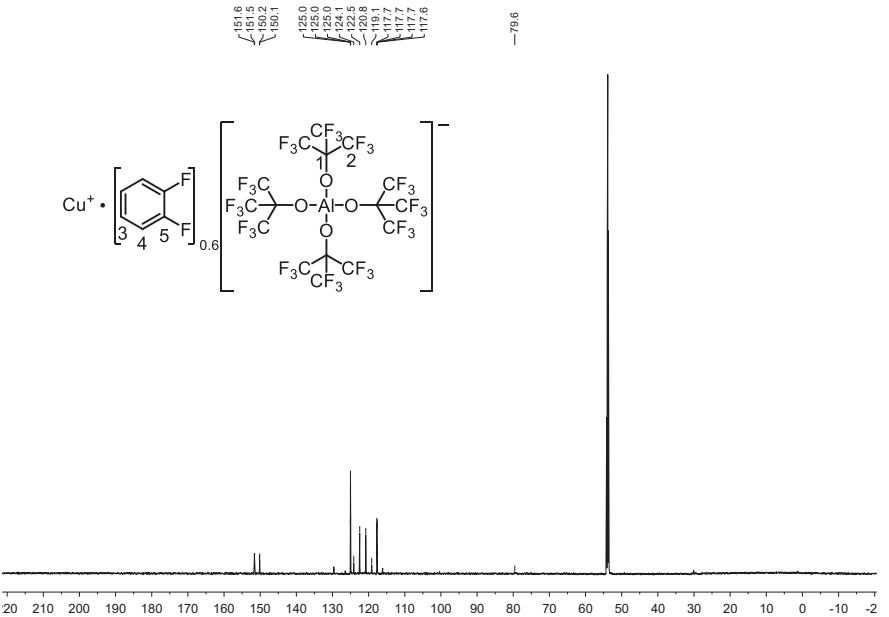

Figure S63. ^{13}C NMR of [Cu(1,2-difluorobenzene)$_{0.6}$][Al(OC(CF$_3$)$_3$)$_4$] in DCM-d$_2$.

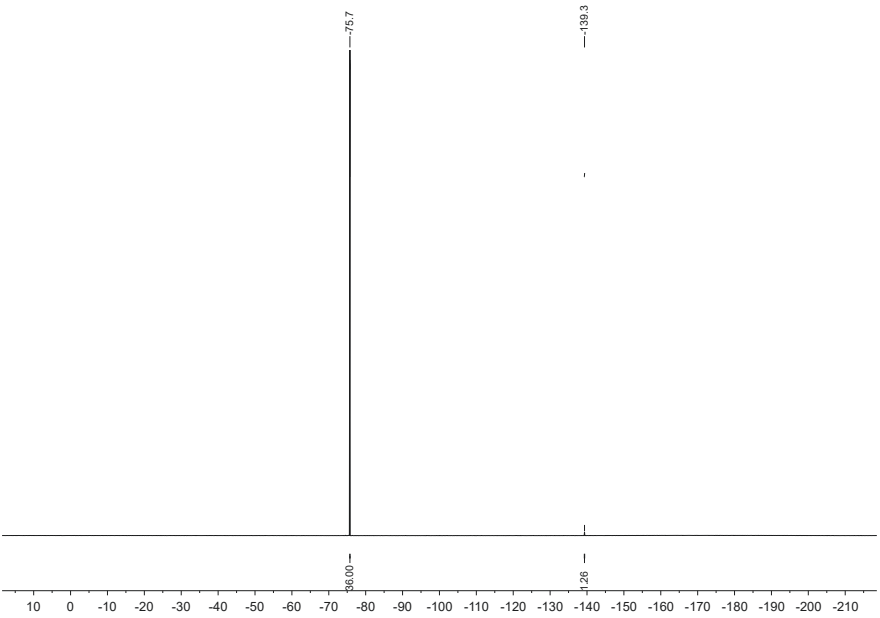

Figure S64: ^{19}F NMR of $[Cu(1,2\text{-difluorobenzene})_{0.6}][Al(OC(CF_3)_3)_4]$ in DCM-d_2.

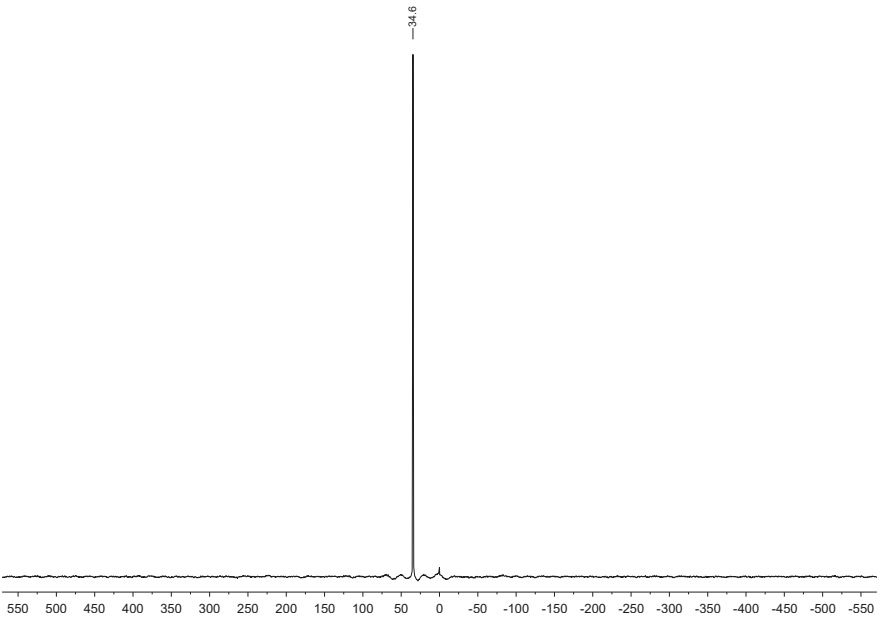

Figure S65: ^{27}Al NMR of $[Cu(1,2\text{-difluorobenzene})_{0.6}][Al(OC(CF_3)_3)_4]$ in DCM-d_2.

$Ag[B(C_6F_5)_4] \bullet (toluene)_2$

$Ag[B(C_6F_5)_4] \bullet (toluene)_2$ was prepared according to literature with minor modifications.[15]

$Ag[B(C_6F_5)_4] \bullet Et_2O$

To a separation funnel $Li[B(C_6F_5)_4] \bullet (Et_2O)_{2.5}$ (0.95 g, 1.09 mmol) dissolved in Et_2O (15 mL) and $AgNO_3$ (0.37 g, 2.18 mmol) in H_2O (4 mL, acidified with one drop of HNO_3) were added and shaken under light exclusion. Subsequently, the ethereal layer was separated and washed with H_2O (1 × 2 mL). After separation, the solvent was removed *in vacuo* and the product was dried under dynamic vacuum for three hours at 50 °C yielding a brownish oil (917 mg, 1.06 mmol, 98%). The product was used without additional analysis.

$Ag[B(C_6F_5)_4] \bullet (toluene)_2$

To $Ag[B(C_6F_5)_4] \bullet Et_2O$ (916.8 mg, 1.06 mmol) toluene (10 mL) was added, resulting in a brownish oil layer and a clear upper layer. The mixture was stirred for 30 min after which the solvent was removed *in vacuo* yielding a brownish oil. The oil was cooled to 235 K yielding colorless crystals (443 mg, 0.46 mmol, 43%).

$AgF_{20}C_{38}BH_{16}$ ($971.19 \frac{g}{mol}$)

^{1}H NMR(600.13 MHz, DCM-d_2): 7.39 – 7.23 (m, 4H), 7.17 (m, 1H), 2.39 (s, 3H).

^{11}B NMR(192.55 MHz, DCM-d_2): -16.6.

^{13}C NMR(150.92 MHz, DCM-d_2): 148.6 (m, C-2), 141.1 (s, C-8), 138.7 (dt, ^1J = 244.9 Hz, ^3J = 13.3 Hz, C-4), 136.8 (m, C-3), 129.6 (s, $C_{toluene}$), 127.1 (s, $C_{toluene}$), 124.4 (m, C-1), 123.1 (s, C-5), 21.7 (s, C-9).

^{19}F NMR(564.63 MHz, DCM-d_2): -133.1 (m, F-2), -163.6 (t, ^3J = 20.3 Hz, F-3), -167.5 (m, F-1).

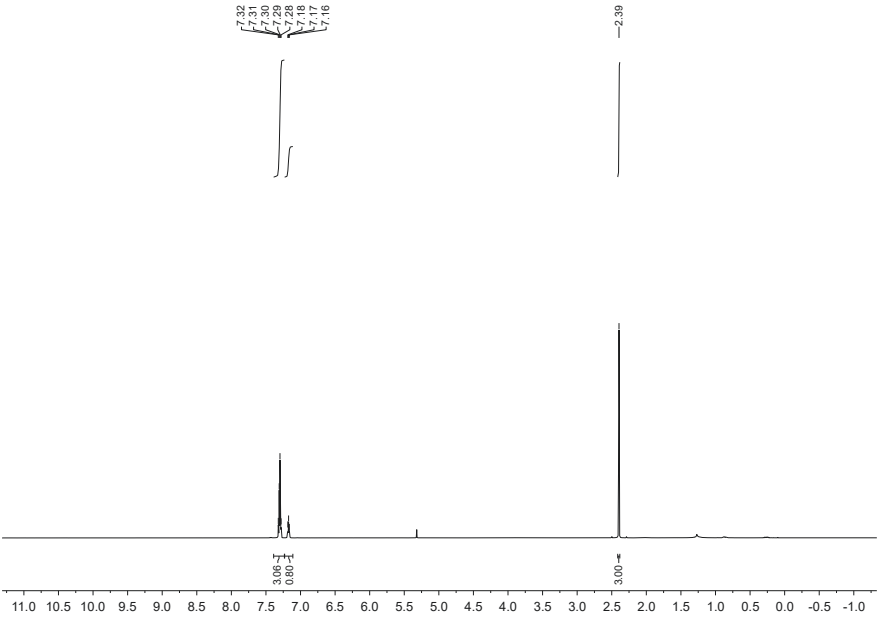

Figure S66. ^{1}H NMR of $Ag[B(C_6F_5)_4] \bullet (toluene)_2$ in DCM-d_2.

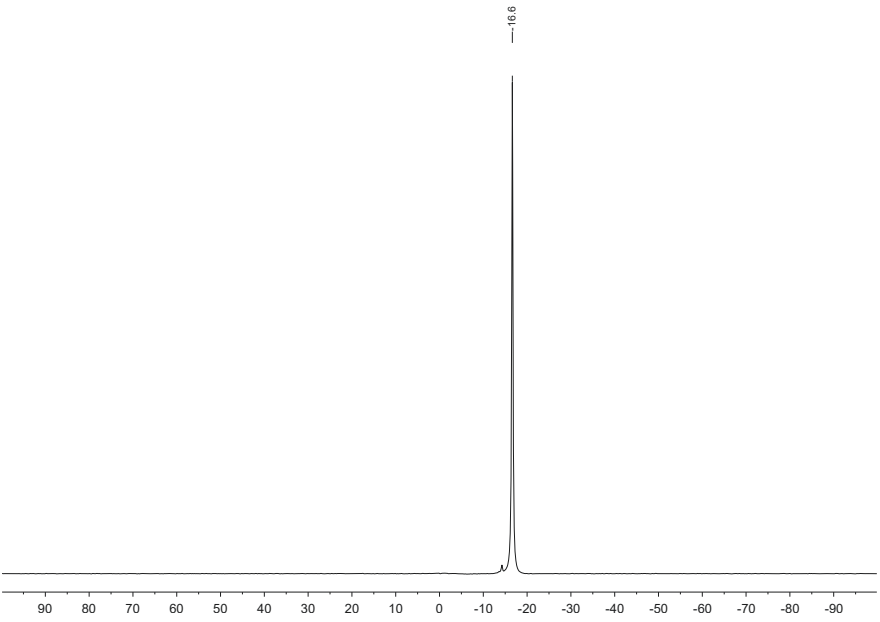

Figure S67. ^{11}B NMR of $Ag[B(C_6F_5)_4] \bullet (toluene)_2$ in DCM-d_2.

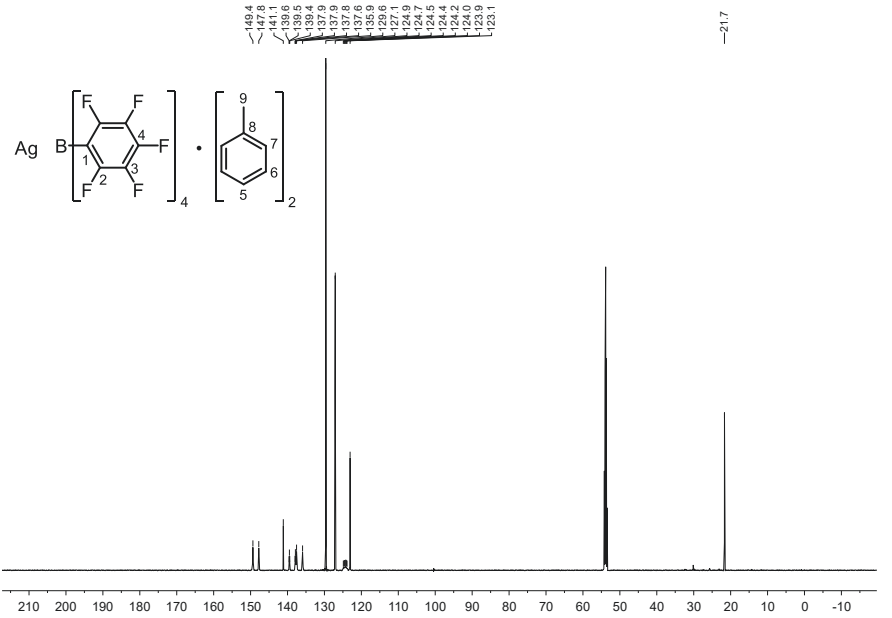

Figure S68: ^{13}C NMR of $Ag[B(C_6F_5)_4] \bullet (toluene)_2$ in DCM-d_2.

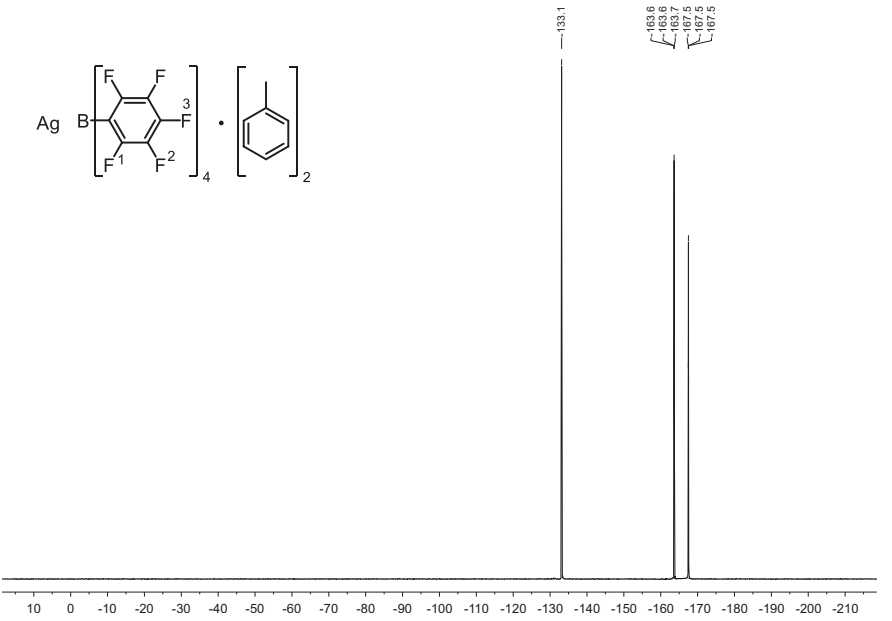

Figure S69: ^{19}F NMR of $Ag[B(C_6F_5)_4] \bullet (toluene)_2$ in DCM-d_2.

4 NMR Studies

In a glovebox, **BNB1** (1.0 equiv.) and AgWCA (1.0 equiv.) were dissolved in DCM-d_2 (20 mM) in a dried J. Young NMR tube and measured *via* NMR spectroscopy. Samples containing **BND1** were prepared according to GP-B, and were measured at low temperature (235 K, 270 K).

BNB1•Ag[Al(OC(CF$_3$)$_3$)$_4$]

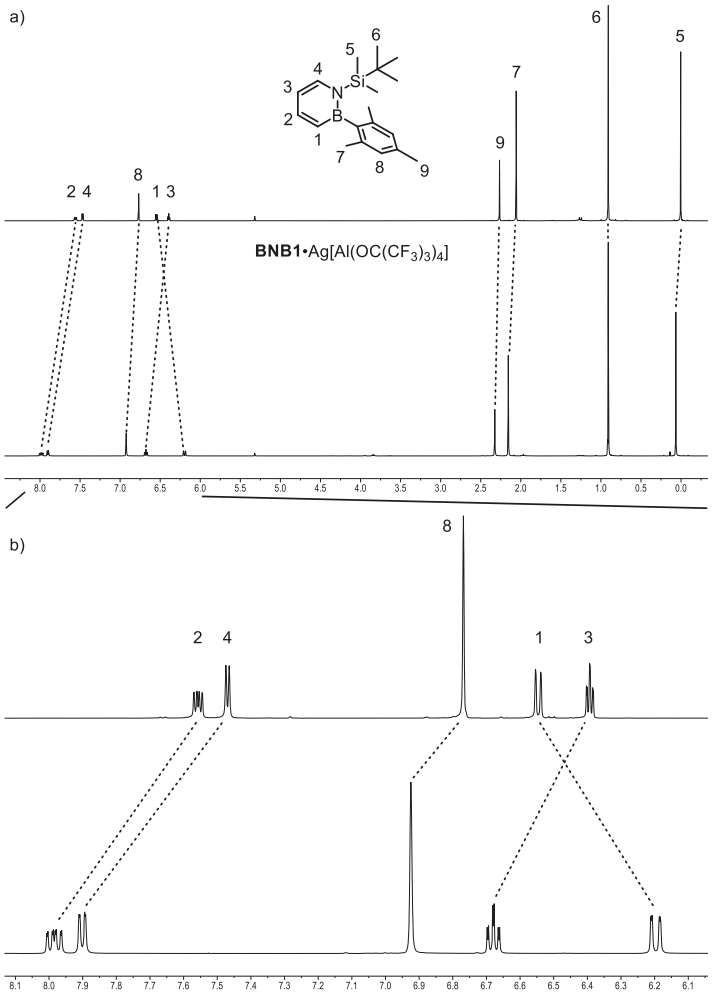

Figure S70. ^{1}H NMR spectrum of **BNB1**•Ag[Al(OC(CF$_3$)$_3$)$_4$] compared to pure **BNB1** in DCM-d_2 at rt. b) displays the magnified aromatic region of a).

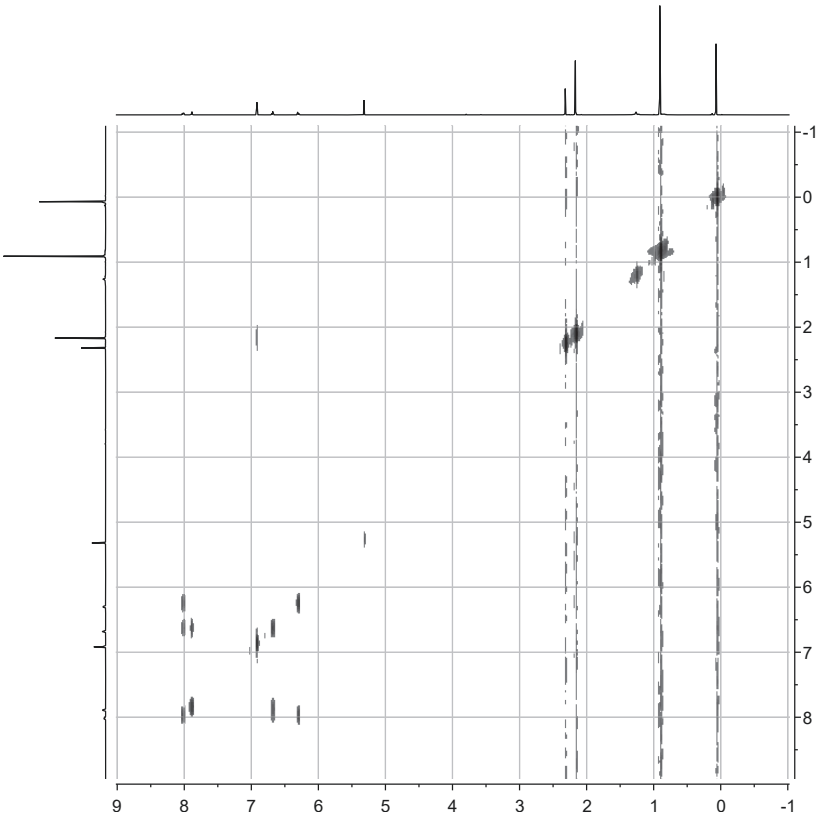

Figure S71. $^{1}H,^{1}H$-COSY of **BNB1**•Ag[Al(OC(CF_3)$_3$)$_4$] in DCM-d_2 at rt.

BND1•Ag[Al(OC(CF$_3$)$_3$)$_4$]

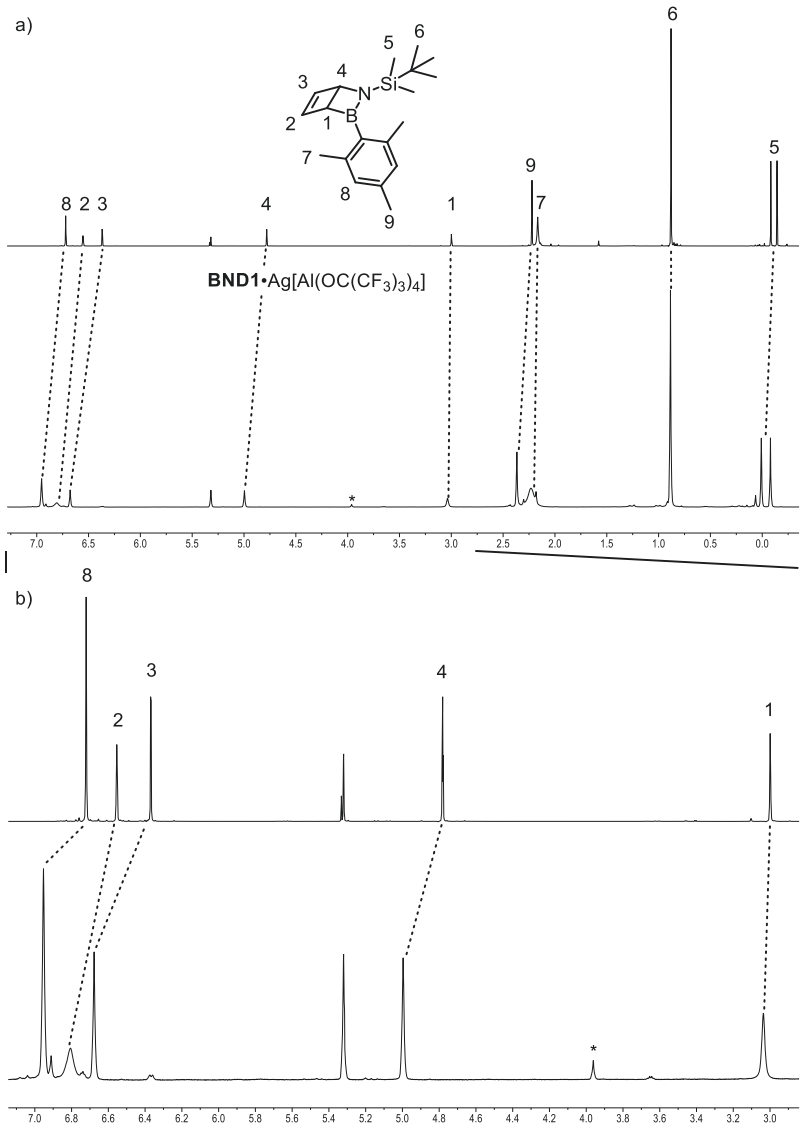

Figure S72. ^{1}H NMR spectrum of **BND1•**Ag[Al(OC(CF$_3$)$_3$)$_4$] compared to pure **BND1** in DCM-d$_2$ at 270 K. The signal denoted by *, is probably due to a different species of **BND1•**Ag[Al(OC(CF$_3$)$_3$)$_4$]. b) displays a magnified spectral range of a).

[BNB1AgSbF$_6$]$_2$

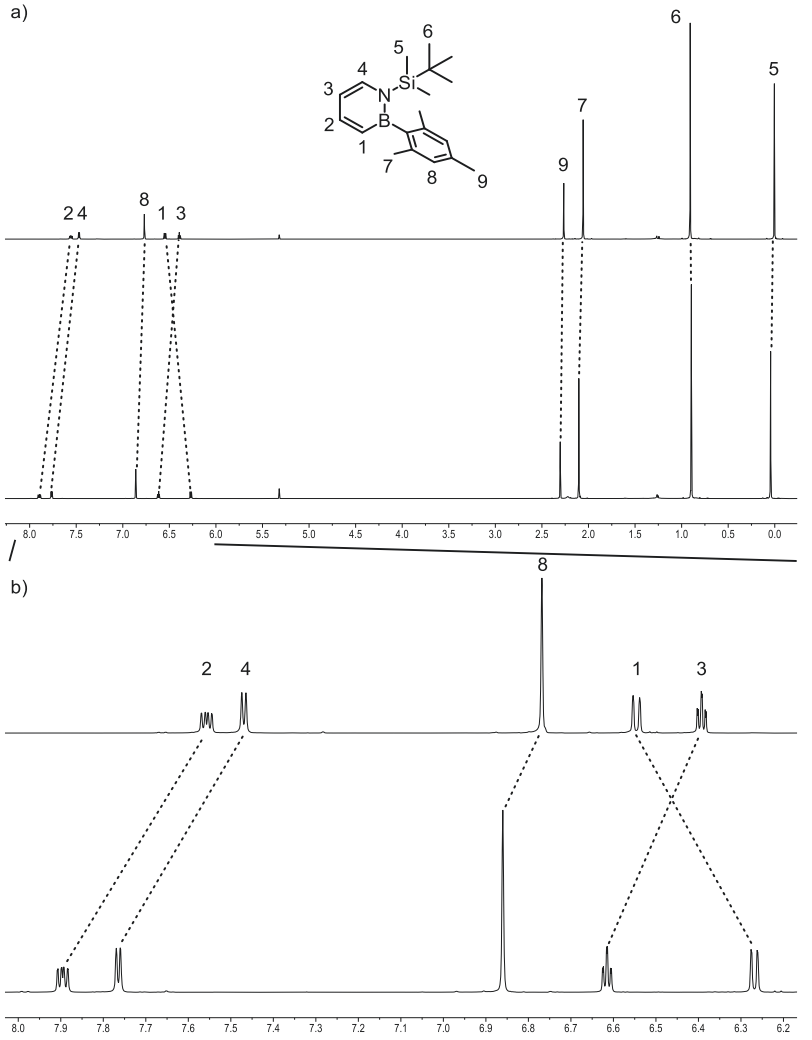

Figure S73. ^{1}H NMR spectrum of [**BNB1**AgSbF$_6$]$_2$ compared to pure **BNB1** in DCM-d$_2$ at rt. b) displays the magnified aromatic region of a).

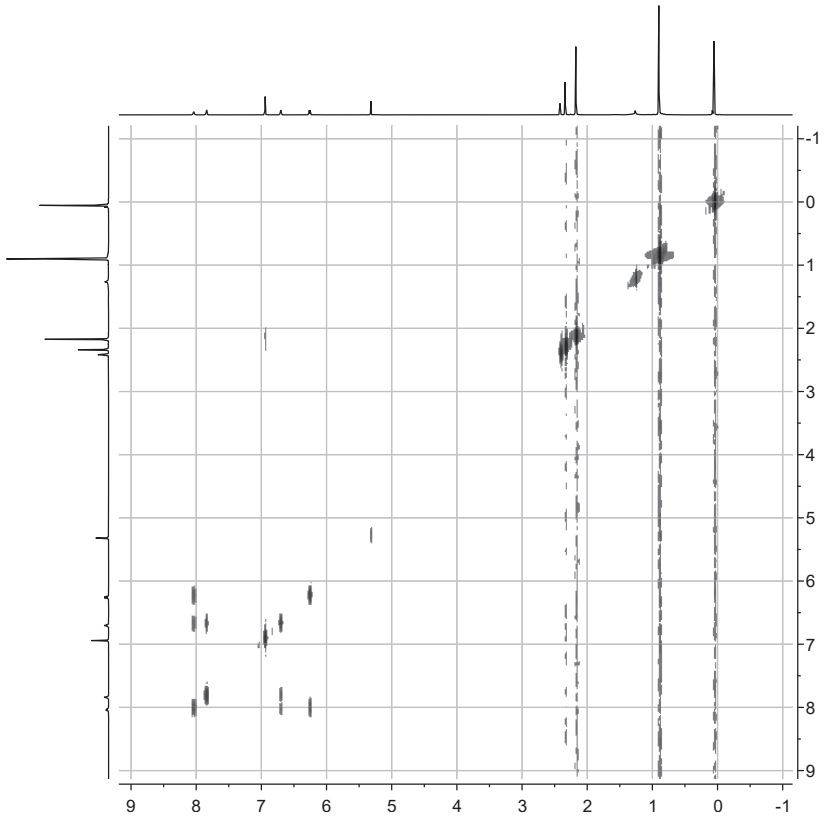

Figure S74. $^{1}H,^{1}H$-COSY of [**BNB1**$AgSbF_6]_2$ in DCM-d_2 at rt.

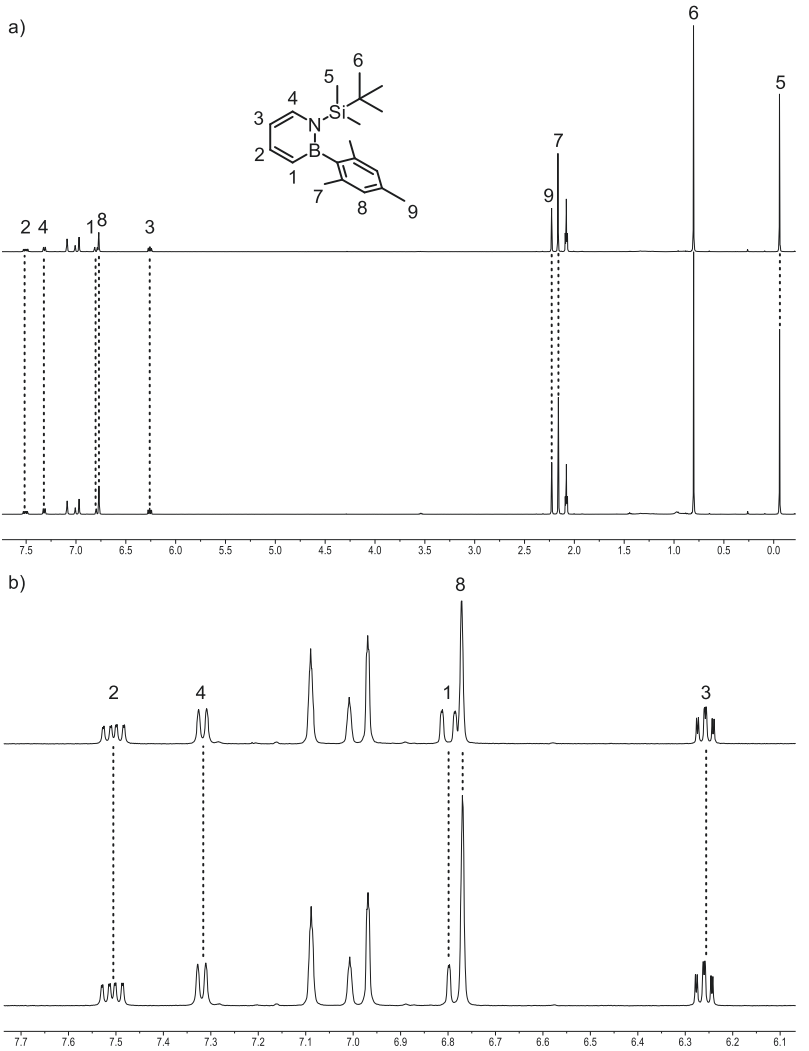

Figure S75. ^{1}H NMR spectrum of [**BNB1**AgSbF$_6$]$_2$ compared to pure **BNB1** in toluene-d$_8$ at rt. b) displays the magnified aromatic region of a).

The spectra measured in toluene-d$_8$ lack the distinct difference in chemical shifts (Figure S75) caused by the coordination of **BNB1** to AgSbF$_6$ in DCM-d$_2$ (Figure S73). This implies that Ag^+ is coordinated by toluene-d$_8$, therefore reducing its catalytic activity.

[BND1AgSbF$_6$]$_2$

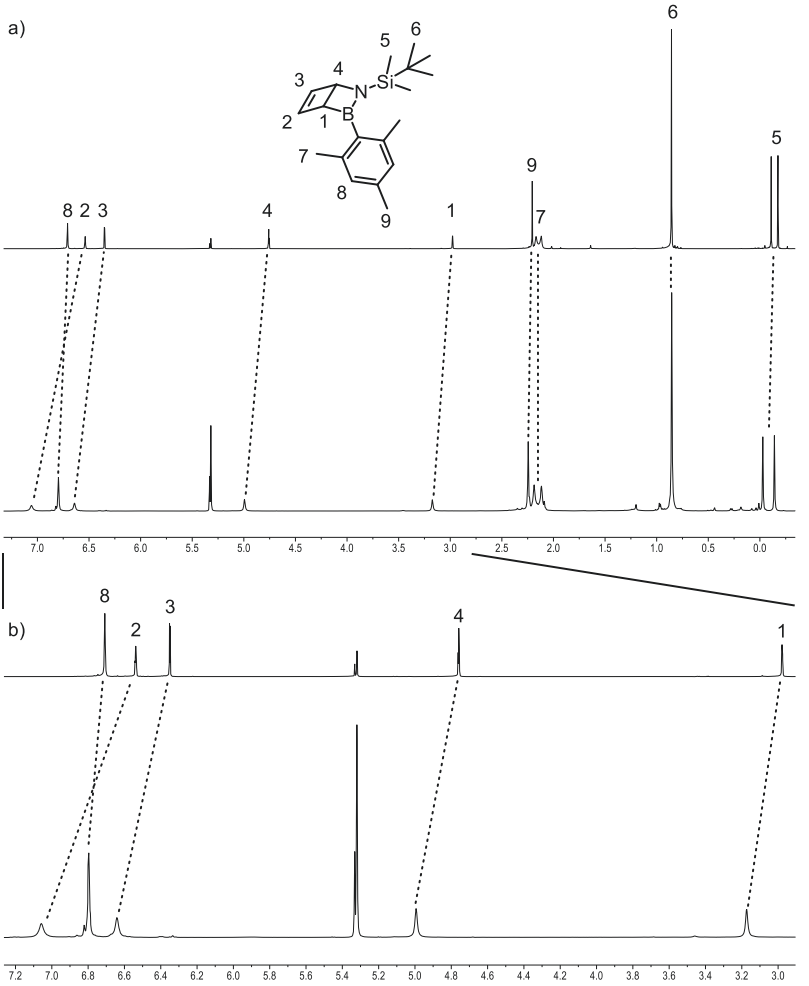

Figure S76. ^{1}H NMR spectrum of [**BND1**AgSbF$_6$]$_2$ compared to pure **BND1** in DCM-d$_2$ at 235 K. b) displays a magnified spectral range of a).

5 Crystal structures

Crystals for X-ray structure analyses, except 1,2-dihydro-1-*tert*-butyldimethylsilyl-2-mesityl-1,2-azaborinine (**BNB1**), were selected in a glovebox, coated with Parabar 10312 oil, and fixed on a nylon/loop glass fibre unless denoted otherwise. X-ray diffraction data, except for **BNB1**, were measured at 100 K employing a Bruker APEX II DUO instrument, featuring an IμS microfocus sealed tube along with QUAZAR optics, utilizing Mo-K_α ($\lambda = 0.71073$ Å) radiation. Raw data processing utilized SAINT[18] and APEX,[19] while corrections for absorption effects were applied using SADABS.[20] Subsequently, the structures were solved *via* direct methods, followed by refinement against all data using full-matrix least-squares methods on F2, employing SHELXTL[21] and SHELXLE.[22] For **BNB1** data was collected on a Rigaku XtaLAB Synergy-S single-crystal X-ray diffractometer equipped with HyPix-6000HE detector and monochromated Cu-K_α radiation (λ=1.54184 Å) at 100 K. Absorption corrections for X-ray intensities were executed through a numerical method employing CrysAlisPro 1.171.42.49 (Rigaku Oxford Diffraction, 2022). The structure was solved by direct methods (SHELXS),[23] followed by full-matrix least-squares structure refinements, performed with SHELXL-2018,[21] implemented in Olex2 1.5.[24] The graphical representations were generated utilizing CCDC Mercury 2022.2.0.[25] Additional details pertaining to refinement procedures and crystallographic data for each crystal structure are listed below and in their respective CIF file.

[(BND1)Ag(SbF_6)]$_2$

In a glovebox **BND1** (150.0 mg, 1.0 equiv) and $AgSbF_6$ (165.5 mg, 1.0 equiv) were dissolved in DCM (5 mL) at 235 K. The mixture was stirred until $AgSbF_6$ was completely dissolved, at which point precooled *n*-hexane (5 mL, 235 K) was added. The residual solvent was removed from the remaining precipitate, which was washed once with *n*-hexane (2 mL, 235 K). Subsequently, a saturated DCM solution of the precipitate at 235 K was prepared, from which [(**BND1**)Ag(SbF_6)]$_2$ was crystallized via vapor diffusion (*n*-hexane, 235 K).

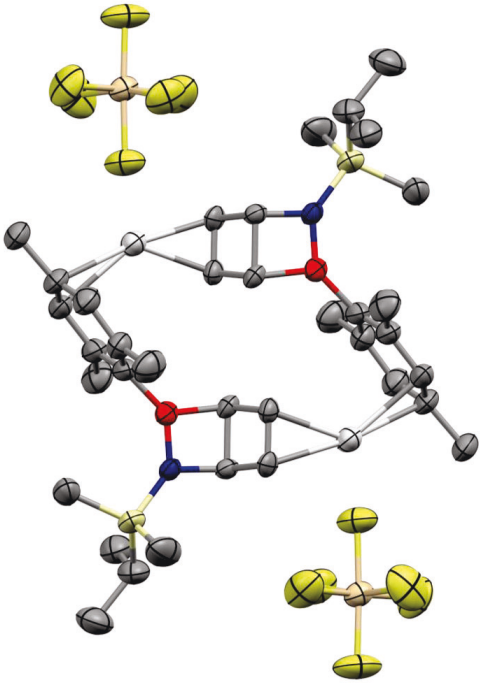

Figure S77. Crystal structure of [(**BND1**)Ag(SbF_6)]$_2$ (DCM). Hydrogen atoms are omitted for clarity and the thermal ellipsoids are drawn at 50% probability level.

Table S1. Crystal data and structure refinement for [(**BND1**)Ag(SbF_6)]$_2$.

Compound	[(**BND1**)Ag(SbF_6)]$_2$
CCDC	2337845
Empirical Formula	$C_{38}H_{60}Ag_2B_2F_{12}N_2Sb_2Si_2$
Formula weight	1309.92
Temperature [K]	100(2)
Crystal system	Orthorhombic
Space group	Pbca
a [Å]	12.8255(4)
b [Å]	15.7137(6)
c [Å]	24.4380(4)
α [°]	90
β [°]	90
γ [°]	90
Volume [Å^3]	4923.1(3)
Z	4
ρ_{calc} [Mg/m^3]	1.767
μ [mm^{-1}]	1.992
F(000)	2576
Crystal size [mm^3]	0.125 × 0.082 × 0.065
Radiation [nm]	MoK$_\alpha$(λ = 0.71073)
Θ range for data collection [°]	1.613 – 30.776
Index ranges	-16 ≤ h ≤ 15, -19 ≤ k ≤ 19, -30 ≤ l ≤ 30
Reflections collected	78033
Independent reflexions	5051 [R_{int} = 0.1484]
Data/restraints/parameters	5051 / 1004 / 436
Goodness-of-fit[a]	1.028
Final R indexes [I>=2σ (I)][b][c]	R_1 = 0.0504, wR_2 = 0.0930
Final R indexes [all data]	R_1 = 0.1185, wR_2 = 0.1165
Largest diff. peak/hole [eÅ^{-3}]	0.570 / -0.637

[a]$GOF = [\sum w(F_0^2 - F_c^2)^2/(n_0 - n_p)]^{1/2}$. [b]$R_1 = \Sigma(||F_0| - |F_c||)/\Sigma|F_0|, F_0 > 4\sigma(F_0)$. [c]$wR_2 = \{\Sigma[w({F_0}^2 - {F_c}^2)^2]/\Sigma[w({F_0}^2)^2]\}^{1/2}$.

Table S2. Atomic coordinates (× 10^4) and equivalent isotropic displacement parameters ($Å^2 \times 10^3$) for [(**BND1**)Ag(SbF_6)]$_2$. U(eq) is defined as one third of the trace of the orthogonalized U_{ij} tensor.

	x	y	z	U(eq)
C(5)	5828(5)	4829(5)	3810(2)	49(2)
C(6)	6024(5)	5662(5)	3669(3)	54(2)
C(7)	7051(5)	5951(5)	3606(3)	59(2)
C(8)	7897(5)	5405(4)	3651(3)	53(2)
C(9)	7685(5)	4559(4)	3775(2)	47(2)
C(10)	6670(5)	4261(4)	3858(2)	50(2)
C(11)	5142(5)	6293(5)	3581(3)	78(2)
C(12)	8998(5)	5712(5)	3531(3)	63(2)
C(13)	6475(5)	3338(4)	3990(3)	68(2)
C(14)	4569(5)	4195(5)	2616(3)	58(2)
C(15)	2332(5)	4699(5)	2888(4)	93(3)
C(16)	2860(30)	3000(30)	3020(20)	70(4)
C(17)	3650(30)	2340(30)	3239(18)	76(5)
C(18)	1800(30)	2980(30)	3344(16)	74(5)
C(16A)	3065(10)	2778(9)	2981(6)	63(2)
C(17A)	4055(8)	2226(7)	2990(5)	72(3)
C(18A)	2349(9)	2468(8)	3433(5)	81(3)
C(19)	2543(6)	2687(5)	2423(3)	86(3)
Si(1)	3430(1)	3965(1)	3057(1)	58(1)
C(1)	3265(8)	4096(8)	4245(5)	35(2)
C(2)	2628(9)	4927(7)	4375(5)	43(3)
C(3)	3426(8)	5281(7)	4658(4)	40(2)
C(4)	4186(8)	4514(7)	4569(5)	36(2)
Ag(1)	2197(3)	4877(3)	5297(2)	50(1)
B(1)	4750(13)	4454(9)	3991(8)	39(3)
F(1)	1138(6)	3592(5)	5202(3)	78(2)
F(2)	819(10)	2434(7)	4736(7)	82(3)
F(3)	492(8)	3726(7)	4191(4)	93(3)
F(4)	-1114(8)	2805(6)	4400(5)	91(3)
F(5)	-743(9)	4181(5)	4971(4)	107(3)

F(6)	-535(19)	2755(15)	5434(6)	87(4)
N(1)	3868(12)	4089(7)	3735(6)	37(3)
Sb(1)	-14(3)	3198(2)	4810(1)	46(1)
C(1A)	2951(16)	4663(16)	4202(9)	46(4)
C(2A)	3054(16)	3969(14)	4537(9)	51(4)
C(3A)	3856(16)	4342(13)	4835(9)	51(4)
C(4A)	3879(18)	5050(16)	4520(10)	50(4)
Ag(1A)	2238(5)	4584(4)	5365(3)	46(1)
B(1A)	4600(30)	4730(20)	3978(18)	53(6)
F(1A)	489(10)	4033(9)	5227(6)	76(4)
F(2A)	640(20)	2118(13)	4664(11)	85(6)
F(3A)	-157(12)	3698(13)	4216(6)	92(5)
F(4A)	-1285(17)	2409(14)	4606(9)	107(6)
F(5A)	-1510(10)	3956(9)	5010(5)	75(4)
F(6A)	-560(30)	2720(30)	5610(11)	79(6)
N(1A)	3760(20)	4398(15)	3695(12)	51(5)
Sb(1A)	-369(5)	3256(4)	4898(2)	53(1)

[(BNB1)Ag(SbF$_6$)]$_2$

In a glovebox **BNB1** (50.0 mg, 1.0 equiv) and AgSbF$_6$ (55.2 mg, 1.0 equiv) were dissolved in DCM (2 mL). The mixture was stirred until AgSbF$_6$ was completely dissolved, at which point *n*-hexane (2 mL) was added. The residual solvent was removed from the remaining precipitate, which was washed once with *n*-hexane (1 mL) and dissolved in DCM. Subsequently, [(**BNB1**)Ag(SbF$_6$)]$_2$ was crystallized from DCM at 235 K.

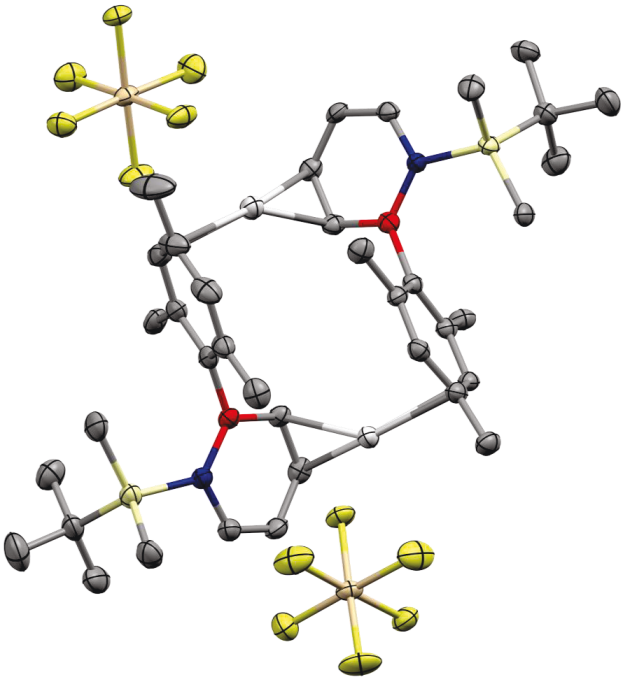

Figure S78. Crystal structure of [(**BNB1**)Ag(SbF$_6$)]$_2$ (DCM). Hydrogen atoms are omitted for clarity and the thermal ellipsoids are drawn at 50% probability level.

Table S3. Crystal data and structure refinement for [(**BNB1**)$Ag(SbF_6)]_2$.

Compound	[(**BNB1**)$Ag(SbF_6)]_2$
CCDC	2337844
Empirical Formula	$C_{38}H_{60}Ag_2B_2F_{12}N_2Sb_2Si_2$
Formula weight	1309.92
Temperature [K]	100(2)
Crystal system	Triclinic
Space group	P-1
a [Å]	9.9600(2)
b [Å]	13.7979(3)
c [Å]	19.9553(4)
α [°]	107.0990(10)
β [°]	98.6090(10)
γ [°]	103.4640(10)
Volume [$Å^3$]	2477.94(9)
Z	2
ρ_{calc} [Mg/m^3]	1.756
μ [mm^{-1}]	1.979
F(000)	1288
Crystal size [mm^3]	0.136 × 0.130 × 0.069
Radiation [nm]	$MoK_\alpha(\lambda = 0.71073)$
Θ range for data collection [°]	1.613 – 30.776
Index ranges	$-14 \leq h \leq 14, -19 \leq k \leq 19, -28 \leq l \leq 28$
Reflections collected	71103
Independent reflexions	14756 [$R_{int} = 0.0620$]
Data/restraints/parameters	14756 / 0 / 557
Goodness-of-fit[a]	1.034
Final R indexes [I>=2σ (I)][b][c]	$R_1 = 0.0416$, $wR_2 = 0.0874$
Final R indexes [all data]	$R_1 = 0.0728$, $wR_2 = 0.0999$
Largest diff. peak/hole [$eÅ^{-3}$]	1.529 / -1.104

Table S4. Atomic coordinates (× 10^4) and equivalent isotropic displacement parameters (Å^2 × 10^3) for [(**BNB1**)Ag(SbF_6)]$_2$. U(eq) is defined as one third of the trace of the orthogonalized U_{ij} tensor.

	x	y	z	U(eq)
C(1)	5079(4)	9087(3)	2311(2)	22(1)
C(2)	6500(4)	9736(3)	2514(2)	23(1)
C(3)	7162(4)	10282(3)	3244(2)	23(1)
C(4)	6456(4)	10182(3)	3793(2)	26(1)
C(5)	5094(4)	9474(3)	3580(2)	25(1)
C(6)	4383(4)	8941(3)	2857(2)	25(1)
C(7)	7327(4)	9889(3)	1958(2)	28(1)
C(8)	7060(4)	10890(3)	4567(2)	32(1)
C(9)	2883(4)	8250(3)	2670(2)	32(1)
C(10)	4630(4)	7496(3)	1049(2)	25(1)
C(11)	3855(4)	6943(3)	342(2)	26(1)
C(12)	2732(4)	7266(3)	52(2)	26(1)
C(13)	2469(4)	8172(3)	438(2)	25(1)
C(14)	789(4)	9676(3)	1364(2)	34(1)
C(15)	3666(4)	10867(3)	2380(2)	28(1)
C(16)	3246(4)	10851(3)	836(2)	31(1)
C(17)	4847(4)	11083(4)	868(2)	41(1)
C(18)	2901(5)	11909(3)	1118(2)	46(1)
C(19)	2422(4)	10313(3)	36(2)	38(1)
C(20)	4900(4)	5866(3)	2756(2)	25(1)
C(21)	4332(4)	5161(3)	2037(2)	28(1)
C(22)	2858(4)	4772(3)	1747(2)	34(1)
C(23)	1901(4)	5075(4)	2165(2)	40(1)
C(24)	2476(4)	5772(4)	2868(2)	39(1)
C(25)	3929(4)	6167(3)	3173(2)	30(1)
C(26)	5299(4)	4749(3)	1585(2)	34(1)
C(27)	323(5)	4599(5)	1868(3)	71(2)
C(28)	4438(4)	6901(3)	3941(2)	36(1)
C(29)	7435(4)	7114(3)	2783(2)	23(1)
C(30)	8876(4)	7562(3)	3091(2)	27(1)
C(31)	9517(4)	7339(3)	3687(2)	30(1)
C(32)	8751(4)	6600(3)	3916(2)	29(1)
C(33)	4819(4)	4211(3)	3529(2)	40(1)
C(34)	7075(5)	5471(3)	4917(2)	39(1)
C(35)	7788(5)	3955(3)	3622(2)	36(1)

C(36)	9393(5)	4435(4)	3811(2)	47(1)
C(37)	7441(6)	3119(4)	3989(3)	59(1)
C(38)	7300(5)	3389(4)	2795(2)	45(1)
Ag(1)	2997(1)	6159(1)	1249(1)	31(1)
Ag(2)	7507(1)	8742(1)	3588(1)	29(1)
B(1)	4289(4)	8482(3)	1487(2)	24(1)
B(2)	6557(4)	6324(3)	3067(2)	24(1)
Si(1)	2733(1)	10046(1)	1432(1)	24(1)
Si(2)	6739(1)	4926(1)	3918(1)	30(1)
F(1)	6853(3)	8029(2)	5889(1)	54(1)
F(2)	7606(3)	10055(2)	5988(1)	55(1)
F(3)	10069(2)	9915(2)	5732(1)	37(1)
F(4)	9386(3)	7920(2)	5651(1)	43(1)
F(5)	7701(2)	8575(2)	4825(1)	34(1)
F(6)	9251(3)	9398(2)	6811(1)	52(1)
F(7)	3343(2)	3979(2)	-141(1)	44(1)
F(8)	1647(2)	2568(2)	-1363(1)	41(1)
F(9)	-496(2)	3328(2)	-1062(1)	32(1)
F(10)	1225(2)	4716(2)	186(1)	41(1)
F(11)	943(2)	2693(2)	-111(1)	38(1)
F(12)	1918(2)	4629(2)	-1052(1)	47(1)
N(1)	3202(3)	8816(2)	1124(2)	22(1)
N(2)	7321(3)	6036(2)	3615(2)	24(1)
Sb(1)	8466(1)	8972(1)	5824(1)	27(1)
Sb(2)	1422(1)	3641(1)	-600(1)	26(1)

BNB1

Crystals from **BNB1** were obtained from *n*-hexane at 253 K.

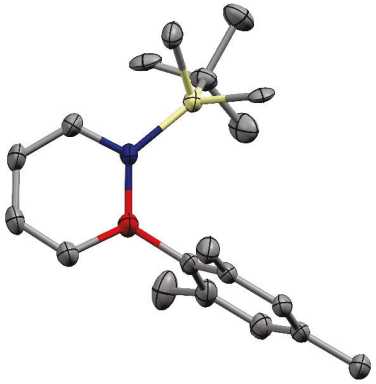

Figure S79. Crystal structure of **BNB1** (*n*-hexane). Hydrogen atoms are omitted for clarity and the thermal ellipsoids are drawn at 50% probability level.

Table S5. Crystal data and structure refinement for **BNB1**.

Compound	**BNB1**
CCDC	2298028
Empirical Formula	$C_{19}H_{30}BNSi$
Formula weight	311.34
Temperature [K]	100.00(11)
Crystal system	monoclinic
Space group	$P2_1/n$
a [Å]	12.3870(3)
b [Å]	9.10838(15)
c [Å]	17.8632(4)
α [°]	90
β [°]	109.277(3)
γ [°]	90
Volume [Å^3]	1902.42(7)
Z	4
r_{calc} [Mg/m^3]	1.087
μ [mm^{-1}]	1.033

Crystal size [mm^3]	0.12 × 0.12 × 0.10
Radiation [nm]	$CuK_\alpha(\lambda = 1.54184)$
Θ range for data collection [°]	3.824 – 66.599
Reflections collected	68327
Independent reflexions	3356 [R_{int} = 0.0366]
Data/restraints/parameters	3356 / 12 / 274
Goodness-of-fit[a]	1.053
Final R indexes [I>=2σ (l)][b][c]	R_1 = 0.0429, wR_2 = 0.1164
Final R indexes [all data]	R_1 = 0.0462, wR_2 = 0.1195
Largest diff. peak/hole [eÅ^{-3}]	0.322 / -0.291

[a]GOF = $[\sum w(F_0^2 - F_c^2)^2/(n_0 - n_p)]^{1/2}$. [b]$R_1 = \Sigma(||F_0| - |F_c||)/\Sigma|F_0|$, $F_0 > 4\sigma(F_0)$. [c]$wR_2 = \{\Sigma[w({F_0}^2 - {F_c}^2)^2]/\Sigma[w({F_0}^2)^2]\}^{1/2}$.

Table S6. Atomic coordinates (× 10^4) and equivalent isotropic displacement parameters (Å^2 × 10^3) for **BNB1**. U(eq) is defined as one third of the trace of the orthogonalized U_{ij} tensor.

	x	y	z	U(eq)
C(2)	4278.2(15)	-1272.2(17)	1967.9(10)	37.8(4)
H(2)	3940(16)	-2110(2)	1670(11)	44(5)
C(3)	5005.7(14)	-1380.2(16)	2754.0(10)	36.1(4)
H(3)	5181.88	-2316.80	2997.89	43
C(4)	5461.7(14)	-150.1(16)	3170.5(9)	35.0(4)
H(4)	5945.73	-235.52	3706.22	42
C(5)	5761.1(13)	2792.8(15)	3255.3(8)	29.2(3)
C(6)	5243.8(12)	3563.6(15)	3726.7(8)	27.9(3)
C(7)	5737.2(12)	4860.9(15)	4106.5(8)	28.8(3)
H(7)	5362.91	5389.73	4408.24	35
C(8)	6755.5(13)	5394.5(15)	4054.5(8)	27.9(3)
C(9)	7302.5(14)	4580.1(16)	3626.5(9)	32.4(3)
H(9)	8016.67	4910.13	3600.28	39
C(10)	6826.2(14)	3291.2(16)	3235.4(9)	33.6(4)
C(11)	4183.2(14)	2978.4(17)	3861.7(10)	37.1(4)
H(11A)	3721.77	2435.36	3391.28	56
H(11B)	3735.23	3798.49	3959.54	56
H(11C)	4403.84	2321.42	4321.96	56
C(12)	7274.7(14)	6804.1(16)	4461.3(9)	34.5(4)
H(12A)	7947.55	6577.24	4921.33	52
H(12B)	6710.50	7329.07	4636.94	52
H(12C)	7503.08	7420.62	4089.49	52
C(13)	7482.3(18)	2429(2)	2804.5(12)	50.8(5)

H(13A)	7839.99	1573.90	3123.08	76
H(13B)	8075.47	3054.38	2719.84	76
H(13C)	6957.16	2099.74	2291.06	76
B(1)	5209.1(16)	1346.3(18)	2793.0(10)	32.6(4)
Si(1A)	3426.9(8)	2970.9(10)	1464.0(5)	24.00(17)
N(1A)	4156(3)	1401(4)	2032(2)	24.6(5)
C(1A)	3768(5)	0069(8)	1661(4)	33.1(8)
H(1A)	3134.94	0067.38	1183.03	40
C(14A)	1931(19)	2420(3)	1014(13)	36(3)
H(14A)	1668.82	1936.58	1413.89	54
H(14B)	1863.07	1730.88	577.77	54
H(14C)	1459.23	3285.43	808.46	54
C(15A)	2657(3)	4486(5)	1798(2)	28.7(7)
H(15A)	1832.20	4396.93	1522.09	43
H(15B)	2924.00	5438.78	1673.69	43
H(15C)	2813.61	4410.36	2371.19	43
C(16A)	4104(3)	3432(4)	685(2)	31.1(8)
C(17A)	3211(4)	4299(5)	18(2)	44.3(10)
H(17A)	2555.03	3664.60	-241.63	66
H(17B)	3558.45	4627.45	-372.75	66
H(17C)	2953.79	5154.55	0246.27	66
C(18A)	5159(4)	4423(5)	1044(3)	43.5(10)
H(18A)	4914.59	5373.15	1189.74	65
H(18B)	5548.39	4572.89	0653.66	65
H(18C)	5684.92	3951.82	1518.18	65
C(19A)	4231(5)	2116(10)	256(4)	32.4(16)
H(19A)	4795.12	1460.64	616.07	49
H(19B)	4490.20	2392.17	-186.65	49
H(19C)	3493.45	1609.63	51.78	49
Si(1)	4258.1(5)	2893.2(7)	1276.9(4)	24.00(17)
N(1)	4648.4(19)	1346(3)	1951.5(14)	24.6(5)
C(1)	4203(3)	18(5)	1592(3)	33.1(8)
H(1	3814.86	28.30	1035.85	40
C(14)	5237(2)	4494(3)	1607.2(17)	31.4(5)
H(14D)	5239.98	4815.93	2131.26	47
H(14E)	4973.95	5299.42	1226.85	47
H(14F)	6013.27	4207.44	1637.37	47
C(15)	4525(4)	2197(6)	363(3)	28.7(7)
H(15D)	5237.29	1630.50	517.80	43
H(15E)	4588.82	3030.45	33.37	43

H(15F)	3887.94	1567.71	62.27	43
C(16)	2730(2)	3499(3)	1136.8(14)	28.3(5)
C(17)	3284(5)	4602(4)	2043(2)	65.1(12)
H(17D)	2949.01	5587.29	1947.02	98
H(17E)	4118.28	4674.93	2194.17	98
H(17F)	3081.55	4132.58	2472.22	98
C(18)	1923(14)	2180(2)	1083(10)	44(3)
H(18D)	1903.54	1568.30	629.17	67
H(18E)	1150.63	2544.67	1015.26	67
H(18F)	2200.78	1603.43	1571.53	67
C(19)	2282(3)	4359(4)	360.9(18)	48.6(8)
H(19D)	2800.49	5176.88	371.01	73
H(19E)	1518.14	4742.68	298.91	73
H(19F)	2239.70	3708.58	-85.00	73

6 Kinetic analysis

6.1 Temperature dependence of reaction rate constant

Reaction rates were determined by ^{1}H NMR measuring samples prepared according to GP-B at their respective temperature. Hereby, four temperatures were measured thrice, and data points were selected between 10% and 90% conversion of **BND1**, ensuring a sufficient signal to noise ratio. The relative concentration of the selected data was normalized ($[\mathbf{BND1}]_{\mathrm{rel},t_0} = 1$) and the negative natural logarithm was plotted against relative time (Figure S80). Linear regression through the origin was carried out in Python 3.10, employing the statsmodels 0.14.0 module, with the slope corresponding to the respective reaction constant. Subsequently, the reaction constants were plotted according to Arrhenius (T^{-1} vs. ln(k)) and Eyring (T^{-1} vs. ln(kT^{-1})), determining E_a, lnA, $\Delta H^{\ddagger}$ and $\Delta S^{\ddagger}$. Under the assumption of an underlying Gaussian distribution, the given errors correspond to the standard deviation of linear regression with their respective error propagation.[26]

$$E_A = -\beta R\ ;\ \varepsilon(E_A) = \sigma(\beta)R\ ;\ \Delta H^{\ddagger} = -\beta' R\ ;\ \varepsilon(\Delta H^{\ddagger}) = \sigma(\beta')R\ ;\ \Delta S^{\ddagger} = \left(\beta'_0 + \ln\left(\frac{h}{k_B}\right)\right)R\ ;$$

$$\varepsilon(\Delta S^{\ddagger}) = \sigma(\beta'_0)R;\ \Delta G^{\ddagger} = \Delta H^{\ddagger} - T\Delta S^{\ddagger};\ \varepsilon(\Delta G^{\ddagger}) = R\sqrt{\mathrm{var}(\beta') + T^2\mathrm{var}(\beta'_0)}$$

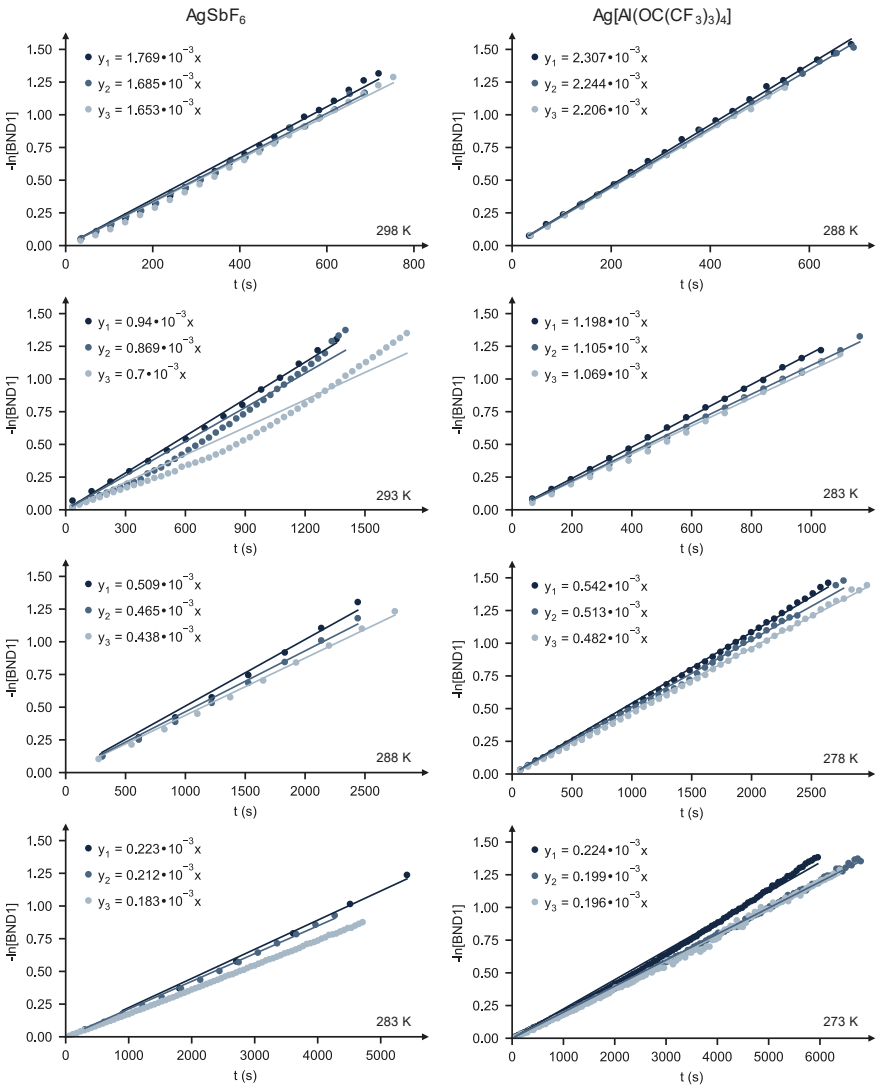

Figure S80. Determination of the reaction constants of the cycloreversion of **BND1** mediated by $Ag[Al(OC(CF_3)_3)_4]$ and $AgSbF_6$ in DCM-d_2 at different temperatures.

Table S7. Parameters of the linear regressions for the determination of the reaction constants of the cycloreversion of **BND1** mediated by $Ag[Al(OC(CF_3)_3)_4]$ and $AgSbF_6$ (Figure S80).

AgWCA	T [K]	y	regression coefficient [10^{-3}]	σ [10^{-3}]	R^2
$AgSbF_6$	298	y_1	1.76866	0.01744	0.9982
		y_2	1.68528	0.01248	0.9990
		y_3	1.65330	0.01656	0.9980
	293	y_1	0.94025	0.00717	0.9992
		y_2	0.86949	0.01322	0.9911
		y_3	0.69982	0.01079	0.9887
	288	y_1	0.50912	0.00979	0.9978
		y_2	0.46560	0.00759	0.9984
		y_3	0.43794	0.00454	0.9991
	283	y_1	0.22327	0.00320	0.9992
		y_2	0.21190	0.00171	0.9992
		y_3	0.18327	0.00026	0.9998
$Ag[Al(OC(CF_3)_3)_4]$	288	y_1	2.30721	0.00865	0.9997
		y_2	2.24396	0.00584	0.9999
		y_3	2.20591	0.00653	0.9999
	283	y_1	1.19836	0.00310	0.9999
		y_2	1.10470	0.00448	0.9997
		y_3	1.06879	0.00916	0.9988
	278	y_1	0.54154	0.00167	0.9996
		y_2	0.51296	0.00223	0.9993
		y_3	0.48192	0.00127	0.9997
	273	y_1	0. 22379	0.00082	0.9986
		y_2	0. 19913	0.00034	0.9997
		y_3	0.19604	0.00063	0.9989

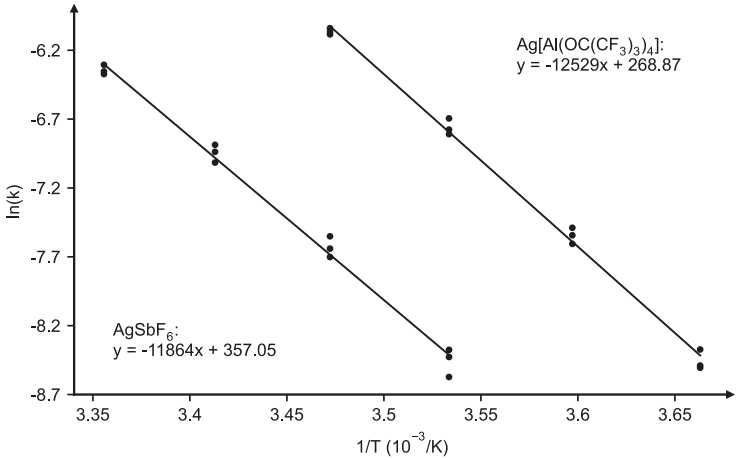

Figure S81. Arrhenius plot for the cycloreversion of **BND1** in DCM-d_2 mediated by $Ag[Al(OC(CF_3)_3)_4]$ and $AgSbF_6$.

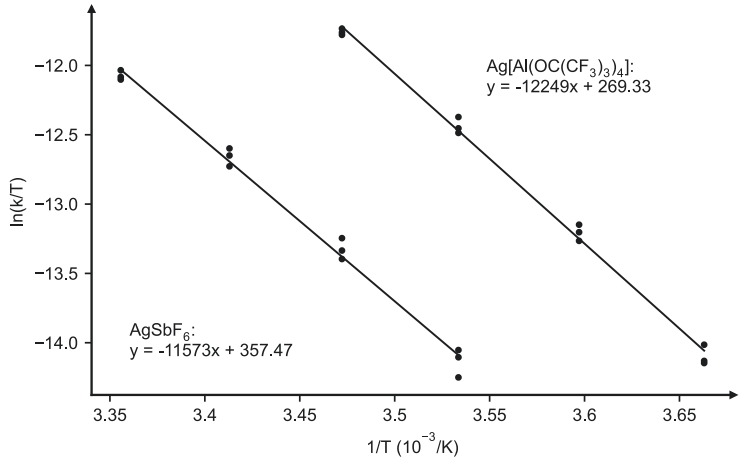

Figure S82. Eyring plot for the cycloreversion of **BND1** in DCM-d_2 mediated by $Ag[Al(OC(CF_3)_3)_4]$ and $AgSbF_6$.

Table S8. Parameters of the linear regressions from Figure S81 (Arrhenius plot) and Figure S82 (Eyring plot) regarding the Ag^+ mediated cycloreversion of **BND1**.

Plot	AgWCA	Intercept a	σ(a)	Regression coefficient b	σ(b)	R^2
Arrhenius	$AgSbF_6$	33.48	1.23	-11863.65	357.05	0.9910
	$Ag[Al(OC(CF_3)_3)_4]$	37.45	0.96	-12529.17	268.87	0.9954
Eyring	$AgSbF_6$	26.81	1.23	-11573.31	357.47	0.9906
	$Ag[Al(OC(CF_3)_3)_4]$	30.81	0.96	-12248.82	269.33	0.9952

Table S9. Thermochemistry values determined from kinetic analysis of **BND1**•$AgSbF_6$ and **BNB1**•$Ag[Al(OC(CF_3)_3)_4]$.

	BND1•$AgSbF_6$		**BNB1**•$Ag[Al(OC(CF_3)_3)_4]$	
	Value	**Error**	**Value**	**Error**
E_a [kcal/mol]	23.6	0.7	24.9	0.5
lnA	33.5	1.2	37.4	1.0
$\Delta H^{\ddagger}$ [kcal/mol]	23.0	0.7	24.3	0.5
$\Delta S^{\ddagger}$ [cal/(mol•K)]	6.1	2.4	14.0	1.9
$\Delta G^{\ddagger}(298\ K)$ [kcal/mol]	21.2	1.0	20.2	0.8

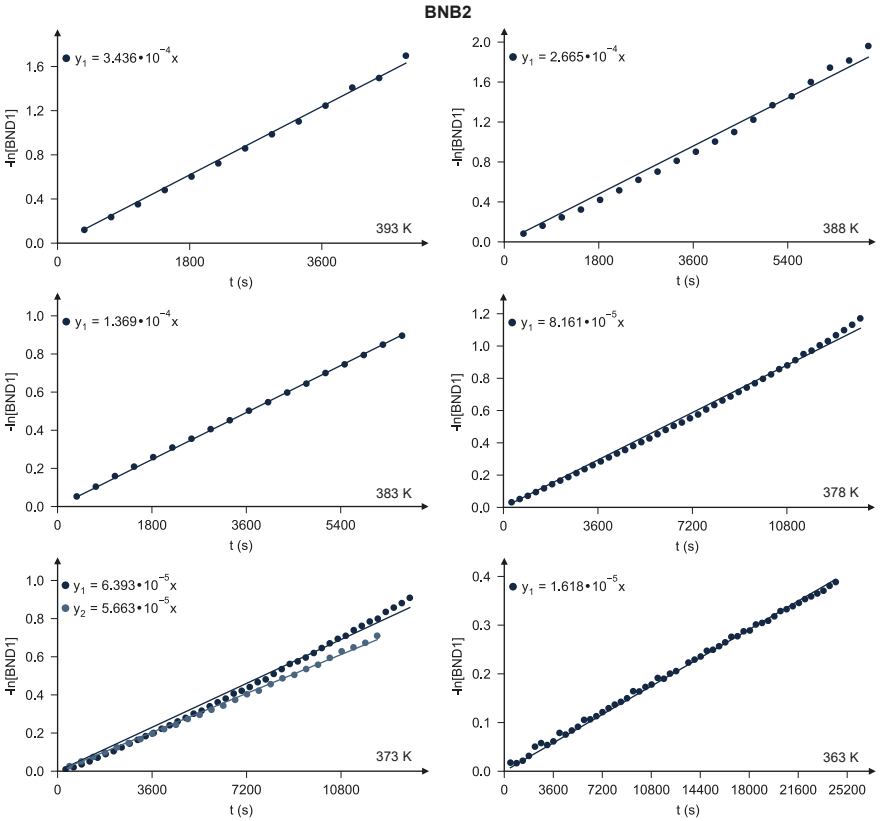

Figure S83. Determination of the reaction constants of the thermal cycloreversion of **BND2** in TCE-d_2 at different temperatures.

Table S10. Parameters of the linear regressions for the determination of the reaction rate of the thermal ring opening of **BND2** (Figure S83).

T [K]	y	Regressioncoefficient [10^{-4}]	σ [10^{-4}]	R^2
393	y_1	3.43584	0.02724	0.9996
388	y_1	2.66548	0.03502	0.9984
383	y_1	1.36911	0.00344	0.9999
378	y_1	0.81607	0.00424	0.9994
373	y_1	0.63925	0.00510	0.9986
	y_2	0.56628	0.00244	0.9998
263	y_1	0.16183	0.00056	0.9997

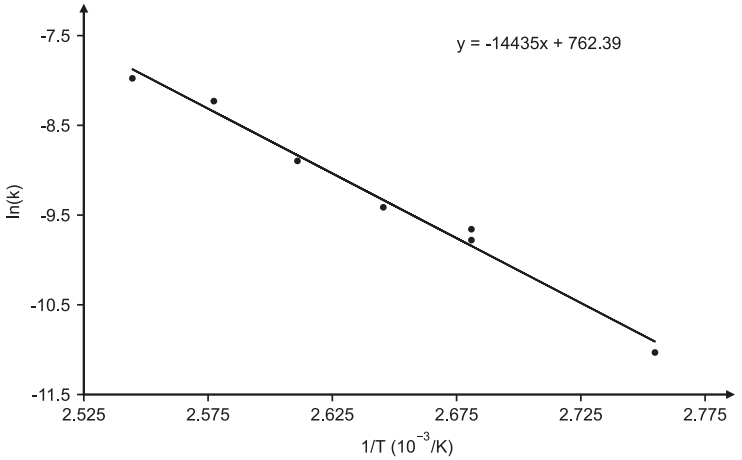

Figure S84. Arrhenius plot for the thermal cycloreversion of **BND2** in TCE-d_2.

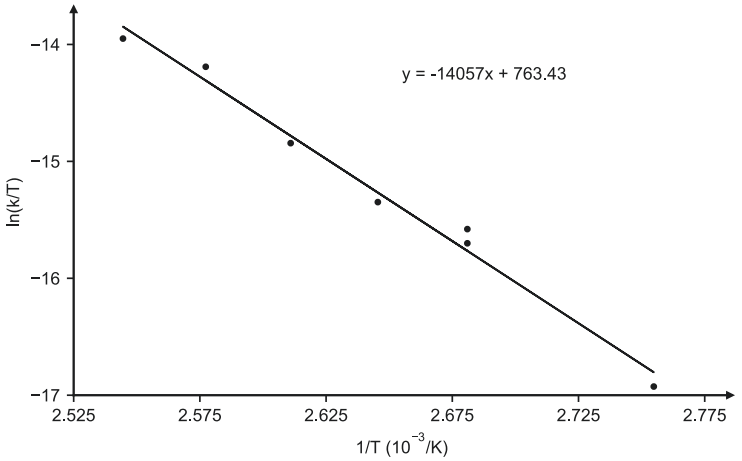

Figure S85. Eyring plot for the thermal cycloreversion of **BND2** in TCE-d_2.

Table S11. Parameters of the linear regressions from Figure S84 (Arrhenius plot) and Figure S85 (Eyring plot) regarding the thermal cycloreversion of **BND2**.

Plot	Intercept a	σ(a)	Regression coefficient b	σ(b)	R^2
Arrhenius	28.85	2.01	-14434.59	762.39	0.9931
Eyring	21.92	2.02	-14056.69	763.43	0.9927

Table S12. Thermochemistry values determined from kinetic analysis for the thermal ring opening of **BND2**.

BND2	Value	Error
E_a [kcal/mol]	28.7	1.5
lnA	28.9	2.0
$\Delta H^{\ddagger}$ [kcal/mol]	27.9	1.5
$\Delta S^{\ddagger}$ [cal/(mol•K)]	-3.7	4.0
$\Delta G^{\ddagger}(298\ K)$ [kcal/mol]	29.0	1.9

6.2 Secondary kinetic isotope effect

Kinetic data for the determination of the secondary kinetic isotope effect was measured by ^{11}B NMR at 293 K of three samples for each [**BND1**$AgSbF_6$]$_2$ and [**BND1d1**$AgSbF_6$]$_2$, which were prepared according to GP-B. Data points were selected between 10% and 90% conversion of **BND1**/**BND1d1**, ensuring a sufficient signal to noise ratio. The relative concentration of the selected data was normalized ($[\mathbf{BND1/BND1d1}]_{\mathrm{rel},t_0} = 1$) and the negative natural logarithm was plotted against relative time (Figure S86). Linear regression through the origin was carried out in Python 3.10, employing the statsmodels 0.14.0 module, with the slope corresponding to the respective reaction constant. Subsequently, the arithmetic mean of all reaction constants of **BNB1** and **BNB1d1** was determined and the secondary kinetic isotope effect was calculated. Under the assumption of an underlying Gaussian distribution, the given errors correspond to the standard deviation of linear regression with their respective error propagation.[26]

$$k_X = \frac{\sum k_{X,i}}{N};\ sKIE = \frac{k_H}{k_D};\ \varepsilon(sKIE) = \frac{\sqrt{\sum var(k_{H,i}) + sKIE^2 \sum var(k_{D,i})}}{\sum k_{D,i}}$$

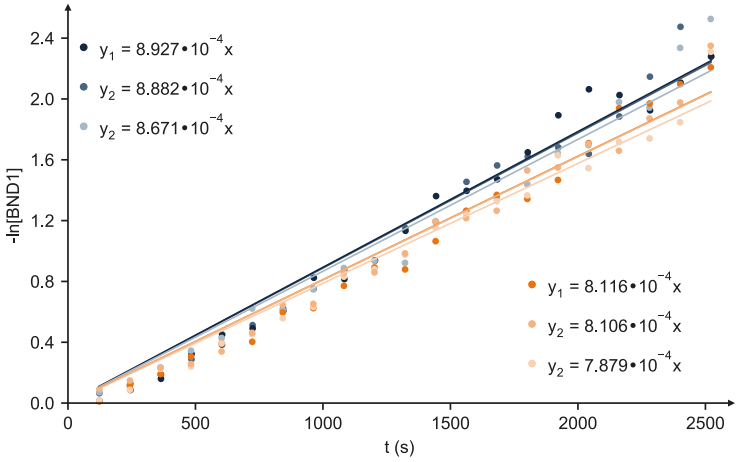

Figure S86. Determination of the reaction rate constants for the $AgSbF_6$ mediated cycloreversion of **BND1** and **BND1d1** in DCM-d_2 at 293 K.

Table S13. Parameters of the linear regressions for the determination of the reaction rate of the $AgSbF_6$ mediated ring opening of **BND1** and **BND1d1** (Figure S86).

	y	Regressioncoefficient [10^{-4}]	σ [10^{-4}]	R^2
	y_1	8.92654	0.17283	0.9963
BND1	y_2	8.88199	0.18401	0.9957
	y_3	8.67136	0.19158	0.9952
	y_4	8.11587	0.17645	0.9953
BND1d1	y_5	8.10560	0.15333	0.9964
	y_6	7.87920	0.15464	0.9961

sKIE = 1.10 ± 0.02.

7 Catalyst screening

BNB1 was irradiated according to GP-A. **BND1** (32 – 150 µmol) was dissolved in DCM-d_2 or toluene-d_8 (0.5 mL) and the respective amount of catalyst was added from a stock solution, prepared in a Schlenk round bottom flask with DCM-d_2 or toluene-d_8. After 24 h, the yield was determined by $^1H/^{11}B$ NMR.

Table S14. Catalyst screening for the ring opening of **BND1** to **BNB1** in DCM-d_2/toluene-d_8 at rt within 24 h.

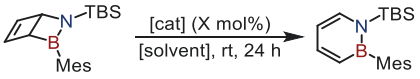

BND1 **BNB1**

Entry	Catalyst	Loading [mol%]	Solvent	Yield [%]
1	$Na[BAr^F_4]$	10	DCM-d_2	/
2	V_2O_5	10	toluene-d_8	/
3	$(FeCl_3)_2(TMEDA)_3$	3	DCM-d_2	/
4	$Fe(acac)_3$ + 2 PPh_3	10	DCM-d_2	/
5	$FeCl_3$	10	DCM-d_2	/
6	$FeCl_2$	10	DCM-d_2	/
7	$Fe(CO)_5$	10	toluene-d_8	/
8	$[Ru(p\text{-cymene})Cl_2]_2$	3	DCM-d_2	/
9	$RuCl_2(PPh_3)_3$	3	DCM-d_2	/
10	Hoveyda-Grubbs II	3	DCM-d_2	/[a]
11	Co(II)-pthalocyanin	3	DCM-d_2	/
12		3	toluene-d_8	/
13	Salcomin	3	toluene-d_8	/
14	$CoCl_2(PPh_3)_2$	3	DCM-d_2	/
15	$CoCl(PPh_3)_3$	3	DCM-d_2	/
16	$Co_2(CO)_8$	3	DCM-d_2	/
17	$Co_2(CO)_8$	10	toluene-d_8	/
18	$[RhCp^*Cl_2]_2$	3	DCM-d_2	/
19	$Rh(CO)_2(acac)$	3	DCM-d_2	/
20	$Rh_2(OAc)_4$	3	DCM-d_2	1
21	$NiCl_2(PPh_3)_2$	3	DCM-d_2	/
22	$Ni(cod)_2$	3	DCM-d_2	2

23	$Ni(cod)_2$ + 2 PPh_3	3	DCM-d_2	2
24	$Ni(cod)_2$ + dppf	10	DCM-d_2	1
25	$Ni(cod)_2$ + xantphos	10	DCM-d_2	/
26	$Ni(cod)_2[Al(OC(CF_3)_3)_4]$	20	DCM-d_2	/[b]
27	Pd/C	10	DCM-d_2	/
28	$PdCl_2(MeCN)_2$	10	DCM-d_2	50
29	CuI	3	DCM-d_2	/
30	CuBr	3	DCM-d_2	/
31	[Cu(1,2-difluorobenzene)$_{0.6}$] $[Al(OC(CF_3)_3)_4]$	5	DCM-d_2	quant.
32	$AgNO_3$	5	DCM-d_2	/
33	AgOPiv	5	DCM-d_2	/
34	$AgCF_3CO_2$	5	DCM-d_2	/
35	$AgCF_3SO_3$	5	DCM-d_2	traces
36	$AgPF_6$	5	DCM-d_2	/
37	$Ag[BAr^F_4]$	5	DCM-d_2	/
38	$Ag[B(C_6F_5)_4](C_6H_6)_n$	5	DCM-d_2	10
39	$AgClO_4$	5	DCM-d_2	43
40	$AgBF_4$	5	DCM-d_2	51
41	$AgNTf_2$	10	DCM-d_2	38
42		5	DCM-d_2	quant.[c]
43	$AgSbF_6$	5	DCM-d_2	quant.
44		50	toluene-d_8	34[d]
45	$Ag[Al(OC(CF_3)_3)_4]$	5	DCM-d_2	quant. (99)[e]
46	Ag nanoparticles[f]	/[g]	DCM-d_2	/
47	AuCl	1 equiv.	DCM-d_2	23[h]
48	$AuClPPh_3$	3	DCM-d_2	/

[a] Polymerization. [b] Decomposition. Synthesized according to literature.[27] [c] rt ≈ 303 K. [d] Quant. Conversion after 10 d. [e] Isolated yield [f] abcr, APS 20 – 40 nm, surfactant free. [g] 100 weight%. [h] Yield determined by GC-FID. Decomposition of **BND1** observed.

8 GC-FID calibration

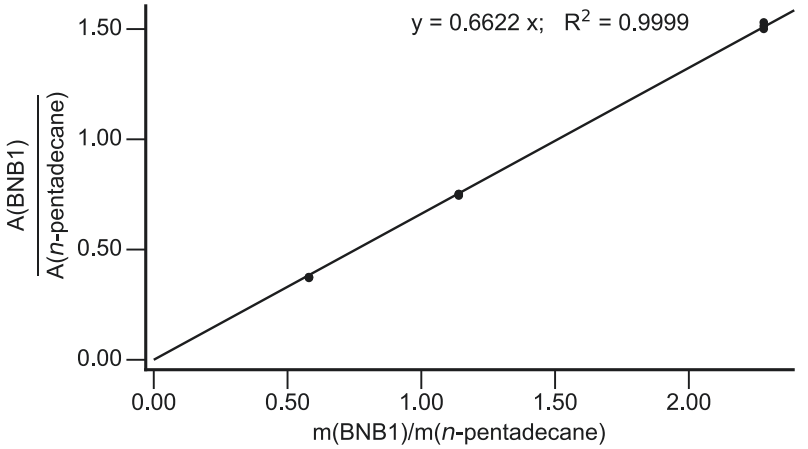

Figure S87. Calibration of **BNB1** with *n*-pentadecane on GC-FID.

Table S15. Values for the calibration of **BNB1** with *n*-pentadecane on GC-FID.

Entry	m(BNB1) [mg]	m(*n*-pentadecane) [mg]	A(BNB1)	A(*n*-pentadecane)
1	2.72	4.67	5608.0	14979.0
2	2.72	4.67	5441.2	14651.5
3	2.72	4.67	5509.3	14686.4
4	2.72	2.38	5243.5	7042.5
5	2.72	2.38	5313.3	7065.2
6	2.72	2.38	5362.1	7135.6
7	5.43	2.38	10605.3	7066.6
8	5.43	2.38	10343.2	6831.2
9	5.43	2.38	10230.9	6685.5

9 Computations

All reported computations were conducted utilizing the Gaussian 16 program package.[28] Molecular geometries were optimized using the M06-2X density functional in conjunction with the def2-SVP basis set.[29] The effect of DCM solvent was taken into account employing the polarizable continuum solvent model (PCM).[30] Verification of the stationary points involved analytical frequency computations, confirming minima with zero imaginary vibrational frequencies and one imaginary vibrational frequency for transition states. Intrinsic reaction coordinates (IRC) were computed starting from the transition states by using the local quadratic approximation.[31] Free energies were computed using standard thermochemistry equations implemented in Gaussian.[32] In addition, single-point energy calculations were executed at the M06-2X/def2-QZVPP[33] level of theory for each optimized structure utilizing the PCM solvation model with DCM as a solvent.

In the images of the molecules given below, hydrogen atoms except those bound directly to the 1,2-dihydro-1,2-azaborinine backbone are omitted for clarity. In this section, total energies are given in Hartree, Cartesian coordinates in Å.

9.1 BNB1

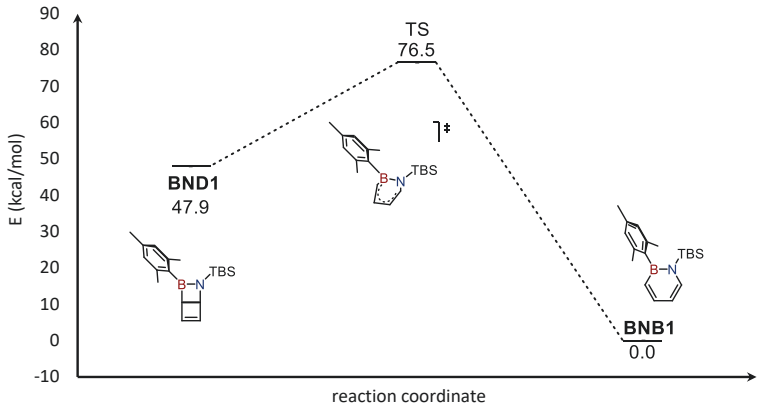

Figure S88. Free energy profile of the thermal cycloreversion of **BND1** at the M06-2X(PCM:DCM)/def2-QVPP//M06-2X(PCM:DCM)/def2-SVP level of theory.

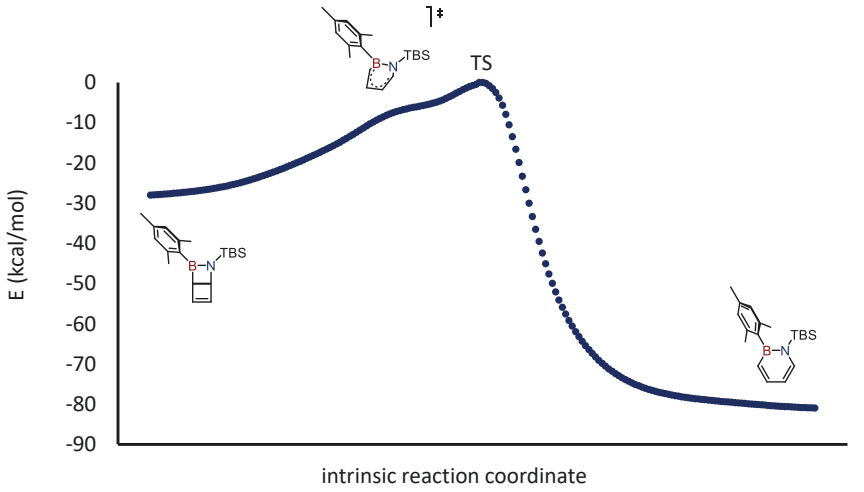

Figure S89. Electronic energies for the irc path of the thermal ring opening of **BND1** calculated at the M06-2X(PCM:DCM)/def2-SVP level of theory.

BND1:

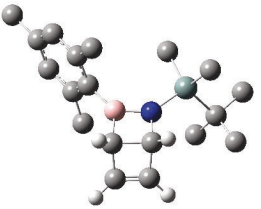

C	-0.04553200	2.67779100	0.63621200
B	0.40255300	1.14809200	0.35411400
N	-0.91641000	0.64545900	0.50222500
C	-1.45588100	2.01577100	0.79457900
C	-1.88203900	2.85852800	-0.39605900
C	-0.68349200	3.44251400	-0.50487000
H	-2.01516100	2.09593000	1.72619600
H	0.40779300	3.24223400	1.45068000
H	-0.27753800	4.17415400	-1.19285700
H	-2.79037500	2.90299100	-0.98190100
Si	-1.74489600	-0.90851100	0.57860300
C	-0.48316400	-2.25026700	0.21991000
H	0.37355500	-2.17197500	0.89080500
H	-0.92858200	-3.23725400	0.36410500
H	-0.09991300	-2.20153000	-0.80050800
C	-2.40100900	-1.11659700	2.33247100
H	-2.96841600	-2.04368300	2.44251100

H	-1.57269100	-1.15163700	3.04404300
H	-3.05489300	-0.29395500	2.62921300
C	-3.19896800	-0.99597700	-0.67206900
C	-2.71615300	-0.61336500	-2.08247600
H	-3.54225600	-0.68795000	-2.79869500
H	-2.33639900	0.40889900	-2.12125900
H	-1.92272200	-1.27676100	-2.43523700
C	-3.74933800	-2.43545600	-0.71253800
H	-3.00252200	-3.15117500	-1.06191000
H	-4.10323300	-2.77085700	0.26554500
H	-4.60050200	-2.49166600	-1.40014200
C	-4.34335800	-0.05303300	-0.25605900
H	-5.15738100	-0.10293200	-0.98799700
H	-4.76359800	-0.32604000	0.71423000
H	-4.02428600	0.98890600	-0.19865500
C	1.78081700	0.44788500	0.09461200
C	2.58821300	0.04097300	1.17367400
C	2.26512000	0.26607400	-1.21443800
C	3.82699800	-0.54947000	0.93307600
C	3.50850200	-0.32832000	-1.41951700
C	4.30513400	-0.75024100	-0.35880000
H	4.43624800	-0.85680700	1.77689600
H	3.86630100	-0.46090800	-2.43545200
C	2.13035900	0.24513600	2.59854300
H	1.19363300	-0.28007500	2.80211500
H	2.87462300	-0.11742700	3.30793900
H	1.95495300	1.30255700	2.81442600
C	5.63149500	-1.42174100	-0.60163400
H	6.32623400	-1.24046600	0.21997200
H	5.51255900	-2.50557400	-0.69427200
H	6.09514900	-1.06635200	-1.52322400
C	1.45844900	0.72480800	-2.40573200
H	1.95692100	0.46942100	-3.34119900
H	0.46454500	0.27220200	-2.42156200
H	1.31168800	1.80815300	-2.39370000

M06-2X(PCM:DCM)/def2-SVP: -1110.55719

M06-2X(PCM:DCM)/def2-QVPP: -1111.23144

$G_{corr.}$: 0.38678

TS:

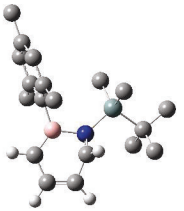

C	-0.41098200	3.00791600	0.42738800
B	-0.37640200	1.53834700	0.25656100
N	1.04175200	0.77314900	0.09380300
C	1.44683300	1.75551100	-0.70296800
C	1.87912400	3.05340200	-0.09706500
C	0.84393700	3.73107400	0.44750200
H	1.57871600	1.58634900	-1.79025300
H	-1.35716200	3.54377000	0.55662200
H	0.96782300	4.69424800	0.95700900
H	2.94756500	3.23643400	0.05801700
Si	1.42500800	-0.98696500	-0.17810200
C	0.49857800	-2.04389900	1.06436400
H	-0.58748700	-1.99580600	0.90374400
H	0.81310800	-3.09307800	0.94134500
H	0.70980800	-1.74729500	2.10278300
C	0.98623300	-1.50397800	-1.93811000
H	1.38877300	-2.50957500	-2.14251800
H	-0.10657800	-1.55017900	-2.06163700
H	1.39220900	-0.82411300	-2.70342000
C	3.32968300	-1.10014600	0.12156900
C	3.68538900	-0.57024900	1.52604800
H	4.77247800	-0.65985000	1.70321400
H	3.41326000	0.48998500	1.64590700
H	3.17700200	-1.13729600	2.32263600
C	3.74857000	-2.58437400	0.02028400
H	3.25371800	-3.20946000	0.78050900
H	3.52559300	-3.01626200	-0.96902000
H	4.83770900	-2.68011000	0.17872800
C	4.10741800	-0.29521500	-0.93740800
H	5.19465300	-0.39555700	-0.76767600
H	3.90296100	-0.64353900	-1.96271300
H	3.88519700	0.78413900	-0.89656000
C	-1.66642100	0.61916800	0.11083000
C	-2.31071600	0.40090300	-1.13452100
C	-2.25656300	0.07797700	1.27980800
C	-3.47585100	-0.37814300	-1.19164800
C	-3.42589500	-0.69335900	1.18488000
C	-4.04681300	-0.94615600	-0.04414200
H	-3.95895500	-0.53768700	-2.16117300

H	-3.86531900	-1.10508600	2.09931100
C	-1.79291400	1.03465700	-2.40705500
H	-0.76011200	0.72802800	-2.63514600
H	-2.41714500	0.76324100	-3.27127800
H	-1.77869000	2.13332300	-2.32482500
C	-5.28154500	-1.81035600	-0.13750000
H	-5.98918300	-1.42467900	-0.88835400
H	-5.02442100	-2.84121600	-0.43911900
H	-5.80583100	-1.87382100	0.82804200
C	-1.67465500	0.35740000	2.64916600
H	-2.03786100	-0.36554600	3.39522600
H	-0.57513700	0.32655200	2.64766400
H	-1.95751600	1.36501600	2.99840000

M06-2X(PCM:DCM)/def2-SVP: -1110.5122

M06-2X(PCM:DCM)/def2-QVPP: -1111.18134

$G_{corr.}$: 0.38225

BNB1:

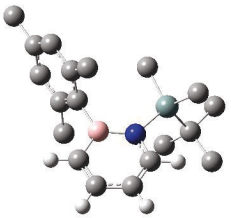

C	0.37581700	2.85656000	-0.72109800
B	0.26723600	1.41314400	-0.22767500
N	-1.06101600	0.97899700	0.20965300
C	-2.08850300	1.90260800	0.21401300
C	-1.96956000	3.20098600	-0.20962900
C	-0.72246900	3.68323800	-0.69697900
H	-3.05468100	1.56450800	0.59283000
H	1.32479800	3.26492500	-1.08577100
H	-0.66373800	4.72431300	-1.03692200
H	-2.84444000	3.85245700	-0.16176900
Si	-1.60448100	-0.69409400	0.76158500
C	-0.16296400	-1.88244700	0.96251800
H	0.58373500	-1.50036800	1.67161300
H	-0.56299400	-2.82487900	1.37122500
H	0.35373400	-2.10743400	0.01912500
C	-2.40486400	-0.45753000	2.45702700
H	-2.70628500	-1.43466400	2.86805300
H	-1.67839000	-0.01246500	3.15671100
H	-3.29665800	0.18711000	2.44361300

C	-2.86990400	-1.43260000	-0.50823500
C	-2.24346600	-1.49979100	-1.91521100
H	-2.94971100	-1.96630900	-2.62571400
H	-2.00137800	-0.49779300	-2.30395800
H	-1.32113300	-2.10245900	-1.93196500
C	-3.20807100	-2.86829600	-0.04098900
H	-2.32467500	-3.52535800	-0.02891200
H	-3.65588100	-2.88561000	0.96630400
H	-3.94218700	-3.32254800	-0.73036500
C	-4.18764800	-0.63413900	-0.59092000
H	-4.90384000	-1.16444000	-1.24443000
H	-4.67208600	-0.51751700	0.39238800
H	-4.04374800	0.36816800	-1.02181800
C	1.58921100	0.52880400	-0.15408200
C	2.34327900	0.49140600	1.04655500
C	2.12349400	-0.10833500	-1.29974400
C	3.56071100	-0.20285200	1.09351800
C	3.34323200	-0.79928000	-1.21781900
C	4.07645500	-0.86870600	-0.02691000
H	4.12640700	-0.21973900	2.03107700
H	3.73577000	-1.29019600	-2.11441500
C	1.85552800	1.20725600	2.28876100
H	0.90462300	0.78830600	2.65875200
H	2.58768800	1.13839600	3.10689900
H	1.66712500	2.27558500	2.09148300
C	5.37162400	-1.64131500	0.05474400
H	6.10865500	-1.12970600	0.69390200
H	5.21194500	-2.64405200	0.48943600
H	5.82122600	-1.78503700	-0.93958200
C	1.40494800	-0.03977200	-2.63005600
H	1.95580100	-0.58034800	-3.41413600
H	0.39407800	-0.47242400	-2.57293000
H	1.27880400	1.00343300	-2.96490300

M06-2X(PCM:DCM)/def2-SVP: -1110.64299

M06-2X(PCM:DCM)/def2-QVPP: -1111.30961

$G_{corr.}$: 0.38855

9.2 [BNB1Ag]$^+$

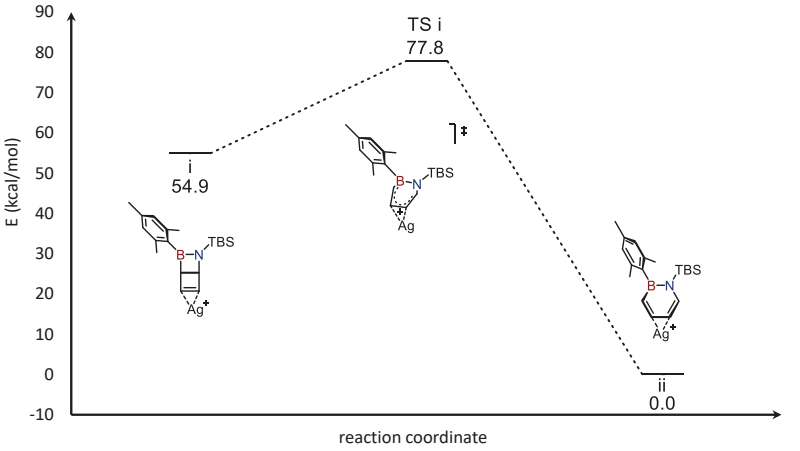

Figure S90. Free energy profile of the Ag$^+$-catalyzed cycloreversion of **BND1** at the M06-2X(PCM:DCM)/def2-QVPP//M06-2X(PCM:DCM)/def2-SVP level of theory.

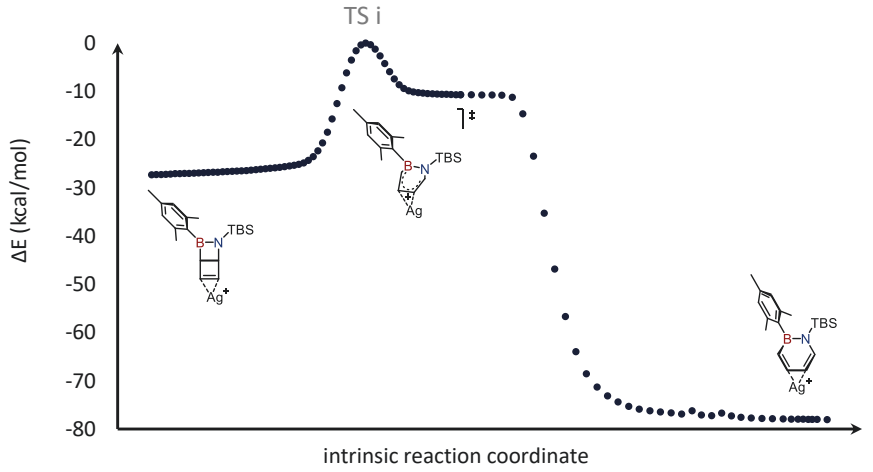

Figure S91. Electronic energies for the irc path of the Ag$^+$-catalyzed cycloreversion of **BND1** calculated at the M06-2X(PCM:DCM)/def2-SVP level of theory.

i:

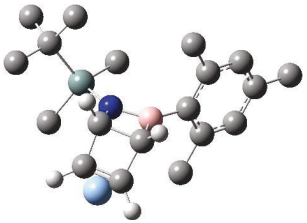

C	-1.45072700	-0.22964200	1.80272400
C	-0.18864200	-0.95572400	2.36610700
C	-2.09132300	-1.60225000	1.65677000
H	-3.08762000	-1.93766600	1.35264900
C	-0.98783700	-2.22284300	2.15015100
H	-0.76262000	-3.26733000	2.38569100
H	-1.97010100	0.52226600	2.41112200
H	0.17896400	-0.76359000	3.38128500
C	1.96991900	-0.00093000	0.57497300
C	2.66636000	1.14217200	1.01198500
C	2.59000400	-0.87899500	-0.33234300
C	3.95800400	1.38795300	0.53731700
C	3.88037500	-0.60829100	-0.79226900
C	4.58130300	0.52616500	-0.36922500
H	4.49350300	2.27536900	0.88514600
H	4.35464600	-1.29821100	-1.49578100
B	0.50940700	-0.23170700	1.09446200
C	1.85182500	-2.09178600	-0.84760200
H	1.34619400	-2.62869100	-0.02373300
H	1.11705200	-1.78828900	-1.61954500
H	2.52626200	-2.81096300	-1.32934800
C	2.01016700	2.10071100	1.97548600
H	2.70455500	2.88589900	2.29968000
H	1.13808400	2.58813600	1.51202000
H	1.64520700	1.57758200	2.87334400
C	5.96506100	0.81018300	-0.89230300
H	6.59785700	-0.08716500	-0.84564100
H	5.92567100	1.12677100	-1.94565600
H	6.45201700	1.60891700	-0.31839800
N	-0.72275900	0.28931400	0.61948700
C	0.24150500	1.80609100	-1.69761600
H	-0.04345500	2.31957300	-2.62787000
H	0.82884000	2.50206200	-1.07993000
H	0.89431900	0.95934400	-1.95794600
C	-2.27391000	0.01783800	-1.87230900
H	-1.60575800	-0.68735400	-2.39911800
H	-3.02570800	-0.53770500	-1.28577800
H	-2.82517700	0.55089400	-2.66278600
C	-2.40371800	2.63418800	-0.21804100

C	-1.71360900	3.40974700	0.91153000
H	-2.35117300	4.24733300	1.24081400
H	-1.51659100	2.77426400	1.78916600
H	-0.75353500	3.83714400	0.58107400
C	-2.65276000	3.57978200	-1.40311900
H	-3.11324200	3.05860800	-2.25760200
H	-3.34069800	4.38691000	-1.10026000
H	-1.72114900	4.05040000	-1.75214600
C	-3.75069200	2.08166900	0.27088900
H	-4.38358700	2.90610100	0.64012600
H	-4.30087700	1.57981600	-0.53968400
H	-3.63662100	1.36155900	1.09628800
Si	-1.28709300	1.21506000	-0.79756100
Ag	-1.15833000	-2.43884500	-0.52869500

M06-2X(PCM:DCM)/def2-SVP: -1256.88948

M06-2X(PCM:DCM)/def2-QVPP: -1258.02105

$G_{corr.}$: 0.394967

TS i:

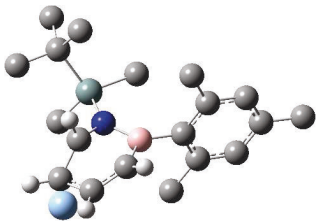

C	-1.19926197	2.62915126	0.00000000
C	0.24649403	1.53124026	0.71903200
C	-2.01211597	1.40345826	-0.13771800
H	-3.01661997	1.38754926	0.29336600
C	-1.01113197	0.90927126	0.77774800
H	-1.28712297	0.35055426	1.68203000
H	-1.40892097	3.35527726	0.79447600
H	0.85040903	1.47196026	1.63036200
C	2.26712403	2.25573926	-1.11565400
C	3.22736103	3.17890326	-0.66391400
C	2.61714703	1.30496226	-2.09089900
C	4.51952703	3.13934526	-1.19372000
C	3.91674803	1.28954926	-2.60373300
C	4.88364203	2.19967426	-2.16406400
H	5.26250503	3.86104126	-0.84323900
H	4.18346603	0.55093326	-3.36457700
B	0.80296103	2.29159426	-0.56134400
C	1.57654503	0.33731926	-2.60045600

H	1.06687703	-0.17449874	-1.76714800
H	0.80505603	0.87073626	-3.18352400
H	2.01576703	-0.42801674	-3.25267900
C	2.84548803	4.21974026	0.35960200
H	3.71839103	4.78843126	0.70399900
H	2.11966103	4.93480326	-0.05952500
H	2.37054403	3.75988826	1.24054500
C	6.29122203	2.14985026	-2.69811600
H	6.92430603	1.51047326	-2.06337400
H	6.31753603	1.73560526	-3.71465900
H	6.74587603	3.14935126	-2.71500900
N	-0.31666497	2.99870926	-1.05060200
C	0.99828203	4.35230026	-3.30187700
H	0.84270903	4.97699326	-4.19438100
H	1.69665703	4.87123626	-2.62886200
H	1.47281003	3.41228426	-3.61927900
C	-1.81368697	3.12824426	-3.65282500
H	-1.31900397	2.24287226	-4.08594700
H	-2.74145997	2.82183226	-3.14439400
H	-2.09795697	3.78025526	-4.49355400
C	-1.46957897	5.62126026	-1.83565500
C	-0.63955197	6.19773326	-0.68113700
H	-1.09782697	7.13124326	-0.31446500
H	-0.57286997	5.50297926	0.17096600
H	0.38692003	6.43718526	-1.00048400
C	-1.53428797	6.65090526	-2.97449100
H	-2.09358897	6.27124926	-3.84408900
H	-2.04672197	7.56307326	-2.62586000
H	-0.53000597	6.94465026	-3.31560600
C	-2.89552297	5.31663726	-1.35443100
H	-3.35081097	6.22463126	-0.92497800
H	-3.53970097	4.98116026	-2.18103400
H	-2.92456397	4.54069426	-0.57138400
Si	-0.65207197	4.03777426	-2.48694400
Ag	-2.06814797	0.40535026	-2.14034200

M06-2X(PCM:DCM)/def2-SVP: -1256.84526

M06-2X(PCM:DCM)/def2-QVPP: -1257.97768

$G_{corr.}$: 0.388054

ii:

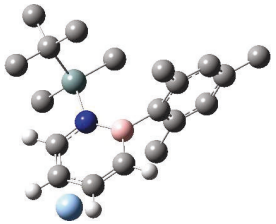

C	-0.62730626	3.49630992	0.00000000
C	0.79078674	1.55591592	1.46489000
C	-1.28079326	2.71008992	0.93145200
H	-2.32152026	2.93772492	1.16909600
C	-0.54312026	1.73862192	1.69288900
H	-1.08431326	1.16509792	2.45083300
H	-1.19312226	4.28510492	-0.50284400
H	1.32316474	0.80471292	2.05430600
C	2.95460874	1.99531792	-0.11387300
C	4.12849274	2.38169292	0.55568900
C	3.05674474	1.17662392	-1.25960600
C	5.37483574	2.00854992	0.03738100
C	4.31213774	0.81010592	-1.74650500
C	5.48878074	1.23350592	-1.11830500
H	6.28338874	2.32549392	0.55870200
H	4.37905774	0.18036492	-2.63810100
B	1.49861974	2.36594592	0.37115400
C	1.80601574	0.69337492	-1.95852300
H	1.16408974	0.12821692	-1.26212100
H	1.20362374	1.53480692	-2.34125200
H	2.04580374	0.03882892	-2.80609200
C	4.08678174	3.18889892	1.83131800
H	4.68165674	2.70021992	2.61670900
H	4.51076674	4.19320792	1.68233900
H	3.06183774	3.30704092	2.21010600
C	6.84402874	0.85132592	-1.65495400
H	7.41865674	0.28598992	-0.90665200
H	6.75612374	0.23322192	-2.55761000
H	7.43266474	1.74531592	-1.90800600
N	0.70081474	3.38064292	-0.30657800
C	2.87192774	4.15011792	-2.39988700
H	3.09370774	4.96878792	-3.10316100
H	3.72474674	4.02715792	-1.71970100
H	2.76360074	3.22749292	-2.98597400
C	-0.09732026	4.67920892	-2.82787000
H	-0.45840526	3.66119292	-3.05033000
H	-0.95782126	5.29129392	-2.52165200
H	0.29707074	5.10578092	-3.76187000
C	1.46611374	6.26787392	-0.62345700

C	2.63165574	6.16138892	0.36732100
H	2.77406374	7.12170592	0.89102100
H	2.43666474	5.39297292	1.13142300
H	3.57936574	5.91081892	-0.13452200
C	1.76680774	7.35519692	-1.66738000
H	0.94705874	7.46118392	-2.39531700
H	1.89319174	8.32902192	-1.16557600
H	2.69388374	7.14892492	-2.22344000
C	0.19361174	6.64979092	0.14342200
H	0.32767274	7.64004492	0.61012700
H	-0.68762726	6.71662692	-0.51478000
H	-0.02899526	5.93709992	0.95249200
Si	1.27773674	4.61560192	-1.54382000
Ag	-1.82382926	1.37259692	-1.09116700

M06-2X(PCM:DCM)/def2-SVP: -1256.96945

M06-2X(PCM:DCM)/def2-QVPP: -1258.1097

$G_{corr.}$: 0.39618

9.3 [BNB1AgSbF$_6$]$_2$

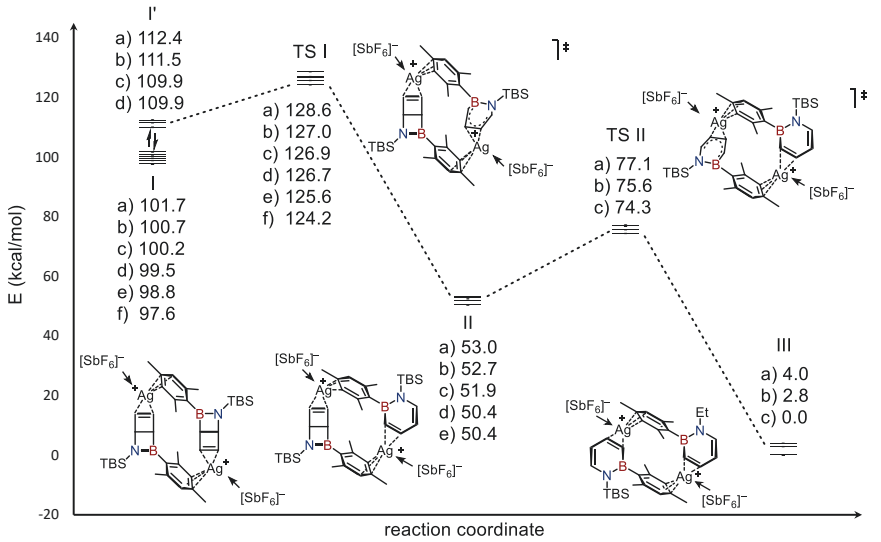

Figure S92. Free energy profile of the $AgSbF_6$ catalyzed cycloreversion of **BND1** at the M06-2X(PCM:DCM)/def2-QVPP//M06-2X(PCM:DCM)/def2-SVP level of theory. Displayed are the free energies of all computed conformers regarding the stepwise ring opening of the dimeric [**BND1**$AgSbF_6$]$_2$.

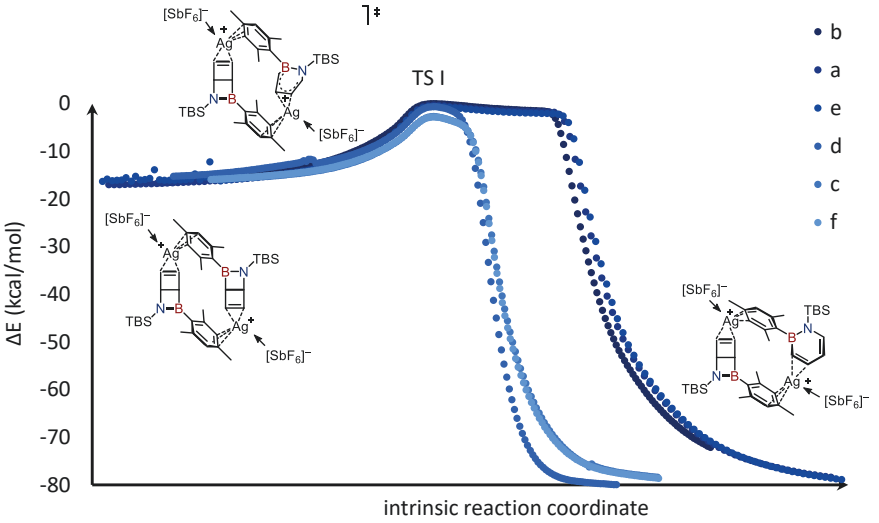

Figure S93. Electronic energies for the IRC paths of the conformers of TS I for the thermal ring opening of [**BND1**AgSbF$_6$]$_2$, calculated at the M06-2X(PCM:DCM)/def2-SVP level of theory.

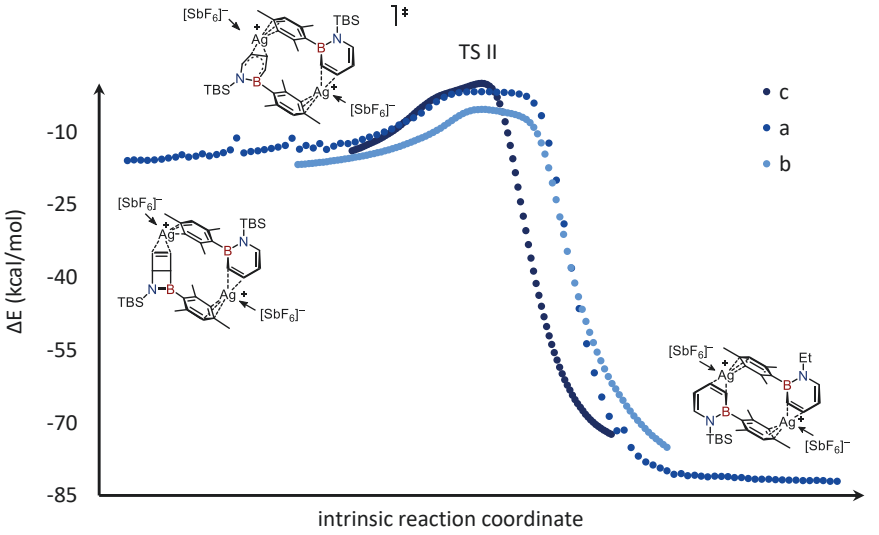

Figure S94. Electronic energies for the IRC paths of the conformers of TS II for the thermal ring opening of [**BND1**AgSbF$_6$]$_2$, calculated at the M06-2X(PCM:DCM)/def2-SVP level of theory.

I a:

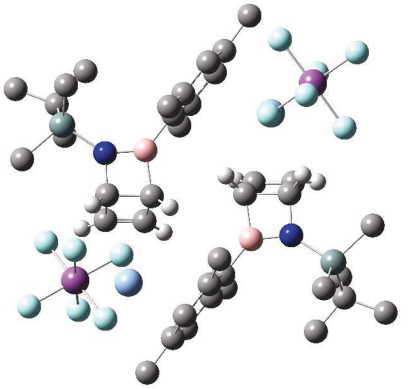

C	2.58238300	-1.85588100	-0.47372200
C	1.33462500	-0.95410100	-0.73628200
C	3.07819100	-1.43791800	-1.85218300
H	3.87816800	-1.80420200	-2.50091800
C	1.98649700	-0.65187100	-2.06750300
H	1.63181000	-0.10766000	-2.94912600
H	3.22463400	-1.68821800	0.39893400
H	1.08176200	-0.12680800	-0.06189000
C	-0.92760100	-2.83522400	-0.58238100
C	-1.58205400	-2.98205200	0.66281600
C	-1.65502100	-3.03735600	-1.76872300
C	-2.92148900	-3.37121700	0.70644200
C	-3.01233100	-3.41528600	-1.70147700
C	-3.65809600	-3.60409000	-0.46534300
H	-3.42634100	-3.46141700	1.67049500
H	-3.55915100	-3.61457400	-2.62833500
B	0.57985800	-2.38662500	-0.61762300
C	-0.99582400	-2.89465000	-3.11857600
H	-1.69828000	-2.50649700	-3.86954100
H	-0.12393300	-2.22384300	-3.07852600
H	-0.63767100	-3.87146000	-3.48072100
C	-0.85203700	-2.65345400	1.93959700
H	-1.43644300	-2.94117900	2.82225800
H	0.12522700	-3.15454000	1.98504500
H	-0.66537900	-1.56874900	2.00207800
C	-5.08485100	-4.08077100	-0.38466600
H	-5.10961400	-5.16837100	-0.21802400
H	-5.60068700	-3.59787400	0.45491300
H	-5.63162300	-3.86937500	-1.31327100
N	1.78141800	-3.10018200	-0.44016800
C	2.08037800	-5.76463100	-1.78693000
C	4.26190600	-4.52292900	0.06387000
H	4.76439400	-4.18271100	-0.85504200

H	4.45733000	-3.77430300	0.84633800
H	4.72565100	-5.47180000	0.37141200
Si	2.42161900	-4.74797400	-0.21645400
C	-2.57462600	1.85834400	-0.44833600
C	-1.31874300	0.93845000	-0.54601500
C	-2.95790600	1.34343000	-1.83165300
H	-3.69434900	1.66932000	-2.57104000
C	-1.86174600	0.53558000	-1.89617500
H	-1.44055700	-0.07749900	-2.70037500
H	-3.28969000	1.75332700	0.37668100
H	-1.12162300	0.16892700	0.21056900
C	0.94386100	2.83265600	-0.47135100
C	1.58623900	3.06596700	0.76523000
C	1.67863600	2.97355200	-1.66319100
C	2.92190000	3.47088700	0.79511500
C	3.03035200	3.37483600	-1.60850700
C	3.66526400	3.63862800	-0.38050800
H	3.41626200	3.62482700	1.75640800
H	3.57771000	3.53938100	-2.54244000
B	-0.56146000	2.37533200	-0.50151100
C	1.02846600	2.75205700	-3.00730300
H	1.75855700	2.41988900	-3.75836600
H	0.22043100	2.00695700	-2.95180200
H	0.58109400	3.68732000	-3.37922600
C	0.84998200	2.80404000	2.05341300
H	1.38299100	3.22432500	2.91546100
H	-0.16627400	3.22277500	2.03010400
H	0.75474000	1.71798900	2.21602500
C	5.09029900	4.12153200	-0.32077700
H	5.11466000	5.21144900	-0.16983200
H	5.61478600	3.65160300	0.52073600
H	5.62906600	3.89668800	-1.25091600
N	-1.76804900	3.10002600	-0.43951900
C	-2.05472400	5.68393500	-1.94308500
C	-4.23681200	4.56936300	-0.01366300
H	-4.74114900	4.14437500	-0.89561000
H	-4.43080400	3.89852200	0.83658000
H	-4.69865400	5.54353100	0.20456500
Si	-2.39662700	4.76258500	-0.31528900
Ag	3.73131200	0.95585400	-1.25480400
Ag	-3.72612400	-0.98815200	-1.21431700
Sb	5.33017000	0.41750700	1.87887000
Sb	-5.37753600	-0.37923900	1.88637000
F	5.76176200	0.97977800	0.06940400
F	5.29223500	2.25259900	2.40077500
F	7.17871900	0.30804000	2.29894600
F	4.80434800	-0.12950500	3.61884400
F	3.48650500	0.52875900	1.31212000
F	5.33685400	-1.39534600	1.26681600
F	-5.38704600	1.43211700	1.27239400

F	-4.87812000	0.16770500	3.63422000
F	-3.52569400	-0.48119700	1.34705400
F	-7.23099600	-0.28394600	2.28759500
F	-5.78836600	-0.94560600	0.07348100
F	-5.32910900	-2.21732200	2.40079200
C	-1.52735300	5.60628100	1.11571200
H	-0.43450500	5.52591300	1.00671800
H	-1.78899700	6.67425600	1.16312000
H	-1.81551800	5.14087900	2.07005900
C	-2.90928400	6.95770300	-1.99898500
H	-2.72177700	7.61675100	-1.13594500
H	-2.67440000	7.53330100	-2.91076800
H	-3.98507100	6.72479000	-2.02041500
C	-0.56906300	6.06379000	-2.00487500
H	-0.31543400	6.81743400	-1.24366300
H	0.08800200	5.19475700	-1.83755300
H	-0.32142400	6.48978200	-2.99275300
C	-2.41127600	4.77675600	-3.12701800
H	-3.47399900	4.48465200	-3.11046200
H	-2.22721400	5.30090800	-4.08072300
H	-1.81034400	3.85401500	-3.12508800
C	1.57066400	-5.51679800	1.26708000
H	0.47627400	-5.47074600	1.15564100
H	1.85853500	-6.57271600	1.38320000
H	1.84823300	-4.98405600	2.18887400
C	0.59331600	-6.13935100	-1.83772500
H	0.32331600	-6.82866100	-1.02302800
H	-0.05830700	-5.25463100	-1.75126800
H	0.35627300	-6.64092100	-2.79216400
C	2.44835300	-4.93645300	-3.02394000
H	3.51154600	-4.64604600	-3.01983200
H	2.26864800	-5.52095300	-3.94274700
H	1.84930400	-4.01463000	-3.08592600
C	2.92835800	-7.04383200	-1.75656200
H	2.70039200	-7.67176400	-2.63492900
H	4.00573600	-6.81831100	-1.77952400
H	2.72721200	-7.64906100	-0.85802700

M06-2X(PCM:DCM)/def2-SVP: -4191.60459

M06-2X(PCM:DCM)/def2-QVPP: -4195.57212

$G_{corr.}$: 0.809389

I b:

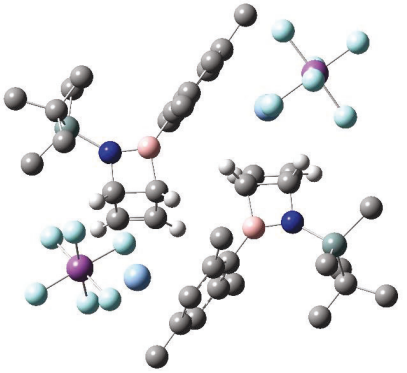

C	2.69720600	1.70835100	0.32286600
C	1.38878700	0.89001400	0.55065600
C	3.06893600	1.36055200	1.76029900
H	3.83231900	1.73858000	2.44551600
C	1.92910700	0.63286300	1.93733500
H	1.48908800	0.15387400	2.81888700
H	3.39252500	1.44658700	-0.48339600
H	1.12696000	0.04339600	-0.09614400
C	-0.75514800	2.88073500	0.20668100
C	-1.41806400	2.84581300	-1.04224400
C	-1.45390400	3.32737700	1.34171900
C	-2.73760300	3.28628300	-1.14746600
C	-2.78845900	3.76874500	1.21224100
C	-3.44303200	3.76513100	-0.03320300
H	-3.25079400	3.22894100	-2.10998200
H	-3.30709700	4.16863000	2.08978100
B	0.72393600	2.35427700	0.31229300
C	-0.79702700	3.37540200	2.70040400
H	-1.50690300	3.10876800	3.49637700
H	0.06607400	2.69511800	2.76303500
H	-0.42839600	4.38955800	2.92023100
C	-0.71017000	2.27796600	-2.24542000
H	-1.29063400	2.42896100	-3.16382800
H	0.28153300	2.73517800	-2.37841300
H	-0.55466700	1.19344900	-2.12153500
C	-4.84384100	4.29630700	-0.18952500
H	-4.81436100	5.33633200	-0.54851000
H	-5.39751900	3.69895700	-0.92496600
H	-5.38755100	4.28315600	0.76452100
N	1.97176200	2.98700900	0.14926600
C	2.39286900	5.79507700	1.14667200
C	4.53854800	4.20961300	-0.45783200
H	4.99564600	3.94918200	0.50977400

H	4.71797200	3.37045800	-1.14621800
H	5.05927600	5.09544800	-0.85061400
Si	2.70764200	4.55852500	-0.26232300
C	-2.65338600	-1.60168400	1.00593200
C	-1.34677000	-0.75654200	0.90148400
C	-2.93057600	-0.86860900	2.31198500
H	-3.64100900	-1.03551300	3.12572900
C	-1.79244900	-0.12786100	2.20020700
H	-1.29917400	0.57455000	2.88031800
H	-3.40742300	-1.58099000	0.21233700
H	-1.15291600	-0.11851900	0.03022200
C	0.80127400	-2.77238400	1.00498000
C	1.50775500	-2.91745500	-0.20377100
C	1.45632000	-3.04670000	2.22567400
C	2.83097300	-3.38195300	-0.18851800
C	2.79279700	-3.47397500	2.21989400
C	3.49407300	-3.67252000	1.01082600
H	3.37390300	-3.49007000	-1.13031300
H	3.28906500	-3.69819300	3.16833600
B	-0.67506900	-2.23208800	1.02772200
C	0.71881700	-2.88270800	3.53149500
H	1.39399700	-2.97542400	4.39164800
H	0.21592000	-1.90442000	3.59006700
H	-0.06708200	-3.64682600	3.62773200
C	0.90022100	-2.52262600	-1.52621500
H	1.00720300	-3.32624800	-2.26903700
H	-0.16897700	-2.27999100	-1.44110800
H	1.42877200	-1.64152400	-1.92244000
C	4.89696000	-4.22480300	0.99865500
H	4.86881600	-5.32426200	0.95816200
H	5.44311900	-3.86469500	0.11764000
H	5.44713500	-3.93819400	1.90526000
N	-1.91873000	-2.87823200	1.15028600
C	-1.63802500	-5.65078500	2.13953200
H	-1.95208700	-6.69450200	1.98846300
H	-0.58165300	-5.56480400	1.83993100
H	-1.71546200	-5.42462200	3.21330100
C	-4.39448700	-4.19407100	1.89254300
H	-4.29986000	-3.80841700	2.91909400
H	-4.96494700	-3.46180400	1.29882500
H	-4.97325500	-5.12836600	1.93279700
C	-2.83702800	-5.02745800	-0.67410400
C	-1.45125600	-5.47228100	-1.15899400
H	-1.47641700	-5.70132700	-2.23825700
H	-0.69530200	-4.68529400	-1.00278400
H	-1.10755600	-6.37627200	-0.63276300
C	-3.82387200	-6.19753000	-0.78257200
H	-4.84620300	-5.89098400	-0.51275500
H	-3.85288900	-6.57560500	-1.81881500
H	-3.53808100	-7.04026600	-0.13208300

C	-3.33110900	-3.85813900	-1.53880500
H	-3.47006800	-4.19119700	-2.58149100
H	-4.29281800	-3.44974100	-1.18894900
H	-2.60475300	-3.02942200	-1.55216600
Si	-2.69965600	-4.47392700	1.13938800
Ag	3.70505800	-1.06414800	1.42685400
Ag	-3.64764800	1.37290600	1.34502500
Sb	5.49340300	-0.79818800	-1.71103200
Sb	-5.45035500	0.23431600	-1.51968600
F	5.78286100	-1.16752800	0.17391200
F	5.38589000	-2.68212900	-2.00807700
F	7.36816100	-0.82131900	-2.01015700
F	5.11977100	-0.44361200	-3.53858100
F	3.61198000	-0.76795000	-1.28041200
F	5.54580400	1.07115600	-1.31044800
F	-5.55742500	-1.35418200	-0.45173500
F	-5.03656300	-0.79482000	-3.06105300
F	-3.57749100	0.35456700	-1.06549700
F	-7.31750400	0.16435300	-1.85638400
F	-5.75607100	1.26330000	0.09792900
F	-5.30460600	1.86912800	-2.49285100
C	1.92170500	5.15362600	-1.85739100
H	0.82442100	5.16748500	-1.76480000
H	2.25658600	6.17019500	-2.11350400
H	2.19053900	4.48481600	-2.68869700
C	0.93661400	6.27526300	1.08531800
H	0.75378900	6.88450400	0.18687100
H	0.22289500	5.43590500	1.06305400
H	0.69909900	6.89799200	1.96543000
C	3.33141400	6.99920500	0.98610400
H	3.11712600	7.75340000	1.76270100
H	4.38805100	6.70759400	1.08786000
H	3.20723000	7.48987600	0.00725400
C	2.66551000	5.11233200	2.49257200
H	3.70733000	4.76020600	2.56600100
H	2.49568000	5.81964200	3.32269800
H	2.00736500	4.24375000	2.64635300

M06-2X(PCM:DCM)/def2-SVP: -4191.60644

M06-2X(PCM:DCM)/def2-QVPP: -4195.57289

$G_{corr.}$: 0.808652

I c:

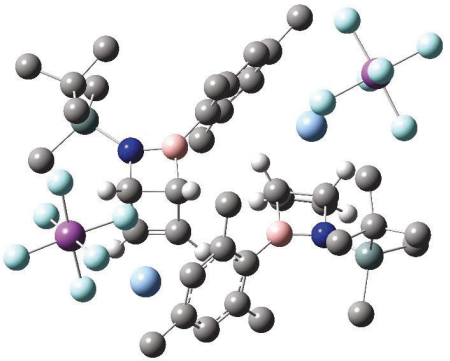

C	-2.69510000	-1.54377000	0.92285900
C	-1.36762900	-0.73458800	0.80631300
C	-2.86504900	-0.91636400	2.30074500
H	-3.52803500	-1.13026400	3.14287100
C	-1.71652000	-0.19337400	2.17130900
H	-1.16979200	0.45440400	2.86541900
H	-3.49649600	-1.42131600	0.18809200
H	-1.19440500	-0.03944100	-0.02455600
C	0.70041700	-2.83006500	0.59410100
C	1.39687500	-2.74328500	-0.62745300
C	1.34700400	-3.39333300	1.71708800
C	2.69769300	-3.25502100	-0.73066600
C	2.66058600	-3.87609900	1.59610600
C	3.34807900	-3.83474900	0.36422500
H	3.23542800	-3.16922200	-1.67820000
H	3.14654700	-4.33107100	2.46418800
B	-0.74774100	-2.23877400	0.75817900
C	0.63654700	-3.47961700	3.04591300
H	1.33410400	-3.71873500	3.85880300
H	0.12237000	-2.53816600	3.29524100
H	-0.13730800	-4.26068200	3.01865600
C	0.80013700	-2.06330300	-1.83429100
H	0.81935800	-2.72650800	-2.71132600
H	-0.24095800	-1.75017900	-1.67059400
H	1.39556400	-1.17216900	-2.08849800
C	4.72240100	-4.43261100	0.21373300
H	4.64151400	-5.48901700	-0.08460800
H	5.28946900	-3.90077000	-0.56025800
H	5.28217500	-4.39342500	1.15783800
N	-2.00714000	-2.85331800	0.89553700
C	-1.84831000	-5.77852900	1.37482900
H	-2.22009700	-6.75803300	1.03815300
H	-0.79144600	-5.69444200	1.07664200

H	-1.90605900	-5.75331800	2.47301400
C	-4.53397200	-4.17647000	1.43399200
H	-4.41571500	-3.95882100	2.50650700
H	-5.08323400	-3.34199300	0.96902100
H	-5.14390700	-5.08642600	1.33675800
C	-3.02987700	-4.61085200	-1.25995200
C	-1.66327900	-4.99421900	-1.84170000
H	-1.71418500	-5.03955800	-2.94318700
H	-0.88747000	-4.25780400	-1.57466100
H	-1.32862800	-5.97938200	-1.48148600
C	-4.04662900	-5.72282900	-1.55202300
H	-5.05616100	-5.44797300	-1.20968000
H	-4.10365200	-5.90983900	-2.63797300
H	-3.76923500	-6.67337000	-1.06788700
C	-3.50818800	-3.30039900	-1.90184200
H	-3.66380500	-3.44338000	-2.98481900
H	-4.45920100	-2.94354500	-1.47549900
H	-2.76661000	-2.49341200	-1.78158600
Si	-2.85761500	-4.39026600	0.62193600
C	2.69509800	1.54378200	0.92285900
C	1.36763200	0.73458900	0.80630900
C	2.86504700	0.91637700	2.30074600
H	3.52802800	1.13028100	3.14287300
C	1.71652500	0.19337600	2.17130600
H	1.16980400	-0.45441100	2.86541400
H	3.49649700	1.42133100	0.18809500
H	1.19441800	0.03944000	-0.02456000
C	-0.70042400	2.83005900	0.59407400
C	-1.39686400	2.74327200	-0.62749300
C	-1.34702900	3.39334200	1.71704200
C	-2.69767700	3.25501200	-0.73073400
C	-2.66060900	3.87611000	1.59603200
C	-3.34808200	3.83474900	0.36414100
H	-3.23539700	3.16920700	-1.67827600
H	-3.14658500	4.33109000	2.46410100
B	0.74773300	2.23877000	0.75817000
C	-0.63660100	3.47966800	3.04588200
H	-1.33420400	3.71865900	3.85877000
H	-0.12228900	2.53828600	3.29518200
H	0.13713700	4.26085000	3.01866900
C	-0.80011000	2.06327600	-1.83431600
H	-0.81930400	2.72647900	-2.71135400
H	0.24097800	1.75013700	-1.67059900
H	-1.39554700	1.17215100	-2.08852900
C	-4.72240200	4.43260700	0.21362500
H	-4.64151400	5.48900700	-0.08473600
H	-5.28946300	3.90075000	-0.56036000
H	-5.28218400	4.39343900	1.15772600
N	2.00712700	2.85332400	0.89553300
C	1.84820300	5.77853500	1.37478400

H	2.21998500	6.75804600	1.03812200
H	0.79135300	5.69442700	1.07655200
H	1.90590500	5.75332700	2.47297100
C	4.53390100	4.17656400	1.43408200
H	4.41560100	3.95891800	2.50659300
H	5.08322200	3.34210800	0.96914500
H	5.14380300	5.08654400	1.33687100
C	3.02990600	4.61086000	-1.25993800
C	1.66332400	4.99420700	-1.84173900
H	1.71426900	5.03953600	-2.94322400
H	0.88751500	4.25778500	-1.57472000
H	1.32864900	5.97937000	-1.48154500
C	4.04665700	5.72284600	-1.55197900
H	5.05617900	5.44800200	-1.20959800
H	4.10371600	5.90985200	-2.63792800
H	3.76923600	6.67338700	-1.06785800
C	3.50825200	3.30040800	-1.90180300
H	3.66391500	3.44338700	-2.98477400
H	4.45924900	2.94355900	-1.47542000
H	2.76667200	2.49341900	-1.78157600
Si	2.85757400	4.39029000	0.62194600
Ag	-3.58493500	1.39933000	1.54540400
Ag	3.58495600	-1.39931100	1.54540300
Sb	-5.59747100	0.47529800	-1.31483100
Sb	5.59747400	-0.47532400	-1.31484800
F	-5.71988500	1.43175800	0.36991300
F	-5.43342400	2.15153700	-2.21341600
F	-7.48702200	0.52091900	-1.49561900
F	-5.37760600	-0.48910800	-2.93628800
F	-3.69072000	0.47484700	-1.02126500
F	-5.70489500	-1.15819400	-0.31646200
F	5.70491500	1.15816400	-0.31647600
F	5.37759400	0.48908400	-2.93630200
F	3.69072400	-0.47485900	-1.02126800
F	7.48702300	-0.52095400	-1.49565500
F	5.71989700	-1.43178300	0.36989700
F	5.43341300	-2.15156700	-2.21342400

M06-2X(PCM:DCM)/def2-SVP: -4191.61032

M06-2X(PCM:DCM)/def2-QVPP: -4195.57416

$G_{corr.}$: 0.809072

I d:

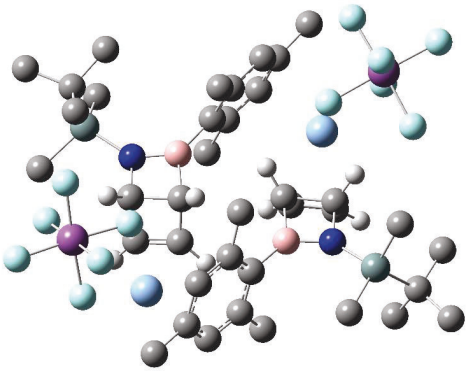

C	2.74519700	1.40810800	1.06520600
C	1.39920600	0.64722800	0.86236600
C	2.90305700	0.62433300	2.36126300
H	3.57418400	0.72470200	3.21812000
C	1.73601800	-0.04945100	2.15908500
H	1.17272800	-0.75400500	2.78061600
H	3.54103700	1.35707900	0.31581200
H	1.21763600	0.04890700	-0.03910100
C	-0.62050100	2.79844300	0.88785000
C	-1.28589800	2.91353100	-0.34817800
C	-1.28781600	3.18936800	2.06988500
C	-2.57943900	3.45163000	-0.39989900
C	-2.59448000	3.69662200	1.99694600
C	-3.25318800	3.85683700	0.75918100
H	-3.09316800	3.52751900	-1.36140600
H	-3.10038500	4.01011400	2.91460300
B	0.81366300	2.16111600	0.98709900
C	-0.60422800	3.05990100	3.40884500
H	-1.30990200	3.20473700	4.23676900
H	-0.12747000	2.07409500	3.52806200
H	0.19604900	3.80821200	3.50625900
C	-0.66445100	2.42561400	-1.63283700
H	-0.64089600	3.22417200	-2.38869400
H	0.36464500	2.06480900	-1.49204200
H	-1.26949100	1.60414700	-2.04734200
C	-4.62008000	4.48509800	0.67169600
H	-4.52576100	5.57052500	0.51577600
H	-5.18077700	4.06767900	-0.17414600
H	-5.19288900	4.32904700	1.59574800
N	2.08542200	2.72578800	1.19657000
C	1.96411900	5.54368300	2.10859900
H	2.35384700	6.55742800	1.93167900
H	0.91230500	5.52091600	1.78268000

H	1.99937200	5.35094900	3.19103600
C	4.62019500	3.89796300	1.98288100
H	4.47112100	3.53196600	3.01021200
H	5.16326600	3.12525000	1.41542400
H	5.25201700	4.79685700	2.03037000
C	3.19228000	4.76318200	-0.64851000
C	1.84938300	5.27018700	-1.18970800
H	1.92356400	5.47409200	-2.27173800
H	1.04729900	4.52766700	-1.04498100
H	1.53660000	6.20232900	-0.69416700
C	4.24520300	5.87487400	-0.75159300
H	5.23944600	5.52029200	-0.43907700
H	4.32957500	6.22287400	-1.79530100
H	3.98506500	6.74903700	-0.13261300
C	3.64849000	3.54860100	-1.47031300
H	3.83579400	3.84737000	-2.51582200
H	4.57675400	3.09952700	-1.08266900
H	2.87997400	2.75851100	-1.48819600
Si	2.96936100	4.26734300	1.17386100
C	-2.71571100	-1.58315000	0.39790800
C	-1.37478600	-0.78746000	0.46190800
C	-2.96299200	-1.11065000	1.82928600
H	-3.68023200	-1.39926200	2.60266500
C	-1.79624600	-0.40640400	1.85877000
H	-1.28064400	0.13755300	2.65758700
H	-3.46723300	-1.36382500	-0.36958500
H	-1.14389700	-0.00243000	-0.26859700
C	0.68004500	-2.88189600	0.14161600
C	1.36622300	-2.77837800	-1.08773500
C	1.31513400	-3.49157200	1.23796500
C	2.65541900	-3.29926600	-1.21504500
C	2.62321800	-3.99744200	1.09192100
C	3.30471200	-3.92038500	-0.13802500
H	3.18926800	-3.19551700	-2.16238900
H	3.09897600	-4.50474600	1.93693100
B	-0.76499500	-2.28475600	0.29064000
C	0.59989700	-3.64299300	2.55844200
H	1.30813900	-3.70981100	3.39540700
H	-0.09030300	-2.80727500	2.75027600
H	-0.00895000	-4.56072300	2.56315000
C	0.70998100	-2.08147000	-2.25158700
H	1.30162700	-2.18491700	-3.16940900
H	-0.29769000	-2.48405900	-2.43945800
H	0.59547400	-1.00435100	-2.04624100
C	4.67129800	-4.52696200	-0.32004400
H	4.57996600	-5.53968300	-0.74145500
H	5.26790100	-3.92213600	-1.01431700
H	5.20598500	-4.60684600	0.63579500
N	-2.03439200	-2.89056200	0.26755200
C	-1.32175400	-5.65773300	-0.36203400

H	-1.68882800	-6.63652000	-0.70498200
H	-0.60865700	-5.27807300	-1.10968400
H	-0.77603300	-5.80495200	0.58203900
C	-3.95310900	-4.97547200	1.20845700
Si	-2.74865400	-4.45913500	-0.16677700
Ag	3.57233300	-1.60983500	1.34008200
Ag	-3.60766100	1.29220100	1.38250000
Sb	5.56329600	-0.45258200	-1.40650800
Sb	-5.43255200	0.88264100	-1.69986600
F	5.71728100	-1.59062500	0.15878200
F	5.36187300	-2.01434100	-2.48454700
F	7.44608300	-0.49112500	-1.64811900
F	5.30092500	0.69316800	-2.89840900
F	3.66616600	-0.46986300	-1.05276500
F	5.72078500	1.05830500	-0.23646400
F	-5.58034300	-0.94303600	-1.14479000
F	-5.07941900	0.35797000	-3.48977300
F	-3.55437000	0.79635300	-1.26205100
F	-7.30388400	0.97779100	-2.00395200
F	-5.69549800	1.41913400	0.14878200
F	-5.22346200	2.72685300	-2.15059300
C	-3.66387600	-4.20167300	-1.78477600
H	-2.94872100	-3.99445400	-2.59498600
H	-4.24787100	-5.09190400	-2.06297600
H	-4.35482700	-3.34770000	-1.71182200
C	-5.18921800	-4.06467200	1.16840000
H	-5.86351300	-4.29958800	2.00973700
H	-4.92826200	-2.99638300	1.23994800
H	-5.75951000	-4.19862600	0.23664100
C	-4.39064400	-6.43017600	0.98958400
H	-3.54048800	-7.12594000	1.06324700
H	-5.12915900	-6.72452300	1.75493000
H	-4.86238300	-6.57309600	0.00430500
C	-3.25756600	-4.85023600	2.56943500
H	-3.94795000	-5.13626500	3.38141700
H	-2.37784000	-5.51037800	2.63583200
H	-2.91764500	-3.81973000	2.75894800

M06-2X(PCM:DCM)/def2-SVP: -4191.60868

M06-2X(PCM:DCM)/def2-QVPP: -4195.57489

$G_{corr.}$: 0.808718

I e:

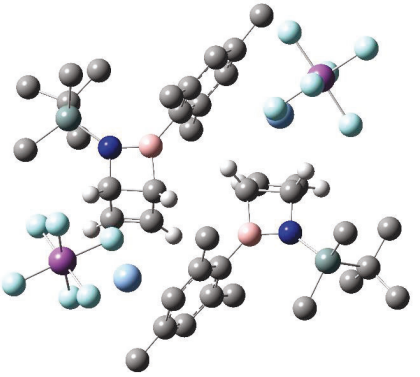

C	2.63955000	-1.68086800	-0.53206300
C	1.33306300	-0.82575200	-0.53897200
C	2.94093400	-1.07120600	-1.90015100
H	3.66717000	-1.30503800	-2.68344300
C	1.80235700	-0.32318500	-1.88246600
H	1.32282800	0.31090700	-2.63530000
H	3.37932000	-1.57939000	0.27174400
H	1.12213000	-0.10739600	0.26313800
C	-0.81358900	-2.85416600	-0.50239100
C	-1.48055800	-3.01403400	0.73045100
C	-1.48366000	-3.16992900	-1.69699800
C	-2.78675800	-3.50632200	0.75903200
C	-2.80917500	-3.64730000	-1.64805800
C	-3.47279300	-3.83471600	-0.41979300
H	-3.30565200	-3.60757400	1.71453600
H	-3.31351300	-3.92744900	-2.57805200
B	0.65687100	-2.30322100	-0.54496900
C	-0.77571900	-3.04401900	-3.02339100
H	-1.48558900	-2.98069600	-3.85892200
H	-0.12148600	-2.15886100	-3.05295600
H	-0.12953300	-3.91885600	-3.19712900
C	-0.78445100	-2.62572500	2.00880700
H	-1.40132200	-2.84700400	2.88834300
H	0.17576300	-3.15470900	2.11433600
H	-0.56145500	-1.54638400	2.01556200
C	-4.86115400	-4.41616000	-0.35522800
H	-4.80819000	-5.49591600	-0.14865000
H	-5.43446100	-3.94472800	0.45294500
H	-5.39804000	-4.28089200	-1.30365700
N	1.89936000	-2.96250700	-0.56154300
C	1.02564100	-5.74016100	-0.32717300
H	1.33197500	-6.78312300	-0.15781200
H	0.34522200	-5.44681000	0.48665500

H	0.46149600	-5.69305000	-1.27106400
C	3.68696300	-5.00791100	-1.81083700
Si	2.52360800	-4.61464400	-0.36097700
C	-2.75181500	1.65064700	-0.50356000
C	-1.43785400	0.82093900	-0.65033200
C	-3.12743000	1.15494000	-1.89464300
H	-3.90049100	1.45004900	-2.60897700
C	-1.98163500	0.42581600	-2.00423200
H	-1.54173400	-0.13452900	-2.83662200
H	-3.44085600	1.47080900	0.32956700
H	-1.17754200	0.04015100	0.07493000
C	0.69060600	2.85145500	-0.46568300
C	1.31180900	2.97889000	0.79924600
C	1.42185700	3.16302100	-1.62436200
C	2.62262400	3.44778600	0.89055600
C	2.74620900	3.63571300	-1.50876700
C	3.35925500	3.79712100	-0.25300500
H	3.10524200	3.51787400	1.86797200
H	3.29215800	3.92340700	-2.41280700
B	-0.78198000	2.30407600	-0.55012300
C	0.81056100	3.02978000	-2.99816500
H	1.54416100	2.65709300	-3.72747000
H	-0.05473800	2.34925400	-2.99787900
H	0.45606900	4.00609300	-3.36441100
C	0.57103100	2.55487900	2.04125700
H	1.13040700	2.80801400	2.95020300
H	-0.42020800	3.02833500	2.09589700
H	0.40996000	1.46413200	2.03978400
C	4.74849300	4.36414800	-0.11960600
H	4.69574800	5.43499300	0.12889200
H	5.29150900	3.85645700	0.68773600
H	5.31539100	4.26187700	-1.05454900
N	-2.03336000	2.94424600	-0.46340000
C	-2.43866200	5.61850800	-1.77882400
C	-4.61204300	4.21806500	-0.04220400
H	-5.05636700	3.86583400	-0.98630400
H	-4.79944200	3.44856000	0.72147100
H	-5.13843800	5.13633300	0.25748100
Si	-2.77811100	4.54917100	-0.24411900
Ag	3.64095700	1.24427500	-1.16091600
Ag	-3.71195200	-1.25237000	-1.28794500
Sb	5.35849300	0.54624200	1.88006700
Sb	-5.48429900	-0.68974200	1.77764300
F	5.70876700	1.26254100	0.10831800
F	5.18705800	2.33662600	2.51952500
F	7.21843800	0.54837800	2.26073200
F	4.91786500	-0.15415400	3.58844200
F	3.49840500	0.56687000	1.36152600
F	5.47992200	-1.21392700	1.13947000
F	-5.58812600	1.10342300	1.11967300

F	-5.07859500	-0.07002000	3.52575500
F	-3.61469600	-0.68424600	1.29677900
F	-7.35233000	-0.70111700	2.11713500
F	-5.79647600	-1.32514700	-0.03146800
F	-5.33826900	-2.50676800	2.34470500
C	-2.02504500	5.32854300	1.28626400
H	-0.92618600	5.33684300	1.21451800
H	-2.36732900	6.36670400	1.41387900
H	-2.30942800	4.76160500	2.18534600
C	-0.98341300	6.10413400	-1.74983100
H	-0.80994000	6.80282500	-0.91701800
H	-0.27123100	5.27118800	-1.63417800
H	-0.73576300	6.63283900	-2.68680700
C	-3.37953200	6.83148500	-1.76924200
H	-3.15345000	7.49405800	-2.62229100
H	-4.43461400	6.52872100	-1.85361700
H	-3.27028100	7.42925300	-0.84994200
C	-2.68758600	4.78858500	-3.04405500
H	-3.72580200	4.42182300	-3.09327800
H	-2.50963900	5.40087100	-3.94496600
H	-2.02073500	3.91408700	-3.09060400
C	3.46081400	-4.64331800	1.26460600
H	2.76410300	-4.52071900	2.10728700
H	4.00059200	-5.59231100	1.40202100
H	4.19405000	-3.82321100	1.30717700
C	4.97719900	-4.18762100	-1.66550100
H	5.63027300	-4.34518900	-2.54091500
H	4.78267500	-3.10587700	-1.58710400
H	5.54399800	-4.48360100	-0.76966300
C	4.03728200	-6.50230700	-1.79757500
H	3.14674000	-7.13036400	-1.95421100
H	4.75262600	-6.73171000	-2.60594200
H	4.50509200	-6.80622300	-0.84759900
C	2.99197500	-4.65975200	-3.13293200
H	3.65937900	-4.87359900	-3.98536100
H	2.07458100	-5.25347400	-3.27481400
H	2.71245700	-3.59529400	-3.17883200

M06-2X(PCM:DCM)/def2-SVP: -4191.60570

M06-2X(PCM:DCM)/def2-QVPP: -4195.57381

$G_{corr.}$: 0.806497

I f:

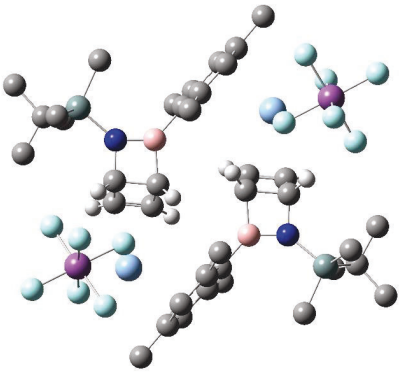

C	2.72924400	-1.56342900	-0.51006100
C	1.38342800	-0.77343100	-0.48483500
C	2.96591800	-0.94673500	-1.88704000
H	3.68272700	-1.14810300	-2.68793900
C	1.79337800	-0.25469700	-1.84137500
H	1.26748800	0.35563200	-2.58360700
H	3.48458600	-1.42109900	0.27131600
H	1.16272600	-0.06152300	0.31993200
C	-0.66100100	-2.90259100	-0.38668000
C	-1.31996300	-3.02069600	0.85548600
C	-1.31951100	-3.31181900	-1.55988600
C	-2.61020300	-3.55216700	0.91456200
C	-2.62737800	-3.83147600	-1.48014200
C	-3.28580500	-3.96771200	-0.24260000
H	-3.12519000	-3.61627600	1.87556200
H	-3.12336300	-4.17890700	-2.39167000
B	0.78081000	-2.28343800	-0.46618300
C	-0.62187800	-3.23690400	-2.89584300
H	-1.33871900	-3.22807700	-3.72766800
H	0.01654600	-2.34335900	-2.97568900
H	0.03952400	-4.10696400	-3.03223000
C	-0.63029500	-2.55417900	2.11105300
H	-1.25231400	-2.71957000	2.99916300
H	0.32716200	-3.07946900	2.25395300
H	-0.40092300	-1.47793100	2.05381100
C	-4.65781500	-4.58202400	-0.14580700
H	-4.57634800	-5.64817100	0.11515800
H	-5.24344100	-4.08518900	0.63787900
H	-5.19797000	-4.50880400	-1.09912500
N	2.05341100	-2.88046500	-0.51368800
C	1.33904900	-5.70041700	-0.24295700
H	1.70382300	-6.72083800	-0.05331300
H	0.64606400	-5.42832700	0.56776100

H	0.77035200	-5.70572400	-1.18517800
C	3.94233700	-4.83043500	-1.76110400
Si	2.77091800	-4.49310400	-0.30402500
C	-2.72926400	1.56345200	-0.50999700
C	-1.38347500	0.77341600	-0.48452900
C	-2.96574500	0.94669400	-1.88698100
H	-3.68241000	1.14805900	-2.68801100
C	-1.79324200	0.25460700	-1.84109200
H	-1.26726500	-0.35580000	-2.58319800
H	-3.48472300	1.42117900	0.27128500
H	-1.16288800	0.06157100	0.32032700
C	0.66100600	2.90253500	-0.38630100
C	1.31987100	3.02061500	0.85592000
C	1.31960200	3.31181600	-1.55943800
C	2.61007700	3.55215000	0.91512700
C	2.62744800	3.83152000	-1.47956100
C	3.28576100	3.96774900	-0.24196200
H	3.12497000	3.61626600	1.87617600
H	3.12348200	4.17903500	-2.39103100
B	-0.78081300	2.28340600	-0.46591800
C	0.62208900	3.23696900	-2.89546300
H	1.33901600	3.22793200	-3.72721300
H	-0.01653100	2.34356500	-2.97531900
H	-0.03909400	4.10717500	-3.03197300
C	0.63017900	2.55383700	2.11137400
H	-0.32812800	3.07779200	2.25345200
H	0.40244100	1.47721600	2.05457400
H	1.25147300	2.72058800	2.99973600
C	4.65773300	4.58212000	-0.14505500
H	4.57619900	5.64824300	0.11599000
H	5.24334700	4.08525200	0.63861700
H	5.19793400	4.50900100	-1.09835500
N	-2.05339400	2.88046900	-0.51361100
C	-1.33898000	5.70037500	-0.24258600
H	-1.70375600	6.72081400	-0.05305100
H	-0.64626500	5.42823700	0.56834700
H	-0.76998800	5.70565000	-1.18462900
C	-3.94188200	4.83060800	-1.76149800
Si	-2.77089000	4.49313400	-0.30410500
Ag	3.57157600	1.43336400	-1.23846200
Ag	-3.57165100	-1.43328700	-1.23837100
Sb	5.43352100	0.75948700	1.74393800
Sb	-5.43364700	-0.75955300	1.74403400
F	5.68637400	1.52499700	-0.02222400
F	5.22518600	2.52590800	2.43752700
F	7.30602700	0.82384000	2.05240100
F	5.08798700	0.00332300	3.45093100
F	3.55517200	0.72108900	1.29793100
F	5.59659100	-0.98040900	0.96255900
F	-5.59665000	0.98050000	0.96300500

F	-5.08808700	-0.00375700	3.45118500
F	-3.55529900	-0.72112700	1.29803300
F	-7.30615400	-0.82390400	2.05248700
F	-5.68652900	-1.52472500	-0.02227300
F	-5.22536100	-2.52613000	2.43724400
C	-3.72296000	4.45379800	1.31253500
H	-3.02778000	4.36060700	2.16022200
H	-4.31476900	5.37064000	1.45403800
H	-4.41102300	3.59482800	1.33960100
C	-5.18407400	3.93632600	-1.63303500
H	-5.83469100	4.05807300	-2.51595200
H	-4.92954400	2.86726600	-1.55216100
H	-5.77753100	4.19744000	-0.74362600
C	-4.37705300	6.30243500	-1.74103100
H	-3.52206300	6.98125000	-1.88392300
H	-5.09640600	6.49730700	-2.55488300
H	-4.87053600	6.57173900	-0.79358800
C	-3.21641600	4.53262200	-3.07947700
H	-3.88833400	4.71120600	-3.93646000
H	-2.33520300	5.18114900	-3.21030900
H	-2.87269900	3.48730700	-3.12889200
C	3.72253200	-4.45381900	1.31288400
H	3.02712000	-4.36063200	2.16037800
H	4.31428500	-5.37067600	1.45452700
H	4.41060700	-3.59486600	1.34015700
C	5.18446300	-3.93611700	-1.63221400
H	5.83527000	-4.05766900	-2.51501700
H	4.92989700	-2.86707700	-1.55115500
H	5.77774200	-4.19739400	-0.74273300
C	4.37755700	-6.30224900	-1.74061700
H	3.52263500	-6.98108300	-1.88382400
H	5.09716700	-6.49703200	-2.55426300
H	4.87075700	-6.57160700	-0.79304200
C	3.21722500	-4.53239300	-3.07926600
H	3.88937100	-4.71095200	-3.93607600
H	2.33603600	-5.18090000	-3.21035700
H	2.87353000	-3.48707600	-3.12873700

M06-2X(PCM:DCM)/def2-SVP: -4191.60735

M06-2X(PCM:DCM)/def2-QVPP: -4195.57560

$G_{corr.}$: 0.806377

I' a:

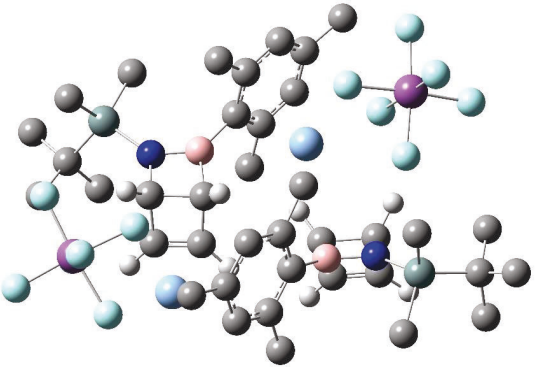

C	-0.27131783	2.82945751	0.00000000
C	-1.74991283	2.31437051	-0.04419700
C	-0.14989883	2.10487951	1.33587700
H	0.61287517	2.10527551	2.11811900
C	-1.43401283	1.66019051	1.28329600
H	-2.06838983	1.13036651	2.00214600
H	0.43363217	2.58433351	-0.80217800
H	-2.09621183	1.68695351	-0.87693300
C	-3.35225883	4.77250651	-0.11563500
C	-3.82110583	5.23593651	-1.37454700
C	-4.09677983	5.07211451	1.05119700
C	-5.01763283	5.95708651	-1.43943600
C	-5.28595683	5.80281751	0.94475700
C	-5.76717283	6.24252751	-0.29141100
H	-5.38591183	6.28821951	-2.41393600
H	-5.86144783	6.01586751	1.84909200
B	-2.03669383	3.91361351	-0.01102400
C	-3.58316183	4.64907451	2.40545200
H	-2.90920383	5.41869351	2.81382800
H	-4.40401183	4.50580551	3.12054200
H	-3.00258283	3.71466251	2.35362800
C	-3.01282183	4.98053951	-2.62366300
H	-2.14195283	5.65391551	-2.66317800
H	-2.62303283	3.95160851	-2.65621300
H	-3.61230383	5.14849751	-3.52698800
C	-7.08572883	6.95511651	-0.40981500
H	-6.98864783	7.86608251	-1.01705200
H	-7.81362383	6.29986151	-0.91074000
H	-7.48306183	7.22975551	0.57530200
N	-0.67861383	4.25000051	0.07139400
Si	0.32239617	5.72157251	0.01642900
C	-6.32360483	0.67334151	1.61476300
C	-4.80614883	1.05911251	1.71801700

C	-6.29466583	0.49011351	3.11808800
H	-7.03383283	0.13412451	3.83766800
C	-5.00140583	0.83637351	3.20484400
H	-4.29617283	0.91338051	4.03627400
H	-7.03961483	1.37151851	1.16027100
H	-4.42574183	2.06311851	1.44375900
C	-3.50219983	-0.88183149	-0.08425800
C	-3.34822283	-0.58916149	-1.45513700
C	-2.57373783	-1.73894549	0.54367600
C	-2.27167883	-1.13033449	-2.16787900
C	-1.51425683	-2.29042849	-0.20177700
C	-1.34338283	-1.98483549	-1.56662700
H	-2.15195183	-0.88044249	-3.22552300
H	-0.84105383	-3.01174849	0.27380900
B	-4.66572283	-0.23701849	0.75454500
C	-2.74994883	-2.09755549	1.99876900
H	-3.62159783	-2.75760749	2.12689600
H	-1.86901883	-2.61515749	2.40015400
H	-2.93690183	-1.20152049	2.61122500
C	-4.28972083	0.35094851	-2.17429900
H	-5.24006883	0.49288551	-1.63249400
H	-3.79977983	1.32690651	-2.35679900
H	-4.55352283	-0.02793749	-3.17197300
C	-0.21483983	-2.57794849	-2.36597100
H	-0.60766883	-3.28490849	-3.11175400
H	0.33435317	-1.79526749	-2.90678900
H	0.49542517	-3.11126049	-1.72220700
N	-6.03864083	-0.53163549	0.79889900
C	-6.10230183	-3.45358249	0.71669200
H	-6.64079583	-4.35879549	0.39637200
H	-5.10234783	-3.47527849	0.25383200
H	-5.98087383	-3.49178949	1.80955400
C	-8.76319883	-1.85996349	0.92892300
Si	-7.01225083	-1.89587849	0.18364900
Ag	-0.09611883	-0.31206849	0.46907700
Ag	-4.94435683	2.83821751	-0.62148500
Sb	-8.10685083	2.86574151	-1.88289800
Sb	2.56003117	0.25668551	-1.61245300
F	-6.32897883	3.07229251	-2.63990400
F	-8.73101883	2.10061151	-3.50110600
F	-8.56098283	4.62428751	-2.44092200
F	-9.77804983	2.61855951	-1.01887900
F	-7.48364783	1.16060851	-1.24837300
F	-7.32468883	3.58135751	-0.26059500
F	0.66526717	0.55852451	-1.86749900
F	2.96006117	1.82716851	-2.60475700
F	2.58345317	-0.83432049	-3.16910600
F	1.99678617	-1.25256949	-0.53187000
F	4.38682717	-0.11332949	-1.25981100
F	2.41747317	1.29372751	-0.00192700

C	1.48562817	5.71291651	1.51578100
C	-7.04089583	-1.86029249	-1.69173300
H	-7.55337083	-2.75618049	-2.07373600
H	-7.54268683	-0.96357049	-2.07875800
H	-6.00864383	-1.87788549	-2.07443600
C	-9.35869083	-0.44486949	0.93764100
H	-10.43282183	-0.49503649	1.18622100
H	-8.88112983	0.18906051	1.69970800
H	-9.25751183	0.06555451	-0.03148200
C	-9.65301383	-2.77006049	0.06740900
H	-10.65030383	-2.86442649	0.52975900
H	-9.79125183	-2.35970649	-0.94429800
H	-9.23662583	-3.78604249	-0.03126300
C	-8.73027683	-2.40678949	2.36299000
H	-8.42820483	-3.46487549	2.38768800
H	-8.03138683	-1.84384749	3.00218600
H	-9.73251083	-2.33411449	2.81911800
C	-0.88260183	7.15603751	0.06314200
H	-1.59006883	7.10185951	-0.77796500
H	-1.46688483	7.15591451	0.99594800
H	-0.34472683	8.11297951	-0.00771200
C	1.29484117	5.65979951	-1.58692600
H	2.02941417	6.47747851	-1.63912000
H	1.83935217	4.70778651	-1.68281900
H	0.61834517	5.75308651	-2.44944400
C	2.56407617	4.63674651	1.31675800
H	3.18565717	4.54968651	2.22438600
H	2.14657417	3.63972351	1.10208100
H	3.23327317	4.89271851	0.48093500
C	0.67782017	5.42253951	2.78726400
H	1.34135917	5.41870151	3.66884400
H	-0.09671083	6.18714351	2.95878400
H	0.17440917	4.44465251	2.73821200
C	2.16167317	7.08503051	1.64719700
H	2.88146517	7.07373451	2.48347300
H	2.71902117	7.35798951	0.73689100
H	1.42968217	7.88202951	1.85001500

M06-2X(PCM:DCM)/def2-SVP: -4191.59165

M06-2X(PCM:DCM)/def2-QVPP: -4195.55457

$G_{corr.}$: 0.808875

I' b:

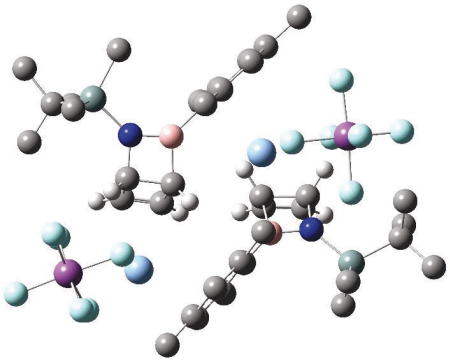

C	-0.27131783	1.24806208	0.00000000
C	-1.74170383	0.71172908	0.04457100
C	-0.05517083	0.51460408	1.31902900
H	0.75613917	0.52080208	2.05093200
C	-1.33437683	0.05318608	1.34443800
H	-1.91716883	-0.48352792	2.10100400
H	0.38314717	1.01848908	-0.84788900
H	-2.11973983	0.08409108	-0.77388200
C	-3.38288383	3.14183508	0.11687100
C	-3.94405083	3.60996008	-1.10215800
C	-4.05577483	3.40544408	1.33376200
C	-5.15183983	4.31059208	-1.07918600
C	-5.26587283	4.11223108	1.31545700
C	-5.82783783	4.57056208	0.12118500
H	-5.59479383	4.64131408	-2.02150600
H	-5.78179083	4.30603508	2.25934500
B	-2.04816583	2.30722808	0.11643200
C	-3.44287183	2.98990208	2.64904400
H	-2.81997783	3.80527208	3.04966600
H	-4.21241283	2.75850508	3.39786500
H	-2.78583183	2.11273908	2.54314000
C	-3.21784683	3.37824708	-2.40393700
H	-2.35084983	4.05287208	-2.48627200
H	-2.83240783	2.34994908	-2.47975200
H	-3.87566783	3.55814008	-3.26258900
C	-7.13633783	5.31184608	0.10275700
H	-7.00100083	6.32658008	-0.29957600
H	-7.84936583	4.78969208	-0.55001500
H	-7.56507683	5.39386908	1.10940600
N	-0.69252083	2.66149508	0.11221600
Si	0.28118417	4.14879808	0.00149600
C	-6.26269283	-0.88744692	1.98096000
C	-4.73462583	-0.55571192	2.05214100

C	-6.13880983	-1.36402592	3.41717900
H	-6.84146083	-1.84445692	4.10008500
C	-4.83791083	-1.04954692	3.48521000
H	-4.08091683	-1.13838692	4.26793500
H	-6.99916883	-0.10627592	1.73975500
H	-4.35998083	0.47878108	1.93792300
C	-3.52224283	-2.42744492	0.10225200
C	-3.33110683	-2.23457192	-1.28445200
C	-2.63231083	-3.26726792	0.80354600
C	-2.25533283	-2.84688992	-1.93358700
C	-1.57386283	-3.89770292	0.11956100
C	-1.36294783	-3.68664692	-1.25664700
H	-2.11020483	-2.67535792	-3.00326100
H	-0.93540483	-4.60684492	0.65667400
B	-4.67301983	-1.71411892	0.90805700
C	-2.80864683	-3.50253892	2.28423900
H	-3.86107683	-3.70142692	2.53753500
H	-2.20330683	-4.35034892	2.62931600
H	-2.50474883	-2.61627692	2.86405600
C	-4.24387983	-1.33556792	-2.08125400
H	-5.26073983	-1.30232092	-1.66643300
H	-3.83685383	-0.30833692	-2.14098100
H	-4.33321583	-1.67338192	-3.12283300
C	-0.24691483	-4.37318992	-1.99849900
H	-0.65812583	-5.12648892	-2.68675400
H	0.32613617	-3.65364992	-2.59969700
H	0.44458517	-4.87469692	-1.30992800
N	-6.06922883	-1.90973192	0.92398100
C	-6.61377283	-4.72265092	1.55190700
H	-7.26202083	-5.59956492	1.40561000
H	-5.58239283	-5.02169892	1.30626200
H	-6.64350783	-4.44208492	2.61590500
C	-8.94288683	-2.82639092	0.70674400
Si	-7.11630583	-3.28285892	0.44991700
Ag	-0.03248383	-1.90867892	0.46935800
Ag	-4.89101983	1.12507808	-0.26116500
Sb	-7.71646683	1.22976008	-2.33780600
Sb	2.50037317	-1.28054192	-1.76182300
F	-5.80380783	1.47139008	-2.54644100
F	-7.98204183	1.34544808	-4.21306100
F	-7.92000483	3.11504508	-2.15116200
F	-9.55988883	0.94612708	-1.98554800
F	-7.40631383	-0.65260992	-2.46068600
F	-7.31361883	1.12530508	-0.43385100
F	0.58282917	-1.04142392	-1.88541300
F	2.77941017	0.24594008	-2.85774200
F	2.43198717	-2.44972392	-3.25970800
F	2.05914217	-2.75028392	-0.57359500
F	4.35708717	-1.59519992	-1.53468800
F	2.45610617	-0.16882092	-0.19849600

C	1.55179917	4.14150408	1.41111300
C	-6.74055183	-3.68810292	-1.33928500
H	-7.27376283	-4.60277392	-1.63924300
H	-7.04139083	-2.86562892	-2.00434600
H	-5.66217683	-3.86991092	-1.46874800
C	-9.30257083	-1.57299492	-0.09911500
H	-10.36855583	-1.32458392	0.04275400
H	-8.71334583	-0.69739392	0.21345800
H	-9.13228683	-1.71370992	-1.17602900
C	-9.79352183	-4.00605592	0.20917400
H	-10.86400483	-3.77885192	0.34918000
H	-9.63457483	-4.20082992	-0.86253800
H	-9.57780583	-4.93418792	0.76161900
C	-9.24963283	-2.58571192	2.19120800
H	-8.97065483	-3.44677992	2.81899300
H	-8.73124783	-1.69558892	2.57803500
H	-10.33144483	-2.41382292	2.32526600
C	-0.93949483	5.56234508	0.15334600
H	-1.70513783	5.50542308	-0.63507400
H	-1.45475683	5.54077508	1.12576200
H	-0.42391383	6.52918108	0.05627100
C	1.13237817	4.11676908	-1.67010700
H	1.84785717	4.94681308	-1.76974500
H	1.68306317	3.17448708	-1.81478500
H	0.39175917	4.20530908	-2.47871200
C	2.62514917	3.08068008	1.12370400
H	3.31581517	2.99813308	1.98044100
H	2.20587317	2.07911908	0.93614500
H	3.22475517	3.34935508	0.24038300
C	0.84247417	3.83001308	2.73525300
H	1.56881817	3.82466108	3.56583800
H	0.07456617	4.58398108	2.97115200
H	0.34708317	2.84702408	2.71257100
C	2.21924517	5.52088108	1.50509300
H	2.99897117	5.51153408	2.28584400
H	2.70458417	5.80827208	0.55868100
H	1.49488417	6.30699008	1.76865800

M06-2X(PCM:DCM)/def2-SVP: -4191.59550

M06-2X(PCM:DCM)/def2-QVPP: -4195.55826

$G_{corr.}$: 0.811162

I' c:

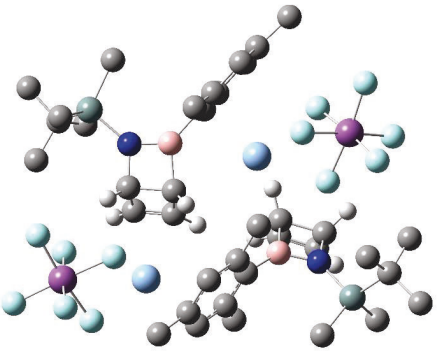

C	-0.50387596	1.49612411	0.00000000
C	-1.99826296	1.04606911	-0.13690400
C	-0.51620796	0.81922011	1.36607200
H	0.18572104	0.82116211	2.20361000
C	-1.81107196	0.42569911	1.23068500
H	-2.52181596	-0.05321489	1.91311100
H	0.24367404	1.18522711	-0.73840700
H	-2.30471596	0.40638911	-0.97599200
C	-3.47367696	3.57969311	-0.32194300
C	-3.99643196	3.89179811	-1.60235100
C	-4.10540696	4.10763111	0.83496200
C	-5.13559396	4.69864411	-1.70071100
C	-5.22957296	4.92123111	0.69212600
C	-5.76877696	5.21213611	-0.56681400
H	-5.54891096	4.91454011	-2.68930100
H	-5.72010196	5.31342311	1.58644100
B	-2.20689796	2.66048011	-0.16398300
C	-3.54041396	3.79723511	2.19993200
H	-3.40379196	2.71278011	2.33999200
H	-2.54977896	4.26020311	2.32746800
H	-4.19734996	4.16337211	2.99842300
C	-3.29623096	3.41200211	-2.85061800
H	-2.47598796	4.09857711	-3.11433500
H	-2.84857696	2.41496411	-2.71962000
H	-3.98662196	3.36914111	-3.70274900
C	-7.05033696	5.98627711	-0.69940000
H	-7.01416296	6.67867711	-1.55132700
H	-7.87888496	5.28282211	-0.87529700
H	-7.27369796	6.55565611	0.21181000
N	-0.84201896	2.93496411	-0.00662900
C	-0.88652396	5.84311511	-0.16790100
H	-0.29602996	6.76441811	-0.28055100
H	-1.56943196	5.76908611	-1.02815800

H	-1.49848896	5.93507311	0.74228000
C	1.36360304	4.34423211	1.42962900
Si	0.23953304	4.34702311	-0.09917900
C	-6.67272096	-1.20214889	2.05376200
C	-5.29627696	-0.47471589	1.94880400
C	-6.30053896	-1.51660689	3.49209600
H	-6.78369096	-2.11372789	4.26729000
C	-5.13301196	-0.86229189	3.40905000
H	-4.31733996	-0.68955489	4.11599100
H	-7.60139496	-0.65440489	1.84999300
H	-5.27221996	0.60870511	1.72795000
C	-3.81452096	-2.18066489	0.00151500
C	-3.63576296	-1.85060089	-1.35351100
C	-2.89491496	-3.06127089	0.61718900
C	-2.55074896	-2.37370489	-2.06946600
C	-1.82974396	-3.59640289	-0.13063700
C	-1.63904196	-3.25435589	-1.48537900
H	-2.41804696	-2.09259289	-3.11783600
H	-1.16771296	-4.33610189	0.33188800
B	-5.02880396	-1.65976189	0.86258400
C	-3.07334696	-3.45144189	2.06523400
H	-4.06694396	-3.89524289	2.23375300
H	-2.31070196	-4.17326289	2.38454000
H	-3.01078596	-2.57104889	2.72367600
C	-4.58687796	-0.91927789	-2.06441600
H	-5.46745696	-0.67894689	-1.44897200
H	-4.07822596	0.01305011	-2.37110600
H	-4.96815696	-1.36825089	-2.99336800
C	-0.51506996	-3.85074989	-2.28834700
H	-0.88956896	-4.68130389	-2.90605800
H	-0.07396596	-3.10294589	-2.95986900
H	0.28005004	-4.23600389	-1.63827900
N	-6.30122996	-2.22442889	1.04706300
C	-5.91617796	-4.83191389	-0.25153000
H	-6.40686396	-5.75220089	-0.60291900
H	-5.43786296	-4.34370989	-1.11366500
H	-5.12351296	-5.11904289	0.45581200
C	-7.82244696	-4.46091989	2.16231800
H	-6.98946096	-4.65979589	2.85412000
H	-8.53334296	-3.78975989	2.66807800
H	-8.33549796	-5.41366789	1.96428900
C	-8.57908996	-3.26339889	-0.62050900
C	-7.98451296	-2.71395389	-1.92317300
H	-8.79068596	-2.44880689	-2.62767400
H	-7.40723596	-1.79717689	-1.73322300
H	-7.32985396	-3.44790089	-2.41942300
C	-9.40179596	-4.52436689	-0.91753100
H	-9.87594696	-4.92725089	-0.00888900
H	-10.20666296	-4.28866289	-1.63471800
H	-8.78689996	-5.32261689	-1.36297400

C	-9.48471096	-2.19326089	0.00249700
H	-10.31445796	-1.95092689	-0.68390100
H	-9.92721996	-2.52809889	0.95443500
H	-8.93093796	-1.26156589	0.18569300
Si	-7.16686496	-3.70095989	0.57404500
Ag	-0.45217096	-1.62002589	0.61825600
Ag	-4.99416796	1.58705411	-0.38535600
Sb	-8.23760496	1.63758611	-1.21454400
Sb	2.30589504	-1.25523189	-1.34459000
F	-6.68761296	1.85997311	-2.35006900
F	-8.98014696	0.38535311	-2.43073600
F	-9.12163496	3.10496811	-2.03030300
F	-9.63768996	1.34053511	0.03287200
F	-7.16836996	0.25001611	-0.37248800
F	-7.34852696	2.81432011	0.02566600
F	0.44279104	-0.89409089	-1.72045300
F	2.80816904	0.29514011	-2.32299000
F	2.39517304	-2.36708289	-2.88229900
F	1.63983404	-2.72816689	-0.27313400
F	4.09816904	-1.66237589	-0.87500600
F	2.08178104	-0.19683889	0.24584000
C	1.24472904	4.15492111	-1.67158000
H	2.01989704	4.93220611	-1.74768700
H	1.74284004	3.17398511	-1.70872300
H	0.58884704	4.23813911	-2.55099200
C	2.37225604	3.19080611	1.31618000
H	2.97239404	3.11989611	2.23949500
H	1.89416604	2.21105411	1.15486500
H	3.06987804	3.35141911	0.47984800
C	2.12554604	5.67465411	1.50751700
H	2.82012404	5.66361411	2.36485400
H	2.72405004	5.85905811	0.60120700
H	1.44281904	6.52755411	1.64414500
C	0.50983604	4.17374011	2.69249400
H	1.15196804	4.16057711	3.58969200
H	-0.20630296	5.00287711	2.81195500
H	-0.06456396	3.23425211	2.67384900

M06-2X(PCM:DCM)/def2-SVP: -4191.59568

M06-2X(PCM:DCM)/def2-QVPP: -4195.55775

$G_{corr.}$: 0.808153

I' d:

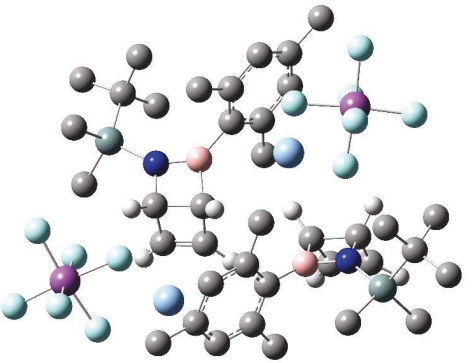

C	-0.42635658	2.24031019	0.00000000
C	-1.90398858	1.75467419	0.15994000
C	-0.13577458	1.54414019	1.31941300
H	0.71314642	1.58363619	2.00618700
C	-1.42062658	1.10629519	1.43514900
H	-1.96030458	0.58746719	2.23469900
H	0.15617542	1.96899819	-0.88738700
H	-2.38091258	1.13120319	-0.61020600
C	-3.45642658	4.23884619	0.17785700
C	-3.93626458	4.74657619	-1.06406400
C	-4.18822058	4.51150519	1.36002600
C	-5.09742058	5.51829519	-1.08952500
C	-5.34671158	5.29969319	1.29095900
C	-5.81629258	5.80633519	0.07867000
H	-5.46908558	5.88561719	-2.04946100
H	-5.90358758	5.50331319	2.20928200
B	-2.14187258	3.36641919	0.20268000
C	-3.72909758	3.98485319	2.69948500
H	-2.88370158	3.28697319	2.60312500
H	-3.40365158	4.81034519	3.35016700
H	-4.54685458	3.46450719	3.21948500
C	-3.17772858	4.46588319	-2.33738900
H	-2.24564658	5.05131219	-2.36992300
H	-2.89606558	3.40473919	-2.41195600
H	-3.77786358	4.72126219	-3.21891900
C	-7.10316458	6.57839719	-0.00438500
H	-6.98862558	7.47451619	-0.62968100
H	-7.87488558	5.94450519	-0.46670700
H	-7.45620458	6.88306919	0.98879100
N	-0.77569458	3.67491219	0.11427200
C	-0.20592558	6.61113419	0.57933800
Si	0.49381742	4.92974719	0.04787200
C	-6.19674458	-0.24300381	1.78745000

C	-4.70613258	0.24039119	1.85155400
C	-6.08282058	-0.52460081	3.27288500
H	-6.75871058	-0.98846981	3.99252900
C	-4.81700658	-0.08519581	3.32932400
H	-4.08259758	-0.01135081	4.13566100
H	-6.98905458	0.42627819	1.42529500
H	-4.38565658	1.27422419	1.61710700
C	-3.28823758	-1.63303881	0.06777200
C	-3.06066458	-1.39439381	-1.30140100
C	-2.37811258	-2.43526581	0.78811900
C	-1.92084858	-1.92188081	-1.92129400
C	-1.25567358	-2.97899981	0.13599400
C	-1.00441658	-2.71866381	-1.22741100
H	-1.74154358	-1.70934981	-2.97862900
H	-0.58771458	-3.65029781	0.68479600
B	-4.51141758	-1.00836081	0.83256200
C	-2.62790358	-2.73316581	2.24591800
H	-3.61208858	-3.20852781	2.38428700
H	-1.86198858	-3.40086781	2.66012900
H	-2.63848758	-1.80921881	2.84470300
C	-4.01617958	-0.56493881	-2.12554900
H	-4.88420758	-0.22311181	-1.54187500
H	-3.51088358	0.31510319	-2.55602400
H	-4.40726958	-1.14942981	-2.97208000
C	0.19273442	-3.30572181	-1.92703200
H	-0.12236758	-4.10294281	-2.61675800
H	0.71695942	-2.54273681	-2.51785700
H	0.90401842	-3.73583281	-1.21006300
N	-5.86959358	-1.37203381	0.88319300
C	-5.60131458	-4.01501781	-0.33731600
H	-6.11992958	-4.94028481	-0.63080800
H	-5.17615458	-3.55481481	-1.24164600
H	-4.76686958	-4.28676381	0.32689200
C	-7.33390558	-3.56279681	2.18231600
H	-6.46644058	-3.66277981	2.85246800
H	-8.07822758	-2.92303881	2.68021400
H	-7.77983758	-4.55982481	2.04858000
C	-8.30043458	-2.47342081	-0.56137900
C	-7.83757758	-2.07369681	-1.96822800
H	-8.70718858	-1.80618681	-2.59317900
H	-7.17514158	-1.19624381	-1.93738000
H	-7.30607658	-2.89697981	-2.47119400
C	-9.17826258	-3.73031681	-0.64505000
H	-9.58206658	-4.01272281	0.33966100
H	-10.03554858	-3.54540481	-1.31474000
H	-8.62625958	-4.59508981	-1.04726800
C	-9.11270358	-1.32447981	0.05011600
H	-10.03264658	-1.15640181	-0.53578200
H	-9.41509658	-1.53640381	1.08862600
H	-8.54481658	-0.38453781	0.03253500

Si	-6.79247658	-2.85170781	0.52741600
Ag	-0.00731758	-0.82049381	0.52449500
Ag	-5.07081858	2.35594519	-0.23170000
Sb	-7.84792258	2.26864419	-2.00444100
Sb	2.67143542	-0.02061781	-1.59960900
F	-6.08661158	2.79519519	-2.59819400
F	-8.01712358	1.08950619	-3.47939600
F	-8.65290958	3.72064619	-2.91745900
F	-9.49836958	1.68535319	-1.27299600
F	-6.88305058	0.90898219	-0.98916700
F	-7.51107158	3.36571719	-0.45220700
F	0.75139942	-0.00194081	-1.84300300
F	2.88233742	1.31913019	-2.93104800
F	2.80667442	-1.41329881	-2.88850700
F	2.29913942	-1.32814881	-0.21414600
F	4.53227842	-0.11274981	-1.24029500
F	2.44989042	1.33445419	-0.26200000
C	1.15290842	4.93325719	-1.70988200
H	1.95013342	5.68224419	-1.82950800
H	1.58458242	3.94753319	-1.94495600
H	0.36447642	5.14768719	-2.44588800
C	1.84229642	4.32945819	1.20548400
H	2.18847442	3.33686619	0.87682900
H	2.70676742	5.00951119	1.18017500
H	1.48942642	4.25523419	2.24508500
C	-0.90034858	6.48138919	1.94071200
H	-0.21977558	6.09374219	2.71498200
H	-1.26158658	7.46810119	2.27749100
H	-1.77068958	5.81049519	1.88343900
C	0.97015542	7.59345119	0.69838100
H	1.51317842	7.70272319	-0.25376400
H	0.59576442	8.59160419	0.98184000
H	1.69142442	7.27816619	1.46769600
C	-1.20532958	7.14665019	-0.45342200
H	-0.75307758	7.24216419	-1.45314100
H	-2.09216958	6.49971319	-0.53343400
H	-1.55749958	8.14794619	-0.15140900

M06-2X(PCM:DCM)/def2-SVP: -4191.59319

M06-2X(PCM:DCM)/def2-QVPP: -4195.55666

$G_{corr.}$: 0.806983

TS I a:

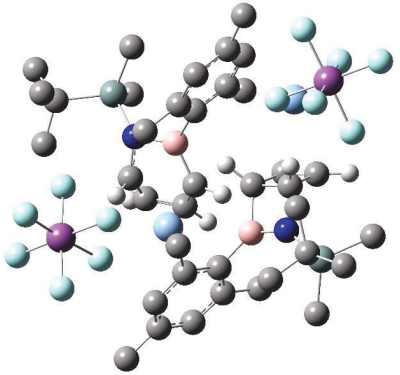

C	1.24806200	3.07751953	0.00000000
C	-0.25292700	2.63341353	0.05454400
C	1.45509400	2.28045953	1.27673800
H	2.27682600	2.22496253	1.99416700
C	0.15286600	1.88619453	1.30632100
H	-0.42821000	1.32712853	2.04747400
H	1.86662200	2.84962253	-0.87330200
H	-0.71840000	2.08058253	-0.77270100
C	-1.73641800	5.14831853	0.14487300
C	-2.27004600	5.60725553	-1.08409800
C	-2.41761900	5.45621153	1.35195900
C	-3.45455600	6.35693253	-1.08525200
C	-3.59989000	6.20192953	1.30926400
C	-4.13346400	6.66145753	0.09731600
H	-3.87800600	6.67886753	-2.03967900
H	-4.12259600	6.42445353	2.24300000
B	-0.44928200	4.24208353	0.17704300
C	-1.84306600	5.00135453	2.67110400
H	-1.48712800	3.95980053	2.62109100
H	-0.97678300	5.62187153	2.94745200
H	-2.58315200	5.07283553	3.47831600
C	-1.61432100	5.27420453	-2.40262900
H	-1.38927800	6.19096653	-2.96630100
H	-0.67431200	4.71883253	-2.27288300
H	-2.29519600	4.66911853	-3.01741900
C	-5.41296200	7.45163753	0.05674200
H	-5.20858900	8.50773953	-0.17593500
H	-6.07106100	7.05933853	-0.72977300
H	-5.93808700	7.41119953	1.01956400
N	0.92939900	4.50764253	0.19357000
C	1.30210100	7.20896753	1.27924800
H	1.93175500	8.11127853	1.27945100
H	0.34446200	7.45972053	0.79693800

H	1.10216800	6.93297853	2.32505800
C	3.53065900	5.01437153	1.36878800
H	3.16179300	4.68220353	2.35117800
H	3.93563500	4.13947653	0.83427600
H	4.35148800	5.72668653	1.53714900
C	2.75228900	6.31625153	-1.34307700
C	1.70184500	7.21979853	-2.00030900
H	1.99778300	7.46182853	-3.03548000
H	0.71612600	6.73013453	-2.04154300
H	1.58427300	8.16910653	-1.45524800
C	4.07435800	7.08332953	-1.20244600
H	4.87760300	6.43814953	-0.81515500
H	4.39776000	7.46270753	-2.18679100
H	3.97961500	7.95125153	-0.52932700
C	2.97433000	5.06974853	-2.21222700
H	3.42432300	5.35497353	-3.17841900
H	3.64699000	4.33700653	-1.73793200
H	2.02261500	4.55910853	-2.43060400
Si	2.14245700	5.79698053	0.38008000
C	-5.38540100	0.85130753	0.55055400
C	-3.48924100	1.27385453	1.49542000
C	-5.74879900	1.00761453	1.96119300
H	-6.66364500	0.66571153	2.44419500
C	-4.56718100	1.40294153	2.48456800
H	-4.38090800	1.67014353	3.52905400
H	-5.49192700	1.69778053	-0.14263200
H	-2.54741300	1.81118653	1.68265700
C	-2.21463200	-0.40830547	-0.31530400
C	-1.92486200	-0.08704447	-1.65959800
C	-1.37043000	-1.29990547	0.37377600
C	-0.80457300	-0.64305047	-2.28535400
C	-0.26636700	-1.87328447	-0.28944000
C	0.03482000	-1.55193047	-1.62740200
H	-0.58427500	-0.37731647	-3.32248300
H	0.33136100	-2.63290747	0.22530900
B	-3.49578400	0.15547053	0.43154400
C	-1.66401600	-1.69786147	1.80027900
H	-2.66200800	-2.15759747	1.88034400
H	-0.92772400	-2.42086147	2.17349600
H	-1.66779200	-0.82603147	2.47036100
C	-2.77766900	0.89578353	-2.42103900
H	-3.83312700	0.85718753	-2.11393700
H	-2.42075300	1.92979053	-2.26183800
H	-2.72798000	0.71566653	-3.50302700
C	1.18884600	-2.19708347	-2.35159800
H	0.81439400	-2.87518147	-3.13268400
H	1.82006100	-1.44389647	-2.84268900
H	1.81645600	-2.78131447	-1.66536200
N	-4.85558400	-0.31959147	0.08624000
C	-4.21544200	-3.00639447	-0.89808300

H	-4.64719500	-3.97462047	-1.19540700
H	-3.81514700	-2.51085847	-1.79457000
H	-3.37745800	-3.20567447	-0.21441600
C	-5.97426200	-2.64693847	1.61363000
H	-5.11276900	-2.56323047	2.29298100
H	-6.81837300	-2.10764647	2.06819300
H	-6.24800200	-3.71050547	1.54017700
C	-7.08395800	-1.77158747	-1.16284800
C	-6.66587600	-1.43933447	-2.60097900
H	-7.56101100	-1.30035647	-3.23099700
H	-6.08528600	-0.50470647	-2.64091500
H	-6.06586600	-2.24693047	-3.04810800
C	-7.87093600	-3.09009547	-1.13514400
H	-8.24116400	-3.32353447	-0.12483600
H	-8.74616700	-3.02001747	-1.80269400
H	-7.26125100	-3.94106047	-1.47930600
C	-7.96302800	-0.63677047	-0.62018200
H	-8.91247500	-0.59571647	-1.18061900
H	-8.21827400	-0.77242047	0.44361300
H	-7.48070600	0.34536053	-0.75363900
Si	-5.53940000	-1.96740047	-0.08178000
Ag	1.38167700	-0.02482347	0.19421900
Ag	-3.56342400	3.28440253	-0.03127500
Sb	-6.19406400	3.77849453	-2.42892500
Sb	4.14497900	0.75014853	-1.89085600
F	-4.26585800	3.66424953	-2.48410600
F	-6.30489200	3.57104453	-4.31136200
F	-6.10282600	5.67345853	-2.60035600
F	-8.07872900	3.84179253	-2.21935600
F	-6.21205100	1.87243153	-2.18703800
F	-5.95117000	3.93906553	-0.50829500
F	2.23191300	0.97505953	-2.08511500
F	4.47195400	2.06174353	-3.22498300
F	4.08344600	-0.64109247	-3.18804400
F	3.66487800	-0.53362047	-0.51300500
F	5.99122900	0.44139853	-1.58013200
F	4.11315900	2.10748553	-0.53658400

M06-2X(PCM:DCM)/def2-SVP: -4191.56424

M06-2X(PCM:DCM)/def2-QVPP: -4195.52890

$G_{corr.}$: 0.80909

TS I b:

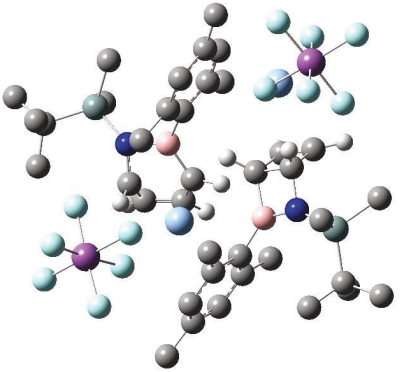

C	-0.34883720	2.08527142	0.00000000
C	-1.81652220	1.60342242	0.23139400
C	-0.00312920	1.42860442	1.32661700
H	0.87970680	1.47410942	1.96833200
C	-1.28273720	1.00395042	1.51455000
H	-1.78285220	0.52472142	2.36327100
H	0.20200080	1.79256142	-0.90051800
H	-2.30927520	0.94694742	-0.49983100
C	-3.39775920	4.05507842	0.25816000
C	-3.94472420	4.52253642	-0.96848000
C	-4.10676920	4.28986042	1.45970900
C	-5.15593320	5.21396542	-0.96563500
C	-5.32293520	4.98972642	1.42205100
C	-5.86201820	5.45541442	0.22206000
H	-5.58690920	5.54044942	-1.91463300
H	-5.86667320	5.15699742	2.35566800
B	-2.06707920	3.21114842	0.23756300
C	-3.57412520	3.80890142	2.78868700
H	-2.68253020	3.17420542	2.67399700
H	-3.29107420	4.66134242	3.42431200
H	-4.33845020	3.23773842	3.33634000
C	-3.21133320	4.26972042	-2.26180300
H	-2.30097220	4.88668542	-2.31762400
H	-2.89673420	3.21768242	-2.34430900
H	-3.84328220	4.50329342	-3.12688800
C	-7.18405720	6.17016542	0.17608900
H	-7.05190520	7.21236742	-0.15070800
H	-7.84453720	5.67855442	-0.55138100
H	-7.67192120	6.17584342	1.15888500
N	-0.70535620	3.52066142	0.08612000
C	-0.12390820	6.44204242	0.56243400
Si	0.54127080	4.78588642	-0.07931600
C	-6.87781620	-0.22298258	0.97478700

C	-4.97119820	0.34200242	1.84567900
C	-7.21884920	0.10856142	2.36209200
H	-8.12213120	-0.19061458	2.89376300
C	-6.04056920	0.58109042	2.82269000
H	-5.84885220	0.96757542	3.82803200
H	-7.02847220	0.51636942	0.17406600
H	-4.03587920	0.91602642	1.94355900
C	-3.71827720	-1.49212458	0.17772300
C	-3.51590020	-1.33079558	-1.21040500
C	-2.80856820	-2.27147658	0.91774600
C	-2.41338420	-1.92805758	-1.82926000
C	-1.72673920	-2.89530958	0.26286800
C	-1.51127820	-2.72878658	-1.11836900
H	-2.25931820	-1.78438258	-2.90180400
H	-1.08412320	-3.58065658	0.82649700
B	-4.98527220	-0.89183958	0.92082300
C	-3.01394020	-2.50535058	2.39548700
H	-3.98496120	-2.99106458	2.58319300
H	-2.22712620	-3.14756958	2.81140700
H	-3.02574320	-1.55981758	2.95636600
C	-4.44976920	-0.48230958	-2.03686800
H	-5.48524520	-0.52480558	-1.66946800
H	-4.13368120	0.57756342	-2.03309600
H	-4.44865420	-0.79411258	-3.08975500
C	-0.37840720	-3.42299558	-1.82680000
H	-0.76995220	-4.21129958	-2.48680000
H	0.18659280	-2.71802858	-2.45153700
H	0.31649280	-3.88727358	-1.11453300
N	-6.33835020	-1.43965558	0.66583200
C	-5.63176820	-4.18560058	-0.09384400
H	-6.03851020	-5.18661158	-0.30549300
H	-5.21050320	-3.77423658	-1.02256800
H	-4.81320620	-4.30072558	0.63166400
C	-7.49405020	-3.64924458	2.30597000
H	-6.64507020	-3.53288058	2.99636900
H	-8.33432320	-3.05651058	2.69683800
H	-7.79179720	-4.70869158	2.30676900
C	-8.49603020	-3.00817658	-0.57643200
C	-8.02371220	-2.76607458	-2.01581700
H	-8.89362520	-2.69978558	-2.69136100
H	-7.46955720	-1.81845058	-2.10033800
H	-7.38165120	-3.58362458	-2.37875300
C	-9.25992620	-4.33793858	-0.49198700
H	-9.66876220	-4.51087158	0.51554400
H	-10.10700820	-4.33062858	-1.19834600
H	-8.62117320	-5.19722958	-0.75238000
C	-9.41916620	-1.85825358	-0.15092700
H	-10.34577720	-1.87860758	-0.74940200
H	-9.71317420	-1.92351758	0.90939000
H	-8.95220820	-0.87698858	-0.33489400

Si	-6.99761620	-3.10055358	0.58129900
Ag	-0.10445420	-1.00662858	0.57627100
Ag	-5.04011720	2.06745642	0.00150200
Sb	-7.72268020	2.48234342	-2.27149400
Sb	2.45947480	-0.43015458	-1.73642000
F	-5.78901020	2.43888142	-2.37020000
F	-7.85465020	2.16904342	-4.13725200
F	-7.70840220	4.36825142	-2.53383900
F	-9.60565520	2.48418942	-2.03796000
F	-7.66619320	0.59282142	-1.91922400
F	-7.45552920	2.74412342	-0.36778100
F	0.53375580	-0.25376758	-1.83494000
F	2.67893880	0.87217242	-3.10157800
F	2.37024780	-1.84553558	-3.00448700
F	2.08550880	-1.68670058	-0.30306400
F	4.32728080	-0.68199258	-1.51826600
F	2.45404780	0.94892042	-0.40561400
C	1.02820080	4.85013042	-1.89133700
H	1.81579180	5.59995242	-2.05998400
H	1.42652480	3.87158642	-2.20245300
H	0.17496880	5.09399842	-2.54048700
C	2.00056480	4.16018342	0.92098600
H	2.28873580	3.15902642	0.56118200
H	2.86988380	4.82299342	0.79738100
H	1.76615480	4.09264542	1.99405100
C	-0.72214820	6.25625542	1.96242600
H	0.01013980	5.83906442	2.67162100
H	-1.05834420	7.22791942	2.36290200
H	-1.59429120	5.58565142	1.93849600
C	1.05043080	7.43037842	0.63495900
H	1.52775280	7.57499942	-0.34731400
H	0.69012180	8.41578342	0.97573900
H	1.82369880	7.09564942	1.34333500
C	-1.19752320	7.00125142	-0.37997700
H	-0.80981320	7.15369142	-1.39941500
H	-2.07415920	6.33733542	-0.43818200
H	-1.55097920	7.97884742	-0.00945500

M06-2X(PCM:DCM)/def2-SVP: -4191.56375

M06-2X(PCM:DCM)/def2-QVPP: -4195.52937

$G_{corr.}$: 0.806947

TS I c:

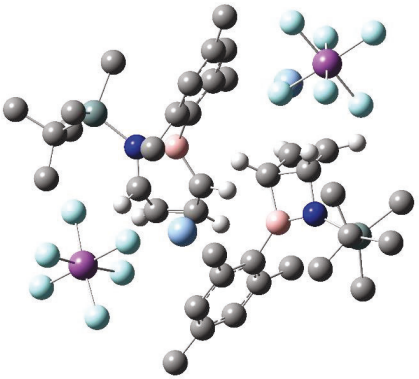

C	0.13178294	1.48062023	0.00000000
C	-1.36582806	1.03473123	0.00019900
C	0.29886494	0.66558223	1.27199100
H	1.09834294	0.59933523	2.01336900
C	-1.00350506	0.27063223	1.25600800
H	-1.61346106	-0.29214177	1.97099900
H	0.78190894	1.26609123	-0.85278000
H	-1.80061506	0.49433323	-0.85126500
C	-2.88658106	3.51337023	0.15581600
C	-3.50920806	3.91159423	-1.05200600
C	-3.52773606	3.79434223	1.38921400
C	-4.75981006	4.55553123	-1.00508700
C	-4.75782206	4.45503623	1.39790400
C	-5.39668406	4.83428823	0.20742500
H	-5.25728606	4.82038323	-1.94183700
H	-5.24823106	4.65563123	2.35393900
B	-1.57659406	2.63963323	0.14974200
C	-2.88618606	3.33777423	2.67544700
H	-1.87822906	3.76431723	2.78680900
H	-3.48365206	3.62561223	3.54932400
H	-2.77090306	2.24047023	2.69022600
C	-2.86616906	3.66288723	-2.39677200
H	-2.52721206	4.61168723	-2.83803000
H	-1.99201706	2.99914523	-2.32381400
H	-3.58919706	3.21572523	-3.09314200
C	-6.73721706	5.51716823	0.22203900
H	-6.61462606	6.61051323	0.18147300
H	-7.32946106	5.21061023	-0.64989500
H	-7.29471306	5.27637223	1.13653900
N	-0.19941706	2.90819323	0.20069800
Si	1.01825994	4.19202823	0.39400300
C	-6.42545406	-0.70169777	0.55962200
C	-4.56571106	-0.13697677	1.33095100

C	-6.74105406	-0.25448477	1.93858000
H	-7.66309006	-0.48334077	2.47425700
C	-5.55140406	0.20016623	2.36566000
H	-5.30072106	0.63334323	3.33715700
H	-6.72288806	-0.10805677	-0.31920000
H	-3.62800106	0.43626423	1.24700800
C	-3.40658706	-2.02151177	-0.30578400
C	-3.13294606	-1.66305477	-1.64254400
C	-2.55112406	-2.92814577	0.35143700
C	-2.02046306	-2.20472377	-2.29611100
C	-1.45393406	-3.48053777	-0.33713100
C	-1.17137106	-3.12712177	-1.67135700
H	-1.81247306	-1.91180277	-3.32843600
H	-0.84304106	-4.24435877	0.15548000
B	-4.63597106	-1.45686577	0.52516000
C	-2.82191206	-3.33243477	1.77974200
H	-3.81308906	-3.80246377	1.86967600
H	-2.07179406	-4.04479377	2.14539600
H	-2.82442806	-2.45743377	2.44762300
C	-3.98400406	-0.65768477	-2.37923700
H	-5.01764406	-0.62350577	-2.00489700
H	-3.54753006	0.35543023	-2.30434700
H	-4.03559406	-0.88444777	-3.45299000
C	-0.02747106	-3.75478677	-2.42585800
H	-0.41254606	-4.46311377	-3.17452800
H	0.56040294	-2.99565477	-2.95899800
H	0.64427994	-4.30398277	-1.75271100
N	-5.99206006	-2.00616677	0.40849600
C	-5.68622406	-4.86421577	-0.11035200
H	-6.08279706	-5.74432777	-0.63909400
H	-4.62457806	-4.75988377	-0.38286000
H	-5.75706906	-5.05104077	0.97088300
C	-8.48370806	-3.44639477	-0.16035900
Si	-6.64257206	-3.33521677	-0.60981900
Ag	0.22029694	-1.63482377	0.15699100
Ag	-4.80835906	1.68786123	-0.39891000
Sb	-7.57669706	2.07372223	-2.57331700
Sb	2.93223394	-0.87210777	-1.99721800
F	-5.64786106	2.06922123	-2.74841400
F	-7.77667906	1.91287223	-4.45187500
F	-7.56616006	3.97633623	-2.67117800
F	-9.44924606	2.03129223	-2.27880800
F	-7.46750406	0.16238023	-2.37537500
F	-7.25434106	2.18383323	-0.66349300
F	1.02149794	-0.59264577	-2.13184700
F	3.25898694	0.48693623	-3.28319600
F	2.80411694	-2.20387477	-3.35081300
F	2.44905994	-2.20068177	-0.66274800
F	4.77661394	-1.24031277	-1.74635600
F	2.97302494	0.42526423	-0.58565200

C	1.63628494	4.69679223	-1.33041600
C	2.39479094	3.40083923	1.39243500
H	2.79711094	2.52180323	0.86280900
H	3.22036994	4.10644423	1.56557800
H	2.01665494	3.07286423	2.37275900
C	-6.41908606	-2.99385577	-2.43877800
H	-6.92720706	-3.78028177	-3.01767000
H	-6.83750206	-2.01969077	-2.73172700
H	-5.35256506	-3.01896477	-2.70650500
C	-9.15781506	-2.07883277	-0.34336600
H	-10.25058106	-2.18056677	-0.23113900
H	-8.83321406	-1.35510077	0.42174600
H	-8.96050406	-1.63403477	-1.33138200
C	-9.15609906	-4.46615177	-1.09215700
H	-10.20863806	-4.60883877	-0.79491500
H	-9.15116706	-4.12577277	-2.13858600
H	-8.66435906	-5.45132777	-1.05080400
C	-8.63873206	-3.90204877	1.29638800
H	-8.25159206	-4.92165977	1.44615200
H	-8.10519606	-3.23194877	1.98932300
H	-9.70422606	-3.90463777	1.58234100
C	0.18486294	5.61492823	1.28230700
H	-0.77741606	5.85848423	0.80579300
H	-0.00499206	5.35599123	2.33435700
H	0.81376894	6.51756223	1.26323500
C	2.94109994	5.49237223	-1.18716700
H	3.75247394	4.86923623	-0.78099900
H	3.26845894	5.86281223	-2.17357300
H	2.82168394	6.36844123	-0.52884200
C	1.89119694	3.44484823	-2.18280200
H	2.56905594	2.72721523	-1.69328000
H	0.95123294	2.91664423	-2.41034200
H	2.34978794	3.72799523	-3.14552100
C	0.57245594	5.56784823	-2.00930100
H	-0.39965106	5.05153323	-2.05505500
H	0.42509894	6.52020823	-1.47693400
H	0.87350894	5.80492223	-3.04408700

M06-2X(PCM:DCM)/def2-SVP: -4191.56806

M06-2X(PCM:DCM)/def2-QVPP: -4195.53263

$G_{corr.}$: 0.810085

TS I d:

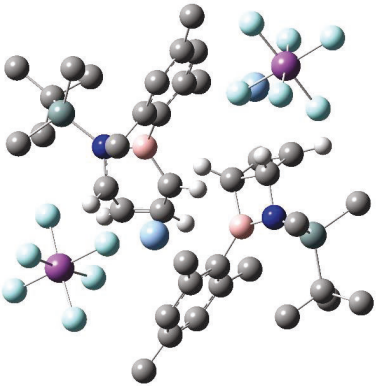

C	-1.15503874	2.17829468	0.00000000
C	-2.63607874	1.73257068	0.22429400
C	-0.81633874	1.44185568	1.28554800
H	0.07103526	1.43137468	1.92258000
C	-2.10664474	1.04402468	1.46243800
H	-2.61254474	0.52735868	2.28546800
H	-0.62665474	1.91312068	-0.92239700
H	-3.16911774	1.14025368	-0.53219100
C	-4.13604674	4.22716968	0.31830700
C	-4.61620874	4.78527068	-0.89687800
C	-4.89604874	4.39521368	1.50037900
C	-5.81213274	5.50329768	-0.90196300
C	-6.10281874	5.11330568	1.45259500
C	-6.57345774	5.67448068	0.26340500
H	-6.19240874	5.90026068	-1.84564900
H	-6.68914574	5.22571368	2.36837400
B	-2.83177974	3.34532468	0.29961200
C	-4.41245974	3.83936168	2.81839200
H	-3.66225274	3.04563268	2.68120800
H	-3.94085574	4.63050668	3.42140400
H	-5.24586374	3.43318068	3.40846400
C	-3.84548574	4.57964668	-2.17627600
H	-2.88462574	5.11564668	-2.14505100
H	-3.61825574	3.51427868	-2.33578000
H	-4.41543874	4.93615768	-3.04254700
C	-7.87792874	6.42036468	0.20627400
H	-7.70611974	7.48661268	-0.00414600
H	-8.49911674	6.01971768	-0.60632500
H	-8.42747674	6.34085168	1.15270100
N	-1.46027174	3.61847868	0.16165700
C	-0.79042774	6.50617568	0.73950100
Si	-0.16820874	4.84458268	0.06705300
C	-7.58838374	-0.15645332	0.62847100

C	-5.77050874	0.37916468	1.60528700
C	-8.00591874	0.25466168	1.98988600
H	-8.96971674	0.01119968	2.43807900
C	-6.85727374	0.68415368	2.54146000
H	-6.70513174	1.07364268	3.55109400
H	-7.79815174	0.46505268	-0.26015400
H	-4.81646374	0.92715368	1.65687400
C	-4.50597374	-1.43052932	-0.03377400
C	-4.23354574	-1.13360732	-1.38578100
C	-3.63492874	-2.28232832	0.67138200
C	-3.10485474	-1.67743432	-2.00610500
C	-2.52204474	-2.84540532	0.01445900
C	-2.24250274	-2.55439732	-1.33493200
H	-2.89998274	-1.43481132	-3.05188200
H	-1.90108374	-3.57490132	0.54487700
B	-5.79018174	-0.89500932	0.73010400
C	-3.91959274	-2.65431132	2.10589800
H	-4.85528774	-3.23102132	2.17494200
H	-3.11331774	-3.26642732	2.52944400
H	-4.04849274	-1.76099832	2.73435000
C	-5.13279274	-0.22009932	-2.17980700
H	-6.18372674	-0.27959632	-1.85885500
H	-4.82045474	0.83543668	-2.08180200
H	-5.09444574	-0.45524232	-3.25182900
C	-1.09488074	-3.20748232	-2.06067400
H	-1.47560874	-3.97979432	-2.74583900
H	-0.53797974	-2.47647432	-2.66137500
H	-0.39748574	-3.68818032	-1.36205600
N	-7.13171974	-1.44739332	0.47826600
C	-6.40857274	-3.70575932	-1.37140200
H	-6.82193374	-4.60880332	-1.84638300
H	-5.96635074	-3.07995932	-2.15954000
H	-5.60427474	-4.01089732	-0.68594600
C	-8.66833674	-3.94488432	0.74911100
Si	-7.79468574	-2.80379332	-0.49470000
Ag	-0.92463774	-0.92048032	0.38357400
Ag	-5.96444874	2.34524668	0.02799500
Sb	-8.33729974	2.87838968	-2.52385900
Sb	1.70337526	-0.22065932	-1.84623100
F	-6.40596274	2.81881968	-2.39815700
F	-8.25283674	2.73994868	-4.41383300
F	-8.28677374	4.78019268	-2.60839800
F	-10.23438374	2.88584468	-2.51045900
F	-8.31889774	0.96696468	-2.34558900
F	-8.29542274	2.96117368	-0.58464600
F	-0.21946074	-0.04627932	-1.98703500
F	1.95322226	1.13006168	-3.15850700
F	1.65210526	-1.58892532	-3.16738700
F	1.29876926	-1.53238532	-0.47226500
F	3.56595326	-0.47418932	-1.58878100

F	1.65811926	1.10890768	-0.46690900
C	0.37354026	4.93854868	-1.72838600
H	1.18809926	5.66766768	-1.85446400
H	0.75264126	3.95619068	-2.05164400
H	-0.45116874	5.22406068	-2.39718300
C	1.24287926	4.14729068	1.08884600
H	1.52303226	3.15743568	0.69428800
H	2.12887426	4.79613268	1.02291900
H	0.96982226	4.03946968	2.14941800
C	-1.44060574	6.30243368	2.11365800
H	-0.75151874	5.82759768	2.82987200
H	-1.74420874	7.27502668	2.53720300
H	-2.34207374	5.67533968	2.03888900
C	0.42093326	7.44136768	0.88015500
H	0.93735226	7.59309068	-0.08111400
H	0.09006426	8.43120068	1.23745000
H	1.15487826	7.05453168	1.60351900
C	-1.80926674	7.14097568	-0.21510200
H	-1.38859274	7.29830068	-1.22071400
H	-2.71551874	6.52330268	-0.31042200
H	-2.12327874	8.12587668	0.17129600
C	-9.00273474	-2.04625432	-1.70634800
H	-9.48138874	-2.83360132	-2.30776400
H	-9.79491174	-1.48152232	-1.19183300
H	-8.49243274	-1.35104832	-2.38837600
C	-9.80227974	-3.17884532	1.44014700
H	-10.29504074	-3.82188032	2.18893400
H	-9.41965674	-2.29104932	1.96780600
H	-10.57257274	-2.85082532	0.72536900
C	-9.24568474	-5.15893832	0.00813900
H	-9.78019574	-5.81416132	0.71670700
H	-9.96438774	-4.86039432	-0.77122200
H	-8.45736174	-5.76201832	-0.46789600
C	-7.66017574	-4.41283532	1.80586600
H	-6.81869274	-4.96425832	1.35673200
H	-7.25206474	-3.55841632	2.36874300
H	-8.15083574	-5.08682432	2.52851000

M06-2X(PCM:DCM)/def2-SVP: -4191.56477

M06-2X(PCM:DCM)/def2-QVPP: -4195.53092

$G_{corr.}$: 0.808079

TS I e:

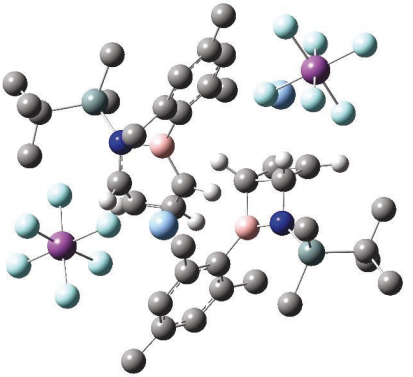

C	0.33333333	2.47286834	0.00000000
C	-1.14182267	1.98533534	0.20698400
C	0.65209333	1.81285634	1.33503500
H	1.52606133	1.83777034	1.98996000
C	-0.62950267	1.39054734	1.50188000
H	-1.13907667	0.90467034	2.34098800
H	0.90278233	2.17533534	-0.88759400
H	-1.62656167	1.32587434	-0.52724500
C	-2.70465167	4.47081834	0.17101500
C	-3.28695967	4.84610134	-1.06657300
C	-3.32161267	4.88025834	1.37773400
C	-4.46270567	5.60178234	-1.07458100
C	-4.50144367	5.63307334	1.33020000
C	-5.08772767	5.99805234	0.11388300
H	-4.92712367	5.85647334	-2.02981700
H	-4.97956067	5.93178534	2.26650500
B	-1.40161467	3.58883334	0.18928800
C	-2.68150767	4.53317134	2.69941600
H	-2.32496867	3.49066534	2.71653700
H	-1.80287067	5.17210434	2.88040000
H	-3.37971167	4.67081834	3.53490700
C	-2.62503567	4.44686734	-2.36170300
H	-1.71523567	5.04441534	-2.53167200
H	-2.31863567	3.38937734	-2.34892400
H	-3.29988867	4.59274834	-3.21335600
C	-6.37357867	6.77681334	0.06382700
H	-6.20616067	7.77692534	-0.36322300
H	-7.09554467	6.25974834	-0.58308100
H	-6.80828667	6.89870934	1.06393300
N	-0.04010167	3.90254234	0.06140400
C	-0.20951067	6.80576634	-0.13184800
H	0.32836833	7.74300834	-0.33774400
H	-1.01426367	6.70468734	-0.87553300

H	-0.67718267	6.88661134	0.86134000
C	2.29689033	5.42368834	1.13514800
Si	0.96321333	5.34624034	-0.21452400
C	-6.21134267	0.20207834	1.13446600
C	-4.26166567	0.73676434	1.92030800
C	-6.48530567	0.50088934	2.54263900
H	-7.36240867	0.19806834	3.11411600
C	-5.28154567	0.95941734	2.95130600
H	-5.03921267	1.33138434	3.95118200
H	-6.38053667	0.96880134	0.36454700
H	-3.31498767	1.29266134	1.99491500
C	-3.08558367	-1.08670566	0.18822500
C	-2.91504067	-0.89790566	-1.20005800
C	-2.16647367	-1.89118466	0.88946100
C	-1.83571067	-1.49535366	-1.85895500
C	-1.10833467	-2.51233066	0.19469700
C	-0.92499967	-2.31932966	-1.18800800
H	-1.70593867	-1.32879166	-2.93143100
H	-0.45844467	-3.21540066	0.72734900
B	-4.32193467	-0.47869066	0.97353300
C	-2.33681467	-2.15099266	2.36745800
H	-3.30228367	-2.64202966	2.56942500
H	-1.53979267	-2.79923166	2.75381500
H	-2.33694067	-1.21515666	2.94446500
C	-3.85352767	-0.01221166	-1.97959200
H	-4.88312567	-0.05531466	-1.59559900
H	-3.52584667	1.04321834	-1.93806500
H	-3.87238067	-0.28354966	-3.04340000
C	0.18414133	-3.00817666	-1.93811200
H	-0.22787367	-3.80772666	-2.57194400
H	0.71166733	-2.30266066	-2.59407700
H	0.91681133	-3.45461666	-1.25373000
N	-5.69150467	-1.00527666	0.76316000
C	-5.04857067	-3.75808366	-0.02645000
H	-5.47779567	-4.75235266	-0.22518200
H	-4.67705367	-3.34089966	-0.97370100
H	-4.19100067	-3.88981666	0.64939900
C	-6.75115067	-3.20486966	2.48832200
H	-5.86622467	-3.07324966	3.12905700
H	-7.57520467	-2.61995566	2.92306900
H	-7.03521567	-4.26782266	2.51272200
C	-7.93131067	-2.56678566	-0.32669900
C	-7.54767367	-2.34722866	-1.79577700
H	-8.45752767	-2.26904166	-2.41507900
H	-6.98059567	-1.41218666	-1.92361200
H	-6.94672267	-3.18111166	-2.19038700
C	-8.70541567	-3.88472166	-0.17681100
H	-9.05399367	-4.03797766	0.85626000
H	-9.59400367	-3.87561266	-0.83018100
H	-8.09494667	-4.75636366	-0.46290400

C	-8.81002567	-1.39913166	0.14219100
H	-9.77345567	-1.41427866	-0.39521900
H	-9.03697367	-1.44763266	1.21986200
H	-8.34283467	-0.42699966	-0.08475900
Si	-6.36241567	-2.66487466	0.73318700
Ag	0.52128233	-0.63850866	0.57728700
Ag	-4.40429467	2.53340034	0.14865100
Sb	-7.15977267	2.88046534	-2.08736300
Sb	3.05810533	-0.16627366	-1.71577600
F	-5.23851167	2.81880134	-2.28102600
F	-7.39799367	2.51811434	-3.93410600
F	-7.14986767	4.75840434	-2.40349600
F	-9.02756467	2.90278934	-1.75213900
F	-7.09841967	1.00037234	-1.68835600
F	-6.79835367	3.19438634	-0.20523200
F	1.14498733	0.10698834	-1.83240400
F	3.35743033	1.27442434	-2.91737800
F	2.94574633	-1.42966966	-3.13244400
F	2.60546233	-1.54714666	-0.42837100
F	4.91087933	-0.50509066	-1.49000700
F	3.05657833	1.04504134	-0.22921600
C	1.74336533	5.15488734	-1.91044500
H	2.46852933	5.95910334	-2.10650800
H	2.27223033	4.19323034	-1.99752600
H	0.97316433	5.19174834	-2.69506700
C	3.34789433	4.33412534	0.87440200
H	4.07135733	4.29734534	1.70696800
H	2.91127633	3.32822534	0.76646100
H	3.91432033	4.53941034	-0.04703300
C	2.97800933	6.79913834	1.10340100
H	3.79527333	6.83420234	1.84406900
H	3.41815733	7.01747134	0.11720300
H	2.27308833	7.60866434	1.34811900
C	1.64784633	5.21122934	2.50871400
H	2.41073333	5.26517734	3.30414600
H	0.89069033	5.98252134	2.72326600
H	1.15367233	4.22994034	2.57961700

M06-2X(PCM:DCM)/def2-SVP: -4191.56466

M06-2X(PCM:DCM)/def2-QVPP: -4195.53054

$G_{corr.}$: 0.805958

TS I f:

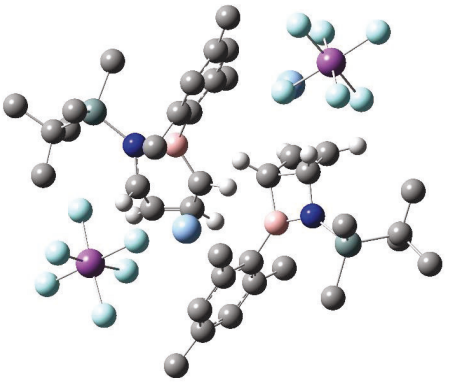

C	-0.44170904	1.04651168	-0.01156656
C	-1.91309004	0.54491568	0.17897744
C	-0.12715704	0.37390868	1.31838944
H	0.74359396	0.39564168	1.97757144
C	-1.40625104	-0.05911632	1.47270244
H	-1.92071404	-0.55287932	2.30442244
H	0.13807896	0.76536668	-0.89776756
H	-2.38624804	-0.10936232	-0.56654456
C	-3.50790804	3.00495868	0.19190544
C	-4.12209404	3.39299568	-1.02619856
C	-4.12108104	3.35742768	1.41891244
C	-5.32850804	4.10305068	-0.99494556
C	-5.32521104	4.07064668	1.41066844
C	-5.94657104	4.44534768	0.21340444
H	-5.81772304	4.36498268	-1.93593856
H	-5.79849704	4.32635168	2.36200644
B	-2.18989704	2.14489368	0.18095044
C	-3.45851804	2.97002068	2.71747244
H	-2.50175504	3.50140968	2.83864644
H	-4.09359604	3.20394668	3.58101144
H	-3.22831204	1.89196568	2.74496544
C	-3.46582304	3.06064168	-2.34377756
H	-2.58674804	3.70345568	-2.50962856
H	-3.11183904	2.01830168	-2.37076256
H	-4.16146304	3.20309868	-3.17917656
C	-7.25832704	5.18152268	0.20594444
H	-7.12217804	6.21382668	-0.14997356
H	-7.95997304	4.68613168	-0.47884456
H	-7.70104604	5.22099768	1.20915944
N	-0.83081604	2.47237768	0.06384144
Si	0.15666896	3.93210468	-0.18621856
C	-6.84987704	-1.24433032	1.08778044
C	-4.97500904	-0.65650332	1.82024544

C	-7.14793604	-0.73029332	2.44700944
H	-8.06673604	-0.92647532	3.00094244
C	-5.95183104	-0.26361332	2.84293644
H	-5.69147004	0.21341168	3.79104344
H	-7.14393704	-0.68704832	0.18355544
H	-4.03443904	-0.09494632	1.70259844
C	-3.86098004	-2.59292232	0.21700244
C	-3.69065004	-2.33595232	-1.15933556
C	-2.93492904	-3.42303832	0.88050944
C	-2.61283804	-2.90443832	-1.84763056
C	-1.87231704	-4.00216432	0.15919544
C	-1.69624904	-3.75183632	-1.21583356
H	-2.48567104	-2.68847032	-2.91152156
H	-1.21024004	-4.71482432	0.66287044
B	-5.06490104	-2.00366032	1.06733744
C	-3.10362904	-3.73237632	2.34813244
H	-4.04700704	-4.27248232	2.52294044
H	-2.28119804	-4.35358132	2.72511744
H	-3.14869504	-2.81098832	2.94789244
C	-4.61246204	-1.40239932	-1.90394256
H	-5.62384504	-1.37264032	-1.47557856
H	-4.20756304	-0.37418632	-1.90842556
H	-4.71308104	-1.69074332	-2.95919556
C	-0.58885304	-4.40668332	-1.99831856
H	-0.99854304	-5.20572232	-2.63438156
H	-0.08884604	-3.68176432	-2.65430056
H	0.16603196	-4.84863432	-1.33564756
N	-6.42458904	-2.55530832	0.99381244
C	-6.07639904	-5.42650132	0.64632344
H	-6.46526404	-6.34973332	0.19085644
H	-5.03085304	-5.30724032	0.32184644
H	-6.09477804	-5.54561232	1.73930244
C	-8.90854604	-4.06625732	0.65393644
Si	-7.09663804	-3.95708732	0.09722444
Ag	-0.26181304	-2.09538132	0.56321344
Ag	-5.24225704	1.09527168	0.00348144
Sb	-8.05011804	1.38646468	-2.15044256
Sb	2.28813996	-1.58972332	-1.70215356
F	-6.12932104	1.40857468	-2.37807256
F	-8.30214104	1.10585968	-4.00903656
F	-8.09976104	3.27810168	-2.36552456
F	-9.91222104	1.32562268	-1.79410756
F	-7.91013504	-0.50906332	-1.84437656
F	-7.67180004	1.61388468	-0.25983356
F	0.37534596	-1.31449232	-1.82646456
F	2.59304896	-0.12134032	-2.86853056
F	2.18690296	-2.82128532	-3.14695256
F	1.82669796	-2.99705232	-0.44694756
F	4.13958896	-1.93186532	-1.47137556
F	2.27640696	-0.41090032	-0.18958156

C	1.49873596	3.99378068	1.15562844
C	-6.98270204	-3.73708832	-1.76072856
H	-7.53423004	-4.55094932	-2.25593456
H	-7.40587004	-2.77704032	-2.09117856
H	-5.93495204	-3.79490332	-2.09035556
C	-9.63176604	-2.74803632	0.34321844
H	-10.70830804	-2.84827532	0.56244944
H	-9.26221104	-1.91630232	0.96513344
H	-9.52978004	-2.44719432	-0.71104756
C	-9.59464004	-5.20907132	-0.10955956
H	-10.63144404	-5.32949532	0.24698844
H	-9.63864904	-5.00931632	-1.19082756
H	-9.07986604	-6.17155432	0.03974144
C	-8.97574404	-4.34489332	2.16105844
H	-8.53847004	-5.32347132	2.41246044
H	-8.43883604	-3.57642232	2.73939144
H	-10.02559304	-4.35211932	2.49984744
C	-1.03307904	5.37475468	-0.06252656
H	-1.84281504	5.27891368	-0.80150956
H	-1.49323304	5.42810568	0.93598344
H	-0.50963204	6.32333968	-0.25287056
C	0.92526396	3.78723568	-1.89182856
H	1.63947796	4.60370068	-2.07687956
H	1.46400096	2.83366968	-2.00364956
H	0.14742196	3.83182768	-2.66851556
C	2.55457796	2.91526068	0.86950244
H	3.28594996	2.87187868	1.69479044
H	2.12416196	1.90766268	0.75221044
H	3.11116396	3.13758068	-0.05396856
C	0.86090696	3.75450868	2.53005944
H	1.62952796	3.79798768	3.32057444
H	0.10220696	4.51857168	2.76415144
H	0.37203096	2.76970568	2.58774144
C	2.17107396	5.37391468	1.14217444
H	2.99216596	5.40225168	1.87884944
H	2.60431096	5.61081568	0.15724844
H	1.46244096	6.17487468	1.40380944

M06-2X(PCM:DCM)/def2-SVP: -4191.56822

M06-2X(PCM:DCM)/def2-QVPP: -4195.53399

$G_{corr.}$: 0.807146

II a:

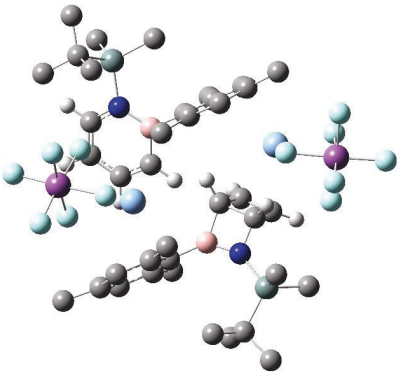

C	-0.79844960	3.23255830	0.00000000
C	-2.25153660	2.81209030	0.39518300
C	-0.35538160	2.70110130	1.35273800
H	0.57673240	2.78872230	1.91510200
C	-1.62192560	2.32573730	1.68130300
H	-2.05429760	1.93545930	2.60872100
H	-0.33211460	2.83636430	-0.90881500
H	-2.81753960	2.09689330	-0.21657000
C	-3.79360860	5.27338230	0.15764300
C	-4.35832760	5.59662330	-1.10294400
C	-4.46166760	5.68084730	1.33860400
C	-5.54992560	6.32482030	-1.15750400
C	-5.64928560	6.41584130	1.24254300
C	-6.20841460	6.74380330	0.00302600
H	-5.99961060	6.53608330	-2.13127600
H	-6.16299460	6.71821830	2.15863600
B	-2.47758160	4.41281230	0.22130100
C	-3.88584960	5.32289030	2.68755800
H	-3.61957960	4.25437330	2.73578700
H	-2.96311460	5.88909230	2.88783100
H	-4.59613960	5.53576030	3.49650500
C	-3.67727960	5.16123630	-2.37705800
H	-2.79124260	5.78383230	-2.57662000
H	-3.32995360	4.11876230	-2.31420100
H	-4.35716160	5.24095930	-3.23354000
C	-7.51647260	7.47809830	-0.10365300
H	-7.37961860	8.45553730	-0.58933300
H	-8.21671560	6.89568230	-0.71907700
H	-7.96715860	7.64262430	0.88319400
N	-1.12242360	4.67780030	-0.04071700
C	-0.49019260	7.64055330	-0.11783700
Si	0.13736440	5.87769630	-0.43535800
C	-7.75150760	0.28728630	1.54210900

C	-5.25772160	1.52291030	1.84497500
C	-7.65144760	1.44577330	2.27068000
H	-8.54648860	1.86229830	2.72908200
C	-6.38801760	2.05579730	2.45007000
H	-6.31681360	2.93069230	3.10593400
H	-8.73106460	-0.18916770	1.45972600
H	-4.28553160	1.95895930	2.09760600
C	-4.10213960	-0.37270670	0.29439000
C	-3.79059160	-0.11919670	-1.05736100
C	-3.22472660	-1.17123970	1.05629900
C	-2.65080860	-0.69059070	-1.63598000
C	-2.09245760	-1.74880070	0.45068300
C	-1.79733960	-1.52970870	-0.91080500
H	-2.42256560	-0.48484670	-2.68490500
H	-1.46776060	-2.43787370	1.02902100
B	-5.38409560	0.25760230	0.98945300
C	-3.52619260	-1.46322270	2.50566200
H	-4.49592060	-1.97699370	2.60696500
H	-2.75504460	-2.09994370	2.95779200
H	-3.60046260	-0.53589470	3.09303300
C	-4.64262060	0.80395330	-1.89323000
H	-5.65569860	0.92374330	-1.48651200
H	-4.18554860	1.80860830	-1.95698000
H	-4.73358060	0.44390430	-2.92750100
C	-0.63712960	-2.21838070	-1.58064000
H	-0.97724860	-3.15281070	-2.05283800
H	-0.19772860	-1.58487570	-2.36065200
H	0.15252140	-2.47409370	-0.86125700
N	-6.70857660	-0.33637670	0.91740900
C	-5.66769260	-2.97288770	-0.29396200
H	-6.04017260	-3.95881770	-0.61311200
H	-5.07561160	-2.54099470	-1.11126400
H	-5.00329960	-3.13298470	0.56642400
C	-8.03927060	-2.86647970	1.58868200
H	-7.43160860	-2.80837370	2.50467300
H	-9.03889660	-2.46855070	1.81498100
H	-8.15295060	-3.92886470	1.32674100
C	-8.33871560	-1.75306670	-1.30416500
C	-7.61420060	-1.10909770	-2.49358000
H	-8.26180760	-1.14784870	-3.38629400
H	-7.39317760	-0.05222070	-2.29718600
H	-6.67519660	-1.62863370	-2.74318900
C	-8.78511360	-3.17382470	-1.69674900
H	-9.32488560	-3.67865170	-0.88060900
H	-9.46932060	-3.11528770	-2.55957400
H	-7.93730160	-3.81006570	-1.99342400
C	-9.58702660	-0.92351170	-0.97216800
H	-10.26751860	-0.92613770	-1.84080300
H	-10.14766760	-1.33946070	-0.11926400
H	-9.33423060	0.12397330	-0.75663900

Si	-7.16986060	-1.96402870	0.18615900
Ag	-0.53314060	0.23222530	0.75668700
Ag	-5.51399760	3.27167030	0.12805400
Sb	-8.22488660	3.36694830	-1.87029600
Sb	2.09422440	0.70424230	-1.57850400
F	-6.33233760	3.54788330	-2.24084900
F	-8.46102160	2.41269930	-3.49420800
F	-8.57007860	5.04304930	-2.69663600
F	-10.04494260	3.11927730	-1.39173200
F	-7.72215260	1.75548430	-0.93900500
F	-7.86746660	4.26596230	-0.19698700
F	0.17236740	0.83582530	-1.74460400
F	2.33672640	1.87592330	-3.05532900
F	2.07766040	-0.82224770	-2.71349200
F	1.69739940	-0.42435870	-0.04839100
F	3.95858740	0.50992430	-1.28125000
F	2.03495940	2.20718730	-0.39110800
C	0.61415840	5.58934830	-2.22868100
H	1.37886340	6.31095730	-2.55361100
H	1.03951440	4.57975030	-2.34288700
H	-0.25063860	5.67611530	-2.90248000
C	1.59593040	5.43693030	0.65985200
H	1.89860540	4.39731430	0.45669700
H	2.45835840	6.08401230	0.44136000
H	1.35171940	5.53160530	1.72873300
C	-1.10708060	7.73889830	1.28265400
H	-0.41298360	7.39910430	2.06781500
H	-1.37643860	8.78549730	1.50513600
H	-2.02715360	7.13911930	1.35095300
C	0.71641840	8.58802730	-0.21260000
H	1.21427940	8.52530930	-1.19341800
H	0.38372140	9.63097330	-0.07697800
H	1.46641740	8.37410430	0.56400300
C	-1.53805160	8.05263330	-1.15913900
H	-1.14743560	7.98586530	-2.18675400
H	-2.44324060	7.42996830	-1.08906100
H	-1.84639460	9.09835830	-0.98805300

M06-2X(PCM:DCM)/def2-SVP: -4191.69296

M06-2X(PCM:DCM)/def2-QVPP: -4195.655025

$G_{corr.}$: 0.814739

II b:

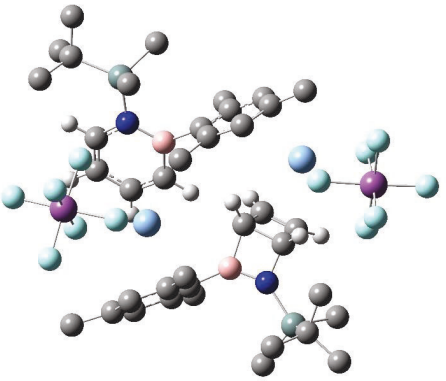

C	-1.71317827	3.75969011	0.00000000
C	-3.21121627	3.33829911	0.16468100
C	-1.44892327	3.07897011	1.33165100
H	-0.59050327	3.07553211	2.00687500
C	-2.75147027	2.70795711	1.46325200
H	-3.29532427	2.23544511	2.28809700
H	-1.13683527	3.44879511	-0.87574000
H	-3.70753427	2.70945611	-0.58591800
C	-4.69167927	5.84919511	0.10763200
C	-5.32954727	6.16262511	-1.11689800
C	-5.29446627	6.25790811	1.32500800
C	-6.55230527	6.85503511	-1.10120000
C	-6.50189927	6.95857111	1.29979700
C	-7.15223227	7.25846311	0.09319700
H	-7.06174127	7.05282311	-2.04800600
H	-6.96379127	7.25847211	2.24403500
B	-3.39849227	4.95187711	0.14562700
C	-4.63187927	5.90215911	2.63240000
H	-3.62402127	6.33933911	2.69479700
H	-5.21569027	6.25648611	3.49103400
H	-4.51261627	4.81016611	2.72816000
C	-4.73364727	5.76752511	-2.44730800
H	-4.42391627	6.66199411	-3.00759100
H	-3.84879227	5.12373311	-2.33407500
H	-5.47856527	5.23843511	-3.05807200
C	-8.47232227	7.97980311	0.07101200
H	-8.33120327	9.04050011	-0.18739900
H	-9.13170227	7.53437411	-0.68577700
H	-8.96776327	7.93392811	1.04938100
N	-2.01875027	5.20484111	0.07414900
Si	-0.79824027	6.49911811	0.10250900
C	-8.95901427	1.27462711	0.95691000
C	-6.37179927	2.14401611	1.57140600

C	-8.78127827	2.30607011	1.84654300
H	-9.65695727	2.78868611	2.27606900
C	-7.47624227	2.73201811	2.17770300
H	-7.35251027	3.51968511	2.92886900
H	-9.97488727	0.98185511	0.70620800
H	-5.37857227	2.46233111	1.89979600
C	-5.32039927	0.32674511	-0.13746600
C	-4.94835527	0.66987911	-1.45597900
C	-4.49800927	-0.56090489	0.58767300
C	-3.81366827	0.09471811	-2.04090600
C	-3.37419327	-1.14443489	-0.02843900
C	-3.02263127	-0.83680789	-1.35855500
H	-3.54102727	0.37068611	-3.06294000
H	-2.80155227	-1.90488689	0.51320600
B	-6.57527627	0.99791211	0.57634500
C	-4.83143427	-0.91792889	2.01538500
H	-5.87601927	-1.25168089	2.10426300
H	-4.18081227	-1.71736689	2.39238900
H	-4.72144327	-0.04501189	2.67699200
C	-5.71357727	1.70833111	-2.24080500
H	-6.74302727	1.84185311	-1.88078500
H	-5.20236327	2.68644111	-2.19132400
H	-5.76697027	1.44942411	-3.30742800
C	-1.87313027	-1.52573189	-2.04782500
H	-2.25313727	-2.32390389	-2.70346200
H	-1.30450327	-0.82305589	-2.66987900
H	-1.18398327	-1.98446289	-1.32581300
N	-7.95331127	0.58514511	0.34816700
C	-7.46077827	-2.33864389	-0.04242000
H	-7.72044227	-3.22814689	-0.63504200
H	-6.37868227	-2.18011589	-0.14370900
H	-7.69133327	-2.55145189	1.01218300
C	-10.30206927	-1.25918689	-0.56035500
Si	-8.42830227	-0.86751989	-0.69085400
Ag	-1.66620827	0.67614511	0.46544300
Ag	-6.56191627	3.95848711	-0.07297300
Sb	-9.41422127	4.17962111	-2.12204700
Sb	1.11462873	1.23971111	-1.66103800
F	-7.50203627	4.23484811	-2.42098000
F	-9.71742427	3.74165711	-3.94441300
F	-9.52587127	6.04257711	-2.51083100
F	-11.26374327	4.08393111	-1.70134000
F	-9.19819827	2.32122711	-1.68830100
F	-8.99097627	4.61763711	-0.28620700
F	-0.78862727	1.49563611	-1.89747700
F	1.49190273	2.47063711	-3.05795600
F	1.04891373	-0.21707289	-2.88291500
F	0.58564873	0.04529611	-0.22231300
F	2.94919573	0.91067511	-1.30352900
F	1.09425173	2.66775011	-0.38210200

C	-0.17539727	6.79787511	-1.66753600
C	0.58115473	5.84235811	1.19081400
H	0.99499073	4.91290211	0.76684100
H	1.39819273	6.57231111	1.28623100
H	0.19926573	5.62425111	2.19989500
C	-8.00140527	-0.54286389	-2.48496600
H	-8.49390927	-1.30371689	-3.10833400
H	-8.35119927	0.44858011	-2.80230900
H	-6.91988027	-0.62236489	-2.65766100
C	-11.17199527	-0.21844889	-1.28665100
H	-12.23110027	-0.52185689	-1.23092100
H	-11.09057427	0.80008111	-0.88271200
H	-10.90056127	-0.15658889	-2.35171600
C	-10.48276627	-2.60069089	-1.30485600
H	-11.55783527	-2.83939689	-1.35422000
H	-10.10867227	-2.56839689	-2.33892700
H	-9.98509527	-3.43136089	-0.78399000
C	-10.79591827	-1.49469089	0.87752500
H	-10.16747527	-2.23074189	1.40260800
H	-10.83047527	-0.58721889	1.49445100
H	-11.82046127	-1.90230789	0.84697200
C	-1.63654727	8.01738511	0.81107000
H	-2.59594327	8.20131211	0.30298300
H	-1.83333427	7.88555111	1.88524400
H	-1.00723727	8.91156511	0.68838800
C	1.13675773	7.59253611	-1.60996900
H	1.94142373	7.01129911	-1.13436100
H	1.46928473	7.84742911	-2.63068700
H	1.02445573	8.53772111	-1.05379400
C	0.07074273	5.45522911	-2.37111200
H	0.72957673	4.78607011	-1.79485000
H	-0.87505027	4.92003311	-2.55324600
H	0.54711973	5.62189611	-3.35223700
C	-1.22722827	7.59641211	-2.44681200
H	-2.20435727	7.08801311	-2.43947500
H	-1.36702127	8.60472711	-2.02737600
H	-0.91840627	7.71124611	-3.49995600

M06-2X(PCM:DCM)/def2-SVP: -4191.69178

M06-2X(PCM:DCM)/def2-QVPP: -4195.65340

$G_{corr.}$: 0.812659

II c:

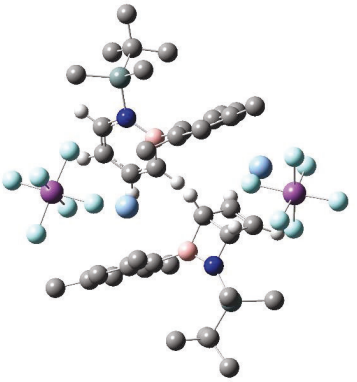

C	-0.50387596	2.70542649	0.00000000
C	-1.97238596	2.26539149	0.31059400
C	-0.10671496	2.03967249	1.30667700
H	0.80618704	2.06653149	1.90597600
C	-1.38565896	1.64483749	1.55723900
H	-1.84898696	1.16234749	2.42458100
H	-0.01574896	2.39251549	-0.92959100
H	-2.53064496	1.62599349	-0.38573100
C	-3.48379796	4.75179449	0.24865700
C	-3.99005796	5.18692449	-1.00458700
C	-4.22115596	5.03127149	1.42443300
C	-5.19006096	5.89880049	-1.05451900
C	-5.42609196	5.74444649	1.33338600
C	-5.92427096	6.18455549	0.10385900
H	-5.59457296	6.19519749	-2.02495800
H	-5.99614896	5.94256649	2.24483700
B	-2.17439496	3.87904649	0.28589000
C	-3.70622696	4.58165249	2.77023800
H	-3.15206196	3.63323449	2.69365600
H	-3.01397496	5.32624849	3.19309100
H	-4.52636596	4.44792549	3.48797600
C	-3.24666896	4.86059649	-2.27576400
H	-2.30065496	5.42060149	-2.33146600
H	-2.99244996	3.79042849	-2.32715000
H	-3.84928096	5.10572249	-3.15834100
C	-7.23656196	6.91113849	-0.00140500
H	-7.07954396	7.95664849	-0.30645200
H	-7.86249996	6.43302249	-0.76736400
H	-7.77430396	6.90962449	0.95518400
N	-0.80952596	4.15139749	0.09044000
C	-0.15433996	7.09432849	0.33802200
Si	0.47296004	5.36882949	-0.14249700
C	-7.58859296	-0.10482451	0.77694500

C	-5.09995196	0.87127749	1.62773100
C	-7.53609296	0.92881949	1.67779500
H	-8.46474996	1.36785649	2.03734100
C	-6.28105796	1.40328349	2.13076700
H	-6.26409596	2.17847049	2.90490800
H	-8.56792696	-0.46038451	0.44909200
H	-4.15459096	1.21881649	2.05713800
C	-3.84076796	-0.88450551	-0.02862300
C	-3.48974096	-0.57432651	-1.36874900
C	-2.97141196	-1.69498251	0.72240800
C	-2.33945196	-1.11588351	-1.94004800
C	-1.83348696	-2.26640951	0.10748200
C	-1.51030296	-2.00216351	-1.23342000
H	-2.08468896	-0.86684551	-2.97324000
H	-1.22435996	-2.97931151	0.67441200
B	-5.16254896	-0.27027251	0.60611600
C	-3.19564996	-2.00148351	2.18471000
H	-4.08608196	-1.50048851	2.58402400
H	-3.30725796	-3.08322551	2.34816700
H	-2.32942696	-1.67345051	2.77928700
C	-4.32233296	0.38035349	-2.18989600
H	-5.39127296	0.35420449	-1.93388800
H	-3.98616696	1.42247649	-2.04039000
H	-4.21878096	0.17672149	-3.26441200
C	-0.35271396	-2.67976151	-1.91893100
H	-0.72645596	-3.46842651	-2.58938300
H	0.21820904	-1.96899351	-2.53023500
H	0.32864804	-3.14641051	-1.19528500
N	-6.49600796	-0.73712651	0.25396900
C	-5.59250496	-2.81654651	-1.88460600
H	-6.01210796	-3.68091651	-2.42354700
H	-5.35782796	-2.04641651	-2.63148900
H	-4.66083196	-3.12807551	-1.39477100
C	-7.27427996	-3.61016651	0.58596000
Si	-6.92862596	-2.25216851	-0.70308200
Ag	-0.22042996	-0.34653451	0.46750000
Ag	-5.26921896	2.81841549	0.10591900
Sb	-7.74366496	3.16106049	-2.33298900
Sb	2.40554204	0.33799449	-1.79620600
F	-5.80821596	3.12770149	-2.33154600
F	-7.77920596	2.74610049	-4.18530000
F	-7.72437596	5.02892849	-2.71295500
F	-9.63784096	3.15954949	-2.20598200
F	-7.68140396	1.29658749	-1.88488900
F	-7.58992296	3.56398749	-0.44456700
F	0.48113104	0.46399549	-1.95205400
F	2.63645004	1.62932749	-3.17106500
F	2.39305704	-1.09196251	-3.05131300
F	2.02074904	-0.91684551	-0.36454500
F	4.27164004	0.13502549	-1.51843800

F	2.32954504	1.73380049	-0.48570100
C	1.00592204	5.26267049	-1.94007900
H	1.79862304	5.99445849	-2.15739100
H	1.41237604	4.26026249	-2.14781900
H	0.17022304	5.44465949	-2.63122400
C	1.89456704	4.80344649	0.94380500
H	2.19581104	3.78738349	0.64341500
H	2.76754604	5.46092949	0.81730500
H	1.61966304	4.79088849	2.00923500
C	-0.80579696	7.04968549	1.72569800
H	-0.12404896	6.64573349	2.49090900
H	-1.09646496	8.06645349	2.04065000
H	-1.71670396	6.43209149	1.71577100
C	1.05641904	8.04032149	0.37162900
H	1.57463604	8.08058349	-0.59975900
H	0.72401704	9.06443949	0.61157400
H	1.78917104	7.74042549	1.13618300
C	-1.17365396	7.61660549	-0.68211600
H	-0.75666296	7.65153749	-1.70091100
H	-2.08294096	6.99634949	-0.69957900
H	-1.48201396	8.64175749	-0.41393000
C	-8.46238796	-1.84050151	-1.70114200
H	-8.56486096	-2.57763851	-2.51124500
H	-9.38921996	-1.86307751	-1.11050400
H	-8.35993296	-0.84125251	-2.14858000
C	-8.41977296	-3.22042551	1.52887700
H	-8.62663596	-4.05131951	2.22452800
H	-8.16897096	-2.33897451	2.13899600
H	-9.35282396	-3.00816551	0.98380300
C	-7.66350296	-4.88755851	-0.17480600
H	-7.89941696	-5.69229251	0.54168400
H	-8.55369296	-4.73403851	-0.80530500
H	-6.84664596	-5.24769051	-0.81829400
C	-6.01207796	-3.86532551	1.41599600
H	-5.14411696	-4.12297351	0.78746900
H	-5.74894996	-2.97986051	2.01404800
H	-6.17756496	-4.70105851	2.11729700

M06-2X(PCM:DCM)/def2-SVP: -4191.69333

M06-2X(PCM:DCM)/def2-QVPP: -4195.65730

$G_{corr.}$: 0.815316

II d:

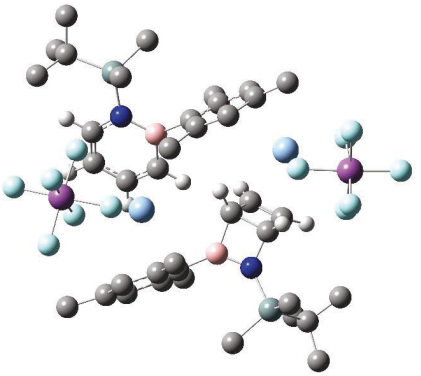

C	-0.19379845	2.28682182	0.00000000
C	-1.67336245	1.86615282	0.29666600
C	0.16029255	1.70264582	1.36070400
H	1.06292755	1.73443182	1.97516200
C	-1.12703845	1.34310582	1.60967300
H	-1.61299845	0.94155082	2.50534800
H	0.32940555	1.91512482	-0.88816800
H	-2.20114845	1.17314982	-0.37278300
C	-3.18644645	4.35910582	0.11330600
C	-3.84255145	4.60010582	-1.11982500
C	-3.75552545	4.86016582	1.30907600
C	-5.05674645	5.30252582	-1.12897400
C	-4.95722345	5.57146182	1.25888400
C	-5.62930645	5.79088682	0.04906000
H	-5.58490745	5.44121482	-2.07562000
H	-5.39583845	5.94251882	2.18881200
B	-1.88930345	3.46928182	0.16574800
C	-3.05712045	4.60329282	2.62094100
H	-2.05933345	5.06870082	2.63221200
H	-3.63048245	4.99710882	3.46946300
H	-2.90687045	3.52273282	2.78218500
C	-3.23122745	4.13900582	-2.42079700
H	-2.52514145	4.89472482	-2.80037500
H	-2.66507245	3.20248982	-2.30225200
H	-4.00417145	3.97919282	-3.18273600
C	-6.94757545	6.51411382	0.00196300
H	-6.81775045	7.53528282	-0.38778000
H	-7.63929545	5.98621782	-0.66820900
H	-7.39914845	6.58683682	0.99961800
N	-0.52289445	3.72984982	-0.02068000
Si	0.51089655	5.11657482	-0.43779700
C	-7.39754445	-0.04028118	1.47575500
C	-4.76543945	0.80447482	1.91040700

C	-7.15747845	1.07011982	2.24844700
H	-8.00264645	1.62117382	2.65623400
C	-5.82976445	1.48635282	2.48883300
H	-5.65665145	2.34339182	3.14875900
H	-8.42982745	-0.32602718	1.29333000
H	-3.75166745	1.12422682	2.16806600
C	-3.82711745	-1.19592218	0.35188300
C	-3.50927045	-0.99193618	-1.00881200
C	-2.98156945	-2.01765518	1.12714700
C	-2.41026445	-1.64284218	-1.58230900
C	-1.88977545	-2.67326318	0.52633500
C	-1.59774845	-2.50979718	-0.84325600
H	-2.18109245	-1.47568018	-2.63788900
H	-1.29756845	-3.37884918	1.11852900
B	-5.03784845	-0.42832218	1.04464400
C	-3.25169745	-2.22166818	2.59748900
H	-4.29572645	-2.52332718	2.76851400
H	-2.59600145	-2.99191618	3.02330300
H	-3.09578545	-1.28865218	3.16051100
C	-4.29430045	-0.02198718	-1.85856900
H	-5.31225245	0.14817782	-1.48219200
H	-3.77745645	0.95389682	-1.90923300
H	-4.37916745	-0.37033818	-2.89726000
C	-0.48767845	-3.28177518	-1.50753100
H	-0.89852145	-4.17168118	-2.00843000
H	0.01903555	-2.67313818	-2.26707200
H	0.26219755	-3.61943118	-0.77982700
N	-6.43467845	-0.81809418	0.90540000
C	-6.03140145	-3.77372818	0.83324400
H	-6.33904245	-4.72138018	0.36743100
H	-4.95105645	-3.66161818	0.66916400
H	-6.22009645	-3.84645318	1.91478100
C	-8.86265145	-2.67753218	0.28213000
Si	-6.98467245	-2.36060118	0.04903200
Ag	-0.17320645	-0.79843118	0.74086600
Ag	-4.95578945	2.42443582	0.06227200
Sb	-7.87686745	2.55149582	-1.89006600
Sb	2.44366455	-0.53073418	-1.57318400
F	-5.97733045	2.53782282	-2.26452100
F	-8.25921645	1.98210782	-3.66053700
F	-7.96645645	4.38226182	-2.41576000
F	-9.71173845	2.53721082	-1.39820700
F	-7.69293245	0.72752282	-1.31675400
F	-7.37457645	3.11303682	-0.10918800
F	0.53795155	-0.21770918	-1.70412300
F	2.76946255	0.70352482	-2.98028200
F	2.27326055	-1.97834318	-2.79538900
F	1.96427755	-1.70347918	-0.10073100
F	4.28685355	-0.90397918	-1.32062200
F	2.52209255	0.89138882	-0.29301800

C	1.87681655	5.27286682	0.87176900
C	-6.61048745	-2.25386918	-1.78258200
H	-7.13232745	-3.07423618	-2.29705700
H	-6.95709045	-1.30041518	-2.20328500
H	-5.53616645	-2.37092718	-1.97758000
C	-9.73110445	-1.68946518	-0.51593100
H	-10.79436845	-1.95992418	-0.40107100
H	-9.61667445	-0.63938718	-0.21373800
H	-9.49108945	-1.73582618	-1.58917800
C	-9.10955945	-4.08053218	-0.31547800
H	-10.19062545	-4.29450718	-0.28794900
H	-8.78893845	-4.15816418	-1.36483900
H	-8.60366045	-4.86959018	0.25939300
C	-9.30639145	-2.75075518	1.75326100
H	-8.68603845	-3.45861518	2.32459600
H	-9.27968445	-1.78709218	2.27859400
H	-10.34638845	-3.11529918	1.80089200
C	-0.62570945	6.60642782	-0.45295500
H	-1.44871445	6.45952882	-1.16844100
H	-1.06881145	6.78111482	0.53944600
H	-0.07395445	7.51086082	-0.74892900
C	1.24032755	4.75690782	-2.12871100
H	1.97734955	5.52121182	-2.41767000
H	1.74474955	3.77821782	-2.14063400
H	0.44604955	4.74116882	-2.88995700
C	2.90434255	4.14885982	0.67236800
H	3.64584055	4.16272882	1.48965700
H	2.44878855	3.14587282	0.65030600
H	3.45277955	4.27296382	-0.27415600
C	1.25689155	5.17395082	2.27141800
H	2.03805855	5.28045682	3.04345800
H	0.51164255	5.96746682	2.44306000
H	0.75644355	4.20566582	2.42770100
C	2.57739255	6.63057082	0.72099100
H	3.41415855	6.70642482	1.43640500
H	2.99483355	6.76846282	-0.28942900
H	1.89116955	7.46764782	0.92238400

M06-2X(PCM:DCM)/def2-SVP: -4191.69182

M06-2X(PCM:DCM)/def2-QVPP: -4195.65478

$G_{corr.}$: 0.810421

II e:

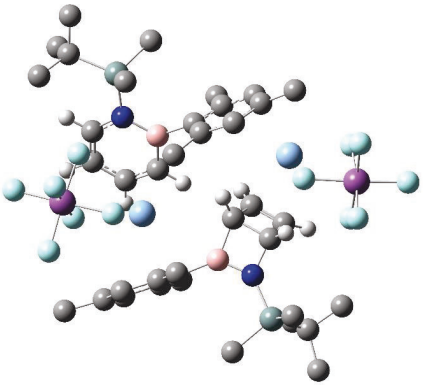

C	0.81395348	2.33333345	0.00000000
C	-0.66564352	1.91265245	0.29646100
C	1.16787748	1.74908145	1.36071400
H	2.07044548	1.78081545	1.97527400
C	-0.11947952	1.38952645	1.60950400
H	-0.60554552	0.98790545	2.50509000
H	1.33724948	1.96169145	-0.88813100
H	-1.19334152	1.21967845	-0.37308900
C	-2.17865152	4.40568445	0.11302800
C	-2.83464852	4.64668645	-1.12016000
C	-2.74777652	4.90684045	1.30873700
C	-4.04879152	5.34919445	-1.12942400
C	-3.94941852	5.61822145	1.25842900
C	-4.62139952	5.83764445	0.04854800
H	-4.57687252	5.48788545	-2.07611500
H	-4.38807252	5.98935045	2.18830900
B	-0.88155352	3.51579945	0.16559000
C	-2.04947952	4.64998345	2.62066300
H	-1.05170252	5.11541345	2.63201900
H	-2.62292152	5.04379145	3.46913300
H	-1.89921652	3.56942745	2.78192300
C	-2.22325952	4.18551445	-2.42107500
H	-1.51723252	4.94126345	-2.80070400
H	-1.65702852	3.24905545	-2.30243900
H	-2.99617652	4.02557245	-3.18301500
C	-5.93961552	6.56096045	0.00132600
H	-5.80971052	7.58206345	-0.38856100
H	-6.63135952	6.03302045	-0.66878800
H	-6.39120252	6.63385545	0.99896100
N	0.48487848	3.77636145	-0.02066100
Si	1.51875148	5.16300145	-0.43785300
C	-6.39008352	0.00680545	1.47549800
C	-3.75793352	0.85135745	1.91026000

C	-6.14996452	1.11720145	2.24818100
H	-6.99510852	1.66832745	2.65592100
C	-4.82223252	1.53333845	2.48861300
H	-4.64908152	2.39038545	3.14851700
H	-7.42238152	-0.27886755	1.29304300
H	-2.74414952	1.17104145	2.16796000
C	-2.81968052	-1.14918455	0.35187500
C	-2.50172152	-0.94532855	-1.00881800
C	-1.97426452	-1.97094255	1.12725000
C	-1.40277352	-1.59641555	-1.58220500
C	-0.88250752	-2.62672155	0.52655200
C	-0.59041352	-2.46342855	-0.84304400
H	-1.17353152	-1.42937455	-2.63778800
H	-0.29041952	-3.33233055	1.11883600
B	-4.03039352	-0.38143655	1.04451200
C	-2.24448152	-2.17480455	2.59759800
H	-3.28860852	-2.47612355	2.76862700
H	-1.58903352	-2.94523955	3.02345600
H	-2.08827552	-1.24181555	3.16058300
C	-3.28658952	0.02463845	-1.85870300
H	-4.30456352	0.19490645	-1.48243300
H	-2.76965952	1.00047745	-1.90938300
H	-3.37139152	-0.32376955	-2.89738000
C	0.51951148	-3.23568155	-1.50724800
H	0.10844748	-4.12545155	-2.00821100
H	1.02644848	-2.62718155	-2.26675800
H	1.26923248	-3.57357055	-0.77950000
N	-5.42725552	-0.77108655	0.90519100
C	-5.02440352	-3.72672555	0.83352500
H	-5.33213852	-4.67445155	0.36792400
H	-3.94401952	-3.61482455	0.66954300
H	-5.21322852	-3.79913855	1.91506100
C	-7.85540352	-2.63021555	0.28162800
Si	-5.97732752	-2.31360255	0.04888200
Ag	0.83448648	-0.75207355	0.74077900
Ag	-3.94802852	2.47109445	0.06194000
Sb	-6.86901252	2.59827645	-1.89056000
Sb	3.45038848	-0.48414455	-1.57402300
F	-4.96945952	2.58452545	-2.26493500
F	-7.25131852	2.02889445	-3.66104200
F	-6.95851652	4.42904045	-2.41627800
F	-8.70390152	2.58405845	-1.39876300
F	-6.68517252	0.77429945	-1.31723100
F	-6.36677052	3.15982245	-0.10967000
F	1.54462048	-0.17098155	-1.70401100
F	3.77552748	0.75129945	-2.98024200
F	3.27937348	-1.93077555	-2.79730000
F	2.97157648	-1.65789355	-0.10220600
F	5.29368348	-0.85761755	-1.32260300
F	3.52939548	0.93697645	-0.29276600

C	2.88479948	5.31910745	0.87159900
C	-5.60275752	-2.20718555	-1.78267100
H	-6.12454052	-3.02760755	-2.29711500
H	-5.94922752	-1.25378155	-2.20359800
H	-4.52840752	-2.32433455	-1.97744300
C	-8.72355852	-1.64195355	-0.51652100
H	-9.78688352	-1.91227355	-0.40189400
H	-8.60903452	-0.59191555	-0.21423100
H	-8.48333652	-1.68825855	-1.58972500
C	-8.10247252	-4.03313755	-0.31609700
H	-9.18356352	-4.24698855	-0.28858200
H	-7.78186952	-4.11070755	-1.36546600
H	-7.59666652	-4.82231155	0.25869600
C	-8.29938452	-2.70344955	1.75268700
H	-7.67930452	-3.41153055	2.32404500
H	-8.27249152	-1.73984455	2.27811900
H	-9.33948752	-3.06771755	1.80013200
C	0.38228348	6.65295845	-0.45292400
H	-0.44076952	6.50613845	-1.16837200
H	-0.06075452	6.82767145	0.53950000
H	0.93410248	7.55734745	-0.74891500
C	2.24800748	4.80328445	-2.12883600
H	2.98514648	5.56747445	-2.41780100
H	2.75224948	3.82450245	-2.14087500
H	1.45367448	4.78774545	-2.89002900
C	3.91214448	4.19495145	0.67209600
H	4.65371848	4.20870645	1.48931800
H	3.45643948	3.19203045	0.65007700
H	4.46051148	4.31898145	-0.27447800
C	2.26497648	5.22026445	2.27130000
H	3.04622648	5.32663345	3.04327600
H	1.51986648	6.01389345	2.44301900
H	1.76438848	4.25205545	2.42760900
C	3.58555448	6.67671245	0.72077700
H	4.42238348	6.75244745	1.43613200
H	4.00294248	6.81455045	-0.28967200
H	2.89946248	7.51388345	0.92222300

M06-2X(PCM:DCM)/def2-SVP: -4191.69182

M06-2X(PCM:DCM)/def2-QVPP: -4195.65477

$G_{corr.}$: 0.810353

TS II a:

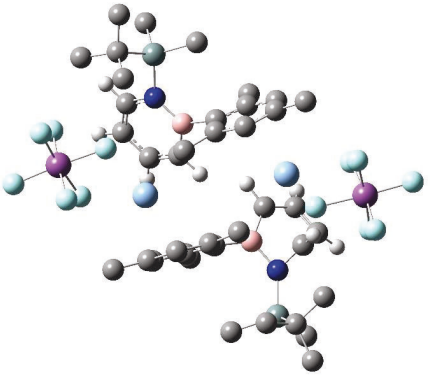

C	-0.58139534	1.49292076	-0.09785119
C	-2.59792134	0.74253076	0.39219781
C	-0.49503334	0.99068276	1.28382781
H	0.28205866	1.28860076	1.98891781
C	-1.69845534	0.42165176	1.50187181
H	-2.02992234	-0.07338624	2.41838981
H	-0.16599534	0.91839676	-0.94231919
H	-3.51877834	0.15824576	0.23852081
C	-3.54758334	2.64756476	-1.36571419
C	-3.47883034	2.50679976	-2.76276019
C	-4.59106434	3.42081176	-0.80130319
C	-4.40754934	3.16615376	-3.58251919
C	-5.52256634	4.05190176	-1.64804319
C	-5.42942434	3.95263776	-3.05184019
H	-4.32500534	3.06348476	-4.66744119
H	-6.28395834	4.70551476	-1.20954019
B	-2.44655234	2.06383376	-0.38498319
C	-4.66327034	3.64720876	0.69232181
H	-4.59820534	2.70214976	1.25047081
H	-3.81988534	4.26929276	1.02920981
H	-5.59423634	4.15706576	0.97349581
C	-2.45500934	1.60306176	-3.39770019
H	-1.49994334	1.60948176	-2.85457519
H	-2.82307434	0.56086876	-3.40890719
H	-2.25573834	1.87826576	-4.44187119
C	-6.39688534	4.69391376	-3.93381519
H	-6.09615334	4.62892376	-4.98692019
H	-7.40997634	4.27885476	-3.83863519
H	-6.44150234	5.75477876	-3.64925219
N	-1.12158334	2.73104076	-0.29874819
C	-1.81579034	5.51751176	-1.00139819
H	-1.39598234	6.51046376	-1.22677819
H	-2.46695334	5.22089176	-1.83687319

H	-2.42702234	5.61143076	-0.09234019
C	0.64207466	4.76615676	0.73489081
H	0.02307366	4.75079776	1.64391081
H	1.46394966	4.04500176	0.86752881
H	1.08243466	5.76823376	0.62870581
C	0.67821266	4.17720376	-2.31496019
C	-0.16311134	4.42994676	-3.57331619
H	0.45092166	4.27343276	-4.47633719
H	-1.02942534	3.75491576	-3.63753319
H	-0.54308634	5.46256276	-3.60238719
C	1.77231666	5.25399876	-2.22815919
H	2.46918266	5.06218476	-1.39866019
H	2.35832066	5.26343476	-3.16254719
H	1.35083466	6.26361976	-2.09249919
C	1.34250966	2.79542376	-2.39954919
H	2.10422966	2.78953076	-3.19764519
H	1.85102066	2.50887776	-1.46415219
H	0.62293066	1.99989476	-2.64740919
Si	-0.40527534	4.31593376	-0.75395219
C	-8.98891334	-0.98144624	0.16998481
C	-6.46172334	0.14042576	0.61850981
C	-8.87477334	0.16141076	0.91980081
H	-9.77784734	0.62556576	1.31045681
C	-7.59690834	0.71277276	1.17368681
H	-7.52250234	1.58213376	1.83604581
H	-9.98719634	-1.39578024	0.01234681
H	-5.48851434	0.55226176	0.90446181
C	-5.31686534	-1.79474724	-0.89844019
C	-4.91570534	-1.50314324	-2.21603619
C	-4.53298134	-2.68045324	-0.12802319
C	-3.80703834	-2.16372824	-2.77592019
C	-3.42671434	-3.32031424	-0.69909319
C	-3.06539134	-3.10923124	-2.04287119
H	-3.54069834	-1.97536924	-3.82042319
H	-2.84904334	-4.03071324	-0.10203319
B	-6.59797734	-1.11363824	-0.25020619
C	-4.89906534	-2.95605824	1.30870681
H	-5.94846234	-3.27965624	1.39644081
H	-4.26101834	-3.73448424	1.74532081
H	-4.79882134	-2.04508624	1.91915681
C	-5.63899634	-0.46398924	-3.03532519
H	-6.71571934	-0.44376924	-2.81876719
H	-5.22800534	0.54146876	-2.82039019
H	-5.51017034	-0.63001624	-4.11365619
C	-1.97503434	-3.92059324	-2.69553319
H	-2.41792834	-4.78841624	-3.20760819
H	-1.41972034	-3.33791724	-3.44266919
H	-1.25929134	-4.29230924	-1.95194119
N	-7.94032834	-1.65131124	-0.39819319
C	-6.95202834	-4.34149024	-1.54795419

H	-7.35686534	-5.30684024	-1.88967919
H	-6.29128534	-3.94289524	-2.32961619
H	-6.35022834	-4.53501624	-0.64979619
C	-9.42392134	-4.12035024	0.18314781
H	-8.83748834	-4.15213524	1.11424081
H	-10.38497434	-3.63407624	0.40154281
H	-9.63144634	-5.15789924	-0.11807219
C	-9.48032634	-2.98957224	-2.72506119
C	-8.69478734	-2.22822624	-3.80001819
H	-9.25370334	-2.24798524	-4.75128019
H	-8.56655234	-1.17552224	-3.51608219
H	-7.70298834	-2.67060324	-3.98933219
C	-9.83293334	-4.39081424	-3.25653719
H	-10.37239334	-4.99621024	-2.51113619
H	-10.48866534	-4.29149224	-4.13754819
H	-8.93935734	-4.94971624	-3.57255419
C	-10.78275934	-2.23417224	-2.43163419
H	-11.38542434	-2.16477924	-3.35294619
H	-11.39575434	-2.74617324	-1.67258519
H	-10.59810234	-1.20585224	-2.09317719
Si	-8.42907434	-3.25892724	-1.15911719
Ag	-1.92428934	-0.91287024	-1.29791019
Ag	-6.78524134	1.87000976	-1.17064919
Sb	-10.13534334	1.92560876	-2.33317519
Sb	1.44120466	-1.41097824	-2.43791319
F	-9.17315934	2.86776076	-0.94460719
F	-8.66234634	0.66193476	-2.25952819
F	-9.11429234	2.90511176	-3.61846119
F	-10.94296734	0.90199576	-3.71606019
F	-11.07903534	0.92229276	-1.01553819
F	-11.50236534	3.24271376	-2.35802519
F	-0.09900634	-0.32803824	-2.93132319
F	0.22431766	-2.25848624	-1.19084319
F	1.81663166	-0.12333524	-1.07343019
F	2.87775666	-2.50990124	-1.86710619
F	2.51876666	-0.44829024	-3.66906819
F	0.93174766	-2.66892524	-3.77188519

M06-2X(PCM:DCM)/def2-SVP: -4191.64874

M06-2X(PCM:DCM)/def2-QVPP: -4195.61324

$G_{corr.}$: 0.811393

TS II b:

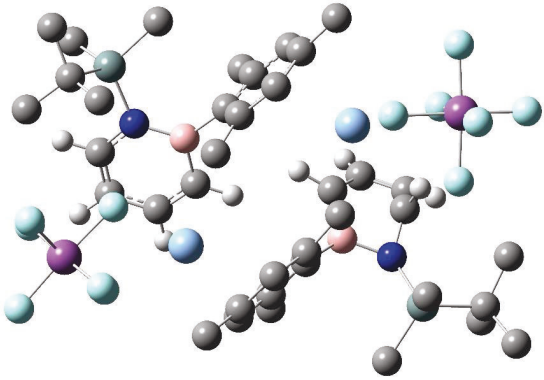

C	-3.74488000	-0.95748700	1.56798400
C	-1.75943600	-0.36739800	1.95265800
C	-3.76020900	-0.56426100	2.99864600
H	-4.53841300	-0.84123200	3.71102400
C	-2.51434200	-0.09468500	3.18247700
H	-2.07347300	0.30693200	4.09822400
H	-4.22904300	-0.34189500	0.79162900
H	-0.86871000	0.23031800	1.69348800
C	-0.97226200	-2.16972600	0.02453500
C	-1.05906900	-1.80219000	-1.32865800
C	0.04793500	-3.06615900	0.42978100
C	-0.16345700	-2.34654000	-2.26336600
C	0.94613600	-3.57747400	-0.52542600
C	0.84017900	-3.23767700	-1.89090800
H	-0.25836400	-2.06336000	-3.31475500
H	1.68793500	-4.32185600	-0.21662600
B	-1.98649800	-1.65835100	1.13147400
C	0.11964500	-3.53971700	1.86322100
H	0.04269700	-2.70126400	2.57139800
H	-0.71955800	-4.21862200	2.07893100
H	1.05305100	-4.08280700	2.06180500
C	-2.05770400	-0.77831000	-1.80037100
H	-2.96497900	-0.76007700	-1.18036400
H	-1.60541300	0.22939500	-1.78216100
H	-2.37201700	-0.96126300	-2.83696000
C	1.76781300	-3.85271200	-2.90303400
H	1.49504100	-3.54768000	-3.92098900
H	2.80787100	-3.55080100	-2.71818800
H	1.72313400	-4.94989200	-2.84627100
N	-3.32751800	-2.24198900	1.28160500
C	-3.06450200	-5.07361900	0.61382900
H	-3.54935700	-5.95479500	0.16684200
H	-2.09628600	-4.93325700	0.10813900

H	-2.88285200	-5.28295200	1.67781100
C	-5.84193500	-3.74218500	1.21889000
Si	-4.14708900	-3.56496600	0.38209000
C	4.62027400	1.00816000	1.96285700
C	2.03132300	-0.02226000	2.25531200
C	4.43557400	-0.20285800	2.57960300
H	5.30731400	-0.75452400	2.92528300
C	3.12640300	-0.70941300	2.75945100
H	2.99584000	-1.63839200	3.32524700
H	5.64095300	1.38344900	1.86123000
H	1.03306100	-0.41109300	2.48324700
C	1.01429700	2.12992700	0.94901200
C	0.62827500	2.02641200	-0.40174400
C	0.25645900	2.94996800	1.81242100
C	-0.43872100	2.80152000	-0.88928000
C	-0.80707200	3.70928900	1.30917600
C	-1.15254200	3.68175000	-0.05533700
H	-0.69842400	2.75039000	-1.95097400
H	-1.36128900	4.36884700	1.98214600
B	2.24643300	1.31140300	1.53170100
C	0.60220600	3.02583800	3.27843600
H	1.66012900	3.29613500	3.42464700
H	-0.01692500	3.76559500	3.80111700
H	0.45729100	2.04868300	3.76491900
C	1.31615600	1.06472200	-1.33762500
H	2.36806600	0.90332300	-1.06625200
H	0.80285400	0.08534200	-1.31827500
H	1.28317600	1.41540500	-2.37841600
C	-2.20712600	4.60431100	-0.61622200
H	-1.72994900	5.48683700	-1.06815500
H	-2.80388900	4.10756500	-1.39212600
H	-2.88557100	4.95580600	0.17246400
N	3.61622900	1.79283900	1.46503400
C	2.78214100	4.65384700	0.65320900
H	3.24119400	5.63262400	0.44360700
H	2.11589100	4.39386300	-0.18047600
H	2.17551300	4.76171500	1.56240300
C	5.21643900	4.08974800	2.35905900
H	4.62142100	4.03524000	3.28371800
H	6.14957500	3.53215900	2.52056600
H	5.47896700	5.14469100	2.19043400
C	5.25048500	3.32541400	-0.66721500
C	4.43963500	2.73390900	-1.82674800
H	5.00709400	2.83745300	-2.76747300
H	4.25718900	1.66291800	-1.66830400
H	3.47201400	3.24348200	-1.96560900
C	5.67226200	4.76144400	-1.02737300
H	6.23020900	5.24949600	-0.21265000
H	6.33227300	4.73677800	-1.91044900
H	4.80805400	5.39416900	-1.27940800

C	6.51275300	2.47917600	-0.45879700
H	7.12157300	2.49020600	-1.37860000
H	7.14078500	2.86763000	0.35896700
H	6.27634500	1.42792300	-0.24577200
Si	4.19615500	3.45460600	0.91343200
Ag	-2.45566800	1.51949500	0.45091000
Ag	2.32184800	-1.58305400	0.31483500
Sb	5.66988800	-1.63680500	-0.86357800
Sb	-5.54444300	1.84554500	-1.25905600
F	4.64949000	-2.69334900	0.39581400
F	4.24537700	-0.33377600	-0.65514500
F	4.63206600	-2.42532100	-2.26159800
F	6.53213300	-0.49172800	-2.11146000
F	6.62948200	-0.82711100	0.57105200
F	6.98704400	-2.99408800	-1.02607800
F	-3.67011500	1.90035700	-1.74818300
F	-4.90162200	1.91413500	0.57322000
F	-5.37368700	-0.06634600	-1.12051100
F	-7.33899600	1.75542000	-0.65284200
F	-6.04919600	1.71024700	-3.08168200
F	-5.58319800	3.74408700	-1.30829200
C	-4.34187200	-3.18308900	-1.44199000
H	-4.95271700	-3.97201700	-1.90721700
H	-4.83186600	-2.21399100	-1.61467300
H	-3.36235700	-3.18138200	-1.94181400
C	-5.66363600	-4.23452400	2.66085900
H	-5.00853100	-3.56390300	3.23951900
H	-6.64035800	-4.27682700	3.17198600
H	-5.22697500	-5.24460100	2.69311800
C	-6.57006700	-2.39003100	1.22481000
H	-7.61086000	-2.52435300	1.56496400
H	-6.10461900	-1.67634000	1.92379300
H	-6.59890800	-1.91637700	0.23072200
C	-6.67839200	-4.75974200	0.42819100
H	-7.63703600	-4.93825900	0.94362000
H	-6.90998500	-4.39668100	-0.58443300
H	-6.16754100	-5.73154500	0.33452800

M06-2X(PCM:DCM)/def2-SVP: -4191.6546

M06-2X(PCM:DCM)/def2-QVPP: -4195.61836

$G_{corr.}$: 0.81404

TS II c:

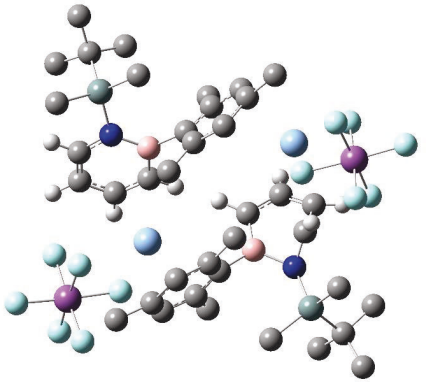

C	-1.75276750	3.49630992	0.00000000
C	-3.88315850	4.50535992	-0.62342300
C	-1.66197250	4.24446492	-1.30065100
H	-0.87400450	3.97984292	-2.01149800
C	-2.86914850	4.82108092	-1.59482800
H	-3.07307550	5.34236192	-2.53627800
H	-1.13849150	3.80408592	0.85874200
H	-4.75285650	5.15278092	-0.49812600
C	-4.73334450	2.89801692	1.33439300
C	-4.54312850	3.33245392	2.66379200
C	-5.91439050	2.19481892	0.99986900
C	-5.53804950	3.10295192	3.61976000
C	-6.90932450	2.00423192	1.98059500
C	-6.73754550	2.45886692	3.29551800
H	-5.38420650	3.45840192	4.64239100
H	-7.82654150	1.47236992	1.71653000
B	-3.70500250	3.26892892	0.18515000
C	-6.08467050	1.56306192	-0.36242100
H	-5.67655950	2.19988592	-1.15974600
H	-5.53845550	0.60644192	-0.39877100
H	-7.14189750	1.36097192	-0.57454100
C	-3.27081650	4.03994592	3.05205900
H	-2.40376250	3.36725192	2.94978700
H	-3.07362350	4.90740892	2.40319800
H	-3.30139850	4.38110792	4.09472400
C	-7.81282150	2.23415392	4.32429600
H	-7.91280350	3.10439792	4.98711500
H	-8.77652250	2.04236992	3.83635100
H	-7.56784150	1.36553092	4.95468100
N	-2.44234150	2.36275292	0.02615800
C	-3.20844550	0.21909492	2.08164500
H	-2.85925750	-0.75088108	2.46889900
H	-3.40025850	0.88077392	2.93767800

H	-4.15917550	0.05659092	1.55450600
C	-1.43750950	-0.31766208	-0.42379300
Si	-1.88039850	0.90467592	0.95990100
C	-8.87064950	7.99204492	0.91771500
C	-7.14106850	6.44997492	-0.66736700
C	-9.37451350	6.95990692	0.17233000
H	-10.43700250	6.73216992	0.20868700
C	-8.50961050	6.20962692	-0.66478600
H	-8.95992050	5.46069192	-1.32519400
H	-9.56303350	8.58702692	1.51726500
H	-6.53143250	5.90711492	-1.39753000
C	-5.01521150	7.85074192	0.39651700
C	-4.39592350	7.52167192	1.63103400
C	-4.23353250	8.43893092	-0.61028100
C	-3.07099250	7.87740992	1.87382100
C	-2.90514150	8.82829592	-0.32888800
C	-2.31840050	8.59925892	0.92652700
H	-2.61553050	7.63954092	2.83855600
H	-2.34250150	9.38112792	-1.08834700
B	-6.57019950	7.56439992	0.22338200
C	-4.75768650	8.69043092	-2.00323200
H	-5.81681550	8.42309592	-2.10361300
H	-4.63902650	9.74542392	-2.28973200
H	-4.19097450	8.08985592	-2.73157700
C	-5.17174350	6.79944792	2.70364500
H	-6.11097350	7.31543892	2.95121900
H	-5.44184750	5.78368792	2.36684600
H	-4.58247250	6.69232192	3.62344000
C	-0.98024250	9.19050492	1.29633700
H	-1.13763750	10.12950892	1.84881500
H	-0.40272950	8.51881892	1.94478700
H	-0.38017350	9.42095492	0.40605100
N	-7.54918650	8.35156692	0.96107100
C	-5.53154350	10.30155192	2.36269200
H	-5.55578350	11.29481992	2.83874400
H	-5.22079250	9.57861592	3.12860200
H	-4.77707750	10.31480492	1.56469900
C	-7.76992450	11.29385292	0.47916200
Si	-7.27831950	9.98561292	1.77043800
Ag	-1.51488850	6.57828092	-0.43908600
Ag	-7.24814050	4.40721392	0.78516300
Sb	-10.62097950	3.05492292	0.84391500
Sb	1.25886950	5.72108792	1.65661000
F	-9.04346350	2.82681092	-0.25370900
F	-9.50298150	4.19305192	1.94147600
F	-10.08452450	1.55897192	1.90677400
F	-12.10389650	3.37333392	1.98715300
F	-11.09275750	4.56023292	-0.23193700
F	-11.62198850	1.90630692	-0.29116500
F	-0.66648850	5.68512092	1.88385900

F	0.89025350	6.92201592	0.18189900
F	1.06054650	4.25822692	0.43325800
F	3.12299150	5.80821892	1.31578800
F	1.46932250	4.50095992	3.09721300
F	1.34639450	7.21374792	2.83536400
C	-0.35639450	1.45611492	1.90453600
H	0.08295550	0.59119092	2.42359200
H	0.40920550	1.88217392	1.23882800
H	-0.58350450	2.21453292	2.66868900
C	-2.71634650	-0.70595108	-1.17759300
H	-3.21198850	0.17822492	-1.60891900
H	-2.47353250	-1.39264708	-2.00598600
H	-3.43716350	-1.21995408	-0.52241100
C	-0.44813950	0.33288592	-1.39883400
H	-0.17531550	-0.38383108	-2.19145400
H	-0.88634550	1.21745992	-1.88628800
H	0.48251650	0.64130992	-0.89724800
C	-0.79844950	-1.56858308	0.19624000
H	-0.55462250	-2.29591008	-0.59634800
H	0.13734450	-1.33094208	0.72543900
H	-1.47520350	-2.06962508	0.90560600
C	-8.39964150	10.02725792	3.27740100
H	-8.08552650	10.86218992	3.92133600
H	-9.46341350	10.17088692	3.04293100
H	-8.29641150	9.09942792	3.86072300
C	-9.22987250	11.13813792	0.03494300
H	-9.48974750	11.94488592	-0.67108100
H	-9.40371750	10.18267592	-0.48303000
H	-9.93095150	11.20439392	0.88178300
C	-6.85747050	11.16276892	-0.74582700
H	-5.79083250	11.24590092	-0.48095000
H	-7.00902650	10.19655392	-1.25147300
H	-7.08385350	11.95740092	-1.47693100
C	-7.58594450	12.68045592	1.11652100
H	-7.88802350	13.46267892	0.40015300
H	-8.20476650	12.80242692	2.01969100
H	-6.53777050	12.87200092	1.39106100

M06-2X(PCM:DCM)/def2-SVP: -4191.64601

M06-2X(PCM:DCM)/def2-QVPP: -4195.61609

$G_{corr.}$: 0.809812

III a:

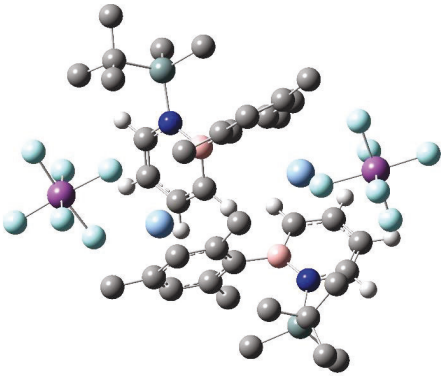

C	4.34345800	1.45464800	2.01943800
C	1.79916400	0.27250800	2.02308000
C	4.14212800	0.27441600	2.68880400
H	4.98496200	-0.19783600	3.18925500
C	2.85233600	-0.30959900	2.71857600
H	2.69892000	-1.21475000	3.31604700
H	5.34366800	1.89137200	2.03249200
H	0.80987000	-0.18851400	2.11033400
C	0.89901200	2.24362900	0.37528600
C	0.87351200	2.11013800	-1.02647700
C	-0.11140100	3.00664800	1.00492100
C	-0.08738400	2.79666900	-1.78351600
C	-1.07923100	3.66655200	0.22398500
C	-1.06202800	3.59642200	-1.18452100
H	-0.07014700	2.70783800	-2.87281000
H	-1.80687000	4.32058200	0.71592100
B	2.04040900	1.56704200	1.24245700
C	-0.11415000	3.18206400	2.50552100
H	-0.10881100	2.21202900	3.02468600
H	0.78950900	3.71682700	2.83797000
H	-0.99027700	3.75170500	2.84182500
C	1.82822900	1.18282600	-1.73645000
H	2.82152400	1.14955100	-1.26704900
H	1.42210700	0.15428300	-1.73298500
H	1.95833100	1.45929900	-2.79121400
C	-2.05860800	4.37218500	-2.00339500
H	-1.72764400	4.45194600	-3.04657300
H	-3.04176500	3.88067600	-1.99654100
H	-2.18710700	5.38549900	-1.59874300
N	3.37444100	2.13870400	1.33752600
C	2.44885900	4.96215100	0.48097900
H	2.88116600	5.95424700	0.26975700
H	1.81786900	4.67382100	-0.37021200

H	1.81817300	5.06009700	1.37565800
C	4.88191600	4.49560900	2.22604100
H	4.31238300	4.36776100	3.15913400
H	5.86701100	4.02520200	2.35425400
H	5.04706700	5.57261400	2.07322000
C	4.98681400	3.70705800	-0.79557700
C	4.12810000	3.91717100	-2.05137500
H	4.75618900	3.81638900	-2.95236800
H	3.31348900	3.18433700	-2.13081700
H	3.67734900	4.92093600	-2.06940100
C	6.02168200	4.84304300	-0.72671000
H	6.72175400	4.71117900	0.11129100
H	6.61259900	4.85910000	-1.65778600
H	5.54583100	5.83176200	-0.62184700
C	5.71972100	2.36365900	-0.88436600
H	6.35054900	2.33855800	-1.78919100
H	6.38094400	2.18851400	-0.02203500
H	5.02792400	1.51045800	-0.94149200
Si	3.90216700	3.81889900	0.77181000
C	-4.62514700	-1.41665000	1.78812000
C	-2.11695700	-0.27012700	2.27036600
C	-4.53237700	-0.27839800	2.54787300
H	-5.44478300	0.17159600	2.93335300
C	-3.26359100	0.28418900	2.82037400
H	-3.20450400	1.14681800	3.49311300
H	-5.61700800	-1.84110600	1.61744200
H	-1.15406900	0.15122700	2.57460900
C	-0.93658600	-2.19006100	0.75096400
C	-0.52994500	-1.88996300	-0.56297200
C	-0.15818100	-3.08457200	1.51670900
C	0.57801100	-2.55153300	-1.12516100
C	0.94856200	-3.72133600	0.94500000
C	1.31690100	-3.50102900	-0.39417600
H	0.84634400	-2.35946000	-2.16863900
H	1.52499900	-4.43442100	1.54025100
B	-2.22830700	-1.51988000	1.39114800
C	-0.53356900	-3.37479300	2.94832100
H	-1.58080100	-3.70849500	3.02453600
H	0.10711600	-4.15187200	3.38364700
H	-0.44680800	-2.46872500	3.56800900
C	-1.25473600	-0.84500100	-1.37289100
H	-2.33844200	-0.86644000	-1.19704600
H	-0.89046400	0.16478600	-1.10147200
H	-1.07727500	-0.96400300	-2.45052400
C	2.41975400	-4.30070600	-1.04099700
H	1.99836800	-5.20362700	-1.50874100
H	2.93801300	-3.72787400	-1.82141900
H	3.16519600	-4.61747500	-0.30079400
N	-3.56361200	-2.07146200	1.22672800
C	-2.54307800	-4.74462500	0.05829600

H	-2.93885900	-5.70919000	-0.29602000
H	-1.88111200	-4.33254700	-0.71539300
H	-1.94462100	-4.94349600	0.95739300
C	-5.02065400	-4.56165700	1.78364900
H	-4.43340400	-4.60088400	2.71395400
H	-5.98432600	-4.08363600	2.00853400
H	-5.22223000	-5.59685300	1.47052500
C	-5.08079200	-3.41079400	-1.11662900
C	-4.30474700	-2.62609600	-2.18153700
H	-4.86166300	-2.64354600	-3.13401300
H	-4.19256200	-1.57479100	-1.88594300
H	-3.30618900	-3.05182300	-2.37343600
C	-5.40692400	-4.81267600	-1.66341200
H	-5.93604000	-5.43619700	-0.92555600
H	-6.06323300	-4.71585200	-2.54426000
H	-4.50274700	-5.35138000	-1.98415700
C	-6.39781900	-2.68147700	-0.82212800
H	-6.99917500	-2.61875300	-1.74477700
H	-7.00288800	-3.20907100	-0.06738700
H	-6.23403600	-1.65125100	-0.47856800
Si	-4.03106600	-3.67877500	0.45125000
Ag	2.46937400	-1.25813100	0.25148200
Ag	-2.41850600	1.51600800	0.52567400
Sb	-5.74413100	1.48550000	-0.72757400
Sb	5.83562400	-1.79228500	-0.77401900
F	-4.82460200	2.45371900	0.67233700
F	-4.24960600	0.25232200	-0.61285300
F	-4.71735000	2.47299900	-2.00196300
F	-6.50579400	0.43498400	-2.11658500
F	-6.69896600	0.47891100	0.57951100
F	-7.13247600	2.77883200	-0.79096200
F	4.27767900	-0.77560000	-1.34088600
F	4.63245600	-2.57459800	0.52810000
F	6.24551500	-0.41995600	0.48503100
F	7.28249800	-2.85129700	-0.14831300
F	6.89379400	-0.92170500	-2.08981900
F	5.33468100	-3.14777800	-2.01557900

M06-2X(PCM:DCM)/def2-SVP: -4191.77710

M06-2X(PCM:DCM)/def2-QVPP: -4195.74018

$G_{corr.}$: 0.821726

III b:

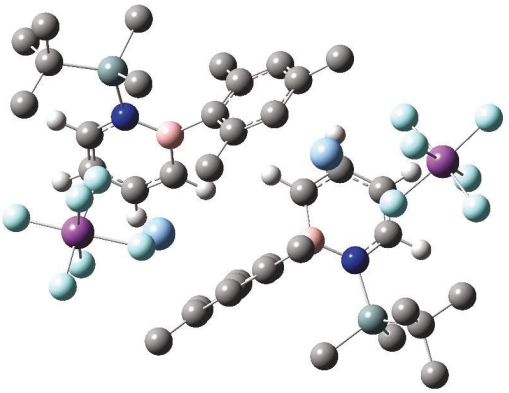

C	1.18555570	2.27033640	-0.07497757
C	3.85900670	3.09786740	-0.04916857
C	1.55675970	3.35092040	0.68982343
H	0.79809470	3.87084240	1.27189443
C	2.90515370	3.77124040	0.70513843
H	3.18756370	4.61787940	1.34031043
H	0.13749670	1.98160340	-0.07874957
H	4.90018470	3.42112440	0.04337343
C	4.55657470	1.03859740	-1.64278957
C	4.95945770	1.34753440	-2.95746557
C	5.25754570	0.03714840	-0.93431657
C	6.00429870	0.62372340	-3.56319657
C	6.28481770	-0.68035060	-1.55970557
C	6.66471070	-0.42191560	-2.88785657
H	6.27195770	0.83703240	-4.60270457
H	6.79762570	-1.47294160	-1.00854957
B	3.44338070	1.87890740	-0.87528657
C	4.93839470	-0.23578160	0.51471343
H	5.38241470	0.54383840	1.15504843
H	3.85546870	-0.22368460	0.70190243
H	5.33758670	-1.20551560	0.83863143
C	4.28375970	2.44609240	-3.73931157
H	3.23646370	2.57896140	-3.43591057
H	4.80325970	3.40974140	-3.59745457
H	4.29519070	2.24247540	-4.81921457
C	7.68917270	-1.27687860	-3.59040957
H	7.18115270	-2.04193260	-4.19688257
H	8.32413670	-0.67957360	-4.25860957
H	8.33541370	-1.78926860	-2.86689957
N	2.03094270	1.52955340	-0.84219257
C	1.95942170	-1.42596260	-1.05677857
H	1.46759870	-2.30423560	-1.50043157
H	3.04019470	-1.52048760	-1.23822157

H	1.78358470	-1.44659860	0.02906143
C	-0.61958230	0.14831240	-1.76890757
Si	1.29795570	0.15125840	-1.82906257
C	10.44154070	3.95969940	-0.33189057
C	7.79059670	3.08424040	-0.12687457
C	10.17285670	2.73577540	0.22636243
H	11.00154170	2.12059740	0.57063243
C	8.83293170	2.30233540	0.35448743
H	8.63354570	1.35415340	0.86549143
H	11.48334270	4.28281040	-0.38414357
H	6.77031070	2.73558640	0.06355743
C	6.91390570	5.32152340	-1.37222357
C	6.58118970	5.30585340	-2.74186857
C	6.12946270	6.09784340	-0.49276457
C	5.51048070	6.07955140	-3.21585957
C	5.07275270	6.87440840	-0.98869257
C	4.75438970	6.89741840	-2.35978557
H	5.27631570	6.07331440	-4.28411157
H	4.49861670	7.50088140	-0.30039857
B	8.09916470	4.43013140	-0.79447157
C	6.44117970	6.11741440	0.98306043
H	7.49461370	6.38619040	1.16087243
H	5.80863870	6.83631240	1.51888043
H	6.29003170	5.12369240	1.43342443
C	7.35645470	4.46056340	-3.72051557
H	8.40822870	4.35309740	-3.42808457
H	6.92672170	3.44327040	-3.79071557
H	7.32058370	4.88127840	-4.73462557
C	3.69274170	7.81849240	-2.90860057
H	4.15720470	8.74260940	-3.28444357
H	3.15526370	7.34901040	-3.74334057
H	2.96550370	8.09548540	-2.13469857
N	9.50010470	4.81871640	-0.82658557
C	8.86365870	7.69164540	-1.71704957
H	9.36459870	8.65839640	-1.88062057
H	8.27276770	7.44865440	-2.61016657
H	8.17355170	7.81144540	-0.87056257
C	11.11312170	7.03337740	0.21195643
H	10.43775770	6.98718640	1.07985443
H	12.00718570	6.43692840	0.44344743
H	11.42812870	8.07964340	0.08578243
C	11.40934070	6.27930940	-2.79794257
C	10.68460170	5.85114340	-4.08049457
H	11.37101770	5.94460840	-4.93934557
H	10.37456770	4.79952540	-4.02325957
H	9.80107770	6.47391040	-4.29305557
C	12.00790970	7.68336240	-3.00722857
H	12.54811970	8.04185040	-2.11739557
H	12.72917170	7.64985140	-3.84060057
H	11.24024070	8.42787540	-3.26733257

C	12.55720470	5.29634840	-2.53274657
H	13.26531270	5.32497040	-3.37814457
H	13.12252370	5.55158540	-1.62171057
H	12.20384470	4.25977140	-2.44693257
Si	10.20539070	6.44708240	-1.32601157
Ag	3.39548670	4.74757140	-1.80758157
Ag	7.95483470	1.70007040	-2.14023957
Sb	11.22963970	1.34813240	-3.40012657
Sb	0.65858170	4.86994240	-3.79790457
F	10.08782170	0.30647940	-2.23529357
F	10.01281870	2.81117140	-3.02872257
F	10.07691170	0.86549140	-4.84898057
F	12.24593870	2.48628440	-4.53402657
F	12.28603270	1.85953740	-1.89803357
F	12.34537870	-0.15125460	-3.73315857
F	2.53153470	4.99187540	-4.27242757
F	1.15844370	5.91858840	-2.24968557
F	1.17222770	3.33390840	-2.75247457
F	-1.12992530	4.74375740	-3.17415057
F	0.30554170	3.73326740	-5.27914957
F	0.28891570	6.44142540	-4.79268957
C	1.81935670	0.27434040	-3.62364757
H	1.33766270	-0.55088160	-4.16825757
H	1.49999770	1.22382040	-4.07651957
H	2.90268470	0.15671140	-3.74771757
C	-1.17817930	-0.24400760	-0.39005457
H	-0.94645630	0.46977640	0.41261743
H	-2.27696530	-0.31922960	-0.44894557
H	-0.79877130	-1.22794260	-0.07410957
C	-1.25125630	1.45485040	-2.27797257
H	-2.34533530	1.32848640	-2.34267057
H	-1.05531130	2.32763540	-1.64122957
H	-0.88616030	1.70831640	-3.28496457
C	-1.04924930	-0.96570960	-2.74953957
H	-2.14094630	-1.10111160	-2.67925057
H	-0.81771830	-0.70830260	-3.79235057
H	-0.58390030	-1.93701260	-2.52057857

M06-2X(PCM:DCM)/def2-SVP: -4191.77982

M06-2X(PCM:DCM)/def2-QVPP: -4195.73954

$G_{corr.}$: 0.81931

III c:

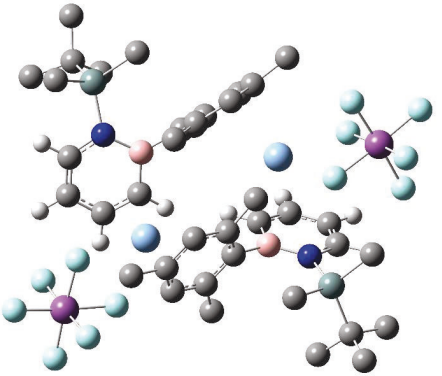

C	-2.42635655	3.34108544	0.00000000
C	-4.96832555	4.51203744	0.02562500
C	-2.73116855	4.31969944	-0.91117300
H	-1.96090155	4.65370844	-1.60367300
C	-4.02443455	4.89946244	-0.91574700
H	-4.26327155	5.64690644	-1.67962600
H	-1.40912555	2.94703044	0.00709200
H	-5.96900855	4.95563444	-0.03024100
C	-5.71123255	3.00693844	2.12485200
C	-5.66422255	3.48125344	3.45288700
C	-6.82317755	2.22799244	1.72356300
C	-6.70170055	3.18704544	4.34646200
C	-7.85500755	1.94776744	2.64386800
C	-7.81019455	2.42674244	3.96491600
H	-6.64401955	3.56557444	5.37090000
H	-8.68882155	1.31034344	2.33821300
B	-4.62162355	3.41680744	1.04288000
C	-6.89088855	1.62381344	0.34012700
H	-6.66344055	2.36715044	-0.43808900
H	-6.14672455	0.81934144	0.24214700
H	-7.88503555	1.20481544	0.14182400
C	-4.51362955	4.32860744	3.93509700
H	-3.56362255	4.06017644	3.45447600
H	-4.69579555	5.39828244	3.71944900
H	-4.38926055	4.24946844	5.02368700
C	-8.91228155	2.09589544	4.93534300
H	-9.22804955	2.98947944	5.49149300
H	-9.77961455	1.67928644	4.40863200
H	-8.56472055	1.35591844	5.67199900
N	-3.29362955	2.84398944	0.93234200
C	-3.69227355	0.90241844	3.29045500
H	-3.17557355	0.07662044	3.80351100
H	-3.86725855	1.69293344	4.03110400

H	-4.66658955	0.53730544	2.93585300
C	-2.24212255	0.02025944	0.71608900
Si	-2.56020755	1.47396144	1.91440500
C	-10.90842555	7.32824644	1.59527800
C	-8.87866955	6.07724744	0.11522300
C	-11.20389455	6.22845944	0.83295300
H	-12.21632155	5.83156244	0.82182500
C	-10.19001055	5.62110044	0.05000500
H	-10.47897655	4.80142444	-0.61587500
H	-11.71368255	7.79988644	2.16286900
H	-8.14896555	5.63869244	-0.57482900
C	-7.05453655	7.79700244	1.20442800
C	-6.40041355	7.63157844	2.44608500
C	-6.35241755	8.41338944	0.14702300
C	-5.11269455	8.16276844	2.64275100
C	-5.07087755	8.93912044	0.36670300
C	-4.44088855	8.86091444	1.61644400
H	-4.64802555	8.09496444	3.63148900
H	-4.55406255	9.44539544	-0.45282900
B	-8.54200255	7.27352844	1.01469100
C	-6.92536755	8.49170744	-1.24688200
H	-8.02136055	8.46233744	-1.25130000
H	-6.59880955	9.40626144	-1.75992200
H	-6.57310455	7.63564244	-1.84483700
C	-7.06821655	6.89811244	3.58453500
H	-8.09884755	7.24290344	3.74839400
H	-7.12477555	5.81534344	3.37422400
H	-6.51072255	7.01944744	4.52301700
C	-3.12584655	9.55071044	1.87462300
H	-3.30888155	10.53866144	2.32410900
H	-2.49187955	8.97598944	2.56257700
H	-2.57302555	9.70195644	0.93888900
N	-9.66634455	7.89642144	1.69781200
C	-8.02882155	10.22561144	2.98255400
H	-8.22187755	11.21024744	3.43707800
H	-7.55913655	9.59668544	3.74998100
H	-7.32097555	10.35778544	2.15267400
C	-10.46026355	10.72236744	1.14432000
Si	-9.70387655	9.57272044	2.46272800
Ag	-3.89693955	6.31224144	1.35352600
Ag	-8.66110355	4.14442144	1.63040500
Sb	-11.72017355	2.17130644	1.39379300
Sb	-0.38283755	6.09211344	1.86302700
F	-10.07880255	2.29886844	0.37881900
F	-10.93980255	3.51333644	2.55151600
F	-10.90959255	0.82637744	2.48582500
F	-13.29075455	2.13809144	2.46114100
F	-12.45600155	3.55221444	0.29938700
F	-12.38685355	0.84276844	0.21094300
F	-1.95555355	5.05150844	2.30500500

F	-1.53467155	6.98030644	0.58615800
F	0.09632045	4.79514944	0.54743500
F	1.08422845	7.19247044	1.37437300
F	0.62371445	5.15664944	3.17557100
F	-0.96435955	7.35973044	3.17265200
C	-0.97146855	2.14909144	2.64572600
H	-0.40192755	1.33302144	3.11555300
H	-0.32430355	2.63727844	1.90302800
H	-1.20292455	2.89626444	3.41845200
C	-3.53635755	-0.33377156	-0.02709400
H	-3.88516055	0.50261844	-0.65386000
H	-3.36872355	-1.19999356	-0.68926200
H	-4.34584355	-0.60416156	0.66954100
C	-1.13697055	0.31224044	-0.30946500
H	-0.89434055	-0.61259456	-0.85959900
H	-1.44936955	1.05635744	-1.05617100
H	-0.20883755	0.66635544	0.16691900
C	-1.80335955	-1.18469656	1.56704100
H	-1.57467055	-2.03829156	0.90741600
H	-0.89528055	-0.96908256	2.15234600
H	-2.59116955	-1.50791256	2.26299700
C	-10.77049555	9.44711944	4.00153900
H	-10.73304055	10.41247644	4.52888000
H	-11.82639955	9.21728044	3.80609300
H	-10.36968855	8.68059944	4.68220000
C	-11.95855355	10.46195144	0.94065400
H	-12.36090755	11.17751144	0.20383300
H	-12.15523855	9.45190244	0.55060300
H	-12.53045555	10.59075644	1.87259900
C	-9.72746855	10.51644744	-0.18699600
H	-8.63606155	10.63547944	-0.08272400
H	-9.92563655	9.51369444	-0.59837000
H	-10.07326255	11.25435844	-0.93034400
C	-10.26899355	12.17335144	1.61575000
H	-10.75417255	12.86179444	0.90393500
H	-10.72119655	12.34953044	2.60523000
H	-9.20567355	12.44957844	1.67143400

M06-2X(PCM:DCM)/def2-SVP: -4191.77898

M06-2X(PCM:DCM)/def2-QVPP: -4195.74386

$G_{corr.}$: 0.819116

10 Literature

[1] M. J. O'Neil, 14th ed., The Merck index : an encyclopedia of chemicals, drugs, and biologicals, Merck Whitehouse Station, N.J., **2006**.

[2] B. Thiedemann, P. J. Gliese, J. Hoffmann, P. G. Lawrence, F. D. Sönnichsen, A. Staubitz, *Chem. Commun.* **2017**, *53*, 7258-7261.

[3] A. J. V. Marwitz, M. H. Matus, L. N. Zakharov, D. A. Dixon, S.-Y. Liu, *Angew. Chem. Int. Ed.* **2009**, *48*, 973-977.

[4] a) A. W. Baggett, M. Vasiliu, B. Li, D. A. Dixon, S.-Y. Liu, *J. Am. Chem. Soc.* **2015**, *137*, 5536-5541; b) J. E. Borger, M. S. Bakker, A. W. Ehlers, M. Lutz, J. Chris Slootweg, K. Lammertsma, *Chem. Commun.* **2016**, *52*, 3284-3287; c) K. Edel, X. Yang, J. S. A. Ishibashi, A. N. Lamm, C. Maichle-Mössmer, Z. X. Giustra, S.-Y. Liu, H. F. Bettinger, *Angew. Chem. Int. Ed.* **2018**, *57*, 5296-5300.

[5] H. Doi, T. Sakai, K.-i. Yamada, K. Tomioka, *Chem. Commun.* **2004**, 1850-1851.

[6] A. W. Baggett, F. Guo, B. Li, S.-Y. Liu, F. Jäkle, *Angew. Chem. Int. Ed.* **2015**, *54*, 11191-11195.

[7] M. Schäfer, J. Schäfer, R. D. Dewhurst, W. C. Ewing, M. Krahfuß, M. W. Kuntze-Fechner, M. Wehner, C. Lambert, H. Braunschweig, *Chem.-Eur. J.* **2016**, *22*, 8603-8609.

[8] A. N. Lamm, S.-Y. Liu, *Mol. Biosyst.* **2009**, *5*, 1303-1305.

[9] E. R. Abbey, L. N. Zakharov, S.-Y. Liu, *J. Am. Chem. Soc.* **2008**, *130*, 7250-7252.

[10] Y. Naruta, Y. Nishigaichi, K. Maruyama, *Chem. Lett.* **2006**, *15*, 1857-1860.

[11] K. S. Dunne, S. E. Lee, V. Gouverneur, *J. Organomet. Chem.* **2006**, *691*, 5246-5259.

[12] P. J. Malinowski, T. Jaroń, M. Domańska, J. M. Slattery, M. Schmitt, I. Krossing, *Dalton T.* **2020**, *49*, 7766-7773.

[13] P. J. Malinowski, D. Himmel, I. Krossing, *Angew. Chem. Int. Ed.* **2016**, *55*, 9259-9261.

[14] G. Santiso-Quiñones, A. Higelin, J. Schaefer, R. Brückner, C. Knapp, I. Krossing, *Chem.-Eur. J.* **2009**, *15*, 6663-6677.

[15] M. Kuprat, M. Lehmann, A. Schulz, A. Villinger, *Organometallics* **2010**, *29*, 1421-1427.

[16] I. Krossing, *Chem.-Eur. J.* **2001**, *7*, 490-502.

[17] A. Decken, C. Knapp, G. B. Nikiforov, J. Passmore, J. M. Rautiainen, X. Wang, X. Zeng, *Chem.-Eur. J.* **2009**, *15*, 6504-6517.

[18] SAINT, v. 8.38A; Bruker AXS Inc., Madison, WI 2017.

[19] APEX 3, v. 2016.2015-2010; Bruker AXS Inc., Madison, WI 2017.

[20] L. Krause, R. Herbst-Irmer, G. M. Sheldrick, D. Stalke, *J. Appl. Crystallogr.* **2015**, *48*, 3-10.

[21] G. Sheldrick, *Acta Crystallogr., Sect. C* **2015**, *71*, 3-8.

[22] C. B. Hubschle, G. M. Sheldrick, B. Dittrich, *J. Appl. Crystallogr.* **2011**, *44*, 1281-1284.

[23] G. M. Sheldrick, *Acta Crystallogr., Sect. A* **2008**, *64*, 112-122.

[24] O. V. Dolomanov, L. J. Bourhis, R. J. Gildea, J. A. K. Howard, H. Puschmann, *J. Appl. Crystallogr.* **2009**, *42*, 339-341.

[25] C. F. Macrae, I. Sovago, S. J. Cottrell, P. T. A. Galek, P. McCabe, E. Pidcock, M. Platings, G. P. Shields, J. S. Stevens, M. Towler, P. A. Wood, *J. Appl. Crystallogr.* **2020**, *53*, 226-235.

[26] H. H. Ku, *J. Res. Nbs. C Eng. Inst.* **1966**, *70C*, 263.

[27] M. M. Schwab, D. Himmel, S. Kacprzak, D. Kratzert, V. Radtke, P. Weis, K. Ray, E.-W. Scheidt, W. Scherer, B. de Bruin, S. Weber, I. Krossing, *Angew. Chem. Int. Ed.* **2015**, *54*, 14706-14709.

[28] M. J. Frisch, G. W. Trucks, H. B. Schlegel, G. E. Scuseria, M. A. Robb, J. R. Cheeseman, G. Scalmani, V. Barone, G. A. Petersson, H. Nakatsuji, X. Li, M. Caricato, A. V. Marenich, J. Bloino, B. G. Janesko, R. Gomperts, B. Mennucci, H. P. Hratchian, J. V. Ortiz, A. F. Izmaylov, J. L. Sonnenberg, Williams, F. Ding, F. Lipparini, F. Egidi, J. Goings, B. Peng, A. Petrone, T. Henderson, D. Ranasinghe, V. G. Zakrzewski, J. Gao, N. Rega, G. Zheng, W. Liang, M. Hada, M. Ehara, K. Toyota, R. Fukuda, J. Hasegawa, M. Ishida, T. Nakajima, Y. Honda, O. Kitao, H. Nakai, T. Vreven, K. Throssell, J. A. Montgomery Jr., J. E. Peralta, F. Ogliaro, M. J. Bearpark, J. J. Heyd, E. N. Brothers, K. N. Kudin, V. N. Staroverov, T. A. Keith, R. Kobayashi, J. Normand, K. Raghavachari, A. P. Rendell, J. C. Burant, S. S. Iyengar, J. Tomasi, M. Cossi, J. M. Millam, M. Klene, C. Adamo, R. Cammi, J. W. Ochterski, R. L. Martin, K. Morokuma, O. Farkas, J. B. Foresman, D. J. Fox, Wallingford, CT, **2016**.

[29] a) Y. Zhao, D. G. Truhlar, *Theor. Chem. Acc.* **2008**, *120*, 215-241; b) F. Weigend, R. Ahlrichs, *Phys. Chem. Chem. Phys.* **2005**, *7*, 3297-3305.

[30] J. Tomasi, B. Mennucci, R. Cammi, *Chem. Rev.* **2005**, *105*, 2999-3094.

[31] M. Page, C. Doubleday, J. W. McIver, Jr., *Chem. Phys.* **1990**, *93*, 5634-5642.

[32] D. A. McQuarrie, J. D. Simon, *Molecular Thermodynamics*, University Science Books, **1999**.

[33] F. Weigend, *Phys. Chem. Chem. Phys.* **2006**, *8*, 1057-1065.

OL Organic Letters

pubs.acs.org/OrgLett

Letter

Stereoselective [2 + 2 + 2] Cycloaddition of Benzocyclobutanones and Norbornadienes through Nickel-Catalyzed C−C Bond Activation

Robert C. Richter, Ivo H. Lindenmaier, David Schray, Markus Ströbele, and Ivana Fleischer*

Cite This: *Org. Lett.* 2025, 27, 5385−5389

Read Online

ACCESS | Metrics & More | Article Recommendations | Supporting Information

ABSTRACT: We report a nickel-catalyzed stereoselective [2 + 2 + 2] cycloaddition between norbornadienes and benzocyclobutanones via C−C activation. This transformation generates four stereocenters, producing nortricyclane scaffolds that introduce three-dimensional architecture. The reaction proceeds with high stereoselectivity while allowing precise steric control of the reaction site, offering a versatile approach for constructing intricate stereochemical frameworks.

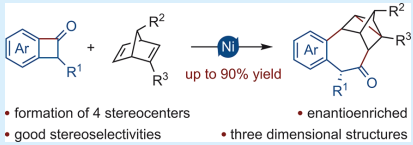

The development of metal-catalyzed C−C bond cleavage reactions has gained exceeding attention in modern synthetic chemistry, enabling atom-efficient and step-economical routes to complex, three-dimensional scaffolds commonly present in natural products.[1] Ring expansion reactions involving three- and four-membered rings have been particularly instrumental in overcoming the inherently inert nature of the C−C bond, as demonstrated by Huffman and Liebeskind,[2] Nishimura et al.,[3] Murakami et al.,[4] and others.[5]

Benzocyclobutanones (BCBs), represent well-studied compounds in C−C activation reactions, contributing to numerous transformations, including natural product synthesis.[6] Traditionally, the strain-driven reactivity of BCBs has been harnessed through noble metal catalysis activating the C^1-C^8 or C^1-C^2 bond.[7] However, these generally intramolecular transformations often require elevated temperatures, carbonyl preactivation, and precious metals, which limit their economic feasibility.[8] When these challenges are addressed, nickel catalysis provides a versatile and economically attractive expansion, especially for intermolecular reactions.[7,9] Seminal work by Martin and colleagues demonstrated nickel-catalyzed C^1-C^2 activation of BCBs, enabling the insertion of 1,3-conjugated dienes and alkynes with excellent diastereoselectivity at ambient temperatures (Scheme 1a).[10] Based on these findings, Shi and co-workers showed that alkynes could also be inserted into the C^1-C^8 bond utilizing steric control.[11]

Inspired by these advances, we sought to explore further substrate classes and report here the intermolecular [2 + 2 + 2] insertion of norbornadiene (NBD) into BCBs. NBD is known to engage in homo-Diels−Alder (HDA) reactions with dieneophiles,[12] forming nortricyclane frameworks either thermally or catalytically (e.g., Ni and Co; Scheme 1b).[13] This approach enables the construction of four stereocenters in a single step and can be achieved enantioselectively, offering a powerful pathway to complex carbon frameworks.[14] Additionally, by introduction of a substituent in the 3-position of BCB, the regioselectivity can be varied, broadening the scope of accessible scaffolds (Scheme 1c).

Scheme 1. Nickel-Catalyzed Activation of BCB Combined with the HDA of NBD

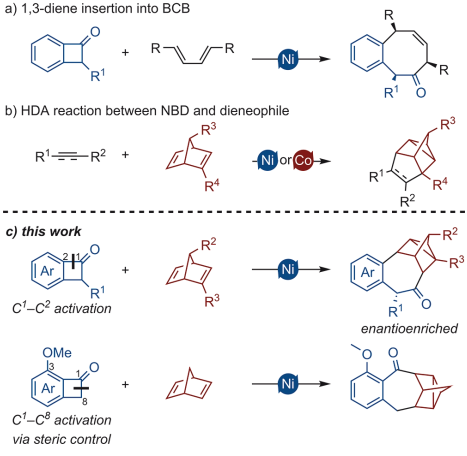

Received: April 2, 2025
Revised: May 7, 2025
Accepted: May 14, 2025
Published: May 16, 2025

To begin our investigation, we optimized the nickel-catalyzed reaction between BCB (**1a**) and NBD (**2a**) to yield product **3aa** in 91%, employing (*R*)-MonoPhos as the ligand in 1,3-dimethyl-2-imidazolidinone (DMI) at 80 °C (Table 1, entry 1). Reducing the reaction temperature to 50 °C

Table 1. Optimization of Reaction Conditions

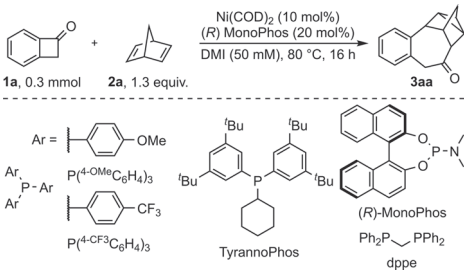

entry	variation from standard conditions[a]	yield (%)[b]
1	none	91
2	50 °C	96
3	12 mol % (*R*)-MonoPhos	63
4	150 mM	78
5	toluene, 150 mM	55
6	*n*-hexane, 150 mM	73
7	1,4-dioxane, 150 mM	63
8[c]	THF	24
9[c]	$P(^{4\text{-}OMe}C_6H_4)_3$, 40 °C	55
10[c]	dppe	29
11[c]	TyrannoPhos	27
12	toluene, $P(^{4\text{-}CF_3}C_6H_4)_3$, 50 °C	11
13	toluene, without ligand or nickel, 50 °C	0

[a]Reaction conditions: **1a** (0.3 mmol), **2a** (1.3 equiv), $Ni(COD)_2$ (10 mol %), and (*R*)-MonoPhos (20 mol %) in DMI (6 mL) at 80 °C for 16 h. [b]GC−FID yields utilizing *n*-pentadecane as an internal standard. [c]**1a** (0.1 mmol).

led to comparable yields (Table 1, entry 2). However, 80 °C was selected as the standard reaction condition due to the shorter reaction time (80 °C, 3 h; 50 °C, 10 h; see the Supporting Information for further details) and increased robustness. Attempts to reduce the catalyst loading to 5 mol % resulted in inconsistent yields. Similarly, varying the ligand-to-catalyst ratio proved unfavorable (Table 1, entry 3). The solvent appeared to play a crucial role in stabilizing the catalytic species, as increased reaction concentrations led to slightly lower yields (Table 1, entry 4), and for some solvents, the formation of a black precipitate was observed, indicating catalyst decomposition. Dimethylimidazolidinone (DMI) proved to be the most robust solvent, although various others, including apolar and etherical solvents, afforded fair to good yields (Table 1, entries 5−8) (see the Supporting Information for details).

Likewise, the developed system accepted various ligands, including electron-rich, bidentate, and sterically demanding phosphines, albeit with reduced yields (Table 1, entries 9 − 11). Electron-poor phosphines performed poorly, especially compared to the literature-known nickel-catalyzed insertion of 1,3-dienes into BCBs (Table 1, entry 12).[10] Other screened phosphoramidite-type ligands gave inferior yields (see the Supporting Information for further information). Changing the nickel(0) source from $Ni(COD)_2$ to $Ni(^{4\text{-}tBu}stb)_3$ reduced the yield, and a control reaction in toluene without either ligand or nickel confirmed their essential role (Table 1, entry 13).

With the optimized reaction conditions in hand, the scope of the reaction was investigated (Table 2). Product **3aa** was isolated in 90% yield with 34% enantiomeric excess (ee) at 50 °C. With exploitation of the modularity provided by phosphoramidite-type ligands and employment of Monophos **2**,[15] product **3aa** was obtained with up to 71% ee at the cost of the yield. Modifying the aromatic ring of **1a**, by extending the π system or adding simple substituents, was tolerated. Electron-donating methoxy and dioxole substituents were also tolerated, requiring elevated temperatures for **1d** (150 °C). Despite the high temperature, 20% ee was still observed. Product **3ea** showcased a minor amount of the regioisomeric C^1-C^8 activation due to steric strain imposed by the pseudo-*ortho* substituent. Electron-withdrawing pseudo-*o*-fluorine-substituted **1f** resulted in 39% of **3fa** (29% ee) requiring 100 °C. Similar to **3ea**, minor quantities of the regioisomer were observed on the account of the pseudo-*ortho* substituent. We were pleased to see that, in the benzylic position, substituted BCBs displayed good to excellent diastereoselectivity and furnished moderate to good yields (39−67%). Hereby, a higher catalyst loading of 20 mol % was necessary for **3ha** and **3ia**. Additionally, **1l** derived from ibuprofen, combining a benzylic and aromatic substituent, and spirocyclic **1k** were tolerated.

The scope of dienes was investigated as well. NBDs substituted in the 7 position extended the scope with good yields (77−87%). Hereby, the diastereoselectivity strongly depends on the steric bulk (**3a**(**b**,**c**)) and was inverted by a phenyl substituent (**3ad**, *vide infra*). Although the observed selectivities were evident through thorough NMR characterization, we unambiguously could ascribe selected structures (**3**(**b**,**f**,**h**,**i**,**m**)**a** and **3ad**) by X-ray crystallography. Finally, the reaction of 2-hexyl NBD with **1a** furnished two constitutional isomers (*vide infra*) in a fair yield (50%). Hereby, the addition of PhCN was necessary, most likely due to competing coordination of cyclooctadiene (COD) with sterically hindered norbornadiene **2e**.[16]

The influence of structural elements on the regioselectivity was explored in more detail. A methyl group in the 3 position of benzocylobutanone enabled addressing the C^1-C^8 bond by sterically encumbering the activation of the C^1-C^2 bond.[11] The product was obtained with good selectivity (81:19). Generally, increasing steric demand in the 3 position resulted in more C^1-C^8 activation product (**3ma** > **3ea** > **3fa**). A OMe substituent in the 3 position almost completely inhibited the reaction. After further optimization, $Ni(COD)_2$ with PCy_3 in toluene was found to be suitable for this transformation, yielding 66% of the [2 + 2 + 2] cycloaddition product (**3na**) with good chemoselectivity ([2 + 2] cycloadduct as the side product). Unfortunately, other 1,4-dienes deviating from the NBD scaffold as well as methyl bicyclo[2.2.1]hepta-2,5-diene-2-carboxylate were not tolerated. Simple cyclobutanone also did not furnish any product (see the Supporting Information for unsuccessful substrates).[17]

To demonstrate the synthetic utility of the established catalytic system, **3aa** was synthesized on a 10 mmol scale in 83% yield (Table 2). Derivatization reactions could be carried out, showcasing reduction with $NaBH_4$ (89%), Johnson−

https://doi.org/10.1021/acs.orglett.5c01324
Org. Lett. 2025, 27, 5385−5389

Table 2. Substrate Scope of BCBs and NBDs[i]

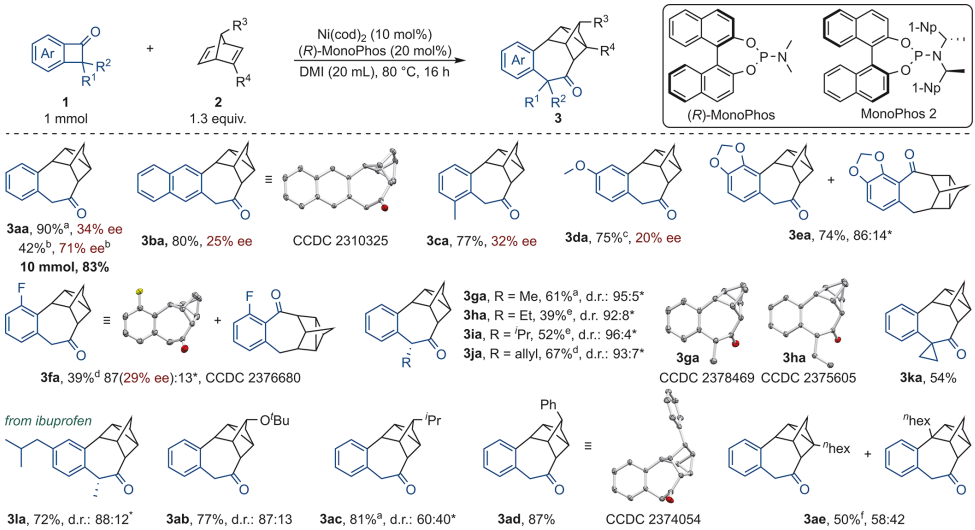

[a]At 50 °C for 24 h. [b]MonoPhos **2** (12 mol %) and *n*-hexane (20 mL) at 70 °C for 16 h. [c]At 150 °C. [d]At 100 °C. [e]**2** (3.0 equiv), $Ni(COD)_2$ (20 mol %), and (*R*)-MonoPhos (40 mol %). [f]PhCN (2 equiv) as an additive. [g]**1n** (1 mmol), **2** (1.3 equiv), $Ni(COD)_2$ (10 mol %), and PCy_3 (20 mol %) in toluene (20 mL) at 100 °C for 16 h. [h]The isomer ratio was determined by GC–FID assuming identical response factors or ^1H NMR. The ee values were determined by GC–MS on the chiral stationary phase. Hydrogen atoms of ORTEP structures are omitted for clarity, and the thermal ellipsoids are drawn at 50% probability level. [i]Standard reaction conditions: **1** (1 mmol), **2** (1.3 equiv), $Ni(COD)_2$ (10 mol %), and (*R*)-MonoPhos (20 mol %) in DMI (20 mL) at 80 °C for 16 h.

Corey–Chaykovsky epoxidation (81%), 1,2-addition of a Grignard reagent (65%), and Baeyer–Villinger oxidation (54%). To our delight, all reactions displayed excellent diastereo- and chemoselectivities furnishing the corresponding products (Scheme 2).

The analysis of the observed stereoisomers formed in the [2 + 2 + 2] cycloaddition provided tentative mechanistic insights. Based on previous experimental and computational findings,

Scheme 2. Synthetic Utility of the Cycloaddition Product

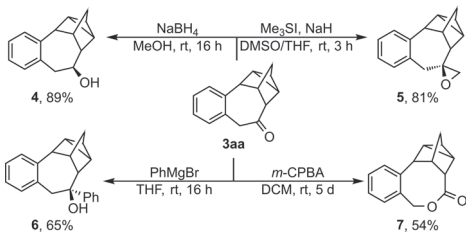

C–C bond activation of BCB likely proceeds via a $Ni(0)L_2$ complex, resulting in an oxidative addition complex with two ligands.[11,18] In this scenario, one ligand must dissociate to enable NBD coordination. When a benzylic substituent is present, the ligand on the same side is sterically favored to dissociate, allowing *syn*-NBD insertion relative to the benzylic substituent (Figure 1, I), in agreement with the *syn*-diastereoselectivity observed for conjugated 1,3-diene insertions in BCBs.[10]

In the presence of **2b** or **2c**, the substituent in the 7 position is oriented distal to the nickel center, minimizing strain during insertion (Figure 1, II). For NBD **2d**, the inverted selectivity is explained by a favorable π interaction between the phenyl substituent and the nickel center. These results suggest that the insertion of NBD occurs in the C^1–Ni bond. The two constitutional isomers observed for **3ae** allowed us to deduce the NBD approach path toward the oxidative addition complex. Upon dissociation of one ligand, **2e** approaches opposite the remaining ligand with the unsubstituted double bond facing nickel. The *n*-hexyl group positions distally from the benzylic CH_2 group of ketone **1a**. As **2e** is now orthogonal with respect to product orientation, a clockwise or

https://doi.org/10.1021/acs.orglett.5c01324
Org. Lett. 2025, 27, 5385–5389

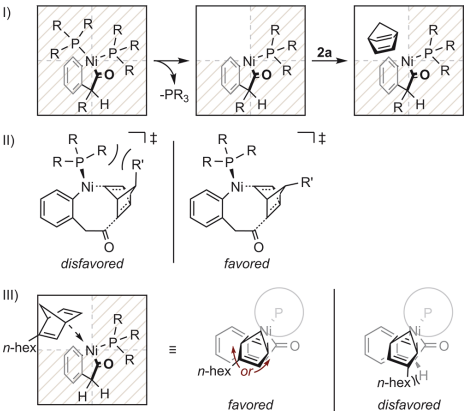

Figure 1. Proposed models, explaining the diastereoselectivity of benzylic-substituted BCBs (I) and NBDs carrying a non-coordinative substituent in the 7 position (II) as well as the constitutional isomer ratio of product **3ae** (III).

anticlockwise rotation occurs, explaining the observed pseudo-C_2 axis differentiating the product (**3ae**) constitutional isomers (Figure 1, III).

To gain further insights into the mechanism, we conducted ^{31}P NMR studies, indicating that Ni(**2a**)((*R*)-MonoPhos)$_2$ is likely the resting state. Furthermore, a possible poisoned catalyst species was identified as a Ni(0) carbonyl complex (see the Supporting Information for details), which was observed previously during nickel-catalyzed BCB activation.[11] Based on these findings and prior studies, a preliminary mechanism was proposed (Figure 2). The reaction initiates

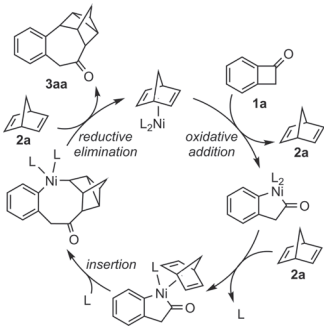

Figure 2. Proposed mechanism for the insertion of **2a** in **1a** subsequent to C^1–C^2 activation.

with the coordination of **1a** to Ni(0)L_2, initiating oxidative addition into the C^1–C^2 bond. One ligand is then replaced by **2a**, enabling insertion into the C^1–Ni bond. After ligand saturation, **3aa** is reductively eliminated, closing the cycle by releasing Ni(0)L_2.

In conclusion, we report the nickel-catalyzed stereoselective intermolecular insertion of norbornadienes into benzocyclobutanones via C–C bond activation. This transformation efficiently constructs complex nortricyclane scaffolds with good stereoselectivity and tunable regioselectivity, broadening the synthetic utility of BCBs. The substrate screening highlights the tolerance of various substitution patterns, providing valuable mechanistic insights. Furthermore, the successful upscale experiment and subsequent derivatization demonstrate the practical applicability of this methodology in complex molecule synthesis.

■ ASSOCIATED CONTENT

Data Availability Statement

The data underlying this study are available in the published article and its Supporting Information.

Supporting Information

The Supporting Information is available free of charge at https://pubs.acs.org/doi/10.1021/acs.orglett.5c01324.

Experimental procedures and compound characterization: ^{1}H, ^{13}C, ^{19}F, and ^{31}P NMR spectra, structural assignments made with COSY, HSQC, HMBC, and NOESY experiments, HRMS for all new compounds, IR, and X-ray crystallographic data (PDF)

Accession Codes

Deposition numbers 2310325, 2374054, 2375605, 2376680, 2378469, 2383238, 2409660, and 2412014 contain the supplementary crystallographic data for this paper. These data can be obtained free of charge via the joint Cambridge Crystallographic Data Centre (CCDC) and Fachinformationszentrum Karlsruhe Access Structures service.

■ AUTHOR INFORMATION

Corresponding Author

Ivana Fleischer – *Institute of Organic Chemistry, Faculty of Science, Eberhard Karls Universität Tübingen, 72076 Tübingen, Germany*; orcid.org/0000-0002-2609-6536; Email: ivana.fleischer@uni-tuebingen.de

Authors

Robert C. Richter – *Institute of Organic Chemistry, Faculty of Science, Eberhard Karls Universität Tübingen, 72076 Tübingen, Germany*

Ivo H. Lindenmaier – *Institute of Organic Chemistry, Faculty of Science, Eberhard Karls Universität Tübingen, 72076 Tübingen, Germany*

David Schray – *Institute of Organic Chemistry, Faculty of Science, Eberhard Karls Universität Tübingen, 72076 Tübingen, Germany*

Markus Ströbele – *Institute of Inorganic Chemistry, Faculty of Science, Eberhard Karls Universität Tübingen, 72076 Tübingen, Germany*; orcid.org/0000-0002-5147-5677

Complete contact information is available at: https://pubs.acs.org/10.1021/acs.orglett.5c01324

Notes

The authors declare no competing financial interest.

■ ACKNOWLEDGMENTS

The authors thank the analytical facilities of the Institute of Organic Chemistry at the University of Tübingen, Studienstiftung des deutschen Volkes (scholarship to Robert C.

Richter) and Fonds der Chemischen Industrie (scholarship to Ivo H. Lindenmaier).

REFERENCES

(1) Xue, Y.; Dong, G. Deconstructive Synthesis of Bridged and Fused Rings via Transition-Metal-Catalyzed "Cut-and-Sew" Reactions of Benzocyclobutenones and Cyclobutanones. *Acc. Chem. Res.* **2022**, *55* (16), 2341−2354.

(2) Huffman, M. A.; Liebeskind, L. S. Rhodium (I)-catalyzed intramolecular carbocyclic ring fusion: a new approach to medium-sized-ring ketones. *J. Am. Chem. Soc.* **1993**, *115* (11), 4895−4896.

(3) Nishimura, T.; Ohe, K.; Uemura, S. Palladium(II)-Catalyzed Oxidative Ring Cleavage of *tert*-Cyclobutanols under Oxygen Atmosphere. *J. Am. Chem. Soc.* **1999**, *121* (11), 2645−2646.

(4) Murakami, M.; Itahashi, T.; Ito, Y. Catalyzed Intramolecular Olefin Insertion into a Carbon−Carbon Single Bond. *J. Am. Chem. Soc.* **2002**, *124* (47), 13976−13977.

(5) (a) Murakami, M.; Ito, Y. Cleavage of carbon−carbon single bonds by transition metals. In *Activation of Unreactive Bonds and Organic Synthesis*; Murai, S., et al., Eds.; Springer: Berlin, Germany, 1999; Vol. 3, pp 97−129, DOI: 10.1007/3-540-68525-1_5. (b) Murakami, M.; Ishida, N. Potential of Metal-Catalyzed C−C Single Bond Cleavage for Organic Synthesis. *J. Am. Chem. Soc.* **2016**, *138* (42), 13759−13769.

(6) (a) Mori, K.; Ohmori, K.; Suzuki, K. Stereochemical Relay via Axially Chiral Styrenes: Asymmetric Synthesis of the Antibiotic TAN-1085. *Angew. Chem., Int. Ed.* **2009**, *48* (31), 5633−5637. (b) Takahashi, N.; Kanayama, T.; Okuyama, K.; Kataoka, H.; Fukaya, H.; Suzuki, K.; Matsumoto, T. Enantioselective Total Synthesis of (−)-Euxanmodin B: An Axially Chiral Natural Product with an Anthraquinone−Xanthone Composite Structure. *Chem. - Asian J.* **2011**, *6* (7), 1752−1756. (c) Flores-Gaspar, A.; Martin, R. Recent Advances in the Synthesis and Application of Benzocyclobutenones and Related Compounds. *Synthesis* **2013**, *45* (05), 563−580.

(7) Murakami, M.; Ishida, N. Cleavage of Carbon−Carbon σ-Bonds of Four-Membered Rings. *Chem. Rev.* **2021**, *121* (1), 264−299.

(8) (a) Chtchemelinine, A.; Rosa, D.; Orellana, A. Palladium-Catalyzed Selective Carboelimination and Cross-Coupling Reactions of Benzocyclobutenols with Aryl Bromides. *J. Org. Chem.* **2011**, *76* (21), 9157−9162. (b) Ko, H. M.; Dong, G. Cooperative activation of cyclobutanones and olefins leads to bridged ring systems by a catalytic [4 + 2] coupling. *Nat. Chem.* **2014**, *6* (8), 739−744. (c) Huffman, M. A.; Liebeskind, L. S.; Pennington, W. T., Jr. Synthesis of metal-lacyclopentenones by insertion of rhodium into cyclobutenones. *Organometallics* **1990**, *9* (8), 2194−2196.

(9) (a) Ambler, B. R.; Turnbull, B. W. H.; Suravarapu, S. R.; Uteuliyev, M. M.; Huynh, N. O.; Krische, M. J. Enantioselective Ruthenium-Catalyzed Benzocyclobutenone−Ketol Cycloaddition: Merging C−C Bond Activation and Transfer Hydrogenative Coupling for Type II Polyketide Construction. *J. Am. Chem. Soc.* **2018**, *140* (29), 9091−9094. (b) Ochi, S.; Zhang, Z.; Xia, Y.; Dong, G. Rhodium-Catalyzed (4 + 1) Cycloaddition between Benzocyclobutenones and Styrene-Type Alkenes. *Angew. Chem., Int. Ed.* **2022**, *61* (22), No. e202202703.

(10) Juliá-Hernández, F.; Ziadi, A.; Nishimura, A.; Martin, R. Nickel-Catalyzed Chemo-, Regio- and Diastereoselective Bond Formation through Proximal C C Cleavage of Benzocyclobutenones. *Angew. Chem., Int. Ed.* **2015**, *54* (33), 9537−9541.

(11) Guo, J.-H.; Liu, Y.; Lin, X.-C.; Tang, T.-M.; Wang, B.-Q.; Hu, P.; Zhao, K.-Q.; Song, F.; Shi, Z.-J. Site-Selective C−C Cleavage of Benzocyclobutenones Enabled by a Blocking Strategy Using Nickel Catalysis. *Angew. Chem., Int. Ed.* **2021**, *60* (35), 19079−19084.

(12) Kiselev, V. D.; Shakirova, I. I.; Kornilov, D. A.; Kashaeva, H. A.; Potapova, L. N.; Konovalov, A. I. Homo-Diels−Alder reaction of a very inactive diene, bicyclo[2,2,1]hepta-2,5-diene, with the most active dienophile, 4-phenyl-1,2,4-triazolin-3,5-dione. Solvent, temperature, and high pressure influence on the reaction rate. *J. Phys. Org. Chem.* **2013**, *26* (1), 47−53.

(13) (a) Yoshikawa, S.; Aoki, K.; Kui, J.; Furukawa, J. An Evaluation of the Effects of the Phosphorus Ligands on the Stereoselectivity of a Nickel-catalyzed Reaction. The Reaction of Norbornadiene with Acrylonitrile. *Bull. Chem. Soc. Jpn.* **1975**, *48* (11), 3239−3242. (b) Schrauzer, G. N.; Glockner, P. Über die katalytische Anlagerung von Olefinen und Alkinen an Norbornadien mit Ni0-Verbindungen und einem neuen NiII-Komplex. *Chem. Ber.* **1964**, *97* (9), 2451−2462. (c) Pardigon, O.; Tenaglia, A.; Buono, G. Influence of aluminum Lewis acids on the diastereoselectivity of the nickel-catalyzed [2 + 2 + 2] cycloaddition of norbornadiene and electron deficient alkenes. *Tetrahedron Lett.* **2000**, *41* (21), 4089−4092. (d) Gugelchuk, M. M.; Doherty-Kirby, A. L. Kinetic and Modeling Studies on the Nickel-Catalyzed Homo-Diels−Alder Addition of 7-Substituted Norbornadienes. *J. Org. Chem.* **1996**, *61* (10), 3490−3495. (e) Lautens, M.; Edwards, L. G.; Tam, W.; Lough, A. J. Nickel-catalyzed [2.pi. + 2.pi. + 2.pi.] (homo-Diels-Alder) and [2.pi. + 2.pi.] cycloadditions of bicyclo[2.2.1]hepta-2,5-dienes. *J. Am. Chem. Soc.* **1995**, *117* (41), 10276−10291. (f) Pardigon, O.; Tenaglia, A.; Buono, G. Enantioselective Syntheses of Monofunctionalized Deltacyclenes Using a [CoI2/Zn] Catalytic System. *J. Org. Chem.* **1995**, *60* (6), 1868−1871. (g) Lautens, M.; Tam, W.; Edwards, L. G. Stereoselectivity in the homo-Diels−Alder reaction: effect of a remote 7-substituent on nickel-catalysed cycloadditions. *J. Chem. Soc., Perkin Trans.* **1994**, *1* (15), 2143−2150.

(14) (a) Brunner, H.; Prester, F. Asymmetrische Katalysen: LXX. Die hochenantioselektive Co-katalysierte Homo-Diels-Alder-Reaktion von Norbornadien mit Acetylenen. *J. Organomet. Chem.* **1991**, *414* (3), 401−409. (b) Chen, Y.; Snyder, J. K. Opening the [4 + 2 + 2] Cycloadducts of Bicyclo[2.2.1]hepta-2,5-dienes (Norbornadienes) to Cis-Fused Bicyclo[5.3.0]decanes1. *J. Org. Chem.* **2001**, *66* (21), 6943−6957. (c) Lautens, M.; Lautens, J. C.; Smith, A. C. Catalytic asymmetric induction in the homo Diels-Alder reaction. *J. Am. Chem. Soc.* **1990**, *112* (14), 5627−5628.

(15) Liu, L.; Ishida, N.; Murakami, M. Atom- and Step-Economical Pathway to Chiral Benzobicyclo[2.2.2]octenones through Carbon−Carbon Bond Cleavage. *Angew. Chem., Int. Ed.* **2012**, *51* (10), 2485−2488.

(16) (a) Clevenger, A. L.; Stolley, R. M.; Staudaher, N. D.; Al, N.; Rheingold, A. L.; Vanderlinden, R. T.; Louie, J. Comprehensive Study of the Reactions Between Chelating Phosphines and Ni(cod)2. *Organometallics* **2018**, *37* (19), 3259−3268. (b) Yin, G.; Kalvet, I.; Englert, U.; Schoenebeck, F. Fundamental Studies and Development of Nickel-Catalyzed Trifluoromethylthiolation of Aryl Chlorides: Active Catalytic Species and Key Roles of Ligand and Traceless MeCN Additive Revealed. *J. Am. Chem. Soc.* **2015**, *137* (12), 4164−4172. (c) Ge, S.; Green, R. A.; Hartwig, J. F. Controlling First-Row Catalysts: Amination of Aryl and Heteroaryl Chlorides and Bromides with Primary Aliphatic Amines Catalyzed by a BINAP-Ligated Single-Component Ni(0) Complex. *J. Am. Chem. Soc.* **2014**, *136* (4), 1617−1627.

(17) Fickes, G. N.; Metz, T. E. Scope of the homo-Diels-Alder reaction. *J. Org. Chem.* **1978**, *43* (21), 4057−4061.

(18) (a) Zhang, M.; Yang, J.; Rong, W.; Li, J. Nickel-catalyzed selective C1−C8 bond cleavage of benzocyclobutenones: theoretical insights into mechanism, substituent effects on regioselectivity, ligand effects on reactivity, and chemoselectivity. *Org. Chem. Front.* **2023**, *10* (20), 5216−5230. (b) Zou, H.; Wang, Z.-L.; Huang, G. Mechanism and Origins of the Chemo- and Regioselectivities in Nickel-Catalyzed Intermolecular Cycloadditions of Benzocyclobutenones with 1,3-Dienes. *Chem. - Eur. J.* **2017**, *23* (51), 12593−12603.

https://doi.org/10.1021/acs.orglett.5c01324
Org. Lett. 2025, 27, 5385−5389

SUPPORTING INFORMATION

Stereoselective [2+2+2] Cycloaddition of Benzocyclobutanones and Norbornadienes through Nickel Catalyzed C–C Bond Activation

Robert C. Richter,[a] Ivo H. Lindenmaier,[a] David Schray,[a] Markus Ströbele,[b] Ivana Fleischer*[a]

[a] Institute of Organic Chemistry, Faculty of Science, Eberhard Karls Universität Tübingen, Auf der Morgenstelle 18, 72076 Tübingen, Germany. E-mail: ivana.fleischer@uni-tuebingen.de

[b] Institute of Inorganic Chemistry, Faculty of Science, Eberhard Karls Universität Tübingen, Auf der Morgenstelle 18, 72076 Tübingen, Germany.

Contents

1 General information

1.1 Chemicals and general techniques

All reactions requiring an inert atmosphere were carried out under argon employing standard Schlenk technique or a glovebox (GS MEGA E-Line, Glovebox Systemtechnik, <5 ppm O_2, <0.1 ppm H_2O) with pre-dried glassware. Solvents (except DMI) were dried via a commercially available solvent purification system (MB SPS-5). DMI was dried *via* an activated neutral Al_2O_3 column. Solvents for the catalytic reaction were degassed by passing through argon and were stored over 3 Å MS from abcr (activated *in vacuo* at 280 °C for 30 min). Solvents employed during chromatography were HPLC grade or distilled prior to use. Column chromatography was performed with silica (35 – 70 µm, 60A) from Thermo Fischer. Flash chromatography was carried out using the Interchim Puriflash XS420 system with FlashPure EcoFlex Silica 25 g columns (50 µm, irregular). Preparative HPLC was conducted using an Agilent 1260 Infinity II preparative binary pump, a 1260 Infinity II preparative autosampler, a 1290 Infinity II column holder, a 1260 Infinity II DAD and a 1260 Infinity II preparative fraction collector. A Kinetex C18 column from *Phenomenex*, with 5 µm particle size, 100 Å pore size, 250 mm length and a 21.2 mm diameter was used. HPLC grade solvents with 0.1% (volume) formic acid as an additive were used. For separations, the gradients are given as a binary eluent combination X:Y (Y is the more polar solvent) with X + Y = 100. Chemicals including ligands L1 – L17 were purchased from abcr, BLDpharm, Sigma-Aldrich, Thermo Fischer, Acros or TCI and were used without further purification. Ligand L18 was kindly provided by Dielman and co-workers.[1] Low reaction temperatures were achieved employing the Julabo FT902 Cryostat or a liquid nitrogen acetone cooling bath.

1.2 Analytical techniques

NMR spectra were recorded using the Bruker Avance III HDX 700, Bruker Avance III HDX 600 or Bruker Avance 400 spectrometers. ^{13}C NMR and ^{19}F NMR experiments were proton-decoupled (not denoted explicitly). Chemical shifts are reported in parts per million relative to tetramethyl silane using the residual NMR solvent signals[2] (chloroform-d: ^{1}H δ = 7.26 and ^{13}C δ = 77.16; acetone-d_6: ^{1}H δ = 2.06) and the J coupling constants are given in Hertz with the usual designations for splitting patterns (s = singlet, d = doublet, dm = doublet of multiplet, t = triplet, q = quartet, sep = septet, m = multiplet). Structural assignments were made with additional information from gCOSY, gHSQC, and gHMBC experiments.

Information on the crystal structures is found in section 5.

HR-MS (ESI/APCI-TOF) measurements were carried out by the mass spectrometry department of the Institute of Organic Chemistry, University of Tübingen. Measurements were carried out using maXis 4G from Bruker (ESI/APCI-TOF). The molecular ion $[M+H/Na]^+$ is given in m/z units.

GC-LR-MS (EI) analysis was carried out with an Agilent 7820A/5977B GC-system/MSD employing an Agilent 190915-433UI column (30 m × 250 µm × 0.25 µm). Program: 50 °C – 280 °C over 15 minutes.

GC-FID analysis was performed on an Agilent 7820A system with an Agilent 19091J-431 column (30 m × 320 µm × 0.25 µm), utilizing H_2 as the carrier gas. The program used heated from 50 °C to 280 °C within 15 min.

FT-IR spectra were measured by a Cary 630 FTIR by applying the neat sample on a diamond ATR sampler.

Melting points were determined either by visual detection employing a Büchi B-540 (heating rate 5 °C/min).

Thin layer chromatography (TLC) was performed on aluminum plates coated with 0.20 mm silica gel 60 with fluorescence indicator UV_{254} from Macherey-Nagel and compounds were detected under UV light (254 nm) or using an anisaldehyde stain (4 mL anisaldehyde, 3 mL glacial acetic acid, 10 mL H_2SO_4 (96%), 200 mL EtOH).

2 General procedures

General Procedure A (GP-A): Nickel catalyzed insertion of benzocyclobutanones (BCB´s) into norbornadienes (NBD´s) for product isolation:

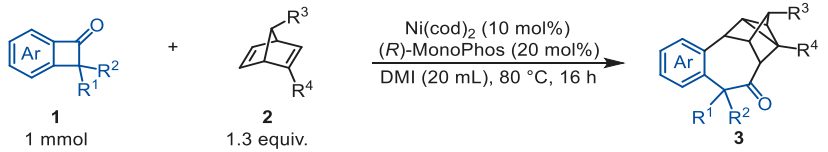

In a glove box, $Ni(COD)_2$ (0.1 mmol, 10 mol%) and (*R*)-(+)-(3,5-dioxa-4-phosphacyclohepta[2,1-a;3,4-a']dinaphthalen-4-yl)dimethylamine ((*R*)-MonoPhos, 0.2 mmol, 20 mol%) were added to a dried 50 mL Schlenk round bottom flask (RBF). 20 mL of 1,3-dimethyl-2-imidazolidinone (DMI) were added and the reaction was stirred for 5 min at rt. Subsequently, first the respective NBD (1.3 mmol, 1.3 equiv.) and then the respective BCB (1.0 mmol, 1.0 equiv.) were added, after which the reaction was transferred to a preheated (80 °C) oil bath and stirred for 16 h. The reaction was diluted with ethyl acetate (EA) (20 mL) and washed once with $HCl_{(aq.)}$ (1M, 50 mL). The aqueous phase was extracted with EA (3 × 20 mL) and the combined organic phases were washed once with brine (50 mL), dried over $MgSO_4$, followed by the removal of solvent *in vacuo*. The crude product was purified by flash column chromatography.

General Procedure B (GP-B): Nickel catalyzed insertion of *ortho* substituted benzocyclobutanones (BCB´s) into norbornadienes (NBD´s) for product isolation:

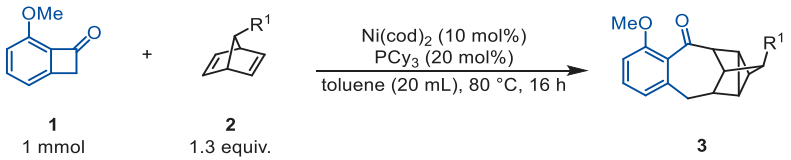

In a glove box, $Ni(COD)_2$ (0.1 mmol, 10 mol%) and PCy_3 (0.2 mmol, 20 mol%) were added to a dried 50 mL Schlenk round bottom flask (RBF). 20 mL of toluene were added and the reaction was stirred for 5 min at rt. Subsequently, first the respective NBD (1.3 mmol, 1.3 equiv.) and then **1** (1.0 mmol, 1.0 equiv.) were added, after which the reaction was transferred to a preheated (100 °C) oil bath and stirred for 16 h. The reaction was diluted with ethyl acetate (EA) (20 mL) and washed once with $HCl_{(aq.)}$ (1M, 50 mL). The aqueous phase

was extracted with EA (3 × 20 mL) and the combined organic phases were washed once with brine (50 mL), dried over $MgSO_4$, followed by the removal of solvent *in vacuo*. The crude product was purified by flash column chromatography.

General Procedure C (GP-C): Nickel catalyzed insertion of benzocyclobutanones (BCB´s) into norbornadienes (NBD´s) for screening reactions:

In a glove box, the respective nickel source (5 – 20 µmol, 5 – 20 mol%) and ligand were added to a dried Schlenk tube. The respective solvent (50.0 mM) was added, and the reaction was stirred for 5 min at rt. Subsequently, first NBD (100 – 300 µmol, 1.3 – 3.0 equiv.) and then the respective BCB (100 – 300 µmol, 1.0 equiv.) were added, after which the reaction was transferred to a preheated metal block and stirred for the respective time. *n*-Pentadecane (30 – 50 µL) was added after which the reaction was diluted with EA (2 mL) and quenched with $HCl_{(aq.)}$ (1M, 2 mL). The organic phase was separated and filtered through Celite, Al_2O_3 and $MgSO_4$, before being quantified by GC-FID.

General Procedure D (GP-D): Weinreb amide formation:

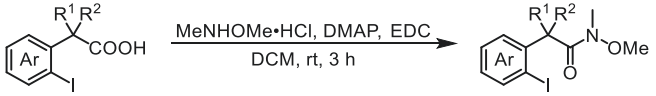

Weinreb amides were synthesized according to literature.[3] 2-(2-Iodophenyl)acetic acid derivatives (2.9 – 75.2 mmol, 1.0 equiv.) and *N*,*O*-dimethylhydroxylamine hydrochloride (4.4 – 113.3 mmol, 1.5 equiv.) were dissolved in DCM (25 mL) in a RBF. Subsequently, DMAP (4.4 – 113.3 mmol, 1.5 equiv.) and EDC (4.4 – 113.3 mmol, 1.5 equiv.) were added and the reaction was stirred for 3 h at rt. Afterwards, the mixture was diluted with 1 M $HCl_{(aq.)}$ (25 mL) and the aqueous phase was extracted with DCM (3 × 20 mL). The combined organic phases were washed with 1 M $HCl_{(aq.)}$ (20 mL), $NaHCO_{3(aq.)}$ (20 mL), and brine (20 mL) and dried over Na_2SO_4. The filtrate was concentrated *in vacuo* and purified *via* column chromatography.

General Procedure E (GP-E): Benzylic substituted Weinreb amide formation:

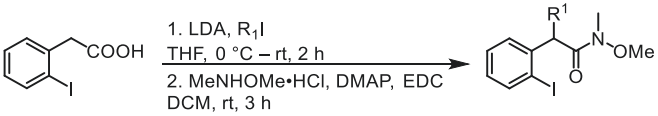

Substitution of the benzylic position was carried out following literature procedure.[3] In a predried Schlenk RBF, a THF (1 M) solution of 2-(2-iodophenyl)acetic acid (10.0 – 11.4 mmol, 1.0 equiv.) was added dropwise into freshly prepared LDA (22.0 – 25.1 mmol, 2.2 equiv., THF, 0.7 M) at 0 °C. The mixture was stirred for 1 h at 0 °C before the alkyl iodide (50.0 – 57.0 mmol, 5.0 equiv.) was slowly added. The reaction was allowed to warm to rt and was stirred for 2 h. Subsequently, the reaction was quenched with 0.5 M $NH_4OAc_{(aq.)}$ (15 mL). Afterwards, 6 M $HCl_{(aq.)}$ (7.5 mL) was added and the aqueous phase was extracted wit EA (3 × 30 mL). The combined organic phases were washed with sat. $NaS_2O_{3(aq.)}$ (45 mL), brine (45 mL) and dried over Na_2SO_4. The solvent was removed *in vacuo* and the product was transformed to the respective Weinreb amide according to **GP-D** without further purification.

General Procedure F (GP-F): Palladium catalyzed *ortho* iodination of phenyl acetic acids followed by Weinreb amide formation:

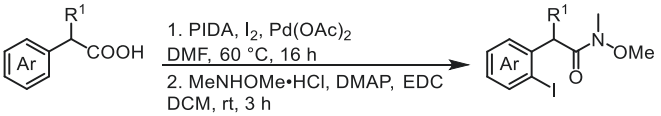

The palladium catalyzed *ortho* iodination of phenyl acetic acids was conducted according to literature.[4] In a 50 mL RBF, the phenylacetic acid derivative (10.0 mmol, 1.0 equiv.), $Pd(OAc)_2$ (0.5 mmol, 5 mol%), (Diacetoxyiodo)benzene (PIDA, 7.5 mmol, 0.75 equiv.), I_2 (7.5 mmol, 0.75 equiv.) were dissolved in anhydrous DMF (0.17 M) under air. The reaction was stirred at 60 °C for 16 h under light exclusion. Subsequently, the mixture was quenched with Na_2SO_3, and the aqueous phase was extracted wit EA (3 × 15 mL), concentrated *in vacuo* and the crude product was directly transformed to the respective Weinreb amide according to **GP-D**.

General Procedure G (GP-G): Synthesis of Kobayashi aryne precursors:

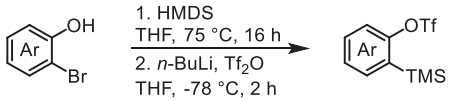

Kobayashi precursors were synthesized according to literature.[5] In a predried Schlenk RBF, Hexamethyldisilazane (HMDS, 24.6 – 28.9 mmol, 1.05 equiv.) was added to a THF (0.3 M)

solution of the *o*-bromo phenol derivate (23.5 – 27.5 mmol, 1.0 equiv.) at rt, after which the solution was stirred at 75 °C for 16 h. Subsequently, all volatiles were removed *in vacuo* and the residue was redissolved in THF (0.15 M) and cooled to -78 °C. *n*-BuLi (35.3 – 41.3 mmol, 2.5 M in *n*-hexane, 1.5 equiv.) was added dropwise over 5 min and the mixture was stirred for 1 h. Afterwards Tf_2O (28.2 – 33.0 mmol, 1.2 equiv.) was added and the mixture was stirred for 1 h. The reaction was quenched with sat. $NaHCO_{3(aq.)}$ (20 mL) and the aqueous phase was extracted with EA (3 × 30 mL). The combined organic extracts were washed with brine (1 × 30 mL), dried over Na_2SO_4 and the solvent was removed *in vacuo*. The crude material was purified *via* column chromatography.

General Procedure H (GP-H): Synthesis of BCB´s from 2-(2-iodophenyl)acetic acid Weinreb amides:

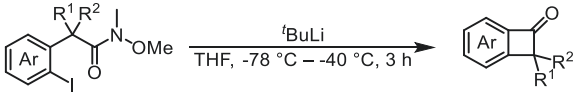

BCB´s were synthesized following a literature procedure with slight modifications.[6] In a predried Schlenk RBF, the respective 2-(2-iodophenyl)acetic acid Weinreb amide (1.9 – 72.5 mmol, 1.0 equiv.) was dissolved in THF (0.3 M) and cooled to -78 °C. *t*BuLi (4.0 – 152.3 mmol, 1.7 M in *n*-pentane, 2.1 equiv.) was added dropwise over 10 min, the mixture was allowed to warm to -40 °C and stirred for 2 h at -40 °C. Afterwards, sat. $NH_4Cl_{(aq.)}$ (12 mL) was added to quench the reaction and the aqueous phase was extracted with EA (3 × 20 mL). The combined organic phases were washed with brine (25 mL) and dried over $MgSO_4$. The filtrate was concentrated *in vacuo* and purified *via* flash chromatography.

General Procedure I (GP-I): Synthesis of BCB´s *via* [2+2] cycloaddition:

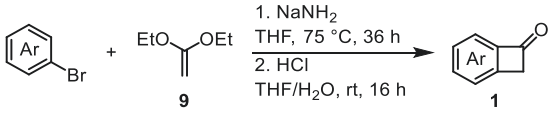

BCB´s were synthesized following a literature procedure with slight modifications.[7] In a predried Schlenk RBF, aryl bromide (20.0 mmol, 1.0 equiv.) and $NaNH_2$ (40.0 mmol, 2.0 equiv.) were suspended in THF (1 M). **9** (80.0 mmol, 4.0 equiv.) was added, and the reaction mixture was heated to 75 °C for 16 h. Reaction progress was monitored by GC-MS. If aryl bromide was still present $NaNH_2$ (20.0 mmol, 2.0 equiv.) was added, and the reaction

was stirred at 75 °C for further 24 h. The cooled mixture was poured on ice, and the organic phase was separated. The aqueous phase was extracted with DCM (3 × 30 mL) and the combined organic phases were washed with brine (1 × 30 mL), after which the solvent was removed *in vacuo*. The obtained black tar was dissolved in equal parts THF and H_2O (0.5 M). $HCl_{(aq.)}$ (conc., 80 mmol, 4 equiv.) was added and the reaction mixture was stirred at rt for 16 h. The organic phase was separated, and the aqueous phase was extracted with DCM (3 × 30 mL). The combined organic extracts were washed with brine (1 × 30 mL), dried over $MgSO_4$ and the solvent was removed *in vacuo*. The crude product was purified *via* column chromatography.

Note: After the first aqueous workup, solids might be present, which can be filtered off via silica plug.

General Procedure J (GP-J): Synthesis of BCB´s *via* [2+2] cycloaddition employing Kobayashi precursors:

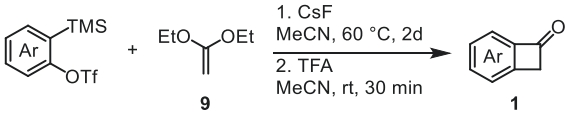

BCB´s were synthesized following a literature procedure.[5] In a Schlenk RBF, CsF (14.4 – 17.3 mmol, 1.5 equiv.) was suspended in MeCN (0.2 M). Subsequently, Kobayashi precursor (9.6 – 11.5 mmol, 1.0 equiv.), and **9** (19.2 – 23 mmol, 2.0 equiv.) were added, and the reaction was stirred at 60 °C for 2 d. The reaction mixture was cooled to rt, TFA (19.2 – 23 mmol, 2.0 equiv.) was added and the mixture was stirred for 30 min. Subsequently, EA (15 mL) and H_2O (10 mL) were added. The organic phase was separated, and the aqueous phase was extracted with EA (3 × 30 mL). The combined organic extracts were dried over $MgSO_4$ and the solvent was removed *in vacuo*. The crude product was purified *via* column chromatography.

General Procedure K (GP-K): Synthesis of 7-substituted NBD´s:

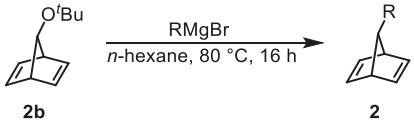

7-substituted NBD´s were synthesized according to literature with slight modifications.[8] In a Schlenk RBF RMgBr (24.0 mmol, 2.0 equiv., 2 M in Et_2O) was added to a solution of **2b**

(12.0 mmol, 1.0 equiv.) in *n*-hexane. At 40 °C with a N_2 stream, the Et_2O was removed (2 h). Subsequently, *n*-hexane (4 mL) was added and the reaction was heated to 80 °C for 16 h. The cooled reaction was quenched with sat. $NH_4Cl_{(aq.)}$ (5 mL) and the aqueous phase was extracted with Et_2O (3 × 5 mL). The combined organic phases were washed with brine (10 mL), dried over $MgSO_4$ and the solvent was carefully removed *in vacuo*. Subsequently the product was purified by vacuum distillation.

3 Optimization

3.1 Optimization of the standard reaction

Ligand screening

Table S 1. Ligand screening for the nickel catalyzed NBD insertion into **1a**.

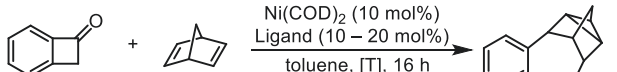

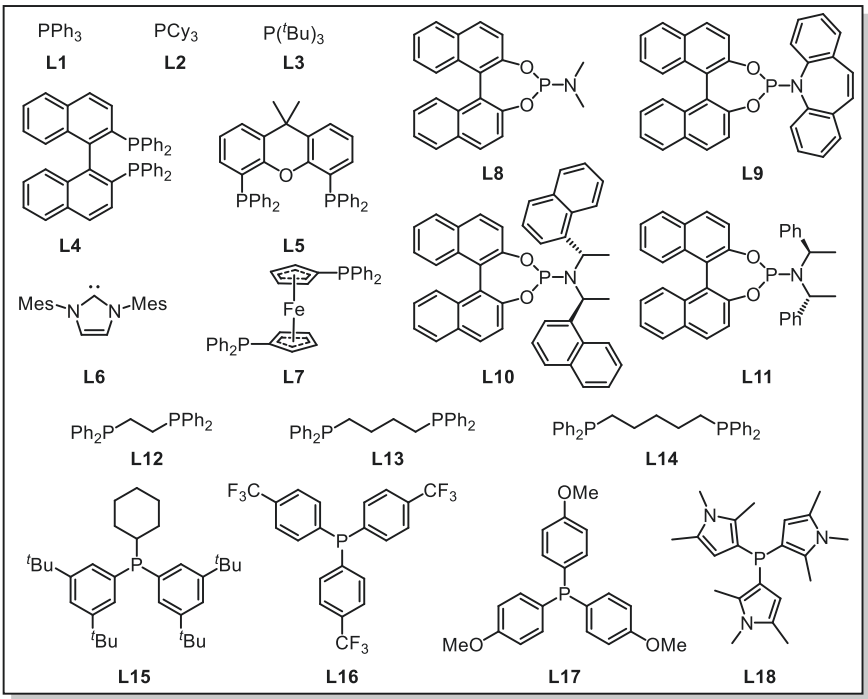

Entry	Ligand	T (°C)	Yield[a] (%)	Conversion[a] (%)
1	dppb (**L13**)	50	44	83
2	dppb (**L13**)	80	55	100
3	P(*p*-OMeC$_6$H$_4$)$_3$ (**L17**)	50	33	100
4	P(*p*-OMeC$_6$H$_4$)$_3$ (**L17**)	40	36	91
5	Tyrannophos (**L15**)	50	30	81

6	Tyrannophos (**L15**)	80	51	100
7	MonoPhos (**L8**)	50	30	70
8	MonoPhos (**L8**)	80	61	100
9	**L9**	80	12	36
10	**L10**	80	28	100
11	**L11**	80	23	47
12	PPh_3 (**L1**)	50	28	100
13	dpppe (**L14**)	50	28	76
14	dpppe (**L14**)	80	50	100
15	dppf (**L7**)	50	22	64
16	BINAP (**L4**)	50	16	70
17	dppe (**L12**)	50	12	95
18	P(*p*-$CF_3C_6H_4)_3$ (**L16**)	50	11	56
19	tmp (**L18**)	50	8	59
20	PCy_3 (**L2**)	50	4	79
21	Xantphos (**L5**)	50	0	51
22	P(^{t}Bu)$_3$ (**L3**)	50	0	31
23	IMes (**L6**)	50	0	35
24	/	50	0	36

Reaction conditions: **1a** (100 µmol, 1.0 equiv.), NBD (1.3 equiv.), $Ni(COD)_2$ (10 mol%), monodentate ligand (20 mol%) / bidentate ligand (10 mol%), toluene (2 mL). [a]GC-FID yields.

A total of 18 ligands were evaluated over a temperature range of 40 – 80 °C. Among these, dppb (**L13**), P(*p*-$OMeC_6H_4)_3$ (**L17**), Tyrannophos (**L15**), MonoPhos (**L8**) and dpppe (**L14**) demonstrated moderate performance, achieving yields of 28 – 44%) (Table S 1, entries 1, 3, 5, 7 and 13). While PPh_3 (**L1**, Table S 1, entry 12) provided a comparable yield of 28%, it displayed complete conversion, indicating the formation of decomposition products. Consequently, ligands **L8**, **13** – **15** were selected to be investigated at a higher temperature of 80 °C, resulting in enhanced yields of 50 – 60% (Table S 1, entries 2, 6, 8 and 14). In contrast, **L17**, which showed full conversion at 50 °C (Table S 1, entry 3), was screened at 40 °C, achieving a yield of 36% (Table S 1, entry 4).

The highest yield (60%) was obtained using the phosphonamidite ligand MonoPhos (Table S 1, entry 8). This prompted the screening of additional phosphonamidite ligands (Table S 1, entries 9 – 11), though all exhibited diminished yields compared to MonoPhos.

Aliphatic bidentate ligands showed promising yields, reaching up to 44% at 50 °C (Table S 1, entry 1). The longer-chain ligands dppb and dpppe (Table S 1, entries 1 and 13) outperformed the short-bridged dppe ligand (Table S 1, entry 17), potentially due to increased flexibility enabling monodentate-like coordination. In contrast, other bidentate ligands such as dppf, BINAP or Xantphos yielded poor results (Table S 1, entries 15, 16 and 21).

Monodentate electron-rich ligands generally afforded poor or negligible yields (Table S 1, entries 19, 20, 22, 23). Similarly, the electron-deficient ligand **L16** provided only a low yield (Table S 1, entry 18). Finally, in the absence of a ligand, no insertion product was observed (Table S 1, entry 24).

Temperature – ligand and catalyst loading screening

As an increased yield was observed by increasing the temperature, a temperature screening was conducted employing the MonoPhos ligand (Table S 2, entries 1 – 5). Hereby, the optimal temperature range at 16 h reaction time was identified as 80 – 90 °C.

Variation of catalyst loading showed minimal impact on the reaction outcome (Table S 2, entries 6 and 7). However, reproducibility issues prompted the selection of a standard catalyst loading of 10 mol% for subsequent experiments. In contrast, altering the ligand loading substantially influenced the catalytic performance.

When the Ni(0) source was replaced with either Ni(^{t}BuStb)$_3$ or Ni(CO)$_2$(PPh$_3$)$_2$, yields decreased substantially to 28% and 11%, respectively (Table S 2, entries 10, 11). Attempts to enhance the yield by employing a large excess of NBD (5.0 equiv.) or adjusting the substrate-to NBD ratio (1.3 equiv. of substrate to 1.0 equiv. of NBD) resulted in only modest improvements (Table S 2, entries 12, 13).

Table S 2. Temperature – ligand and catalyst loading screening for the nickel catalyzed NBD insertion into **1a**.

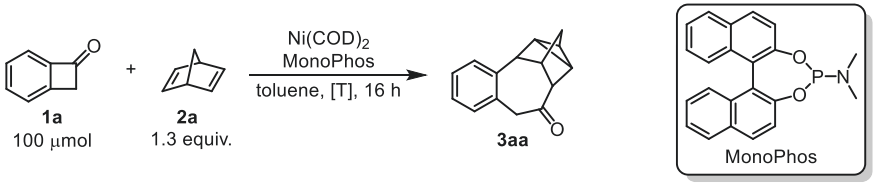

Entry	Catalyst loading (mol%)	Ligand loading (mol%)	T (°C)	Yield[a] (%)	Conversion[a] (%)
1	10	20	60	45	79

2	10	20	70	53	99
3	10	20	80	61	100
4	10	20	90	59	100
5	10	20	100	48	100
6	20	40	80	64	100
7[b]	5	10	80	63	100
8	10	10	80	44	82
9	10	30	80	14	47
10[c]	10	20	80	28	57
11[d]	10	0	80	11	33
12[e]	10	20	80	63	100
13[f]	10	20	80	74	n. d.

Reaction conditions: **1a** (100 µmol, 1.0 equiv.), NBD (1.3 equiv.), toluene (2 mL). [a]GC-FID yields. [b] **1a** (200 µmol, 1.0 equiv.). [c] Ni(ᵗBuStb)$_3$ instead of Ni(COD)$_2$. [d] Ni(CO)$_2$(PPh$_3$)$_2$ instead of Ni(COD)$_2$. [e] 3 equiv. NBD. [f] 1.3 equiv. **1a**.

Solvent screening

17 solvents were evaluated, with the most promising ones being screened at several temperatures and applied to the most promising ligands.

Table S 3. Solvent screening for the nickel catalyzed NBD insertion into **1a**.

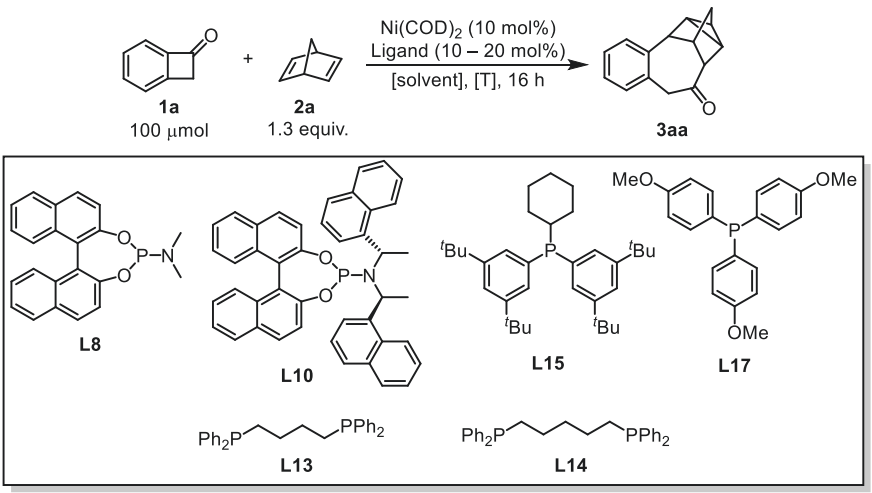

Entry	Solvent	Ligand	T (°C)	Yield (%)[a]	Conversion (%)[a]

1	DMI	MonoPhos (**L8**)	80	85	n. d.
2	DMI	Tyrannophos (**L15**)	80	25	n. d.
3	DMI	dpppe (**L14**)	80	27	n. d.
4	DMI	P(*p*-OMeC$_6$H$_4$)$_3$ (**L17**)	40	52	n. d.
5	DMI	MonoPhos (**L8**)	60	72	n. d.
6	DMI	MonoPhos (**L8**)	100	28	n. d.
7	DMPU	MonoPhos (**L8**)	80	37	68
8	DMF	MonoPhos (**L8**)	80	78	100
9	DMF	Tyrannophos (**L15**)	80	74	100
10	DMF	dppb (**L13**)	80	62	100
11	DMF	dpppe (**L14**)	80	74	100
12	DMF	**L10**[b]	80	17	100
13	DMF	P(*p*-OMeC$_6$H$_4$)$_3$ (**L17**)	40	61	100
14	DMF	P(*p*-OMeC$_6$H$_4$)$_3$ (**L17**)	25	11	31
15	DMA	MonoPhos (**L8**)	80	71	100
16	*n*-hexane	MonoPhos (**L8**)	80	73	100
17	*n*-hexane	Tyrannophos (**L15**)	80	62	100
18	*n*-hexane	dppb (**L13**)	80	60	100
19	*n*-hexane	dpppe (**L14**)	80	63	100
20	*n*-hexane	**L10**[b]	80	50	100
21	*n*-hexane	P(*p*-OMeC$_6$H$_4$)$_3$ (**L17**)	40	52	100
22	*n*-hexane	MonoPhos (**L8**)	30	41	58
23	*n*-hexane	MonoPhos (**L8**)	60	71	100
24	*n*-hexane	MonoPhos (**L8**)	70	66	100
25	*n*-hexane	MonoPhos (**L8**)	90	72	100
26	*n*-hexane	MonoPhos (**L8**)	100	71	100
27[c]	*n*-octane	MonoPhos (**L8**)	80	80	100
28	*n*-octane	**L10**[b]	80	48	100
29	*n*-octane	MonoPhos (**L8**)	60	52	78
30	*n*-octane	MonoPhos (**L8**)	100	51	83
31	*n*-pentane	MonoPhos (**L8**)	80	63	100
32	1,4-dioxane	MonoPhos (**L8**)	80	70	100
33	1,4-dioxane	Tyrannophos (**L15**)	80	62	100

34	1,4-dioxane	dppb (**L13**)	80	55	100
35	1,4-dioxane	dpppe (**L14**)	80	66	100
36	1,4-dioxane	**L10**[b]	80	29	49
37	1,4-dioxane	P(*p*-OMeC$_6$H$_4$)$_3$ (**L17**)	40	61	100
38	1,4-dioxane	MonoPhos (**L8**)	60	68	100
39	1,4-dioxane	MonoPhos (**L8**)	70	69	100
40	1,4-dioxane	MonoPhos (**L8**)	90	70	100
41	1,4-dioxane	MonoPhos (**L8**)	100	70	100
42	2-MeTHF	MonoPhos (**L8**)	80	50	73
43	THF	MonoPhos (**L8**)	80	23	32
44	Et_2O	MonoPhos (**L8**)	80	49	100
45	MTBE	MonoPhos (**L8**)	80	46	100
46	DME	MonoPhos (**L8**)	80	0	0
47	EtOH	MonoPhos (**L8**)	80	72	100
48	Toluene	MonoPhos (**L8**)	80	61	100
49[d]	MeCN	MonoPhos (**L8**)	80	25	51
50	DCE	MonoPhos (**L8**)	80	6	20

Reaction conditions: **1a** (100 µmol, 1.0 equiv.), NBD (1.3 equiv.), Ni(COD)$_2$ (10 mol%), Ligand (modentate: 10 mol%, bidentate: 20 mol%), solvent (2 mL). [a]GC-FID yields. [b] **L10** (12 mol%). [c] **1** (85 µmol, 1.0 equiv.), NBD (1.3 equiv.), Ni(COD)$_2$ (10 mol%), **L8** (20 mol%), *n*-octane (2 mL). [d] **1** (100 µmol, 1.0 equiv.), NBD (1.3 equiv.), Ni(COD)$_2$ (10 mol%), **L8** (20 mol%), MeCN (2.5 mL).

The highest yield of 85% was achieved using DMI as the solvent with the MonoPhos ligand (Table S 3, entry 1). Attempts to vary the temperature resulted in decreased yields (Table S 3, entries 5, 6). Interestingly, substituting DMI with the structurally similar solvent DMPU led to a substantial drop in yield to 37% (Table S 3, entry 7). Using DMF, another solvent with an amide group, resulted in 78% yield (Table S 3, entry 8). Comparable yields were obtained with other promising ligands in DMF (Table S 3, entries 9–11, 13). The structurally similar solvent **DMA** provided analoglous results to DMF for the MonoPhos ligand (Table S 3, entry 15).

When the solvent was changed to the nonpolar *n*-hexane, MonoPhos afforded a yield of 73% (Table S 3, entry 16). Other ligands produced slightly lower yields in *n*-hexane (Table S 3, entries 17–21), though the 50% yield observed with **L10** was notable, as this ligand holds potential for improved enantioselectivity.[9] Varying the reaction temperature between 30 °C and 100 °C with MonoPhos (Table S 3, entries 22–26) revealed consistent yields between

60 °C and 100 °C, while decreasing the temperature to 30 °C led to a decline in yield, in correspondence with lower conversion rates.

While screening etheric solvents, 1,4-dioxane emerged as the most promising, yielding 70% of the product at 80 °C with MonoPhos (Table S 3, entry **32**). Other promising ligands showed slightly reduced yields under the same conditions (Table S 3, entries 33–37). Temperature variation between 60 °C and 100 °C in 1,4-dioxane did not affect the yield (Table S 3, entries 38–41) substantially. In contrast, switching to 2-MeTHF reduced the yield to 50% (Table S 3, entry 42), while THF resulted in a much lower yield of 23% (23%, Table S 3, entry 43). Solvents such as Et_2O and MTBE yielded approximately 50% (Table S 3, entries 44, 45), whereas DME completely inhibited the reaction (Table S 3, entry 46).

Polar protic EtOH, performed surprisingly well, yielding 72% (Table S 3, entry 47). In comparison, MeCN and DCE gave poor results, with yields of only 25% and 6%, respectively (Table S 3, entries 49, 50).

Table S 4. Screening for the Ni catalyzed NBD insertion into **1a** at 300 µmol scale.

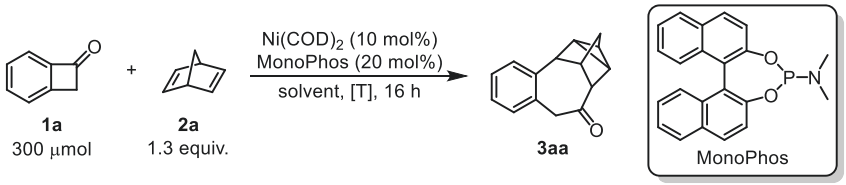

Entry	Solvent	T [°C]	Yield (%)[a]	Conversion (%)[a]
1	DMI	80	91	n. d
2	DMI	70	83	n. d
3	DMI	60	85	n. d
4[b]	DMI	50	96	n. d
5[b]	DMI	40	45	n. d
6[c]	DMI	80	86	n. d
7[d]	DMI	80	74	n. d
8[d]	*n*-hexane	80	69	100
9[d]	DMF	80	68	100
10[d]	1,4-dioxane	80	59	90
11[d]	toluene	80	55	100
12[e]	DMI	80	89	n. d

13[f]	DMI	80	67	n. d
14[g]	DMI	80	69	n. d
15[h]	DMI	80	63	n. d
16[i]	DMI	80	43	n. d
17	*n*-hexane/DMF	80	78	100
18	*n*-hexane/1,4-dioxane	80	77	100
19	*n*-hexane/DMI	80	69	n. d

Reaction conditions: **1a** (300 µmol, 1.0 equiv.), NBD (1.3 equiv.), $Ni(COD)_2$ (10 mol%), MonoPhos (20 mol%), solvent (6 mL). [a]GC-FID yields. [b] 24 h. [c] 5 mol% $Ni(COD)_2$ [d] solvent (2 mL). [e] slow addition of **1a**. [f] slow addition of NBD. [g] slow addition of **1a** and NBD. [h] 12 mol% MonoPhos. [i] 5 mol% MonoPhos.

Final screening reactions were performed on a 300 µmol scale to confirming the standard conditions (Table S 4, entry 1). Additionally, it was demonstrated that a lower reaction temperature could be employed if the reaction time was extended (Table S 4, entry 4). Modifications such as increasing the reaction concentration or reducing the catalyst loading resulted in a slight decrease in product yield (Table S 4, entries 6, 7). Consequently, these conditions were deemed unsuitable for the substrate screening. Attempts to optimize the reaction through adjustments in the mode of compound addition or the use of solvent mixtures also furnished unfavourable yields (Table S 4, entries 12 – 19).

3.2 Optimization of 3-OMe BCB

Table S 5. Ligand screening for the nickel catalyzed NBD insertion into **1n**.

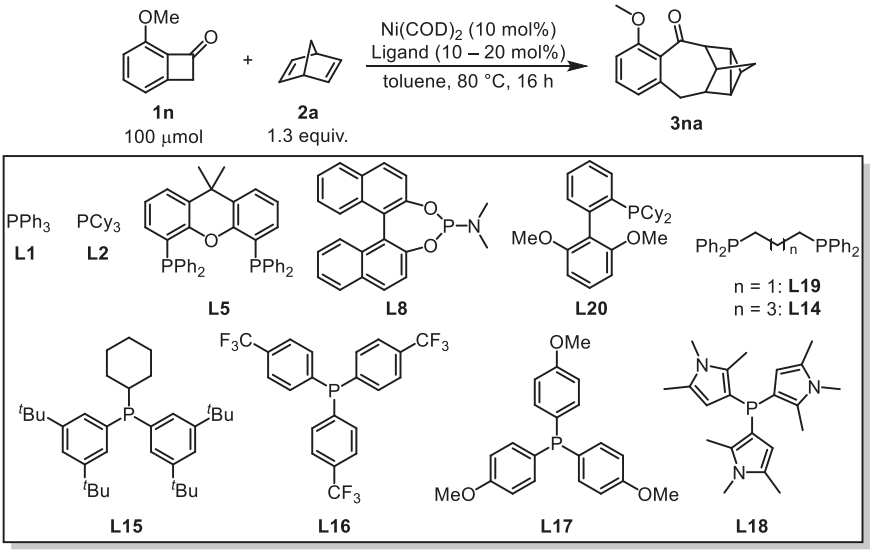

Entry	Ligand	Yield[a] (%)
1	PCy_3 (**L2**)	56
2	Tyrannophos (**L15**)	48
3	PPh_3 (**L1**)	47
4	$P(p\text{-}OMeC_6H_4)_3$ (**L17**)	46
5	dpppe (**L14**)	31
6	tmp (**L18**)	17
7[b]	MonoPhos (**L8**)	13
8[b]	$P(p\text{-}CF_3C_6H_4)_3$ (**L16**)	8
9[b]	Xantphos (**L5**)	7
10[b]	dppp (**L19**)	5
11[b]	SPhos (**L20**)	2
12	/	0

Reaction conditions: **1n** (100 μmol, 1.0 equiv.), NBD (1.3 equiv.), $Ni(COD)_2$ (10 mol%), monodentate ligand (20 mol%) / bidentate ligand (10 mol%), toluene (2 mL). [a]GC-FID yields. [b] NBD (3.0 equiv.).

The screening revealed that electron-rich ligands provided the best performance, with PCy_3 delivering the highest yield (Table S 5, entry 1). Thus, subsequent optimization efforts focused on reactions employing PCy_3 as the ligand.

Table S 6. Solvent and temperature screening for the Ni catalyzed NBD insertion into **1n**.

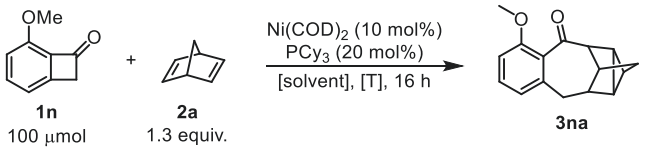

1n 100 μmol | **2a** 1.3 equiv. | **3na**

Entry	Solvent	T (°C)	Yield (%)[a]
1	toluene	80	56
2[b]	toluene	40	32
3	toluene	100	74
4[c]	toluene	100	78
5	THF	80	57
6	*n*-hexane	80	53
7	1,4-dioxane	80	51
8	DMI	80	46
9	DMF	80	44
10	EtOH	80	7

Reaction conditions: **1n** (100 μmol, 1.0 equiv.), NBD (1.3 equiv.), $Ni(COD)_2$ (10 mol%), PCy_3 (20 mol%), solvent (2 mL). [a]GC-FID yields. [b] 64 h. [c] NBD (3.0 equiv.).

A correlation between reaction temperature and yield was observed, with lower temperatures resulting in reduced, and higher temperatures in enhanced yields (Table S 6, entries 2, 3). Increasing the excess of NBD provided only a marginal improvement in yield (Table S 6, entry 4). Based on these findings, the standard reaction conditions were established as 1.3 equiv. of NBD at 100 °C in toluene (Table S 6, entry 3).

Similar to the solvent screening conducted for **1a**, several solvents were found to be tolerated with the reaction, delivering yields comparable to toluene (Table S 6, entries 5 – 9). Only, the use of the polar protic solvent EtOH resulted in a significantly lower yield, contrasting with the results observed during the optimization of the reaction with **1a**.

4 Synthesis

4.1 Weinreb amides

2-(2-iodophenyl)-*N*-methoxy-*N*-methylacetamide

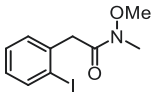

8a

8a was synthesized according to **GP-D** employing 2-(2-iodophenyl)acetic acid (19.7 g, 75.2 mmol, 1.0 equiv.), *N*,*O*-dimethylhydroxylamine hydrochloride (11.0 g, 113mmol, 1.50 equiv.), DMAP (13.8 g, 113mmol, 1.50 equiv.), and EDC (17.5 g, 113 mmol, 1.5 equiv.). Purification *via* column chromatography (80:20 *n*-hexane/EA) afforded **8a** (22.9 g, 75.2 mmol, 97%) as a yellow oil. The analytical data is in accordance with literature.[10]

$C_{10}H_{12}NO_2I$ (305.12 $\frac{g}{mol}$)

R$_f$: 0.41 (*n*-hexane/EA = 80:20) [UV]

^{1}H NMR(700.21 MHz, $CDCl_3$): δ = 7.84 (d, ^3J = 7.9 Hz, 1H), 7.31 (m, 1H), 7.28 (dd, ^3J = 7.6 Hz, ^4J = 1.7 Hz, 1H), 6.94 (m, 1H), 3.93 (s, 2H), 3.72 (s, 3H), 3.23 (s, 3H).

^{13}C NMR(176.08 MHz, $CDCl_3$): δ = 171.5, 139.4, 138.5, 130.5, 128.6, 128.4, 101.4, 61.5, 44.5, 32.5.

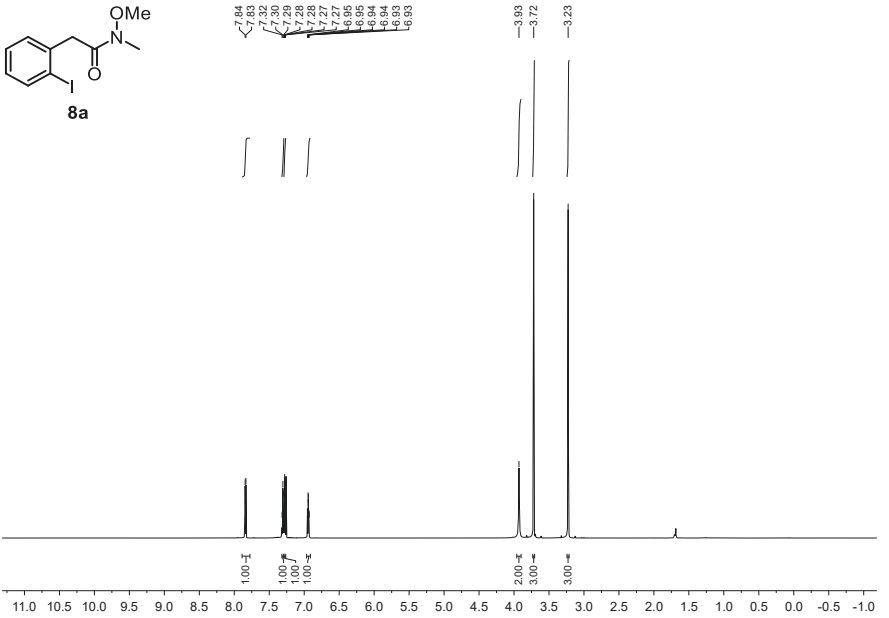

Figure S 1. ^{1}H NMR of **8a** in $CDCl_3$ measured at 700.21 MHz.

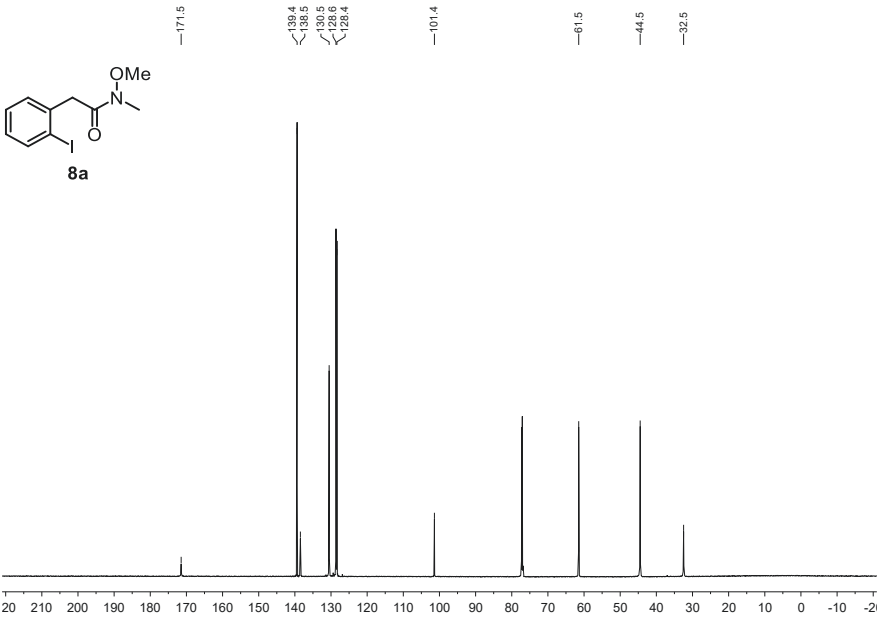

Figure S 2. ^{13}C NMR of **8a** in $CDCl_3$ measured at 176.08 MHz.

2-(2-iodo-6-methylphenyl)-*N*-methoxy-*N*-methylacetamide

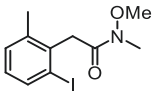

8c

8c was synthesized according to **GP-F** employing *o*-tolylacedic acid (1.50 g, 10.0 mmol, 1.00 equiv.), $Pd(OAc)_2$ (113 mg, 500 µmol, 5 mol%), PIDA (2.42 g, 7.50 mmol, 0.75 equiv.), I_2 (1.90 g, 7.50 mmol, 0.75 equiv.), N,O-dimethylhydroxylamine hydrochloride (1.50 g, 15.0 mmol, 1.50 equiv.), DMAP (1.83 g, 15.0 mmol, 1.50 equiv.), and EDC (2.33 g, 15.0 mmol, 1.50 equiv.). Purification *via* column chromatography (70:30 *n*-hexane/EA) afforded **8c** (1.18 g, 3.70 mmol, 37%) as a yellow oil over two steps.

$C_{11}H_{14}NO_2I$ (319.14 $\frac{g}{mol}$)

mp: 75.0 °C.

Rf: 0.27 (*n*-hexane/EA = 80:20) [UV]

^{1}H NMR(400.16 MHz, $CDCl_3$): δ = 7.70 (d, ^3J = 7.9 Hz, 1H), 7.14 (d, ^3J = 7.5 Hz, 1H), 6.85 (m, 1H), 4.05 (s, 2H), 3.80 (s, 3H), 3.24 (s, 3H), 2.33 (s, 3H).

^{13}C NMR(100.62 MHz, $CDCl_3$): δ = 171.0, 139.0, 137.3, 137.0, 130.4, 128.8, 103.4, 61.5, 42.2, 32.7, 21.7.

HRMS (APCI-TOF) m/z: $[M+H]^+$ Calcd for $C_{11}H_{14}NO_2IH$ 320.0142; Found 320.0143.

IR (ATR, ṽ): 1649 cm^{-1} (s, *CO*NMeOMe).

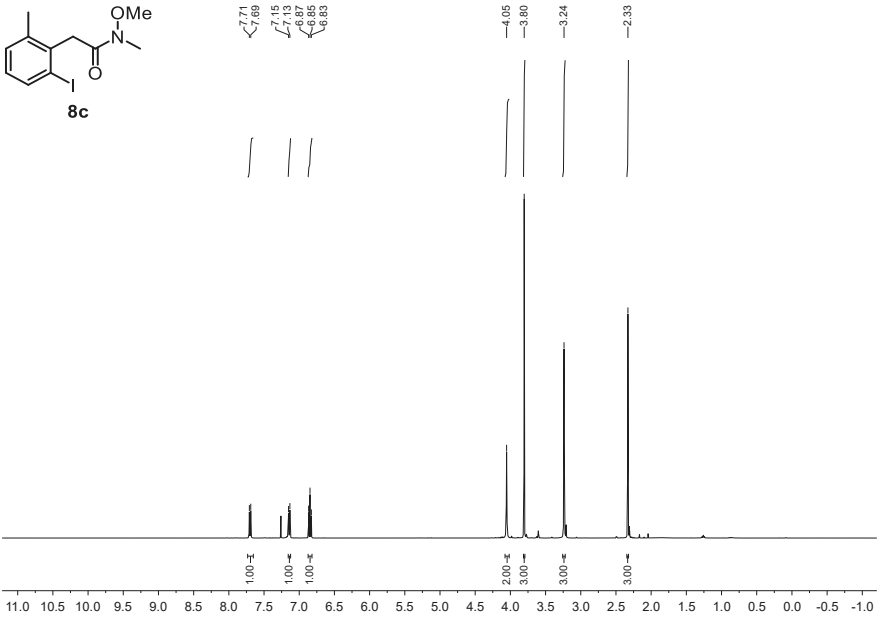

Figure S 3. ^{1}H NMR of **8c** in $CDCl_3$ measured at 400.16 MHz.

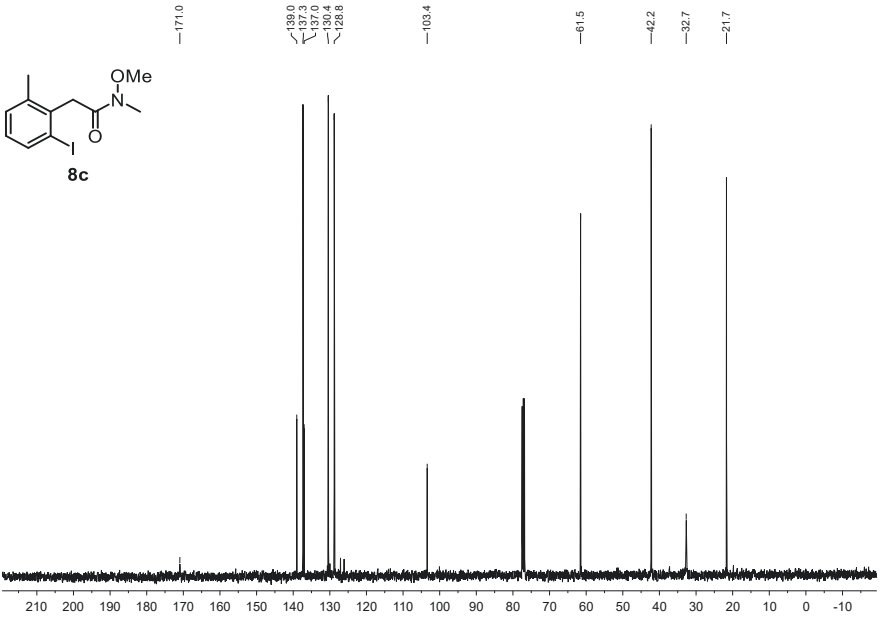

Figure S 4. ^{13}C NMR of **8c** in $CDCl_3$ measured at 100.63 MHz.

2-(2-iodophenyl)-*N*-methoxy-*N*-methylpropanamide

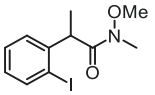

8g

8g was synthesized according to **GP-E** employing 2-(2-iodophenyl)acetic acid (2.99 g, 11.4 mmol, 1.00 equiv.), diisopropylamine (3.20 mL, 22.8 mmol, 2.00 equiv.), *n*-BuLi (9.12 mL, 2.50 M, 2.00 equiv.), methyl iodide (3.55 mL, 57.0 mmol 5.00 equiv.), N,O-dimethylhydroxylamine hydrochloride (1.67 g, 17.1 mmol, 1.50 equiv.), DMAP (2.09 g, 17.1 mmol, 1.50 equiv.), and EDC (2.65 g, 17.1 mmol, 1.50 equiv.). Purification *via* column chromatography (67:33 *n*-hexane/EA) afforded **8g** (1.92 g, 6.02 mmol, 53%) as a yellow oil. The analytical data is in accordance with literature.[11]

$C_{11}H_{14}NO_2I$ (319.14 $\frac{g}{mol}$)

R$_f$: 0.75 (*n*-hexane/EA = 80:20) [UV]

^{1}H NMR(400.16 MHz, $CDCl_3$): δ = 7.84 (d, ^3J = 8.5 Hz, 1H), 7.29 (m, 2H), 6.90 (m, 1H), 4.38 (m, 1H), 3.38 (s, 3H), 3.15 (s, 3H), 1.34 (d, ^3J = 7.0 Hz, 3H).

^{13}C NMR(176.08 MHz, $CDCl_3$): δ = 175.1, 145.0, 139.7, 128.9, 128.5, 127.4, 100.9, 61.3, 47.1, 32.6, 18.5, 1.1.

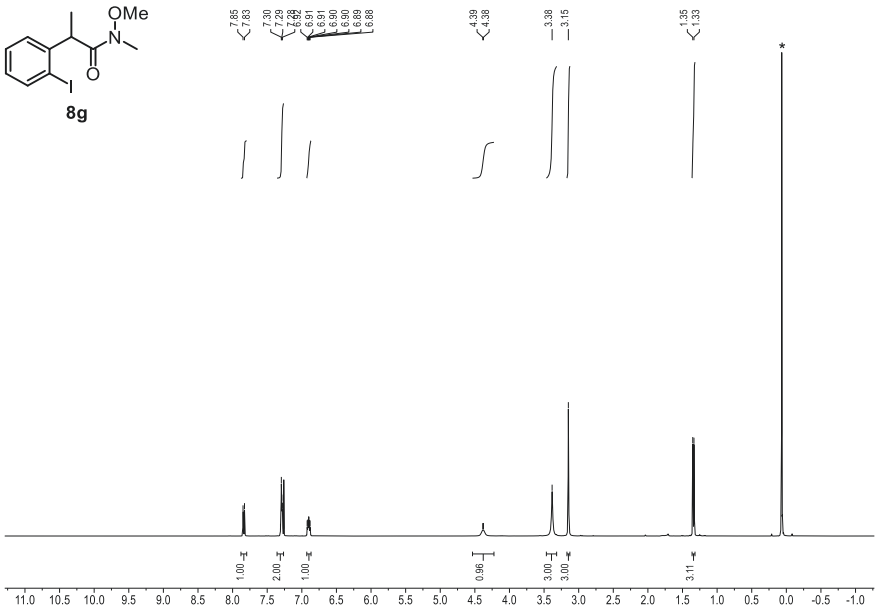

Figure S 5. ^{1}H NMR of **8g** in $CDCl_3$ measured at 700.21 MHz. * Denotes residual grease.

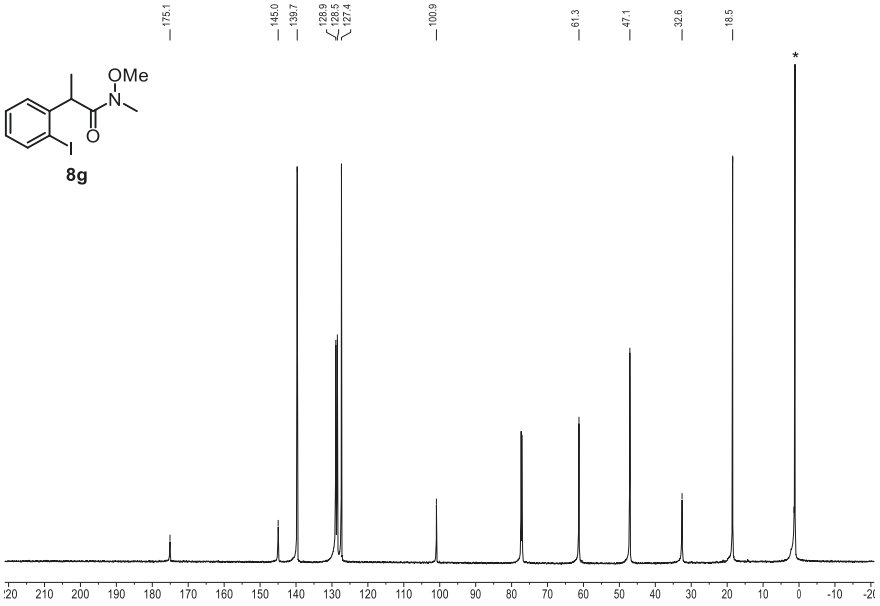

Figure S 6. ^{13}C NMR of **8g** in $CDCl_3$ measured at 176.08 MHz. * Denotes residual grease.

2-(2-iodophenyl)-*N*-methoxy-*N*-methylbutanamide

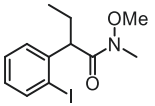

8h

8h was synthesized according to **GP-E** employing 2-(2-iodophenyl)acedic acid (2.62 g, 10.0 mmol, 1.00 equiv.), diisopropylamine (3.09 mL, 22.0 mmol, 2.20 equiv.), *n*-BuLi (13.8 mL, 1.60 M, 2.20 equiv.), ethyl iodide (4.02 mL, 50.0 mmol 5.00 equiv.), N,O-dimethylhydroxylamine hydrochloride (1.46 g, 15.0 mmol, 1.50 equiv.), DMAP (1.83 g, 15.0 mmol, 1.50 equiv.), and EDC (2.33 g, 15.0 mmol, 1.50 equiv.). Purification *via* flash chromatography (23 g SiO_2, gradient from 100:0 to 50:50 *n*-hexane/EA over 10 CV) afforded **8h** (2.53 g, 7.93 mmol, 79%) as a yellow oil. The analytical data is in accordance with literature.[3]

$C_{12}H_{16}NO_2I$ (333.17 $\frac{g}{mol}$)

R_f: 0.48 (*n*-hexane/EA = 80:20) [UV]

^{1}H NMR(400.16 MHz, $CDCl_3$): δ = 7.84 (dd, ^3J = 7.9 Hz, ^4J = 1.2 Hz, 1H), 7.34 (dd, ^3J = 7.8 Hz, ^3J = 1.7 Hz, 1H), 7.27 (m, 1H), 6.89 (m, 1H), 4.23 (m, 1H), 3.46 (s, 3H), 3.15 (s, 3H), 1.99 (m, 1H), 1.65 (m, 1H), 0.95 (t, ^3J = 7.4 Hz, 3H).

^{13}C NMR(100.62 MHz, $CDCl_3$): δ = 174.2, 143.4, 139.6, 128.8, 128.5, 127.9, 102.0, 61.5, 53.3, 32.5, 27.4, 12.5.

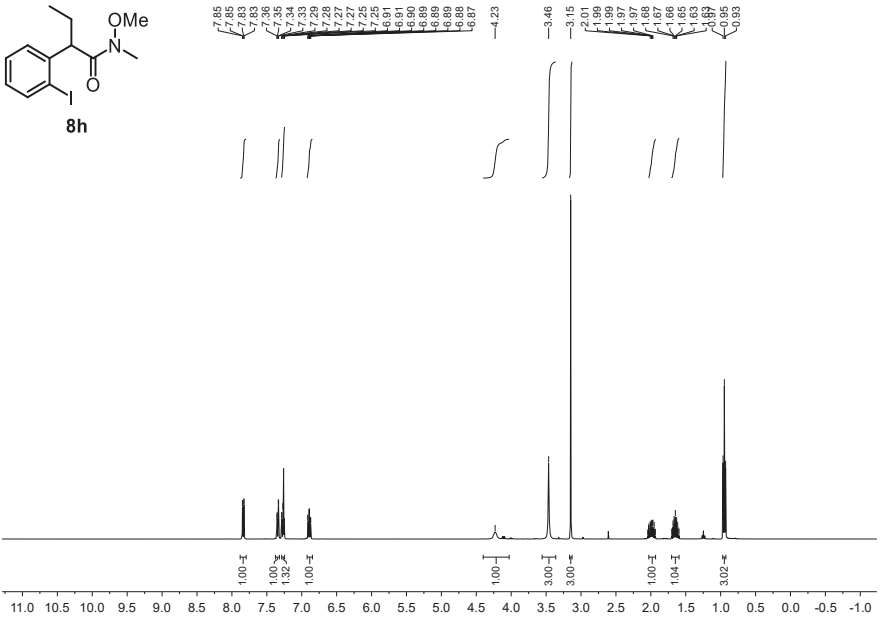

Figure S 7. ^{1}H NMR of **8h** in $CDCl_3$ measured at 400.16 MHz.

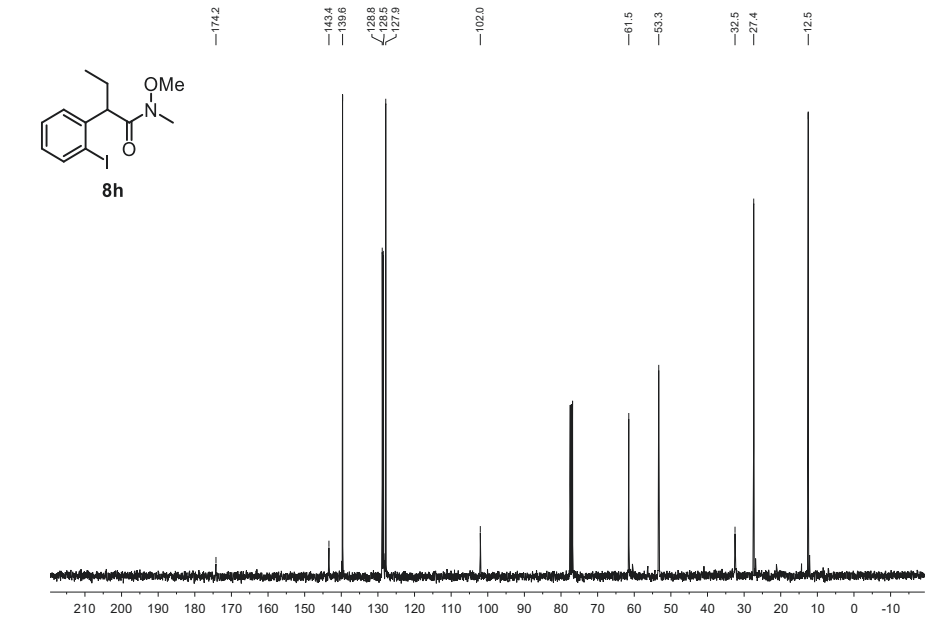

Figure S 8. ^{13}C NMR of **8h** in $CDCl_3$ measured at 100.63 MHz.

2-(2-iodophenyl)-*N*-methoxy-*N*,3-dimethylbutanamide

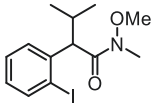

8i

8i was synthesized according to **GP-E** employing 2-(2-iodophenyl)acedic acid (2.99 g, 11.4 mmol, 1.00 equiv.), diisopropylamine (3.20 mL, 22.8 mmol, 2.00 equiv.), *n*-BuLi (9.12 mL, 2.50 M, 2.00 equiv.), isopropyl iodide (5.70 mL, 57.0 mmol 5.00 equiv.), N,O-dimethylhydroxylamine hydrochloride (1.67 g, 17.1 mmol, 1.50 equiv.), DMAP (2.09 g, 17.1 mmol, 1.50 equiv.), and EDC (2.09 g, 17.1 mmol, 1.50 equiv.). Purification *via* column chromatography (67:33 *n*-hexane/EA) afforded **8i** (1.75 g, 5.48 mmol, 48%) as a yellow oil.

$C_{13}H_{18}NO_2I$ (347.20 $\frac{g}{mol}$)

Rf: 0.90 (*n*-hexane/EA = 80:20) [UV]

^{1}H NMR(400.16 MHz, $CDCl_3$): δ = 7.84 (dd, ^3J = 8.0 Hz, ^4J = 1.2 Hz, 1H), 7.51 (dd, ^3J = 7.8 Hz, ^4J = 1.5 Hz, 1H), 7.29 (m, 1H), 6.90 (m, 1H), 4.10 (dm, ^3J = 10.1 Hz, 1H), 3.62 (s, 3H), 3.14 (s, 3H), 2.39 (dqq, ^3J = 10.1 Hz, ^3J = 6.9 Hz, ^3J = 6.4 Hz, 1H), 1.07 (d, ^3J = 6.4 Hz, 3H), 0.77 (d, ^3J = 6.9 Hz, 3H).

^{13}C NMR(100.62 MHz, $CDCl_3$): δ = 174.2, 142.2, 139.7, 128.8, 128.7, 128.6, 103.4, 61.9, 57.6, 33.5, 32.4, 22.0, 19.4.

HRMS (ESI-TOF): m/z $[M+Na]^+$ Calcd for $C_{13}H_{18}NO_2INa$ 370.0274; Found 370.0275.

IR (ATR, $\tilde{\nu}$): 1653 cm^{-1} (s, *CO*NMeOMe).

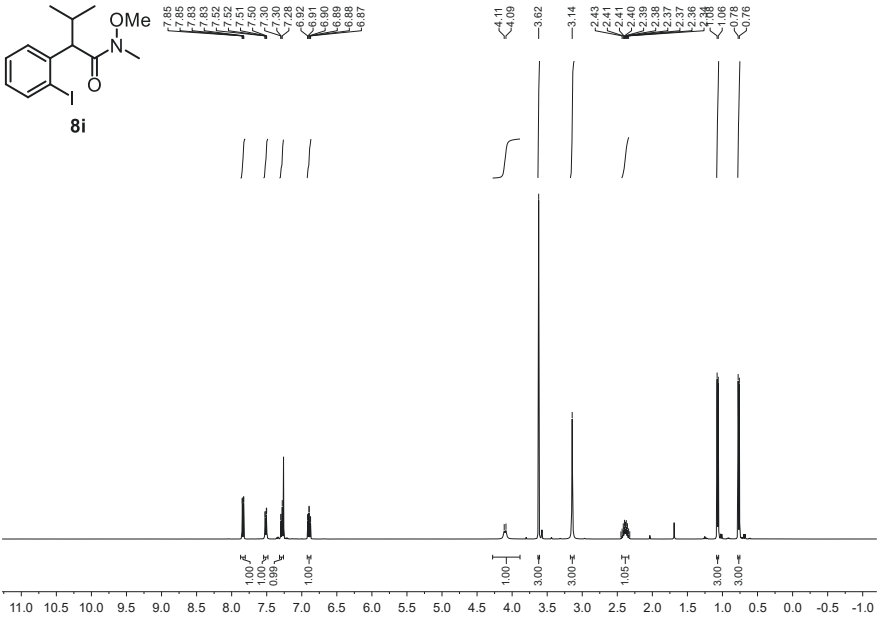

Figure S 9. ^{1}H NMR of **8i** in $CDCl_3$ measured at 400.16 MHz.

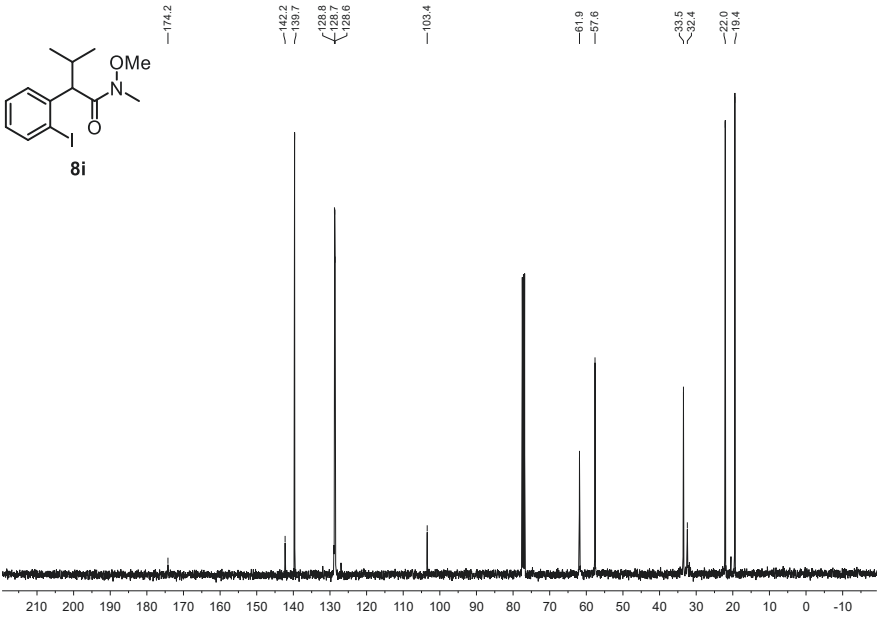

Figure S 10. ^{13}C NMR of **8i** in $CDCl_3$ measured at 100.63 MHz.

2-(2-iodophenyl)-*N*-methoxy-*N*-methylpent-4-enamide

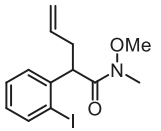

8j

8j was synthesized according to **GP-E** employing 2-(2-iodophenyl)acedic acid (2.99 g, 11.4 mmol, 1.00 equiv.), diisopropylamine (3.20 mL, 22.8 mmol, 2.00 equiv.), *n*-BuLi (9.12 mL, 2.50 M, 2.00 equiv.), allyl iodide (5.20 mL, 57.0 mmol 5.00 equiv.), N,O-dimethylhydroxylamine hydrochloride (1.67 g, 17.1 mmol, 1.50 equiv.), DMAP (2.09 g, 17.1 mmol, 1.50 equiv.), and EDC (2.65 g, 17.1 mmol, 1.50 equiv.). Purification *via* column chromatography (67:33 *n*-hexane/EA) afforded **8j** (768 mg, 2.41 mmol, 21%) as a yellow oil.

$C_{13}H_{16}NO_2I$ (344.18 $\frac{g}{mol}$)

R_f: 0.84 (*n*-hexane/EA = 80:20) [UV]

^{1}H NMR(400.16 MHz, $CDCl_3$): δ = 7.85 (dd, ^3J = 7.9 Hz, ^4J = 1.2 Hz, 1H), 7.36 (dd, ^3J = 7.8 Hz, ^4J = 1.7 Hz, 1H), 7.29 (m, 1H), 6.91 (m, 1H), 5.85 (dddd, ^3J = 17.1 Hz, ^3J = 10.2 Hz, ^3J = 6.9 Hz, ^3J = 6.9 Hz, 1H), 5.09 (dm, ^3J = 17.1 Hz, 1H), 5.00 (dm, ^3J = 10.2 Hz, 1H), 4.42 (m, 1H), 3.46 (s, 3H), 3.15 (s, 3H), 2.72 (m, 1H), 2.34 (m, 1H).

^{13}C NMR(100.62 MHz, $CDCl_3$): δ = 173.7, 142.7, 139.7, 135.9, 128.9, 128.7, 128.0, 116.9, 101.8, 61.5, 51.9, 37.9, 32.5.

HRMS (ESI-TOF) m/z: $[M+Na]^+$ Calcd for $C_{13}H_{16}NO_2INa$ 368.0118; Found 368.0124.

IR (ATR, $\tilde{\nu}$): 1657 cm^{-1} (s, *CO*NMeOMe).

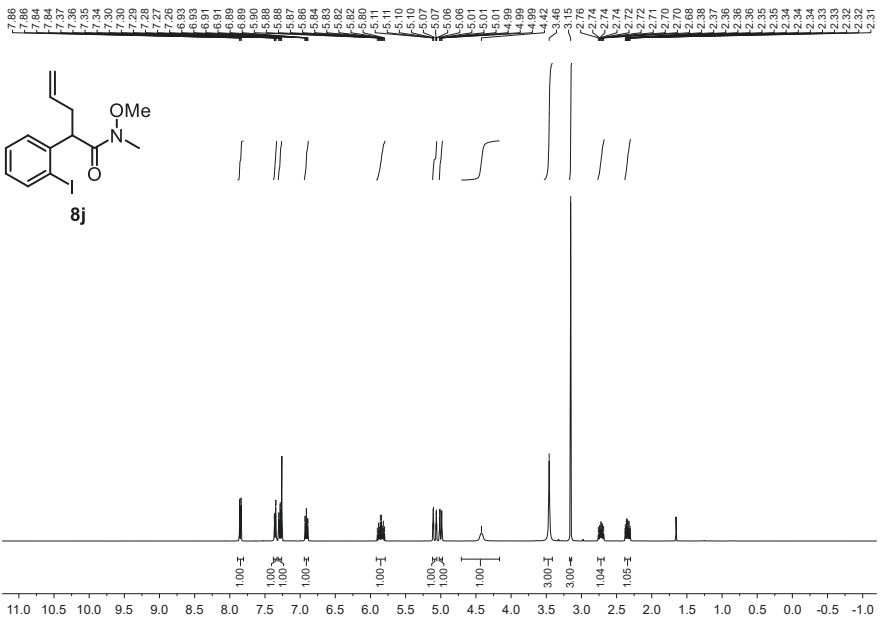

Figure S 11. ^{1}H NMR of **8j** in $CDCl_3$ measured at 400.16 MHz.

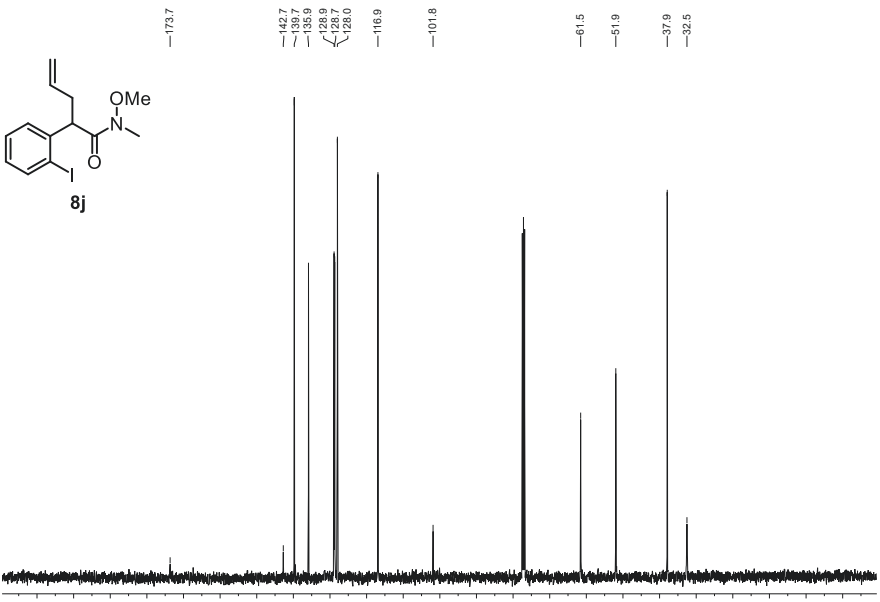

Figure S 12. ^{13}C NMR of **8j** in $CDCl_3$ measured at 100.63 MHz.

1-(2-bromophenyl)-*N*-methoxy-*N*-methylcyclopropane-1-carboxamide

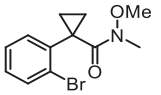

8k

8k was synthesized according to **GP-D** employing 1-(2-bromophenyl)cyclopropanecarboxylic acid (699 mg, 2.90 mmol, 1.00 equiv.), N,O-dimethylhydroxylamine hydrochloride (424 mg, 4.35 mmol, 1.50 equiv.), DMAP (531 mg, 4.35 mmol, 1.50 equiv.), and EDC (675 mg, 4.35 mmol, 1.50 equiv.). Purification *via* column chromatography (90:10 *n*-hexane/EA) afforded **8k** (651 mg, 2.04 mmol, 70%) as a yellow oil. The analytical data is in accordance with literature.

$C_{12}H_{14}NO_2Br$ (284.15 $\frac{g}{mol}$)

mp: 80.0 °C.

R_f: 0.73 (*n*-hexane/EA = 80:20) [UV]

^{1}H NMR(700.21 MHz, $CDCl_3$): δ = 7.54 (dd, ^3J = 7.9 Hz, ^4J = 1.1 Hz, 1H), 7.33 (dd, ^3J = 7.8 Hz, ^3J = 1.6 Hz, 1H), 7.27 (m, 1H), 7.09 (m, 1H), 3.10 (s, 3H), 2.90 (s, 3H), 1.69 (m, 2H), 1.11 (m, 2H).

^{13}C NMR(176.08 MHz, $CDCl_3$): δ = 173.4, 141.5, 132.5, 131.0, 128.0, 127.0, 126.9, 59.8, 33.8, 31.0, 16.1.

HRMS (ESI-TOF) m/z: $[M+Na]^+$ Calcd for $C_{12}H_{14}NO_2BrNa$ 306.0100; Found 306.0100.

IR (ATR, ṽ): 1654 cm^{-1} (s, *CO*NMeOMe).

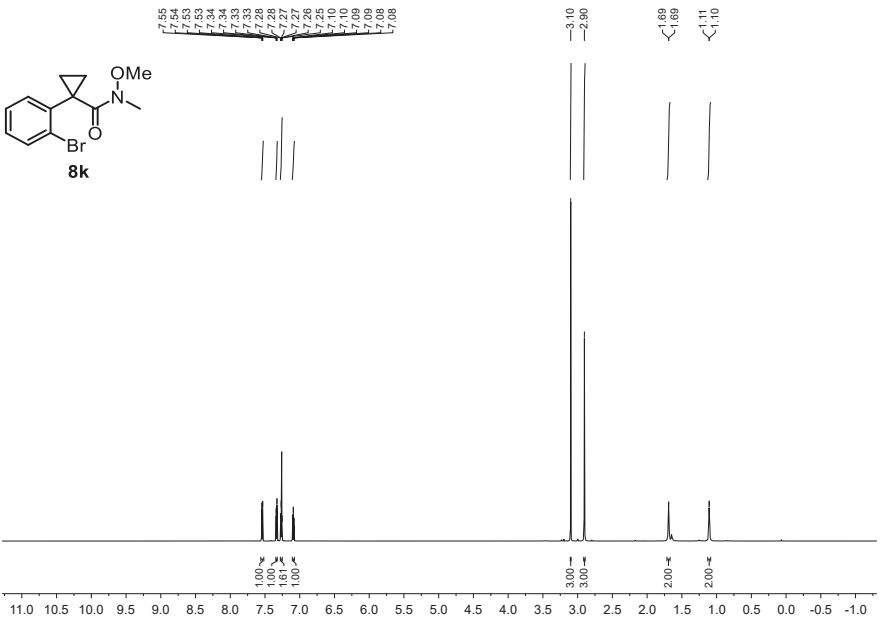

Figure S 13. ^{1}H NMR of **8k** in $CDCl_3$ measured at 700.21 MHz.

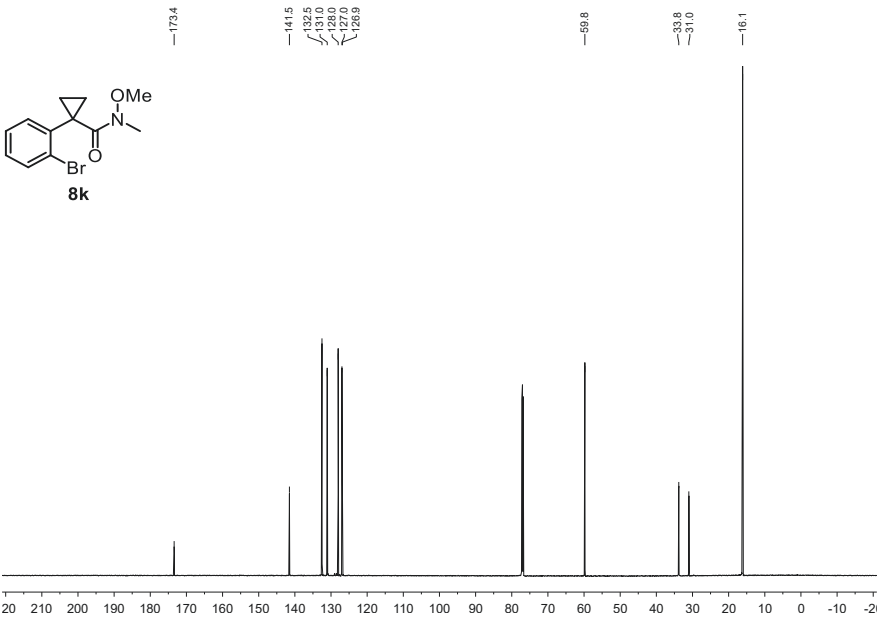

Figure S 14. ^{13}C NMR of **8k** in $CDCl_3$ measured at 176.08 MHz.

2-(2-iodo-4-isobutylphenyl)-*N*-methoxy-*N*-methylpropanamide

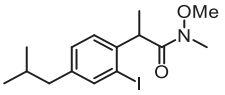

8l

8l was synthesized according to **GP-F** employing ibuprofen (2.06 g, 10.0 mmol, 1.00 equiv.), $Pd(OAc)_2$ (112 mg, 500 µmol, 5 mol%), PIDA (2.42 g, 7.50 mmol, 0.75 equiv.), I_2 (1.90 g, 7.50 mmol, 0.75 equiv.), N,O-dimethylhydroxylamine hydrochloride (1.46 g, 15.0 mmol, 1.50 equiv.), DMAP (1.83 g, 15.0 mmol, 1.50 equiv.), and EDC (2.33 g, 15.0 mmol, 1.50 equiv.). Purification *via* column chromatography (80:20 *n*-hexane/EA) afforded 1.51 g of a mixture of **8l** (1.22 g, 3.30 mmol) and N-methoxy-N-methyl-2-(4-isobutylphenyl)propenamide (78:22) as a yellow oil corresponding to 33% yield over two steps.

$C_{15}H_{22}NO_2I$ (375.25 $\frac{g}{mol}$)

R$_f$: 0.88 (*n*-hexane/EA = 80:20) [UV]

^{1}H NMR(700.21 MHz, $CDCl_3$): δ = 7.63 (d, ^4J = 1.8 Hz, 1H), 7.19 (d, ^3J = 7.8 Hz, 1H), 7.06 (dd, ^3J = 7.8 Hz, ^4J = 1.8 Hz, 1H), 4.36 (m, 1H), 3.36 (s, 3H), 3.15 (s, 3H), 2.37 (d, ^3J = 7.2 Hz, 2H), 1.82 (m, 1H), 1.33 (d, ^3J = 7.0 Hz, 3H), 0.88 (d, ^3J = 6.6 Hz, 3H), 0.88 (d, ^3J = 6.6 Hz, 3H).

^{13}C NMR(176.08 MHz, $CDCl_3$): δ = 175.4, 142.3, 142.1, 140.0, 129.8, 126.9, 100.8, 61.2, 46.7, 44.4, 32.6, 30.2, 22.4, 22.4, 18.6.

HRMS (APCI-TOF) m/z: $[M+Na]^+$ Calcd for $C_{15}H_{22}NO_2INa$ 398.0588; Found 398.0589.

IR (ATR, ṽ): 1649 cm^{-1} (s, *CO*NMeOMe).

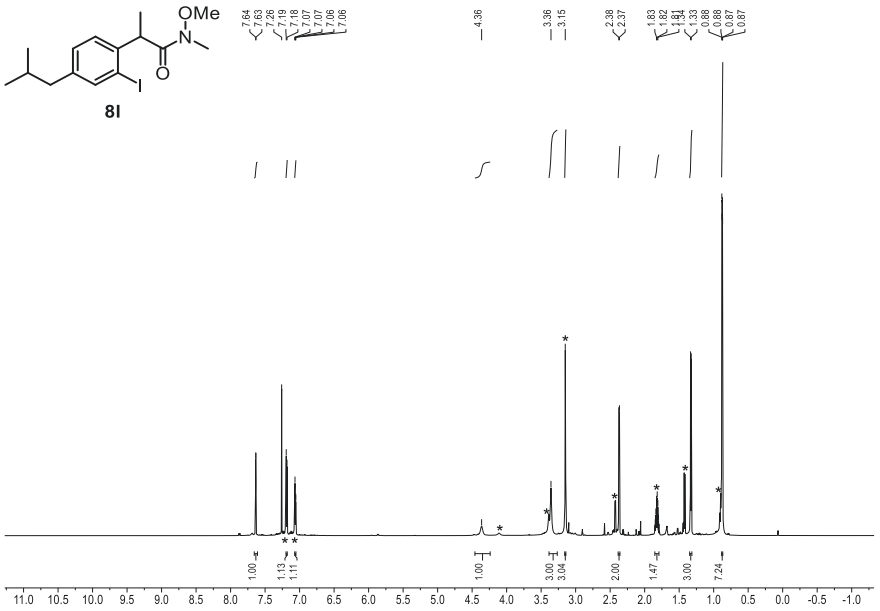

Figure S 15. ^{1}H NMR of **8l** in $CDCl_3$ measured at 700.21 MHz. Signals denoted by * correspond to N-Methoxy-N-methyl-2-(4-isobutylphenyl)propanamide.[12]

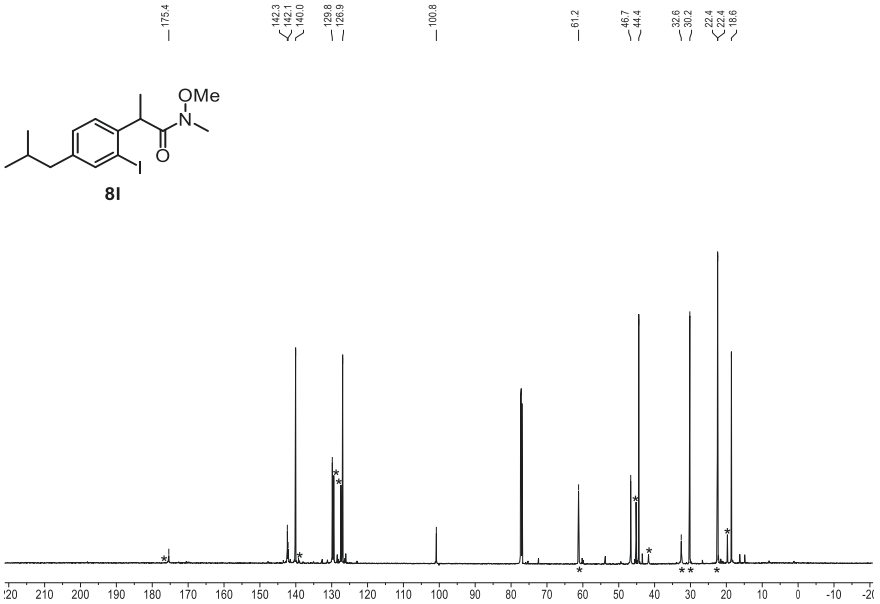

Figure S 16. ^{13}C NMR of **8l** in $CDCl_3$ measured at 176.08 MHz. Signals denoted by * correspond N-Methoxy-N-methyl-2-(4-isobutylphenyl)propanamide.[12]

4.2 Kobayashi and ketene precursors

1,1-diethoxyethene

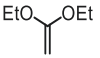

9

9 was synthesized according to literature.[13] In a dried two necked Schlenk RBF (500 mL) KO^{t}Bu (93.0 g, 829 mmol, 1.00 equiv.) was cooled to 0 °C and 2-bromo-1,1-diethoxyethane (129 mL, 829 mmol, 1.00 equiv.) was added dropwise until white mist formed (about 10 mL). The remaining 2-bromo-1,1-diethoxyethane was added dropwise after disappearance of the mist, whilst stirring manually. ^{t}BuOH (50 mL) was added and the mixture was heated to 50 °C and stirred for 1 h. Subsequently, ^{t}BuOH was distilled off (oil bath: 130 – 145 °C, 1.0 atm), after which **9** was obtained *via* vacuum distillation (oil bath: 60 – 120 °C, 30 – 10 mbar) as a colorless liquid (84.8 g, 730 mmol, 88%). The analytical data is in accordance with literature.[13]

$C_6H_{12}O_2$ (116.16 $\frac{g}{mol}$)

b.p. (28 mbar): 35 °C.

^{1}H NMR(400.16 MHz, $CDCl_3$): δ = 3.81 (q, ^3J = 7.1 Hz, 4H), 3.07 (d, ^2J = 4.2 Hz, 2H), 1.31 (t, ^3J = 7.1 Hz, 6H).

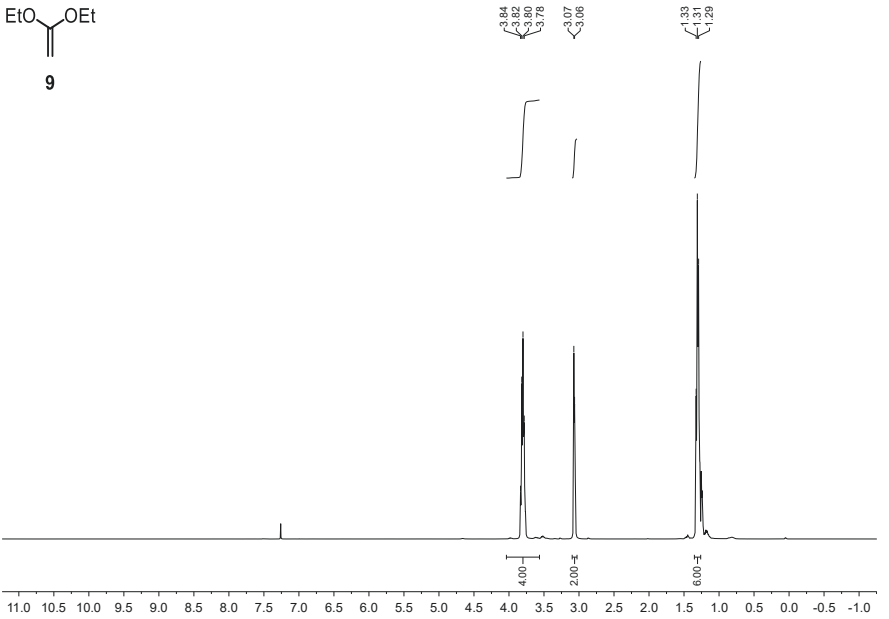

Figure S 17. ^{1}H NMR of **9** in $CDCl_3$ measured at 400.16 MHz.

3-(trimethylsilyl)naphthalen-2-yl trifluoromethanesulfonate

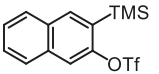

10b

10b was synthesized according to **GP-G** employing 3-bromo-2-naphthol (5.23 g, 23.5 mmol, 1.00 equiv.), HMDS (5.13 mL, 24.6 mmol, 1.05 equiv.), *n*-BuLi (14.1 mL, 2.50 M, 1.50 equiv.) and Tf_2O (4.72 mL, 28.1 mmol, 1.20 equiv.). Purification *via* column chromatography (98:02 *n*-hexane/EA) afforded **10b** (4.20 g, 12.1 mmol, 52%) as a colorless oil. The analytical data is in accordance with literature.[5]

$C_{14}H_{15}O_3F_3SSi$ (348.41 $\frac{g}{mol}$)

R$_f$: 0.56 (*n*-hexane/EA = 98:2) [UV]

^{1}H NMR(700.21 MHz, $CDCl_3$): δ = 8.02 (s, 1H), 7.88 (d, ^3J = 7.8 Hz, 1H), 7.84 (d, ^3J = 7.7 Hz, 1H), 7.82 (s, 1H), 7.56 (m, 2H), 0.46 (m, 9H).

^{13}C NMR(176.08 MHz, $CDCl_3$): δ = 152.7, 137.7, 134.2, 131.9, 131.2, 128.1, 127.9, 127.1, 118.7 (q, ^1J = 320.2 Hz), 116.6, -0.6.

^{19}F NMR(658.79 MHz, $CDCl_3$): δ =-73.7.

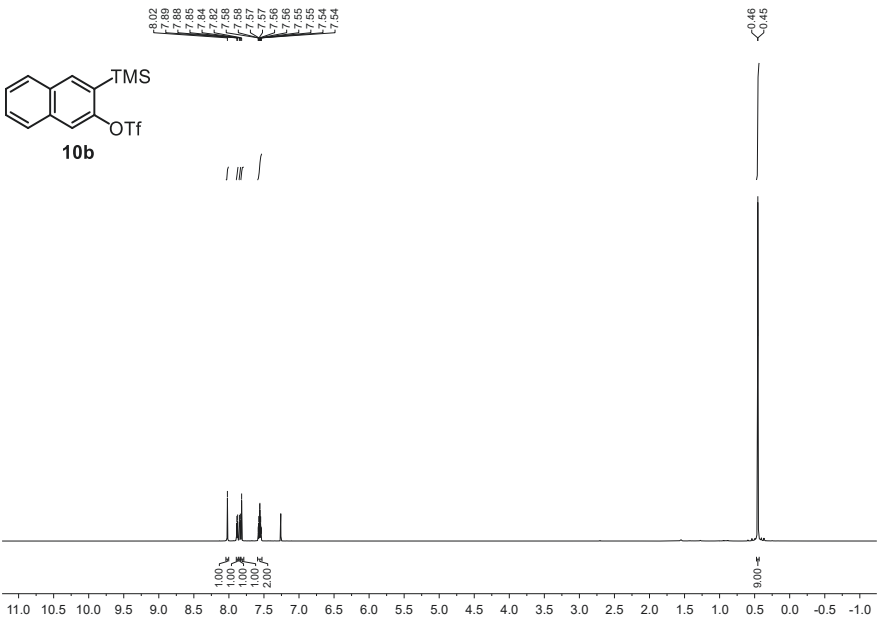

Figure S 18. ^{1}H NMR of **10b** in $CDCl_3$ measured at 700.21 MHz.

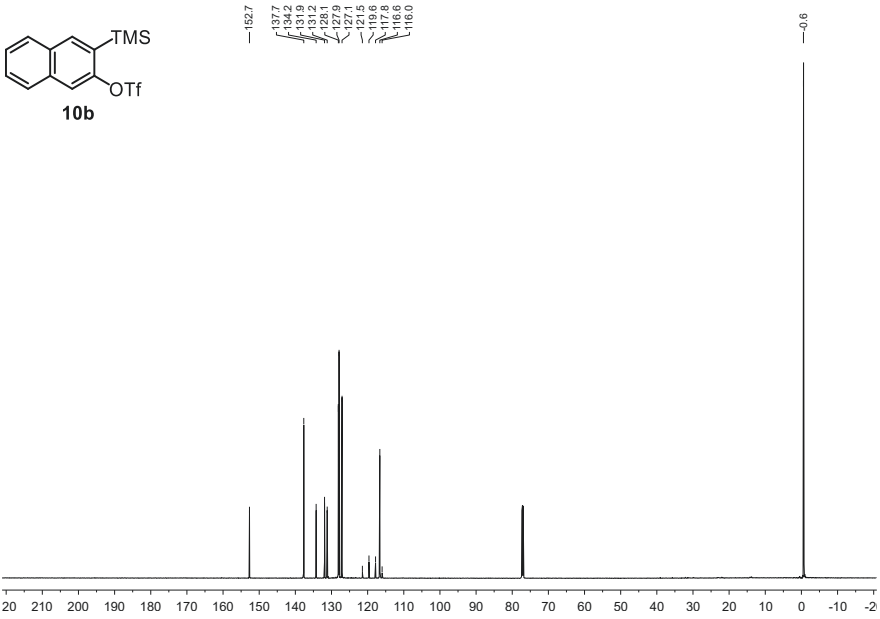

Figure S 19. ^{13}C NMR of **10b** in $CDCl_3$ measured at 176.08 MHz.

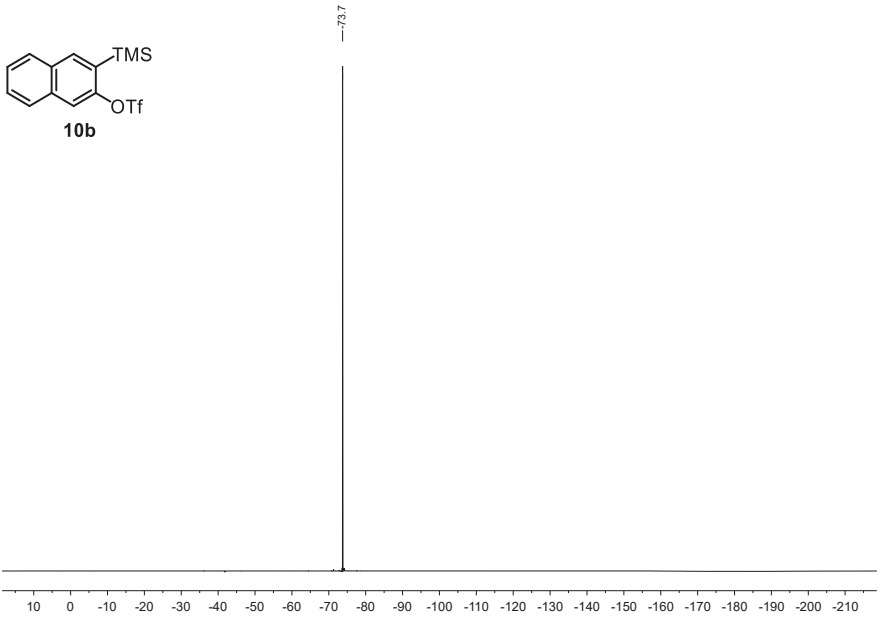

Figure S 20. ^{19}F NMR of **10b** in $CDCl_3$ measured at 658.79 MHz.

3-methyl-2-(trimethylsilyl)phenyl trifluoromethanesulfonate

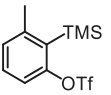

10m

10m was synthesized according to **GP-G** employing 2-bromo-3-methylphenol (5.15 g, 27.5 mmol, 1.00 equiv.), HMDS (6.03 mL, 28.9 mmol, 1.05 equiv.), *n*-BuLi (25.8 mL, 1.60 M, 1.50 equiv.) and Tf_2O (5.55 mL, 33.0 mmol, 1.20 equiv.). Purification *via* column chromatography (98:02 *n*-hexane/EA) afforded **10m** (3.26 g, 10.4 mmol, 38%) as a colorless oil. The analytical data is in accordance with literature.[14]

$C_{11}H_{15}O_3F_3SSi$ ($312.38\ \frac{g}{mol}$)

R_f: 0.71 (*n*-hexane/EA = 98:2) [UV]

^{1}H NMR(700.21 MHz, $CDCl_3$): δ = 7.30 (m, 1H), 7.15 (m, 2H), 2.50 (s, 3H), 0.44 (s, 9H).

^{13}C NMR(176.08 MHz, $CDCl_3$): δ = 155.4, 146.9, 131.2, 130.6, 130.2, 118.7 (q, ^1J = 320.4 Hz), 117.6, 24.3, 2.0.

^{19}F NMR(658.79 MHz, $CDCl_3$): δ =-73.1.

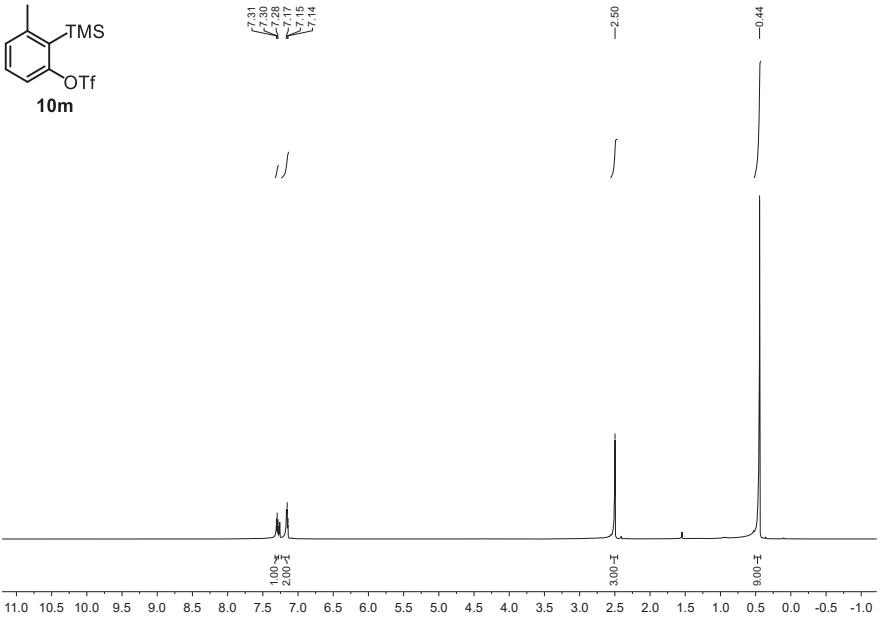

Figure S 21. ^{1}H NMR of **10m** in $CDCl_3$ measured at 700.21 MHz.

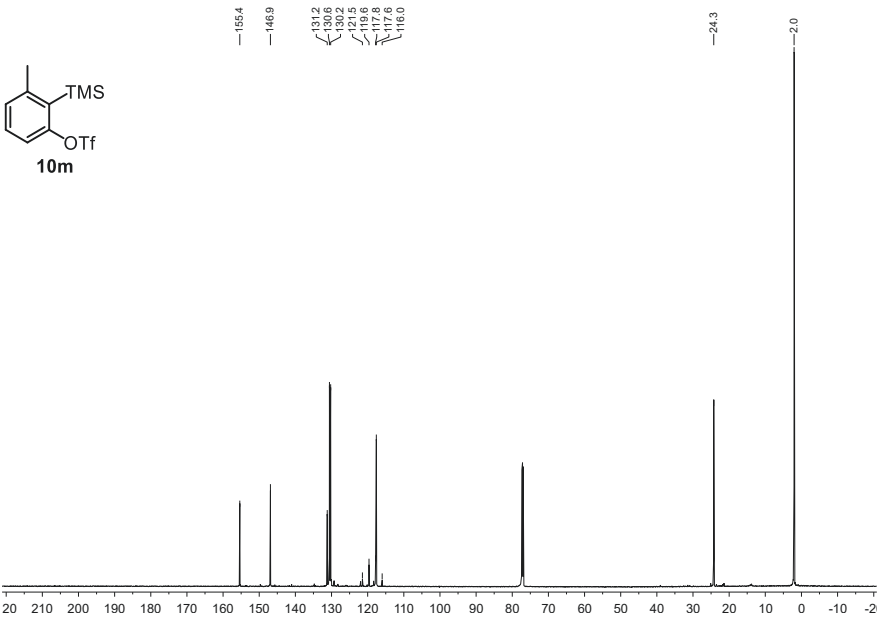

Figure S 22. ^{13}C NMR of **10m** in $CDCl_3$ measured at 176.08 MHz.

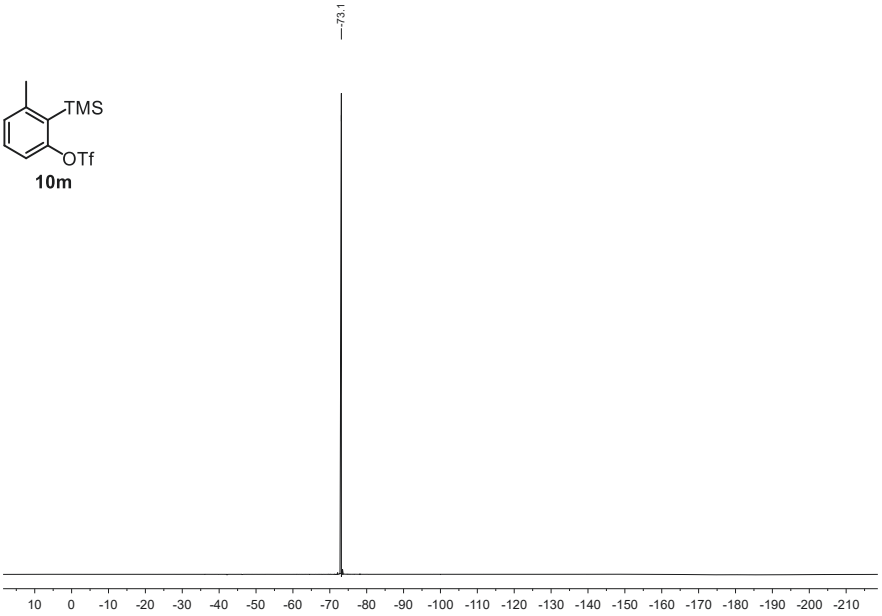

Figure S 23. ^{19}F NMR of **10m** in $CDCl_3$ measured at 658.79 MHz.

4.3 Benzocyclobutanones

bicyclo[4.2.0]octa-1,3,5-trien-7-one

1a

1a was synthesized according to **GP-H** employing 2-(2-iodophenyl)acetic acid (22.1 g, 72.5 mmol, 1.00 equiv.) and ^{t}BuLi (89.6 mL, 1.70 M, 2.10 equiv.). Purification *via* flash chromatography (80 g SiO_2, gradient from 100:0 to 93:07 *n*-hexane/EA over 15 CV) afforded **1a** (2.74 g, 23.2 mmol, 32%) as a pale yellow oil. Subsequent vacuum distillation at 2.8 mbar, 54 °C (70 °C water bath) furnished **1a** (2.32 g, 19.6 mmol, 27%) as a colorless oil. The analytical data is in accordance with literature.[15]

C_8H_6O (118.14 $\frac{g}{mol}$)

b.p. (2.8 mbar): 54 °C.

R$_f$: 0.66 (*n*-hexane/EA = 80:20) [UV]

^{1}H NMR(700.21 MHz, $CDCl_3$): δ = 7.53 (m, 2H), 7.40 (m, 1H), 7.34 (d, ^3J = 7.6 Hz, 1H), 3.98 (s, 2H).

^{13}C NMR(176.08 MHz, $CDCl_3$): δ = 188.9, 151.4, 148.1, 135.3, 128.8, 123.8, 120.7, 52.5.

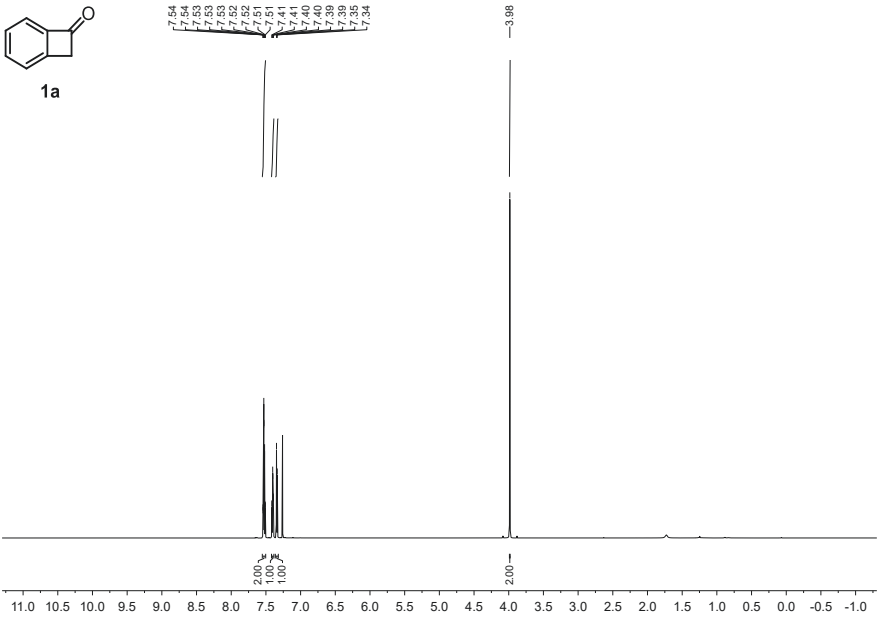

Figure S 24. ^{1}H NMR of **1a** in $CDCl_3$ measured at 700.21 MHz.

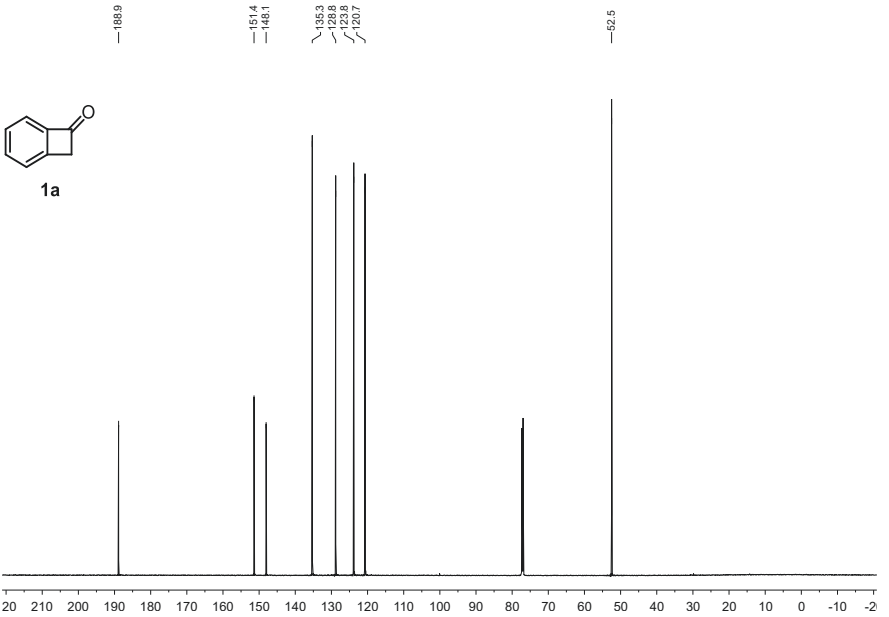

Figure S 25. ^{13}C NMR of **1a** in $CDCl_3$ measured at 176.08 MHz.

cyclobuta[b]naphthalen-1(2H)-one

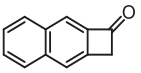

1b

1b was synthesized according to **GP-J** employing **10b** (4.01 g, 11.5 mmol, 1.0 equiv.), **9** (3.41 mL, 23.0 mmol, 2.00 equiv.), CsF (2.62 g, 17.3 mmol, 1.50 equiv.), and TFA (1.76 mL, 23.0 mmol, 2.00 equiv.). Purification *via* column chromatography (gradient from 100:0 to 85:15 *n*-hexane/EA) and recrystallisation from *n*-hexane/EA (80:20) afforded **1b** (630 mg, 3.74 mmol, 33%) as colorless crystals. The analytical data is in accordance with literature.[5]

$C_{12}H_8O$ (168.20 $\frac{g}{mol}$)

R$_f$: 0.50 (*n*-hexane/EA = 90:10) [UV]

^{1}H NMR(400.16 MHz, $CDCl_3$): δ = 7.95 (d, ^3J = 8.5 Hz, 1H), 7.87 (m, 3H), 7.60 (ddd, ^3J = 8.2 Hz, ^3J = 6.9 Hz, ^4J = 1.3 Hz, 1H), 7.50 (m, 1H), 4.19 (s, 2H).

^{13}C NMR(100.62 MHz, $CDCl_3$): δ = 190.7, 146.5, 143.5, 137.8, 133.6, 130.9, 128.6, 128.4, 126.2, 121.6, 120.2, 53.1.

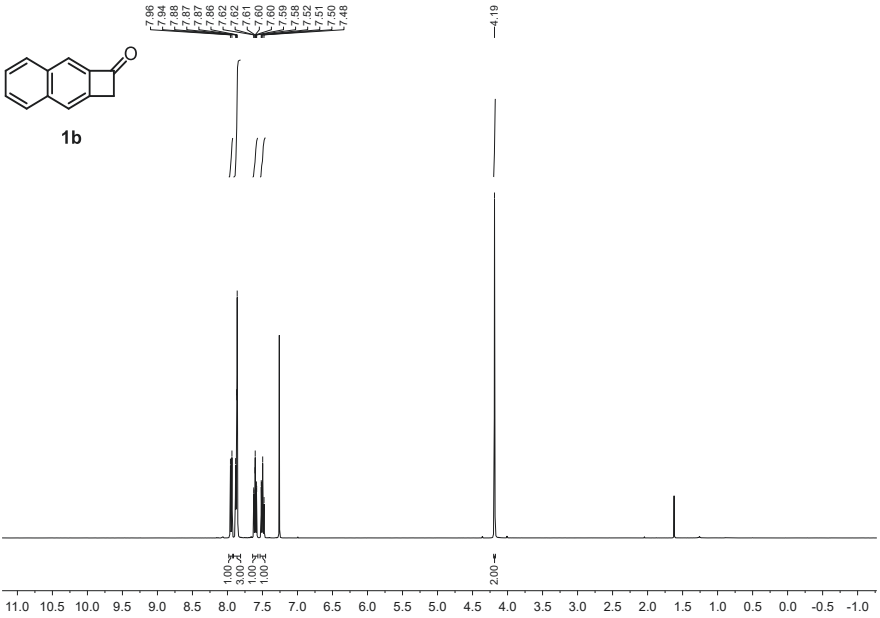

Figure S 26. ^{1}H NMR of **1b** in $CDCl_3$ measured at 400.16 MHz.

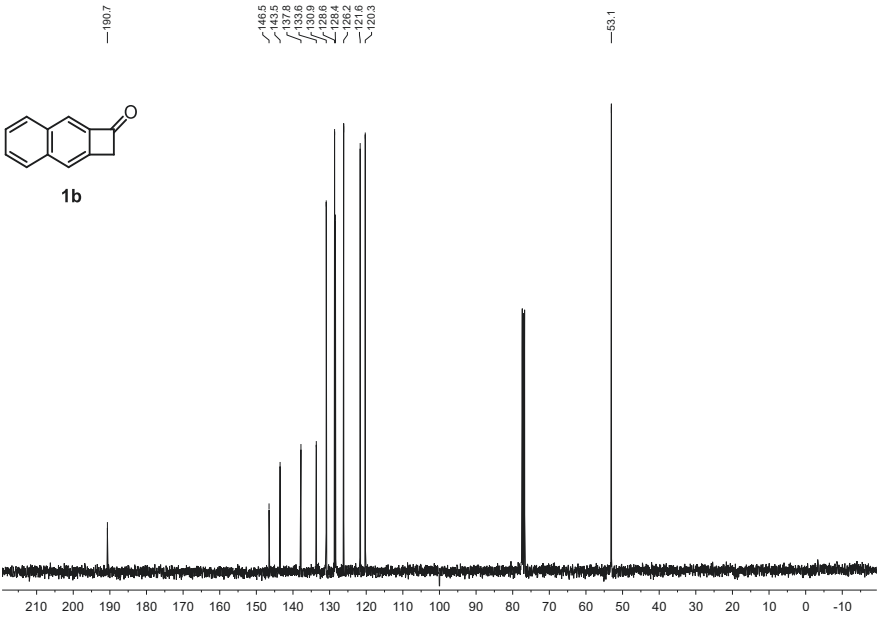

Figure S 27. ^{13}C NMR of **1b** in $CDCl_3$ measured at 100.63 MHz.

2-methylbicyclo[4.2.0]octa-1,3,5-trien-7-one

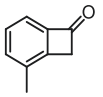

1c

1c was synthesized according to **GP-H** employing **8c** (851 mg, 2.67 mmol, 1.00 equiv.) and ^{t}BuLi (3.14 mL, 1.70 M, 2.00 equiv.). Purification *via* flash chromatography (23 g SiO_2, gradient from 100:0 to 80:20 *n*-hexane/EA over 15 CV) afforded **1c** (281 mg, 2.13 mmol, 80%) as a colorless soid. The analytical data is in accordance with literature**.** The analytical data is in accordance with literature.[6]

C_9H_8O (132.16 $\frac{g}{mol}$)

R$_f$: 0.68 (*n*-hexane/EA = 80:20) [UV]

^{1}H NMR(700.21 MHz, $CDCl_3$): δ = 7.31 (m, 2H), 7.16 (m, 1H), 3.91 (s, 2H), 2.37 (s, 3H).

^{13}C NMR(176.08 MHz, $CDCl_3$): δ = 188.7, 150.5, 147.6, 136.1, 134.2, 129.6, 118.0, 51.2, 17.8.

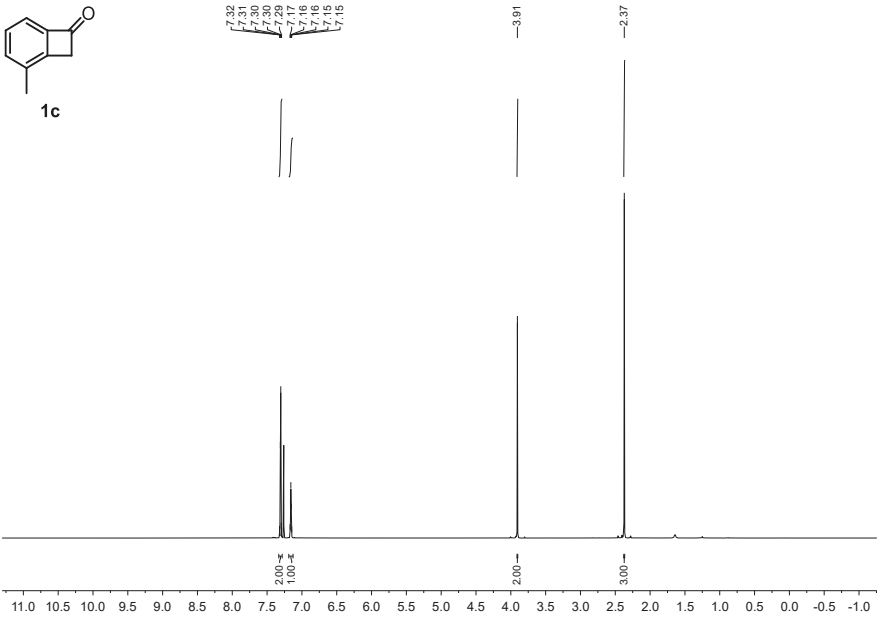

Figure S 28. ^{1}H NMR of **1c** in $CDCl_3$ measured at 700.21 MHz.

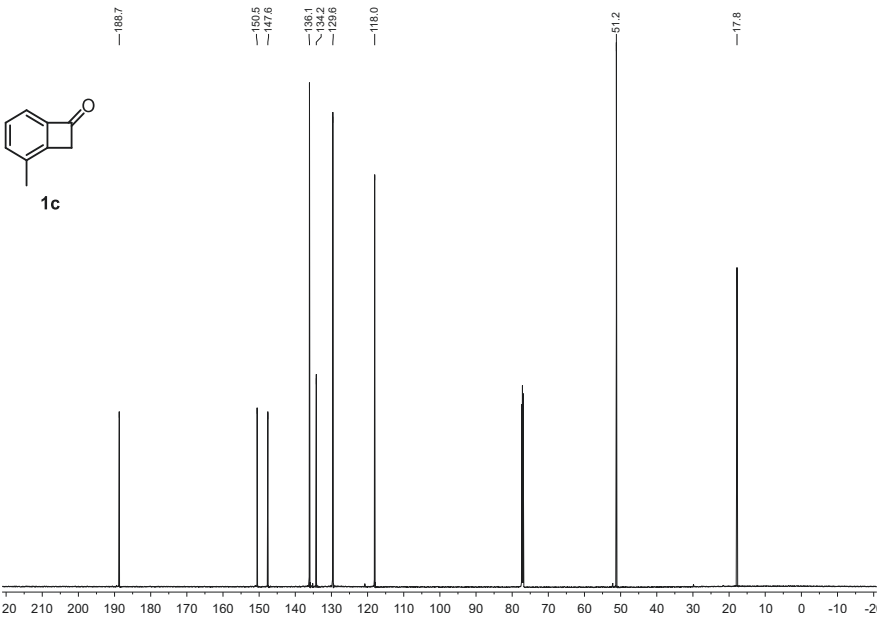

Figure S 29. ^{13}C NMR of **1c** in $CDCl_3$ measured at 176.08 MHz.

4-methoxybicyclo[4.2.0]octa-1,3,5-trien-7-one

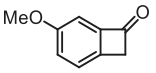

1d

1d was synthesized according to **GP-I** employing 4-bromo anisole (3.74 g, 20.0 mmol, 1.00 equiv.), $NaNH_2$ (3.12 g, 80.0 mmol. 4.00 equiv.), and **9** (10.6 mL, 80.0 mmol, 4.00 equiv.). Purification *via* flash chromatography (40 g SiO_2, gradient from 100:0 to 92:08 *n*-hexane/EA over 11 CV) afforded **1d** (0.633 g, 4.27 mmol, 21%) as a yellow solid. The analytical data is in accordance with literature.[6]

$C_9H_8O_2$ (148.16 $\frac{g}{mol}$)

R$_f$: 0.59 (*n*-hexane/EA = 80:20) [UV]

^{1}H NMR(400.16 MHz, $CDCl_3$): δ = 7.41 (dm, ^3J = 8.1 Hz, 1H), 7.09 (dd, ^3J = 8.1 Hz, ^4J = 2.2 Hz, 1H), 6.82 (d, ^4J = 2.2 Hz, 1H), 3.87 (s, 2H), 3.79 (s, 3H).

^{13}C NMR(100.62 MHz, $CDCl_3$): δ = 188.2, 160.8, 148.8, 144.0, 124.7, 124.1, 103.1, 55.8, 51.1.

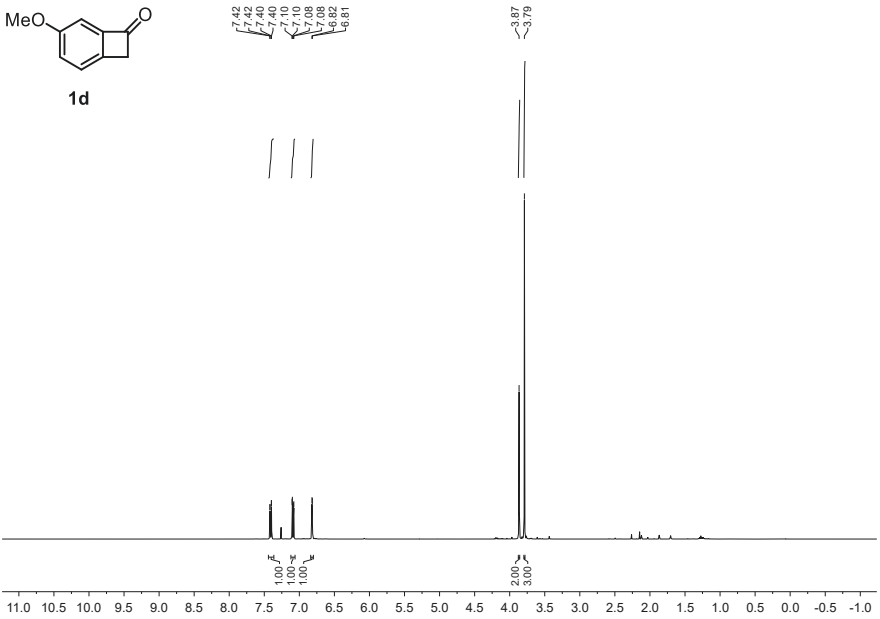

Figure S 30. ^{1}H NMR of **1d** in $CDCl_3$ measured at 400.16 MHz.

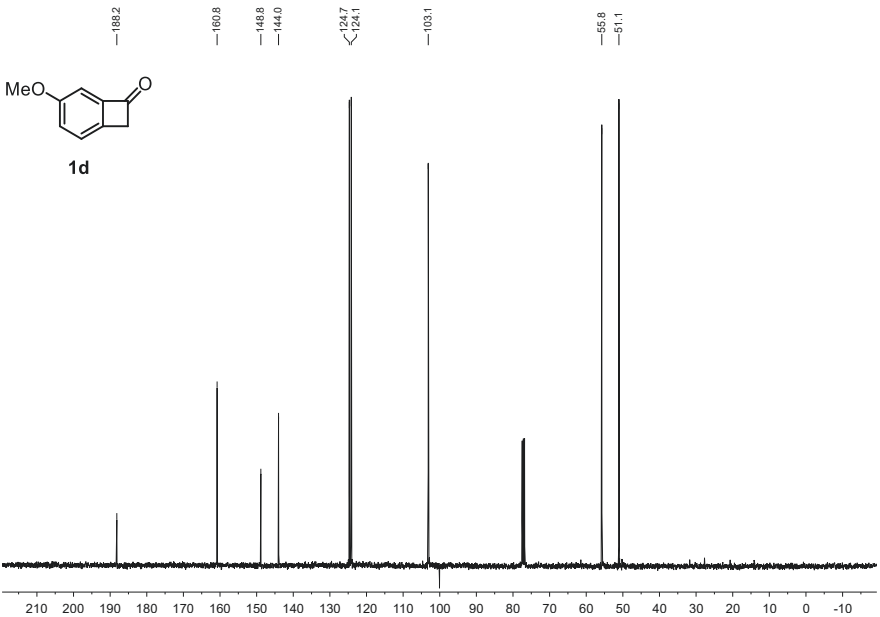

Figure S 31. ^{13}C NMR of **1d** in $CDCl_3$ measured at 100.63 MHz.

cyclobuta[3,4]benzo[1,2-d][1,3]dioxol-7(6H)-one

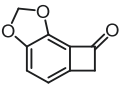

1e

1e was synthesized according to **GP-I** employing 5-bromo 1,3-benzodioxole (4.02 g, 20.0 mmol, 1.00 equiv.), $NaNH_2$ (3.12 g, 80.0 mmol. 4.00 equiv.), and **9** (11.9 mL, 80.0 mmol, 4.00 equiv.). Purification *via* flash chromatography (40 g SiO_2, gradient from 100:0 to 90:10 *n*-hexane/EA over 10 CV) afforded **1e** (1.72 g, 10.61 mmol, 53%) as a pale yellow solid. The analytical data is in accordance with literature.[7]

$C_9H_6O_3$ (162.14 $\frac{g}{mol}$)

R$_f$: 0.52 (*n*-hexane/EA = 80:20) [UV]

^{1}H NMR(400.16 MHz, $CDCl_3$): δ = 6.97 (m, 1H), 6.92 (m, 1H), 6.06 (s, 2H), 3.90 (d, ^4J = 0.8 Hz, 2H).

^{13}C NMR(100.62 MHz, $CDCl_3$): δ = 184.4, 149.1, 141.6, 137.7, 128.2, 115.6, 115.0, 102.6, 52.2.

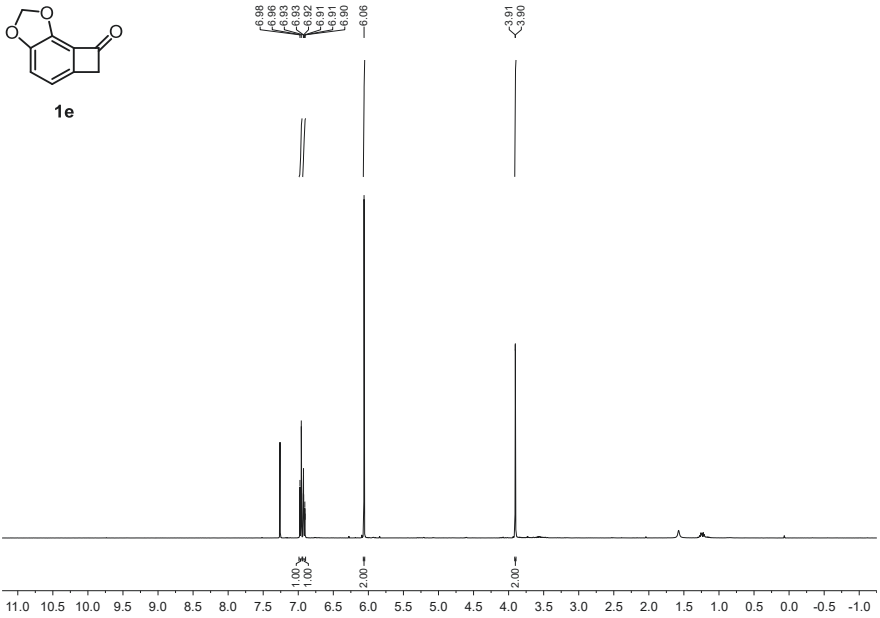

Figure S 32. ^{1}H NMR of **1e** in $CDCl_3$ measured at 400.16 MHz.

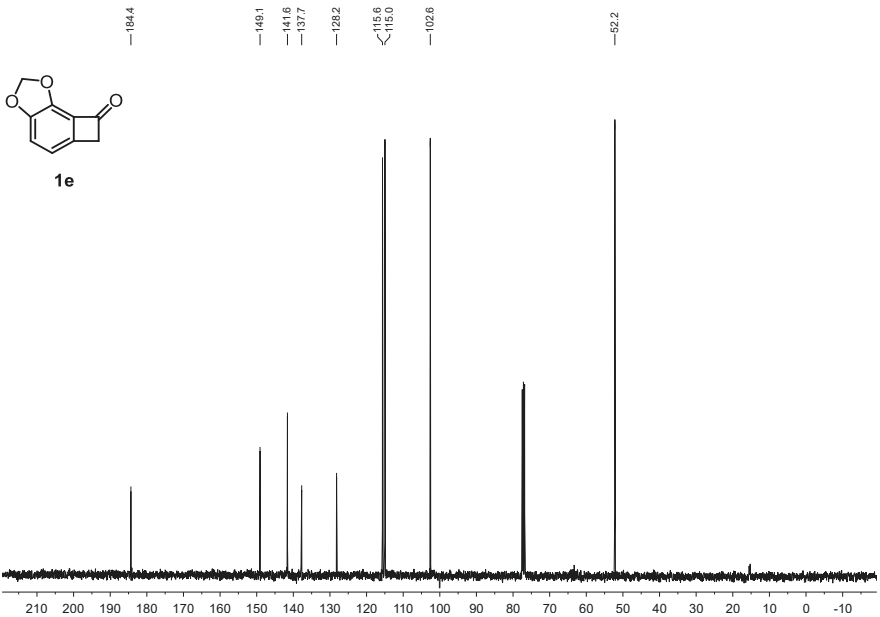

Figure S 33. ^{13}C NMR of **1e** in $CDCl_3$ measured at 100.63 MHz.

5-Fluorobicyclo[4.2.0]octa-1,3,5-trien-7-one

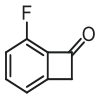

1f

1f was synthesized according to **GP-I** employing 1-bromo-2-fluorobenzene (3.50 g, 20.0 mmol, 1.00 equiv.), $NaNH_2$ (1.56 g, 40.0 mmol. 2.00 equiv.), and **9** (11.9 mL, 80.0 mmol, 4.00 equiv.). Purification *via* flash chromatography (40 g SiO_2, gradient from 100:0 to 85:15 *n*-hexane/EA over 10 CV) afforded **1f** (551 mg, 4.05 mmol, 20%) as a yellow solid.[7]

C_8H_5OF (136.13 $\frac{g}{mol}$)

Rf: 0.59 (*n*-hexane/EA = 80:20) [UV]

^{1}H NMR(700.21 MHz, $CDCl_3$): δ = 7.55 (m, 1H), 7.32 (dm, ^3J = 7.3 Hz, 1H), 6.99 (m, 1H), 3.99 (m, 2H).

^{13}C NMR(176.08 MHz, $CDCl_3$): δ = 183.2, 151.9 (d, ^4J = 4 Hz), 151.3 (d, ^1J = 267 Hz), 138.2 (d, ^3J = 7 Hz), 134.3 (d, ^2J = 17 Hz), 120.0 (d, ^3J = 5 Hz), 115.5 (d, ^2J = 20 Hz), 52.8.

^{19}F NMR(658.79 MHz, $CDCl_3$): δ =-106.8.

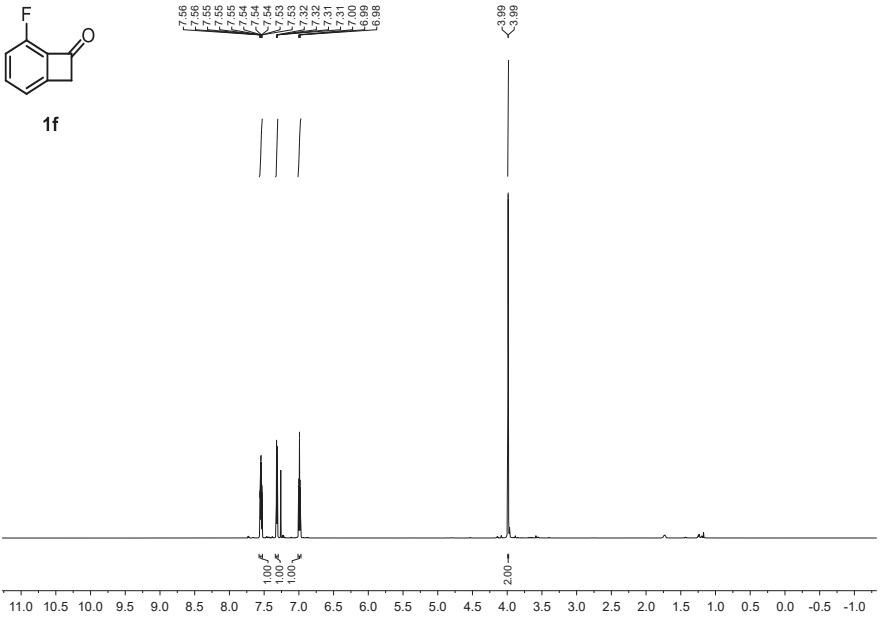

Figure S 34. ^{1}H NMR of **1f** in $CDCl_3$ measured at 700.21 MHz.

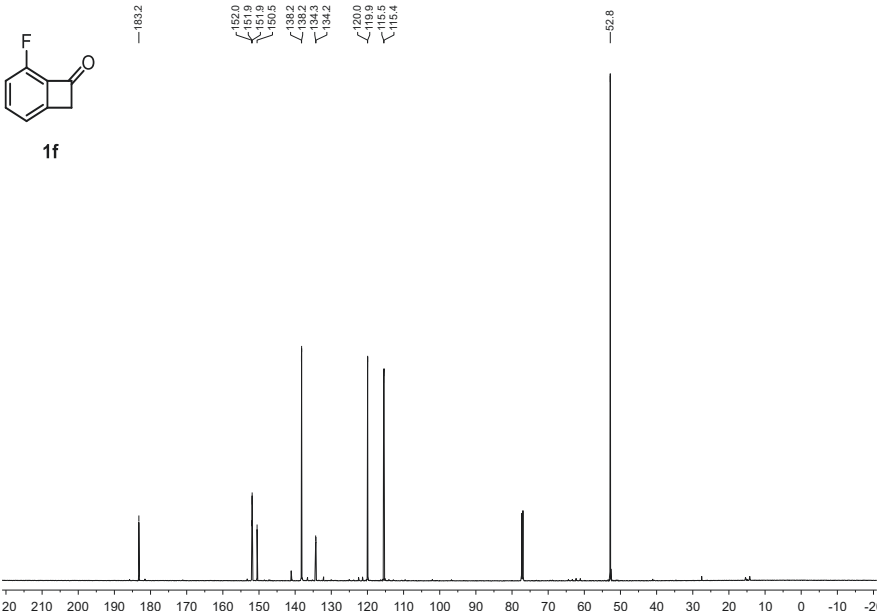

Figure S 35. ^{13}C NMR of **1f** in $CDCl_3$ measured at 176.08 MHz.

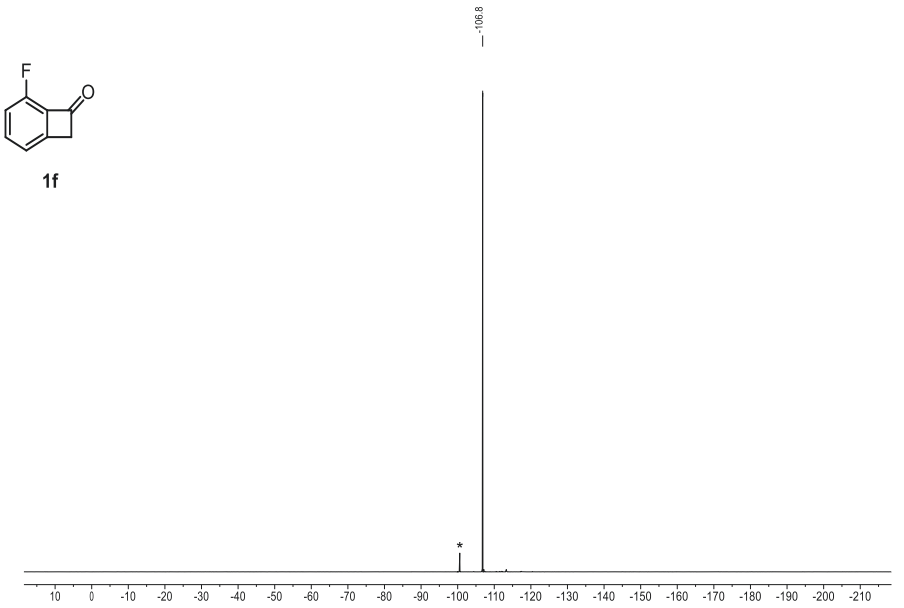

Figure S 36. ^{19}F NMR of **1f** in $CDCl_3$ measured at 658.79 MHz. * Denotes an unknown impurity.

8-methylbicyclo[4.2.0]octa-1,3,5-trien-7-one

1g

1g was synthesized according to **GP-H** employing **8g** (1.63 g, 5.10 mmol, 1.00 equiv.) and ^{t}BuLi (6.00 mL, 1.7 M, 2.00 equiv.). Purification *via* flash chromatography (23 g SiO_2, gradient from 100:0 to 80:20 *n*-hexane/EA over 10 CV) afforded **1g** (514 mg, 3.89 mmol, 76%) as a pale yellow oil. The analytical data is in accordance with literature.[6]

C_9H_8O (132.16 $\frac{g}{mol}$)

Rf: 0.68 (*n*-hexane/EA = 80:20) [UV]

^{1}H NMR(400.16 MHz, $CDCl_3$): δ = 7.51 (m, 2H), 7.41 (m, 1H), 7.35 (dm, ^{3}J = 7.5 Hz, 1H), 4.27 (q, ^{3}J = 7.2 Hz, 1H), 1.45 (d, ^{3}J = 7.2 Hz, 3H).

^{13}C NMR(100.62 MHz, $CDCl_3$): δ = 193.3, 157.7, 146.4, 135.3, 129.2, 122.9, 121.1, 59.7, 15.2.

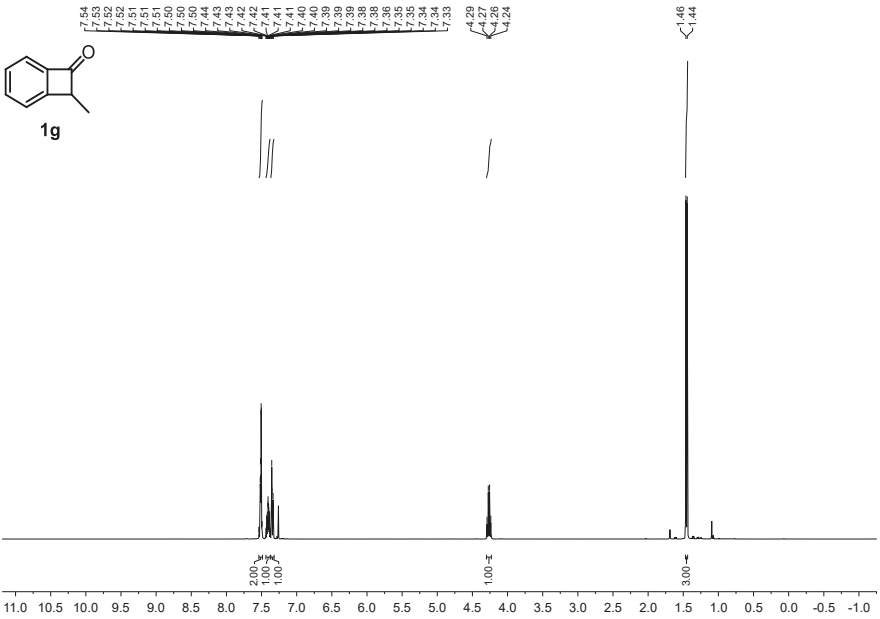

Figure S 37. ^{1}H NMR of **1g** in $CDCl_3$ measured at 400.16 MHz.

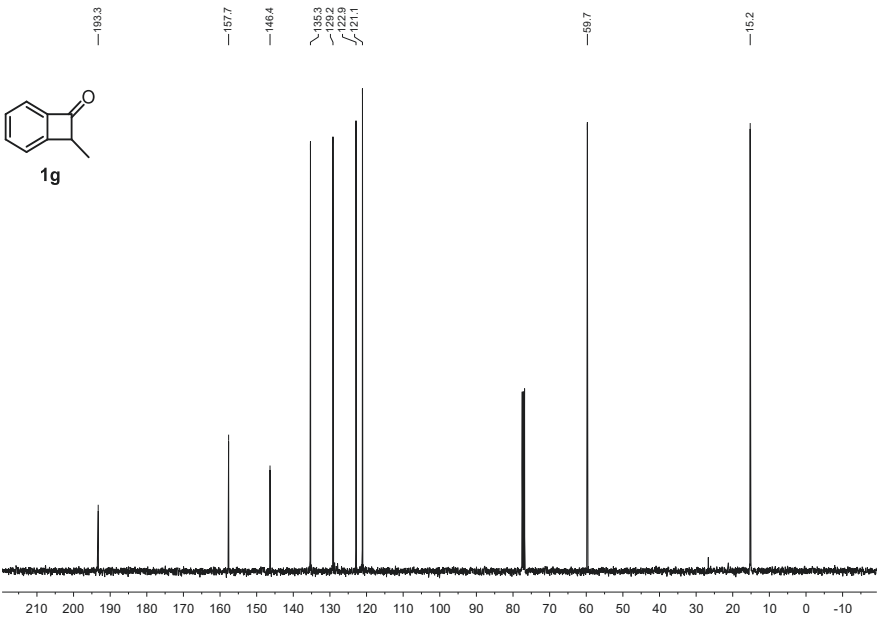

Figure S 38. ^{13}C NMR of **1g** in $CDCl_3$ measured at 100.63 MHz.

8-ethylbicyclo[4.2.0]octa-1,3,5-trien-7-one

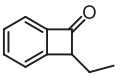

1h

1h was synthesized according to **GP-H** employing **8h** (2.10 g, 6.30 mmol, 1.00 equiv.) and ^{t}BuLi (7.78 mL, 1.70 M, 2.10 equiv.). Purification *via* flash chromatography (23 g SiO_2, gradient from 100:0 to 80:20 *n*-hexane/EA over 10 CV) afforded **1h** (587 mg, 4.01 mmol, 64%) as a pale yellow oil. The analytical data is in accordance with literature.[3]

$C_{10}H_{10}O$ (146.19 $\frac{g}{mol}$)

Rf: 0.77 (*n*-hexane/EA = 80:20) [UV]

^{1}H NMR(700.21 MHz, $CDCl_3$): δ = 7.52 (m, 2H), 7.42 (m, 1H), 7.36 (d, ^{3}J = 7.6 Hz, 1H), 4.21 (t, ^{3}J = 6.9 Hz, 1H), 1.94 (m, 1H), 1.81 (m, 1H), 1.05 (t, ^{3}J = 7.5 Hz, 3H).

^{13}C NMR(176.08 MHz, $CDCl_3$): δ = 193.2, 156.7, 146.9, 135.2, 129.2, 123.5, 120.9, 66.5, 23.6, 11.8.

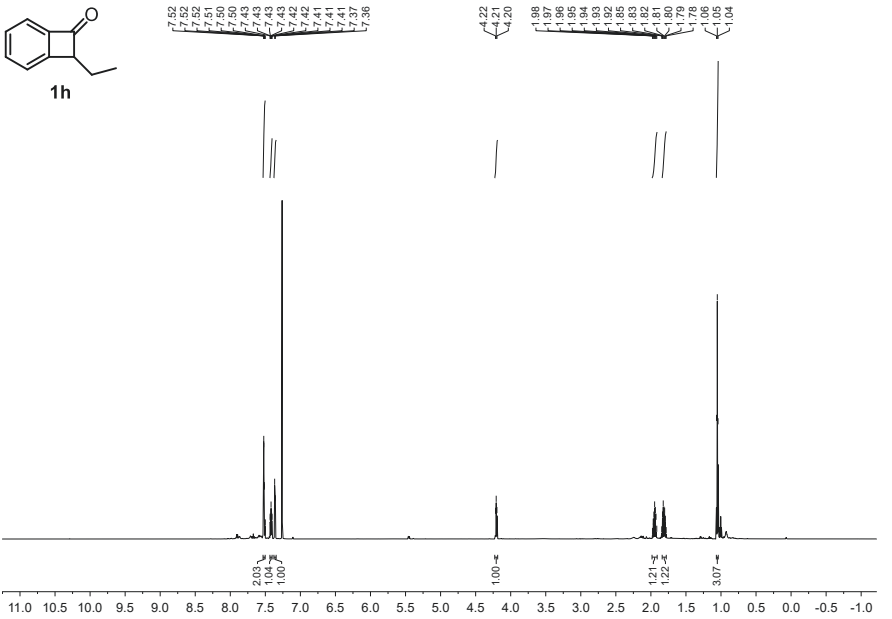

Figure S 39. ^{1}H NMR of **1h** in $CDCl_3$ measured at 700.21 MHz.

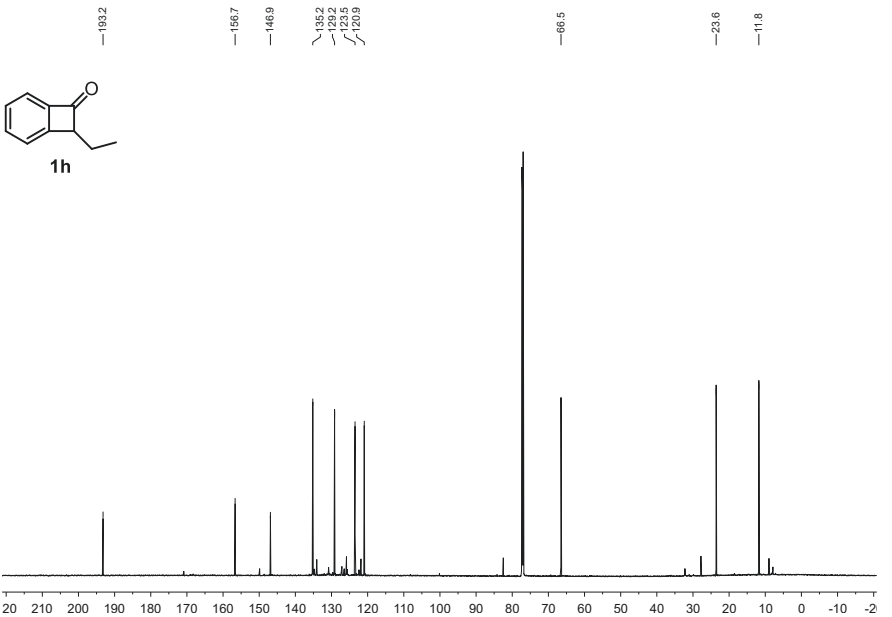

Figure S 40. ^{13}C NMR of **1h** in $CDCl_3$ measured at 176.08 MHz.

8-isopropylbicyclo[4.2.0]octa-1,3,5-trien-7-one

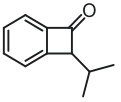

1i

1i was synthesized according to **GP-H** employing **8i** (1.70 g, 4.90 mmol, 1.00 equiv.) and ^{t}BuLi (5.76 mL, 1.70 M, 2.00 equiv.). Purification *via* flash chromatography (23 g SiO_2, gradient from 100:0 to 85:15 *n*-hexane/EA over 10 CV) afforded **1i** (701 mg, 4.38 mmol, 89%) as a pale yellow oil. The analytical data is in accordance with literature.[16]

$C_{11}H_{12}O$ (160.22 $\frac{g}{mol}$)

R$_f$: 0.80 (*n*-hexane/EA = 80:20) [UV]

^{1}H NMR(400.16 MHz, $CDCl_3$): δ = 7.52 (m, 2H), 7.41 (m, 1H), 7.35 (dm, ^3J = 7.5 Hz, 1H), 4.06 (d, ^3J = 7.3 Hz, 1H), 2.14 (dqq, ^3J = 7.3 Hz, ^3J = 6.8 Hz, ^3J = 6.7 Hz, 1H), 1.11 (d, ^3J = 6.8 Hz, 3H), 1.00 (d, ^3J = 6.7 Hz, 3H).

^{13}C NMR(100.62 MHz, $CDCl_3$): δ = 192.9, 155.9, 147.2, 135.0, 129.1, 123.9, 120.6, 71.9, 29.9, 21.0, 20.1.

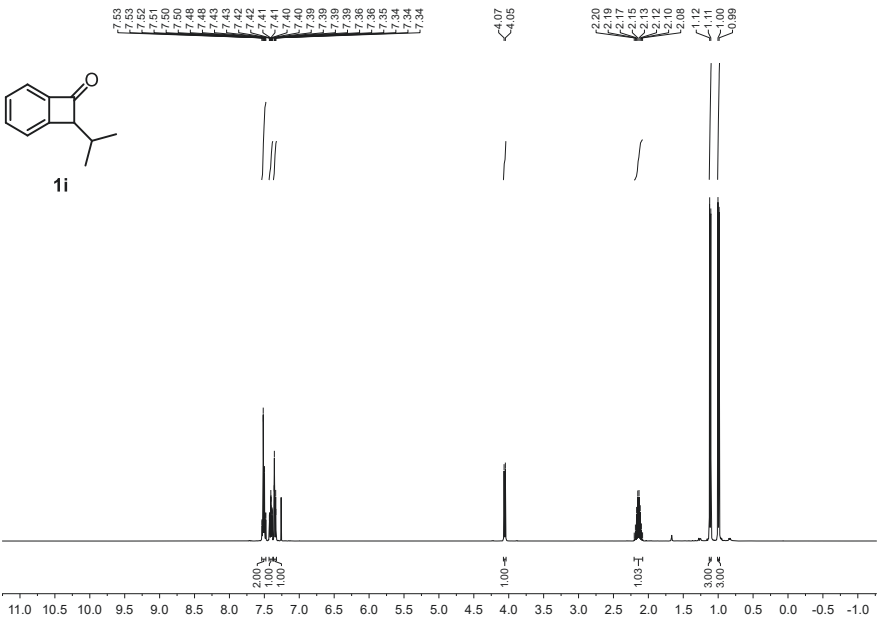

Figure S 41. ^{1}H NMR of **1i** in $CDCl_3$ measured at 400.16 MHz.

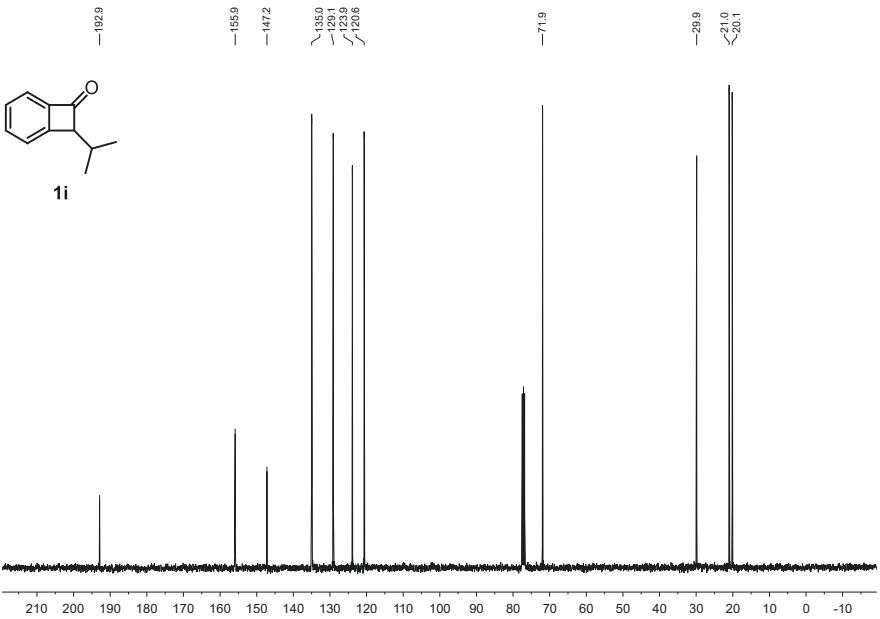

Figure S 42. ^{13}C NMR of **1i** in $CDCl_3$ measured at 100.63 MHz.

8-allylbicyclo[4.2.0]octa-1,3,5-trien-7-one

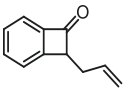

1j

1j was synthesized according to **GP-H** employing **8j** (783 mg, 2.27 mmol, 1.00 equiv.) and ^{t}BuLi (2.67 mL, 1.70 M, 2.00 equiv.). Purification *via* flash chromatography (23 g SiO_2, gradient from 100:0 to 90:10 *n*-hexane/EA over 7 CV) afforded **1j** (283 mg, 1.79 mmol, 79%) as a pale yellow oil. The analytical data is in accordance with literature.[3]

$C_{11}H_{10}O$ (158.20 $\frac{g}{mol}$)

Rf: 0.75 (*n*-hexane/EA = 80:20) [UV

^{1}H NMR(400.16 MHz, $CDCl_3$): δ = 7.51 (m, 2H), 7.42 (m, 1H), 7.36 (dm, ^{3}J = 7.5 Hz, 1H), 5.89 (dddd, ^{3}J = 17.1 Hz, ^{3}J = 10.2 Hz, ^{3}J = 7.6 Hz, ^{3}J = 6.5 Hz, 1H), 5.13 (dm, ^{3}J = 17.1 Hz, 1H), 5.09 (dm, ^{3}J = 10.2 Hz, 1H), 4.30 (dd, ^{3}J = 8.8 Hz, ^{3}J = 5.8 Hz, 1H), 2.71 (ddddd, ^{2}J = 14.6 Hz, ^{3}J = 6.5 Hz, ^{3}J = 5.8 Hz, ^{4}J = 1.5 Hz, ^{4}J = 1.5 Hz, 1H), 2.46 (ddddd, ^{2}J = 14.6 Hz, ^{3}J = 8.8 Hz, ^{3}J = 7.6 Hz, ^{4}J = 1.1 Hz, ^{4}J = 1.1 Hz, 1H).

^{13}C NMR(100.62 MHz, $CDCl_3$): δ = 192., 156.2, 146.9, 135.2, 134.9, 129.3, 123.7, 121.0, 117.1, 64.1, 34.7.

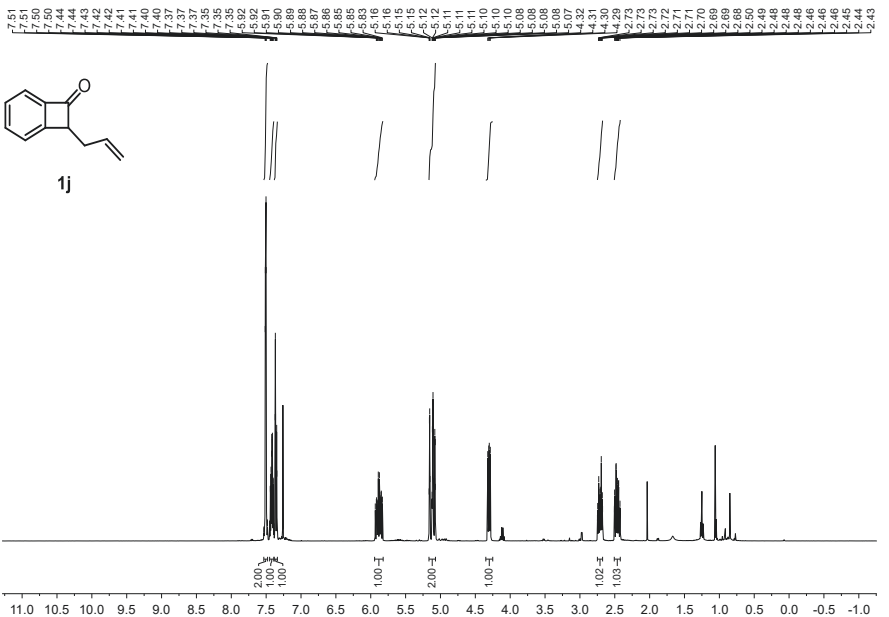

Figure S 43. ^{1}H NMR of **1j** in $CDCl_3$ measured at 400.16 MHz.

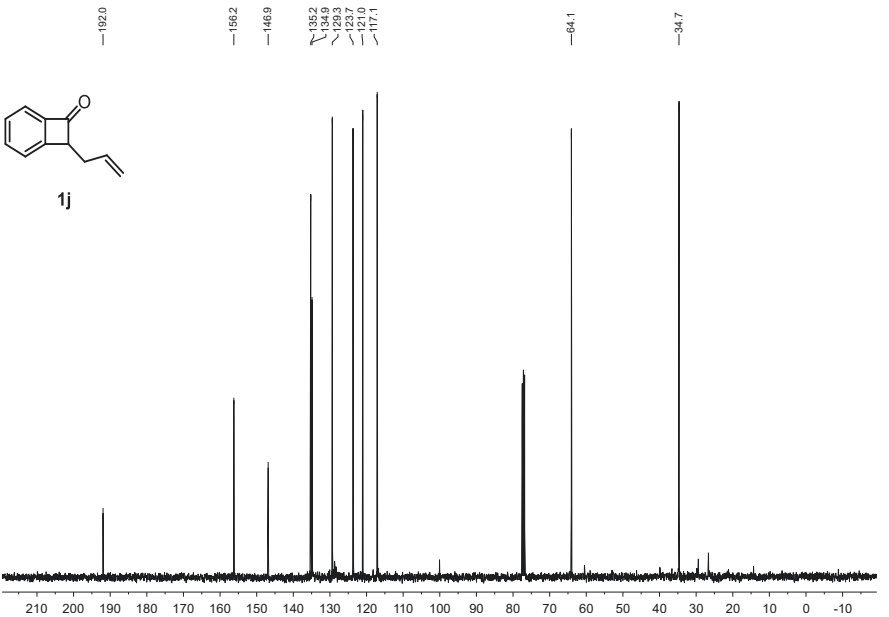

Figure S 44. ^{13}C NMR of **1j** in $CDCl_3$ measured at 100.63 MHz.

spiro[bicyclo[4.2.0]octane-7,1'-cyclopropane]-1,3,5-trien-8-one

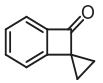

1k

1k was synthesized according to **GP-H** employing **8k** (540 mg, 1.90 mmol, 1.00 equiv.) and ^{t}BuLi (2.35 mL, 1.70 M, 2.10 equiv.). Purification *via* flash chromatography (23 g SiO_2, gradient from 100:0 to 90:10 *n*-hexane/EA over 15 CV) afforded **1k** (262 mg, 1.82 mmol, 96%) as a colorless solid, which was recrystallized from *n*-hexane yielding **1k** (223 mg, 1.54 mmol, 81%) as colorless crystals.

$C_{10}H_8O$ (144.17 $\frac{g}{mol}$)

mp: 86.9 °C.

R$_f$: 0.75 (*n*-hexane/EA = 80:20) [UV]

^{1}H NMR(400.16 MHz, $CDCl_3$): δ = 7.44 (m, 1H), 7.32 (m, 1H), 7.27 (dm, ^{3}J = 7.5 Hz, 1H), 7.17 (d, ^{3}J = 7.4 Hz, 1H), 1.47 (m, 2H), 1.24 (m, 2H).

^{13}C NMR(100.62 MHz, $CDCl_3$): δ = 195.0, 158.0, 148.1, 135.3, 128.1, 119.6, 119.3, 47.1, 13.1.

HRMS (ESI-TOF) m/z: $[M+Na]^+$ Calcd for $C_{10}H_8ONa$ 167.0467; Found 167.0466.

IR (ATR, ṽ): 1739 cm^{-1} (s, *CO*).

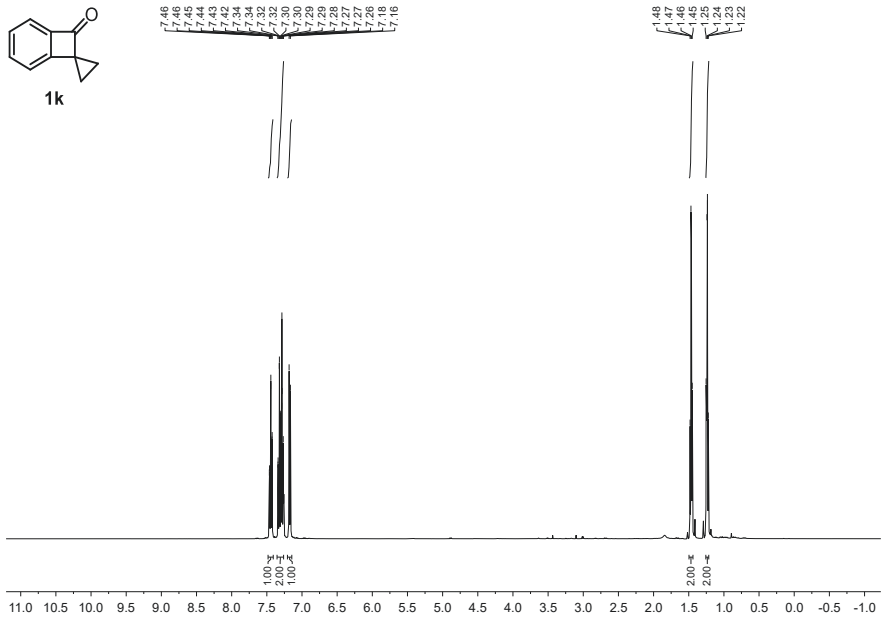

Figure S 45. ^{1}H NMR of **1k** in $CDCl_3$ measured at 400.16 MHz.

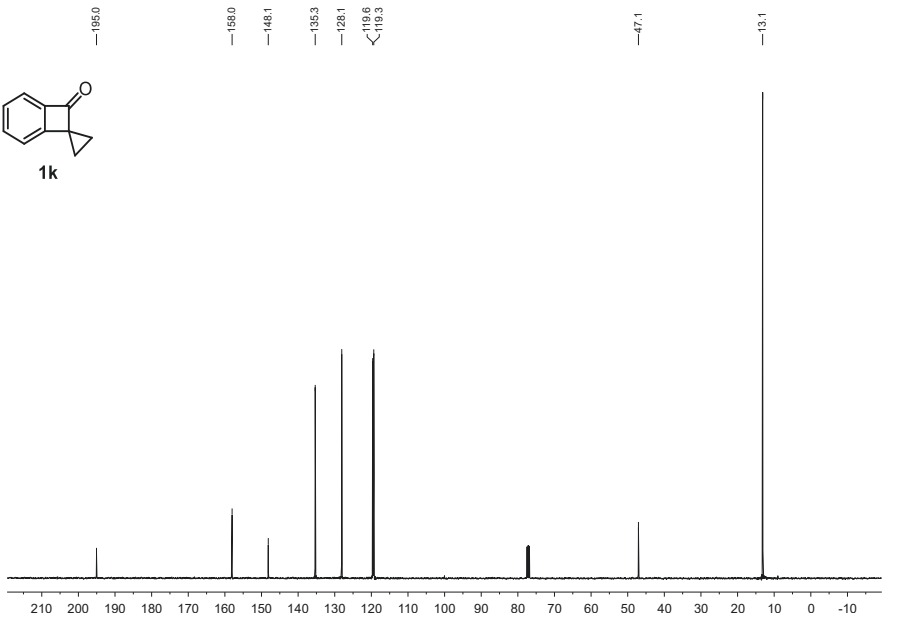

Figure S 46. ^{13}C NMR of **1k** in $CDCl_3$ measured at 100.63 MHz.

4-isobutyl-8-methylbicyclo[4.2.0]octa-1,3,5-trien-7-one

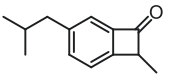

1l

1l was synthesized according to **GP-H** employing **8l** (1.34 g, 3.57 mmol, 1.00 equiv.) and ^{t}BuLi (4.41 mL, 1.70 M, 2.10 equiv.). Purification *via* flash chromatography (23 g SiO_2, gradient from 100:0 to 85:15 *n*-hexane/EA over 15 CV) afforded **1l** (436 mg, .2.32 mmol, 65%) as a pale colorless oil.

$C_{13}H_{16}O$ (188.27 $\frac{g}{mol}$)

R$_f$: 0.61 (*n*-hexane/EA = 80:20) [UV]

^{1}H NMR(700.21 MHz, $CDCl_3$): δ = 7.41 (d, ^3J = 7.6 Hz, 1H), 7.30 (dd, ^3J = 7.6 Hz, ^3J = 1.2 Hz, 1H), 7.12 (s, 1H), 4.20 (q, ^3J = 7.2 Hz, 1H), 2.51 (d, ^3J = 7.2 Hz, 2H), 1.83 (tsep, ^3J = 7.2 Hz, ^3J = 6.7 Hz, 1H), 1.43 (d, ^3J = 7.2 Hz, 3H), 0.89 (d, ^3J = 6.7 Hz, 6H).

^{13}C NMR(176.08 MHz, $CDCl_3$): δ = 193.5, 155.3, 146.5, 143.1, 136.7, 122.4, 121.1, 58.9, 45.6, 30.5, 22.3, 15.4.

HRMS (ESI-TOF) m/z: $[M+Na]^+$ Calcd for $C_{13}H_{16}ONa$ 211.1093; Found 211.1091.

IR (ATR, $\tilde{\nu}$): 1757 cm^{-1} (vs, *CO*).

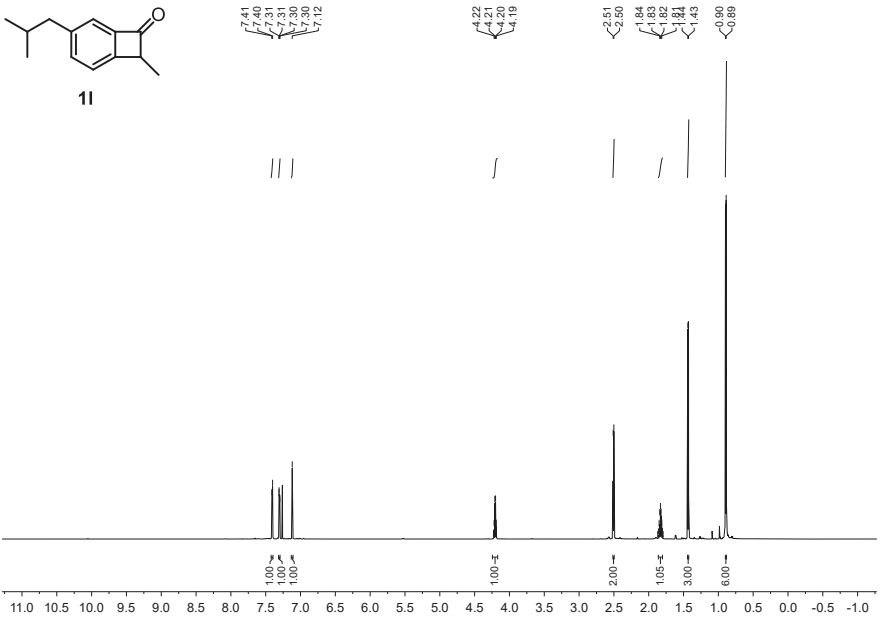

Figure S 47. ^{1}H NMR of **1l** in $CDCl_3$ measured at 700.21 MHz.

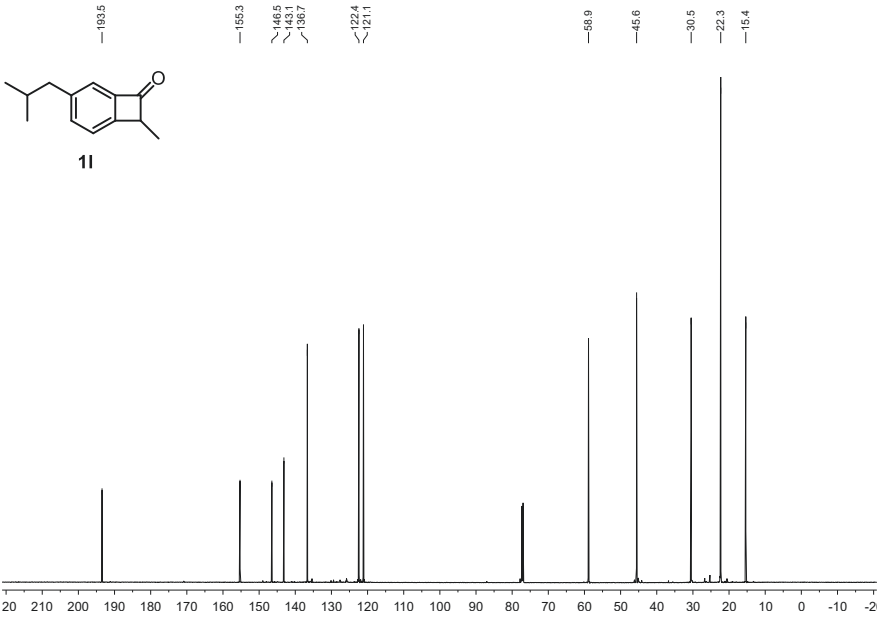

Figure S 48. ^{13}C NMR of **1l** in $CDCl_3$ measured at 176.08 MHz.

5-methylbicyclo[4.2.0]octa-1,3,5-trien-7-one

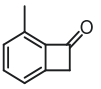

1m

1m was synthesized according to **GP-J** employing **10m** (3.00 g, 9.60 mmol, 1.00 equiv.), **9** (2.85 mL, 19.2 mmol, 2.00 equiv.), CsF (2.19 g, 14.4 mmol, 1.50 equiv.), and TFA (1.47 mL, 19.2 mmol, 2.00 equiv.). Purification *via* flash chromatography (23 g SiO_2, gradient from 100:0 to 88:12 *n*-hexane/EA over 12 CV) and recrystallisation from *n*-hexane afforded **1m** (157 mg, 1.15 mmol, 12%) as a colorless solid. The analytical data is in accordance with literature.[17]

C_9H_8O ($132.16\,\frac{g}{mol}$)

R$_f$: 0.55 (*n*-hexane/EA = 90:10) [UV]

^{1}H NMR(600.13 MHz, $CDCl_3$): δ = 7.40 (m, 1H), 7.32 (d, ^3J = 7.3 Hz, 1H), 7.14 (d, ^3J = 7.6 Hz, 1H), 3.93 (s, 2H), 2.41 (s, 3H).

^{13}C NMR(150.90 MHz, $CDCl_3$): δ = 189.3, 151.0, 146.7, 135.1, 133.7, 129.6, 120.6, 52.1, 17.7.

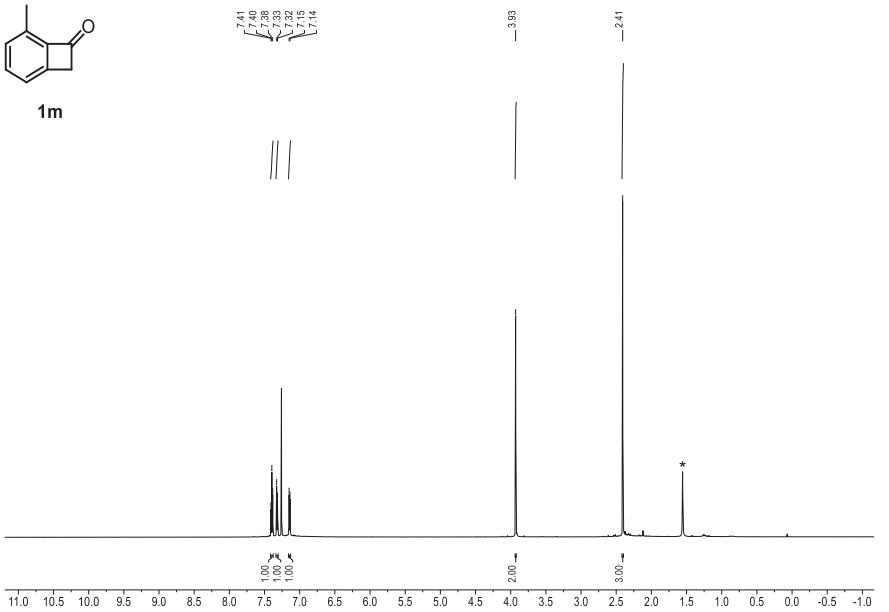

Figure S 49. ^{1}H NMR of **1m** in $CDCl_3$ measured at 600.13 MHz.

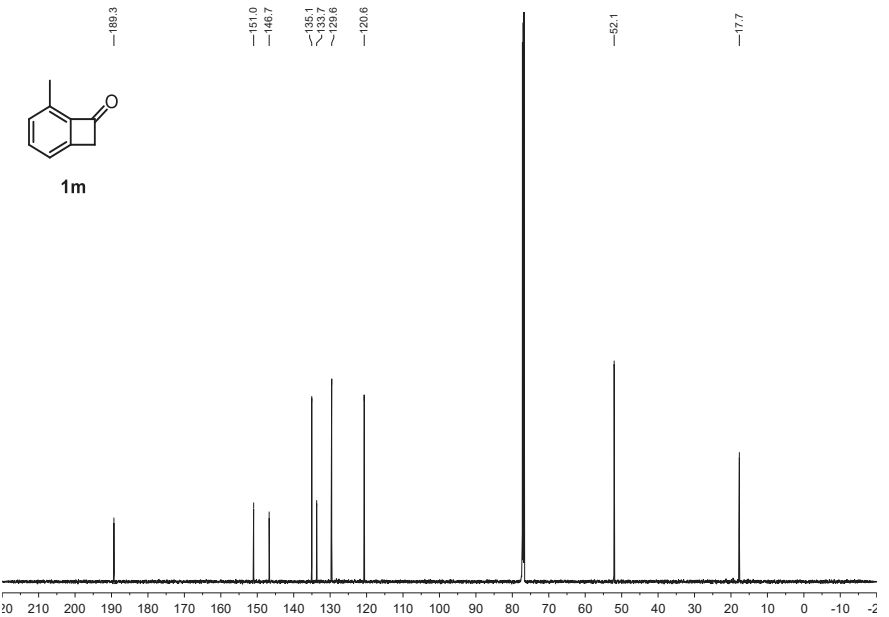

Figure S 50. ^{13}C NMR of **1m** in $CDCl_3$ measured at 150.92 MHz.

5-methoxybicyclo[4.2.0]octa-1,3,5-trien-7-one

1n

1n was synthesized according to **GP-I** employing 2-bromo anisole (3.74 g, 20.0 mmol, 1.00 equiv.), $NaNH_2$ (3.12 g, 80.0 mmol. 4.00 equiv.), and **9** (11.9 mL, 80.0 mmol, 4.00 equiv.). Purification *via* flash chromatography (40 g SiO_2, gradient from 100:0 to 90:10 *n*-hexane/EA over 10 CV) afforded **1n** (1.53 g, 10.3 mmol, 52%) as a colorless solid. The analytical data is in accordance with literature.[7]

$C_9H_8O_2$ (148.16 $\frac{g}{mol}$)

R$_f$: 0.25 (*n*-hexane/EA = 80:20) [UV]

^{1}H NMR(700.21 MHz, $CDCl_3$): δ = 7.42 (dd, ^3J = 8.4 Hz, ^3J = 7.1 Hz, 1H), 7.02 (d, 7.0 Hz, 1H), 6.79 (d, ^3J = 8.4 Hz, 1H), 4.10 (s, 3H), 3.91 (s, 2H).

^{13}C NMR(176.08 MHz, $CDCl_3$): δ = 185.0, 153.5, 150.7, 137.7, 132.5, 115.9, 115.2, 59.9, 51.4.

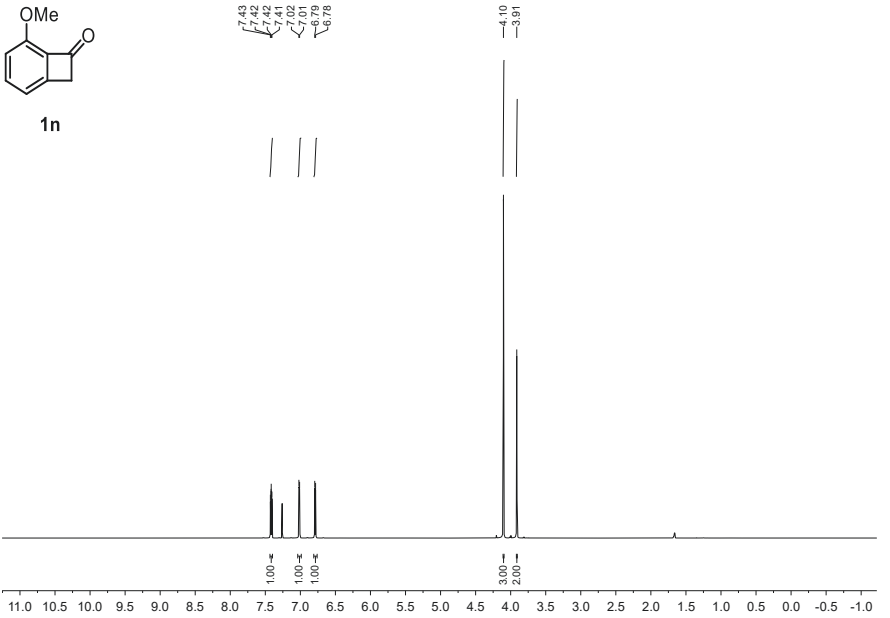

Figure S 51. ^{1}H NMR of **1n** in $CDCl_3$ measured at 700.21 MHz.

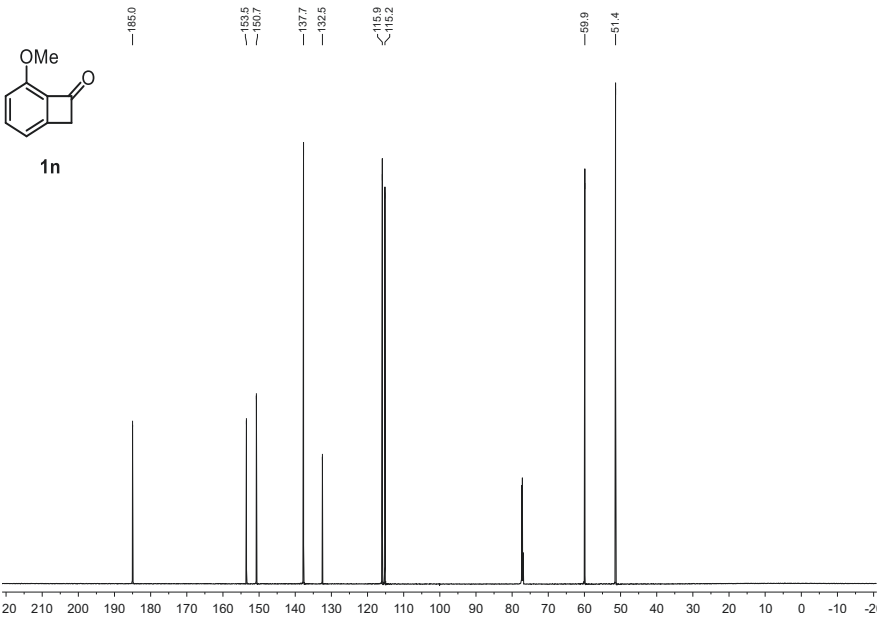

Figure S 52. ^{13}C NMR of **1n** in $CDCl_3$ measured at 176.08 MHz.

4.4 Norbornadienes

7-(*tert*-butoxy)bicyclo[2.2.1]hepta-2,5-diene

2b

2b was synthesized according to literature.[18] In a RBF NBD (98.9 mL, 0.98 mol, 2.6 equiv.) and CuBr (215 mg, 1.50 mmol, 0.4 mol%) were dissolved in benzene (160 mL) and heated to a reflux. *tert*-Butyl perbenzoate (71.5 mL, 0.38 mol, 1.00 equiv.) dissolved in benzene (25 mL) was added dropwise over 1 h. Afterwards, the mixture was refluxed for 1 h, cooled to rt and washed with brine (3 × 100 mL), $NaOH_{(aq.)}$ (3 × 100 mL, 10%) and again with brine (50 mL). The solution was dried over $MgSO_4$ and carefully concentrated *in vacuo*. **2b** (12.9 g, 78.5 mmol, 21%) was obtained upon vacuum distillation (7 mbar, 62 °C, 80 °C oil bath) as a colorless oil. The analytical data is in accordance with literature.[19]

$C_{11}H_{16}O$ (164.25 $\frac{g}{mol}$)

b.p. (7 mbar): 62 °C.

^{1}H NMR(400.16 MHz, $CDCl_3$): δ = 6.64 (dd, ^3J = 2.7 Hz, ^3J = 2.2 Hz, 2H), 6.58 (m, 2H), 3.78 (m, 1H), 3.39 (m, 2H), 1.14 (s, 9H).

^{13}C NMR(100.62 MHz, $CDCl_3$): δ = 140.0, 137.4, 104.5, 73.7, 55.6, 28.5.

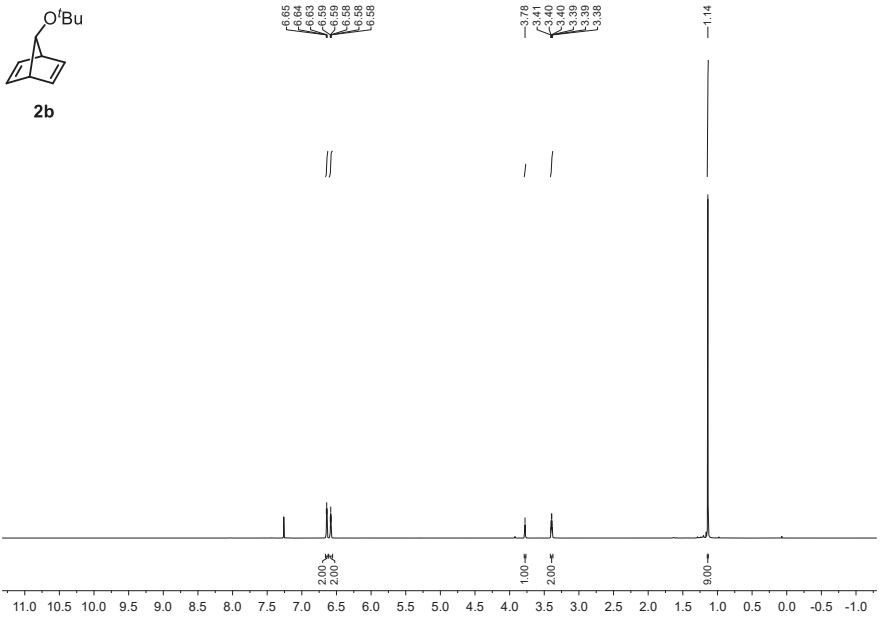

Figure S 53. ^{1}H NMR of **2b** in $CDCl_3$ measured at 400.16 MHz.

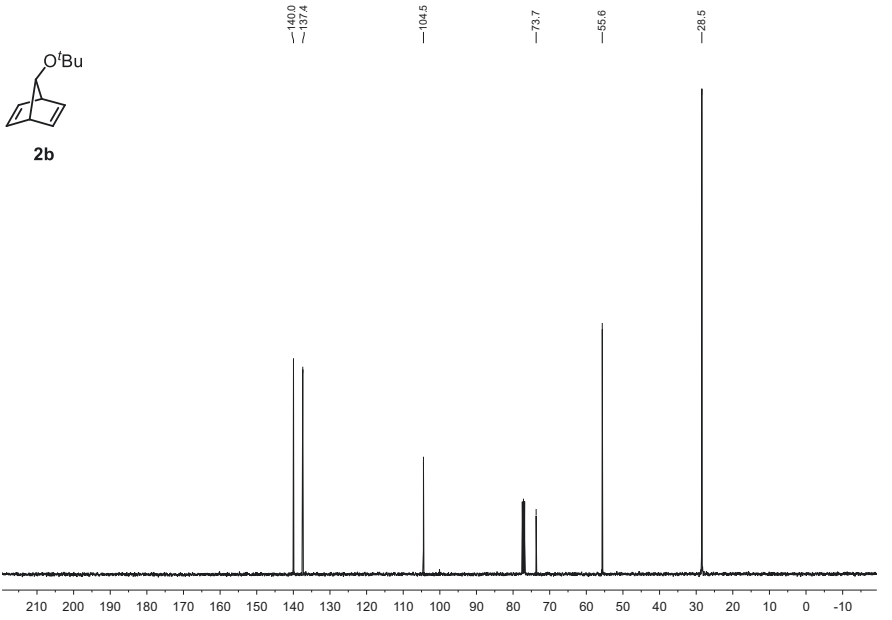

Figure S 54. ^{13}C NMR of **2b** in $CDCl_3$ measured at 100.63 MHz.

7-(isopropyl)bicyclo[2.2.1]hepta-2,5-diene

2c

2c was synthesize d according to **GP-K** employing **2b** (1.97 g, 12.0 mmol, 1.00 equiv.), and ^{i}PrMgBr (8.00 mL, 3.00 M, 2.00 equiv.). Vacuum distillation furnished **2c** (0.21 g, 1.56 mmol, 13%) as a colorless oil. The analytical data is in accordance with literature.[20]

$C_{10}H_{14}$ (134.22 $\frac{g}{mol}$)

^{1}H NMR(700.21 MHz, $CDCl_3$): δ = 6.81 (dd, ^{3}J = 2.4 Hz, ^{3}J = 1.9 Hz, 2H), 6.58 (dd, ^{3}J = 2.4 Hz, ^{3}J = 1.9 Hz, 2H), 3.42 (ddd, ^{3}J = 3.8 Hz, ^{3}J = 1.9 Hz, ^{3}J = 1.9 Hz, 2H), 2.09 (d, ^{3}J = 9.8 Hz, 1H), 1.62 (dsep, ^{3}J = 9.8 Hz, ^{3}J = 6.7 Hz, 1H), 0.75 (d, ^{3}J = 6.7 Hz, 6H).

^{13}C NMR(176.08 MHz, $CDCl_3$): δ = 144.9, 140.0, 96.3, 52.7, 27.2, 21.3.

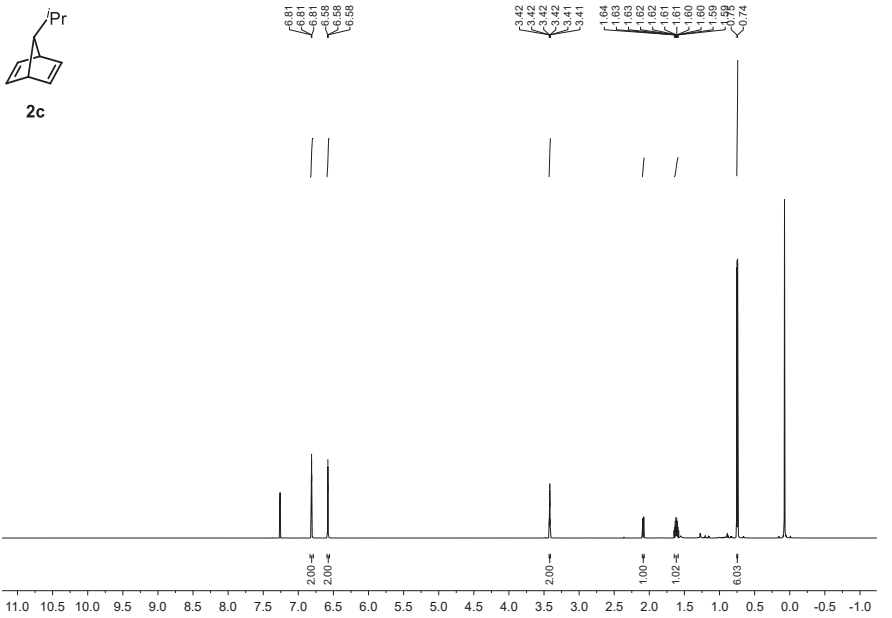

Figure S 55. ^{1}H NMR of **2c** in $CDCl_3$ measured at 700.21 MHz. * Denotes residual grease.

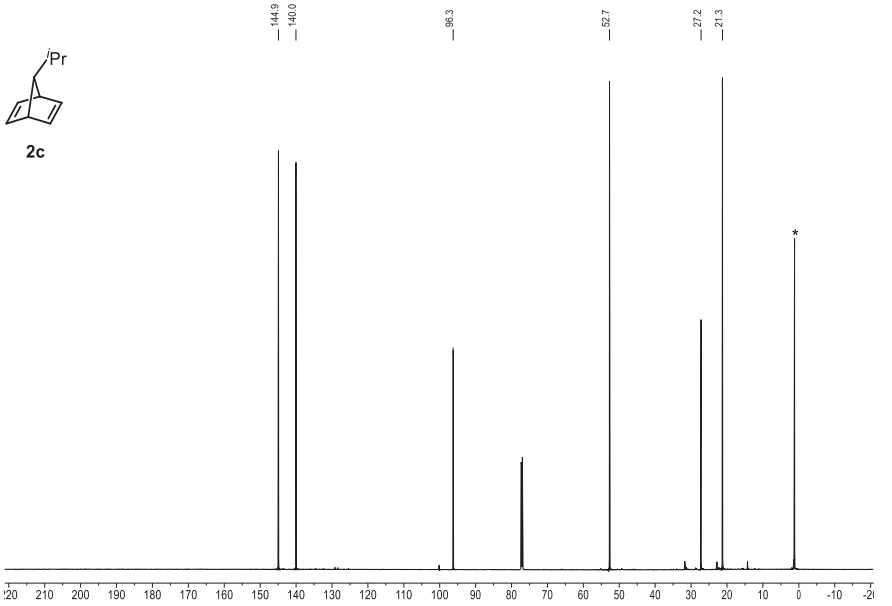

Figure S 56. ^{13}C NMR of **2c** in $CDCl_3$ measured at 176.08 MHz. * Denotes residual grease.

7-(phenyl)bicyclo[2.2.1]hepta-2,5-diene

2d

2d was synthesized according to **GP-K** employing **2b** (1.97 g, 12.0 mmol, 1.00 equiv.), and PhMgBr (8.00 mL, 3.00 M, 2.00 equiv.). Vacuum distillation (15 mbar, 110 C) furnished **2d** (1.09 g, 6.48 mmol, 54%) as a colorless oil. The analytical data is in accordance with literature.[20]

$C_{13}H_{12}$ ($168.24\ \frac{g}{mol}$)

b.p. (15 mbar): 110 °C.

^{1}H NMR(700.21 MHz, $CDCl_3$): δ = 7.26 (m, 2H), 7.17 (t, ^{3}J = 7.3 Hz, 1H), 7.08 (d, ^{3}J = 7.4 Hz, 2H), 6.96 (dd, ^{3}J = 1.9 Hz, ^{3}J = 1.9 Hz, 2H), 6.58 (dd, ^{3}J = 1.9 Hz, ^{3}J = 1.9 Hz, 2H), 3.87 (m, 2H), 3.83 (s, 1H).

^{13}C NMR(176.08 MHz, $CDCl_3$): δ = 144.4, 141.4, 139.9, 128.2, 127.7, 125.7, 87.7, 53.7.

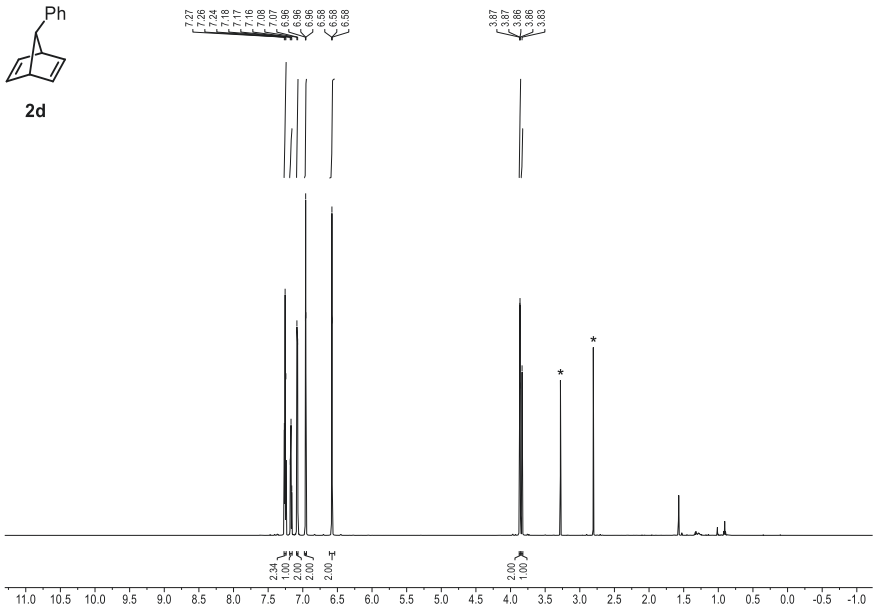

Figure S 57. ^{1}H NMR of **2d** in $CDCl_3$ measured at 700.21 MHz. * Denotes DMI.

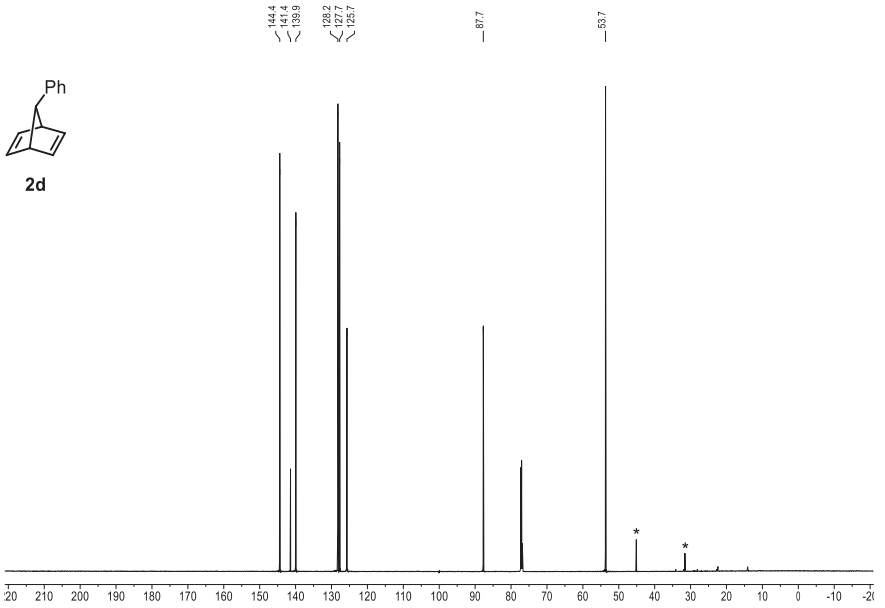

Figure S 58. ^{13}C NMR of **2d** in $CDCl_3$ measured at 176.08 MHz. * Denotes DMI.

2-hexylbicyclo[2.2.1]hepta-2,5-diene

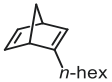

2e

2e was synthesized according to literature.[21] In a predried Schlenk RBF, a solution of NBD (2.03 mL, 20.0 mmol, 1.82 equiv.) in THF (50 mL) was added to a solution of KO^{t}Bu (1.23 g, 11.0 mmol, 1.00 equiv.) in THF (60 mL) at -78 °C. Subsequently, ^{n}BuLi (6.87 mL, 1.60 M, 1.00 equiv.) was added dropwise over 45 min. After complete addition the reaction was first allowed to slowly warm to -35 °C and then cooled down to -70 °C, before 1-bromohexane (2.00 mL, 14.3 mmol, 1.30 equiv.) was added over 2 min. After complete addition the reaction was stirred at -40 °C for 2 h, before stirring at 0 °C for further 2 h. The reaction was allowed to warm to rt and was quenched with $NH_4Cl_{(aq.)}$ (25 mL). The layers were separated, and the aqueous phase was extracted with DCM (3 × 10 mL). The combined organic phases were washed with H_2O (2 × 25 mL), dried over $MgSO_4$ and the solvent was removed *in vacuo*. **2e** was purified by flash chromatography (23 g SiO_2, *n*-hexane over 10 CV) followed by vacuum distillation (5 mbar, 65 °C, 105 °C oil bath) yielding a colorless oil (1.13 g, 6.41 mmol, 58%). The analytical data is in accordance with literature.[22]

$C_{13}H_{20}$ (176.30 $\frac{g}{mol}$)

b.p. (5 mbar): 65 °C.

R$_f$: 0.63 (*n*-hexane/EA = 80:20) [UV]

^{1}H NMR(400.16 MHz, $CDCl_3$): δ = 6.75 (m, 2H), 6.11 (m, 1H), 3.49 (s, 1H), 3.27 (s, 1H), 2.18 (m, 2H), 1.96 (m, 2H), 1.40 (m, 2H), 1.27 (m, 6H), 0.88 (t, ^2J = 6.8 Hz, 3H).

^{13}C NMR(176.08 MHz, $CDCl_3$): δ = 159.3, 144.0, 142.6, 133.2, 73.6, 53.7, 50.1, 31.9, 31.7, 29.2, 27.4, 22.8, 14.3.

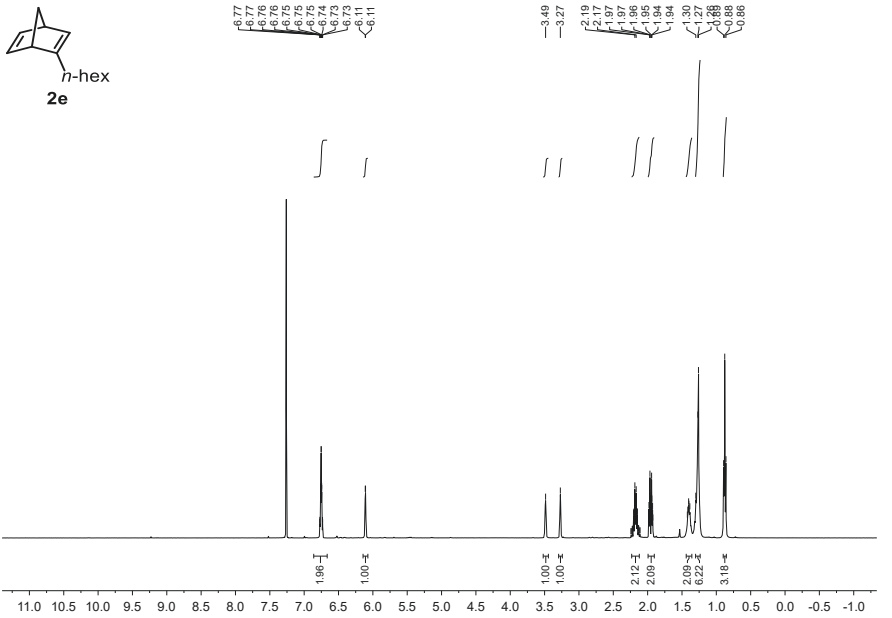

Figure S 59. ^{1}H NMR of **2e** in $CDCl_3$ measured at 400.16 MHz.

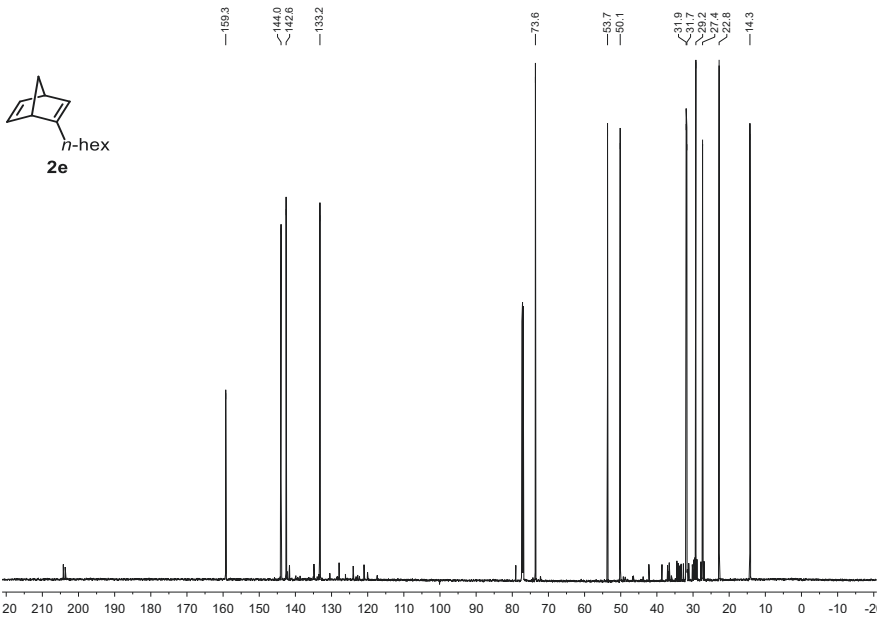

Figure S 60. ^{13}C NMR of **2e** in $CDCl_3$ measured at 176.08 MHz.

4.5 Catalytic Products

***rel*-(1*S*,2*S*,3a*R*,4*R*,10a*S*,11*R*)-2,3,3a,4,9,10a-hexahydro-1,2,4-(epimethanetriyl) benzo[f]azulen-10(1H)-one**

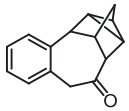

3aa

3aa was synthesized according to **GP-A** employing **1a** (118 mg, 1.00 mmol, 1.00 equiv.) and NBD (132 µL, 1.30 mmol, 1.30 equiv.) at 50 °C instead of 80 °C. Purification *via* flash chromatography (23 g SiO_2, gradient from 100:0 to 70:30 *n*-hexane/EA over 15 CV) afforded **3aa** (190 mg, 904 µmol, 90%, 34% *ee*, $[\alpha]_D^{20}$ +24 (*c* 1.0, $CHCl_3$)) as a pale yellow solid.

Additionally, **3aa** was synthesized in an upscaled reaction according to **GP-A** employing **1a** (1.18 g, 10.0 mmol, 1.00 equiv.) and NBD (1.32 mL, 1.30 mmol, 1.30 equiv.) at 50 °C instead of 80 °C. Hereby all parameters were scaled accordingly. Purification *via* flash chromatography (37 g SiO_2, gradient from 100:0 to 70:30 *n*-hexane/EA over 15 CV) afforded **3aa** (1.75 g, 8.31 mmol, 83%) as a pale yellow solid.

Alternatively, $Ni(COD)_2$ (10 mol%) and 11bS-N,N-bis[(1S)-1-(1-naphthalenyl)ethyl]dinaphtho[2,1-d:1',2'-f][1,3,2]dioxaphosphepin-4-amine (cas: 342813-26-7, 12 mol%) were added to a dried 50 mL Schlenk round bottom flask (RBF) in a glovebox. 20 mL of *n*-hexane were added, and the reaction was stirred for 5 min at rt. Subsequently, first NBD (132 µL, 1.30 mmol, 1.30 equiv.) and then **1a** (118 mg, 1.00 mmol, 1.00 equiv.) were added, after which the reaction was transferred to a preheated (70 °C) oil bath and stirred for 16 h. The workup was conducted according to **GP-A**. Purification *via* flash chromatography (23 g SiO_2, gradient from 100:0 to 70:30 *n*-hexane/EA over 15 CV) afforded **3aa** (87.9 mg, 418 µmol, 42%, 71% *ee*, $[\alpha]_D^{20}$ -60 (*c* 1.0, $CHCl_3$)) as a pale yellow solid.

$C_{15}H_{14}O$ (210.28 $\frac{g}{mol}$)

mp: 65.5 °C.

R_f: 0.45 (*n*-hexane/EA = 80:20) [anisaldehyde]

^{1}H NMR(400.16 MHz, $CDCl_3$): δ = 7.18 (m, 1H, H-10), 7.17 (m, 1H, H-11), 7.16 (m, 1H, H-12), 7.06 (m, 1H, H-13), 4.50 (dd, ^2J = 12.3 Hz, ^4J = 0.6 Hz, 1H, H-15b), 3.36 (dd,

^{2}J = 12.3 Hz, ^{4}J = 1.0 Hz, 1H, H-15a), 2.91 (s, 1H, H-7), 2.65 (m, 1H, H-2), 2.29 (m, 1H, H-8), 1.72 (ddm, ^{3}J = 5.0 Hz, ^{3}J = 5.0 Hz, 1H, H-6), 1.66 (dm, ^{2}J = 10.8 Hz, 1H, H-5a), 1.52 (dm, ^{2}J = 10.8 Hz, 1H, H-5b), 1.51 (m, 1H, H-4), 1.49 (m, 1H, H-3).

^{13}C NMR(100.62 MHz, $CDCl_3$): δ = 209.5 (C-1), 139.7 (C-9), 131.8 (C-14), 131.5 (C-10), 130.4 (C-13), 127.6 (C-12), 127.1 (C-11), 59.1 (C-2), 52.9 (C-7), 49.1 (C-15), 42.1 (C-8), 36.3 (C-5), 17.8 (C-6), 14.9 (C-4), 13.2 (C-3).

HRMS (ESI-TOF) m/z: $[M+H]^+$ Calcd for $C_{15}H_{14}OH$ 211.1117; Found 211.1119.

IR (ATR, ṽ): 1687 cm^{-1} (s, *CO*).

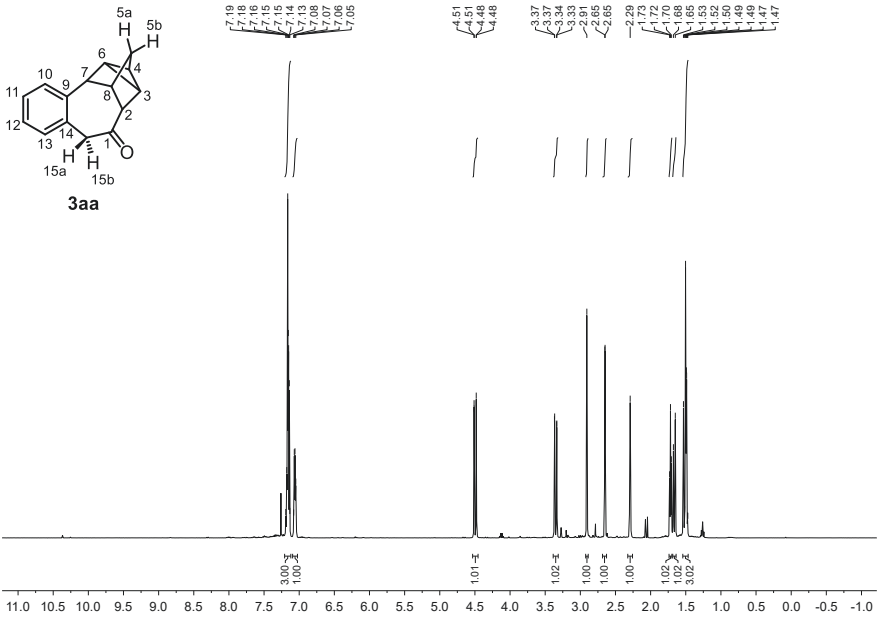

Figure S 61. ^{1}H NMR of **3aa** in $CDCl_3$ measured at 400.16 MHz.

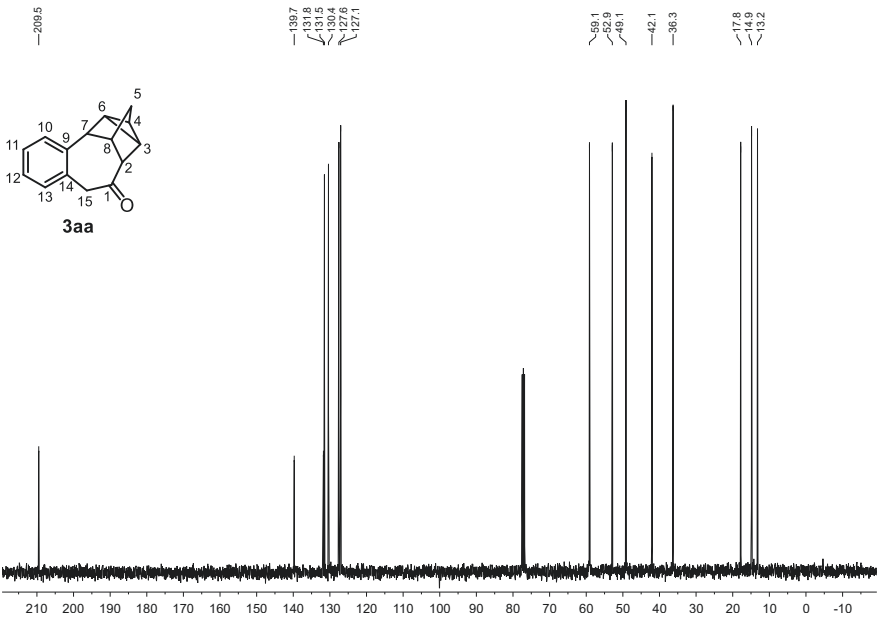

Figure S 62. ^{13}C NMR of **3aa** in $CDCl_3$ measured at 100.63 MHz.

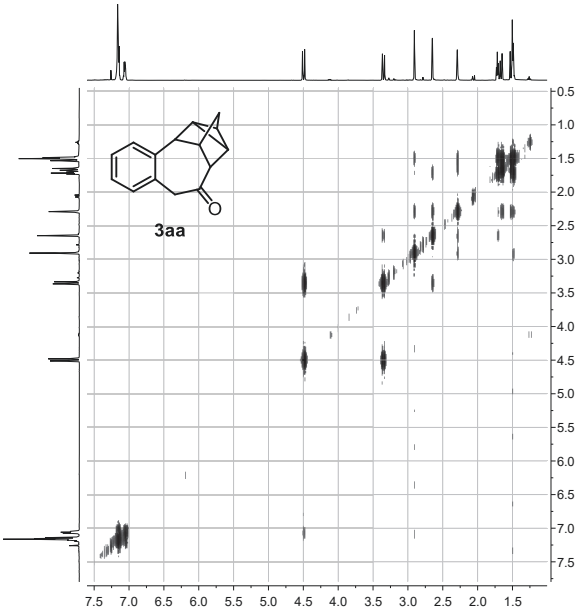

Figure S 63. ^{1}H,^{1}H-COSY of **3aa** in $CDCl_3$ measured at 400.16 MHz.

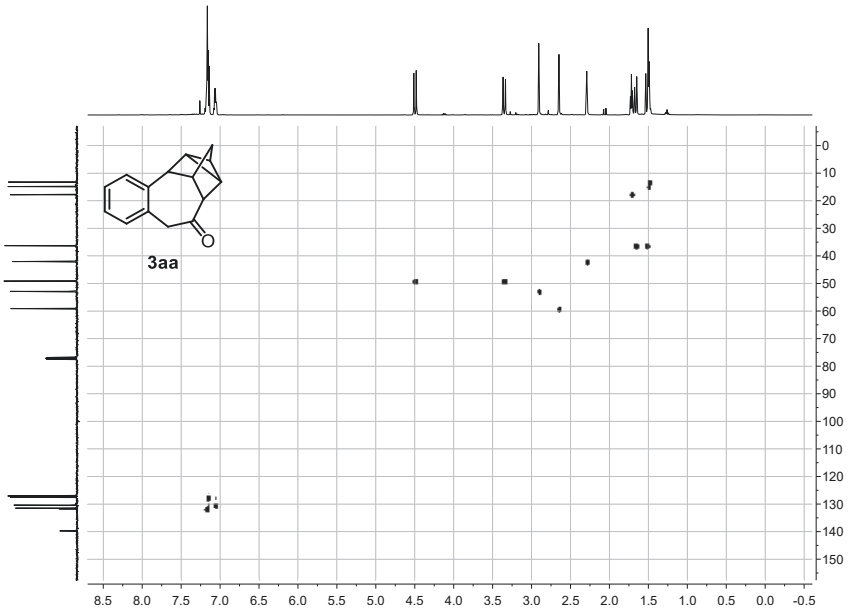

Figure S 64. ^{1}H,^{13}C-HSQC of **3aa** in $CDCl_3$ measured at ^{1}H: 400.16 MHz; ^{13}C: 100.63 MHz.

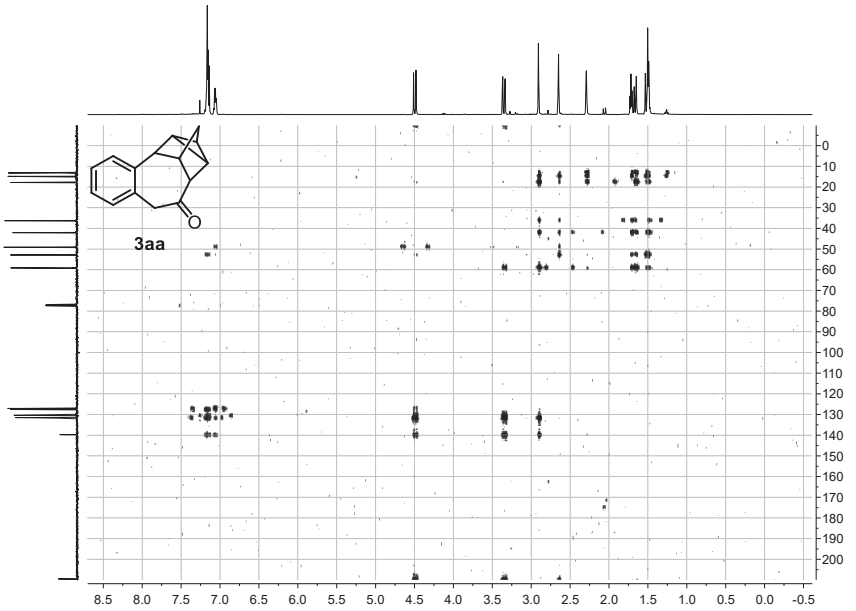

Figure S 65. $^{1}H,^{13}C$-HMBC of **3aa** in $CDCl_3$ measured at ^{1}H: 400.16 MHz; ^{13}C: 100.63 MHz.

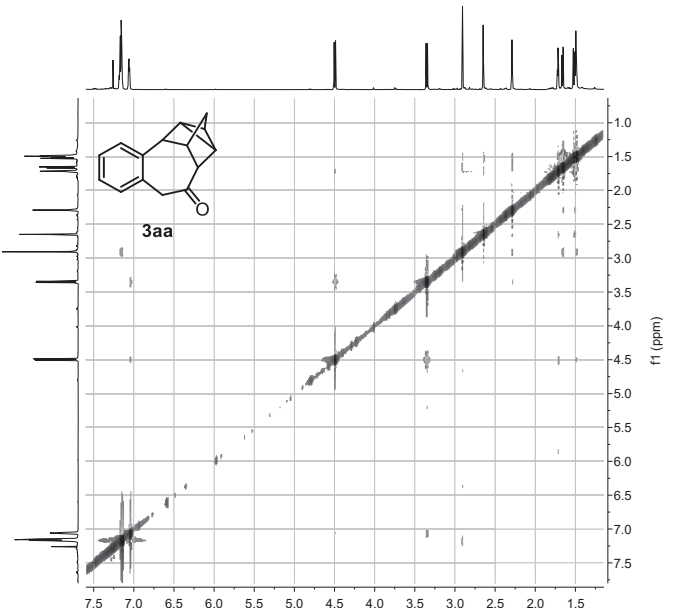

Figure S 66. $^{1}H,^{1}H$-NOESY of **3aa** in $CDCl_3$ measured at 700.21 MHz.

***rel*-(1*S*,2*S*,3a*R*,4*R*,12a*S*,13*R*)-2,3,3a,4,11,12a-hexahydro-1,2,4-(epimethanetriyl) naphtho[2,3-f]azulen-12(1H)-one**

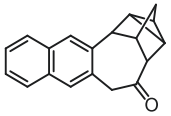

3ba

3ba was synthesized according to **GP-A** employing **1b** (168 mg, 1.00 mmol, 1.00 equiv.) and NBD (132 µL, 1.30 mmol, 1.30 equiv.). Purification *via* flash chromatography (23 g SiO_2, gradient from 98:02 to 80:10 *n*-hexane/EA over 15 CV) afforded **3ba** (209 mg, 802 µmol, 80%, 25% *ee*, $[\alpha]_D^{20}$ -2 (*c* 1.0, $CHCl_3$)) as a pale brown solid.

$C_{19}H_{16}O$ (260.34 $\frac{g}{mol}$)

mp: 144.3 °C.

Rf: 0.57 (*n*-hexane/EA = 80:20) [UV]

^{1}H-NMR (700 MHz, $CDCl_3$) δ = 7.73 (m, 2H, H-12, H-15), 7.67 (s, 1H, H-10), 7.54 (s, 1H, H-17), 7.42 (m, 2H, H-13, H-14), 4.73 (m, 1H, H-19b), 3.48 (m, 1H, H-19a), 3.12 (s, 1H, H-7), 2.69 (s, 1H, H-2), 2.27 (s, 1H, H-8), 1.78 (m, 1H, H-3), 1.73 (m, 1H, H-5a), 1.59 (m, 1H, H-4), 1.56 (m, 2H, H-6, H-5b).

^{13}C-NMR (176 MHz, $CDCl_3$) δ = 210.0 (C-1), 138.1 (C-8), 132.9 (C-11), 132.5 (C-16), 130.2 (C-18), 130.0 (C-10), 128.7 (C-17), 127.2 (C-12), 127.1 (C-15), 126.1 (C-14), 126.1 (C-13), 59.1 (C-2), 53.4 (C-7), 49.3 (C-19), 42.5 (C-8), 36.6 (C-5), 18.3 (C-3), 15.0 (C-4), 13.6 (C-6).

HRMS (ESI-TOF) m/z: $[M+H]^+$ Calcd for $C_{19}H_{16}OH$ 261.1274; Found 261.1273.

IR (ATR, $\tilde{\nu}$): 1687 cm^{-1} (s, *CO*).

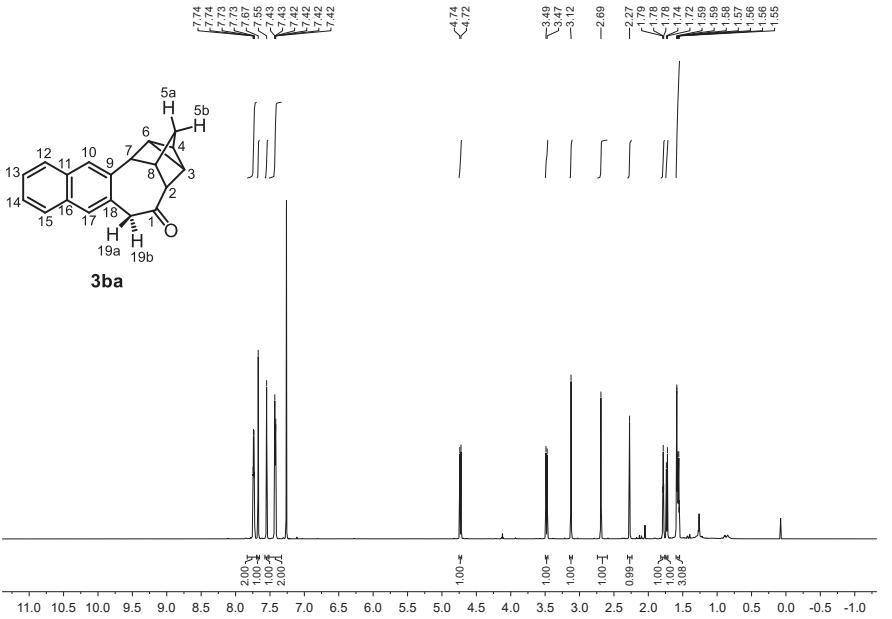

Figure S 67. ^{1}H NMR of **3ba** in $CDCl_3$ measured at 700.21 MHz.

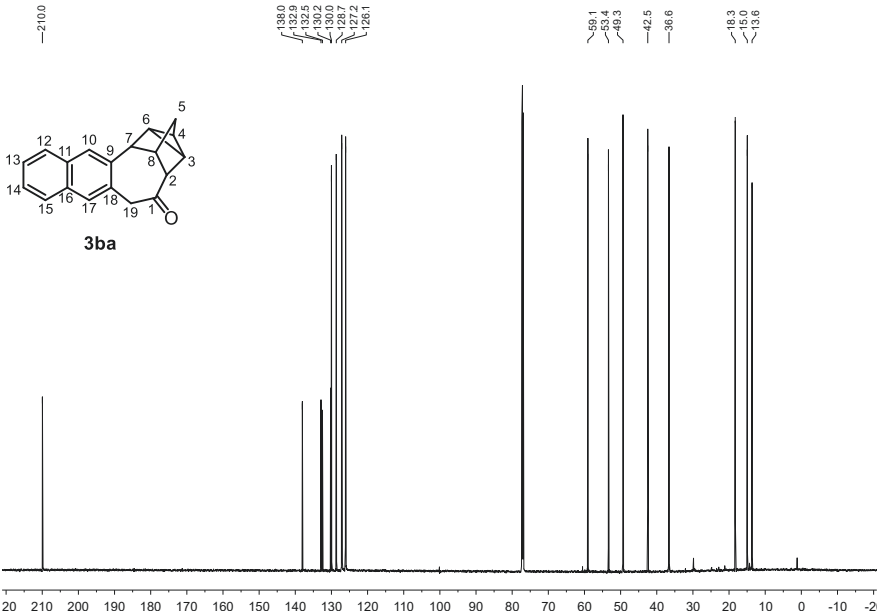

Figure S 68. ^{13}C NMR of **3ba** in $CDCl_3$ measured at 176.08 MHz.

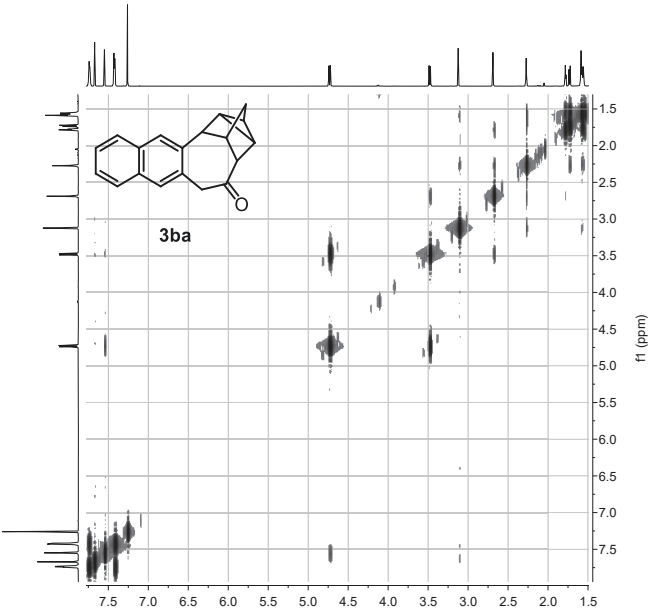

Figure S 69. $^{1}H,^{1}H$-COSY of **3ba** in $CDCl_3$ measured at 700.21 MHz.

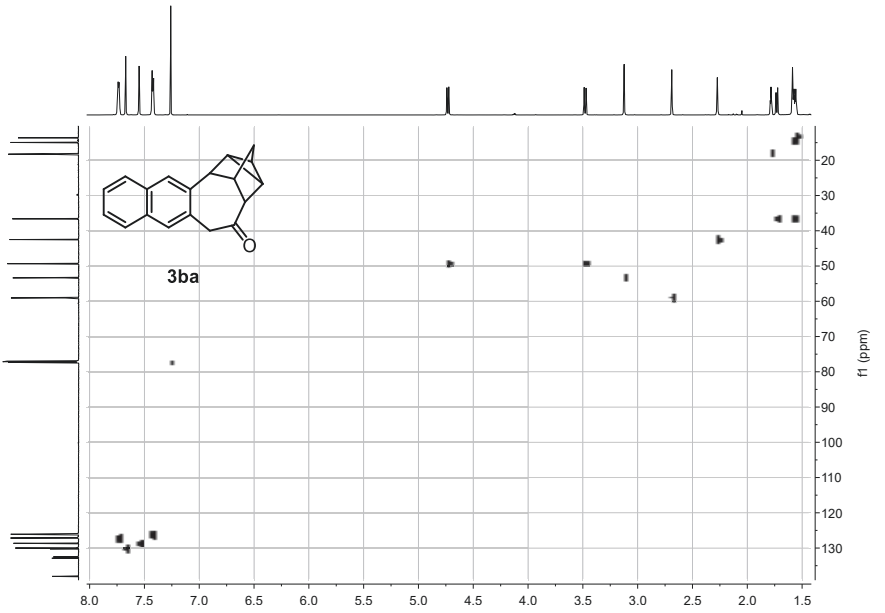

Figure S 70. $^{1}H,^{13}C$-HSQC of **3ba** in $CDCl_3$ measured at ^{1}H: 700.21 MHz; ^{13}C: 176.08 MHz.

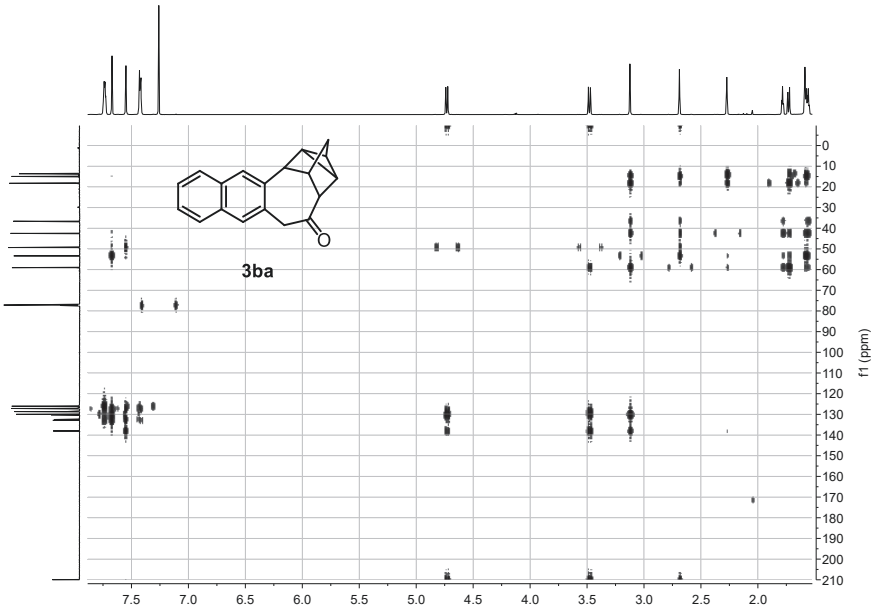

Figure S 71. $^{1}H,^{13}C$-HMBC of **3ba** in $CDCl_3$ measured at ^{1}H: 700.21 MHz; ^{13}C: 176.08 MHz.

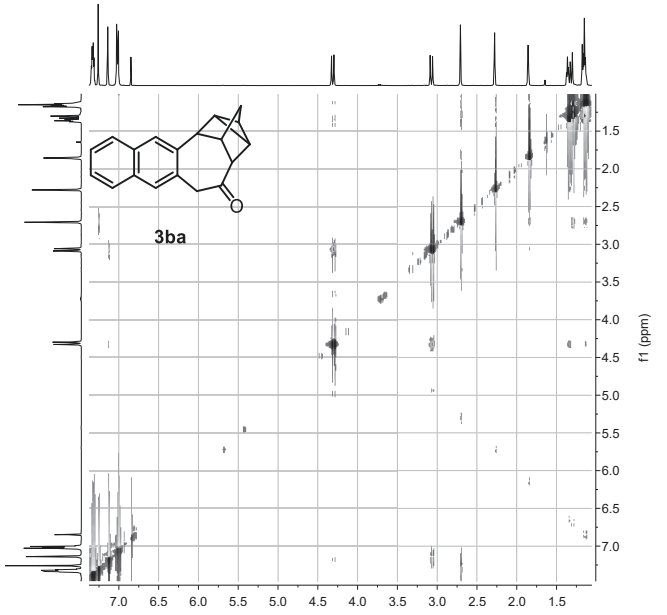

Figure S 72. $^{1}H,^{1}H$-NOESY of **3ba** in $CDCl_3$ measured at 400.16 MHz.

***rel*-(1*S*,2*S*,3a*R*,4*R*,10a*S*,11*R*)-8-methyl-2,3,3a,4,9,10a-hexahydro-1,2,4-(epimethanetriyl) benzo[f]azulen-10(1H)-one**

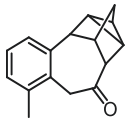

3ca

3ca was synthesized according to **GP-A** employing **1c** (132 mg, 1.00 mmol, 1.00 equiv.) and NBD (132 µL, 1.30 mmol, 1.30 equiv.). Purification *via* flash chromatography (23 g SiO_2, gradient from 98:02 to 75:25 *n*-hexane/EA over 20 CV) afforded **3ca** (174 mg, 774 µmol, 77%, 32% *ee*, $[\alpha]_D^{20}$ +13 (*c* 1.0, $CHCl_3$)) as a colorless oil.

$C_{16}H_{16}O$ (224.30 $\frac{g}{mol}$)

Rf: 0.68 (*n*-hexane/EA = 80:20) [anisaldehyde]

^{1}H NMR(400.16 MHz, $CDCl_3$): δ = 7.07 (m, 1H, H-12), 7.03 (m, 1H, H-10), 7.03 (m, 1H, H-11), 4.33 (d, ^2J = 12.4 Hz, 1H, H-16b), 3.64 (dd, ^2J = 12.4 Hz, ^4J = 0.8 Hz, 1H, H-16a), 2.91 (s, 1H, H-7), 2.64 (m, 1H, H-2), 2,37 (s, 3H, H-14), 2.26 (m, 1H, H-8), 1.74 (ddm, ^3J = 5.1 Hz, ^3J = 5.0 Hz, 1H, H-6), 1.65 (dm, ^2J = 11.0 Hz, 1H, H-5a), 1.52 (dm, ^2J = 11.0 Hz, 1H, H-5b), 1.50 (m, 1H, H-4), 1.49 (m, 1H, H-3).

^{13}C NMR(100.62 MHz, $CDCl_3$): δ = 210.3 (C-1), 140.1 (C-9), 136.3 (C-15), 130.8 (C-13), 129.8, 129.7, 126.5, 59.1 (C-2), 53.4 (C-7), 42.8 (C-16), 42.0 (C-8), 36.2 (C-5), 21.4 (C-14), 18.1 (C-6), 14.5 (C-3), 13.5 (C-4).

HRMS (ESI-TOF) m/z: $[M+H]^+$ Calcd for $C_{16}H_{16}OH$ 225.1274; Found 225.1276.

IR (ATR, ṽ): 1693 cm^{-1} (s, *CO*).

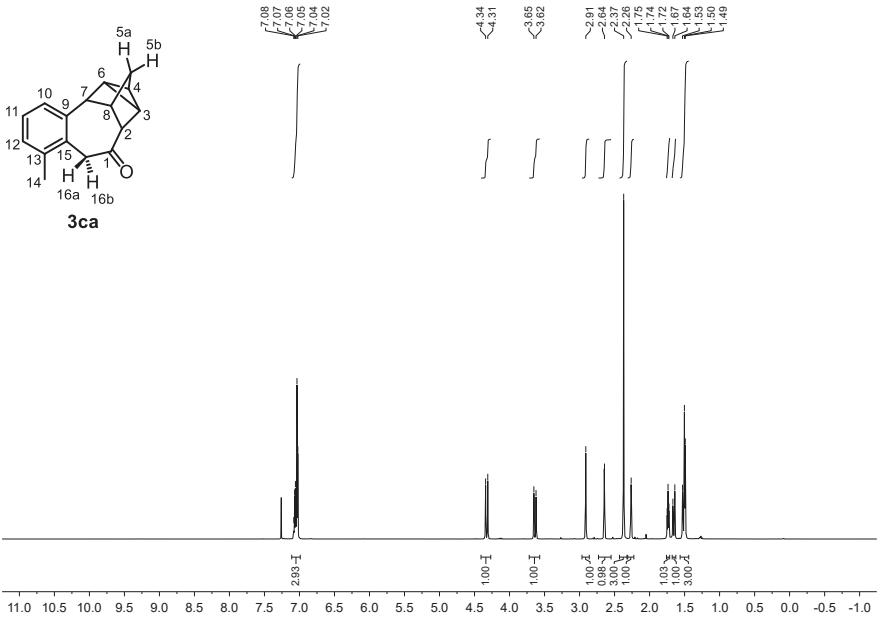

Figure S 73. ^{1}H NMR of **3ca** in $CDCl_3$ measured at 400.16 MHz.

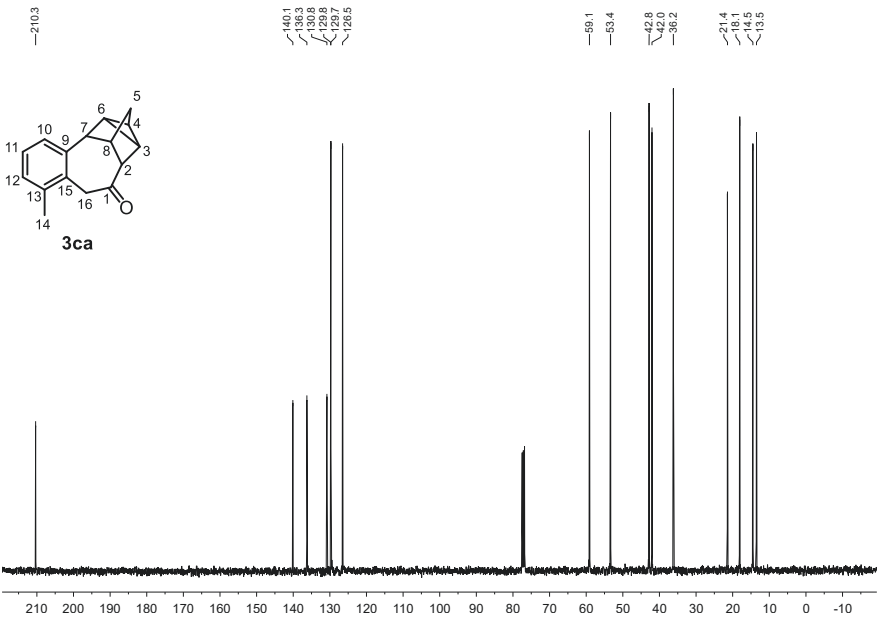

Figure S 74: ^{13}C NMR of **3ca** in $CDCl_3$ measured at 100.63 MHz.

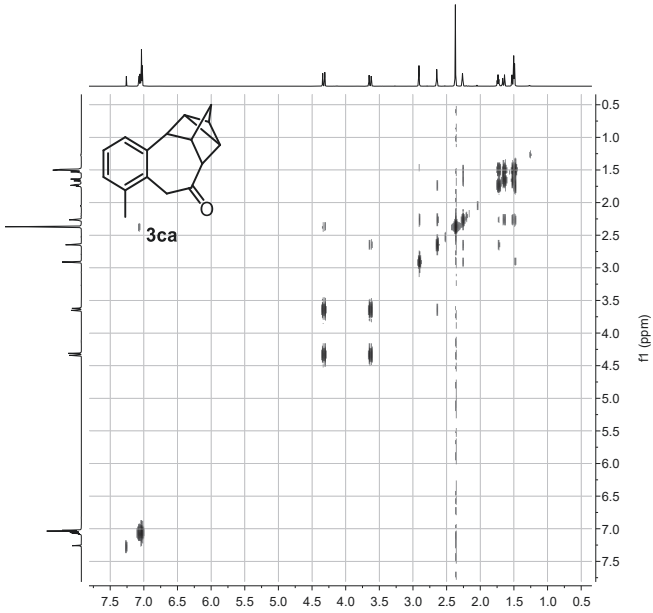

Figure S 75. $^{1}H,^{1}H$-COSY of **3ca** in $CDCl_3$ measured at 400.16 MHz.

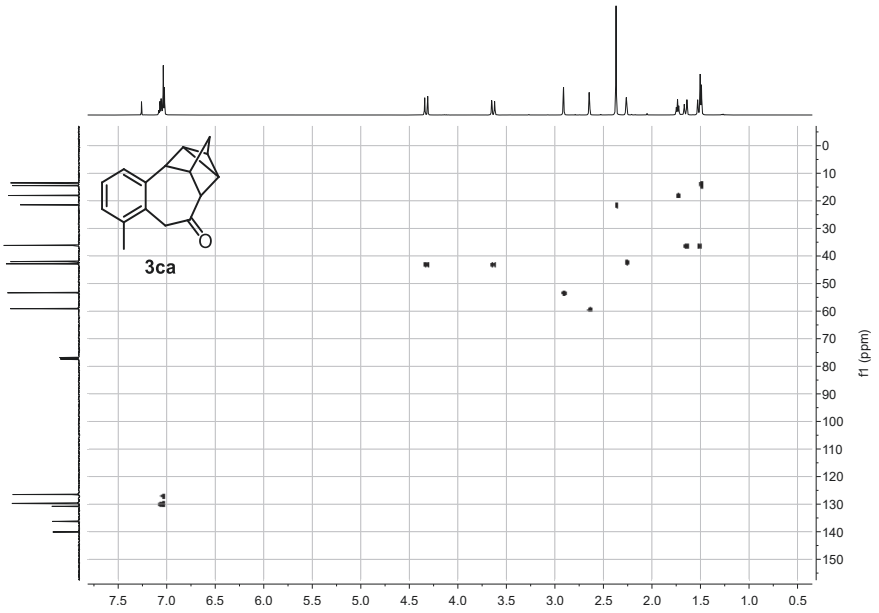

Figure S 76. $^{1}H,^{13}C$-HSQC of **3ca** in $CDCl_3$ measured at ^{1}H: 400.16 MHz; ^{13}C: 100.63 MHz.

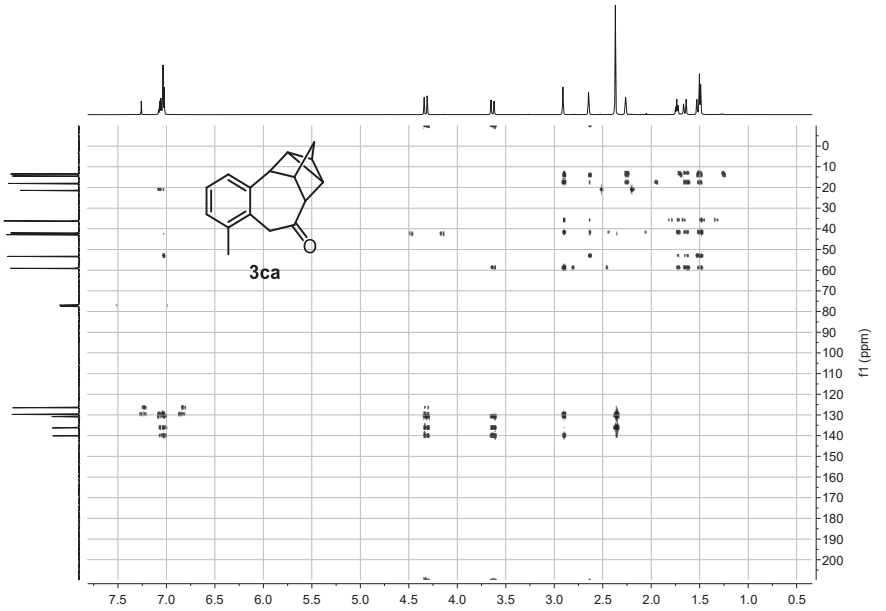

Figure S 77. $^{1}H,^{13}C$-HMBC of **3ca** in $CDCl_3$ measured at ^{1}H: 400.16 MHz; ^{13}C: 100.63 MHz.

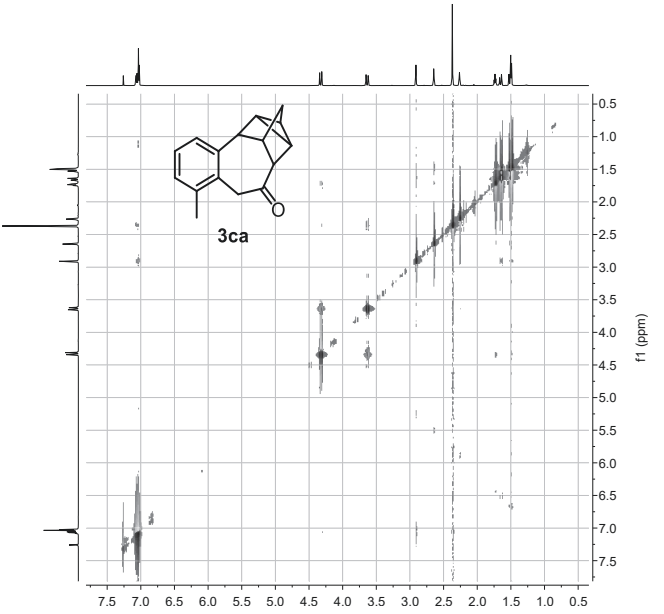

Figure S 78. $^{1}H,^{1}H$-NOESY of **3ca** in $CDCl_3$ measured at 400.16 MHz.

***rel*-7-methoxy-(1*S*,2*S*,3a*R*,4*R*,10a*S*,11*R*)-2,3,3a,4,9,10a-hexahydro-1,2,4-(epimethanetriyl)benzo[f]azulen-10(1H)-one**

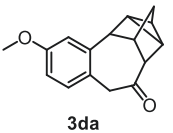

3da

3da was synthesized according to **GP-A** employing **1d** (148 mg, 1.00 mmol, 1.00 equiv.) and NBD (132 µL, 1.30 mmol, 1.30 equiv.) at 150 °C instead of 80 °C. Purification *via* flash chromatography (23 g SiO_2, gradient from 100:0 to 65:35 *n*-hexane/EA over 20 CV) afforded **3da** (179 mg, 746 µmol, 75%, 20% *ee*, $[\alpha]_D^{20}$ +10 (*c* 1.0, $CHCl_3$)) as a colorless solid.

$C_{16}H_{16}O_2$ (240.30 $\frac{g}{mol}$)

mp: 97.3 °C.

Rf: 0.51 (*n*-hexane/EA = 80:20) [anisaldehyde]

^{1}H NMR(400.16 MHz, $CDCl_3$): δ = 6.97 (m, 1H, H-14), 6.74 (m, 1H, H-10), 6.69 (m, 1H, H-13), 4.38 (dd, ^2J = 12.3 Hz, ^4J = 0.5 Hz, 1H, H-16b), 3.78 (s, 3H, H-12) 3.30 (dd, ^2J = 12.3 Hz, ^4J = 1.0 Hz, 1H, H-16a), 2.84 (s, 1H, H-7), 2.62 (m, 1H, H-2), 2.30 (m, 1H, H-8), 1.71 (ddm, ^3J = 5.1 Hz, ^3J = 5.0 Hz, 1H, H-6), 1.65 (dm, ^2J = 10.7 Hz, 1H, H-5a), 1.51 (dm, ^2J = 10.7 Hz, 1H, H-5b), 1.50 (m, 1H, H-3), 1.48 (m, 1H, H-4).

^{13}C NMR(100.62 MHz, $CDCl_3$): δ = 209.8 (C-1), 158.5 (C-11), 141.1 (C-15), 131.4 (C-14), 123.8 (C-9), 117.4 (C-10), 112.2 (C-13), 58.9 (C-2), 55.4 (C-12), 53.1 (C-7), 48.3 (C-16), 42.0 (C-8), 36.3 (C-5), 17.8 (C-6), 15.0 (C-3), 13.2 (C-4).

HRMS (ESI-TOF) m/z: $[M+H]^+$ Calcd for $C_{16}H_{16}O_2H$ 241.1223; Found 241.1226.

IR (ATR, ṽ): 1694 cm^{-1} (s, *CO*).

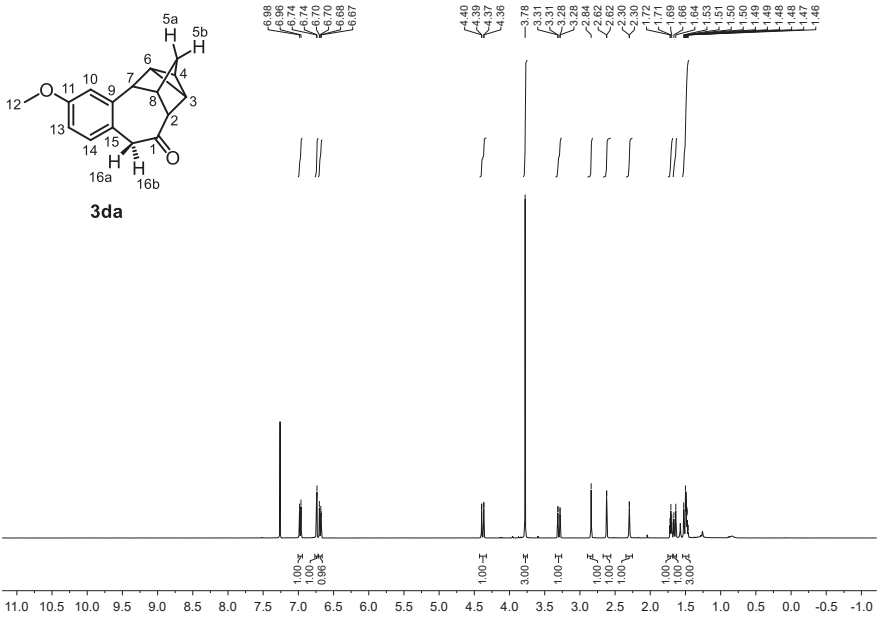

Figure S 79. ^{1}H NMR of **3da** in $CDCl_3$ measured at 400.16 MHz.

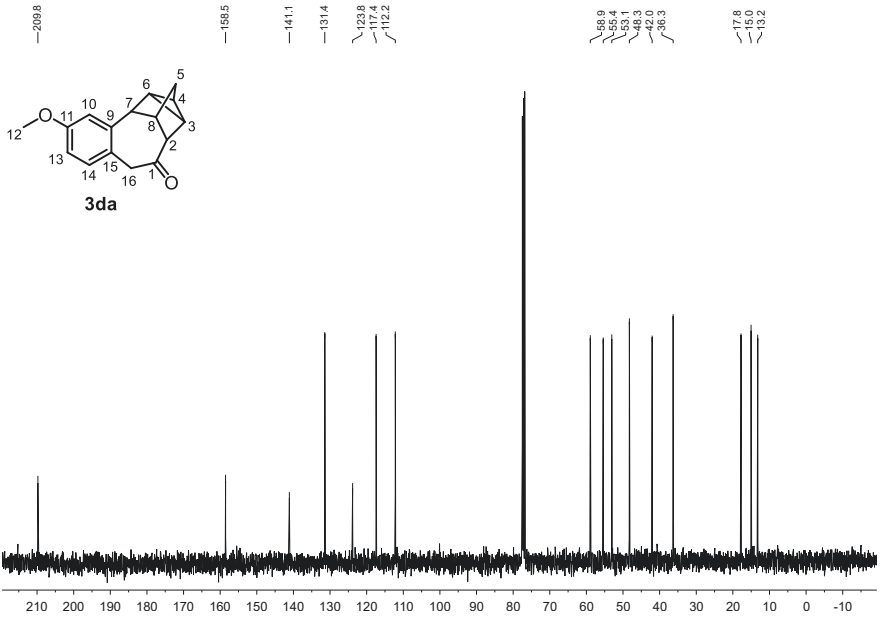

Figure S 80. ^{13}C NMR of **3da** in $CDCl_3$ measured at 100.63 MHz.

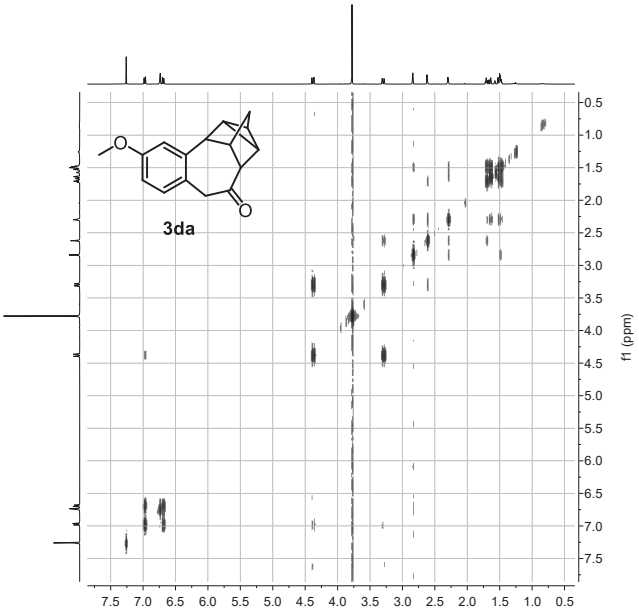

Figure S 81. $^{1}H,^{1}H$-COSY of **3da** in $CDCl_3$ measured at 400.16 MHz.

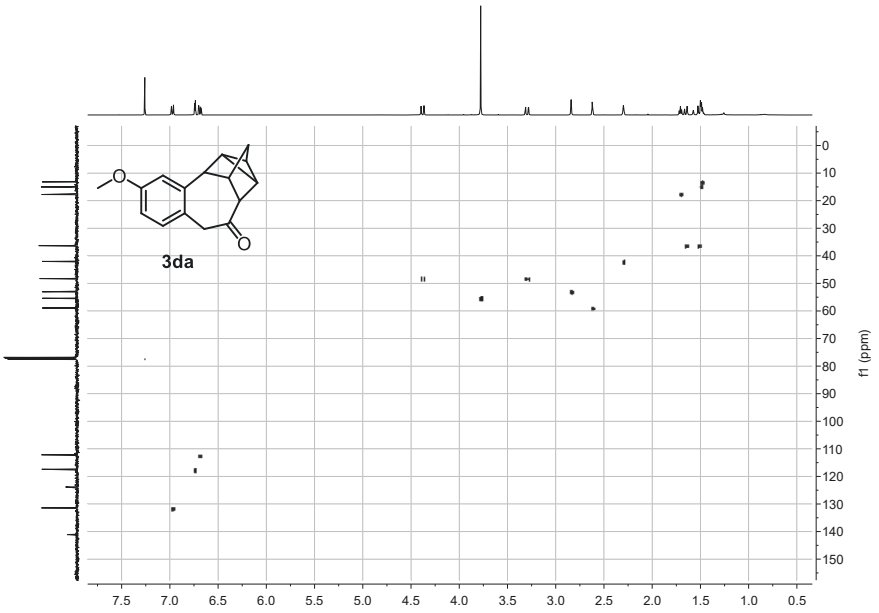

Figure S 82. $^{1}H,^{13}C$-HSQC of **3da** in $CDCl_3$ measured at ^{1}H: 400.16 MHz; ^{13}C: 100.63 MHz.

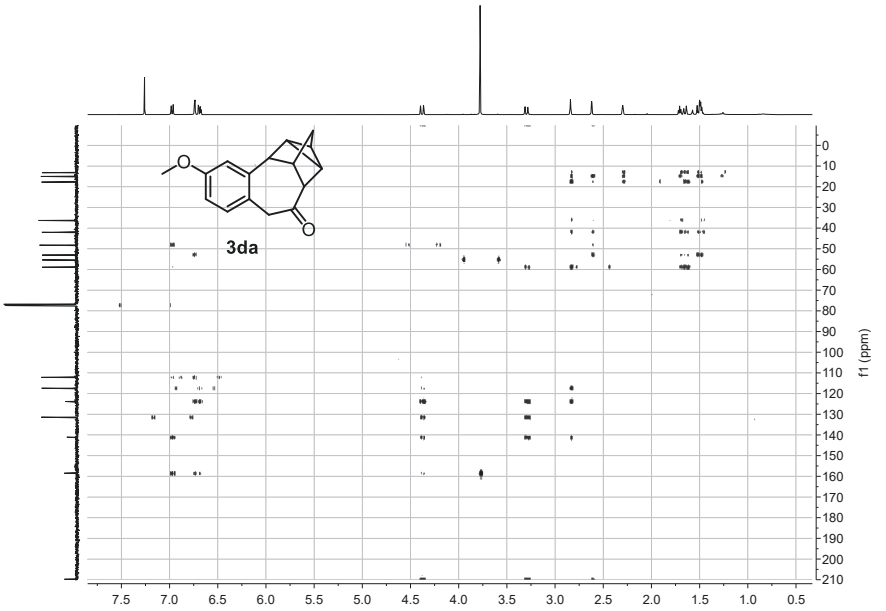

Figure S 83. $^{1}H,^{13}C$-HMBC of **3da** in $CDCl_3$ measured at ^{1}H: 400.16 MHz; ^{13}C: 100.63 MHz.

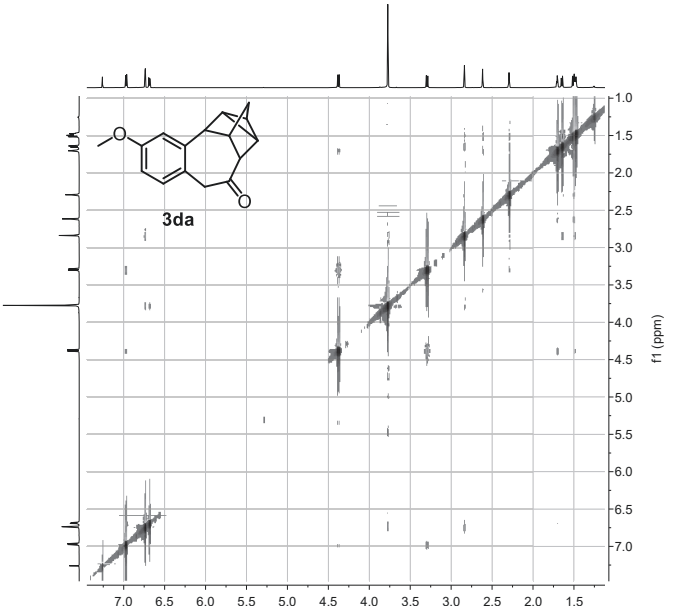

Figure S 84. $^{1}H,^{1}H$-NOESY of **3da** in $CDCl_3$ measured at 700.21 MHz.

***rel*-(7a*R*,8*R*,9*R*,10a*S*,11*S*,12*S*)-7a,8,9,10,10a,11-hexahydro-8,9,11-(epimethanetriyl) azuleno[5',6':3,4]benzo[1,2-d][1,3]dioxol-7(6H)-one**

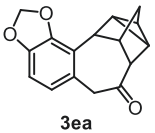

3ea

3ea was synthesized according to **GP-A** employing **1e** (162 mg, 1.00 mmol, 1.00 equiv.) and NBD (132 µL, 1.30 mmol, 1.30 equiv.). Purification *via* flash chromatography (23 g SiO_2, gradient from 90:10 to 70:30 *n*-hexane/EA over 15 CV) afforded **3ea** (187 mg, 737 µmol, 74%, mixture of isomers) as a pale brown solid.

Regioselective ratio: 86:14

$C_{16}H_{14}O_3$ (254.29 $\frac{g}{mol}$)

mp: 59.4 °C.

Rf: 0.53 (*n*-hexane/EA = 80:20) [anisaldehyde]

^{1}H NMR(700.21 MHz, CD_2Cl_2): δ = 6.59 (d, ^3J = 7.8 Hz, 1H, H-13), 6.52 (d, ^3J = 7.8 Hz, 1H, H-14), 5.94 (m, 1H, H-11a), 5.93 (m, 1H, H-11b), 4.27 (d, ^2J = 12.3 Hz, 1H, H-16b), 3.37 (d, ^2J = 12.3 Hz, 1H, H-16a), 3.24 (s, 1H, H-7), 2.62 (s, 1H, H-2), 2.31 (s, 1H, H-8), 1.67 (m, 1H, H-3), 1.67 (d, ^2J = 10.8 Hz, 1H, H-5a), 1.52 (d, ^2J = 10.8 Hz, 1H, H-5b), 1.48 (m, 1H, H-4), 1.48 (m, 1H, H-6).

^{13}C NMR(176.08 MHz, CD_2Cl_2): δ = 209.7 (C-1), 146.7 (C-10), 145.8 (C-12), 125.7 (C-15), 122.8 (C-14), 121.7 (C-9), 106.9 (C-13), 100.9 (C-11), 58.9 (C-2), 48.7 (C-15), 42.7 (C-2), 40.9 (C-8), 36.1 (C-5), 17.2 (C-3), 14.7 (C-6), 13.1 (C-4).

HRMS (ESI-TOF) m/z: $[M+H]^+$ Calcd for $C_{16}H_{14}O_3H$ 255.1016; Found 255.1017.

IR (ATR, ṽ): 1688 cm^{-1} (s, *CO*).

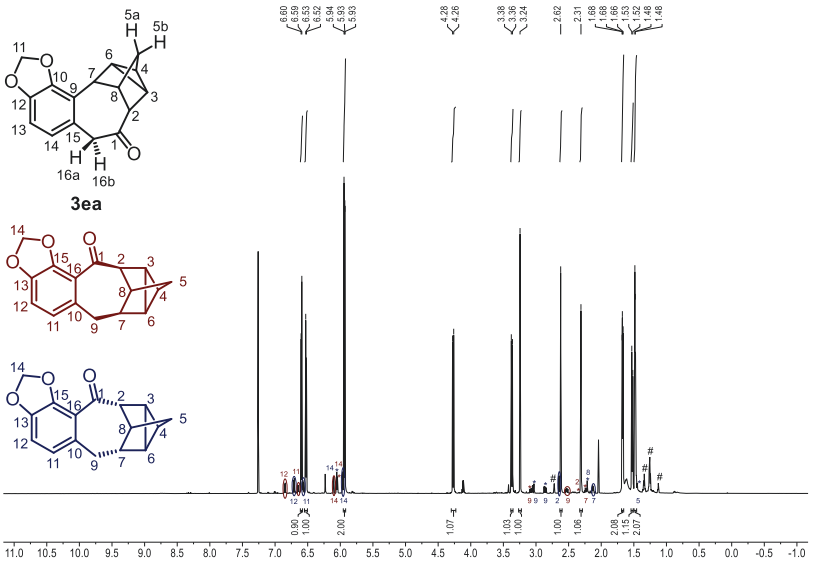

Figure S 85. ^{1}H NMR of **3ea** with the two diastereomers of the respective regioisomer in $CDCl_3$ measured at 700.21 MHz. The assigned signals of the diastereomers are color coded and their ambiguous signals are denoted by #.

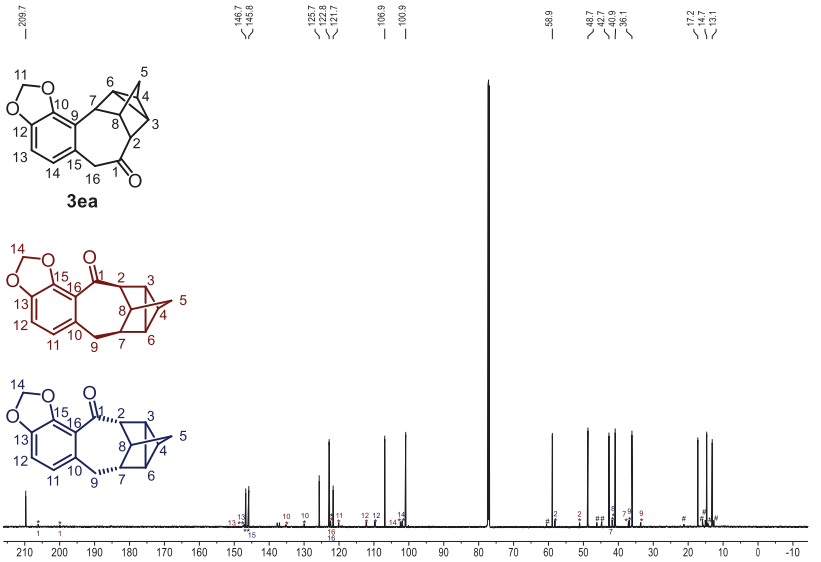

Figure S 86. ^{13}C NMR of **3ea** with the two diastereomers of the respective regioisomer in $CDCl_3$ measured at 176.08 MHz. The assigned signals of the diastereomers are color coded and their ambiguous signals are denoted by #.

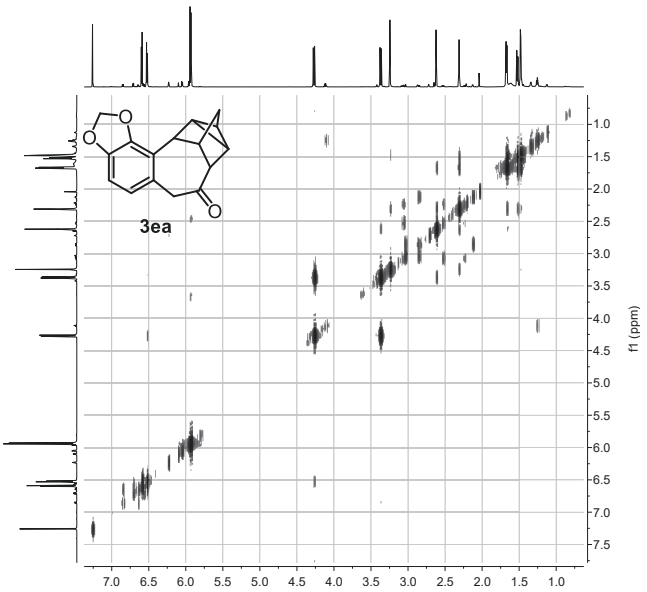

Figure S 87. ^{1}H,^{1}H-COSY of **3ea** with the two diastereomers of the respective regioisomer in $CDCl_3$ measured at 700.21 MHz.

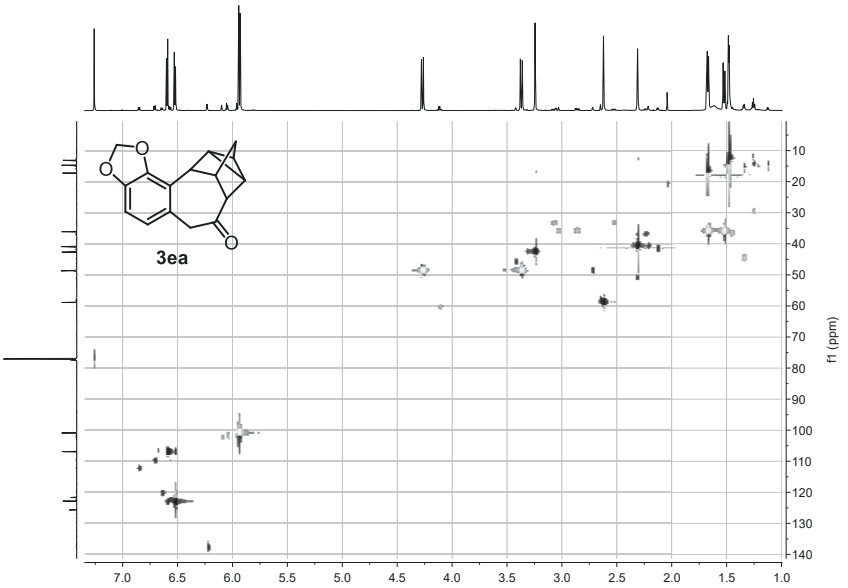

Figure S 88. ^{1}H,^{13}C-HSQC of **3ea** with the two diastereomers of the respective regioisomer in $CDCl_3$ measured at ^{1}H: 700.21 MHz; ^{13}C: 176.08 MHz.

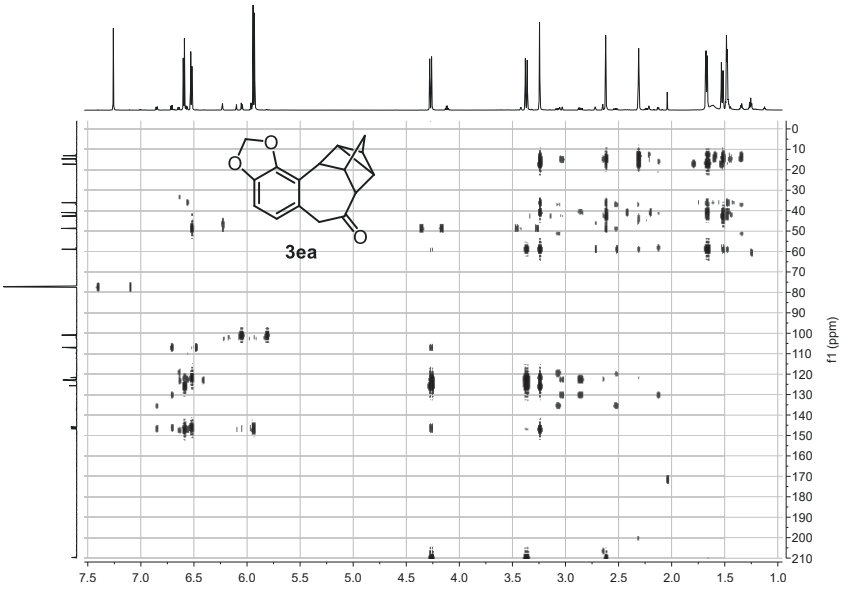

Figure S 89. $^{1}H,^{13}C$-HMBC of **3ea** with the two diastereomers of the respective regioisomer in $CDCl_3$ measured at ^{1}H: 700.21 MHz; ^{13}C: 176.08 MHz.

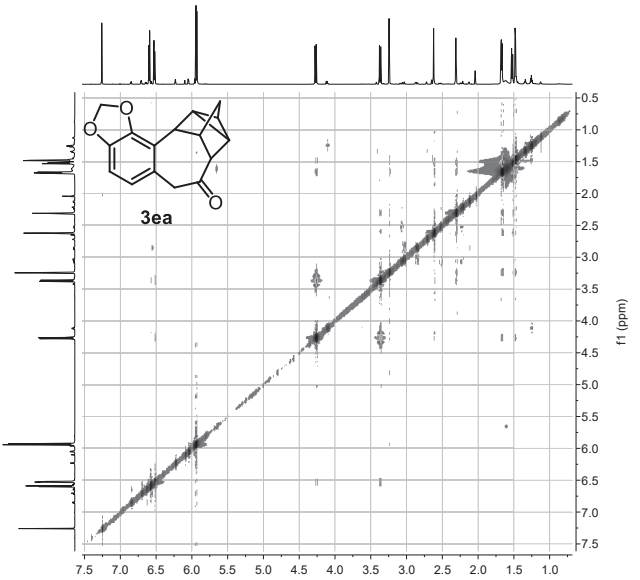

Figure S 90. $^{1}H,^{1}H$-NOESY of **3ea** with the two diastereomers of the respective regioisomer in $CDCl_3$ measured at 700.21 MHz.

***rel*-5-fluoro-(1*S*,2*S*,3a*R*,4*R*,10a*S*,11*R*)-2,3,3a,4,9,10a-hexahydro-1,2,4-(epimethanetriyl) benzo[f]azulen-10(1H)-one**

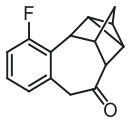

3fa

3fa was synthesized according to **GP-A** employing **1f** (136 mg, 1.00 mmol, 1.00 equiv.) and NBD (132 µL, 1.30 mmol, 1.30 equiv.) at 100 °C instead of 80 °C. Purification *via* flash chromatography (23 g SiO_2, gradient from 100:0 to 60:40 *n*-hexane/EA over 20 CV) afforded **3fa** (89.2 mg, 391 µmol, 39%, 29% *ee*, $[\alpha]_D^{20}$ +8 (*c* 1.0, $CHCl_3$)) as a pale yellow solid.

Regioisomeric ratio: 87:13

$C_{15}H_{13}FO$ (228.27 $\frac{g}{mol}$)

mp: 62.1 °C.

Rf: 0.66 (*n*-hexane/EA = 80:20) [anisaldehyde]

^{1}H NMR(400.16 MHz, $CDCl_3$): δ = 7.09 (m, 1H, H-12), 6.92 (m, 1H, H-11), 6.82 (d, ^3J = 7.6 Hz, 1H, H-13), 4.23 (d, ^2J = 12.4 Hz, 1H, H-15b), 3.58 (d, ^2J = 12.4 Hz, 1H, H-15a), 3.46 (s, 1H, H-7), 2.63 (s, 1H, H-2), 2.35 (s, 1H, H-8), 1.69 (dm, ^2J = 10.7 Hz, 1H, H-5a), 1.66 (ddm, ^3J = 5.5 Hz, ^3J = 5.0 Hz, 1H, H-6), 1.54 (dm, ^2J = 10.7 Hz, 1H, H-5b), 1.48 (m, 1H, H-4), 1.47 (m, 1H, H-3).

^{13}C NMR(100.62 MHz, $CDCl_3$): δ = 208.7 (C-1), 161.4 (d, ^1J = 244 Hz, C-10), 134.0 (d, ^3J = 3 Hz, C-14), 128.1 (d, ^3J = 10 Hz, C-12), 126.8 (d, ^2J = 13 Hz, C-9), 125.9 (d, ^4J = 3 Hz, C-13), 114.1 (d, ^2J = 25 Hz, C-11), 58.6 (C-2), 49.2 (C-15), 41.2 (d, ^3J = 7 Hz, C-7), 39.8 (C-8), 36.0 (C-5), 16.9 (C-6), 15.3 (C-3), 13.1 (C-4).

^{19}F NMR(376.49 MHz, $CDCl_3$): δ = -116.6.

HRMS (ESI-TOF) m/z: $[M+Na]^+$ Calcd for $C_{15}H_{13}FONa$ 251.0843; Found 251.0845.

IR (ATR, ṽ): 1701 cm^{-1} (s, *CO*).

Regiosiomer:

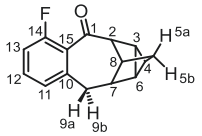

^{1}H NMR(400.16 MHz, $CDCl_3$): δ = 7.23 (ddd, , ^{3}J = 8.2 Hz, ^{3}J = 8.2 Hz, ^{4}J = 5.7 Hz, 1H, H-12), 6.94 (ddm, ^{3}J = 9.8 Hz, ^{3}J = 8.6 Hz, 1H, H-11), 6.90 (d, ^{3}J = 7.5 Hz, 1H, H-13), 3.09 (d, ^{2}J = 15.9 Hz, 1H, H-9a), 2.90 (ddd, ^{2}J = 15.9 Hz, ^{3}J = 7.6 Hz, ^{4}J = 1.2 Hz, 1H, H-9b), 2.65 (m, 1H, H-2), 2.22 (m, 1H, H-8), 2.14 (dm, ^{3}J = 7.6 Hz, 1H, H-7), 1.53 (dm, ^{2}J = 10.7 Hz, 1H, H-5b), 1.47 (dm, ^{3}J = 10.8 Hz, 1H, H-5a), 1.31 (m, 1H, H-4), 1.28 (m, 1H, H-3), 1.07 (m, 1H, H-6).

^{13}C NMR(100.62 MHz, $CDCl_3$): δ = 205.9 (C-1), 159.2 (d, ^{1}J = 252 Hz, C-14), 137.1 (d, ^{2}J = 66 Hz, C-15), 131.2 (d, ^{3}J = 9 Hz, C-12), 128.5 (d, ^{3}J = 14 Hz, C-10), 126.3 (d, ^{4}J = 3 Hz, C-11), 114.4 (d, ^{2}J = 22 Hz, C-13), 57.3 (C-2), 41.7 (C-8), 41.2 (C-7), 36.8 (C-5), 35.8 (C-9), 15.3 (C-4), 15.1 (C-6), 12.9 (C-3).

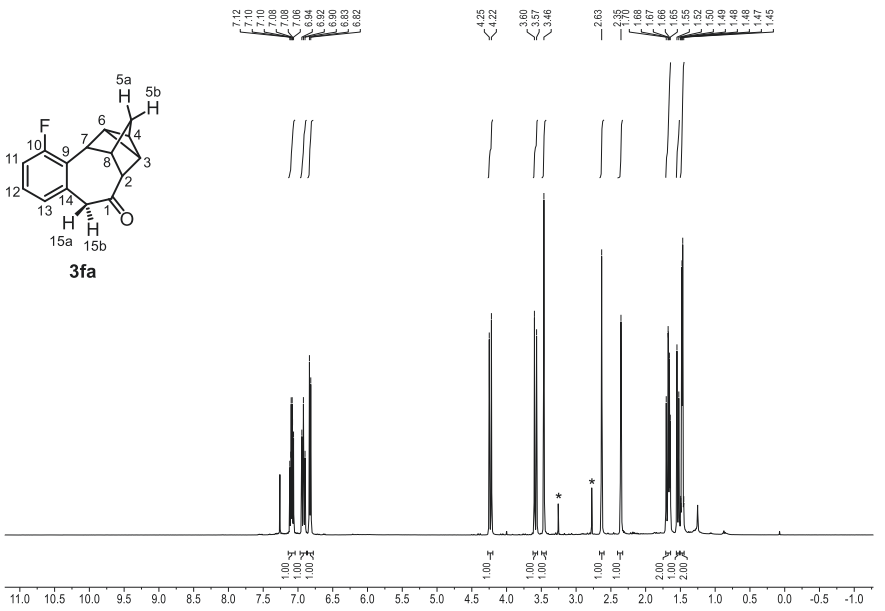

Figure S 91. ^{1}H NMR of **3fa** in $CDCl_3$ measured at 400.16 MHz. * Denotes residual DMI.

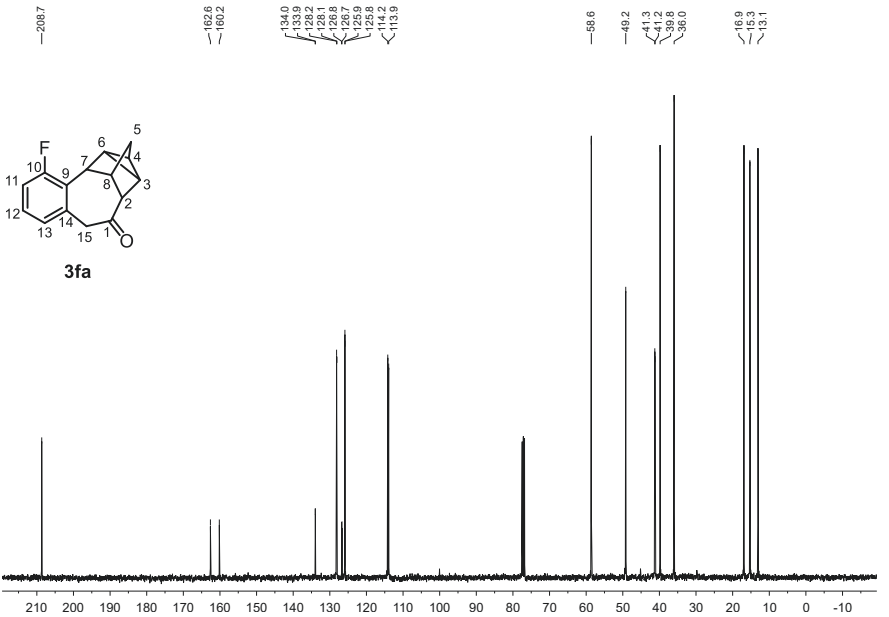

Figure S 92. ^{13}C NMR of **3fa** in $CDCl_3$ measured at 100.63 MHz.

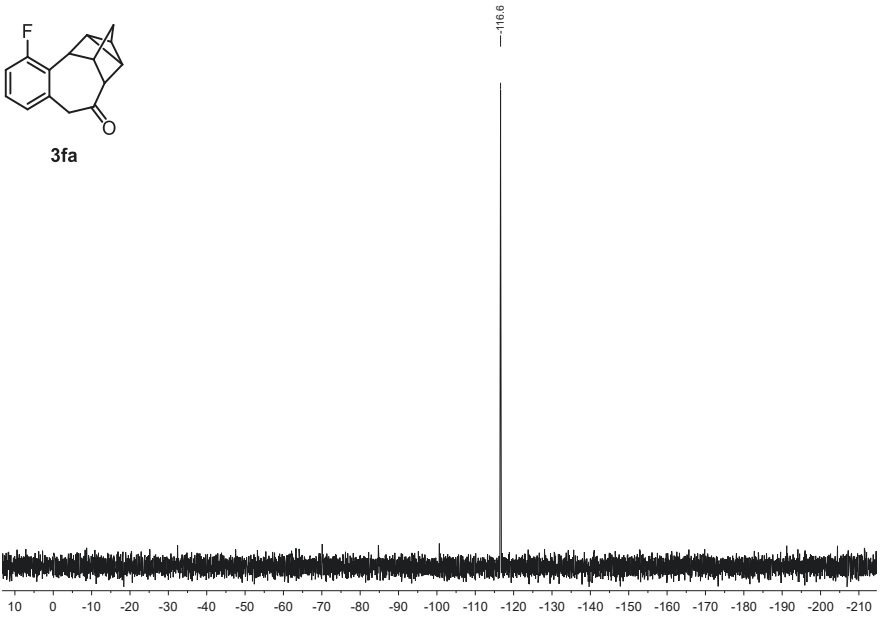

Figure S 93. ^{19}F NMR of **3fa** in $CDCl_3$ measured at 376.49 MHz.

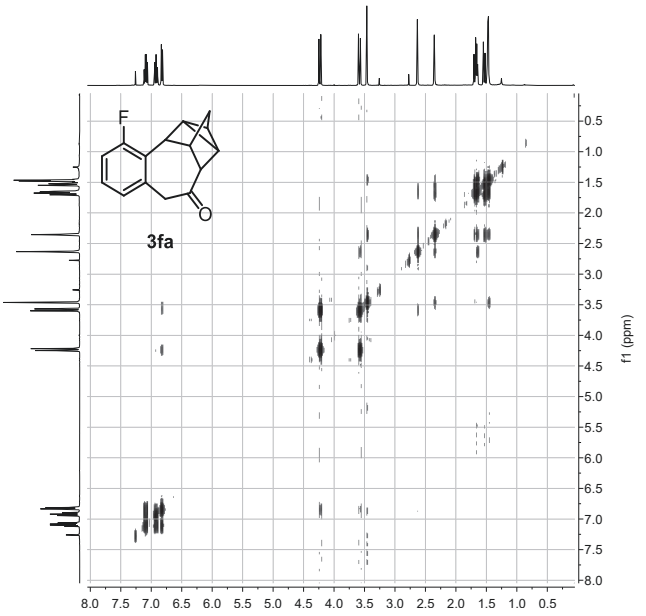

Figure S 94. $^{1}H,^{1}H$-COSY of **3fa** in $CDCl_3$ measured at 400.16 MHz.

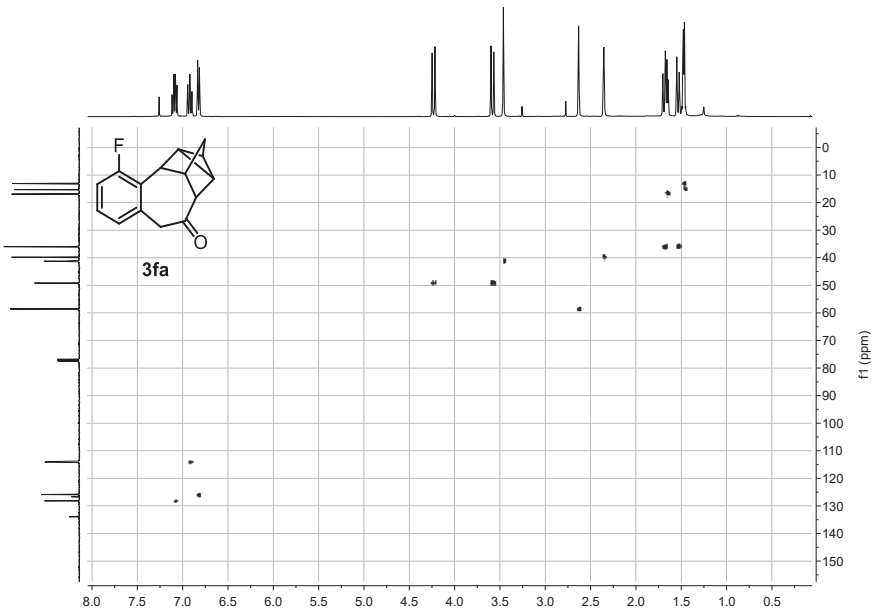

Figure S 95. $^{1}H,^{13}C$-HSQC of **3fa** in $CDCl_3$ measured at ^{1}H: 700.21 MHz; ^{13}C: 176.08 MHz.

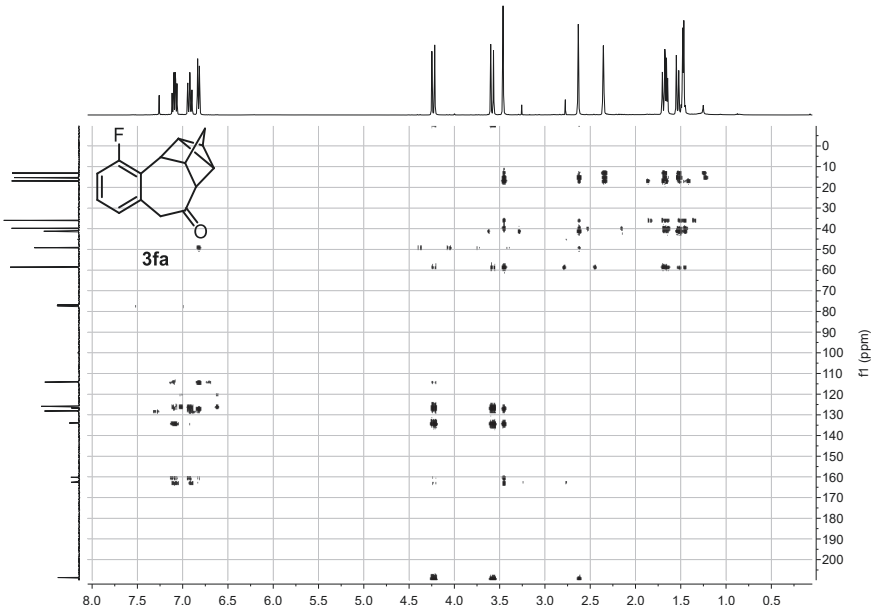

Figure S 96. $^{1}H,^{13}C$-HMBC of **3fa** in $CDCl_3$ measured at ^{1}H: 700.21 MHz; ^{13}C: 176.08 MHz.

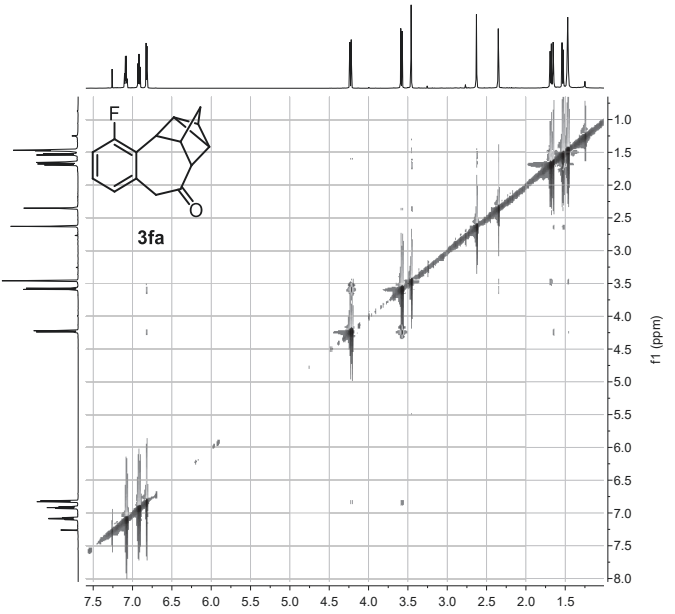

Figure S 97. $^{1}H,^{1}H$-NOESY of **3fa** in $CDCl_3$ measured at 700.21 MHz.

***rel*-(1*R*,2*R*,3a*S*,4*S*,9*R*,10a*R*,11*S*)-9-methyl-2,3,3a,4,9,10a-hexahydro-1,2,4-(epimethanetriyl)benzo[f]azulen-10(1H)-one (mixture of enantiomers)**

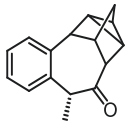

3ga

3ga was synthesized according to **GP-A** employing **1g** (132 mg, 1.00 mmol, 1.00 equiv.) and NBD (132 µL, 1.30 mmol, 1.30 equiv.) at 50 °C instead of 80 °C. Purification *via* flash chromatography (23 g SiO_2, gradient from 100:00 to 90:10 *n*-hexane/EA over 10 CV) afforded **3ga** (137 mg, 610 µmol, 61%, mixture of isomers) as colorless crystals.

d.r.: 95:5

$C_{16}H_{16}O$ (224.30 $\frac{g}{mol}$)

mp: 85.6 °C.

R_f: 0.68 (*n*-hexane/EA = 80:20) [anisaldehyde]

^{1}H NMR(400.16 MHz, $CDCl_3$): δ = 7.22 (m, 1H, H-10), 7.20 (m, 2H, H-11/12), 7.14 (m, 1H, H-13), 4.28 (q, ^3J = 6.9 Hz, 1H, H-15), 3.16 (s, 1H, H-7), 2.70 (m, 1H, H-8), 2.63 (m, 1H, H-2), 1.64 (dm, ^2J = 10.6 Hz, 1H, H-5a), 1.56 (dm, ^2J = 10.6 Hz, 1H, H-5b), 1.53 (m, 1H, H-3), 1.48 (d, ^3J = 6.9 Hz, 3H, H-16), 1.40 (m, 1H, H-4), 1.38 (m, 1H, H-6); *diastereomer* δ = 7.22 (m, 1H), 7.20 (m, 2H), 7.16 (m, 1H, H-10), 4.86 (q, ^3J = 6.8 Hz, 1H, H-15), 2.90 (s, 1H, H-2), 2.71 (m, 1H, H-7), 2.24 (m, 1H, H-8), 1.75 (m, 1H, H-6), 1.65 (dm, ^2J = 11.6 Hz, 1H, H-5a), 1.53 (m, 1H, H-3), 1.52 (dm, ^2J = 11.6 Hz, 1H, H-5b), 1.43 (m, 1H, H-4), 1.42 (d, ^3J = 6.8 Hz, 3H, H-16).

^{13}C NMR(100.62 MHz, $CDCl_3$): δ = 210.7 (C-1), 139.4 (C-9), 134.6 (C-14), 131.2 (C-10), 127.2 (C-12), 126.8 (C-11), 126.6 (C-12), 57.7 (C-2), 52.6 (C-7), 48.6 (C-15), 35.4 (C-8), 35.3 (C-5), 21.2 (C-6), 15.0 (C-16), 14.5 (C-3), 13.5 (C-4) *diastereomer* δ = 139.4 (C-9), 134.5 (C-14), 131.5 (C-10), 127.6, 126.8, 125.2, 53.8 (C-2), 44.2 (C-15), 44.1 (C-8), 36.2 (C-7), 36.2 (C-5), 18.2 (C-6), 14.1 (C-16), 13.7 (C-3), 13.0 (C-4).

HRMS (ESI-TOF) m/z: $[M+Na]^+$ Calcd for $C_{16}H_{16}ONa$ 247.1093; Found 247.1095.

IR (ATR, ṽ): 1699 cm^{-1} (s, *CO*).

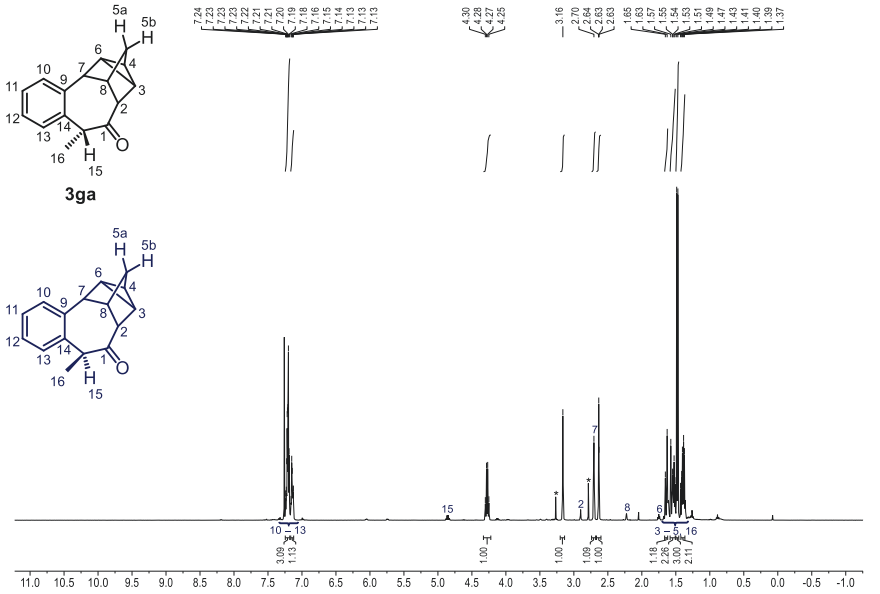

Figure S 98. ^{1}H NMR of **3ga** and the respective diastereomer (blue) in $CDCl_3$ measured at 400.16 MHz. * denotes residual DMI.

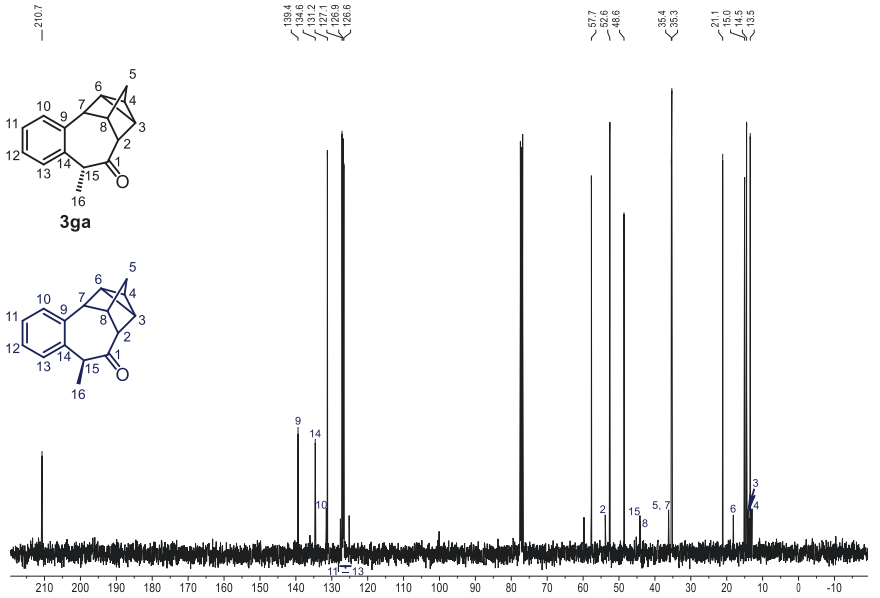

Figure S 99. ^{13}C NMR of **3ga** and the respective diastereomer (blue) in $CDCl_3$ measured at 100.63 MHz.

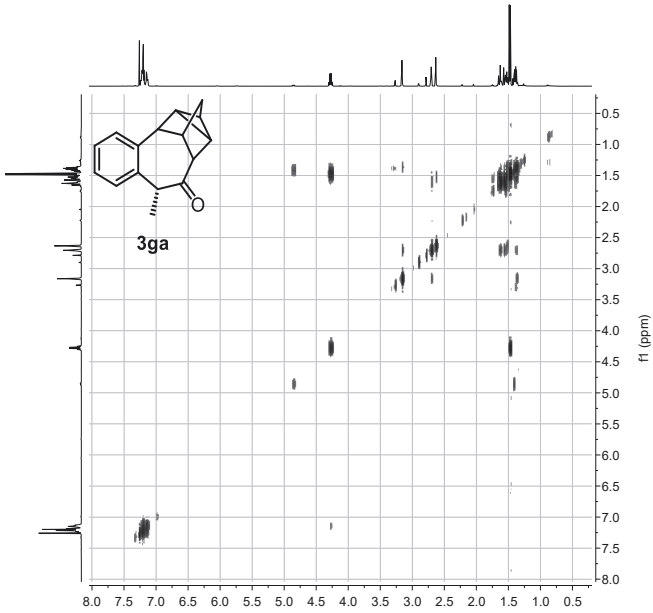

Figure S 100. $^{1}H,^{1}H$-COSY of **3ga** in $CDCl_3$ measured at 400.16 MHz.

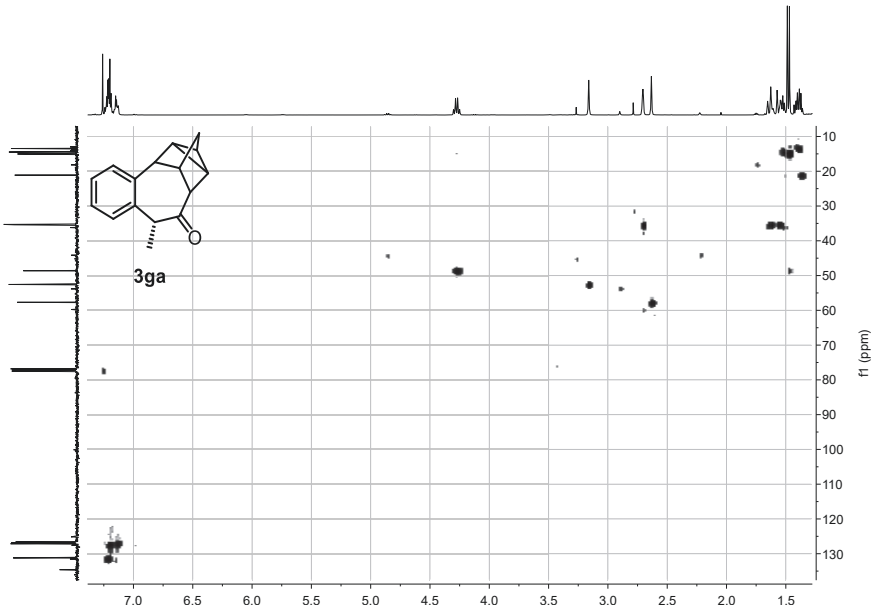

Figure S 101. $^{1}H,^{13}C$-HSQC of **3ga** in $CDCl_3$ measured at ^{1}H: 400.16 MHz; ^{13}C: 100.63 MHz.

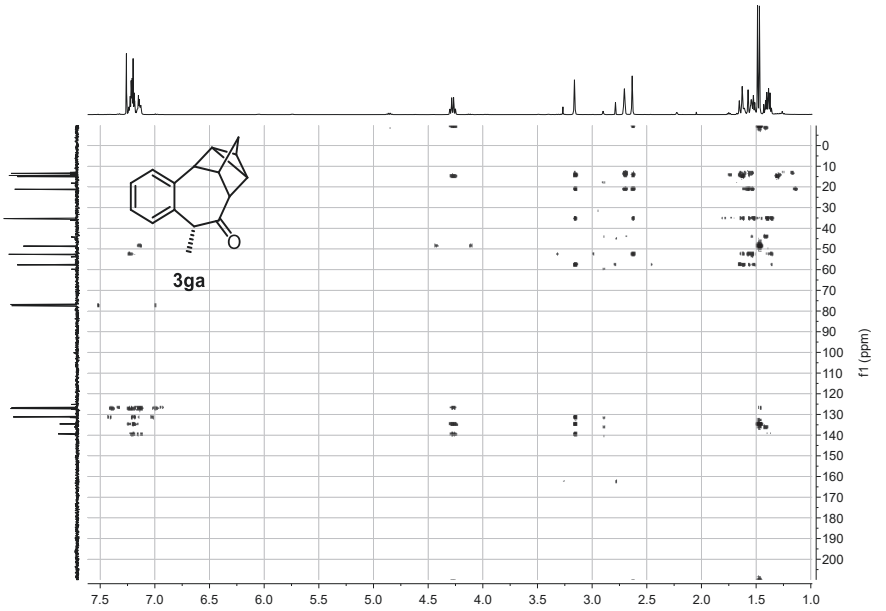

Figure S 102. $^{1}H,^{13}C$-HMBC of **3ga** in $CDCl_3$ measured at ^{1}H: 400.16 MHz; ^{13}C: 100.63 MHz.

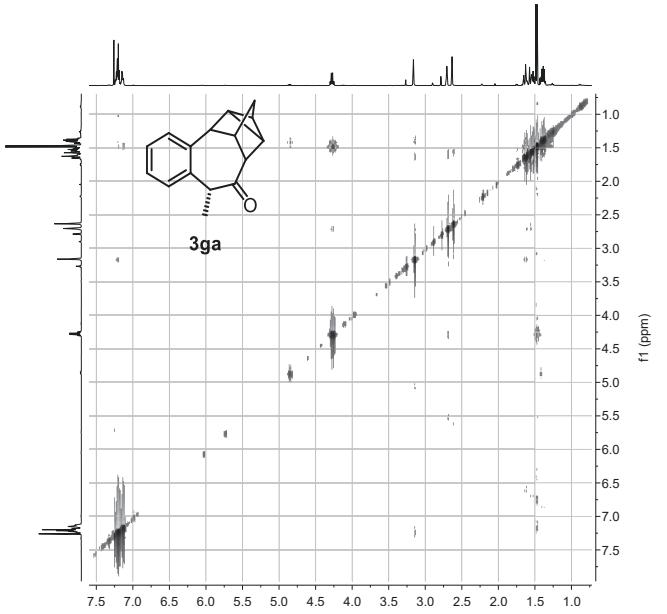

Figure S 103. $^{1}H,^{1}H$-NOESY of **3ga** in $CDCl_3$ measured at 400.16 MHz.

***rel*-(1*R*,2*R*,3a*S*,4*S*,9*R*,10a*R*,11*S*)-9-ethyl-2,3,3a,4,9,10a-hexahydro-1,2,4-(epimethanetriyl)benzo[f]azulen-10(1H)-one (mixture of enantiomers)**

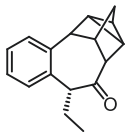

3ha

3ha was synthesized according to **GP-A** employing **1h** (146 mg, 1.00 mmol, 1.00 equiv.), NBD (305 µL, 3.00 mmol, 3.00 equiv.), $Ni(COD)_2$ (20 mol%) and (*R*)-(+)-(3,5-dioxa-4-phosphacyclohepta[2,1-a;3,4-a']dinaphthalen-4-yl)dimethylamine ((*R*)-MonoPhos, 40 mol%). Purification *via* flash chromatography (23 g SiO_2, gradient from 98:02 to 80:20 *n*-hexane/EA over 15 CV) afforded **1ha** (92.0 mg, 386 µmol, 39%, mixture of isomers) as colorless crystals.

d.r.: 92:8

$C_{17}H_{18}O$ (238.33 $\frac{g}{mol}$)

Rf: 0.71 (*n*-hexane/EA = 80:20) [anisaldehyde]

^{1}H NMR(400.16 MHz, $CDCl_3$): δ = 7.21 (m, 1H, H-10), 7.17 (m, 2H, H-11/12), 7.07 (m, 1H, H-13), 3.88 (dd, ^{3}J = 9.6 Hz, ^{3}J = 5.9 Hz, 1H, H-15), 3.06 (s, 1H, H-7), 2.67 (m, 1H, H-2), 2.55 (s, 1H, H-8), 2.24 (ddt, ^{2}J = 20.7 Hz, ^{3}J = 9.6 Hz, ^{3}J = 7.3 Hz, 1H, H-16b), 1.88 (ddt, ^{2}J = 20.7 Hz, ^{3}J = 5.9 Hz, ^{3}J = 7.3 Hz, 1H, H-16a), 1.63 (dm, ^{2}J = 10.7 Hz, 1H, H-5a), 1.55 (dm, ^{2}J = 10.7 Hz, 1H, H-5b), 1.57 (m, 1H, H-6), 1.44 (m, 1H, H-4), 1.43 (m, 1H, H-4), 0.99 (t, ^{3}J = 7.3 Hz, 1H, H-17).

^{13}C NMR(100.62 MHz, $CDCl_3$): δ = 210.8 (C-1), 139.3 (C-9), 135.3 (C-14), 131.7 (C-10), 128.7 (C-13), 127.2 (C-12), 126.9 (C-11), 60.0 (C-15), 59.1 (C-2), 53.0 (C-7), 37.8 (C-8), 35.5 (C-5), 25.4 (C-16), 20.3 (C-4), 15.0 (C-6), 13.9 (C-3), 13.0 (C-17).

HRMS (ESI-TOF) m/z: $[M+H]^+$ Calcd for $C_{17}H_{18}OH$ 239.1430; Found 239.1431.

IR (ATR, ṽ): 1701 cm^{-1} (s, *CO*).

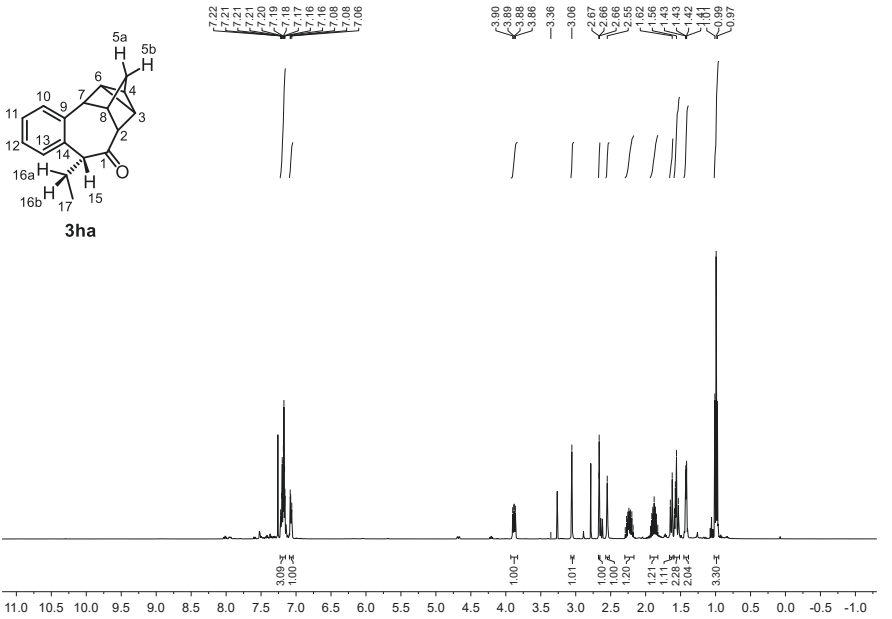

Figure S 104. ^{1}H NMR of **3ha** in $CDCl_3$ measured at 400.16 MHz. * denotes residual DMI.

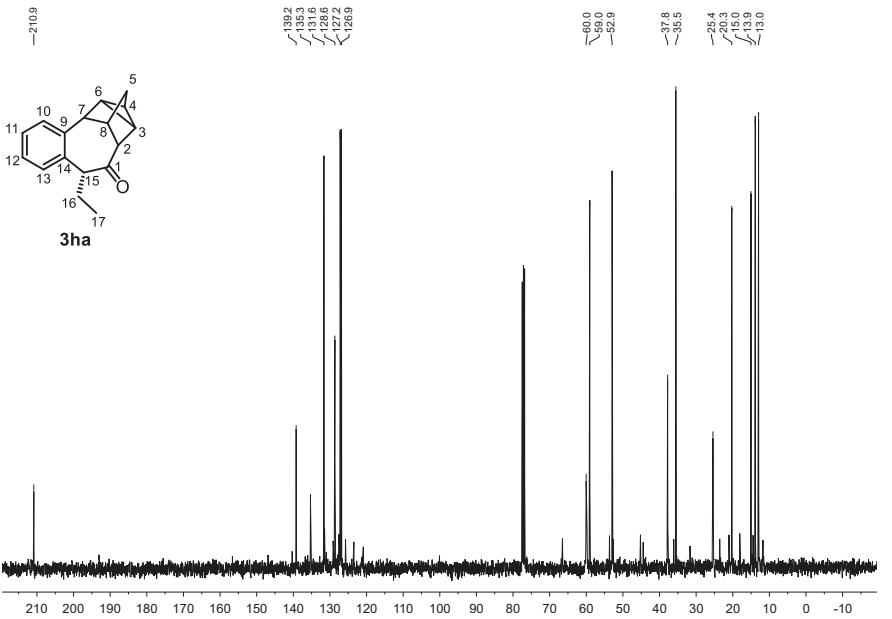

Figure S 105. ^{13}C NMR of **3ha** in $CDCl_3$ measured at 100.63 MHz.

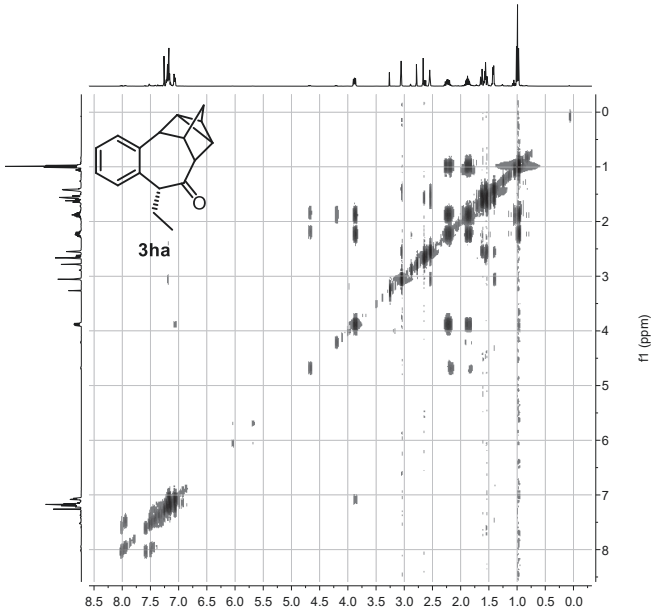

Figure S 106. $^{1}H,^{1}H$-COSY of **3ha** in $CDCl_3$ measured at 400.16 MHz.

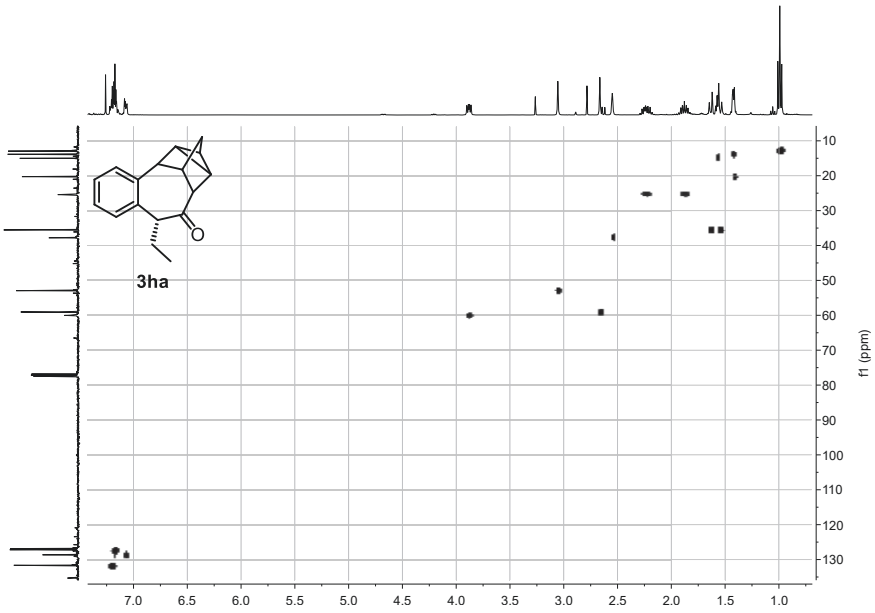

Figure S 107. $^{1}H,^{13}C$-HSQC of **3ha** in $CDCl_3$ measured at ^{1}H: 400.16 MHz; ^{13}C: 100.63 MHz.

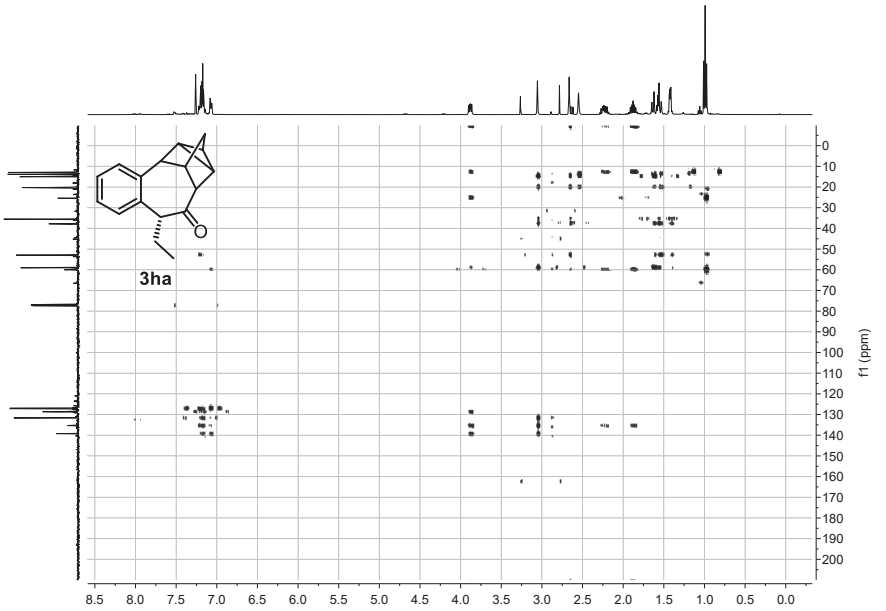

Figure S 108. $^{1}H,^{13}C$-HMBC of **3ha** in $CDCl_3$ measured at ^{1}H: 400.16 MHz; ^{13}C: 100.63 MHz.

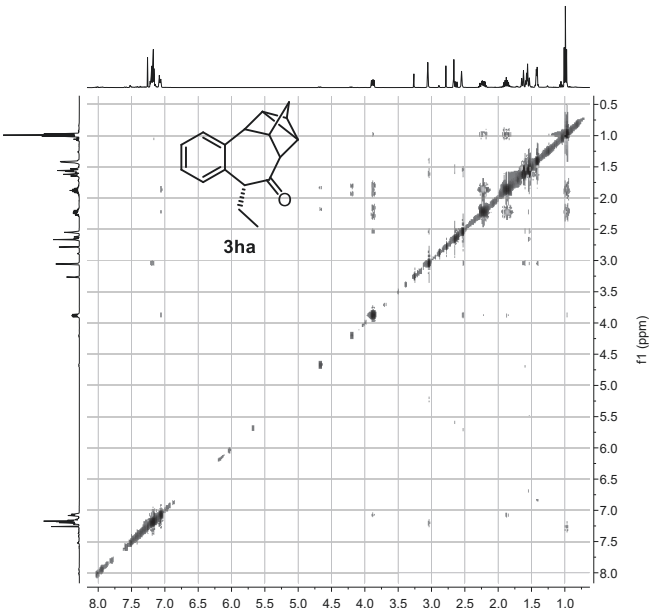

Figure S 109. $^{1}H,^{1}H$-NOESY of **3ha** in $CDCl_3$ measured at 400.16 MHz.

***rel*-(1*R*,2*R*,3a*S*,4*S*,9*R*,10a*R*,11*S*)-9-isopropyl-2,3,3a,4,9,10a-hexahydro-1,2,4-(epimethanetriyl)benzo[f]azulen-10(1H)-one**

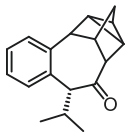

3ia

3ia was synthesized according to **GP-A** employing **1i** (160 mg, 1.00 mmol, 1.00 equiv.), NBD (305 µL, 3.00 mmol, 3.00 equiv.), $Ni(COD)_2$ (20 mol%) and (*R*)-(+)-(3,5-dioxa-4-phosphacyclohepta[2,1-a;3,4-a']dinaphthalen-4-yl)dimethylamine ((*R*)-MonoPhos, 40 mol%). Purification *via* flash chromatography (23 g SiO_2, gradient from 100:00 to 90:10 *n*-hexane/EA over 10 CV) afforded **3ia** (131 mg, 518 µmol, 52%, mixture of isomers) as a yellow solid.

d.r.: 96:4

$C_{18}H_{20}O$ (252.36 $\frac{g}{mol}$)

mp: 104.3 °C.

R$_f$: 0.67 (*n*-hexane/EA = 80:20) [anisaldehyde]

^{1}H NMR(400.16 MHz, $CDCl_3$): δ = 7.19 (m, 1H, H-10), 7.15 (m, 2H, H-11/12), 7.00 (m, 1H, H-13), 3.25 (d, ^3J = 11.1 Hz, 1H, H-15), 2.88 (s, 1H, H-7), 2.76 (m, 1H, H-2), 2.67 (dsep, ^3J = 11.1 Hz, ^3J = 6.5 Hz, 1H, H-16), 2.27 (s, 1H, H-8), 1.67 (m, 1H, H-3), 1.61 (dm, ^2J = 10.7 Hz, 1H, H-5a), 1.53 (m, 1H, H-6), 1.51 (dm, ^2J = 10.7 Hz, 1H, H-5b), 1.48 (m, 1H, H-4), 1.06 (d, ^3J = 6.5 Hz, 1H, H-18), 0.81 (d, ^3J = 6.5 Hz, 1H, H-17).

^{13}C NMR(100.62 MHz, $CDCl_3$): δ = 212.5 (C-1), 139.4 (C-9), 135.5 (C-14), 132.6 (C-13), 132.4 (C-10), 127.0 (C-11/12), 126.7 (C-12/11), 72.0 (C-15), 60.4 (C-2), 53.9 (C-7), 42.4 (C-8), 35.8 (C-5), 31.9 (C-16), 22.4 (C-18), 22.0 (C-17), 18.9 (C-6), 16.1 (C-3), 14.3 (C-4).

HRMS (ESI-TOF) m/z: $[M+H]^+$ Calcd for $C_{18}H_{20}OH$ 253.1587; Found 253.1589.

IR (ATR, ṽ): 1675 cm^{-1} (s, *CO*).

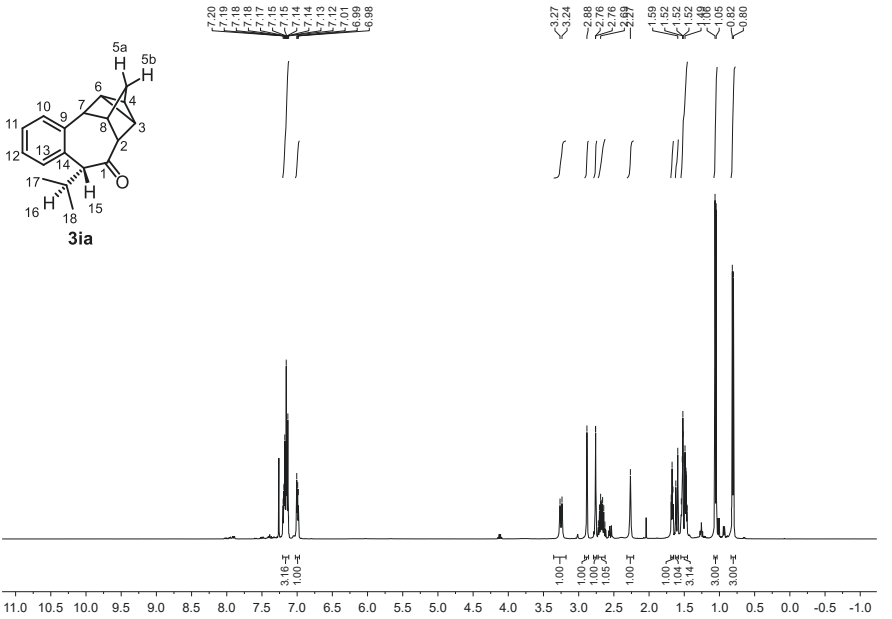

Figure S 110. ^{1}H NMR of **3ia** in $CDCl_3$ measured at 400.16 MHz.

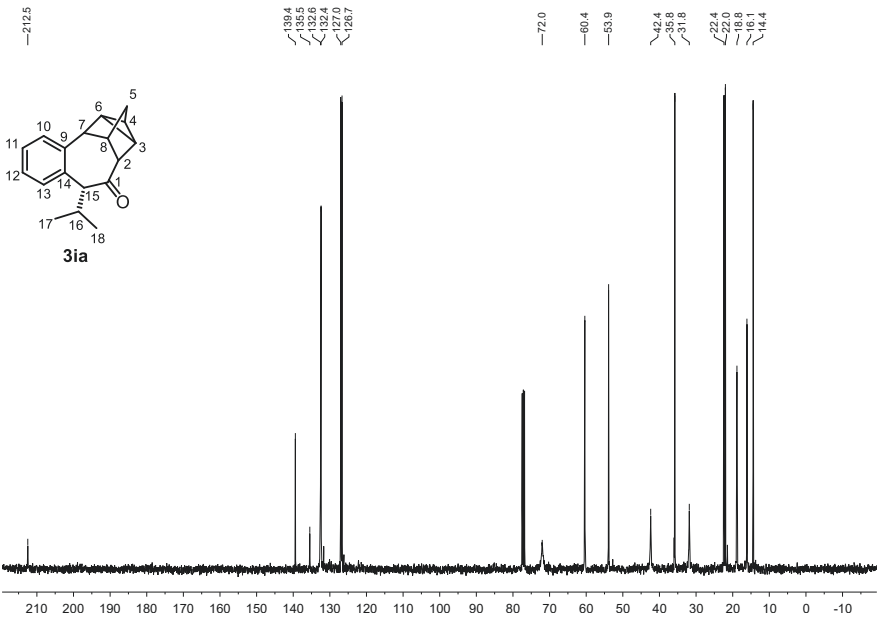

Figure S 111. ^{13}C NMR of **3ia** in $CDCl_3$ measured at 100.63 MHz.

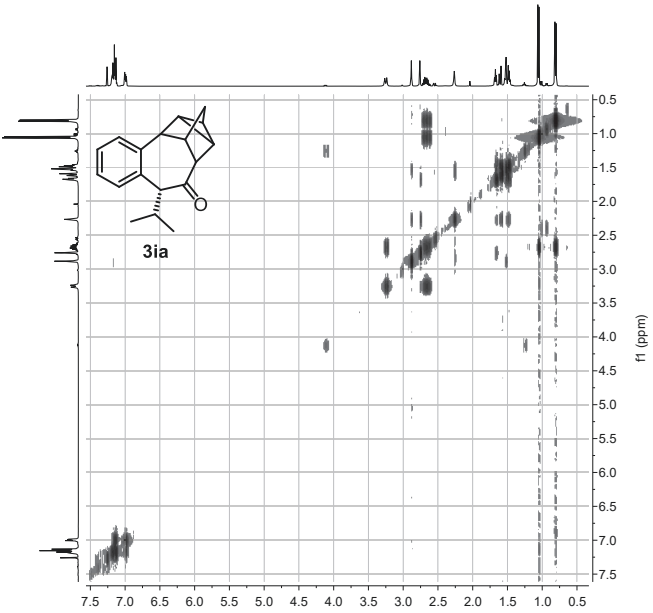

Figure S 112. $^{1}H,^{1}H$-COSY of **3ia** in $CDCl_3$ measured at 400.16 MHz.

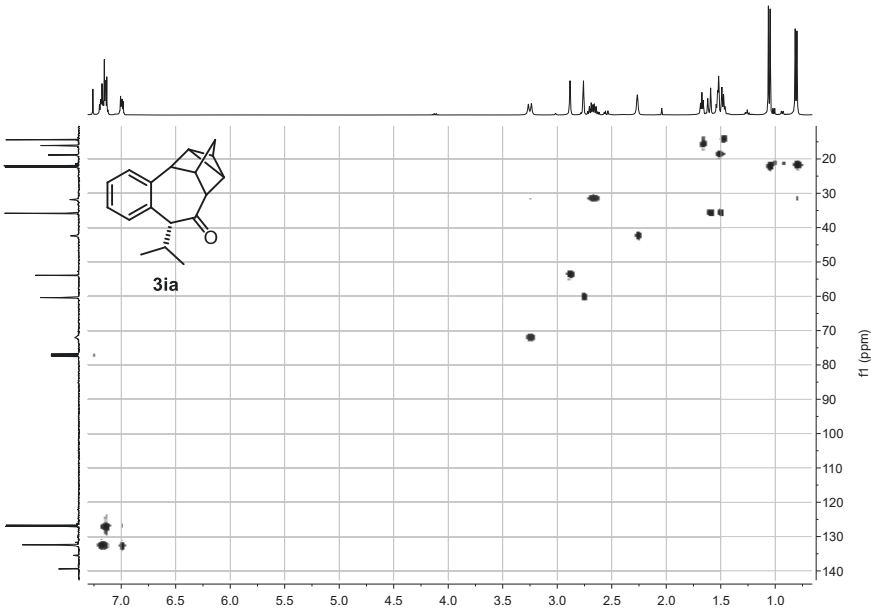

Figure S 113. $^{1}H,^{13}C$-HSQC of **3ia** in $CDCl_3$ measured at ^{1}H: 400.16 MHz; ^{13}C: 100.63 MHz.

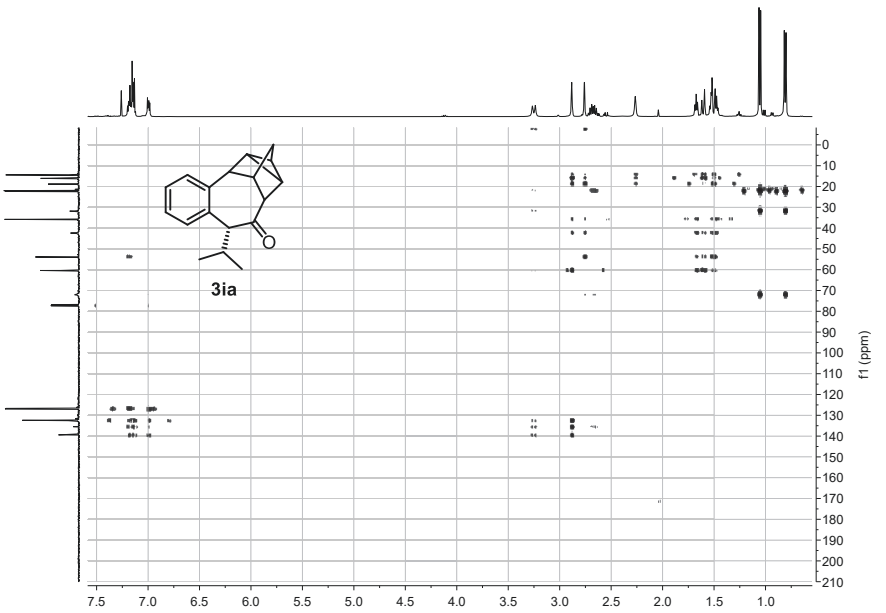

Figure S 114. $^{1}H,^{13}C$-HMBC of **3ia** in $CDCl_3$ measured at ^{1}H: 400.16 MHz; ^{13}C: 100.63 MHz.

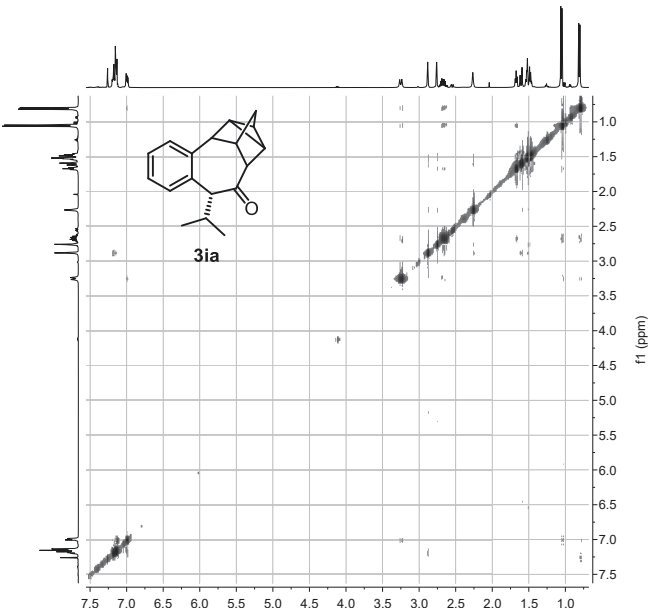

Figure S 115. $^{1}H,^{1}H$-NOESY of **3ia** in $CDCl_3$ measured at 400.16 MHz.

***rel*-(1*R*,2*R*,3a*S*,4*S*,9*R*,10a*R*,11*S*)-9-allyl-2,3,3a,4,9,10a-hexahydro-1,2,4-(epimethanetriyl)benzo[f]azulen-10(1H)-one**

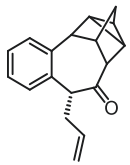

3ja

3ja was synthesized according to **GP-A** employing **1j** (158 mg, 1.00 mmol, 1.00 equiv.) and NBD (132 µL, 1.30 mmol, 1.30 equiv.) at 100 °C instead of 80 °C. Purification *via* flash chromatography (23 g SiO_2, gradient from 100:00 to 90:10 *n*-hexane/EA over 10 CV) afforded **3ja** (168 mg, 670 µmol, 67%, mixture of isomers) as a yellow oil.

d.r.: 93:7

$C_{18}H_{18}O$ (250.33 $\frac{g}{mol}$)

Rf: 0.80 (*n*-hexane/EA = 80:20) [anisaldehyde]

^{1}H NMR(400.16 MHz, $CDCl_3$): δ = 7.23 (m, 1H, H-10), 7.19 (m, 2H, H-11/12), 7.09 (m, 1H, H-13), 5.84 (dddd, ^3J = 17.1 Hz, ^3J = 10.2 Hz, ^3J = 6.7 Hz, ^3J = 6.7 Hz, 1H, H-17), 5.11 (dm, ^3J = 17.1 Hz, 1H, H-18b), 5.07 (dm, ^3J = 10.2 Hz, 1H, H-18a), 4.15 (dd, ^3J = 9.4 Hz, ^3J = 6.0 Hz, 1H, H-15), 3.11 (s, 1H, H-7), 2.95 (dddm, ^2J = 14.2 Hz, ^3J = 9.4 Hz, ^3J = 6.7 Hz, 1H, H-16b), 2.64 (m, 1H, H-2), 2.63 (m, 1H, H-8), 2.63 (ddm, ^2J = 14.2 Hz, ^3J = 6.0 Hz, 1H, H-16a), 1.64 (dm, ^2J = 10.6 Hz, 1H, H-5a), 1.59 (m, 1H, H-3), 1.56 (dm, ^2J = 10.6 Hz, 1H, H-5b), 1.43 (m, 1H, H-4), 1.41 (m, 1H, H-6); *diastereomer* δ = 7.25 – 7.16 (m, 3H, H-10, H-11, H-12), 7.15 (m, 1H, H-13), 5.84 (m, 1H, H-17), 5.15 (m, 1H, H-18b), 5.07 (m, 1H, H-18a), 4.89 (dd, ^3J = 10.0 Hz, ^3J = 5.0 Hz, 1H, H-15), 2.92 (m, 1H, H-16a/b), 2.90 (s, 1H, H-7), 2.67 (m, 1H, H-2), 2.56 (m, 1H, H-16b/a), 2.24 (m, 1H, H-8), 1.74 (m, 1H, H-3) 1.65 (dm, ^2J = 10.7 Hz, 1H, H-5a), 1.58 (m, 1H, H-4/6), 1.51 (dm, ^2J = 10.7 Hz, 1H, H-5b), 1.43 (m, 1H, H-6/4).

^{13}C NMR(100.62 MHz, $CDCl_3$): δ = 209.6 (C-1), 139.3 (C-9), 136.2 (C-17), 134.1 (C-14), 131.5 (C-10), 127.9 (C-13), 127.1 (C-11/12), 127.0 (C-12/11), 116.9 (C-18), 58.5 (C-2), 56.4 (C-15), 52.7 (C-7), 36.8 (C-8), 35.4 (C-5), 35.1 (C-16), 20.6 (C-6), 14.6 (C-3), 13.8 (C-4); *diastereomer* δ = 210.6 (C-1), 140.4 (C-9), 136.5 (C-17), 135.3 (C-14), 131.5 (C-10), 127.6

(C-11/12), 126.8 (C-12/11), 125.5 (C-13), 116.9 (C-18), 59.7 (C-2), 53.7 (C-2), 50.2 (C-15), 44.7 (C-8), 36.1 (C-5), 31.7 (C-16), 18.0 (C-3), 14.4 (C-4/6), 13.7 (C-6/4).

HRMS (ESI-TOF) m/z: $[M+H]^+$ Calcd for $C_{18}H_{18}OH$ 251.1430; Found 251.1433.

IR (ATR, $\tilde{\nu}$): 1705 cm^{-1} (s, *CO*).

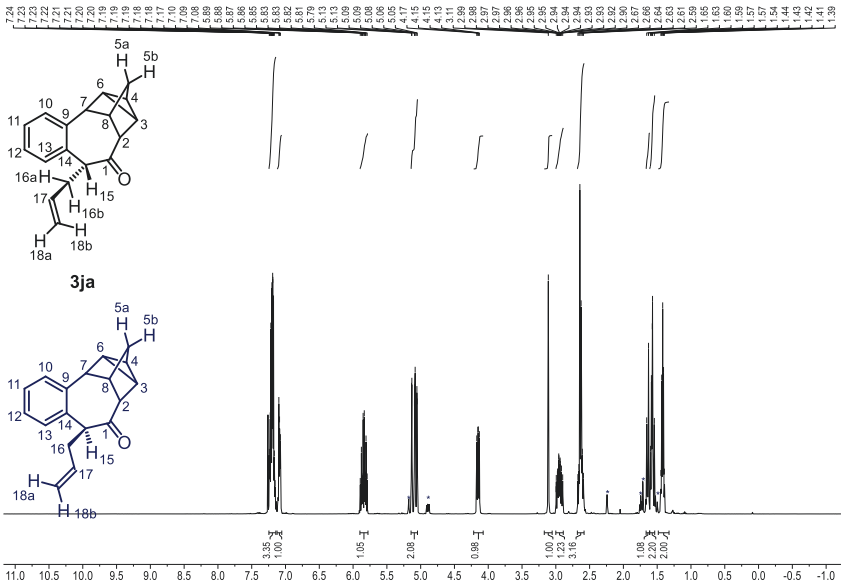

Figure S 116. ^{1}H NMR of **3ja** in $CDCl_3$ measured at 400.16 MHz. * Denotes signals corresponding to the diastereomer marked in blue.

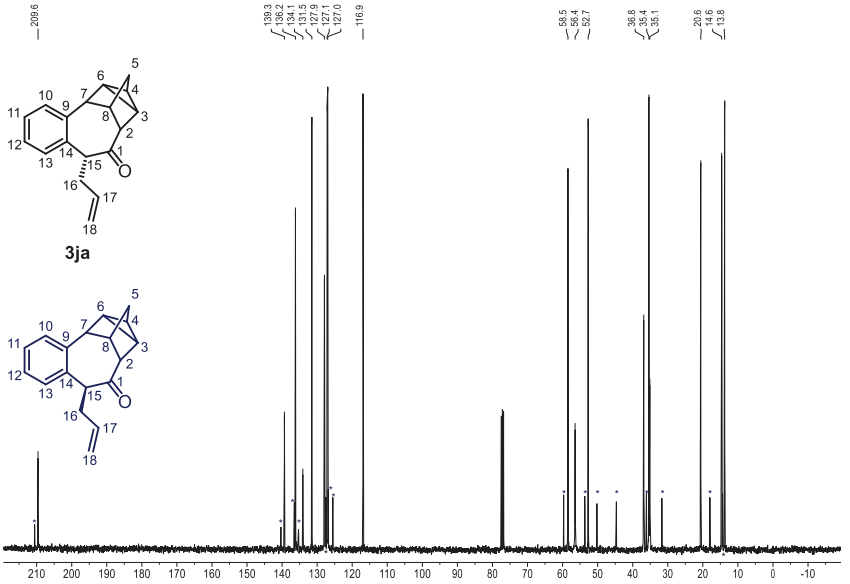

Figure S 117. ^{13}C NMR of **3ja** in $CDCl_3$ measured at 100.63 MHz. * Denotes signals corresponding to the diastereomer marked in blue.

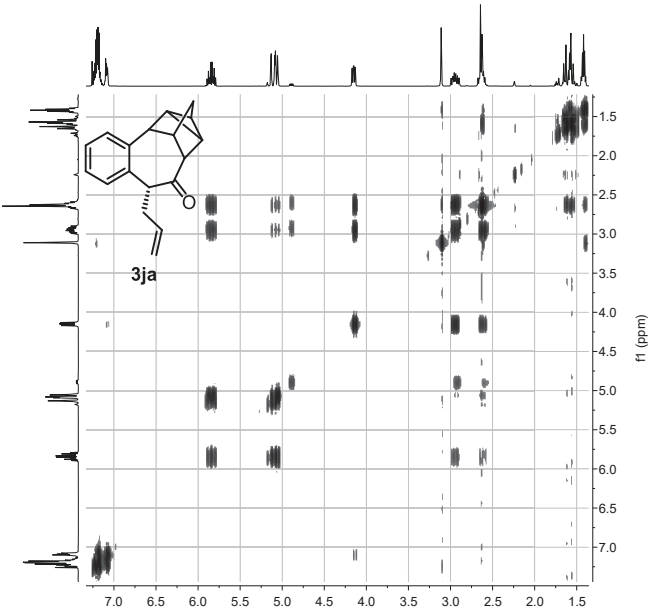

Figure S 118. ^{1}H,^{1}H-COSY of **3ja** and its respective diastereomer in $CDCl_3$ measured at 400.16 MHz.

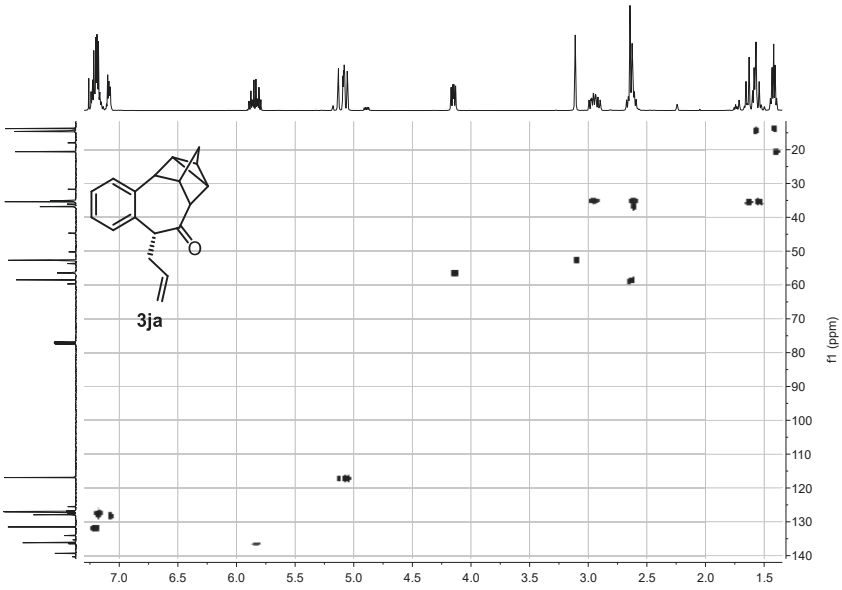

Figure S 119. ^{1}H,^{13}C-HSQC of **3ja** and its respective diastereomer in $CDCl_3$ measured at ^{1}H: 400.16 MHz; ^{13}C: 100.63 MHz.

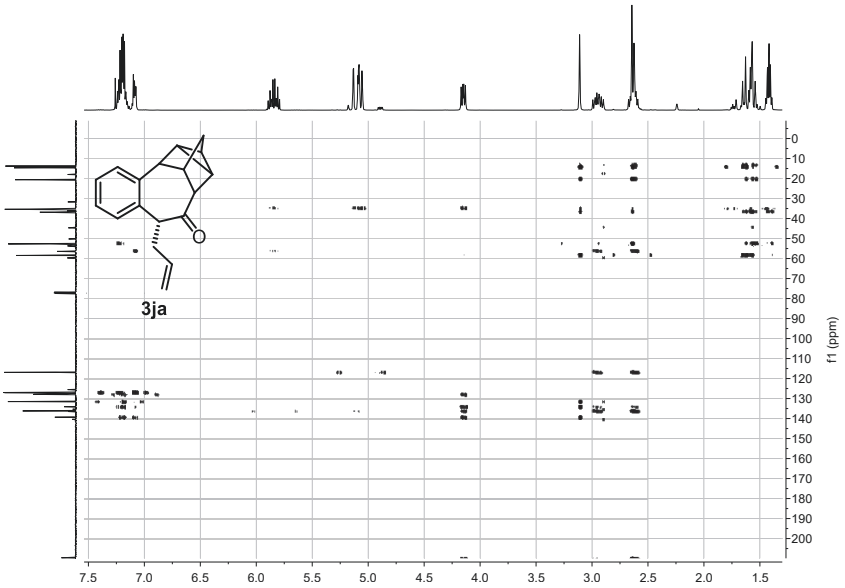

Figure S 120. $^{1}H,^{13}C$-HMBC of **3ja** and its respective diastereomer in $CDCl_3$ measured at ^{1}H: 400.16 MHz; ^{13}C: 100.63 MHz.

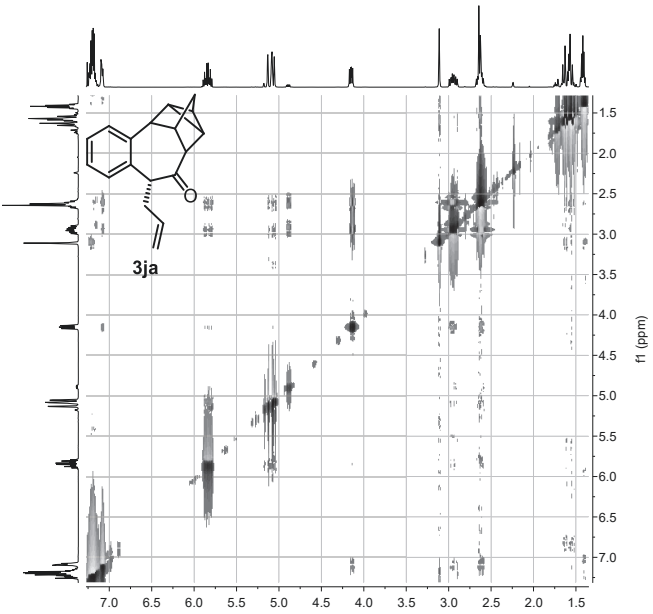

Figure S 121. $^{1}H,^{1}H$-NOESY of **3ja** and its respective diastereomer in $CDCl_3$ measured at 400.16 MHz.

***rel*-(1'*S*,2'*S*,3a'*R*,4'*R*,10a'*S*,11'*R*)-1',2',3',3a',4',10a'-hexahydro-10'H-spiro[cyclopropane-1,9'-[1,2,4](epimethanetriyl) benzo[f]azulen]-10'-one**

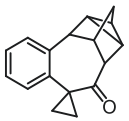

3ka

3ka was synthesized according to **GP-A** employing **1k** (144 mg, 1.00 mmol, 1.00 equiv.) and NBD (132 µL, 1.30 mmol, 1.30 equiv.). Purification *via* flash chromatography (23 g SiO_2, gradient from 100:00 to 90:10 *n*-hexane/EA over 10 CV) afforded **3ka** (127 mg, 537 µmol, 54%) as a pale yellow solid.

$C_{17}H_{16}O$ (236.31 $\frac{g}{mol}$)

mp: 86.1 °C.

Rf: 0.73 (*n*-hexane/EA = 80:20) [anisaldehyde]

^{1}H NMR(600.13 MHz, $CDCl_3$): δ = 7.22 (dd, ^3J = 7.4 Hz, ^4J = 0.7 Hz, 1H, H-10,), 7.03 (td, ^3J = 7.2 Hz, ^4J = 1.3 Hz, 1H, H-11), 7.15 (td, ^3J = 7.6 Hz, ^4J = 1.5 Hz, 1H, H-12), 7.10 (d, ^3J = 7.6 Hz, 1H, H-13), 3.09 (s, 1H, H-7), 2.70 (s, 1H, H-2), 2.60 (s, 1H, H-8), 1.65 (d, ^2J = 10.7 Hz, 1H, H-5a), 1.57 (m, 1H, H-3), 1.53 (d, ^2J = 10.7 Hz, 1H, H-5b), 1.50 (m, 1H, H-6), 1.41 (m, 1H, H-4), 1.37 (m, 1H, H-17b), 1.23 (m, 1H, H-17a), 1.21 (m, 2H, H-16).

^{13}C NMR(150.90 MHz, $CDCl_3$): δ = 209.0 (C-1), 141.6 (C-9), 134.5 (C-14), 131.5 (C-10), 127.4 (C-13), 127.2 (2C, C-11, C-12), 58.8 (C-2), 53.4 (C-7), 38.0 (C-8), 36.5 (C-15), 35.9 (C-5), 18.6 (C-6), 17.3 (C-3), 13.7 (C-17), 13.1 (C-4), 12.9 (C-16).

HRMS (ESI-TOF) m/z: $[M+Na]^+$ Calcd for $C_{17}H_{16}ONa$ 259.1093; Found 259.1098.

IR (ATR, ṽ): 1687 cm^{-1} (s, *CO*).

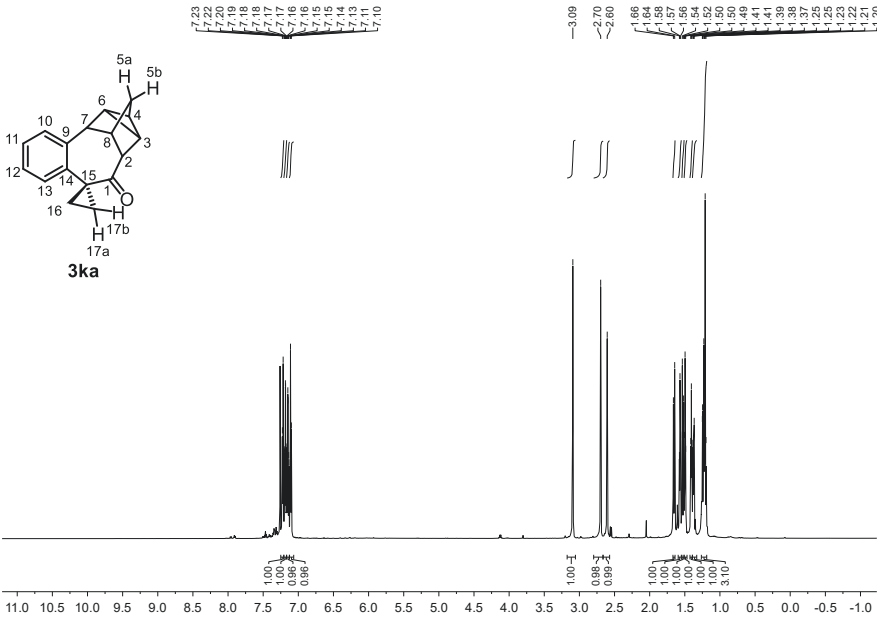

Figure S 122. ^{1}H NMR of **3ka** in $CDCl_3$ measured at 600.13 MHz.

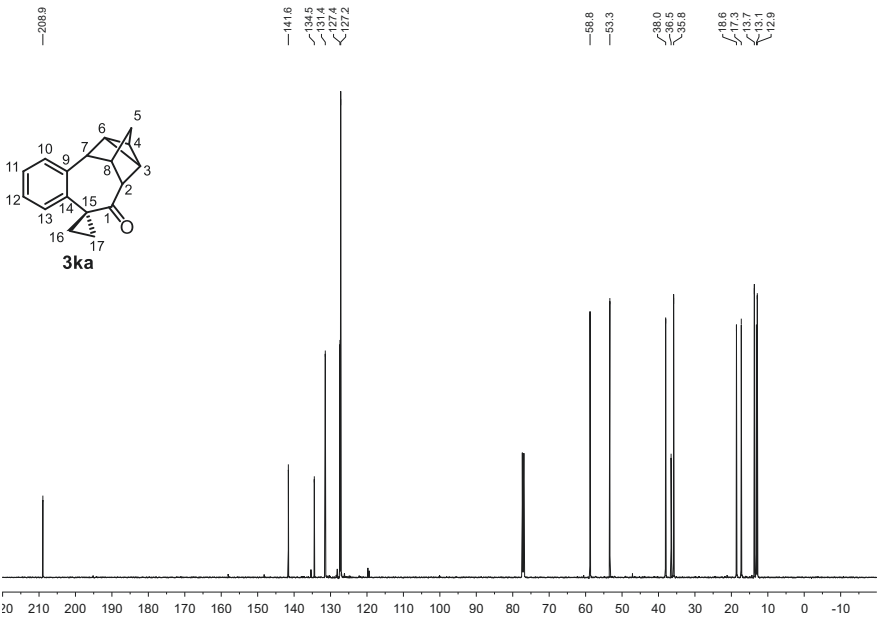

Figure S 123. ^{13}C NMR of **3ka** in $CDCl_3$ measured at 150.92 MHz.

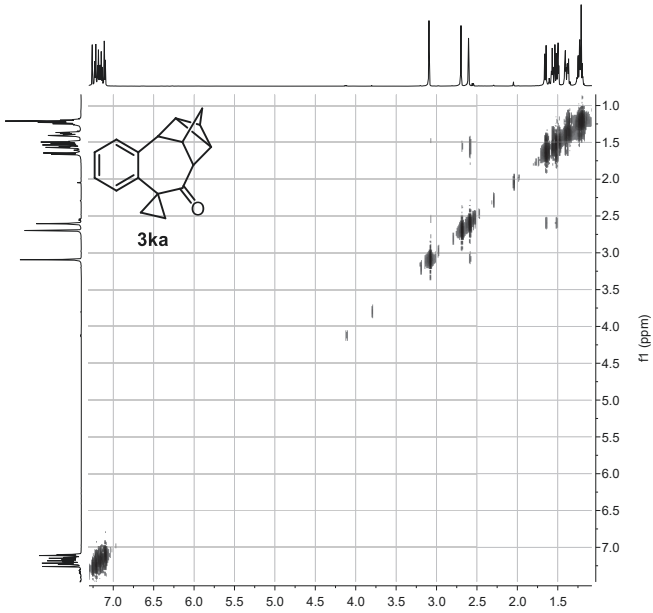

Figure S 124. ^{1}H,^{1}H-COSY of **3ka** in $CDCl_3$ measured at 600.13 MHz.

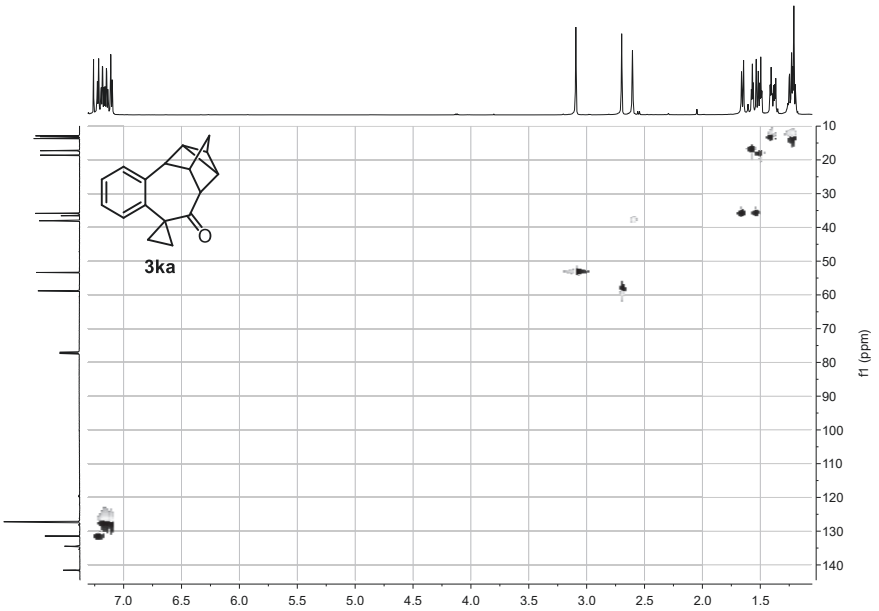

Figure S 125. ^{1}H,^{13}C-HSQC of **3ka** in $CDCl_3$ measured at ^{1}H: 600.13 MHz; ^{13}C: 150.92 MHz..

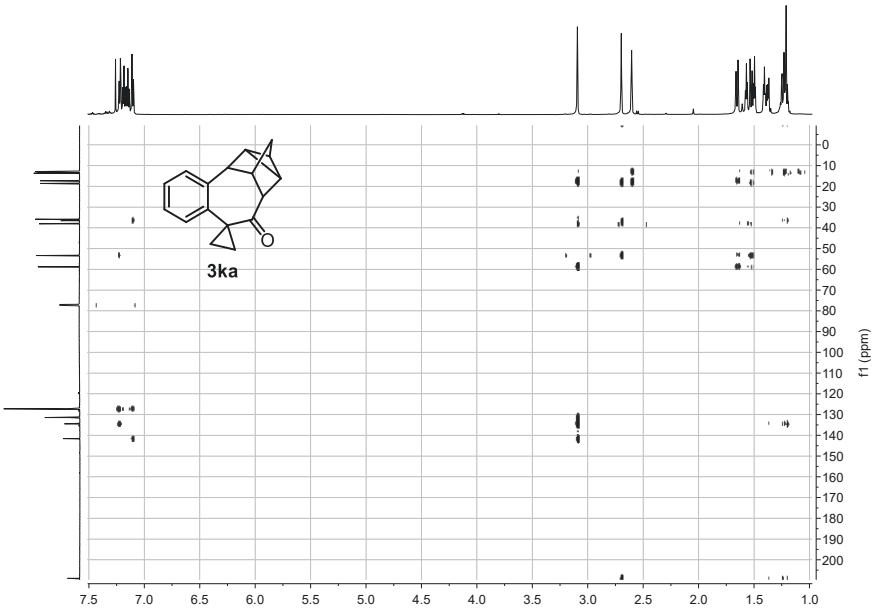

Figure S 126. $^{1}H,^{13}C$-HMBC of **3ka** in $CDCl_3$ measured at ^{1}H: 600.13 MHz; ^{13}C: 150.92 MHz.

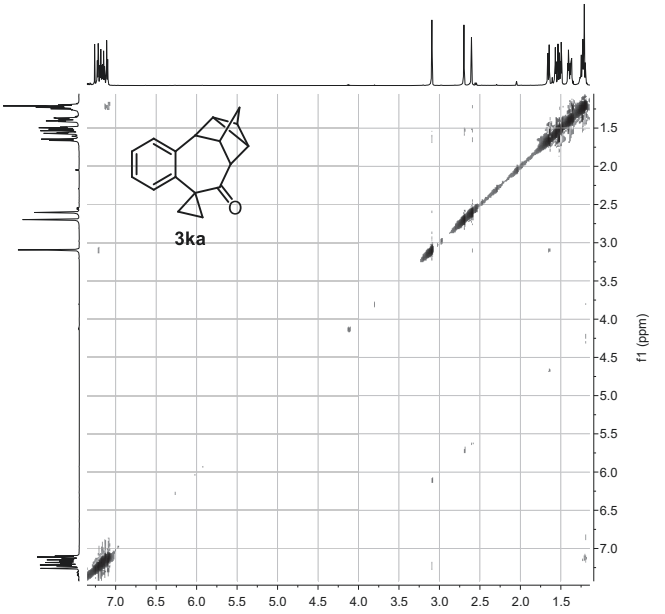

Figure S 127. $^{1}H,^{1}H$-NOESY of **3ka** in $CDCl_3$ measured at 600.13 MHz.

***rel*-(1*R*,2*R*,3a*S*,4*S*,9*R*,10a*R*,11*S*)-6-isobutyl-9-methyl-2,3,3a,4,9,10a-hexahydro-1,2,4-(epimethanetriyl)benzo[f]azulen-10(1H)-one**

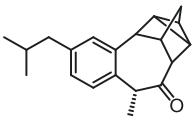

3la

3la was synthesized according to **GP-A** employing **1l** (188 mg, 1.00 mmol, 1.00 equiv.) and NBD (132 µL, 1.30 mmol, 1.30 equiv.). Purification *via* flash chromatography (23 g SiO_2, gradient from 100:00 to 85:15 *n*-hexane/EA over 15 CV) afforded **1la** (202 mg, 721 µmol, 72%, mixture of isomers) as a yellow oil.

d.r.: 88:12

$C_{20}H_{24}O$ (280.41 $\frac{g}{mol}$)

Rf: 0.79 (*n*-hexane/EA = 80:20) [anisaldehyde]

^{1}H NMR(400.16 MHz, $CDCl_3$): δ = 7.05 (m, 1H, H-13), 7.01 (m, 1H, H-10), 6.99 (m, 1H, H-12), 4.25 (q, ^3J = 6.9 Hz, 1H, H-15), 3.14 (s, 1H, H-7), 2.71 (m, 1H, H-8), 2.61 (m, 1H, H-2), 2.43 (m, 2H, H-17), 1.85 (sep, ^3J = 6.7 Hz, 1H, H-18), 1.65 (dm, ^2J = 10.5 Hz, 1H, H-5a), 1.55 (dm, ^2J = 10.5 Hz, 1H, H-5b), 1.52 (m, 1H, H-3), 1.47 (d, ^3J = 6.9 Hz, 3H, H-16), 1.39 (m, 1H, H-4), 1.36 (m, 1H, H-6), 0.92 (d, ^3J = 3.9 Hz, 3H, H-19/20), 0.90 (d, ^3J = 3.9 Hz, 3H, H-20/19); *diastereomer* δ = 7.11 (m, 1H, H-13), 7.00 (m, 1H, H-12), 6.95 (m, 1H, H-10), 4.81 (q, ^3J = 6.8 Hz, 1H, H-15), 2.87 (s, 1H, H-7), 2.69 (m, 1H, H-2), 2.43 (m, 2H, H-17), 2.22 (m, 1H, H-8), 1.83 (m, 1H, H-18), 1.74 (m, 1H, H-3), 1.65 (m, 1H, H-5a), 1.54 (m, 2H, H-4, H-6), 1.51 (m, 1H, H-5b), 1.42 (d, ^3J = 6.9 Hz, 3H, H-16), 0.92 (m, 3H, H-19/20), 0.90 (m, 3H, H-20/19).

^{13}C NMR(100.62 MHz, $CDCl_3$): δ = 210.7 (C-1), 140.1 (C-11), 138.9 (C-9), 131.9 (C-10), 131.7 (C-14), 127.9 (C-12), 126.3 (C-13), 57.5 (C-2), 52.5 (C-7), 48.0 (C-15), 44.8 (C-17), 34.2 (C-8), 35.2 (C-5), 30.2 (C-18), 22.5 (C-19/20), 22.4 (C-20/19), 21.2 (C-6), 14.8 (C-16), 14.4 (C-3), 13.3 (C-4) *diastereomer* δ = 211.9 (C-1), 140.0 (C-11), 139.8 (C-9), 133.2 (C-14), 132.4 (C-10), 128.1 (C-12), 124.9 (C-13), 59.7 (C-2), 53.8 (C-7), 44.1 (C-8), 43.8 (C-15), 43.4 (C-17), 36.2 (C-5), 29.1 (C-18), 22.5 (C-19/20), 22.4 (C-20/19), 18.1 (C-3), 14.0 (C-6), 13.7 (C-4), 13.0 (C-16).

HRMS (ESI-TOF) m/z: $[M+H]^+$ Calcd for $C_{20}H_{24}OH$ 281.1900; Found 281.1903.

IR (ATR, $\tilde{\nu}$): 1705 cm^{-1} (s, *CO*).

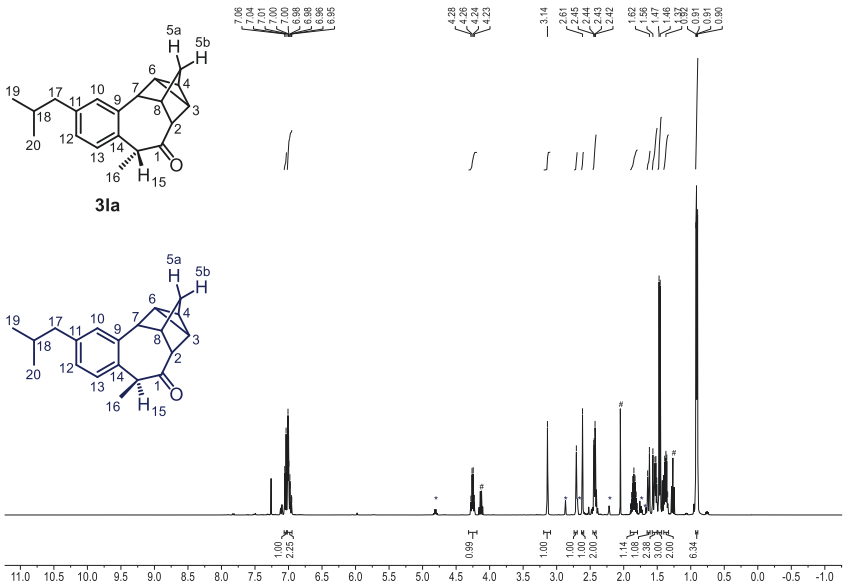

Figure S 128. ^{1}H NMR of **3la** in $CDCl_3$ measured at 400.16 MHz. * Denotes signals of the diastereomer. # Denotes residual EA.

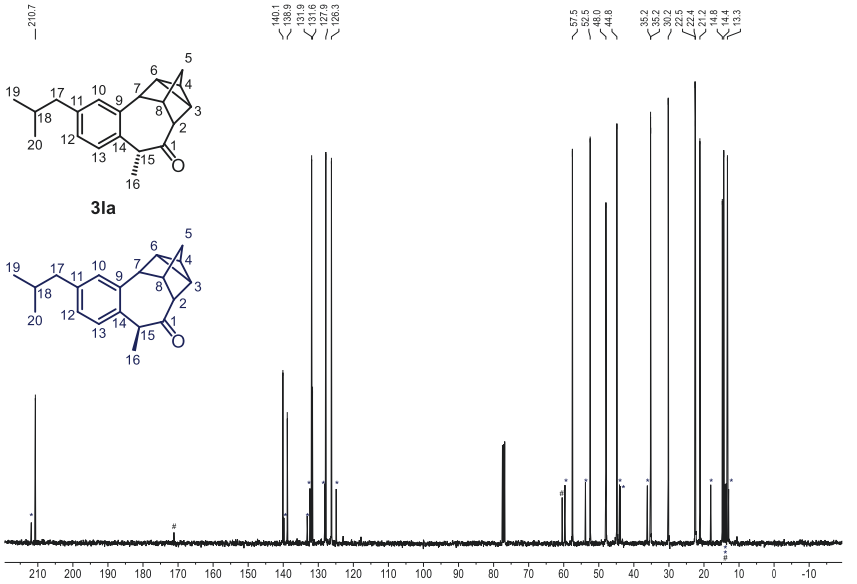

Figure S 129. ^{13}C NMR of **3la** in $CDCl_3$ measured at 100.63 MHz. * Denotes signals of the diastereomer. # Denotes residual EA.

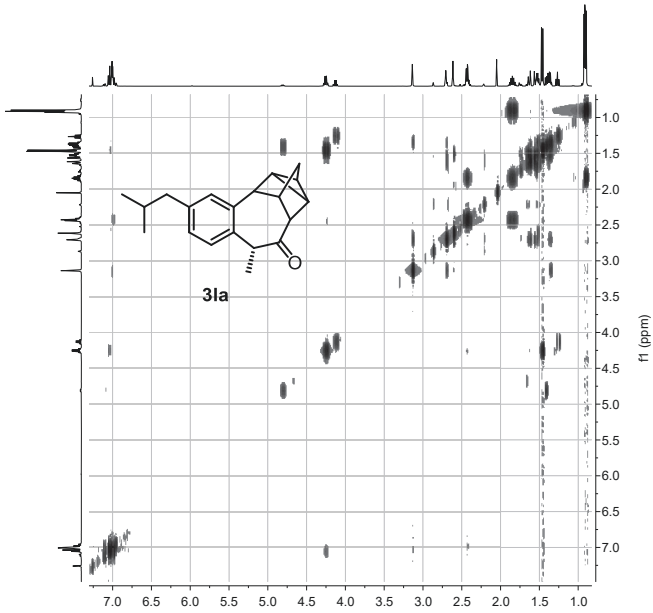

Figure S 130. ^{1}H,^{1}H-COSY of **3la** and its respective diastereomer in $CDCl_3$ measured at 400.16 MHz.

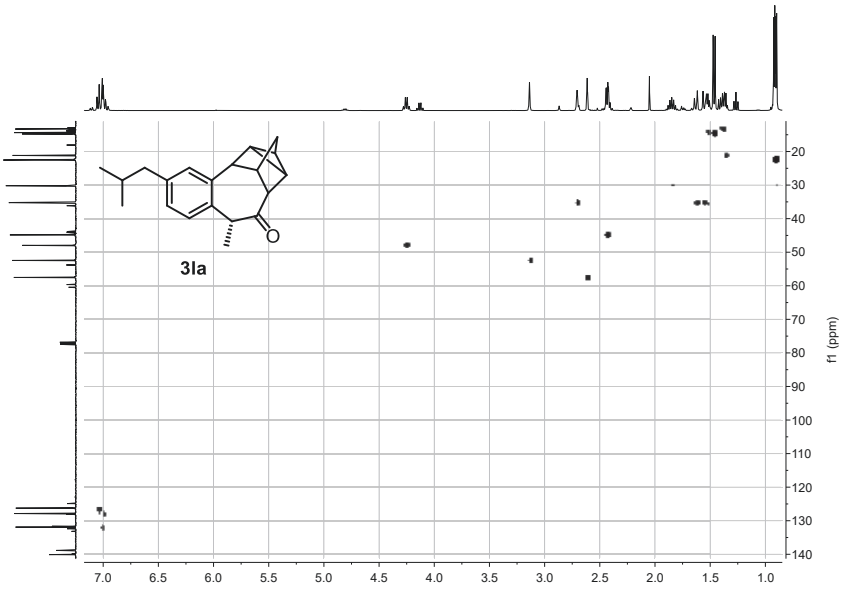

Figure S 131. ^{1}H,^{13}C-HSQC of **3la** and its respective diastereomer in $CDCl_3$ measured at ^{1}H: 400.16 MHz; ^{13}C: 100.63 MHz.

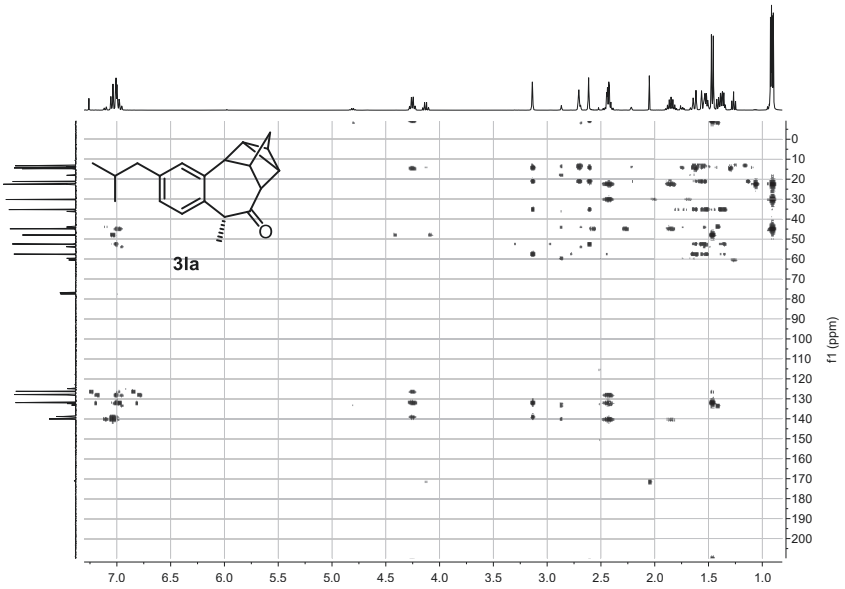

Figure S 132. $^{1}H,^{13}C$-HMBC of **3la** and its respective diastereomer in $CDCl_3$ measured at ^{1}H: 400.16 MHz; ^{13}C: 100.63 MHz.

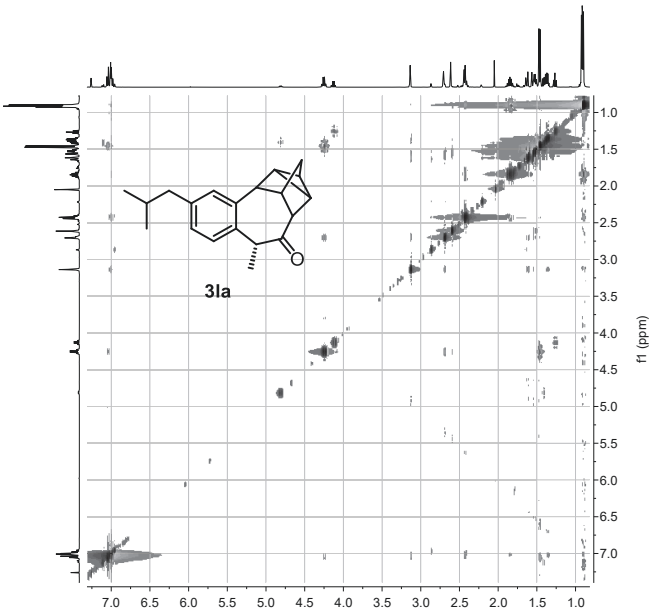

Figure S 133. $^{1}H,^{1}H$-NOESY of **3la** and its respective diastereomer in $CDCl_3$ measured at 400.16 MHz.

***rel*-(1*S*,2*R*,3*S*,3a*S*,4*R*,10a*S*,11*S*)-3-(*tert*-butoxy)-2,3,3a,4,9,10a-hexahydro-1,2,4-(epimethanetriyl)benzo[f]azulen-10(1H)-one**

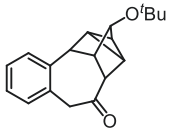

3ab

3ab was synthesized according to **GP-A** employing **1a** (118 mg, 1.00 mmol, 1.00 equiv.) and **2b** (214 mg, 1.30 mmol, 1.30 equiv.). Purification *via* flash chromatography (23 g SiO_2, gradient from 90:10 to 60:40 *n*-hexane/EA over 20 CV) afforded **3ab** (218 mg, 773 µmol, 77%) as a colorless solid.

d.r.: 87:13

$C_{19}H_{22}O_2$ (282.38 $\frac{g}{mol}$)

mp: 111.9 °C.

R$_f$: 0.53 (*n*-hexane/EA = 80:20) [anisaldehyde]

^{1}H NMR(400.16 MHz, $CDCl_3$): δ = 7.16 (m, 1H, H-12), 7.15 (m, 1H, H-11), 7.15 (m, 1H, H-10), 7.08 (m, 1H, H-13), 4.53 (dd, ^2J = 12.3 Hz, ^4J = 0.7 Hz, 1H, H-15b), 3.94 (m, 1H, H-5), 3.38 (dd, ^2J = 12.3 Hz, ^4J = 1.0 Hz, 1H, H-15a), 3.29 (s, 1H, H-2), 2.95 (s, 1H, H-7), 2.20 (s, 1H, H-8), 1.89 (m, 1H, H-3), 1.64 (m, 1H, H-6), 1.43 (m, 1H, H-4), 1.21 (s, 9H, H-17).

^{13}C NMR(100.62 MHz, $CDCl_3$): δ = 210.0 (C-1), 139.2 (C-9), 132.2 (C-14), 131.2 (C-10), 130.5 (C-13), 127.7 (C-12), 127.1 (C-11), 77.7 (C-5), 74.0 (16), 55.6 (C-2), 49.6 (C-15), 49.5 (C-7), 47.9 (C-8), 28.6 (C-17), 18.8 (C-4), 18.6 (C-3), 17.9 (C-6).

HRMS (ESI-TOF) m/z: $[M+H]^+$ Calcd for $C_{19}H_{22}O_2H$ 283.1693; Found 283.1693.

IR (ATR, ṽ): 1687 cm^{-1} (s, *CO*).

Diastereomer (anti):

$C_{19}H_{22}O_2$ (282.38 $\frac{g}{mol}$)

mp: 88.2 °C.

R$_f$: 0.55 (*n*-hexane/EA = 80:20) [anisaldehyde]

^{1}H NMR(700.21 MHz, CD_2Cl_2): δ = 7.30 (dm, ^{3}J = 7.0 Hz, 1H, H-10), 7.17 (m, 1H, H-11), 7.15 (m, 1H, H-12), 7.06 (d, ^{3}J = 6.9 Hz, 1H, H-13), 4.43 (d, ^{2}J = 12.2 Hz, 1H, H-15b), 3.80 (m, 1H, H-5), 3.63 (s, 1H, H-7), 3.33 (d, ^{2}J = 12.4 Hz, 1H, H-15a), 2.65 (s, 1H, H-2), 2.16 (s, 1H, H-8), 1.78 (m, 1H, H-3), 1.60 (m, 1H, H-6), 1.38 (m, 1H, H-4), 1.22 (s, 9H, H-17).

^{13}C NMR(176.08 MHz, CD_2Cl_2): δ = 208.2 (C-1), 140.0 (C-9), 132.3 (C-10), 132.3 (C-14), 130.4 (C-13), 127.7 (C-12), 127.3 (C-11), 78.0 (C-5), 74.2 (C-16), 56.1 (C-2), 49.3 (C-15), 48.4 (C-7), 47.7 (C-8), 28.6 (C-17), 19.7 (C-2), 18.6 (C-4), 16.4 (C-6).

HRMS (ESI-TOF) m/z: $[M+H]^+$ Calcd for $C_{19}H_{22}O_2H$ 283.1693; Found 283.1692.

IR (ATR, ṽ): 1694 cm^{-1} (s, *CO*).

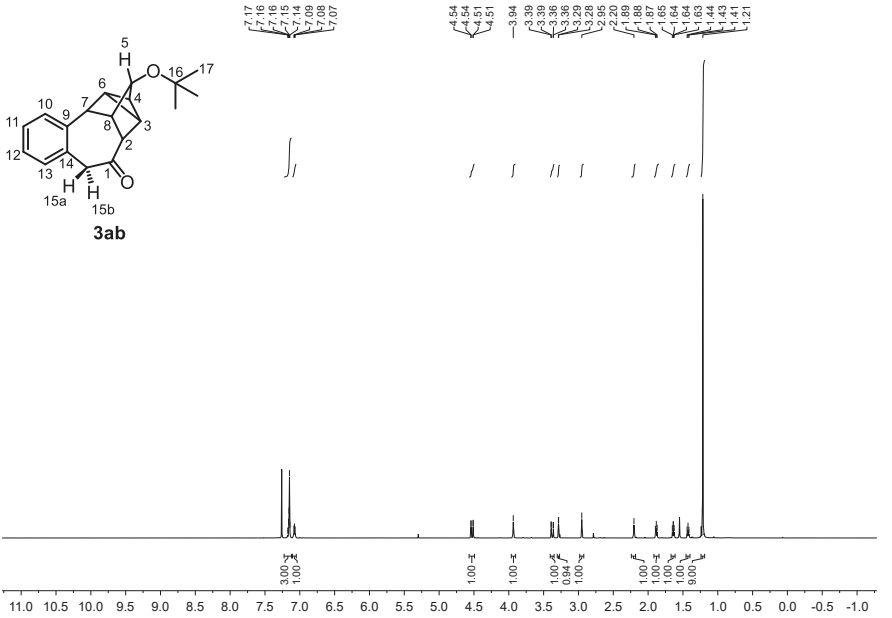

Figure S 134. ^{1}H NMR of **3ab** in $CDCl_3$ measured at 400.16 MHz.

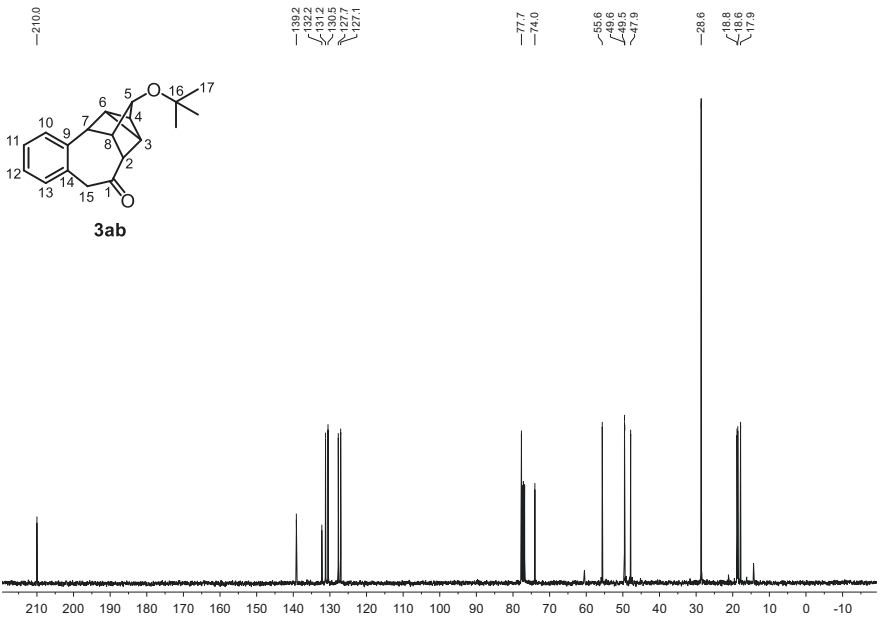

Figure S 135. ^{13}C NMR of **3ab** in $CDCl_3$ measured at 100.63 MHz.

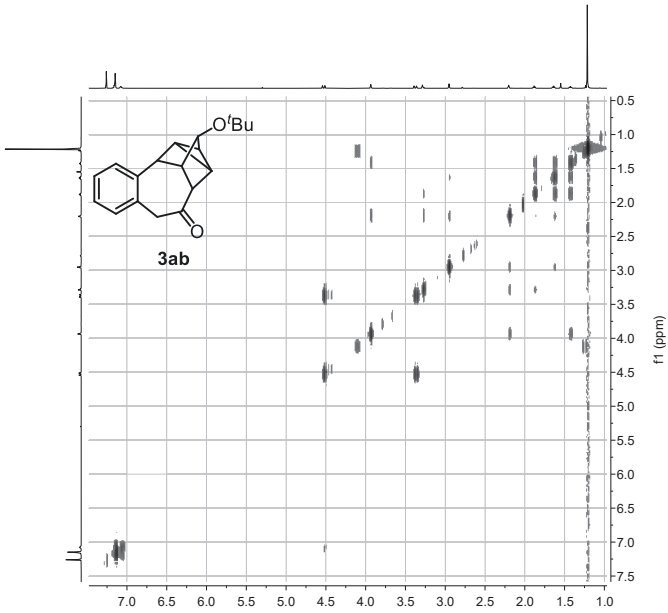

Figure S 136. ^{1}H,^{1}H-COSY of **3ab** in $CDCl_3$ measured at 400.16 MHz.

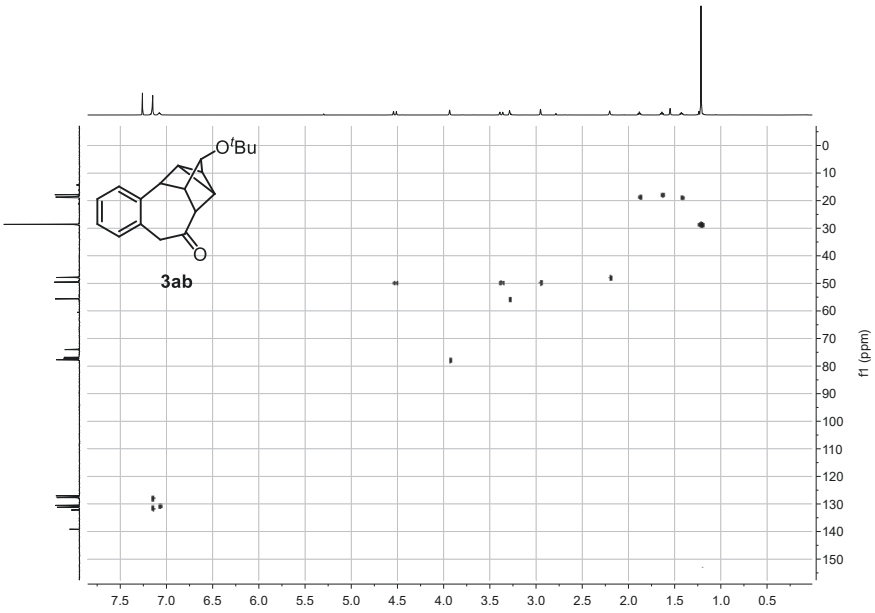

Figure S 137. ^{1}H,^{13}C-HSQC of **3ab** in $CDCl_3$ measured at ^{1}H: 400.16 MHz; ^{13}C: 100.63 MHz.

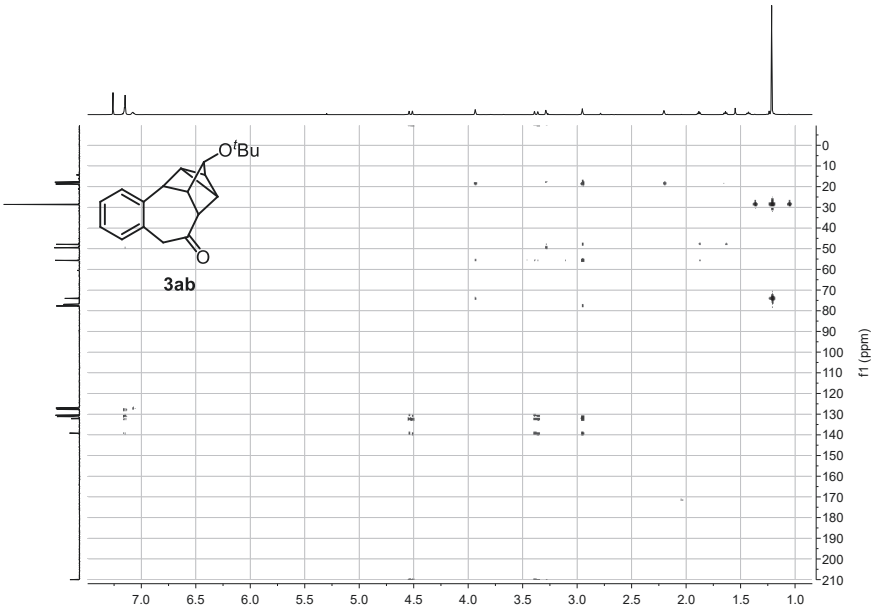

Figure S 138. $^{1}H,^{13}C$-HMBC of **3ab** in $CDCl_3$ measured at ^{1}H: 400.16 MHz; ^{13}C: 100.63 MHz.

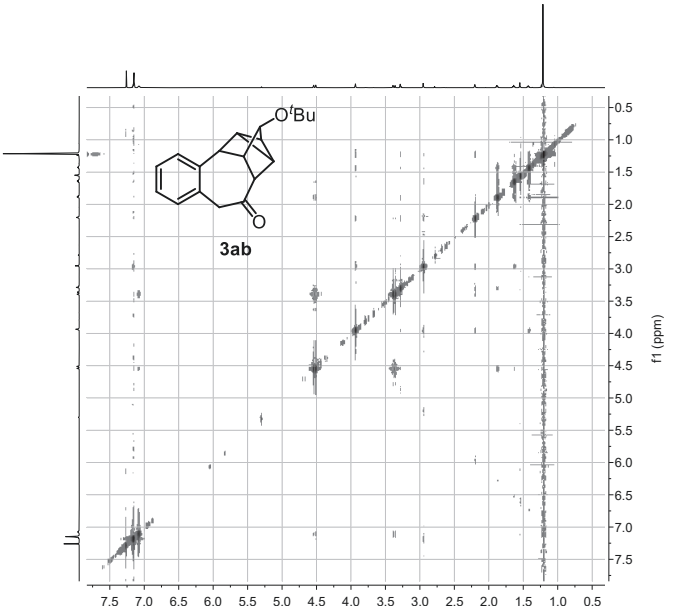

Figure S 139. $^{1}H,^{1}H$-NOESY of **3ab** in $CDCl_3$ measured at 400.16 MHz.

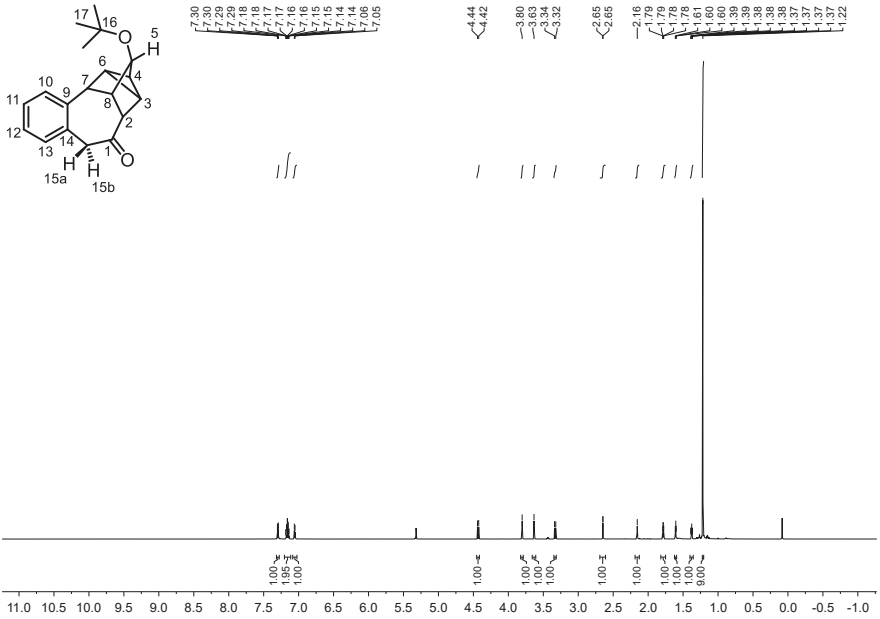

Figure S 140. ^{1}H NMR of the diastereomer of **3ab** in CD_2Cl_2 measured at 700.26 MHz.

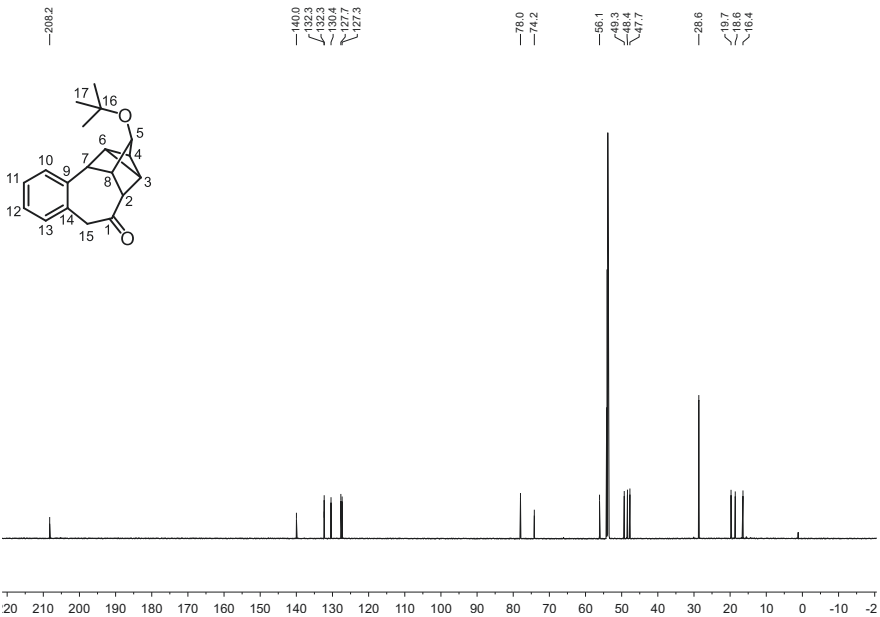

Figure S 141. ^{13}C NMR of the diastereomer of **3ab** in CD_2Cl_2 measured at 176.08 MHz.

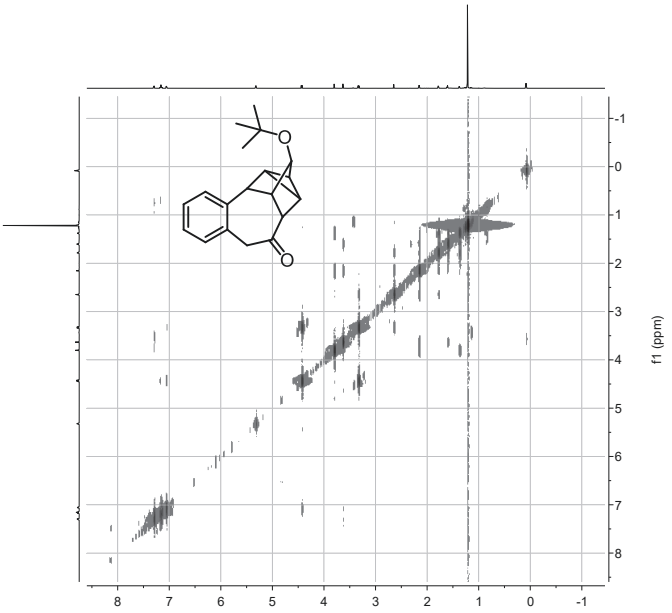

Figure S 142. $^{1}H,^{1}H$-COSY of the diastereomer of **3ab** in CD_2Cl_2 measured at 700.26 MHz.

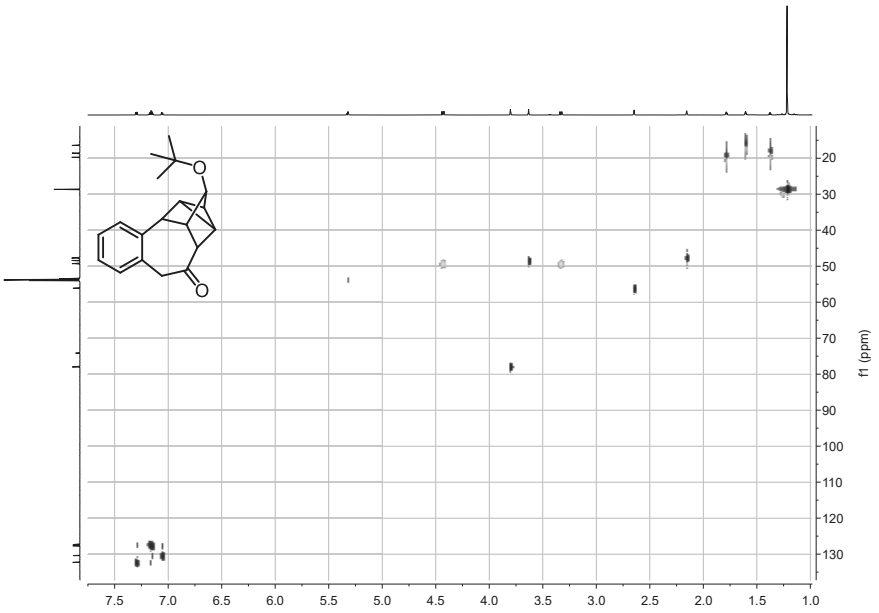

Figure S 143. $^{1}H,^{13}C$-HSQC of the diastereomer of **3ab** in CD_2Cl_2 measured at ^{1}H: 700.26 MHz; ^{13}C: 176.08 MHz.

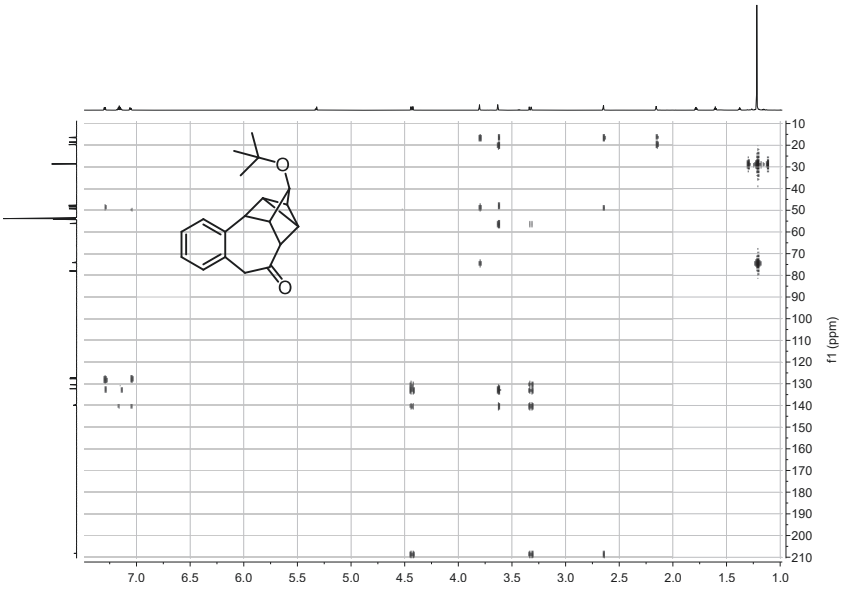

Figure S 144. $^{1}H,^{13}C$-HMBC of the diastereomer of **3ab** in CD_2Cl_2 measured at ^{1}H: 700.26 MHz; ^{13}C: 176.08 MHz.

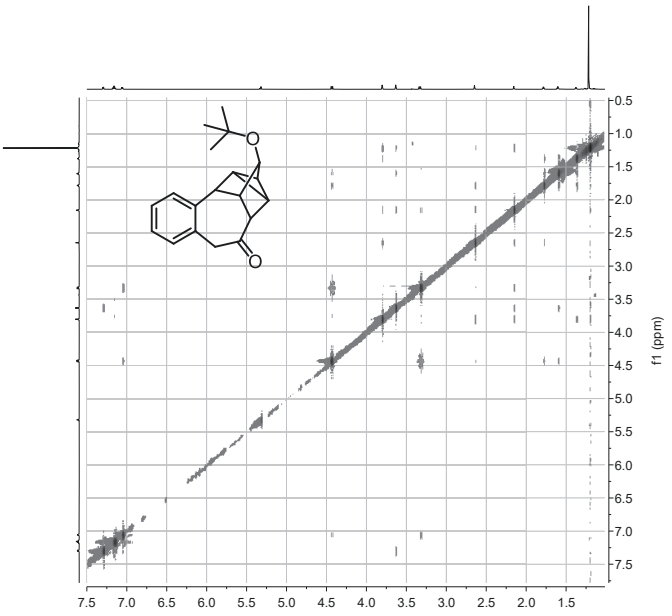

Figure S 145. $^{1}H,^{1}H$-NOESY of the diastereomer of **3ab** in CD_2Cl_2 measured at 700.26 MHz.

***rel*-(1*S*,2*R*,3*S*,3a*S*,4*R*,10a*S*,11*S*)-3-isopropyl-2,3,3a,4,9,10a-hexahydro-1,2,4-(epimethanetriyl)benzo[f]azulen-10(1H)-one**

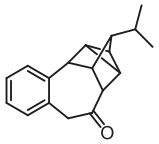

3ac

3ac was synthesized according to **GP-A** employing **1a** (118 mg, 1.00 mmol, 1.00 equiv.) and **2c** (175 mg, 1.30 mmol, 1.30 equiv.) at 50 °C instead of 80 °C. Purification *via* flash chromatography (23 g SiO_2, gradient from 98:02 to 80:20 *n*-hexane/EA over 20 CV) afforded **3ac** 205 mg, 812 µmol, 81%, mixture of isomers) as a pale yellow solid.

d.r.: 60:40

$C_{18}H_{20}O$ (252.36 $\frac{g}{mol}$)

mp: 64.1 °C.

R_f: 0.66 (*n*-hexane/EA = 80:20) [anisaldehyde]

^{1}H NMR(400.16 MHz, $CDCl_3$): *syn* δ = 7.15 (m, 3H, H-10 – 12), 7.07 (m, 1H, H-13), 4.58 (d, ^2J = 12.2 Hz, 1H, H-15b), 3.32 (dd, ^2J = 12.3 Hz, ^4J = 0.9 Hz, 1H, H-15a), 2.85 (s, 1H, H-7), 2.80 (m, 1H, H-2), 2.21 (m, 1H, H-8), 1.70 (m, 1H, H-6), 1.56 (m, 1H, H-4), 1.49 (m, 1H, H-3), 1.48 (m, 1H, H-5), 1.33 (m, 1H, H-16), 0.98 (d, ^3J = 6.5 Hz, 3H, H-18), 0.85 (d, ^3J = 6.5 Hz, 3H, H-17); *anti* δ = 7.20 (m, 1H, H-10), 7.15 (m, 2H, H-11/12), 7.07 (m, 1H, H-13), 4.44 (d, ^2J = 12.2 Hz, 1H, H-15b), 3.40 (d, ^2J = 12.2 Hz, 1H, H-15a), 3.15 (s, 1H, H-7), 2.61 (m, 1H, H-2), 2.26 (m, 1H, H-8), 1.74 (m, 1H, H-6), 1.63 (m, 1H, H-16), 1.47 (m, 1H, H-4), 1.46 (m, 1H, H-3), 1.32 (m, 1H, H-5), 1.01 (d, ^3J = 6.6 Hz, 3H, H-18), 0.89 (d, ^3J = 6.6 Hz, 3H, H-17).

^{13}C NMR(100.62 MHz, $CDCl_3$): *syn* δ = 210.1 (C-1), 140.0 (C-9), 132.1 (C-14), 131.4 (C-10), 130.2 (C-13), 127.6 (C-12), 127.0 (C-11), 56.8 (C-5), 55.6 (C-2), 54.1 (C-7), 49.1 (C-15), 44.7 (C-8), 26.9 (C-16), 21.5 (C-18), 21.0 (C-17), 17.9 (C-6), 17.1 (C-3), 16.7 (C-4); *anti* δ = 209.3 (C-1), 139.7 (C-9), 131.9 (C-10), 131.7 (C-14), 130.4 (C-13), 127.6 (C-12), 127.1 (C-11), 60.2 (C-2), 56.7 (C-5), 49.2 (C-15), 48.4 (C-7), 44.3 (C-8), 27.1 (C-16), 21.8 (C-18), 21.1 (C-17), 19.6 (C-6), 16.4 (C-3), 15.5 (C-4).

HRMS (ESI-TOF) m/z: $[M+H]^+$ Calcd for $C_{18}H_{20}OH$ 253.1587; Found 253.1588.

IR (ATR, $\tilde{\nu}$): 1690 cm^{-1} (s, *CO*).

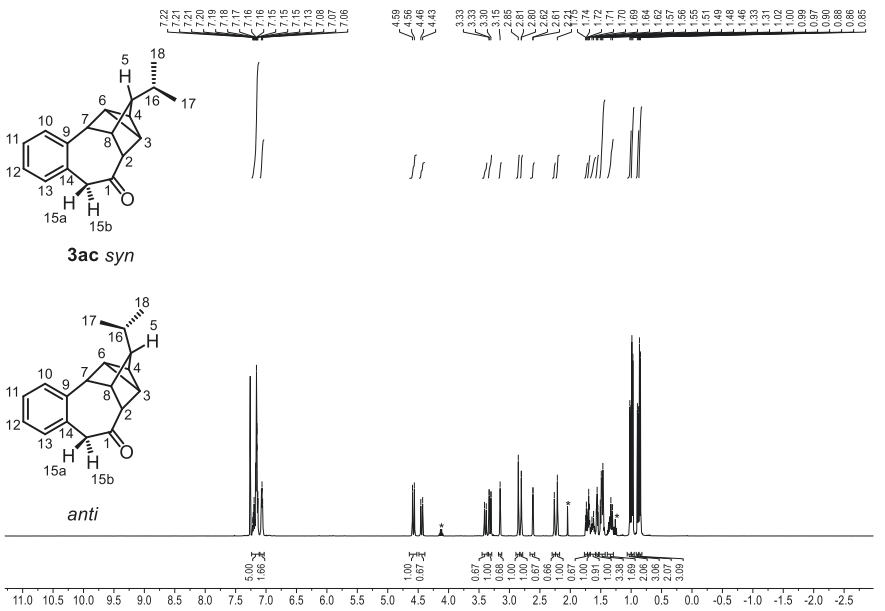

Figure S 146. ^{1}H NMR of **3ac** in $CDCl_3$ measured at 400.16 MHz. * denotes residual EA.

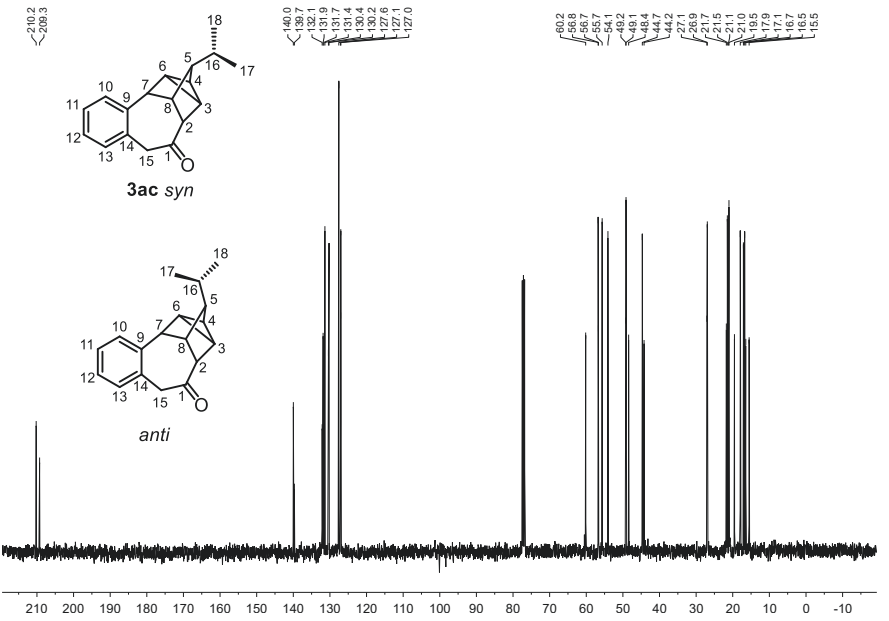

Figure S 147. ^{13}C NMR of **3ac** in $CDCl_3$ measured at 100.63 MHz.

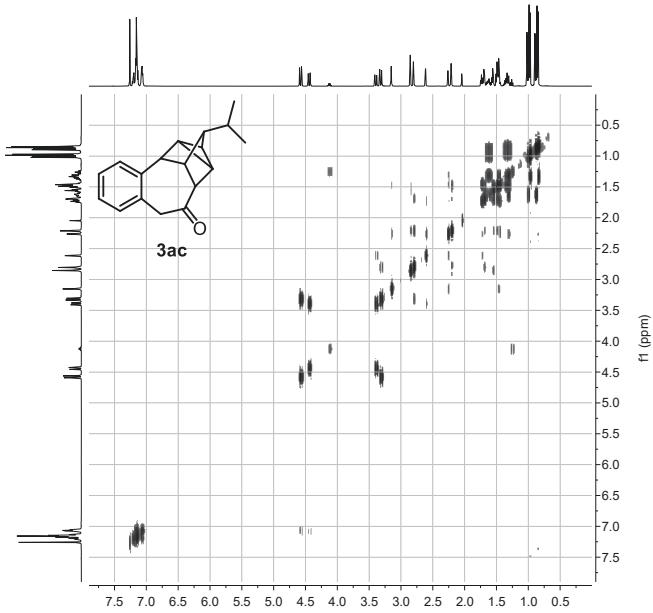

Figure S 148. $^{1}H,^{1}H$-COSY of **3ac** in $CDCl_3$ measured at 400.16 MHz.

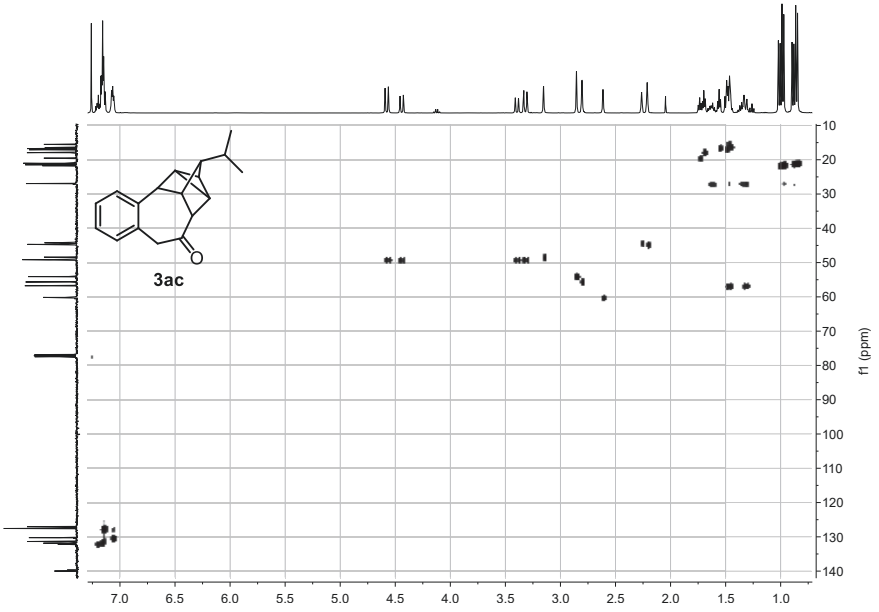

Figure S 149. $^{1}H,^{13}C$-HSQC of **3ac** in $CDCl_3$ measured at ^{1}H: 400.16 MHz; ^{13}C: 100.63 MHz.

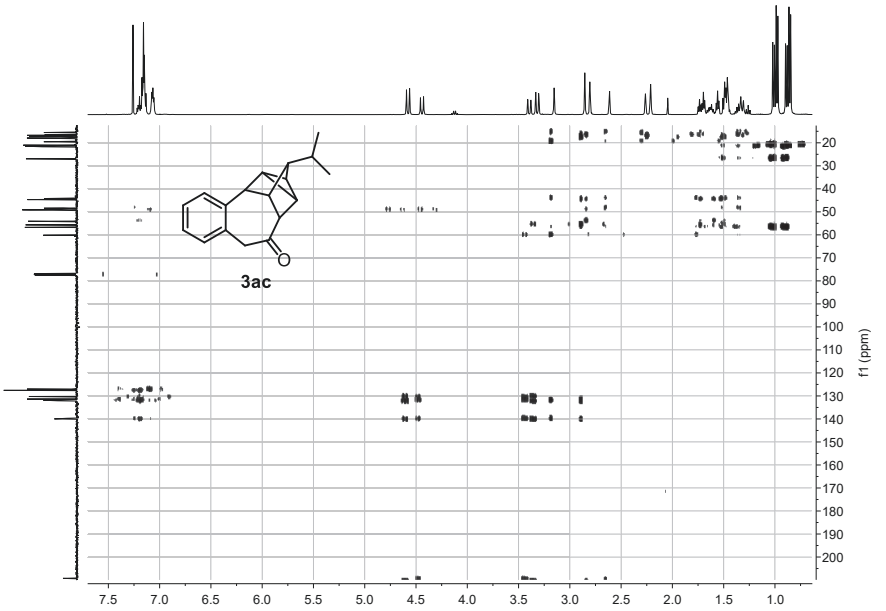

Figure S 150. $^{1}H,^{13}C$-HMBC of **3ac** in $CDCl_3$ measured at ^{1}H: 400.16 MHz; ^{13}C: 100.63 MHz.

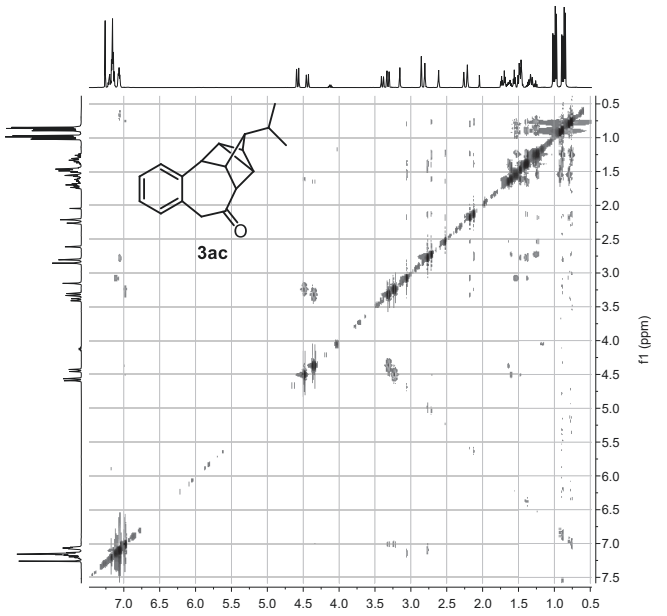

Figure S 151. $^{1}H,^{1}H$-NOESY of **3ac** in $CDCl_3$ measured at 400.16 MHz.

***rel*-(1*R*,2*R*,3*R*,3a*S*,10a*S*,11*S*)-3-phenyl-2,3,3a,4,9,10a-hexahydro-1,2,4-(epimethanetriyl) benzo[f]azulen-10(1H)-one**

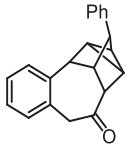

3ad

3ad was synthesized according to **GP-A** employing **1a** (118 mg, 1.00 mmol, 1.00 equiv.) and **2d** (219 mg, 1.30 mmol, 1.30 equiv.). Purification *via* flash chromatography (23 g SiO_2, gradient from 98:02 to 80:20 *n*-hexane/EA over 15 CV) afforded **3ad** (249 mg, 870 µmol, 87%) as a colorless solid.

$C_{21}H_{18}O$ (286.37 $\frac{g}{mol}$)

mp: 156.5 °C.

R_f: 0.64 (*n*-hexane/EA = 80:20) [anisaldehyde]

^{1}H NMR(400.16 MHz, $CDCl_3$): δ = 7.38 (m, 1H, H-19), 7.36 (m, 1H, H-17), 7.34 (m, 1H, H-10), 7.30 (m, 1H, H-18), 7.26 (m, 1H, H-11), 7.13 (m, 1H, H-12), 7.07 (m, 2H, H-13, H-20), 6.94 (m, 1H, H-21), 4.50 (d, ^2J = 12.2 Hz, 1H, H-15b), 3.44 (d, ^2J = 12.2 Hz, 1H, H-15a), 3.14 (s, 1H, H-6), 2.95 (s, 1H, H-5), 2.94 (s, 1H, H-2), 2.43 (m, 1H, H-8), 1.93 (ddm, ^3J = 5.8 Hz, ^3J = 4.8 Hz, 1H, H-3), 1.81 (ddm, ^3J = 5.3 Hz, ^3J = 5.3 Hz, 1H, H-3), 1.71 (ddm, ^3J = 4.8 Hz, ^3J = 4.9 Hz, 1H, H-3).

^{13}C NMR(100.62 MHz, $CDCl_3$): δ = 208.6 (C-1), 140.2 (C-16), 138.9 (C-9), 131.9 (C-21), 131.8 (C-14), 130.3 (C-13), 128.4 (3C, C-10, C-18, C-19), 127.6 (C-12), 127.0 (3C, C-11, C-20), 126.7 (C-17), 60.3 (C-2), 52.0 (C-7), 49.2 (C-15), 47.9 (C-5), 47.2 (C-8), 19.4 (C-6), 19.2 (C-3), 16.3 (C-4).

HRMS (ESI-TOF) m/z: $[M+H]^+$ Calcd for $C_{21}H_{18}OH$ 287.1430; Found 287.1433.

IR (ATR, ṽ): 1694 cm^{-1} (s, *CO*).

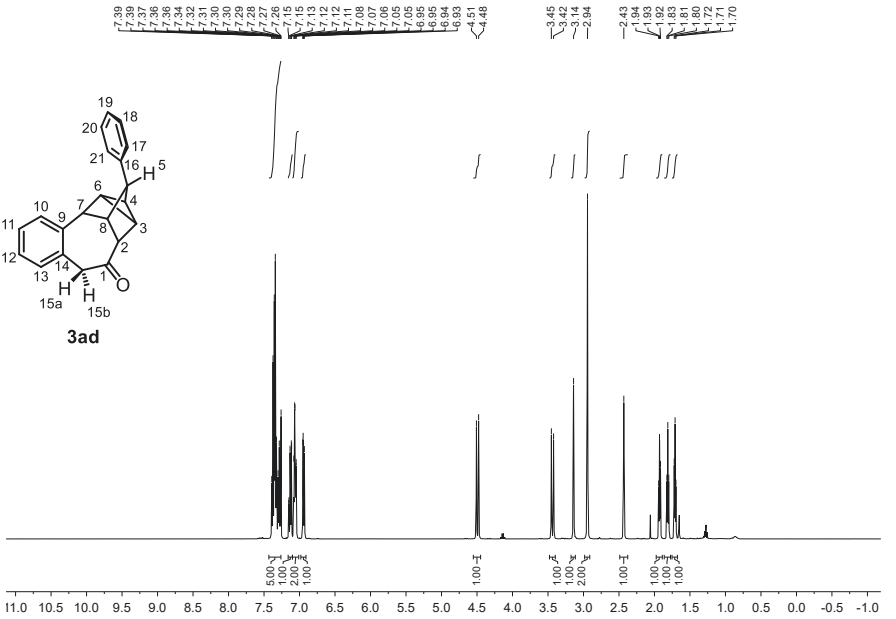

Figure S 152. ^{1}H NMR of **3ad** in $CDCl_3$ measured at 400.16 MHz.

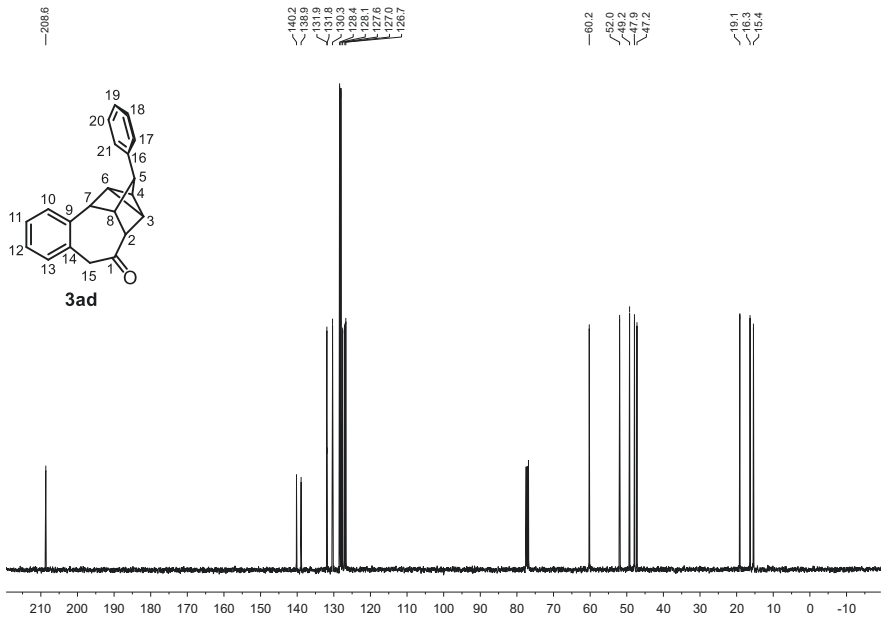

Figure S 153. ^{13}C NMR of **3ad** in $CDCl_3$ measured at 100.63 MHz.

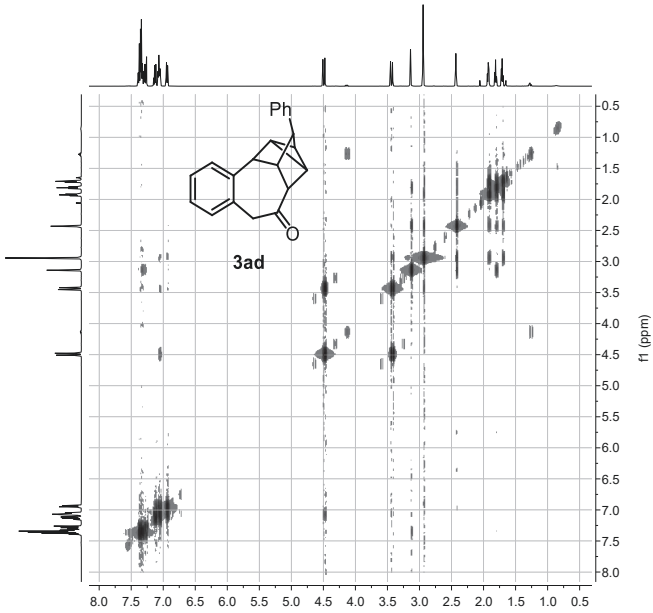

Figure S 154. $^{1}H,^{1}H$-COSY of **3ad** in $CDCl_3$ measured at 400.16 MHz.

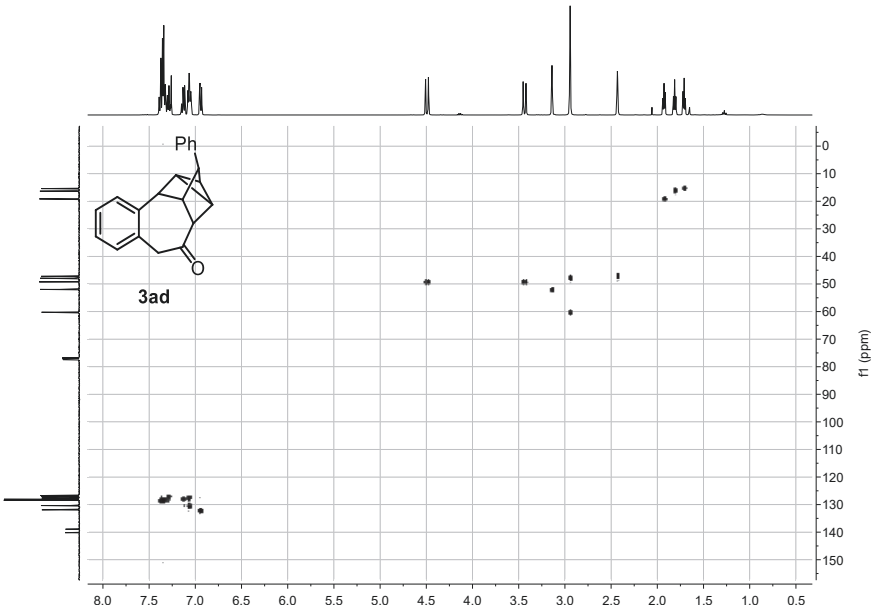

Figure S 155. $^{1}H,^{13}C$-HSQC of **3ad** in $CDCl_3$ measured at ^{1}H: 400.16 MHz; ^{13}C: 100.63 MHz.

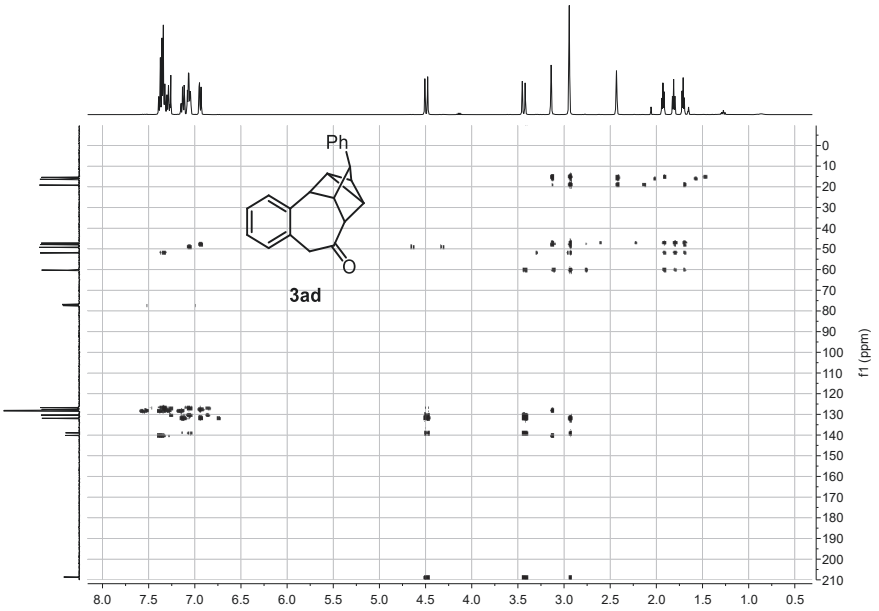

Figure S 156. $^{1}H,^{13}C$-HMBC of **3ad** in $CDCl_3$ measured at ^{1}H: 400.16 MHz; ^{13}C: 100.63 MHz.

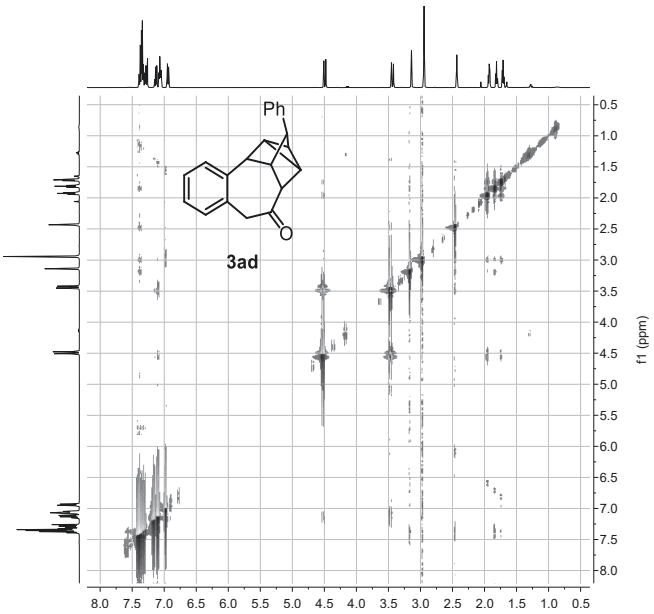

Figure S 157. $^{1}H,^{1}H$-NOESY of **3ad** in $CDCl_3$ measured at 400.16 MHz.

***rel*-(1*R*,2*R*,3a*S*,4*S*,10a*R*,11*R*)-1-hexyl-2,3,3a,4,9,10a-hexahydro-1,2,4-(epimethanetriyl) benzo[f]azulen-10(1H)-one**

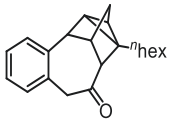

3ae

3ae was synthesized according to **GP-A** employing **1a** (118 mg, 1.00 mmol, 1.00 equiv.) and **2e** (229 mg, 1.30 mmol, 1.30 equiv.). PhCN (206 µL, 2.00 mmol, 2.00 equiv.) was added prior to **1a** and **2e**. Purification *via* flash chromatography (23 g SiO_2, gradient from 100:00 to 85:15 *n*-hexane/EA over 15 CV) afforded **3ae** and the respective isomer (147 mg, 499 µmol, 50%) as a pale yellow oil.

constitumeric ratio: 58:42

$C_{21}H_{26}O$ (294.44 $\frac{g}{mol}$)

R$_f$: 0.63 (*n*-hexane/EA = 80:20) [anisaldehyde]

^{1}H NMR(400.16 MHz, $CDCl_3$): δ = 7.15 (m, 3H, H-10, H-11, H-12), 7.07 (m, 1H, H-13), 4.46 (d, ^2J = 12.3 Hz, 1H, H-15b), 3.27 (d, ^2J = 12.3 Hz, 1H, H-15a), 2.81 (s, 1H, H-7), 2.66 (m, 1H, H-2), 2.26 (s, 1H, H-8), 1.71 (dm, ^2J = 10.5 Hz, 1H, H-5a), 1.71 (m, 1H, H-16a), 1.51 (s, 1H, H-6), 1.51 (dm, ^2J = 10.5 Hz, H-5b), 1.35 (dm, ^3J = 5.2 Hz, H-4), 1.29 (m, 1H, H-16b), 1.26 (m, 2H, H-17), 1.23 (m, 2H, H-18), 1.20 (m, 4H, H-19, H-20), 0.85 (t, ^3J = 6.8 Hz, 3H, H-21).

^{13}C NMR(100.62 MHz, $CDCl_3$): δ = 209.9 (C-1), 138.8 (C-9), 132.2 (C-10), 131.9 (C-14), 130.3 (C-13), 127.6 (C-12), 127.0 (C-11), 60.3 (C-2), 55.4 (C-7), 49.3 (C-15), 44.5 (C-8), 36.5 (C-5), 31.9 (C-19), 29.6 (C-20), 27.9 (C-17), 27.7 (C-16), 25.8 (C-3), 23.9 (C-6), 22.7 (C-18), 18.4 (C-4), 14.2 (C-21).

HRMS (ESI-TOF) m/z: $[M+H]^+$ Calcd for $C_{21}H_{26}OH$ 295.2055; Found 295.2056.

IR (ATR, ṽ): 1693 cm^{-1} (s, *CO*).

Constitumer:

$C_{21}H_{26}O$ (294.44 $\frac{g}{mol}$)

R$_f$: 0.66 (*n*-hexane/EA = 80:20) [anisaldehyde]

^{1}H NMR(400.16 MHz, $CDCl_3$): δ = 7.55 (dd, ^{3}J = 8.1 Hz, ^{4}J = 0.7 Hz, 1H, H-10), 7.23 (ddm, ^{3}J = 7.6 Hz, ^{3}J = 7.6 Hz, 1H, H-11), 7.13 (ddd, ^{3}J = 7.5 Hz, ^{3}J = 7.3 Hz, ^{4}J = 1.3 Hz, 1H, H-12), 6.97 (dm, ^{3}J = 7.6 Hz, 1H, H-13), 4.49 (dm, ^{2}J = 11.5 Hz, 1H, H-15b), 3.20 (d, ^{2}J = 11.5 Hz, 1H, H-15a), 2.66 (s, 1H, H-8), 2.49 (m, 1H, H-2), 2.12 (m, 1H, H-16b), 1.99 (dm, ^{2}J = 11.3 Hz, 1H, H-5a), 1.65 (m, 1H, H-16a), 1.49 (m, 1H, H-4), 1.40 (dm, ^{2}J = 11.3 Hz, H-5b), 1.38 (m, 1H, H-6), 1.32 (m, 1H, H-3), 1.19 (m, 3H, H-17a/b, H-18), 1.18 (m, 4H, H-19, H-20), 0.90 (m, 1H, H-17b/a), 0.83 (t, ^{3}J = 6.8 Hz, 3H, H-21).

^{13}C NMR(100.62 MHz, $CDCl_3$): δ = 207.0 (C-1), 142.3 (C-9), 130.7 (C-13), 130.5 (C-14), 130.0 (C-10), 127.4 (C-11), 127.1 (C-12), 57.3 (C-2), 57.3 (C-7), 50.8 (C-15), 37.5 (C-8), 36.3 (C-16), 33.5 (C-5), 31.8 (C-19), 30.0 (C-20), 26.9 (C-3), 25.6 (C-17), 22.7 (C-18), 16.6 (C-4), 14.2 (C-21), 13.9 (C-6).

HRMS (ESI-TOF) m/z: $[M+H]^+$ Calcd for $C_{21}H_{26}OH$ 295.2056; Found 295.2057.

IR (ATR, $\tilde{\nu}$): 1709 cm^{-1} (s, *CO*).

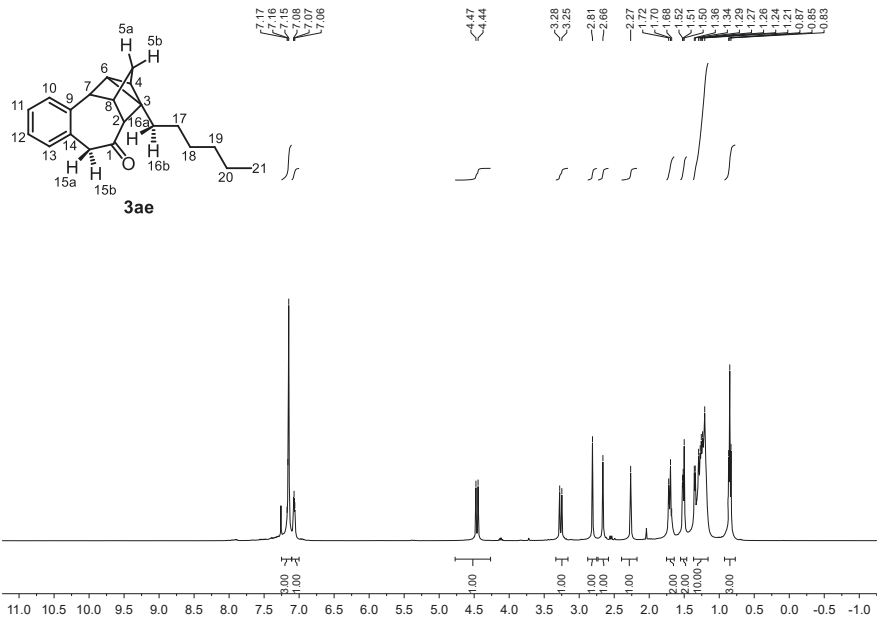

Figure S 158. ^{1}H NMR of **3ae** in $CDCl_3$ measured at 400.16 MHz.

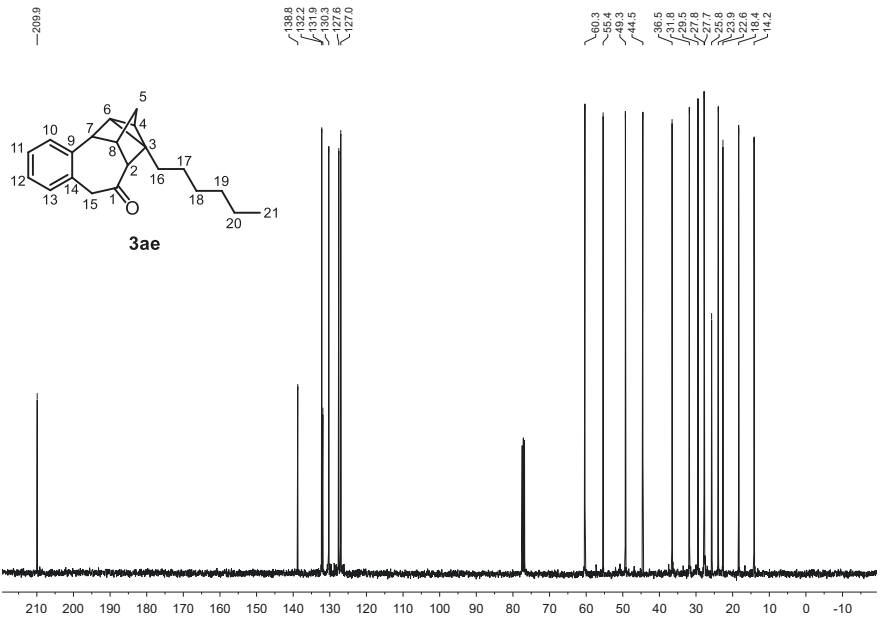

Figure S 159. ^{13}C NMR of **3ae** in $CDCl_3$ measured at 100.63 MHz.

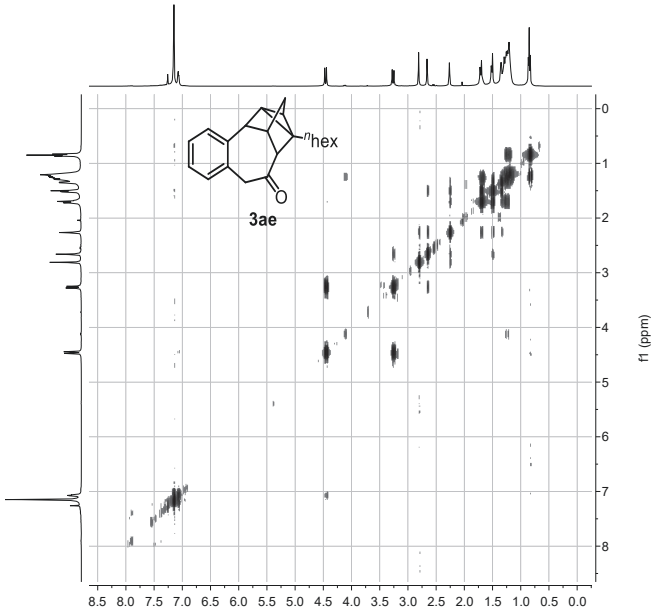

Figure S 160. $^{1}H,^{1}H$-COSY of **3ae** in $CDCl_3$ measured at 400.16 MHz.

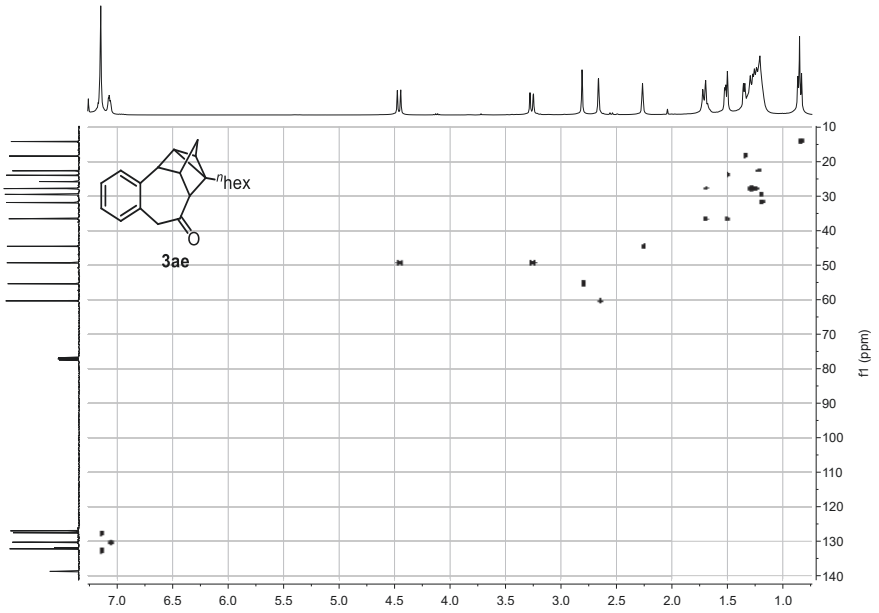

Figure S 161. $^{1}H,^{13}C$-HSQC of **3ae** in $CDCl_3$ measured at ^{1}H: 400.16 MHz; ^{13}C: 100.63 MHz.

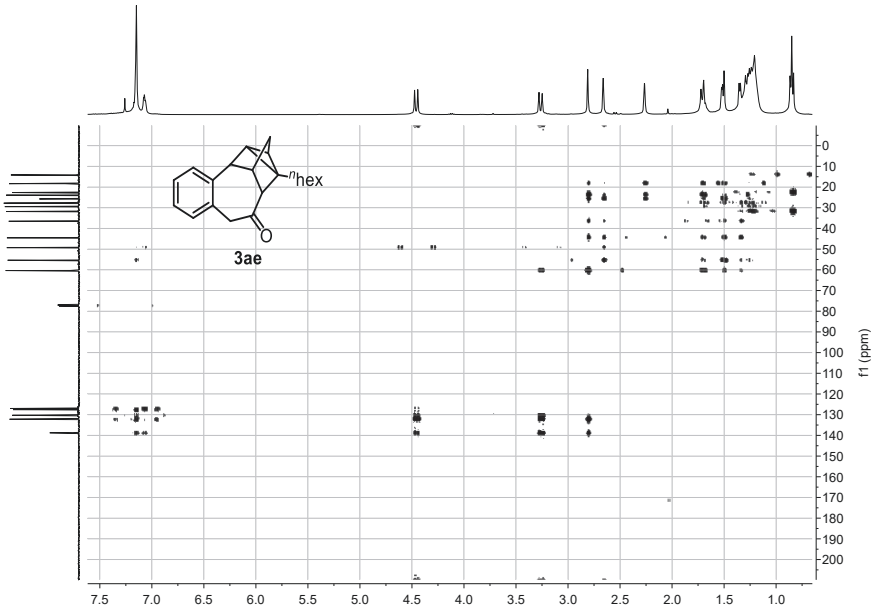

Figure S 162. $^{1}H,^{13}C$-HMBC of **3ae** in $CDCl_3$ measured at ^{1}H: 400.16 MHz; ^{13}C: 100.63 MHz.

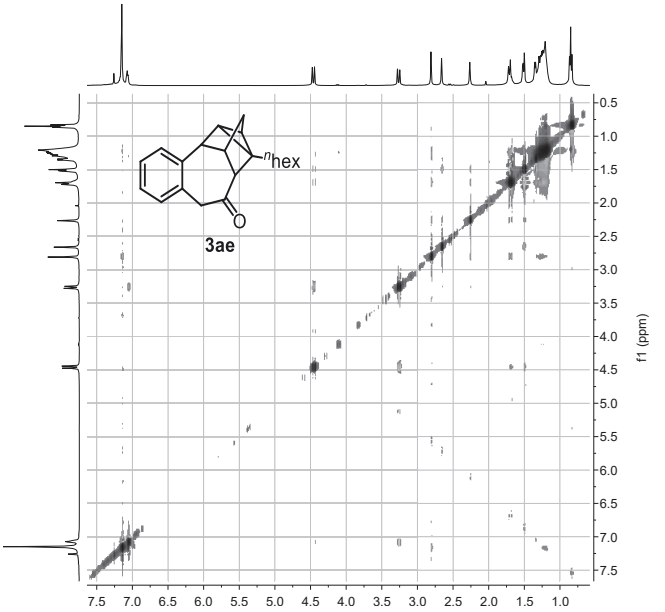

Figure S 163. $^{1}H,^{1}H$-NOESY of **3ae** in $CDCl_3$ measured at 400.16 MHz.

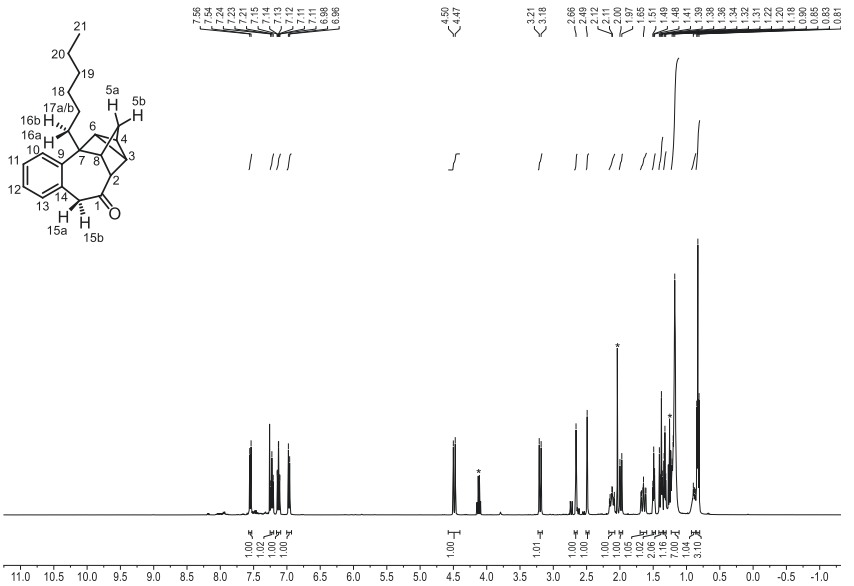

Figure S 164. ^{1}H NMR of the constitutional isomer of **3ae** in $CDCl_3$ measured at 400.16 MHz. * denotes residual EA.

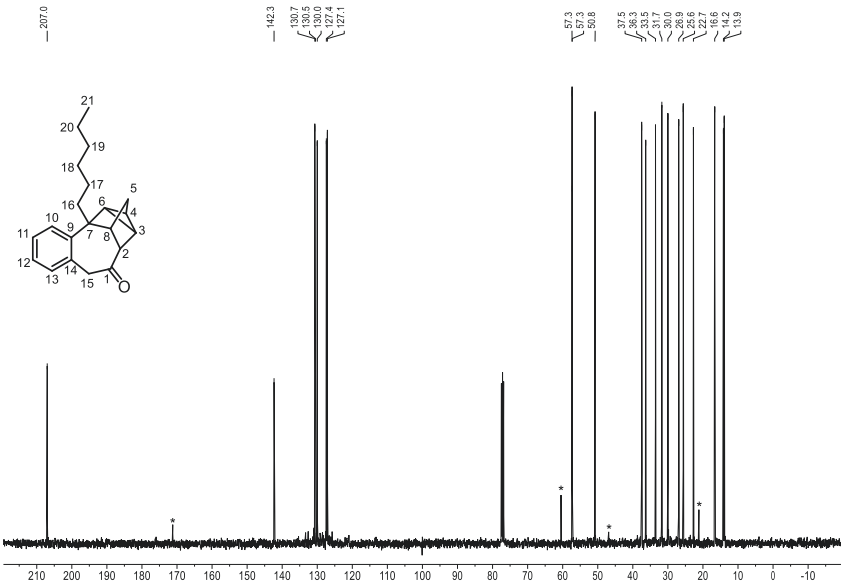

Figure S 165. ^{1}H NMR of the constitutional isomer of **3ae** in $CDCl_3$ measured at 400.16 MHz. * denotes residual EA.

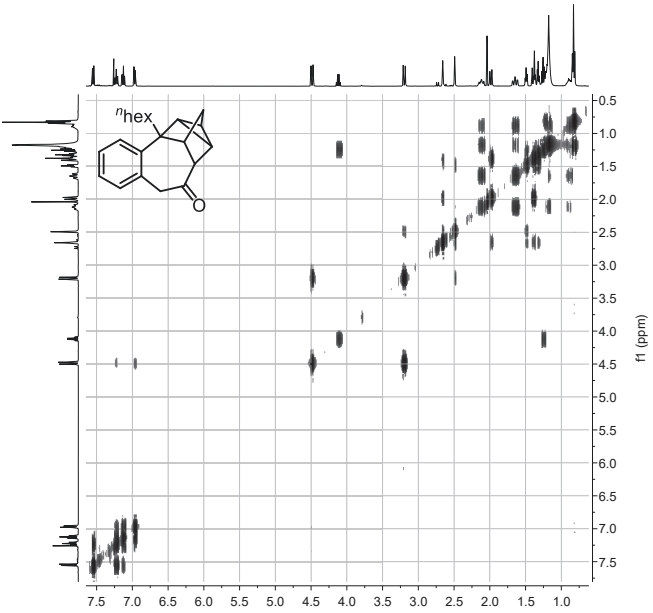

Figure S 166. $^{1}H,^{1}H$-COSY of the constitutional isomer of **3ae** in $CDCl_3$ measured at 400.16 MHz.

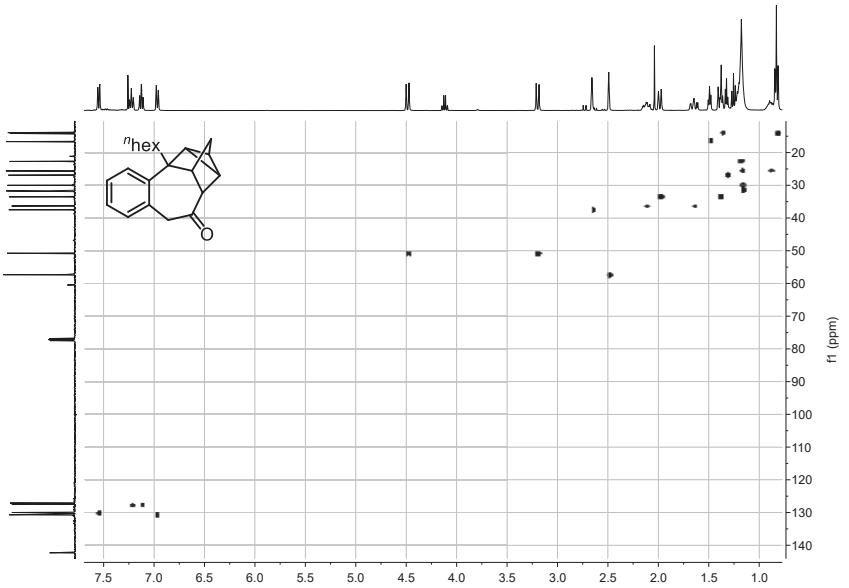

Figure S 167. $^{1}H,^{13}C$-HSQC of the constitutional isomer of **3ae** in $CDCl_3$ measured at ^{1}H: 400.16 MHz; ^{13}C: 100.63 MHz.

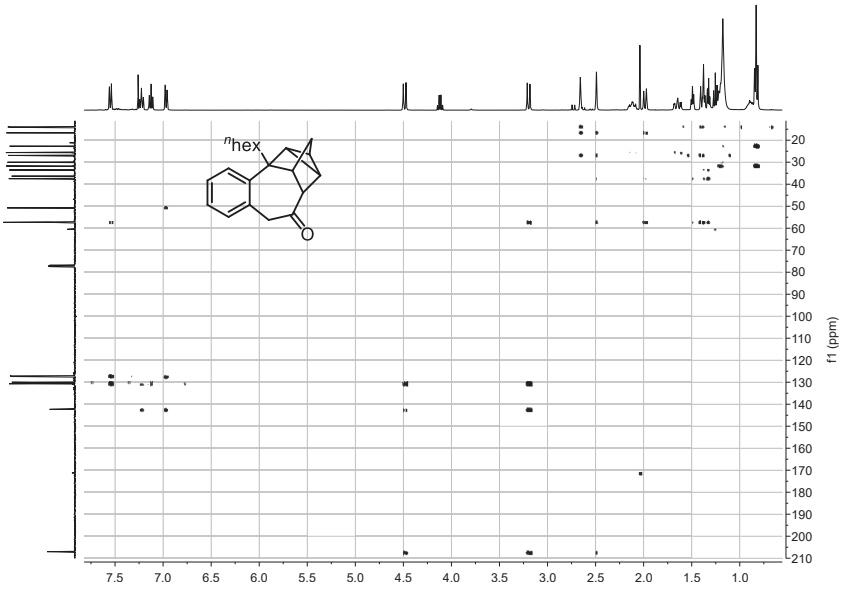

Figure S 168. $^{1}H,^{13}C$-HMBC of the constitutional isomer of **3ae** in $CDCl_3$ measured at ^{1}H: 400.16 MHz; ^{13}C: 100.63 MHz.

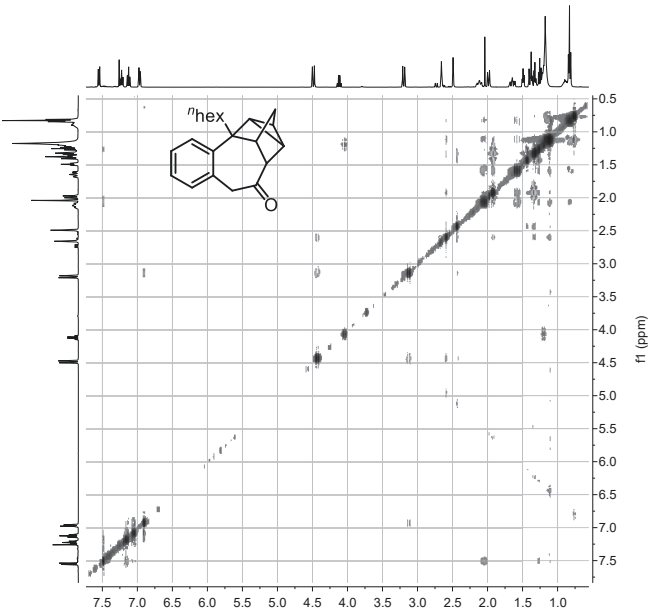

Figure S 169. $^{1}H,^{1}H$-NOESY of the constitutional isomer of **3ae** in $CDCl_3$ measured at 400.16 MHz.

***rel*-(2*S*,3*S*,3a*S*,10*R*,10a*R*,11*S*)-5-methyl-2,3,3a,9,10,10a-hexahydro-2,3,10-(epimethanetriyl)benzo[f]azulen-4(1H)-one**

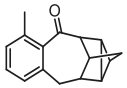

3ma

3ma was synthesized according to **GP-A** employing **1m** (132 mg, 1.00 mmol, 1.00 equiv.) and NBD (132 µL, 1.30 mmol, 1.30 equiv.). Purification *via* flash chromatography (23 g SiO_2, gradient from 100:00 to 85:15 *n*-hexane/EA over 15 CV) afforded **3ma** (167 mg, 745 µmol, 74%, 16% *ee*, $[\alpha]_D^{20}$ +1 (*c* 1.0, $CHCl_3$)) as a pale yellow oil.

isomer ratio: 81:19

$C_{16}H_{16}O$ (224.30 $\frac{g}{mol}$)

Rf: 0.84 (*n*-hexane/EA = 80:20) [UV]

^{1}H NMR(400.16 MHz, $CDCl_3$): δ = 7.13 (t, ^3J = 7.6 Hz, 1H, H-12,), 7.04 (d, ^3J = 7.7 Hz, 1H, H-13), 6.92 (d, ^3J = 7.4 Hz, 1H, H-11), 3.03 (d, ^2J = 15.7 Hz, 1H, H-9a), 2.90 (dd, ^2J = 15.7 Hz, ^3J = 7.7 Hz, 1H, H-9b), 2.57 (m, 1H, H-2), 2.27 (s, 3H, H-16), 2.19 (s, 1H, H-8), 2.11 (dm, ^3J = 7.7 Hz, 1H, H-7), 1.50 (dm, ^2J = 10.6 Hz, 1H, H-5b), 1.45 (dm, ^2J = 10.6 Hz, 1H, H-5a), 1.24 (m, 1H, H-4), 1.19 (m, 1H, H-3), 1.04 (m, 1H, H-6).

^{13}C NMR(100.62 MHz, $CDCl_3$): δ = 211.9 (C-1), 140.5 (C-15), 135.5 (C-10), 134.4 (C-14), 129.2 (C-12), 128.9 (C-13), 127.2 (C-11), 57.1 (C-2), 41.9 (C-8), 41.3 (C-7), 36.5 (C-5), 35.7 (C-9), 19.7 (C-16), 15.4 (C-6), 14.9 (C-3), 13.1 (C-4).

HRMS (ESI-TOF) m/z: $[M+H]^+$ Calcd for $C_{16}H_{16}OH$ 225.1274; Found 225.1278.

IR (ATR, ṽ): 1679 cm^{-1} (s, *CO*).

Regioisomer:

mp: 131.6 °C.

Rf: 0.60 (*n*-hexane/EA = 80:20) [anisaldehyde]

^{1}H NMR(600.13 MHz, $CDCl_3$): δ = 7.08 (d, ^3J = 6.9 Hz, 1H, H-11,), 7.03 (t, ^3J = 7.5 Hz, 1H, H-12), 6.92 (d, ^3J = 7.3 Hz, 1H, H-13), 4.06 (d, ^2J = 12.2 Hz, 1H, H-15b), 3.73 (d, ^2J = 12.2 Hz, 1H, H-15a), 3.27 (s, 1H, H-7), 2.62 (m, 1H, H-2), 2.43 (m, 1H, H-8), 2.41 (s, 3H, H-16), 1.66

(dm, ^{2}J =10.7 Hz, 1H, H-5a), 1.63 (m, 1H, H-3), 1.55 (dm, ^{2}J = 10.7 Hz, 1H, H-5b), 1.47 (m, 1H, H-4), 1.44 (m, 1H, H-6).

^{13}C NMR(150.90 MHz, $CDCl_3$): δ = 209.5 (C-1), 137.5 (C-9), 137.4 (C-14), 134.7 (C-10), 129.7 (C-11), 128.9 (C-13), 127.0 (C-12), 58.0 (C-2), 49.8 (C-15), 46.8 (C-7), 38.7 (C-8), 35.9 (C-5), 21.2 (C-16), 16.6 (C-3), 15.8 (C-6), 13.1 (C-4).

HRMS (ESI-TOF) m/z: $[M+H]^+$ Calcd for $C_{16}H_{16}OH$ 225.1274; Found 225.1277.

IR (ATR, ṽ): 1698 cm^{-1} (s, *CO*).

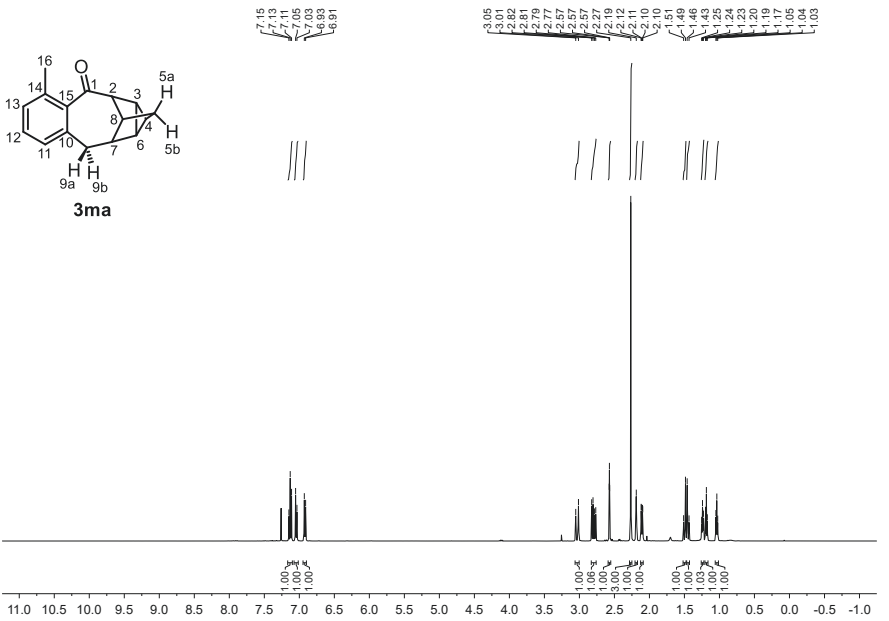

Figure S 170. ^{1}H NMR of **3ma** in $CDCl_3$ measured at 400.16 MHz.

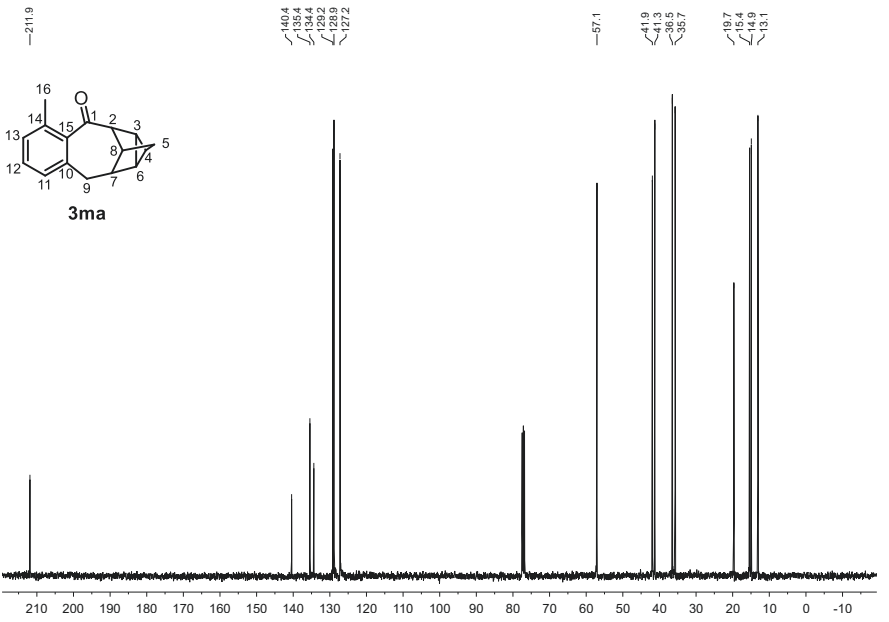

Figure S 171. ^{13}C NMR of **3ma** in $CDCl_3$ measured at 100.63 MHz.

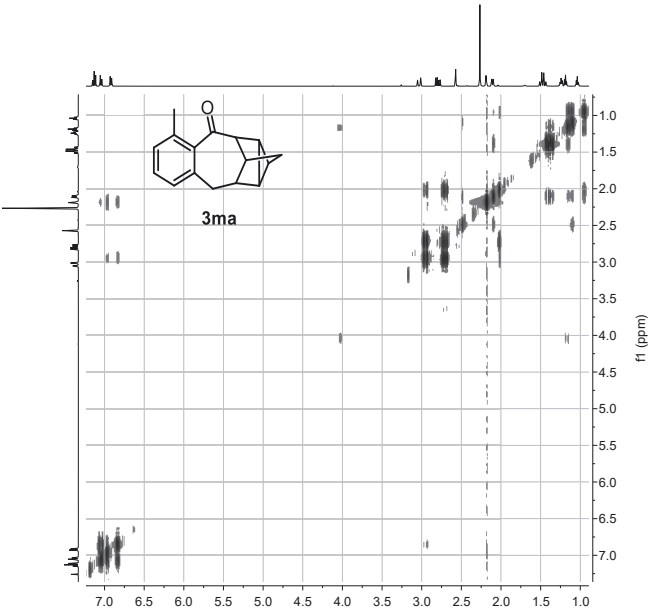

Figure S 172. $^{1}H,^{1}H$-COSY of **3ma** in $CDCl_3$ measured at 400.16 MHz.

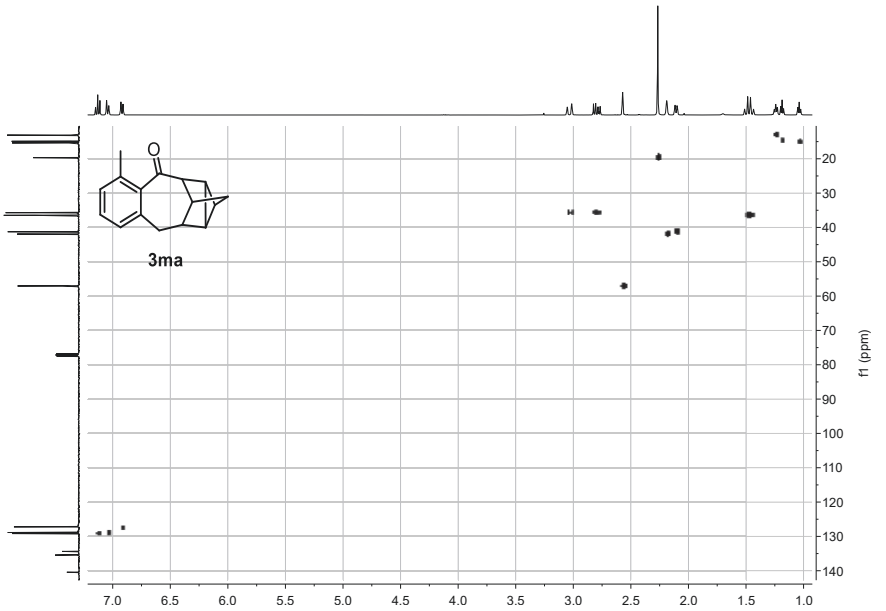

Figure S 173. $^{1}H,^{13}C$-HSQC of **3ma** in $CDCl_3$ measured at ^{1}H: 400.16 MHz; ^{13}C: 100.63 MHz.

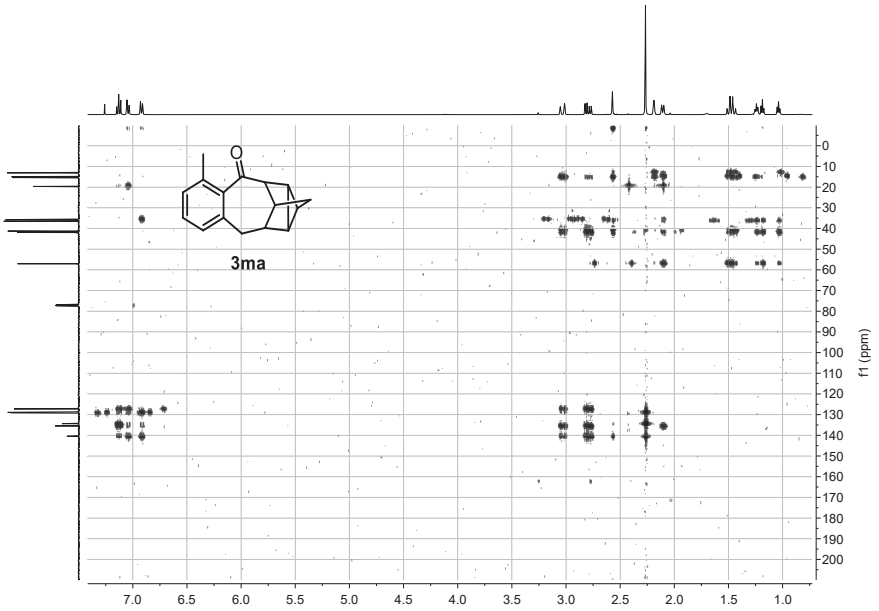

Figure S 174. $^{1}H,^{13}C$-HMBC of **3ma** in $CDCl_3$ measured at ^{1}H: 400.16 MHz; ^{13}C: 100.63 MHz.

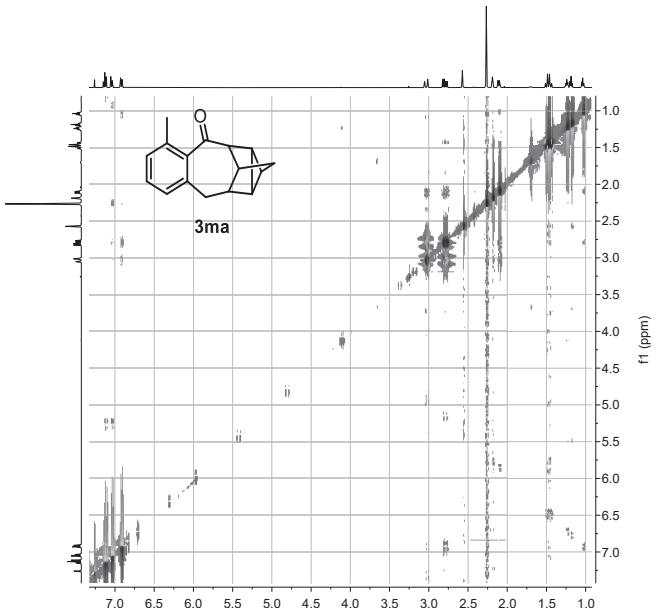

Figure S 175. $^{1}H,^{1}H$-NOESY of **3ma** in $CDCl_3$ measured at 400.16 MHz.

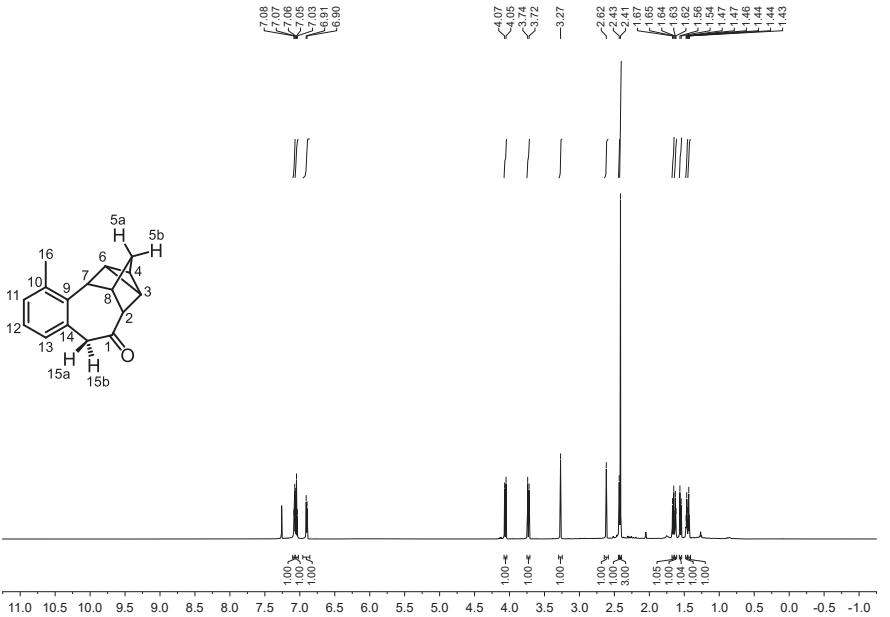

Figure S 176. ^{1}H NMR of the regioisomer of **3ma** in $CDCl_3$ measured at 600.13 MHz.

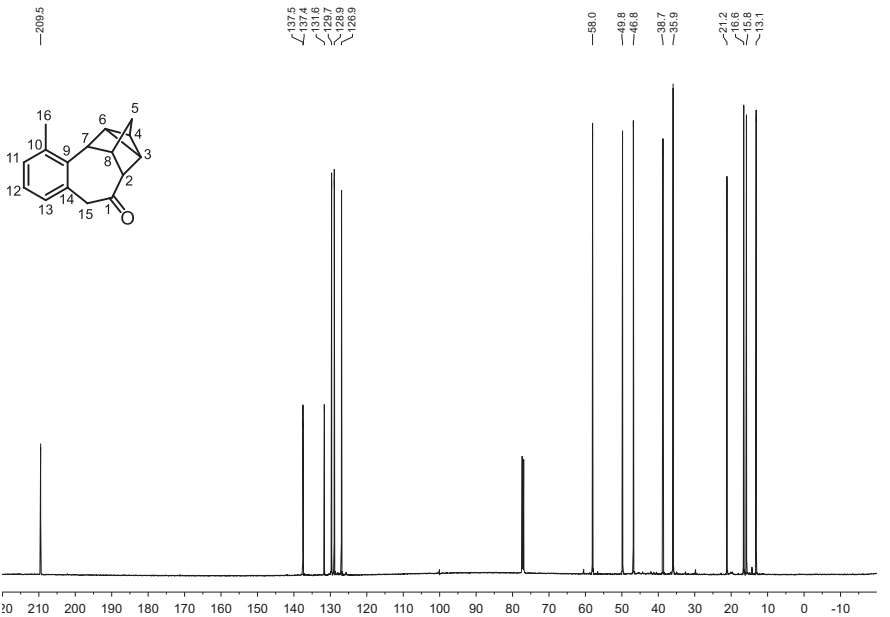

Figure S 177. ^{13}C NMR of the regioisomer of **3ma** in $CDCl_3$ measured at 150.92 MHz.

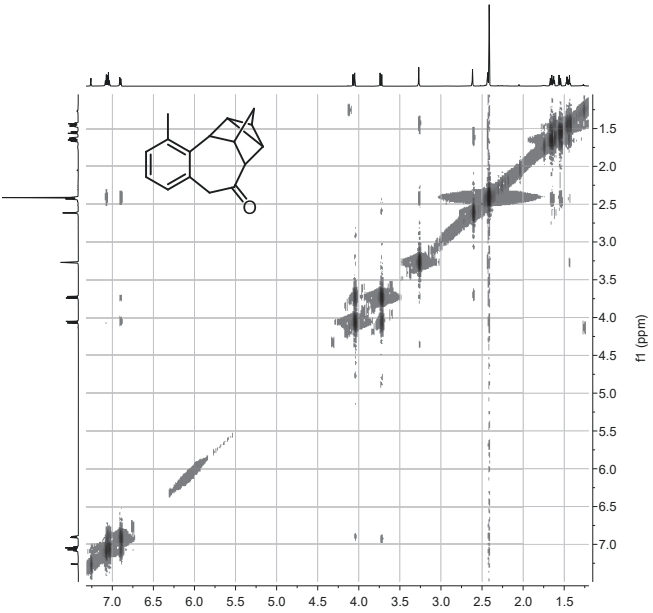

Figure S 178. ^{1}H,^{1}H-COSY of the regioisomer of **3ma** in $CDCl_3$ measured at 600.13 MHz.

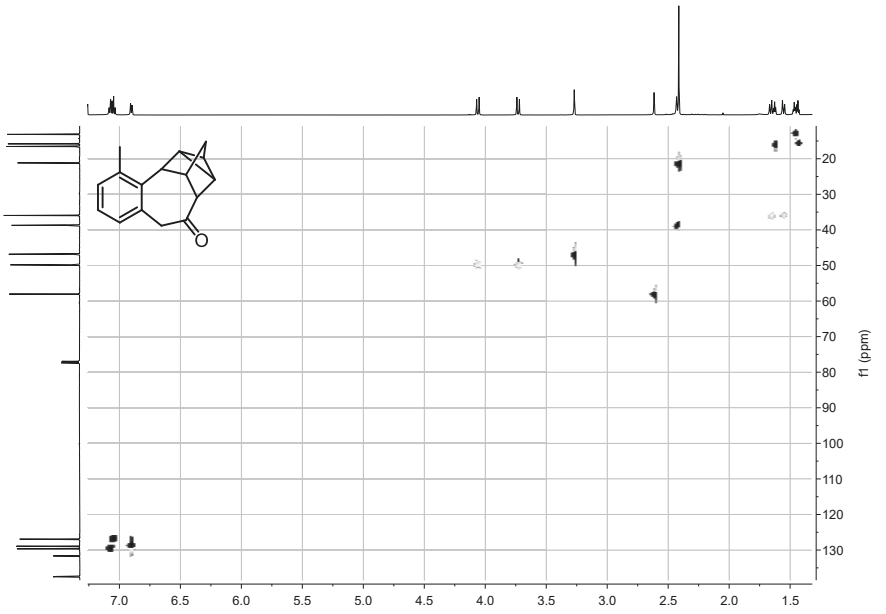

Figure S 179. ^{1}H,^{13}C-HSQC of the regioisomer of **3ma** in $CDCl_3$ measured at ^{1}H: 600.13 MHz; ^{13}C: 150.92 MHz.

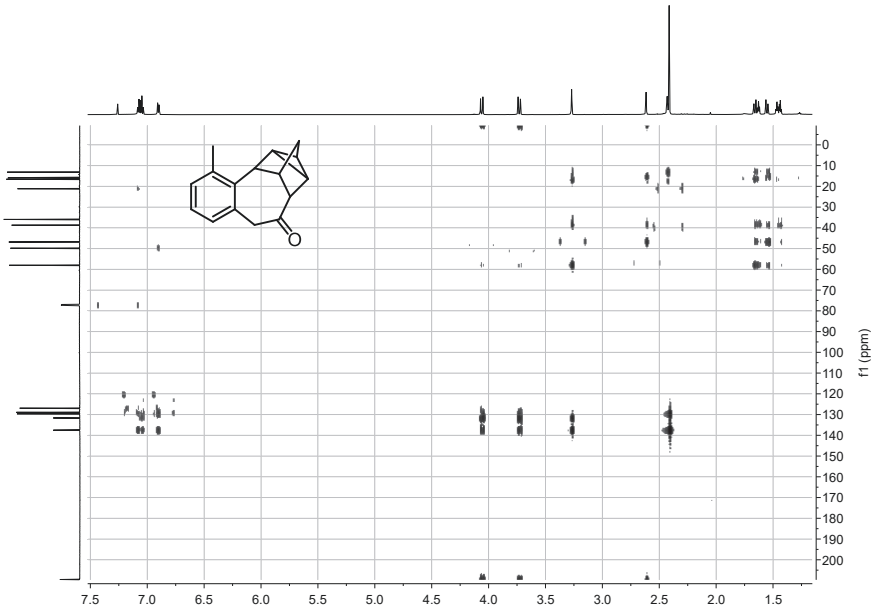

Figure S 180. $^{1}H,^{13}C$-HMBC of the regioisomer of **3ma** in $CDCl_3$ measured at ^{1}H: 600.13 MHz; ^{13}C: 150.92 MHz.

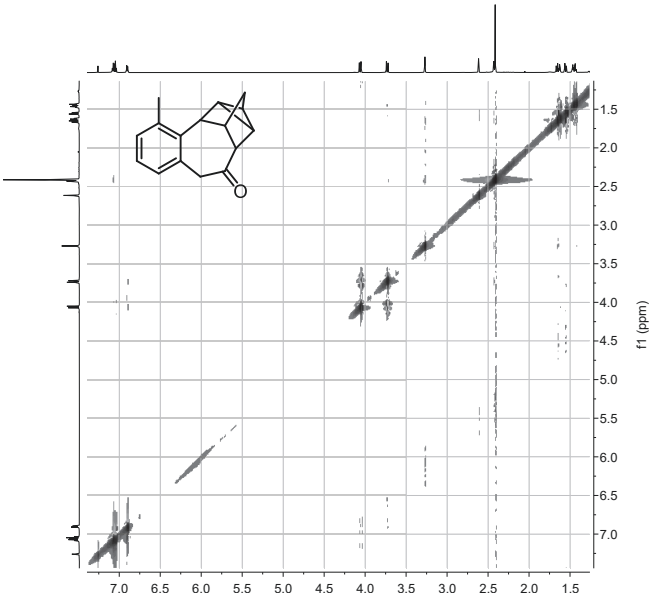

Figure S 181. $^{1}H,^{1}H$-NOESY of the regioisomer of **3ma** in $CDCl_3$ measured at 600.13 MHz.

***rel*-(2*S*,3*S*,3a*S*,10*R*,10a*R*,11*S*)-5-methoxy-2,3,3a,9,10,10a-hexahydro-2,3,10-(epimethanetriyl)benzo[f]azulen-4(1H)-one**

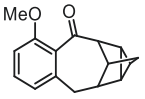

3na

3na was synthesized according to **GP-B** employing **1n** (148 mg, 1.00 mmol, 1.00 equiv.) and NBD (132 µL, 1.30 mmol, 1.30 equiv.). Purification *via* flash chromatography (23 g SiO_2, gradient from 100:00 to 80:20 *n*-hexane/EA over 15 CV) afforded **3na** (240 mg, 663 µmol, 66%, mixture of isomers) as a pale yellow oil.

isomeric ratio: 93:7 ([4+2+2]:[4+2])

$C_{16}H_{16}O_2$ (240.30 $\frac{g}{mol}$)

R$_f$: 0.52 (*n*-hexane/EA = 80:20) [UV]

^{1}H NMR(400.16 MHz, $CDCl_3$): δ = 7.18 (t, ^3J = 7.9 Hz, 1H, H-12,), 6.78 (d, ^3J = 8.4 Hz, 1H, H-13), 6.68 (d, ^3J = 7.6 Hz, 1H, H-11), 3.78 (s, 3H, H-16), 3.01 (d, ^2J = 15.8 Hz, 1H, H-9a), 2.78 (dd, ^2J = 15.8 Hz, ^3J = 7.7 Hz, 1H, H-9b), 2.59 (m, 1H, H-2), 2.16 (s, 1H, H-8), 2.08 (dm, ^3J = 7.7 Hz, 1H, H-7), 1.48 (dm, ^2J = 10.6 Hz, 1H, H-5b), 1.43 (dm, ^2J = 10.6 Hz, 1H, H-5a), 1.25 (m, 1H, H-3), 1.22 (m, 1H, H-4), 1.01 (m, 1H, H-6).

^{13}C NMR(100.62 MHz, $CDCl_3$): δ = 208.7 (C-1), 155.7 (C-14), 137.0 (C-10), 130.3 (C-13), 129.9 (C-15), 122.0 (C-11), 109.7 (C-12), 57.0 (C-2), 56.1 (C-16), 41.9 (C-8), 41.1 (C-7), 36.5 (C-5), 35.4 (C-9), 15.1 (C-6), 14.9 (C-3), 12.9 (C-4).

HRMS (ESI-TOF) m/z: $[M+H]^+$ Calcd for $C_{16}H_{16}O_2H$ 241.1223; Found 241.1224.

IR (ATR, ṽ): 1684 cm^{-1} (s, *CO*), 1583 cm^{-1} (m).

[2+2] insertion product:

^{1}H NMR(400.16 MHz, $CDCl_3$): δ = 7.31 (dd, ^3J = 8.2 Hz, ^3J = 7.7 Hz, 1H, H-12,), 6.80 (d, ^3J = 8.2 Hz, 1H, H-13), 6.75 (d, ^3J = 7.7 Hz, 1H, H-11), 6.18 (m, 2H, H-4, H-6), 3.83 (s, 3H, H-16), 3.48 (m, 1H, H-3), 2.96 (dd, ^2J = 14.8 Hz, ^3J = 6.5 Hz, 1H, H-9), 2.69 (m, 1H, H-7), 2.42 (dd, ^2J = 14.8 Hz, ^3J = 10.8 Hz, 1H, H-9), 2.31 (m, 1H, H-2), 2.25 (dm, ^3J = 10.8 Hz, 1H, H-7), 1.41 (m, 2H, H-5).

^{13}C NMR(100.62 MHz, $CDCl_3$): δ = 201.6 (C-1), 157.1 (C-14), 144.0 (C-15), 137.2 (C-4/6), 136.8 (C-6/4), 133.1 (C-12), 126.1 (C-10), 120.1 (C-11), 109.9 (C-13), 55.9 (C-16), 53.3 (C-2), 47.7 (C-7), 43.5 (C-3), 37.8 (C-8), 34.3 (C-9), 14.3 (C-5).

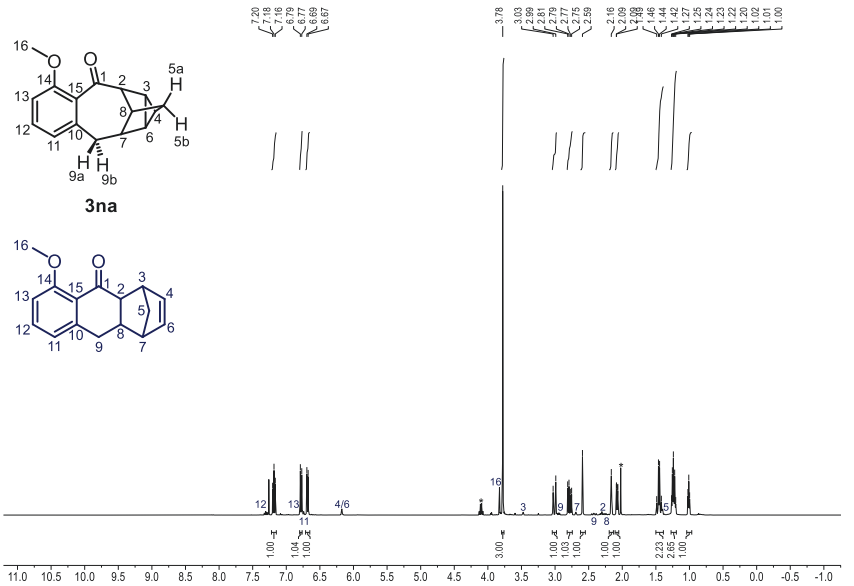

Figure S 182. ^{1}H NMR of **3na** and alken insertion product (blue) in $CDCl_3$ measured at 400.16 MHz. * denotes residual EA.

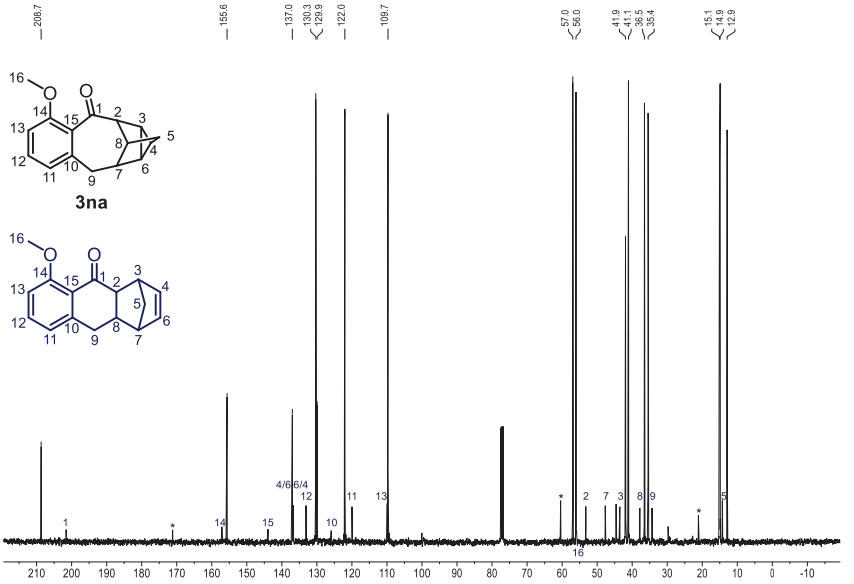

Figure S 183. ^{13}C NMR of **3na** and alken insertion product (blue) in $CDCl_3$ measured at 100.63 MHz. * denotes residual EA.

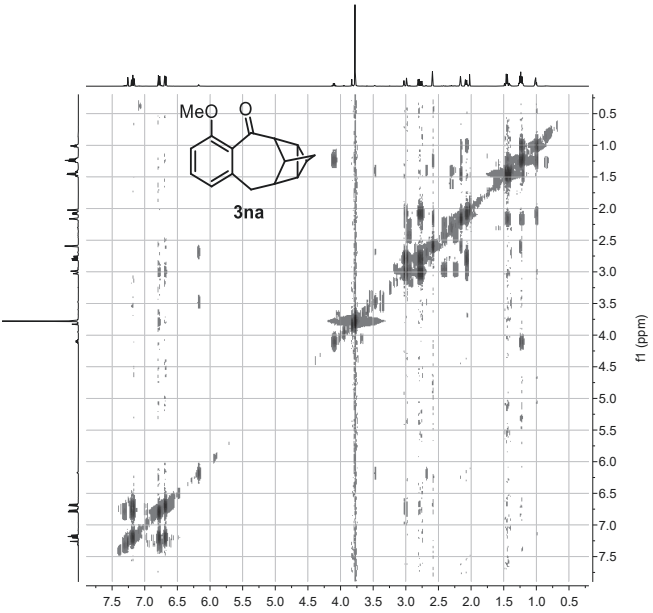

Figure S 184. $^{1}H,^{1}H$-COSY of **3na** in $CDCl_3$ measured at 400.16 MHz.

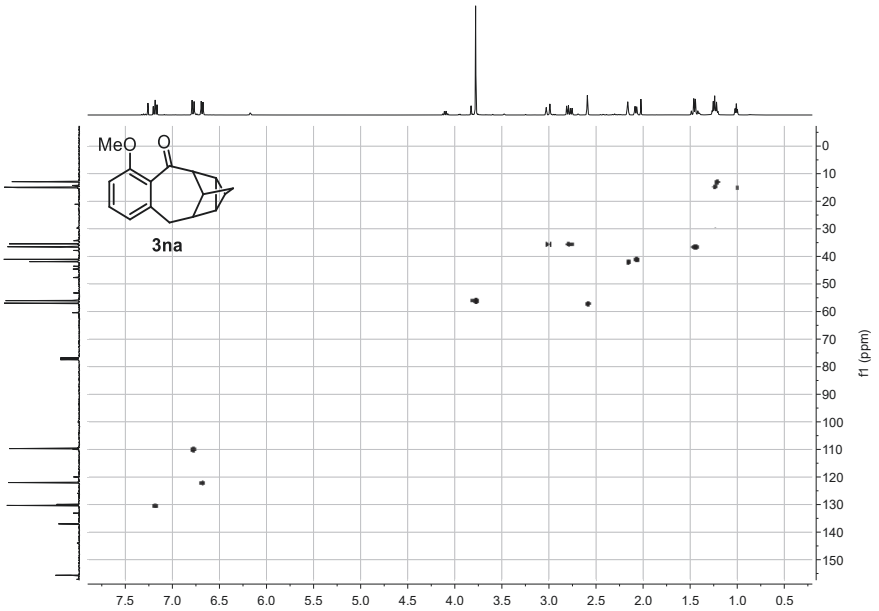

Figure S 185. $^{1}H,^{13}C$-HSQC of **3na** in $CDCl_3$ measured at ^{1}H: 400.16 MHz; ^{13}C: 100.63 MHz.

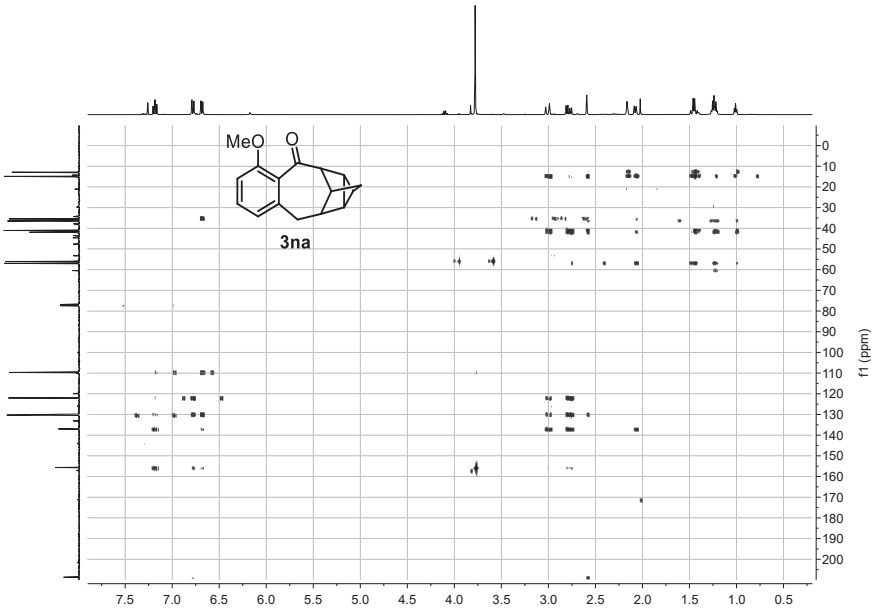

Figure S 186. $^{1}H,^{13}C$-HMBC of **3na** in $CDCl_3$ measured at ^{1}H: 400.16 MHz; ^{13}C: 100.63 MHz.

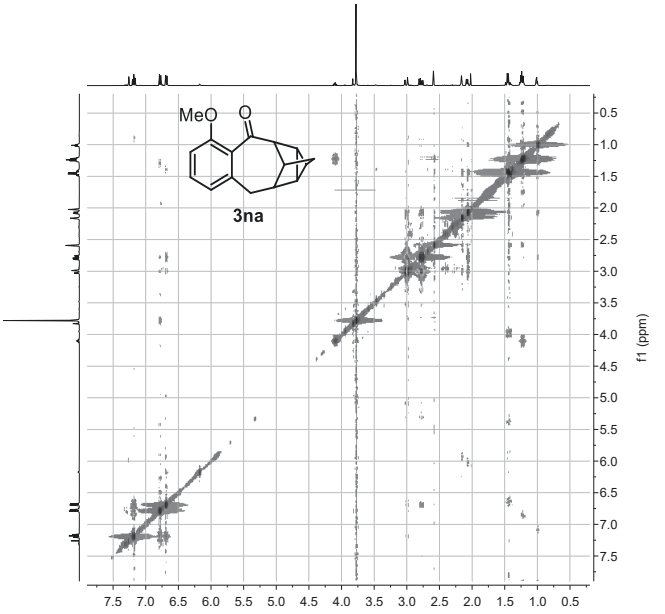

Figure S 187. $^{1}H,^{1}H$-NOESY of **3na** in $CDCl_3$ measured at 400.16 MHz.

***rel*-(1*R*,2*S*,3*R*,3a*R*,10*S*,10a*R*,11*S*)-1-(*tert*-butoxy)-5-methoxy-2,3,3a,9,10,10a-hexahydro-2,3,10-(epimethanetriyl)benzo[f]azulen-4(1H)-one**

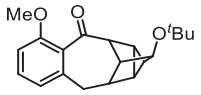

3nb

3nb was synthesized according to **GP-B** employing **1n** (148 mg, 1.00 mmol, 1.00 equiv.) and **2b** (214 mg, 1.30 mmol, 1.30 equiv.). Purification *via* flash chromatography (23 g SiO_2, gradient from 100:00 to 80:20 *n*-hexane/EA over 20 CV) afforded **3nb** as a mixture of isomers (240 mg, 663 µmol, 84%). Further purification by preparative HPLC (Kinetex C18; H_2O/MeOH + 0.1% FA = 32/68, for 10 min, then gradient to 20/80 over 25 min, flow rate = 14.8 mL/min, l = 220 nm) furnished: t_R = 13.5 min (**3nb** + diastereomer (1S)), 18.2 min (regioisomer), 27.1 min (*endo* [2+2] insertion product), and 31.2 min (*exo* [2+2] insertion product). A second preparative HPLC of the mixture of **3nb** and its diastereomer (1S) (Kinetex C18; H_2O/MeOH + 0.1% FA = 70:30 gradient to 0:100, over 30 min, flow rate = 7.5 mL/min, l = 220 nm) furnished: t_R = 31.1 min (**3nb**) and 31.5 min (diastereomer (1S)).

d.r.: 52:48

$C_{20}H_{24}O_3$ (312.41 $\frac{g}{mol}$)

Rf: 0.40 (*n*-hexane/EA = 80:20) [anisaldehyde]

^{1}H NMR(600.13 MHz, $CDCl_3$): δ = 7.18 (t, ^3J = 7.8 Hz, 1H, H-12,), 6.79 (d, ^3J = 8.4 Hz, 1H, H-13), 6.67 (d, ^3J = 7.6 Hz, 1H, H-11), 3.79 (s, 3H, H-16), 3.76 (m, 1H, H-5), 3.26 (m, 1H, H-2), 2.96 (d, ^2J = 15.7 Hz, 1H, H-9a), 2.75 (dd, ^2J = 15.8 Hz, ^3J = 7.7 Hz, 1H, H-9b), 2.16 (m, 1H, H-7), 2.08 (s, 1H, H-8), 1.45 (m, 1H, H-3), 1.19 (s, 9H, H-18), 1.19 (m, 1H, H-4), 1.13 (m, 1H, H-6).

^{13}C NMR(150.90 MHz, $CDCl_3$): δ = 209.6 (C-1), 155.8 (C-14), 136.6 (C-10), 130.7 (C-15), 130.2 (C-12), 122.1 (C-11), 109.9 (C-13), 77.9 (C-5), 73.7 (C-17), 56.1 (C-16), 53.7 (C-2), 47.8 (C-8), 37.9 (C-7), 35.9 (C-9), 28.6 (C-18), 18.8 (C-4), 17.7 (C-6), 16.0 (C-3).

HRMS (ESI-TOF) m/z: $[M+H]^+$ Calcd for $C_{20}H_{24}O_3H$ 313.1804; Found 313.1804.

IR (ATR, ṽ): 1686 cm^{-1} (s, *CO*), 1585 cm^{-1} (m).

Diastereomer (1*S*):

^{1}H NMR(600.13 MHz, $CDCl_3$): δ = 7.21 (t, ^{3}J = 7.8 Hz, 1H, H-12), 6.79 (d, ^{3}J = 8.4 Hz, 1H, H-13), 6.75 (d, ^{3}J = 7.5 Hz, 1H, H-11), 3.80 (s, 3H, H-16), 3.75 (m, 1H, H-5), 3.02 (d, ^{2}J = 15.7 Hz, 1H, H-9a), 2.90 (dd, ^{2}J = 15.7 Hz, ^{3}J = 7.7 Hz, 1H, H-9b), 2.76 (m, 1H, H-7), 2.66 (s, 1H, H-2), 2.08 (s, 1H, H-8), 1.35 (m, 1H, H-3), 1.25 (m, 1H, H-6), 1.20 (s, 9H, H-18), 1.19 (m, 1H, H-4).

^{13}C NMR(150.90 MHz, $CDCl_3$): δ = 207.8 (C-1), 155.9 (C-14), 137.6 (C-10), 130.6 (C-12), 129.5 (C-15), 122.3 (C-11), 109.7 (C-13), 78.2 (C-5), 74.8 (C-17), 56.1 (C-16), 54.0 (C-2), 47.2 (C-8), 37.6 (C-7), 35.2 (C-9), 28.7 (C-18), 18.2 (C-4), 17.1 (C-3), 16.3 (C-6).

HRMS (ESI-TOF) m/z: $[M+H]^+$ Calcd for $C_{20}H_{24}O_3H$ 313.1804; Found 313.1804.

IR (ATR, ṽ): 1683 cm^{-1} (s, *CO*), 1584 cm^{-1} (m).

regioisomer:

regioisomeric ratio: 82:18

mp: 137.8 °C.

^{1}H NMR(600.13 MHz, $CDCl_3$): δ = 7.11 (t, ^{3}J = 8.0 Hz, 1H, H-12), 6.78 (d, ^{3}J = 8.1 Hz, 1H, H-13), 6.66 (d, ^{3}J = 7.6 Hz, 1H, H-11), 4.05 (d, ^{2}J = 12.3 Hz, 1H, H-15b), 3.98 (m, 1H, H-5), 3.83 (s, 3H, H-16), 3.73 (d, ^{2}J = 12.3 Hz, 1H, H-15a), 3.69 (s, 1H, H-2), 3.25 (s, 1H, H-7), 2.26 (s, 1H, H-8), 1.75 (m, 1H, H-3), 1.55 (m, 1H, H-6), 1.38 (m, 1H, H-4), 1.22 (s, 9H, H-18).

^{13}C NMR(150.90 MHz, $CDCl_3$): δ = 209.9 (C-1), 157.8 (C-14), 133.3 (C-10), 127.9 (C-12), 127.4 (C-15), 123.0 (C-13), 109.4 (C-11), 77.9 (C-5), 73.9 (C-17), 55.9 (C-16), 55.0 (C-2), 49.9 (C-15), 44.8 (C-8), 38.8 (C-7), 28.7 (C-18), 19.0 (C-4), 18.9 (C-6), 17.3 (C-3).

HRMS (ESI-TOF) m/z: $[M+H]^+$ Calcd for $C_{20}H_{24}O_3H$ 313.1804; Found 313.1801.

IR (ATR, ṽ): 1702 cm^{-1} (s, *CO*), 1582 cm^{-1} (m).

***endo* [2+2] insertion product:**

d.r.: 95:5 (*endo*:*exo*)

mp: 145.1 °C.

^{1}H NMR(600.13 MHz, $CDCl_3$): δ = 7.28 (t, ^{3}J = 7.9 Hz, 1H, H-12), 6.76 (d, ^{3}J = 8.4 Hz, 1H, H-13), 6.70 (d, ^{3}J = 7.5 Hz, 1H, H-11), 6.24 (dd, ^{3}J = 6.2 Hz, ^{3}J = 3.3 Hz, 1H, H-5), 5.90 (dd, ^{3}J = 6.3 Hz, ^{3}J = 3.5 Hz, 1H, H-6), 3.83 (s, 3H, H-16), 3.54 (m, 1H, H-4), 3.36 (dd,

^{3}J = 10.8 Hz, ^{3}J = 3.8 Hz, 1H, H-2), 3.23 (dddd, ^{3}J = 11.3 Hz, ^{3}J = 10.8 Hz, 1H, ^{3}J = 6.9 Hz, ^{3}J = 3.8 Hz, 1H, H-8), 2.99 (m, 1H, H-3), 2.79 (dd, ^{2}J = 15.0 Hz, ^{3}J = 6.9 Hz, 1H, H-9b), 2.67 (m, 1H, H-7), 2.45 (dd, ^{2}J = 15.0 Hz, ^{3}J = 11.3 Hz, 1H, H-9a), 1.15 (s, 9H, H-18).

^{13}C NMR(150.90 MHz, $CDCl_3$): δ = 202.2 (C-1), 157.1 (C-14), 145.5 (C-10), 137.0 (C-5), 133.4 (C-6), 133.0 (C-12), 125.4 (C-15), 120.1 (C-11), 109.7 (C-13), 84.0 (C-4), 73.6 (C-17), 55.9 (C-16), 52.8 (C-2), 50.7 (C-7), 48.5 (C-3), 36.7 (C-8), 31.6 (C-9), 28.4 (C-18).

HRMS (ESI-TOF) m/z: $[M+H]^+$ Calcd for $C_{20}H_{24}O_3H$ 313.1804; Found 313.1797.

IR (ATR, ṽ): 1694 cm^{-1} (s, *CO*), 1587 cm^{-1} (m).

***exo* [2+2] insertion product:**

^{1}H NMR(600.13 MHz, $CDCl_3$): δ = 7.32 (t, ^{3}J = 8.1 Hz, 1H, H-12), 6.79 (d, ^{3}J = 8.4 Hz, 1H, H-11), 6.77 (d, ^{3}J = 7.5 Hz, 1H, H-13), 6.09 (ddd, ^{3}J = 6.2 Hz, ^{3}J = 3.3 Hz, ^{4}J = 0.9 Hz, 1H, H-5), 6.08 (ddd, ^{3}J = 6.2 Hz, ^{3}J = 3.4 Hz, ^{4}J = 0.9 Hz, 1H, H-6), 3.86 (s, 3H, H-16), 3.67 (dd, ^{2}J = 15.3 Hz, ^{3}J = 11.3 Hz, 1H, H-9a), 3.55 (m, 1H, H-4), 3.46 (m, 1H, H-7), 2.73 (dd, ^{2}J = 15.0 Hz, ^{3}J = 7.5 Hz, 1H, H-9b), 2.48 (m, 1H, H-3), 2.34 (dm, ^{3}J = 10.7 Hz, 1H, H-2), 2.28 (dddm, ^{3}J = 11.3 Hz, ^{3}J = 10.3 Hz, ^{3}J = 7.5 Hz, 1H, H-8), 1.07 (s, 9H, H-18).

^{13}C NMR(150.90 MHz, $CDCl_3$): δ = 198.9 (C-1), 157.9 (C-14), 145.6 (C-10), 135.5 (C-5), 134.4 (C-6), 132.9 (C-12), 125.4 (C-15), 120.3 (C-13), 109.3 (C-11), 84.3 (C-4), 74.2 (C-17), 56.1 (C-16), 51.0 (C-2), 50.2 (C-3), 47.2 (C-7), 37.6 (C-8), 30.7 (C-9), 28.0 (C-18).

HRMS (ESI-TOF) m/z: $[M+H]^+$ Calcd for $C_{20}H_{24}O_3H$ 313.1804; Found 313.1801.

IR (ATR, ṽ): 1732 cm^{-1} (m, *CO*), 1681 cm^{-1} (m), 1664 cm^{-1} (m), 1590 cm^{-1} (m).

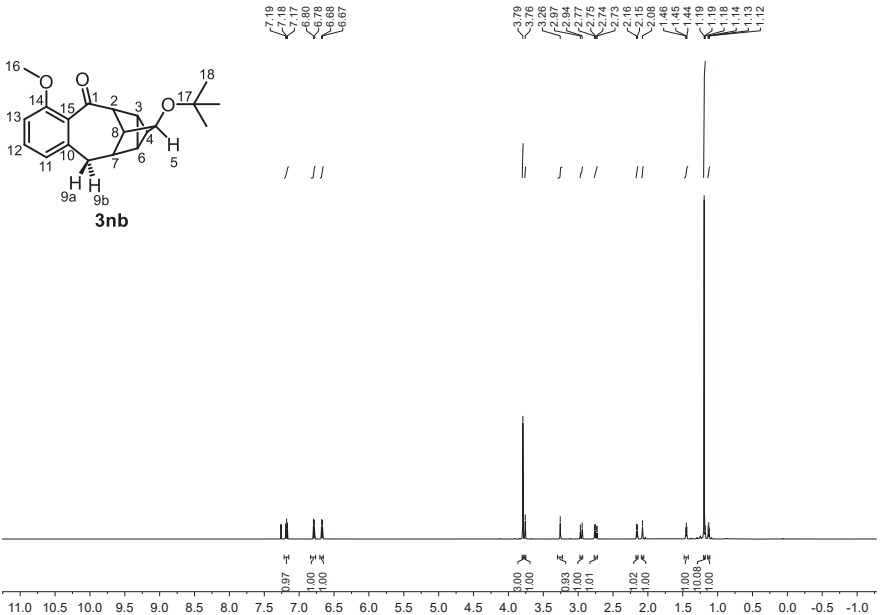

Figure S 188. ^{1}H NMR of **3nb** in $CDCl_3$ measured at 600.13 MHz.

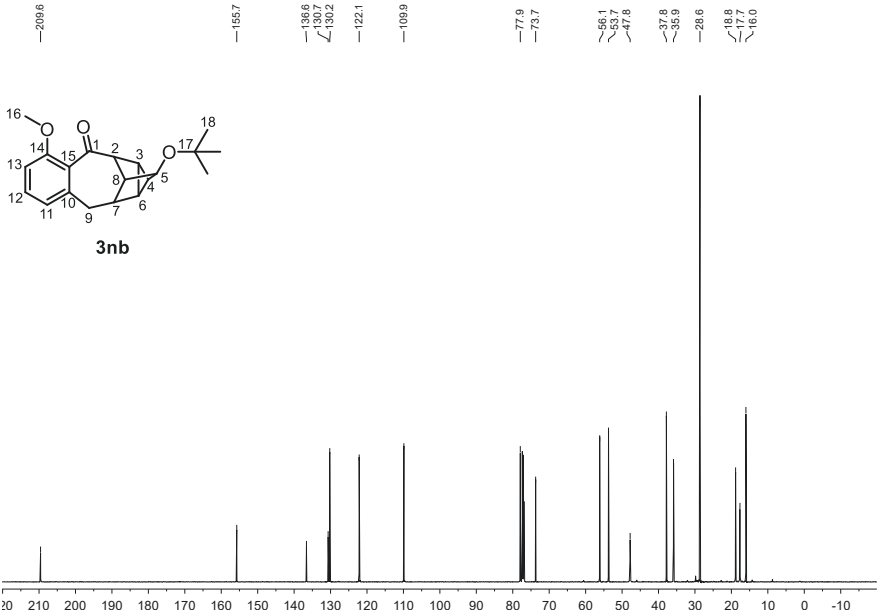

Figure S 189. ^{13}C NMR of **3nb** in $CDCl_3$ measured at 150.92 MHz.

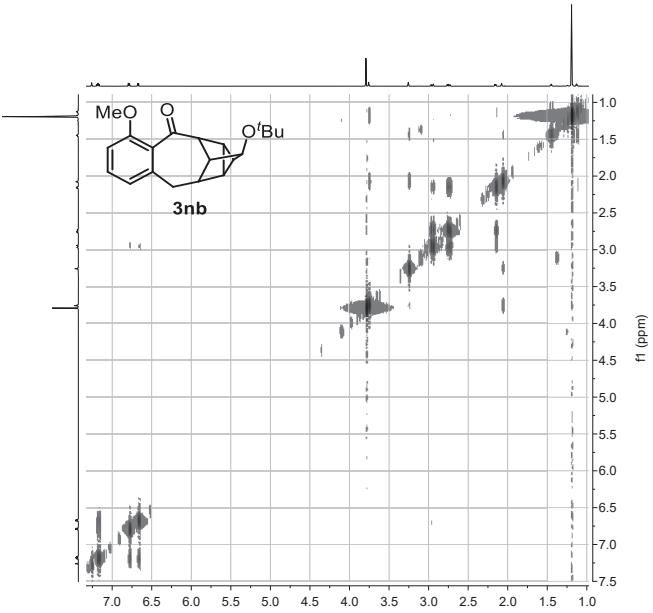

Figure S 190. $^{1}H,^{1}H$-COSY of **3nb** in $CDCl_3$ measured at 600.13 MHz.

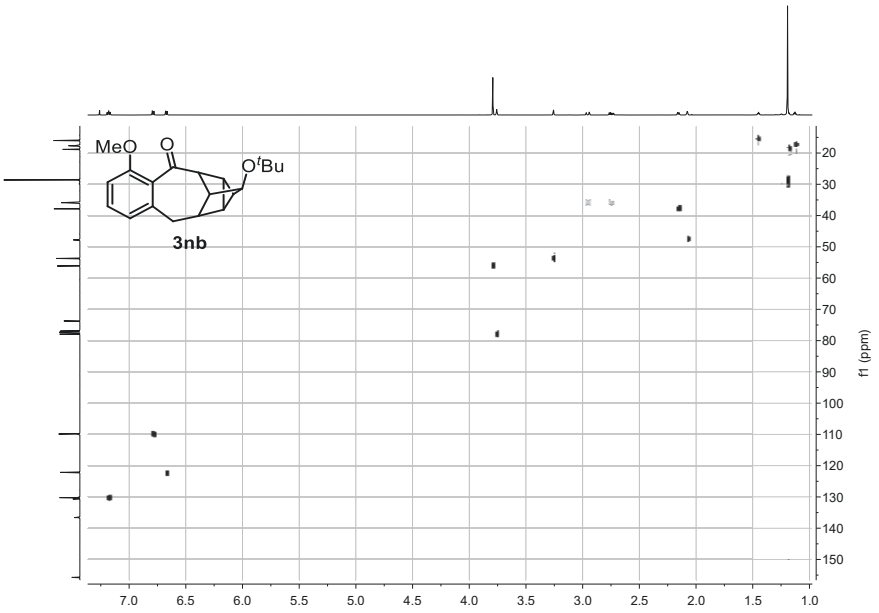

Figure S 191. $^{1}H,^{13}C$-HSQC of **3nb** in $CDCl_3$ measured at ^{1}H: 600.13 MHz; ^{13}C: 150.92 MHz.

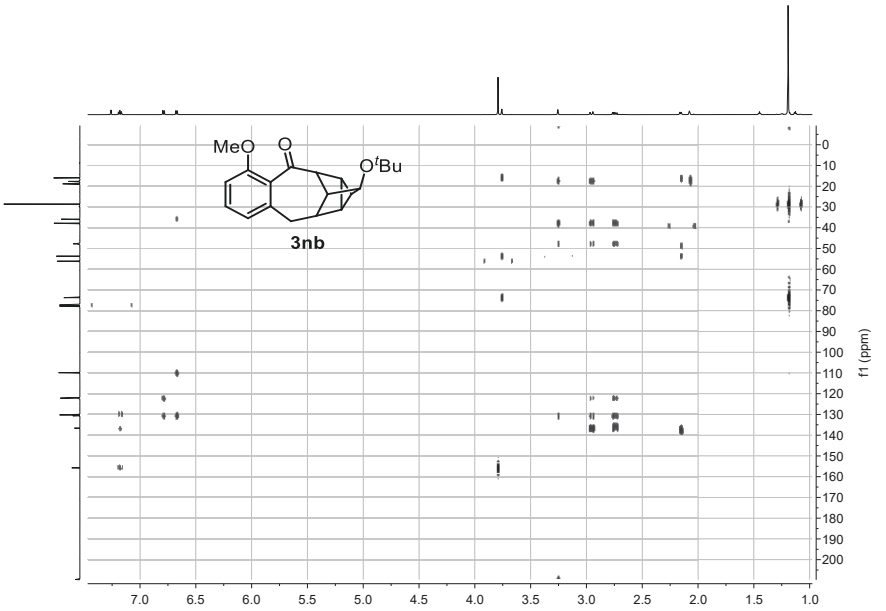

Figure S 192. $^{1}H,^{13}C$-HMBC of **3nb** in $CDCl_3$ measured at ^{1}H: 600.13 MHz; ^{13}C: 150.92 MHz.

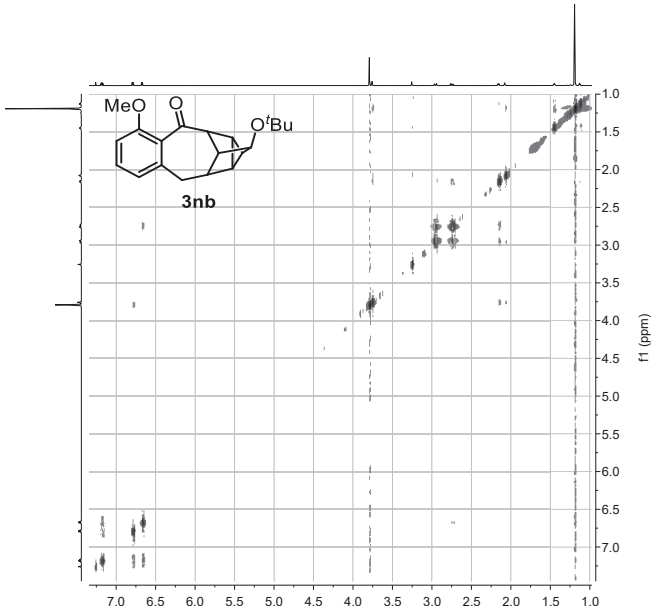

Figure S 193. $^{1}H,^{1}H$-NOESY of **3nb** in $CDCl_3$ measured at 600.13 MHz.

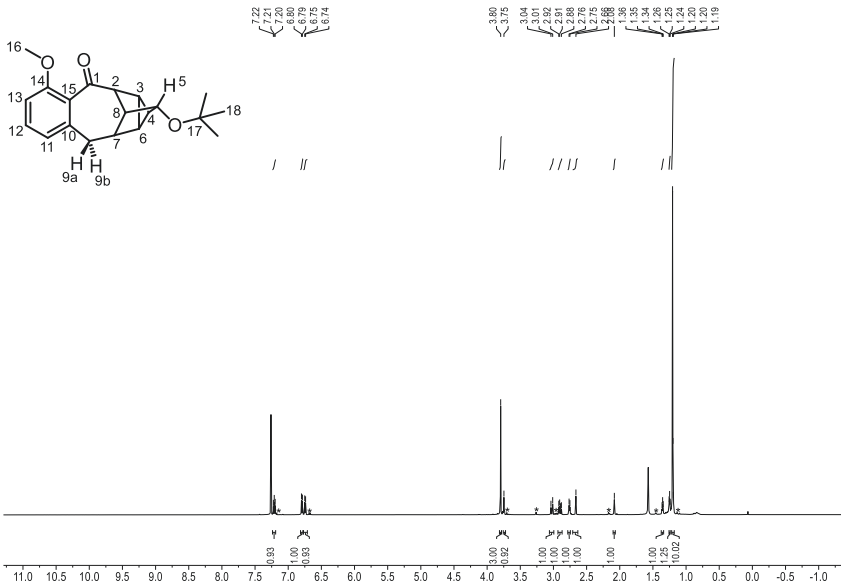

Figure S 194. ^{1}H NMR of the diastereomer (1*S*) of **3nb** in $CDCl_3$ measured at 600.13 MHz. * denotes signals of the *syn* diastereomer.

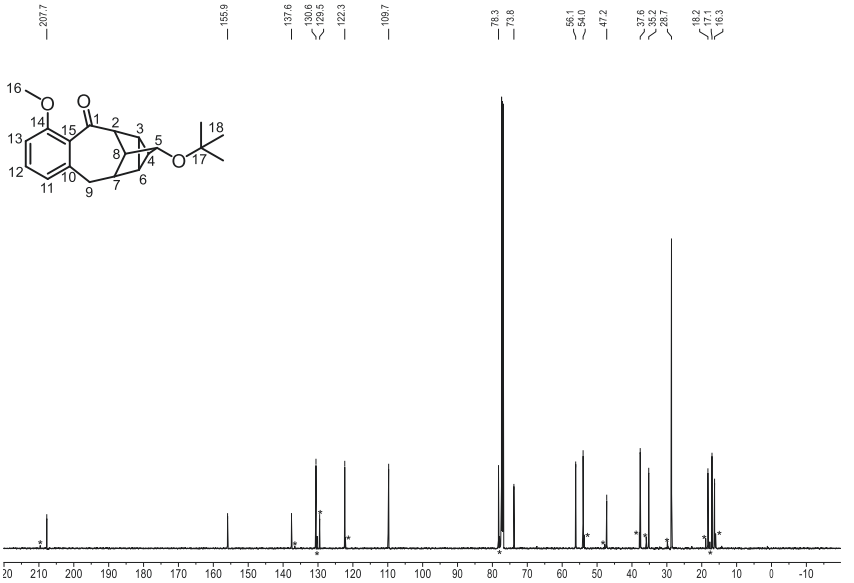

Figure S 195. ^{13}C NMR of the diastereomer (1*S*) of **3nb** in $CDCl_3$ measured at 150.92 MHz. * denotes signals of the *syn* diastereomer.

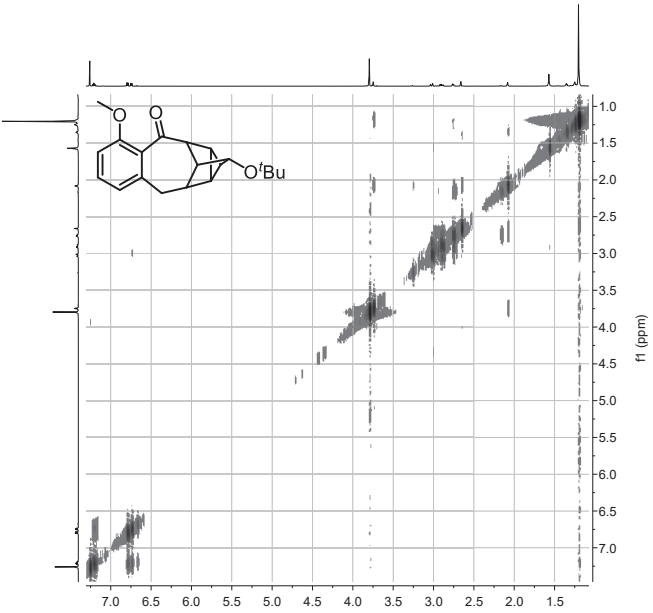

Figure S 196. ^{1}H,^{1}H-COSY of the diastereomer (1*S*) of **3nb** in $CDCl_3$ measured at 600.13 MHz

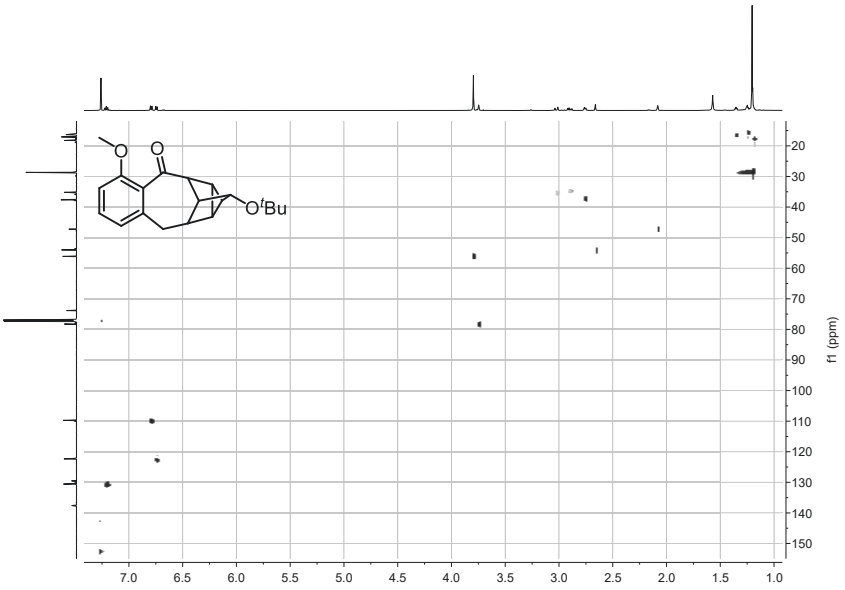

Figure S 197. ^{1}H,^{13}C-HSQC of the diastereomer (1*S*) of **3nb** in $CDCl_3$ measured at ^{1}H: 600.13 MHz; ^{13}C: 150.92 MHz.

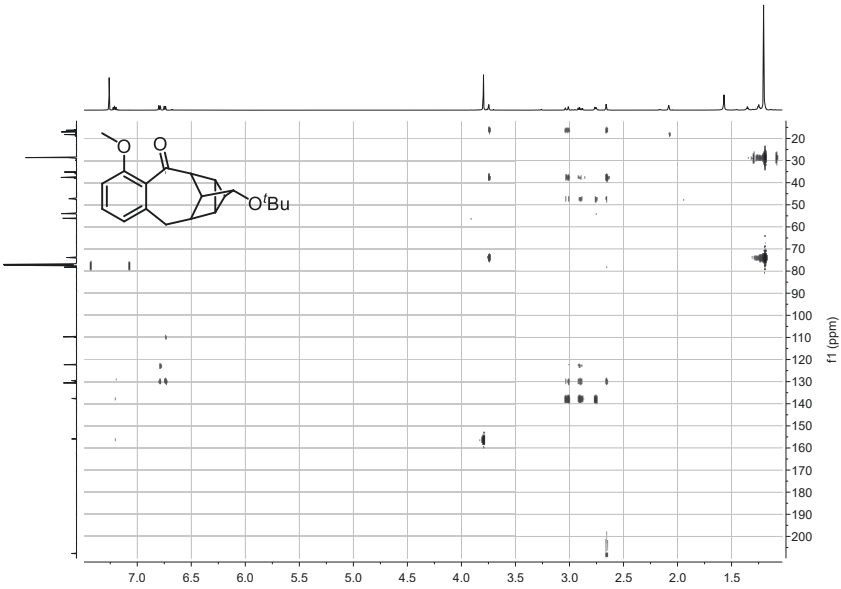

Figure S 198. ^{1}H,^{13}C-HMBC of the diastereomer (1*S*) of **3nb** in $CDCl_3$ measured at ^{1}H: 600.13 MHz; ^{13}C: 150.92 MHz.

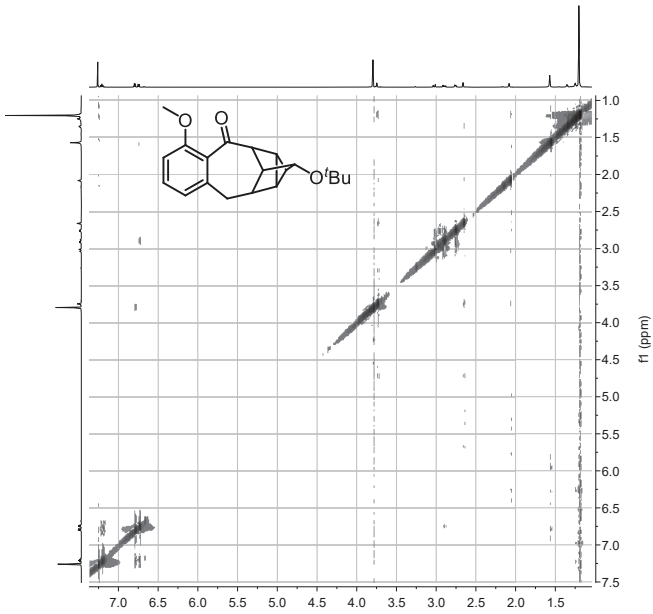

Figure S 199. ^{1}H,^{1}H-NOESY of the diastereomer (1*S*) of **3nb** in $CDCl_3$ measured at 600.13 MHz.

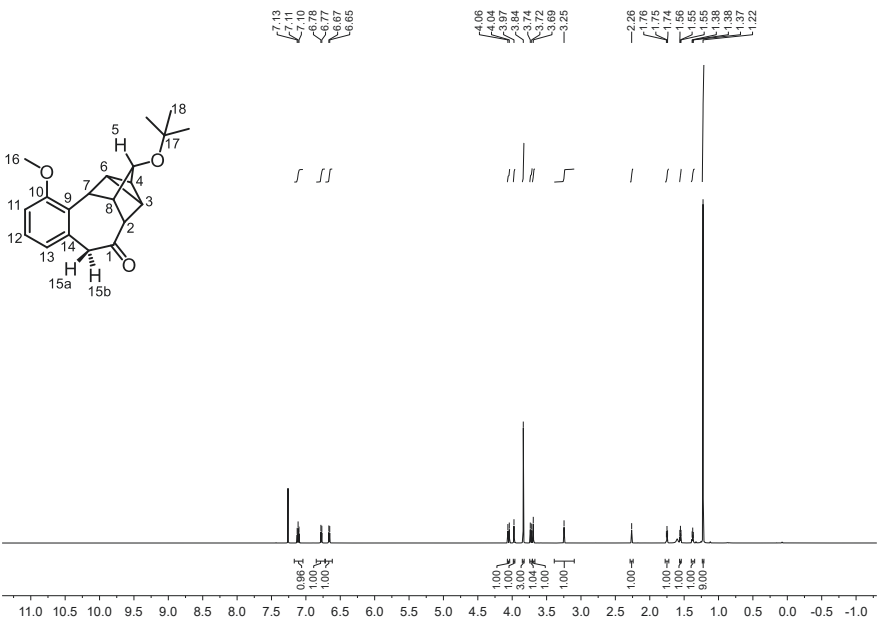

Figure S 200. ^{1}H NMR of the regioisomer of **3nb** in $CDCl_3$ measured at 600.13 MHz.

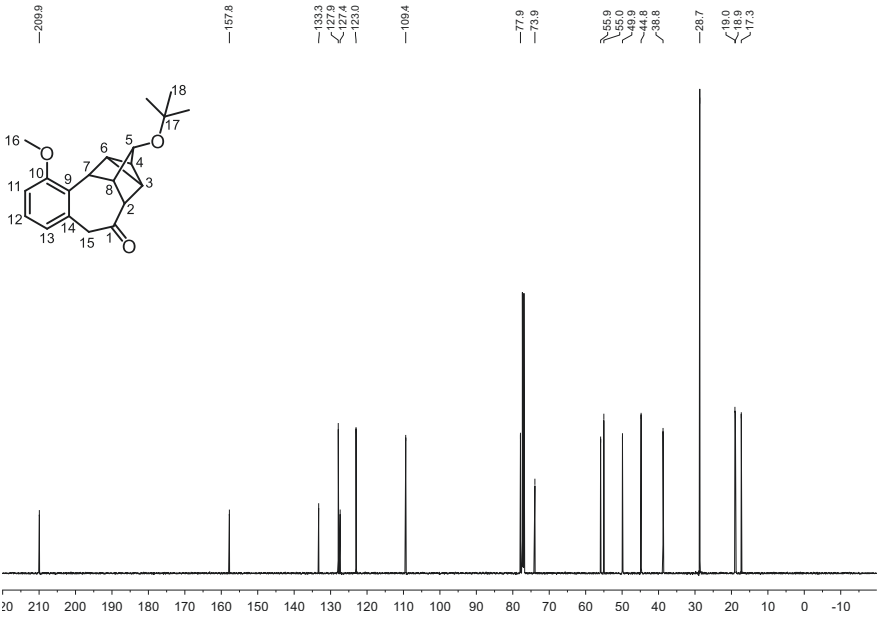

Figure S 201. ^{13}C NMR of the regioisomer of **3nb** in $CDCl_3$ measured at 150.92 MHz.

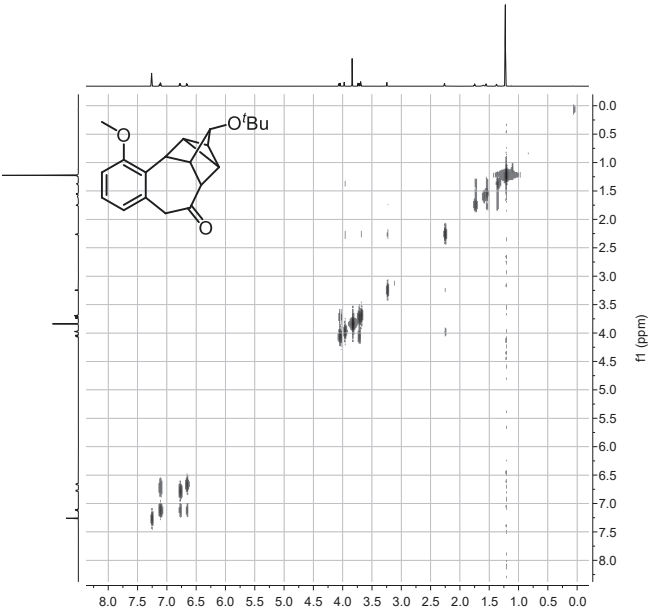

Figure S 202. ^{1}H,^{1}H-COSY of the regioisomer of **3nb** in $CDCl_3$ measured at 600.13 MHz.

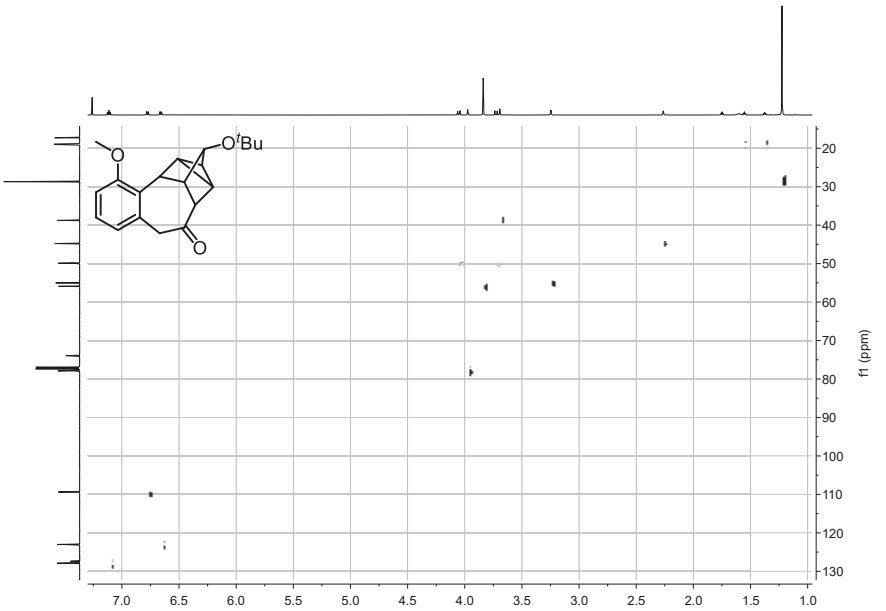

Figure S 203. ^{1}H,^{13}C-HSQC of the regioisomer of **3nb** in $CDCl_3$ measured at ^{1}H: 600.13 MHz; ^{13}C: 150.92 MHz.

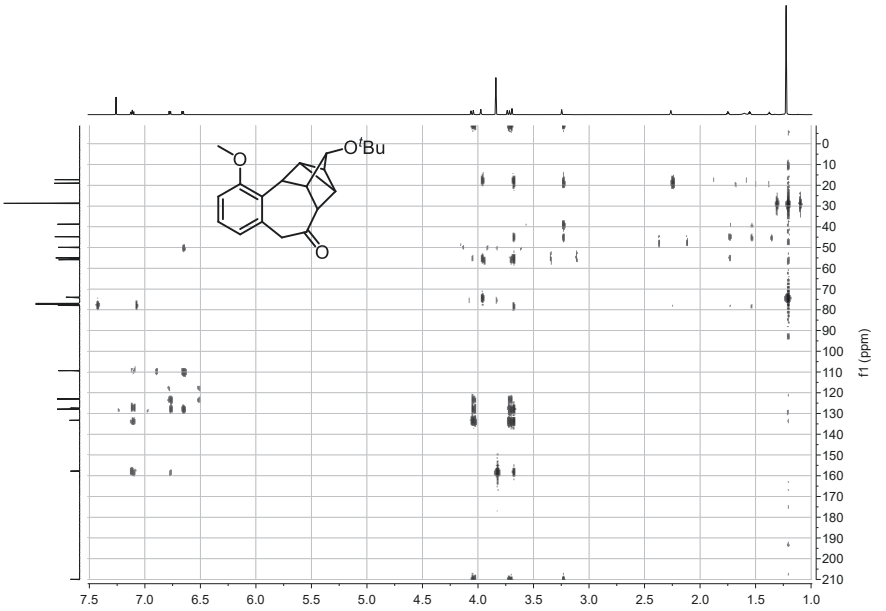

Figure S 204. $^{1}H,^{13}C$-HMBC of the regioisomer of **3nb** in $CDCl_3$ measured at ^{1}H: 600.13 MHz; ^{13}C: 150.92 MHz.

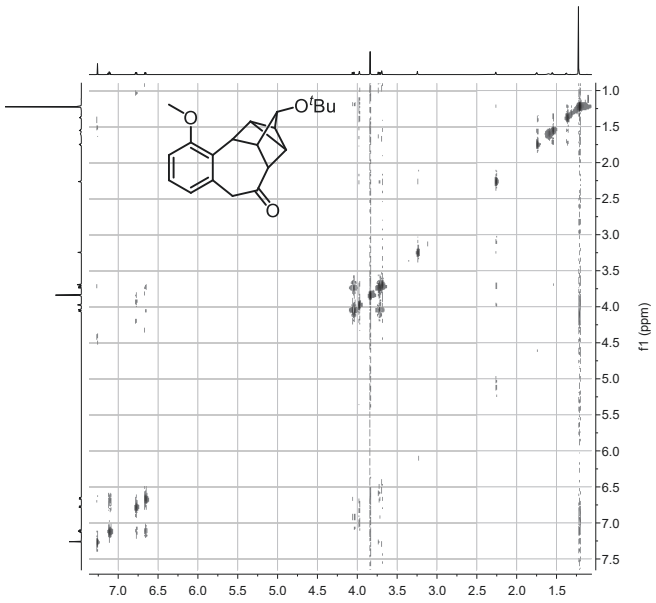

Figure S 205. $^{1}H,^{1}H$-NOESY of the regioisomer of **3nb** in $CDCl_3$ measured at 600.13 MHz.

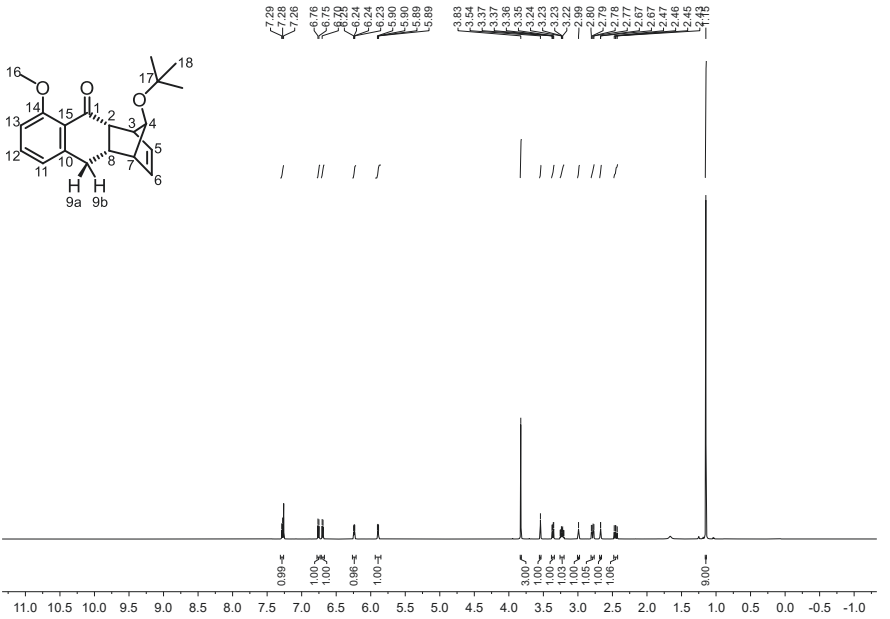

Figure S 206. ^{1}H NMR of the *endo* [2+2] insertion product of **3nb** in $CDCl_3$ measured at 600.13 MHz.

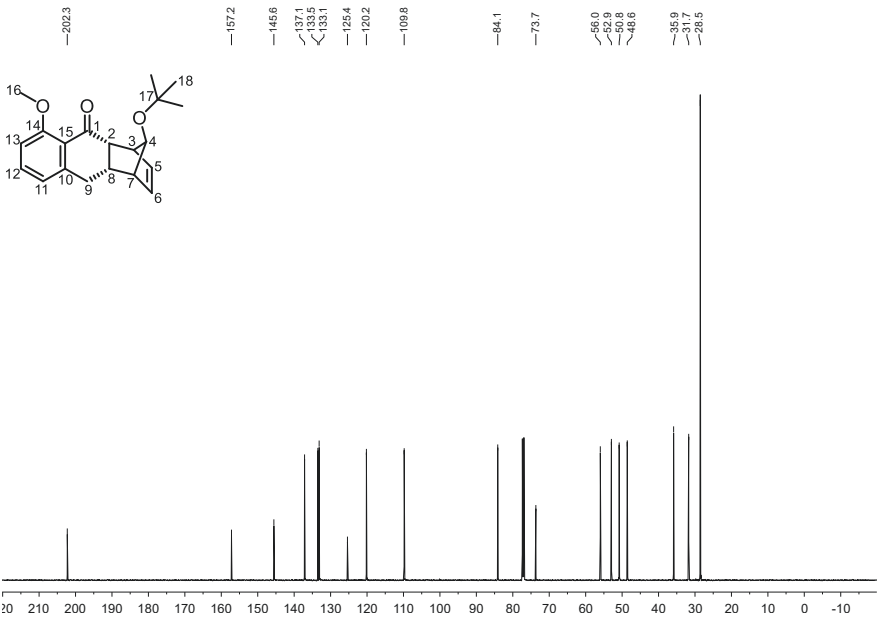

Figure S 207. ^{13}C NMR of the *endo* [2+2] insertion product of **3nb** in $CDCl_3$ measured at 150.92 MHz.

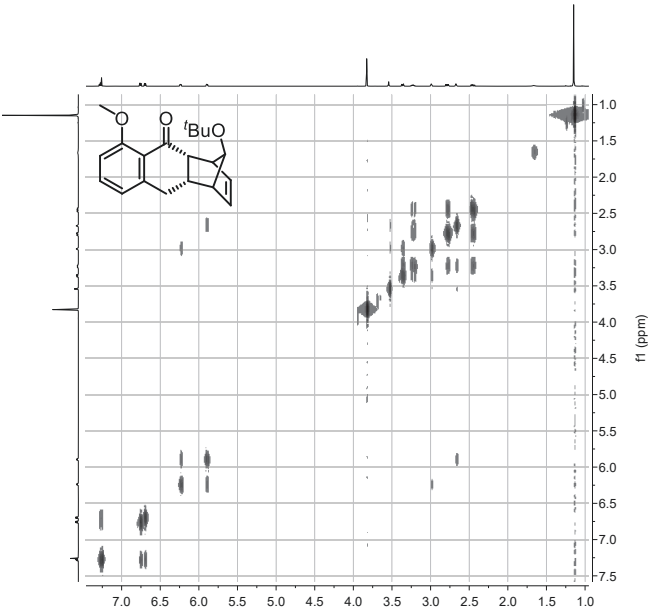

Figure S 208. ^{1}H,^{1}H-COSY of the *endo* [2+2] insertion product of **3nb** in $CDCl_3$ measured at 600.13 MHz.

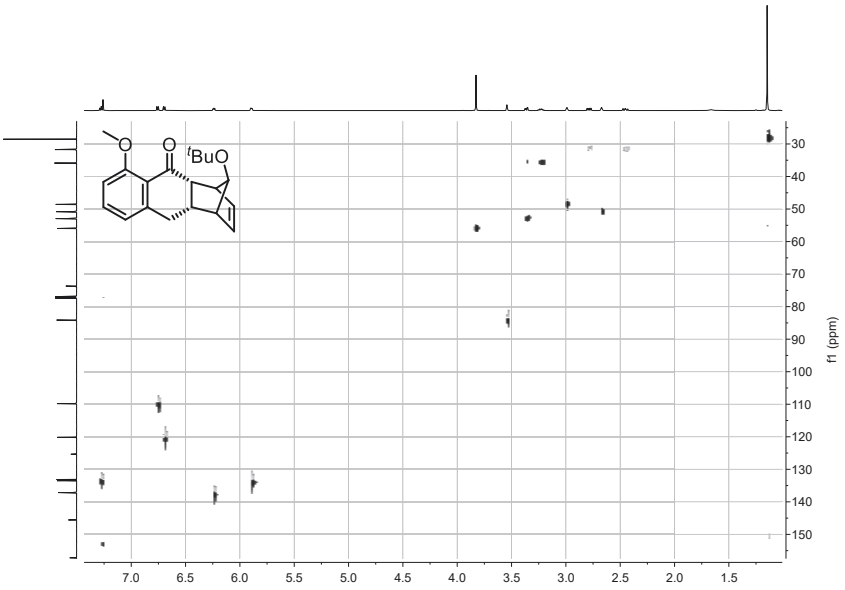

Figure S 209. ^{1}H,^{13}C-HSQC of the *endo* [2+2] insertion product of **3nb** in $CDCl_3$ measured at ^{1}H: 600.13 MHz; ^{13}C: 150.92 MHz.

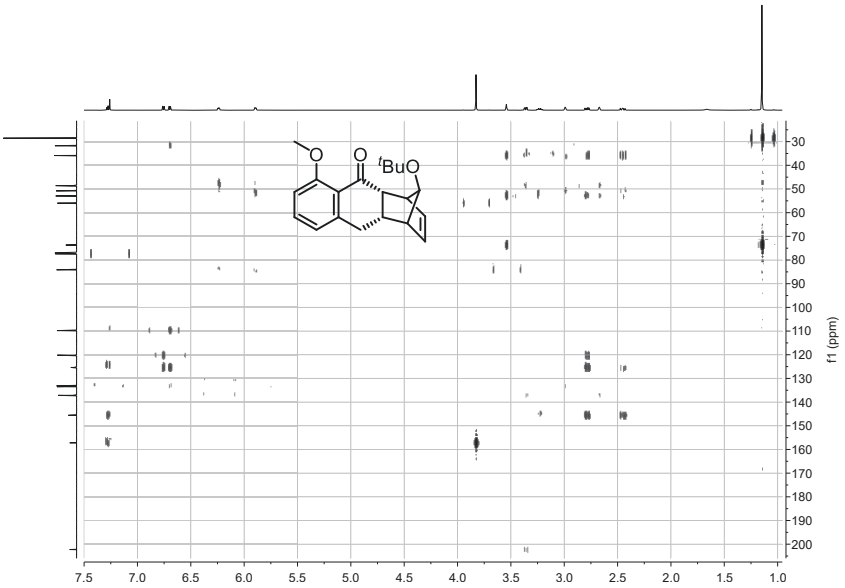

Figure S 210. $^{1}H,^{13}C$-HMBC of the *endo* [2+2] insertion product of **3nb** in $CDCl_3$ measured at ^{1}H: 600.13 MHz; ^{13}C: 150.92 MHz.

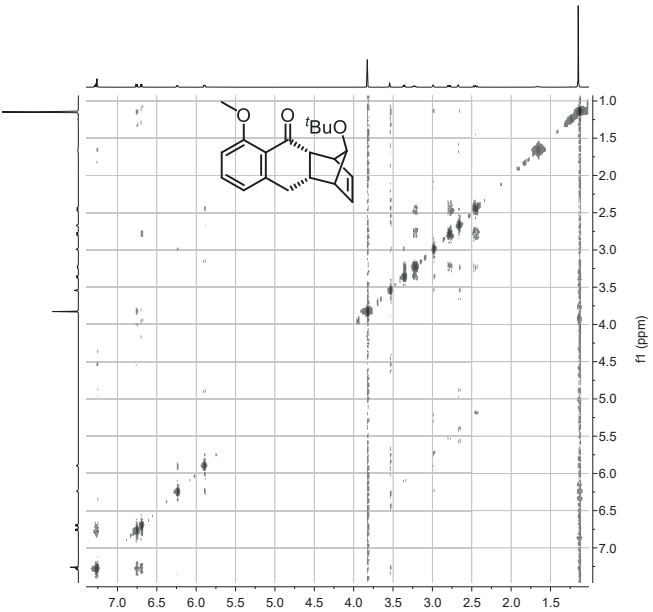

Figure S 211. $^{1}H,^{1}H$-NOESY of the *endo* [2+2] insertion product of **3nb** in $CDCl_3$ measured at 600.13 MHz.

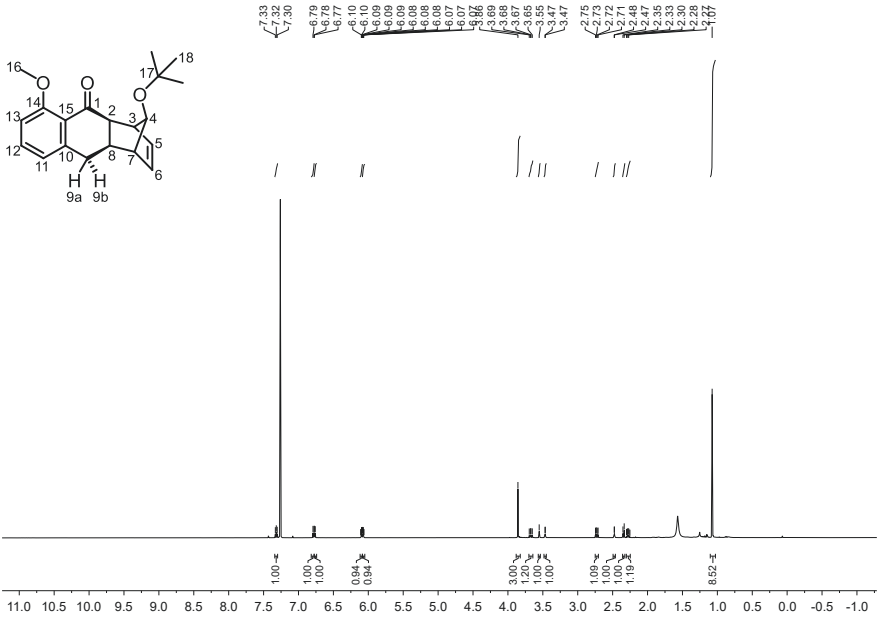

Figure S 212. ^{1}H NMR of the *exo* [2+2] insertion product of **3nb** in $CDCl_3$ measured at 600.13 MHz.

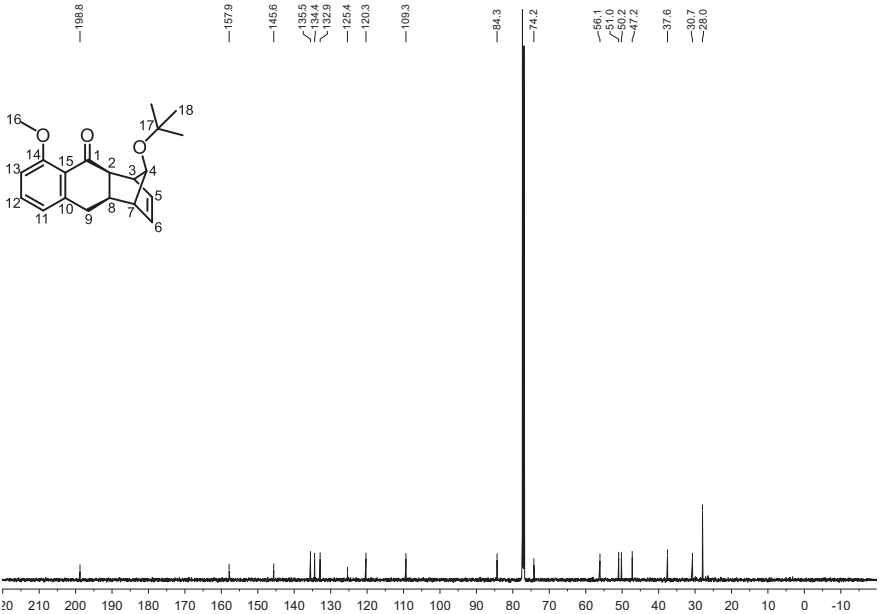

Figure S 213. ^{13}C NMR of the *exo* [2+2] insertion product of **3nb** in $CDCl_3$ measured at 150.92 MHz.

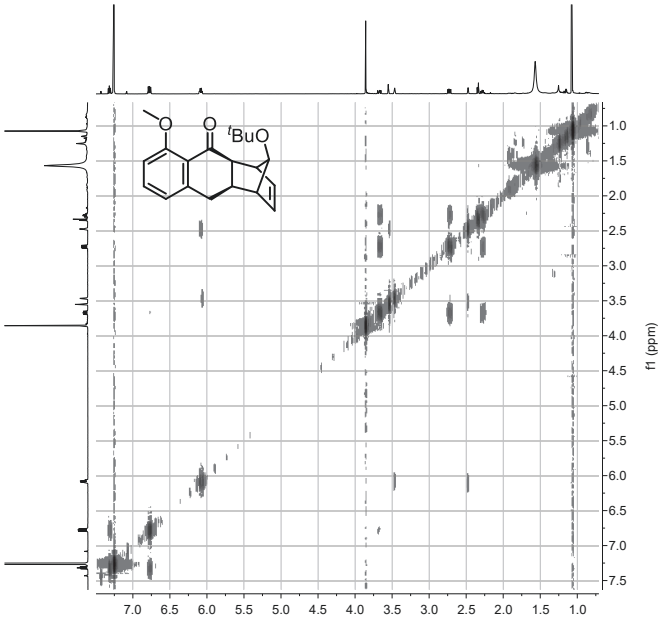

Figure S 214. ^{1}H,^{1}H-COSY of the *exo* [2+2] insertion product of **3nb** in $CDCl_3$ measured at 600.13 MHz.

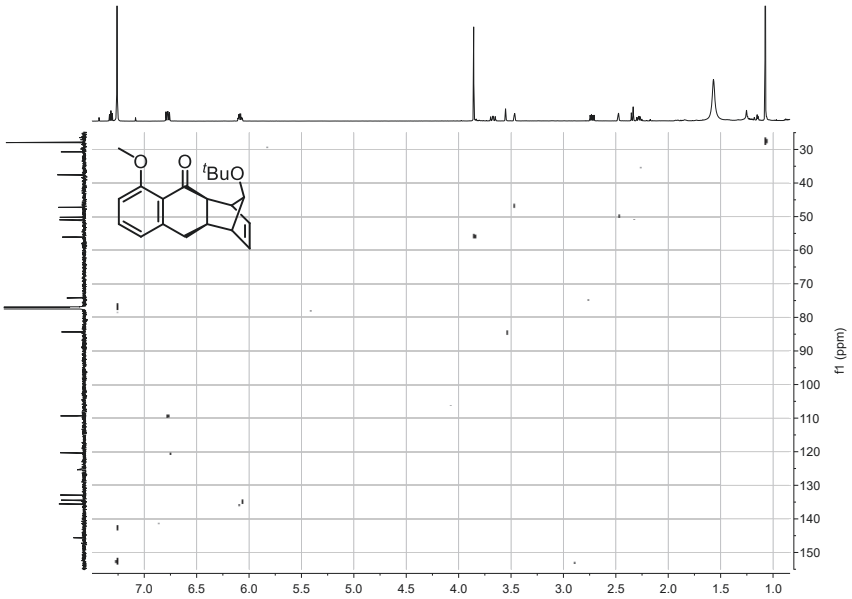

Figure S 215. ^{1}H,^{13}C-HSQC of the *exo* [2+2] insertion product of **3nb** in $CDCl_3$ measured at ^{1}H: 600.13 MHz; ^{13}C: 150.92 MHz.

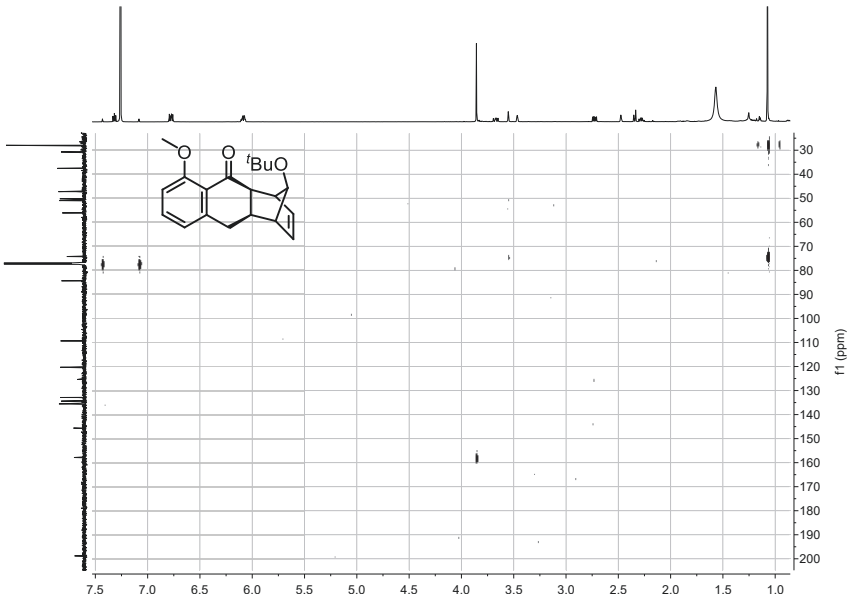

Figure S 216. $^{1}H,^{13}C$-HMBC of the *exo* [2+2] insertion product of **3nb** in $CDCl_3$ measured at ^{1}H: 600.13 MHz; ^{13}C: 150.92 MHz.

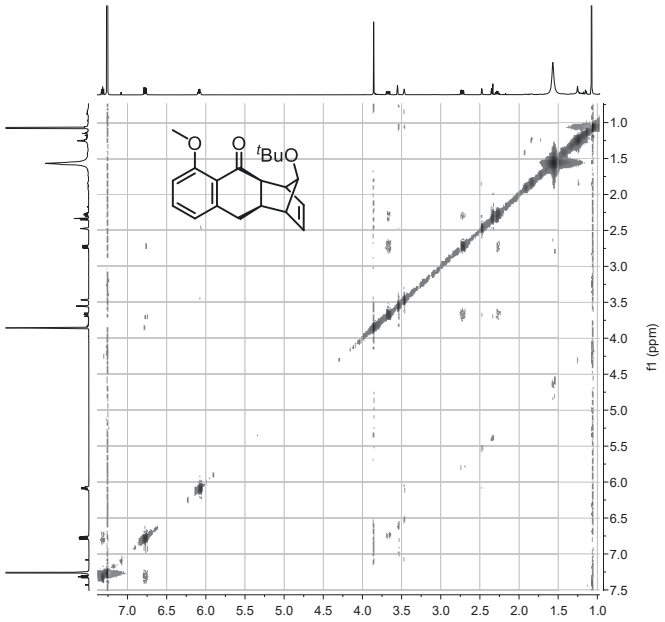

Figure S 217. $^{1}H,^{1}H$-NOESY of the *exo* [2+2] insertion product of **3nb** in $CDCl_3$ measured at 600.13 MHz.

4.6 Derivatisation products

***rel*-1*R*,2*R*,3,3a*S*,4*S*,9,10*S*,10a*R*,11*S*-octahydro-1,2,4-(epimethanetriyl)benzo[f]azulen-10-ol**

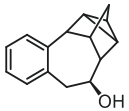

4

4 was synthesized according to a similar literature procedure.[23] $NaBH_4$ (22.7 mg, 600 µmol, 1.20 equiv.) was added to a solution of **3aa** (105 mg, 500 µmol, 1.0 equiv.) in MeOH (5 mL) at rt. The reaction was stirred overnight, quenched with H_2O (5 mL) and the organic phase was extracted with EA (3 × 5 mL). The combined organic phases were dried over Na_2SO_4 and the solvent was removed under reduced pressure. Purification *via* flash chromatography (23 g SiO_2, gradient from 100:00 to 50:50 *n*-hexane/EA over 15 CV) afforded **4** (94.6 mg, 446 µmol, 89%) as a colorless solid.

$C_{15}H_{16}O$ (212.29 $\frac{g}{mol}$)

mp: 103.6 °C.

R_f: 0.33 (*n*-hexane/EA = 80:20) [anisaldehyde]

^{1}H NMR(400.16 MHz, $CDCl_3$): δ = 7.17 (m, 1H, H-10), 7.13 (m, 2H, H-11/H-12), 7.10 (m, 1H, H-13), 4.24 (m, 1H, H-1), 3.59 (dm, ^2J = 14.9 Hz, 1H, H-15b), 2.73 (dd, ^2J = 14.9 Hz, ^3J = 5.7 Hz, 1H, H-15a), 2.69 (m, 1H, H-7), 2.29 (dm, ^3J = 6.2 Hz, 1H, H-2), 1.99 (m, 1H, H-8), 1.52 (dm, ^2J = 10.3 Hz, 1H, H-5a), 1.39 (dm, ^2J = 10.3 Hz, 1H, H-5b), 1.36 (m, 1H, H-4), 1.29 (m, 1H, H-6), 1.28 (m, 1H, H-3).

^{13}C NMR(100.62 MHz, $CDCl_3$): δ = 142.1 (C-9), 135.9 (C-14), 132.4 (C-13), 131.0 (C-10), 126.9 (C-11/C-12), 126.6 (C-12/C-11), 68.9 (C-1), 53.2 (C-7), 50.8 (C-2), 39.8 (C-15), 35.9 (C-5), 35.1 (C-8), 16.2 (C-3), 13.6 (C-6), 12.9 (C-4).

HRMS (ESI-TOF) m/z: $[M+Na]^+$ Calcd for $C_{15}H_{16}ONa$ 235.1093; Found 235.1093.

IR (ATR, ṽ): 3313 cm^{-1} (w, *OH*).

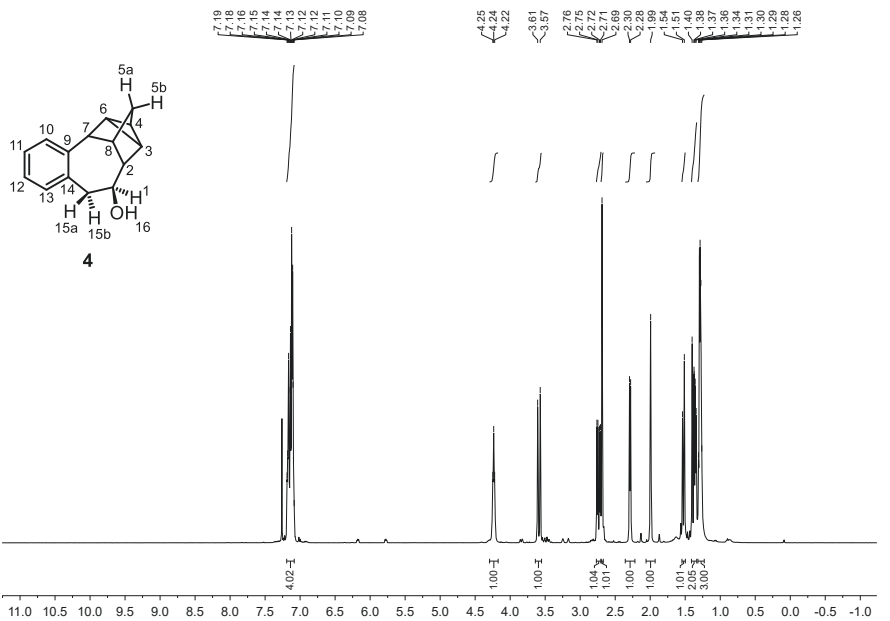

Figure S 218. ^{1}H NMR of **4** in $CDCl_3$ measured at 400.16 MHz.

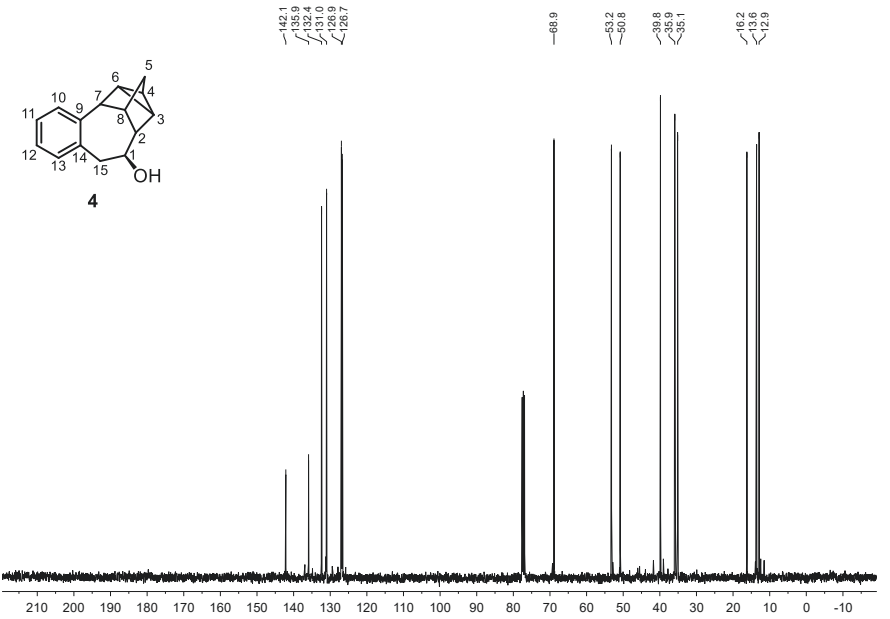

Figure S 219. ^{13}C NMR of **4** in $CDCl_3$ measured at 100.63 MHz.

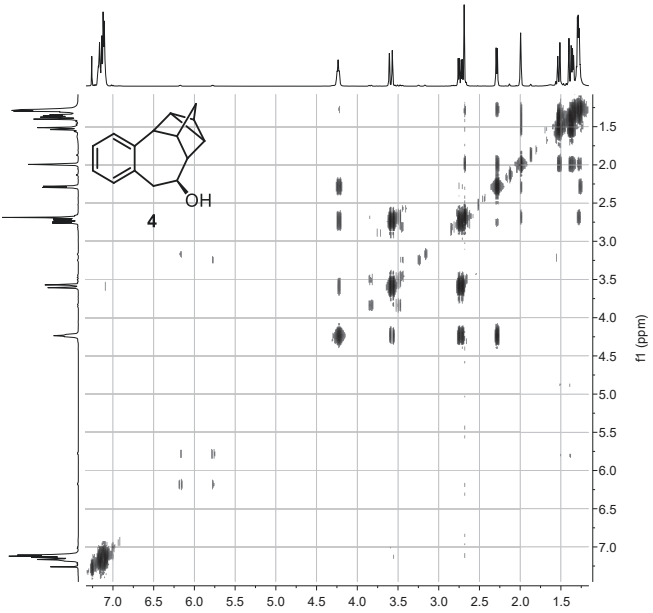

Figure S 220. $^{1}H,^{1}H$-COSY of **4** in $CDCl_3$ measured at 400.16 MHz.

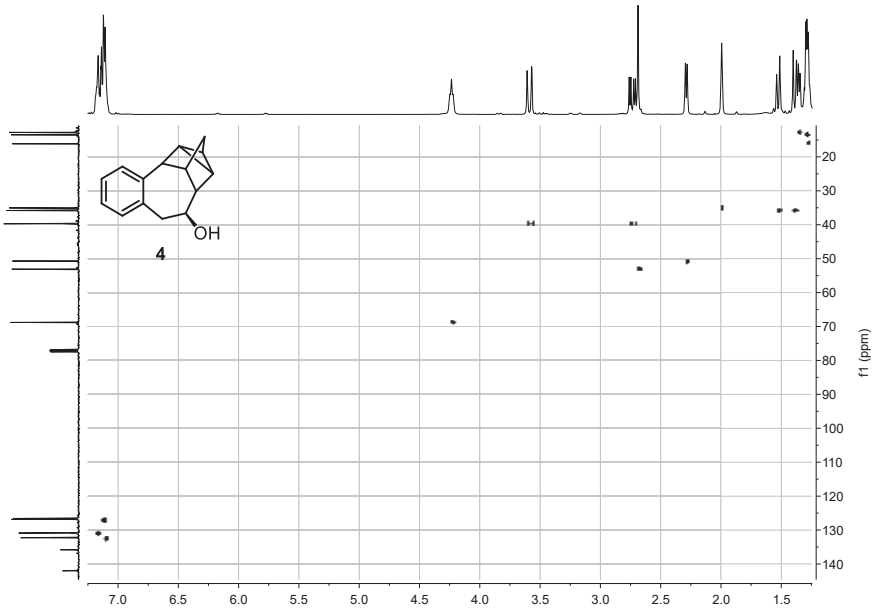

Figure S 221. $^{1}H,^{13}C$-HSQC of **4** in $CDCl_3$ measured at ^{1}H: 400.16 MHz; ^{13}C: 100.63 MHz.

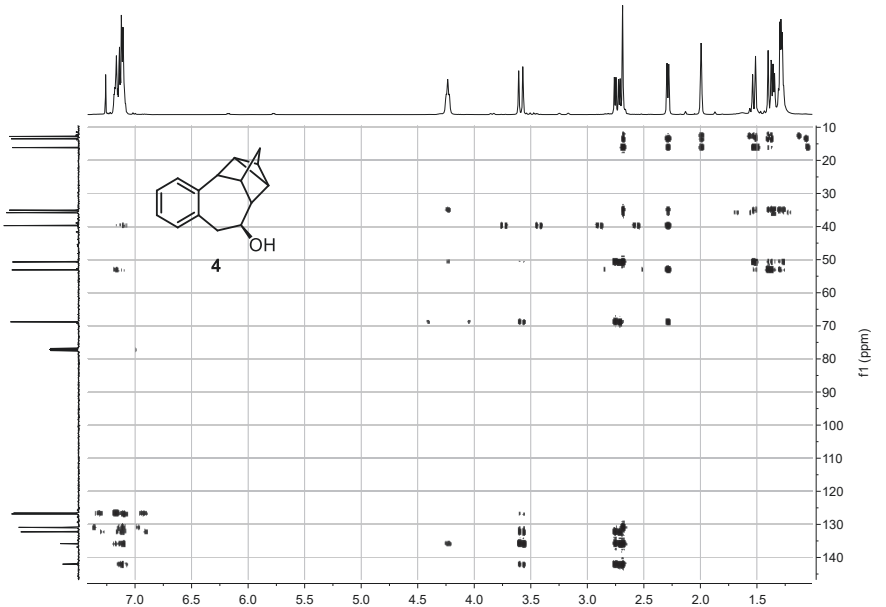

Figure S 222. $^{1}H,^{13}C$-HMBC of **4** in $CDCl_3$ measured at ^{1}H: 400.16 MHz; ^{13}C: 100.63 MHz.

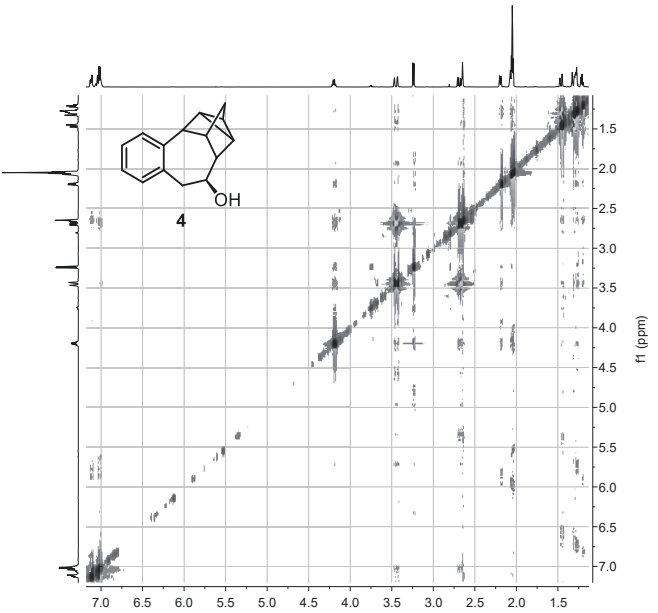

Figure S 223. $^{1}H,^{1}H$-NOESY of **4** in acetone-d6 measured at 400.16 MHz.

***rel*-1*R*,2*S*,2'*R*,3',3a'*S*,4'*S*,9',10a'*S*,11*S*-hexahydro-1'H-spiro[oxirane-2,10'-[1,2,4](epimethanetriyl)benzo[f]azulene]**

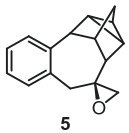

5

5 was synthesized according to a similar literature procedure with slight modifications.[24] In a dried Schlenk tube, a solution of **3aa** (105 mg, 500 µmol, 1.0 equiv.) in dry DMSO/THF (3 mL/1 mL) was slowly added to a cooled (0 °C) solution of NaH (36.0 mg, 1.50 mmol, 3.00 equiv.) in dry THF (1 mL). The reaction was allowed to warm to rt and stirred for 3 h, after which H_2O (5 mL) was added. The aqueous phase was extracted with EA (3 × 5 mL) and the combined organic extracts were washed with brine (3 × 5 mL), dried over $MgSO_4$ and the solvent was removed under reduced pressure. The crude product was recrystallized from *n*-hexane/toluene (98/2) furnishing **5** (91.3 mg, 407 µmol, 81%) as a colorless solid.

*Note: **5** decomposes in contact with silica.*

$C_{16}H_{16}O$ (224.30 $\frac{g}{mol}$)

mp: 102.6 °C.

^{1}H NMR(400.16 MHz, $CDCl_3$): δ = 7.19 (dm, ^3J = 7.1 Hz, 1H, H-10), 7.13 (m, 2H, H-11, H-12), 7.00 (d, ^3J = 6.7 Hz, 1H, H-13), 3.92 (d, ^2J = 15.0 Hz, 1H, H-15b), 2.78 (m, 1H, H-7), 2.77 (d, ^2J = 5.2 Hz, 1H, H-16a), 2.72 (d, ^2J = 5.2 Hz, 1H, H-16b), 2.15 (d, ^2J = 15.0 Hz, 1H, H-15a), 2.12 (m, 1H, H-8), 1.63 (m, 1H, H-2), 1.52 (dm, ^2J = 10.6 Hz, 1H, H-5a), 1.46 (m, 1H, H-3), 1.41 (m, 1H, H-6), 1.38 (dm, ^2J = 10.6 Hz, 1H, H-5b), 1.37 (m, 1H, H-4).

^{13}C NMR(100.62 MHz, $CDCl_3$): δ = 140.8 (C-9), 136.4 (C-14), 131.0 (C-10), 130.8 (C-13), 126.6 (C-11, C-12), 58.3 (C-1), 57.8 (C-16), 52.9 (C-7), 51.5 (C-2), 40.2 (C-15), 37.8 (C-8), 35.4 (C-5), 16.2 (C-3), 14.2 (C-6), 12.6 (C-4).

HRMS (ESI-TOF) m/z: $[M+Na]^+$ Calcd for $C_{16}H_{16}ONa$ 247.1093; Found 247.1093.

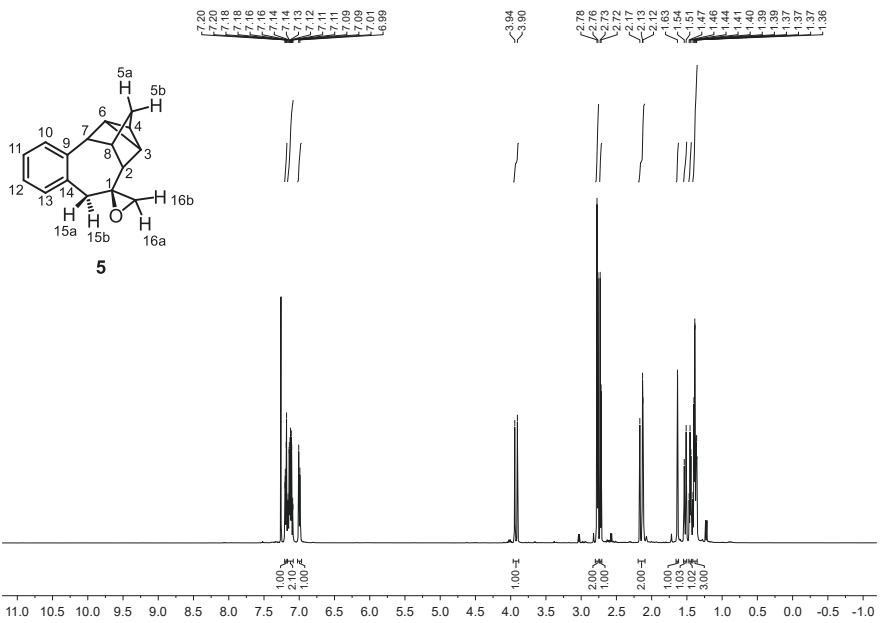

Figure S 224. ^{1}H NMR of **5** in $CDCl_3$ measured at 400.16 MHz.

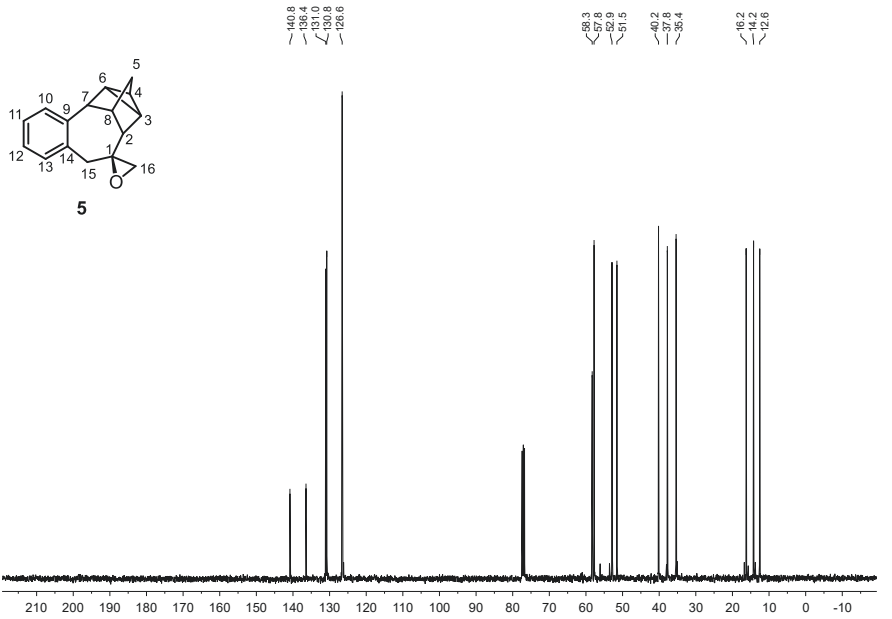

Figure S 225. ^{13}C NMR of **5** in $CDCl_3$ measured at 100.63 MHz.

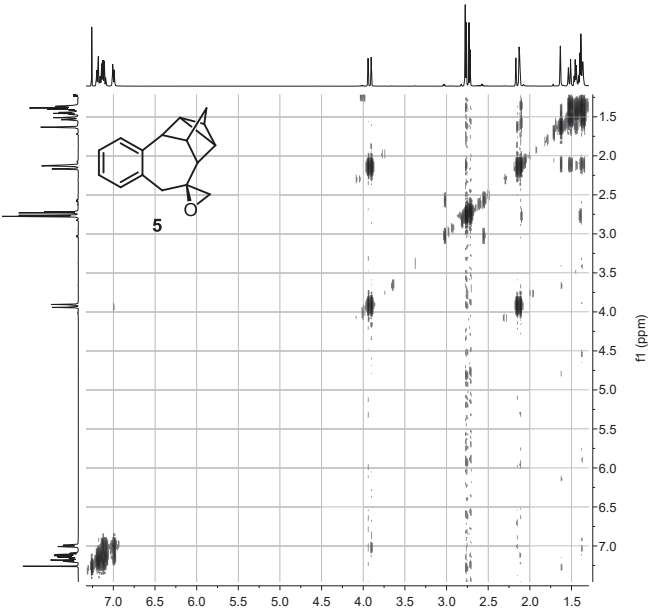

Figure S 226. $^{1}H,^{1}H$-COSY of **5** in $CDCl_3$ measured at 400.16 MHz.

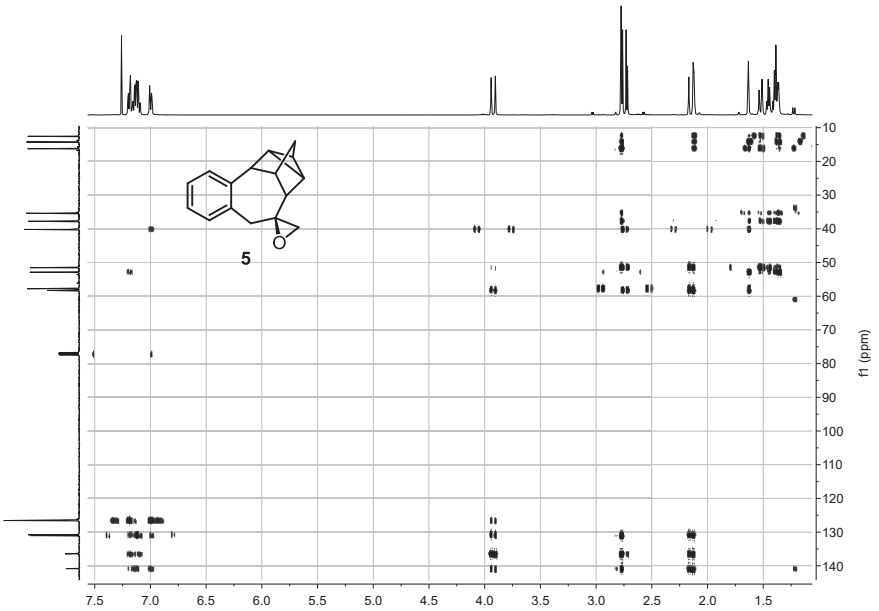

Figure S 227. $^{1}H,^{13}C$-HSQC of **5** in $CDCl_3$ measured at ^{1}H: 400.16 MHz; ^{13}C: 100.63 MHz.

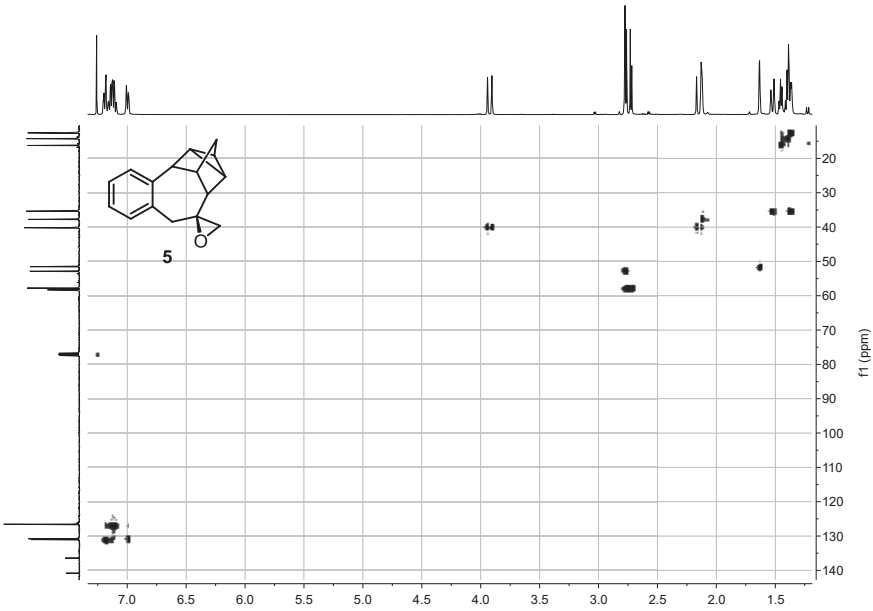

Figure S 228. $^{1}H,^{13}C$-HMBC of **5** in $CDCl_3$ measured at ^{1}H: 400.16 MHz; ^{13}C: 100.63 MHz.

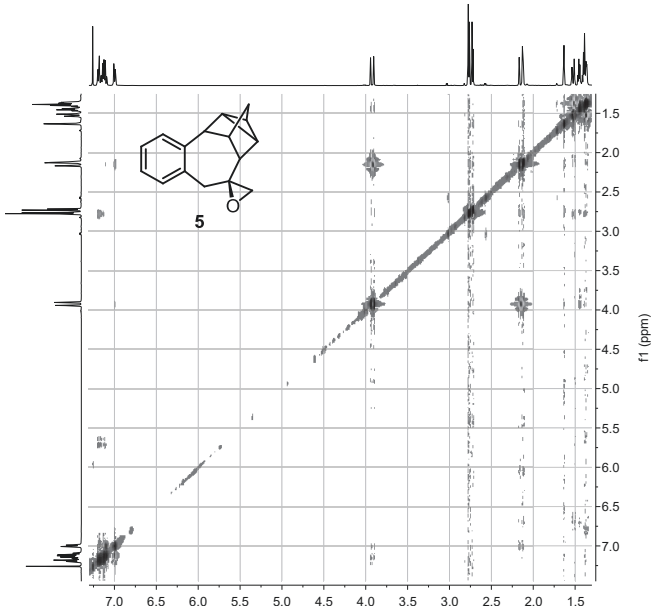

Figure S 229. $^{1}H,^{1}H$-NOESY of **5** in $CDCl_3$ measured at 400.16 MHz.

***rel*-10-phenyl-1*R*,2*R*,3,3a*S*,4*S*,9,10*S*,10a*R*,11*S*-octahydro-1,2,4-(epimethanetriyl)benzo[f]azulen-10-ol**

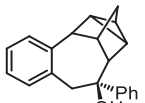

6

In a dried Schlenk tube, PhMgBr (750 µL, 1.00 M, 1.50 equiv.) was added to a solution of **3aa** (105 mg, 500 µmol, 1.0 equiv.) in THF (4 mL). The reaction was stirred for 4 h, after which sat. $NH_4Cl_{(aq.)}$ (2 mL) was added. The aqueous phase was extracted with EA (3 × 5 mL) and the combined organic phases were dried over Na_2SO_4. The solvent was removed *in vacuo*. Purification *via* flash chromatography (23 g SiO_2, gradient from 100:00 to 50:50 *n*-hexane/EA over 15 CV) afforded **5** (93.2 mg, 323 µmol, 65%) as a colorless solid.

$C_{21}H_{20}O$ (288.39 $\frac{g}{mol}$)

mp: 145.3 °C.

Rf: 0.70 (*n*-hexane/EA = 80:20) [anisaldehyde]

^{1}H NMR(600.13 MHz, $CDCl_3$): δ = 7.69 (d, ^3J = 7.7 Hz, 2H, H-17), 7.41 (m, 2H, H-18), 7.31 (m, 1H, H-19), 7.25 (dd, ^3J = 7.5 Hz, ^4J = 1.1 Hz, 1H, H-10), 7.21 (m, 1H, H-11), 7.17 (m, 1H, H-12), 7.11 (d, ^3J = 7.2 Hz, 1H, H-13), 4.26 (d, ^2J = 14.4 Hz, 1H, H-15b), 2.82 (d, ^2J = 14.4 Hz, 1H, H-15a), 2.79 (m, 1H, H-7), 2.21 (m, 1H, H-2), 2.13 (m, 1H, H-8), 1.63 (s, 1H, H-20), 1.55 (dm, ^2J = 10.5 Hz, 1H, H-5a), 1.41 (m, 1H, H-3), 1.37 (dm, ^2J = 10.5 Hz, 1H, H-5b), 1.37 (m, 1H, H-6), 1.32 (m, 1H, H-4).

^{13}C NMR(100.62 MHz, $CDCl_3$): δ = 150.1 (C-16), 141.9 (C-9), 135.5 (C-14), 132.6 (C-13), 131.1 (C-10), 128.3 (C-18), 127.2 (C-11), 126.9 (C-12), 126.9 (C-19), 125.0 (C-17), 73.5 (C-1), 58.0 (C-2), 53.1 (C-7), 44.8 (C-15), 36.9 (C-8), 35.8 (C-5), 16.0 (C-3), 13.4 (C-6), 13.1 (C-4).

HRMS (ESI-TOF) m/z: $[M+Na]^+$ Calcd for $C_{21}H_{20}ONa$ 311.1406; Found 311.1406.

IR (ATR, ṽ): 3577 cm^{-1} (w, *OH*).

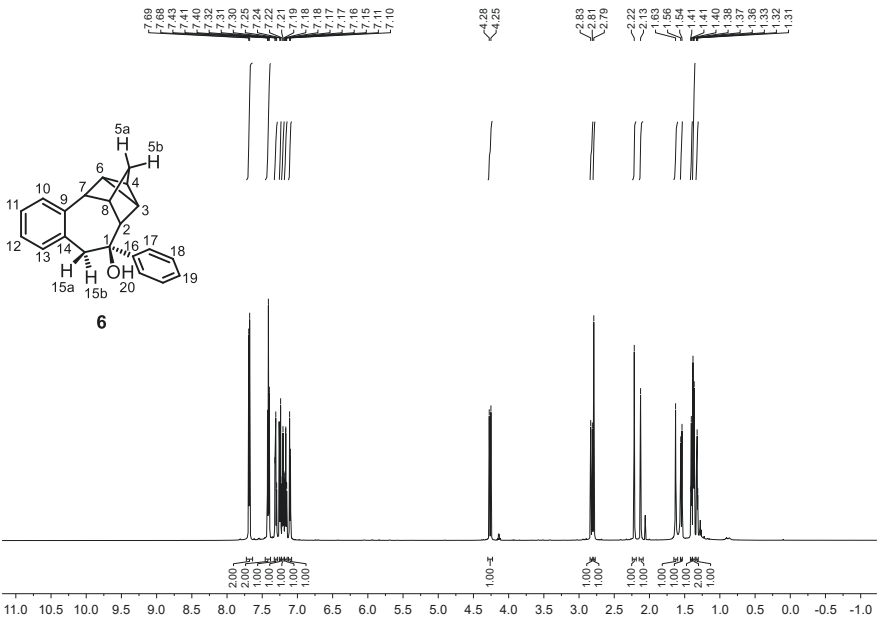

Figure S 230. ^{1}H NMR of **6** in $CDCl_3$ measured at 400.16 MHz.

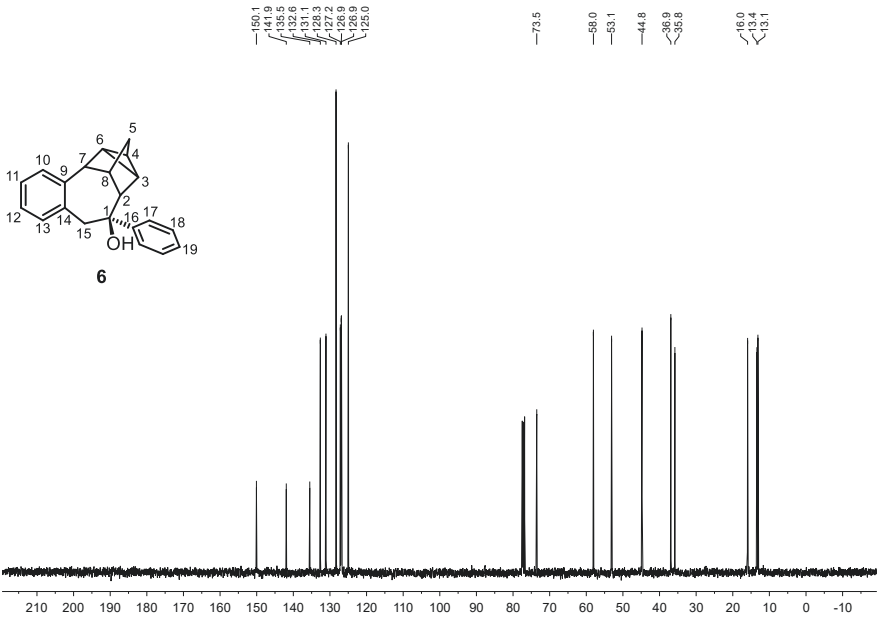

Figure S 231. ^{13}C NMR of **6** in $CDCl_3$ measured at 100.63 MHz.

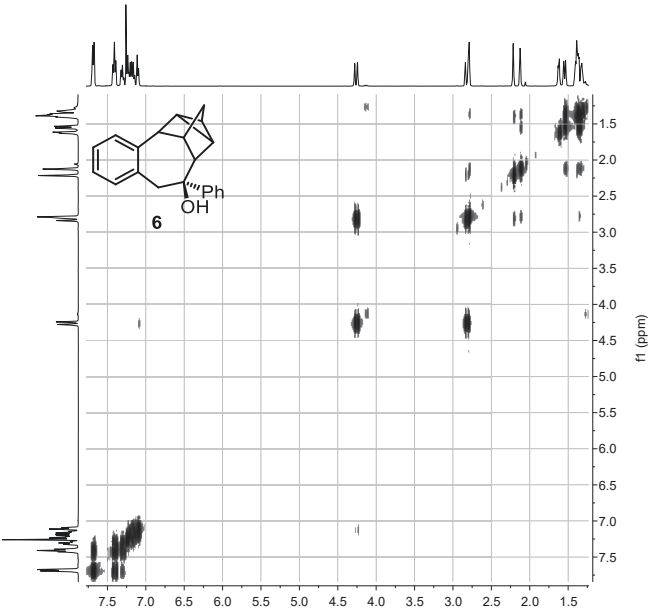

Figure S 232. $^{1}H,^{1}H$-COSY of **6** in $CDCl_3$ measured at 400.16 MHz.

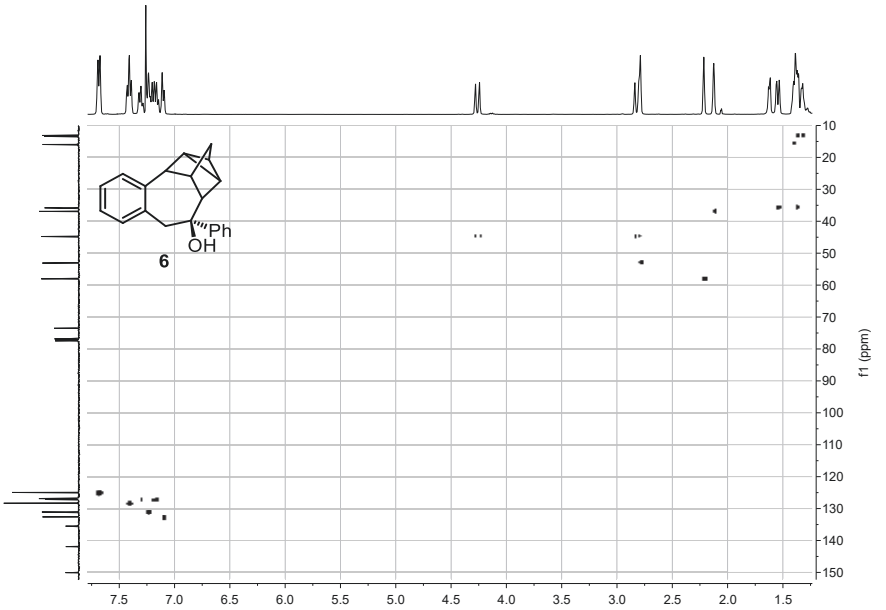

Figure S 233. $^{1}H,^{13}C$-HSQC of **6** in $CDCl_3$ measured at ^{1}H: 400.16 MHz; ^{13}C: 100.63 MHz.

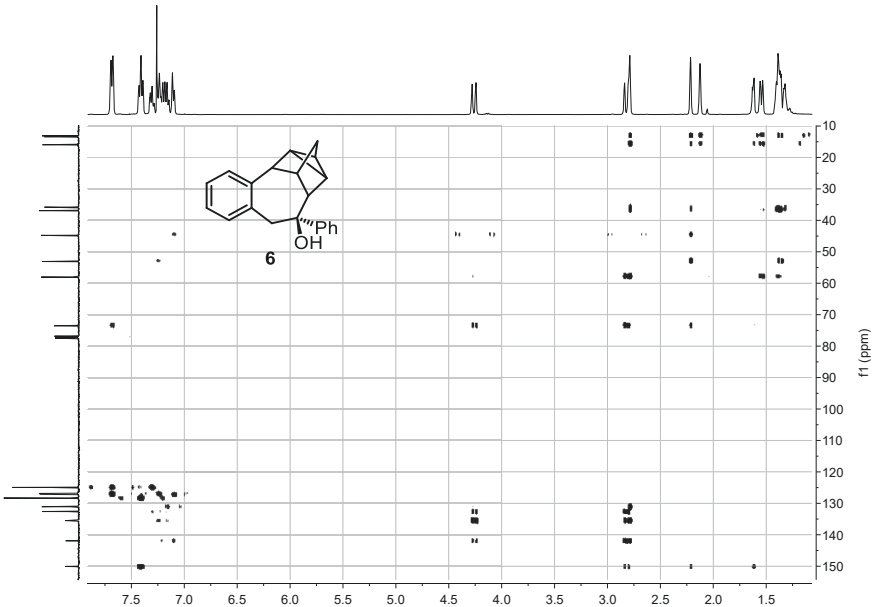

Figure S 234. $^{1}H,^{13}C$-HMBC of **6** in $CDCl_3$ measured at ^{1}H: 400.16 MHz; ^{13}C: 100.63 MHz.

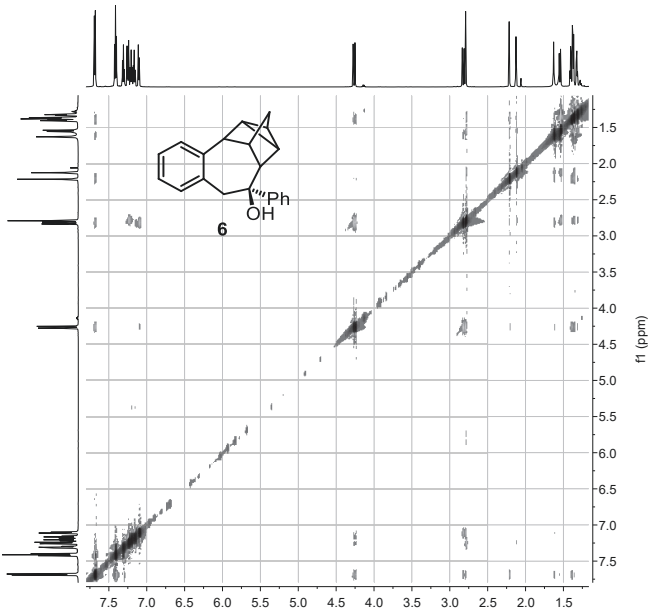

Figure S 235. $^{1}H,^{1}H$-NOESY of **6** in $CDCl_3$ measured at 400.16 MHz.

***rel*-1*S*,2*R*,3,3a*S*,4*R*,7,11b*S*,12*R*-hexahydro-1,2,4-(epimethanetriyl)benzo[c]cyclopenta[e]oxocin-5(1H)-one**

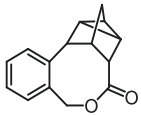

7

7 was synthesized according to a similar literature procedure with slight modifications.[25] **3aa** (105 mg, 500 µmol, 1.0 equiv.) and *m*-CPBA (140 mg, 1.50 mmol, 1.50 equiv.) were dissolved in DCM (2 mL) at 0 °C. The reaction was allowed to warm to rt and stirred for 4 d. Subsequently *m*-CPBA (140 mg, 1.50 mmol, 1.50 equiv.) was added and the reaction was stirred for 1 d. Reaction completion was confirmed by TLC, after which the precipitated was filtered. The organic phase was washed with sat. $NaHCO_{3(aq.)}$, dried over Na_2SO_4 and the solvent was removed *in vacuo*. Purification *via* flash chromatography (23 g SiO_2, gradient from 100:00 to 63:37 *n*-hexane/EA over 18 CV) afforded **7** (60.7 mg, 268 µmol, 54%) as a colorless solid.

$C_{15}H_{14}O_2$ (226.28 $\frac{g}{mol}$)

mp: 110.9 °C.

R$_f$: 0.25 (*n*-hexane/EA = 80:20) [anisaldehyde]

^{1}H NMR(400.16 MHz, $CDCl_3$): δ = 7.26 (m, 4H, H-10, H-11, H-12, H-13), 6.60 (d, ^2J = 12.4 Hz, 1H, H-15b), 4.80 (d, ^2J = 12.4 Hz, 1H, H-15a), 3.02 (s, 1H, H-7), 2.88 (s, 1H, H-2), 2.37 (m, 1H, H-8), 1.85 (m, 1H, H-3), 1.61 (m, 1H, H-4, H-4), 1.60 (m, 1H, H-6), 1.58 (dm, ^2J = 10.7 Hz, 1H, H-5a), 1.50 (dm, ^2J = 10.7 Hz, 1H, H-5b).

^{13}C NMR(100.62 MHz, $CDCl_3$): δ = 175.0 (C-1), 139.9, 135.4, 132.9, 132.5, 129.6, 127.5, 68.7 (C-15), 53.4 (C-7), 51.9 (C-2), 40.9 (C-8), 34.7 (C-5), 16.9 (C-6), 15.0 (C-3), 14.7 (C-3).

HRMS (ESI-TOF) m/z: $[M+H]^+$ Calcd for $C_{15}H_{14}O_2H$ 227.1067; Found 227.1069.

IR (ATR, ṽ): 1701 cm^{-1} (s, *CO*OR).

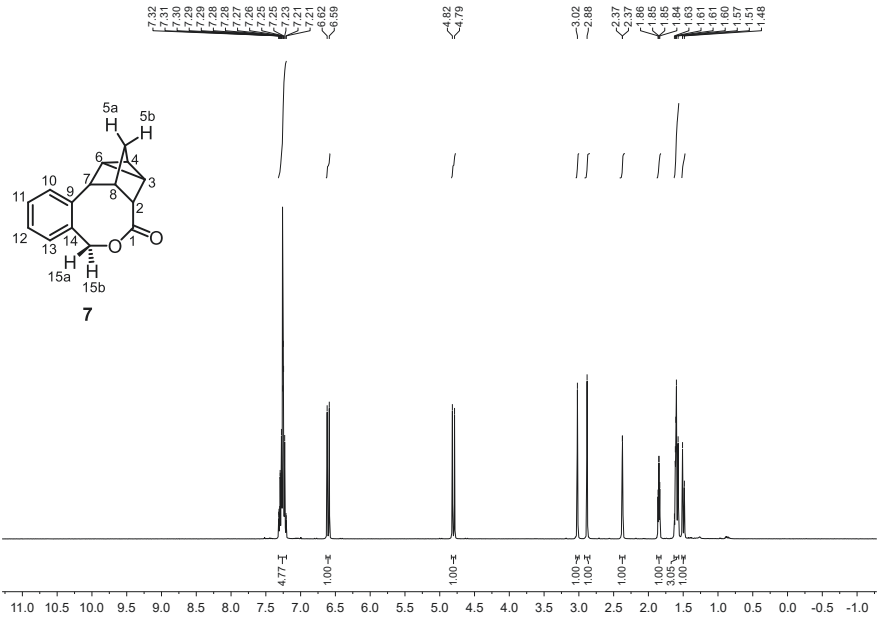

Figure S 236. ^{1}H NMR of **7** in $CDCl_3$ measured at 400.16 MHz.

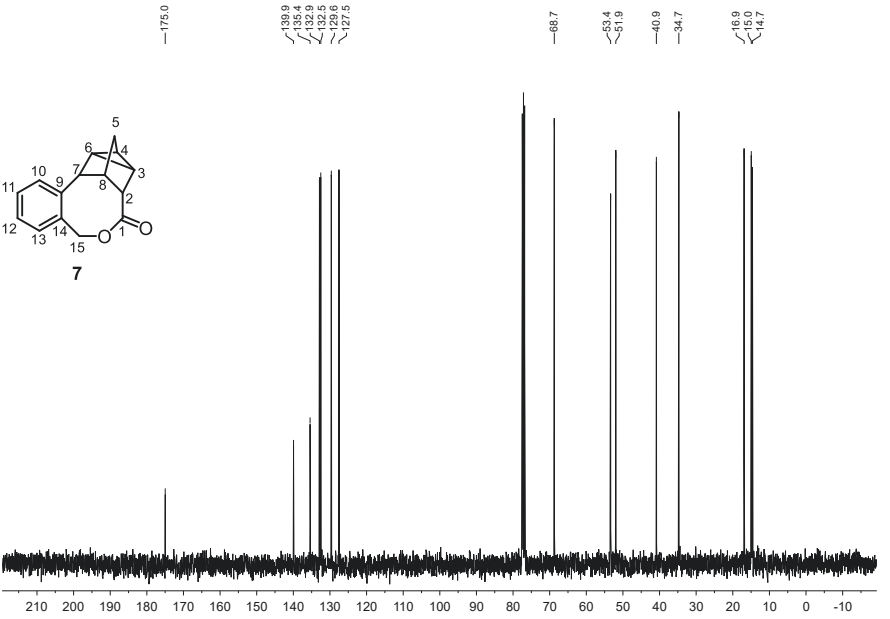

Figure S 237. ^{13}C NMR of **7** in $CDCl_3$ measured at 100.63 MHz.

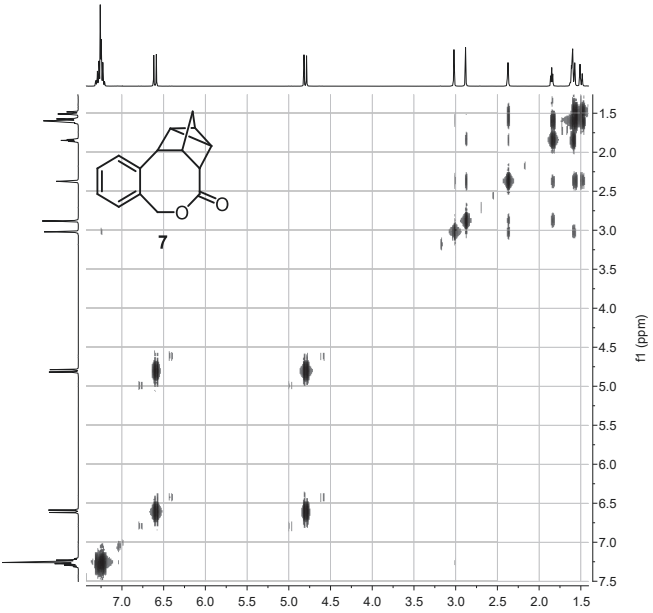

Figure S 238. $^{1}H,^{1}H$-COSY of **7** in $CDCl_3$ measured at 400.16 MHz.

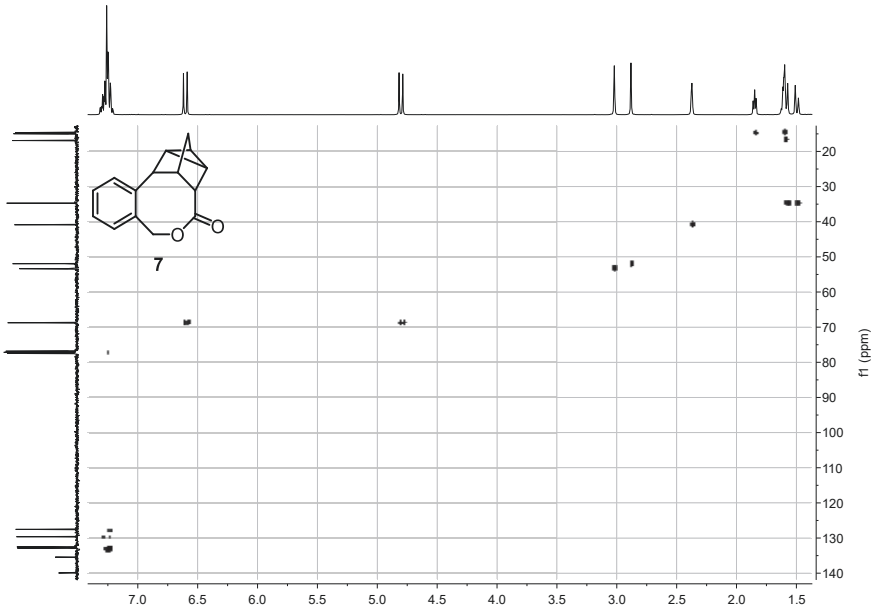

Figure S 239. $^{1}H,^{13}C$-HSQC of **7** in $CDCl_3$ measured at ^{1}H: 400.16 MHz; ^{13}C: 100.63 MHz.

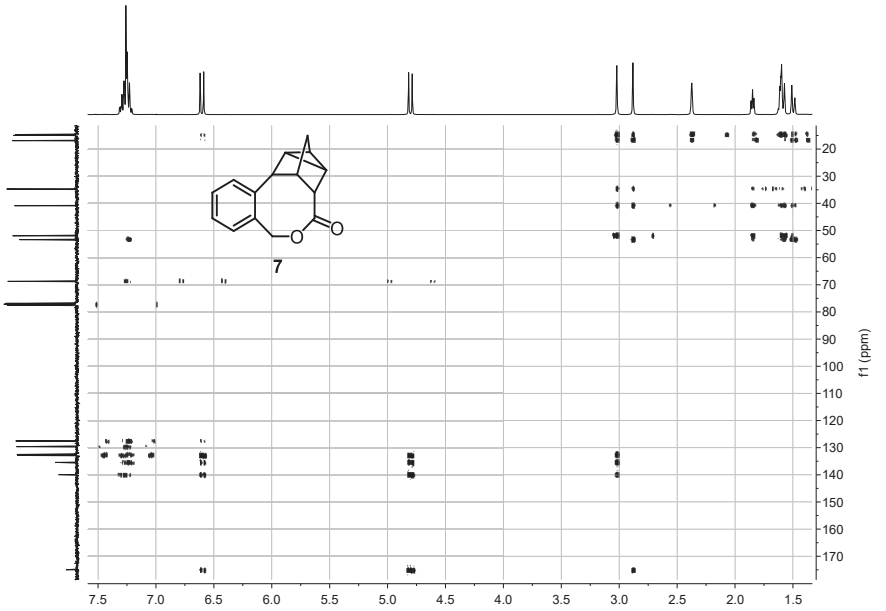

Figure S 240. $^{1}H,^{13}C$-HMBC of **7** in $CDCl_3$ measured at ^{1}H: 400.16 MHz; ^{13}C: 100.63 MHz.

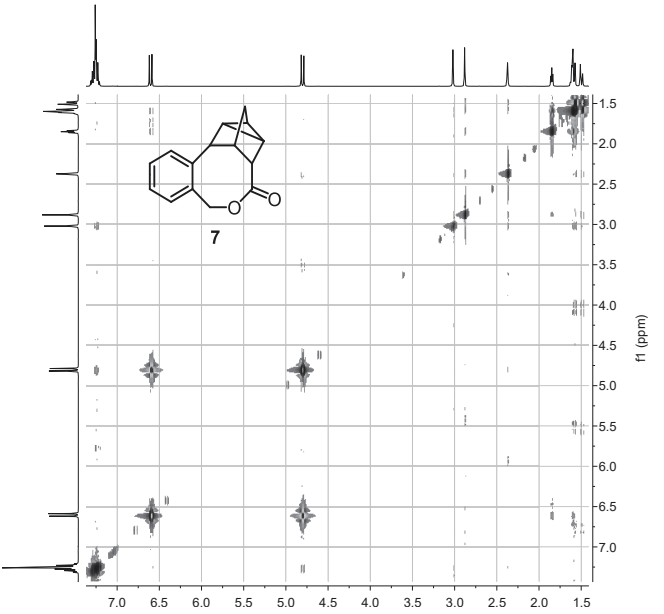

Figure S 241. $^{1}H,^{1}H$-NOESY of **7** in $CDCl_3$ measured at 400.16 MHz.

5 ^{31}P NMR studies

To gain insight into the mechanism of the Ni catalyzed NBD insertion into **1a**, a ^{31}P NMR study was conducted. Hereby, ^{31}P NMR spectra were measured in DMI without locking or shimming the sample.

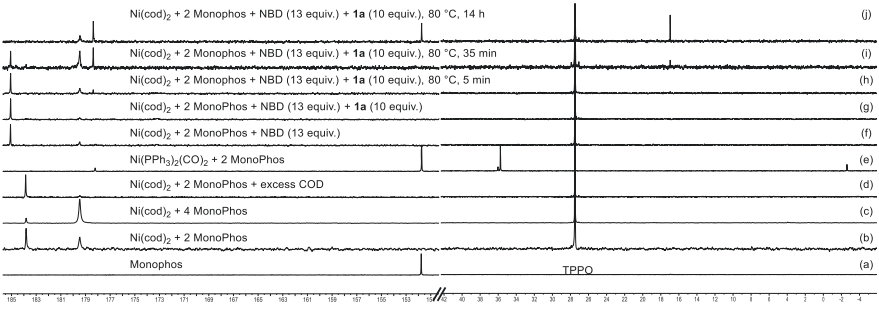

Figure S 242. Mechanistic ^{31}P NMR study of the Ni catalyzed NBD insertion into **1a**. All ^{31}P NMR spectra were measured in DMI without locking or shimming the sample at 300.13 MHz. To all reaction triphenylphosphine oxide (TPPO) was added as an internal standard.

In order to assign measured signals, reference spectra of MonoPhos and the employed catalyst consisting of 1 equiv. of $Ni(COD)_2$ and 2 equiv. of MonoPhos were recorded. Hereby, two distinct signals were observed (Figure S 242, b), which could be assigned to a Ni-species with most likely four MonoPhos ligands (Figure S 242, c) accompanied by a Ni-species with most likely two MonoPhos ligands and one COD ligand (Figure S 242, d), by adding an excess of MonPhos or COD respectively. Additionally, Ni(PPh3)2(CO)2 was mixed with 2 equiv. of MonoPhos giving rise to a signal corresponding to a Ni-carbonyl species with one or more MonoPhos ligands (Figure S 242, e).

To mimic the standard conditions, initially NBD (13 equiv.) was added. As expected, the signals corresponding to the Ni-species with most likely four MonoPhos ligands depleted, while the signal corresponding to the Ni-species with most likely two MonoPhos ligands and one COD ligand was shifted, as COD was replaced by NBD. Upon addition of **1a** (10 equiv.)

6 Kinetic measurements

To gain insight into the reaction kinetics, preliminary experiments were conducted at 50 °C and 80 °C.

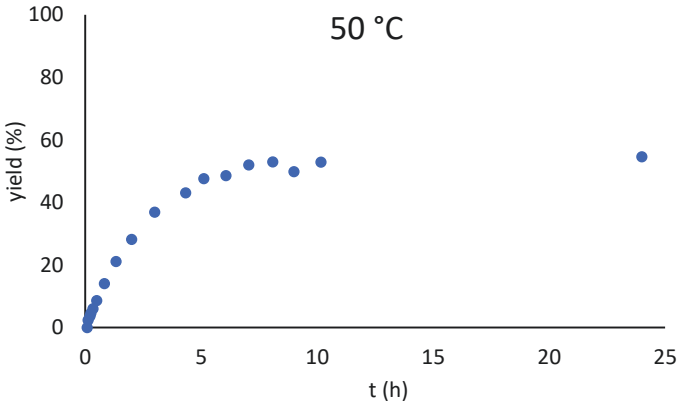

Figure S 243. GC-FID kinetic measurement of the Ni catalyzed NBD insertion into **1a** at 50 °C.

At 50 °C, the reaction achieved only ~50% yield after 10 h (Figure S 243), which was unexpected given the isolated yield of 90% under these conditions. However, the reproducibility of the kinetic measurements suggests that sampling during the reaction adversely affects the outcome. Furthermore, an induction period of approximately 10 min was observed at 50 °C.

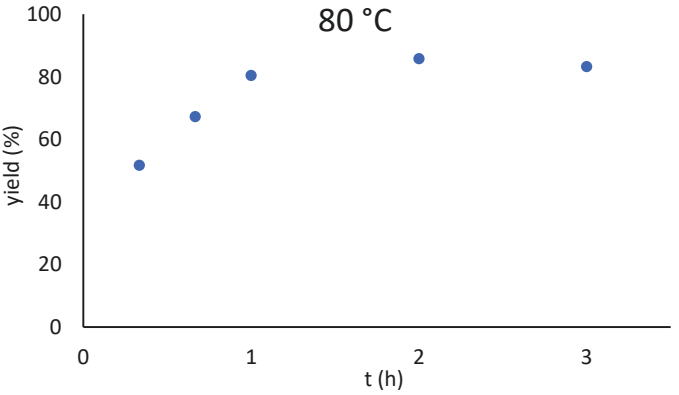

Figure S 244. GC-FID kinetic measurement of the Ni catalyzed NBD insertion into **1a** at 80 °C.

In contrast, the reaction at 80 °C proceeded significantly faster, reaching completion within approximately 2 h. Notably, the overall yield was not affected during this experiment, likely due to the reduced frequency of sampling.

7 Crystal structures

Crystals for X-ray structure analyses, were crystallized from *n*-hexane/EA unless denoted otherwise by slow evaporation of the solvent. Data collection was conducted on a Rigaku XtaLAB Synergy-S single-crystal X-ray diffractometer equipped with HyPix-6000HE detector and monochromated Cu-K_α radiation (λ=1.54184 Å) at 100 K. Absorption corrections for X-ray intensities were executed through a numerical method employing CrysAlisPro 1.171.42.49 (Rigaku Oxford Diffraction, 2022). The structure was solved by direct methods (SHELXS),[26] followed by full-matrix least-squares structure refinements, performed with SHELXL-2018,[27] implemented in Olex2 1.5.[28] The graphical representations were generated utilizing CCDC Mercury 2022.2.0.[29] Additional details pertaining to refinement procedures and crystallographic data for each crystal structure are listed below and in their respective CIF file.

rel-(1_S_,2_S_,3a_R_,4_R_,12a_S_,13_R_)-2,3,3a,4,11,12a-hexahydro-1,2,4-(epimethanetriyl) naphtho[2,3-f]azulen-12(1H)-one (3ba)

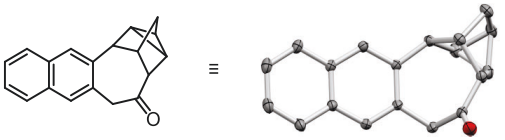

Figure S 245. Crystal structure of **3ba**. Hydrogen atoms are omitted for clarity and the thermal ellipsoids are drawn at 50% probability level.

Table S 7. Crystal data and structure refinement for **3ba**.

Compound	**3ba**		
Formula	$C_{19}H_{16}O$	Z'	1
CCDC	2310325	Wavelength/Å	1.54184
$D_{calc.}$/ g cm^{-3}	1.331	Radiation type	Cu K$_a$
μ/mm^{-1}	0.623	Θ_{min}/°	4.40
Formula Weight	260.338	Θ_{max}/°	79.61
Colour	clear colourless	Measured Refl's.	13687
Shape	plate-shaped	Indep't Refl's	2759
Size/mm^3	0.14×0.13×0.06	Refl's I≥2 s(I)	2618
T/K	149.99(10)	R_{int}	0.0145
Crystal System	monoclinic	Parameters	326
Space Group	$P2_1/c$	Restraints	0
a/Å	10.5666(3)	Largest Peak	0.0855
b/Å	16.0194(3)	Deepest Hole	-0.0781
c/Å	8.0757(2)	GooF	1.2241
α/°	90	wR_2 (all data)	0.0257
β/°	108.119(3)	wR_2	0.0255
γ/°	90	R_1 (all data)	0.0119
V/Å^3	1299.19(6)	R_1	0.0108
Z	4		

rel-5-fluoro-(1_S_,2_S_,3a_R_,4_R_,10a_S_,11_R_)-2,3,3a,4,9,10a-hexahydro-1,2,4-(epimethanetriyl) benzo[f]azulen-10(1H)-one (3fa)

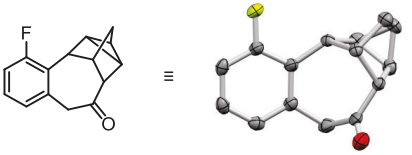

Figure S 246. Crystal structure of **3fa**. Hydrogen atoms are omitted for clarity and the thermal ellipsoids are drawn at 50% probability level.

Table S 8. Crystal data and structure refinement for **3fa**.

Compound	**3fa**		
Formula	$C_{15}H_{13}FO$	Z	4
CCDC	2376680	Z'	2
$D_{calc.}$/ g cm^{-3}	1.409	Wavelength/Å	1.54184
μ/mm^{-1}	0.802	Radiation type	Cu K□
Formula Weight	228.25	Θ_{min}/°	5.253
Colour	clear colourless	Θ_{max}/°	78.844
Shape	plate-shaped	Measured Refl's.	25937
Size/mm^3	0.16×0.10×0.05	Indep't Refl's	4360
T/K	149.99(10)	Refl's I≥2 □(I)	4272
Crystal System	monoclinic	R_{int}	0.0129
Flack Parameter	0.08(14)	Parameters	465
Hooft Parameter	-0.07(2)	Restraints	43
Space Group	$P2_1$	Largest Peak	0.194
a/Å	8.4337(2)	Deepest Hole	-0.163
b/Å	15.1543(2)	GooF	1.036
c/Å	9.2579(2)	wR_2 (all data)	0.0721
α/°	90	wR_2	0.0715
β/°	114.552(2)	R_1 (all data)	0.0265
γ/°	90	R_1	0.0259
V/Å^3	1076.24(4)		

rel-(1*R*,2*R*,3a*S*,4*S*,9*R*,10a*R*,11*S*)-9-methyl-2,3,3a,4,9,10a-hexahydro-1,2,4-(epimethanetriyl)benzo[f]azulen-10(1H)-one (mixture of enantiomers) (3ga)

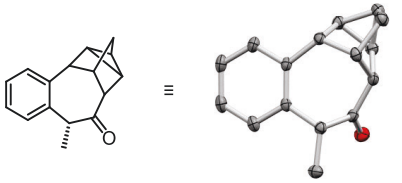

Figure S 247. Crystal structure of **3ga**. Hydrogen atoms are omitted for clarity and the thermal ellipsoids are drawn at 50% probability level.

Table S 9. Crystal data and structure refinement for **3ga**.

Compound	**3ga**		
Formula	$C_{16}H_{16}O$	Z'	2
CCDC	2378469	Wavelength/Å	1.54184
$D_{calc.}$/ g cm^{-3}	1.312	Radiation type	Cu K□
μ/mm^{-1}	0.618	Θ_{min}/°	3.27
Formula Weight	224.305	Θ_{max}/°	79.74
Colour	clear colourless	Measured Refl's.	43228
Shape	plate-shaped	Indep't Refl's	4855
Size/mm^3	0.17×0.12×0.05	Refl's I≥2 s(I)	4550
T/K	150.00(10)	R_{int}	0.0175
Crystal System	triclinic	Parameters	596
Space Group	P-1	Restraints	0
a/Å	9.2433(3)	Largest Peak	0.1920
b/Å	9.3665(3)	Deepest Hole	-0.0984
c/Å	13.9650(5)	GooF	1.0867
α/°	78.015(3)	wR_2 (all data)	0.0407
β/°	79.186(3)	wR_2	0.0401
γ/°	75.965(3)	R_1 (all data)	0.0194
V/Å^3	1135.33(7)	R_1	0.0176
Z	4		

rel-(1_R_,2_R_,3a_S_,4_S_,9_R_,10a_R_,11_S_)-9-ethyl-2,3,3a,4,9,10a-hexahydro-1,2,4-(epimethanetriyl)benzo[f]azulen-10(1H)-one (mixture of enantiomers) (3ha)

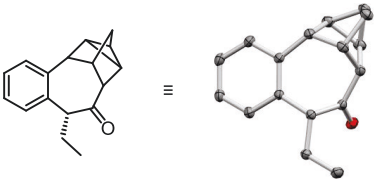

Figure S 248. Crystal structure of **3ha**. Hydrogen atoms are omitted for clarity and the thermal ellipsoids are drawn at 50% probability level.

Table S 10. Crystal data and structure refinement for **3ha**.

Compound	**3ha**		
Formula	$C_{17}H_{18}O$	Z'	1
CCDC	2375605	Wavelength/Å	1.54184
$D_{calc.}$/ g cm^{-3}	1.275	Radiation type	Cu K□
μ/mm^{-1}	0.594	Θ_{min}/°	4.84
Formula Weight	238.332	Θ_{max}/°	79.74
Colour	clear colourless	Measured Refl's.	22390
Shape	block-shaped	Indep't Refl's	2643
Size/mm^3	0.22×0.17×0.07	Refl's I≥2 s(I)	2494
T/K	149.99(10)	R_{int}	0.0160
Crystal System	triclinic	Parameters	326
Space Group	P-1	Restraints	0
a/Å	8.2890(4)	Largest Peak	0.2601
b/Å	8.9537(4)	Deepest Hole	-0.1055
c/Å	8.9537(4)	GooF	1.6571
α/°	76.935(3)	wR_2 (all data)	0.0424
β/°	69.386(4)	wR_2	0.0421
γ/°	66.263(4)	R_1 (all data)	0.0176
V/Å^3	620.84(5)	R_1	0.0163
Z	2		

rel-(1*R*,2*R*,3*R*,3a*S*,10a*S*,11*S*)-3-phenyl-2,3,3a,4,9,10a-hexahydro-1,2,4-(epimethanetriyl) benzo[f]azulen-10(1H)-one (3ad)

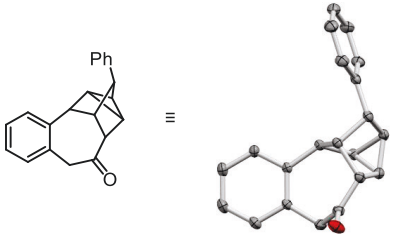

Figure S 249. Crystal structure of **3ad**. Hydrogen atoms are omitted for clarity and the thermal ellipsoids are drawn at 50% probability level.

Table S 11. Crystal data and structure refinement for **3ad**.

Compound	**3ad**		
Formula	$C_{21}H_{18}O$	Z'	1
CCDC	2374054	Wavelength/Å	1.54184
$D_{calc.}$/ g cm^{-3}	1.303	Radiation type	Cu K$_a$
μ/mm^{-1}	0.604	Θ_{min}/°	4.70
Formula Weight	286.376	Θ_{max}/°	79.84
Colour	clear colourless	Measured Refl's.	51022
Shape	block-shaped	Indep't Refl's	3177
Size/mm^3	0.23×0.21×0.13	Refl's I≥2 s(I)	3118
T/K	149.99(10)	R_{int}	0.0186
Crystal System	monoclinic	Parameters	362
Space Group	$P2_1/n$	Restraints	0
a/Å	11.1297(1)	Largest Peak	0.0763
b/Å	7.7608(1)	Deepest Hole	-0.0753
c/Å	16.9009(2)	GooF	1.2584
α/°	90	wR_2 (all data)	0.0291
β/°	91.540(1)	wR_2	0.0289
γ/°	90	R_1 (all data)	0.0127
V/Å^3	1459.29(3)	R_1	0.0123
Z	4		

rel-5-methyl-2,3,3a,4,9,10a-hexahydro-1,2,4-(epimethanetriyl)benzo[f]azulen-10(1H)-one (X)

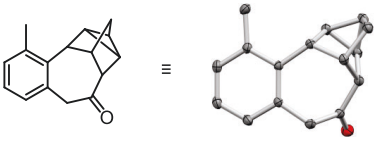

Figure S 250. Crystal structure of the regioisomer of **3ma**. Hydrogen atoms are omitted for clarity and the thermal ellipsoids are drawn at 50% probability level.

Table S 12. Crystal data and structure refinement for the regioisomer of **3ma**.

Compound	regioisomer of **3ma**		
Formula	$C_{16}H_{16}O$	Z'	1
CCDC	2383238	Wavelength/Å	1.54184
$D_{calc.}$/ g cm^{-3}	1.338	Radiation type	Cu K□
μ/mm^{-1}	0.630	Θ_{min}/°	5.59
Formula Weight	224.305	Θ_{max}/°	79.93
Colour	clear colourless	Measured Refl's.	40072
Shape	block-shaped	Indep't Refl's	2415
Size/mm^3	0.28×0.14×0.13	Refl's I≥2 s(I)	2368
T/K	150.00(10)	R_{int}	0.0307
Crystal System	monoclinic	Parameters	299
Space Group	$P2_1/c$	Restraints	0
a/Å	8.7741(2)	Largest Peak	0.1678
b/Å	15.5263(2)	Deepest Hole	-0.0718
c/Å	9.0616(2)	GooF	1.1718
α/°	90	wR_2 (all data)	0.0341
β/°	115.591(2)	wR_2	0.0339
γ/°	90	R_1 (all data)	0.0152
V/Å^3	1113.36(4)	R_1	0.0148
Z	4		

***rel*-(2S)-2',3',3a',4',9',10a'-hexahydro-1'H-spiro[oxirane-2,10'-[1,2,4](epimethanetriyl)benzo[f]azulene]**

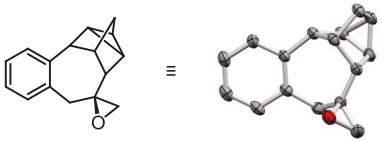

Figure S 251. Crystal structure of **5**. Hydrogen atoms are omitted for clarity and the thermal ellipsoids are drawn at 50% probability level.

Table S 13. Crystal data and structure refinement for **5**.

Compound	**5**		
Formula	$C_{16}H_{16}O$	*Z′*	1
CCDC	2412014	Wavelength/Å	1.54184
$D_{calc.}$/ g cm^{-3}	1.294	Radiation type	Cu K□
μ/mm^{-1}	0.609	Θ_{min}/°	5.00
Formula Weight	224.305	Θ_{max}/°	79.89
Colour	clear colourless	Measured Refl's.	17017
Shape	block-shaped	Indep't Refl's	2444
Size/mm^3	0.09×0.07×0.06	Refl's I≥2 *s*(I)	2369
T/K	150.01(19)	R_{int}	0.0275
Crystal System	monoclinic	Parameters	299
Space Group	-0.06(8)	Restraints	2
a/Å	-0.06(8)	Largest Peak	0.3031
b/Å	$P2_1$	Deepest Hole	-0.1671
c/Å	6.6983(4)	GooF	1.5325
α/°	9.7213(4)	wR_2 (all data)	0.0442
β/°	9.4188(5)	wR_2	0.0440
γ/°	90	R_1 (all data)	0.0197
V/Å^3	110.205(6)	R_1	0.0187
Z	90		

rel-2,3,3a,4,7,11b-hexahydro-1,2,4-(epimethanetriyl)benzo[c]cyclopenta[e]oxocin-5(1H)-one (7)

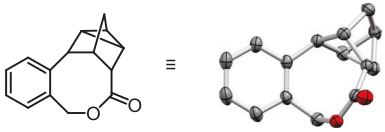

Figure S 252. Crystal structure of **7**. Hydrogen atoms are omitted for clarity and the thermal ellipsoids are drawn at 50% probability level.

Table S 14. Crystal data and structure refinement for **7**.

Compound	**7**		
Formula	$C_{15}H_{14}O_2$	Z'	1
CCDC	2409660	Wavelength/Å	1.54184
$D_{calc.}$/ g cm^{-3}	1.378	Radiation type	Cu K□
μ/mm^{-1}	0.721	Θ_{min}/°	5.16
Formula Weight	226.277	Θ_{max}/°	81.02
Colour	clear colourless	Measured Refl's.	38923
Shape	block-shaped	Indep't Refl's	2378
Size/mm^3	0.08×0.06×0.03	Refl's I≥2 s(I)	2125
T/K	150.01(18)	R_{int}	0.0339
Crystal System	monoclinic	Parameters	280
Space Group	$C2/c$	Restraints	0
a/Å	18.0665(12)	Largest Peak	0.2126
b/Å	8.2079(5)	Deepest Hole	-0.1295
c/Å	15.5222(11)	GooF	1.0650
α/°	90	wR_2 (all data)	0.0611
β/°	108.558(7)	wR_2	0.0594
γ/°	90	R_1 (all data)	0.0296
V/Å^3	2182.1(3)	R_1	0.0255
Z	8		

8 GC on chiral stationary phase

GC-MS spectra were measured on a 8890 GC and 5977B MSD system from Agilent, utilizing a chiral stationary phase: MEGA-DEX DET Beta (film thickness: 0.25 micron, Internal diameter: 0.25 mm; length: 25 m). All measurements were conducted under isocratic conditions with the respective temperature denoted under each measurement.

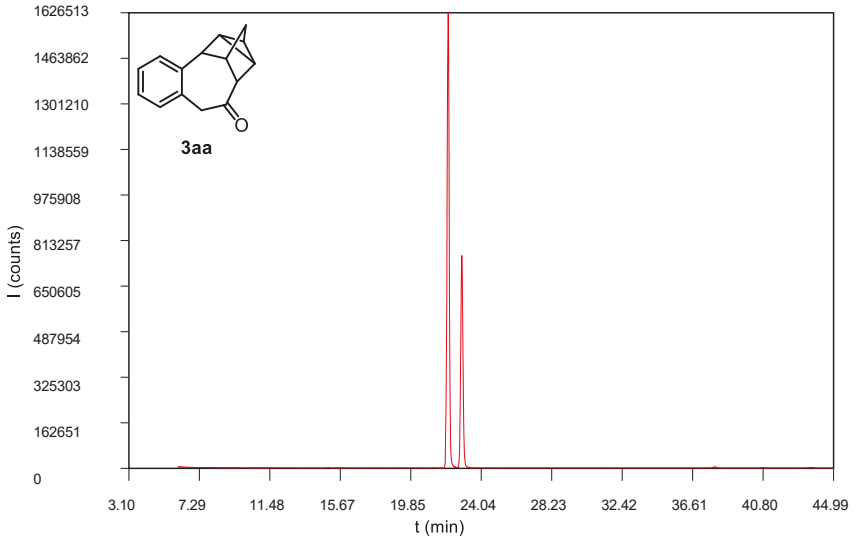

Figure S 253. GC-MS chromatogram measured with a chiral stationary phase of **3aa** (isocratic, 170 °C).

GC-MS (MEGA-DEX DET Beta, He, flow rate = 1.2 mL/min, EI) t_R = 20.39 min (**3aa**, 1); t_R = 21.26 min (**3aa**, 2).

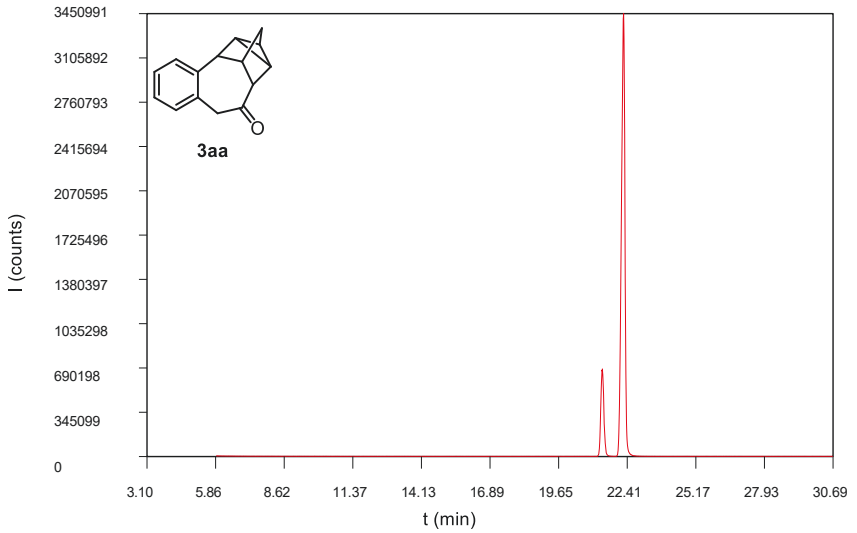

Figure S 254. GC-MS chromatogram measured with a chiral stationary phase of **3aa** (isocratic, 170 °C).

GC-MS (MEGA-DEX DET Beta, He, flow rate = 1.2 mL/min, EI) t_R = 20.37 min (**3aa**, 1); t_R = 21.31 min (**3aa**, 2).

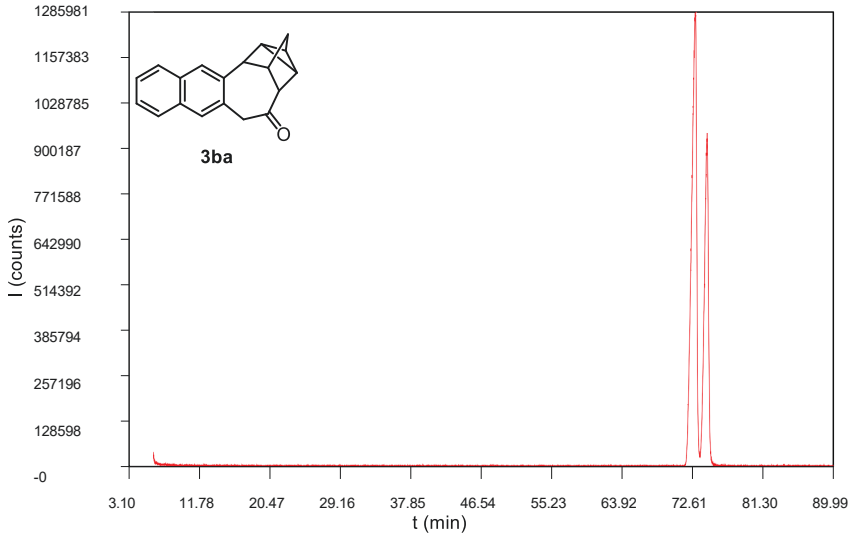

Figure S 255. GC-MS chromatogram measured with a chiral stationary phase of **3ba** (isocratic, 195 °C).

GC-MS (MEGA-DEX DET Beta, He, flow rate = 1.2 mL/min, EI) t_R = 72.36 min (**3ba**, 1); t_R = 73.87 min (**3ba**, 2).

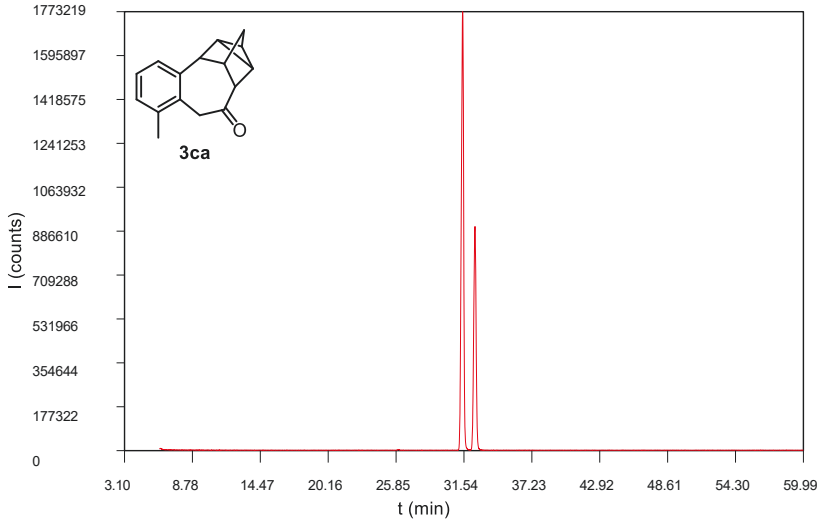

Figure S 256. GC-MS chromatogram measured with a chiral stationary phase of **3ca** (isocratic, 170 °C).

GC-MS (MEGA-DEX DET Beta, He, flow rate = 1.2 mL/min, EI) t_R = 29.88 min (**3ca**, 1); t_R = 30.97 min (**3ca**, 2).

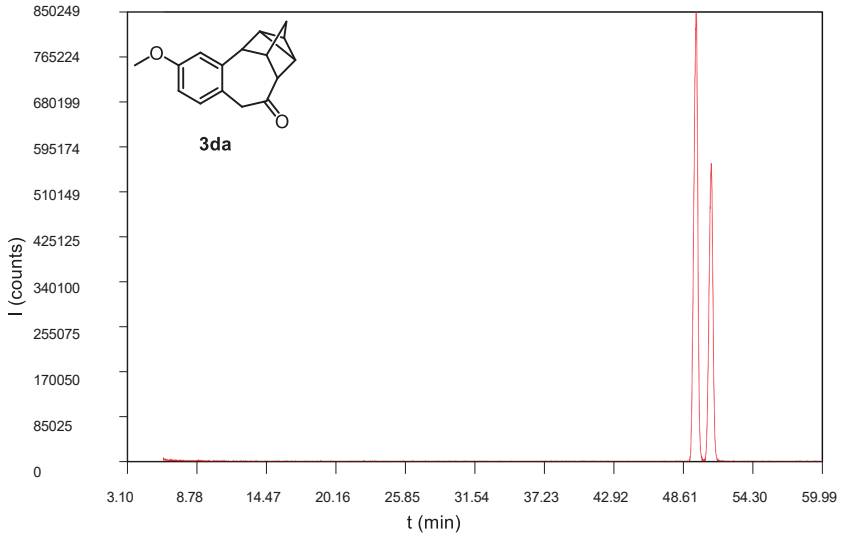

Figure S 257. GC-MS chromatogram measured with a chiral stationary phase of **3da** (isocratic, 175 °C).

GC-MS (MEGA-DEX DET Beta, He, flow rate = 1.2 mL/min, EI) t_R = 49.03 min (**3da**, 1); t_R = 50.33 min (**3da**, 2).

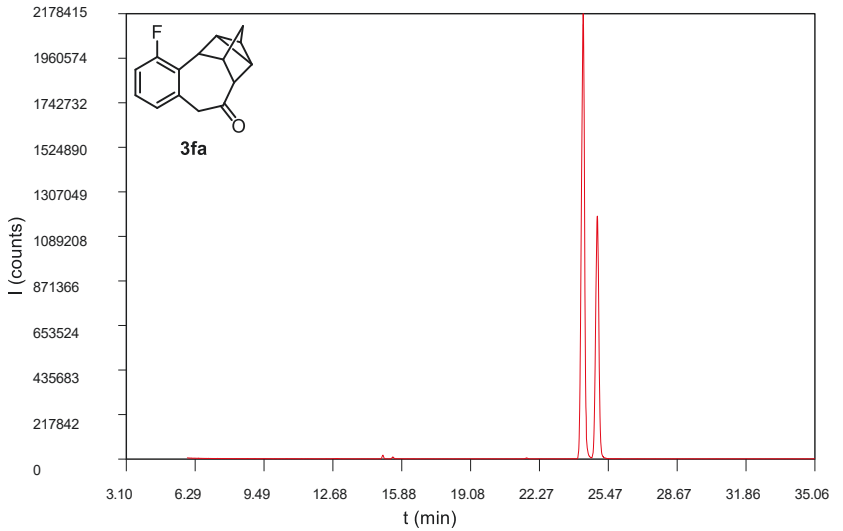

Figure S 258. GC-MS chromatogram measured with a chiral stationary phase of **3fa** (isocratic, 165 °C).

GC-MS (MEGA-DEX DET Beta, He, flow rate = 1.2 mL/min, EI) t_R = 23.26 min (**3fa**, 1); t_R = 23.98 min (**3fa**, 2).

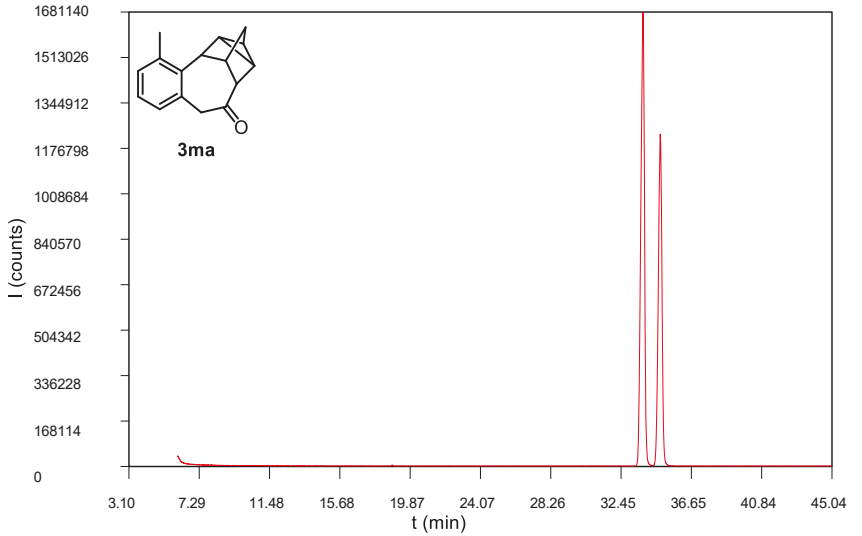

Figure S 259. GC-MS chromatogram measured with a chiral stationary phase of **3ma** (isocratic, 170 °C).

GC-MS (MEGA-DEX DET Beta, He, flow rate = 1.2 mL/min, EI) t_R = 32.93 min (**3ma**, 1); t_R = 34.04 min (**3ma**, 2).

9 GC-FID calibration

GC-FID yields were quantified by addition of *n*-pentadecane as an internal standard, applying the general equation:

$$\frac{A(compound)}{A(n\text{-}pentadecane)} = R \cdot \frac{m(compound)}{m(n\text{-}pentadecane)}$$

R: response factor
A: peak area determined by GC-FID
m: mass of compound

The response factors were determined by GC-FID calibration in EA.

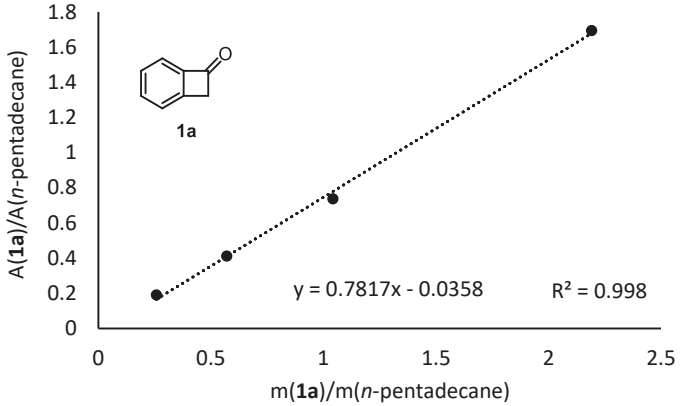

Figure S 260. GC-FID calibration of **1a** with *n*-pentadecane as an internal standard.

Table S 15. Values for the calibration of **1a** with *n*-pentadecane as an internal standard.

Entry	m(1a) (mg)	m(*n*-pentadecane) (mg)	A(1a)	A(*n*-pentadecane)
1	14.9	6.8	9419	5560
2	7.4	7.1	4445	6037
3	7.7	13.5	4575	11114
4	7.1	27.5	3354	17669

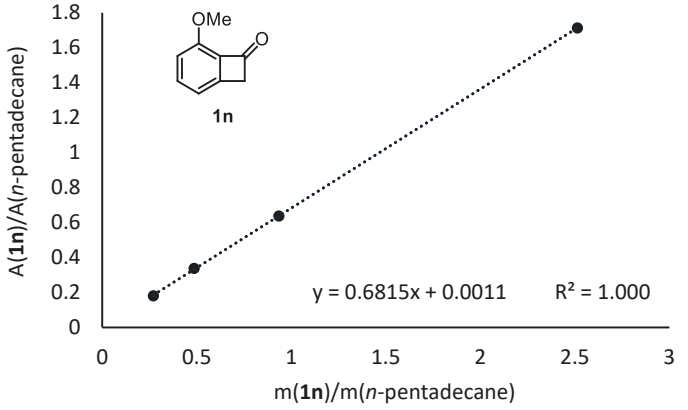

Figure S 261. GC-FID calibration of **1n** with *n*-pentadecane as an internal standard.

Table S 16. Values for the calibration of **1n** with *n*-pentadecane as an internal standard.

Entry	m(1n) (mg)	m(*n*-pentadecane) (mg)	A(1n)	A(*n*-pentadecane)
1	19.1	7.6	10923	6375
2	10.0	10.7	5248	8239
3	8.4	17.3	4564	13524
4	7.6	28.1	2848	15733

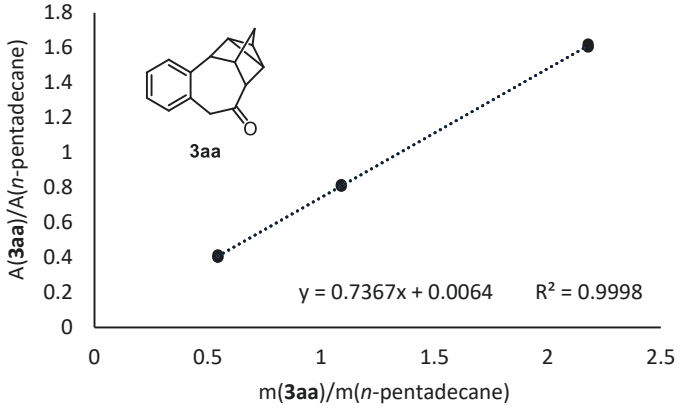

Figure S 262. GC-FID calibration of **3aa** with *n*-pentadecane as an internal standard.

Table S 17. Values for the calibration of **3aa** with *n*-pentadecane as an internal standard.

Entry	m(3aa) (mg)	m(*n*-pentadecane) (mg)	A(3aa)	A(*n*-pentadecane)
1	1.4	2.5	3118	7521
2	1.4	2.5	3100	7716
3	1.4	2.5	3084	7657
4	1.4	1.2	2983	3692
5	1.4	1.2	3214	3936
6	2.7	1.2	6112	3769
7	2.7	1.2	6095	3791
8	2.7	1.2	5759	3590

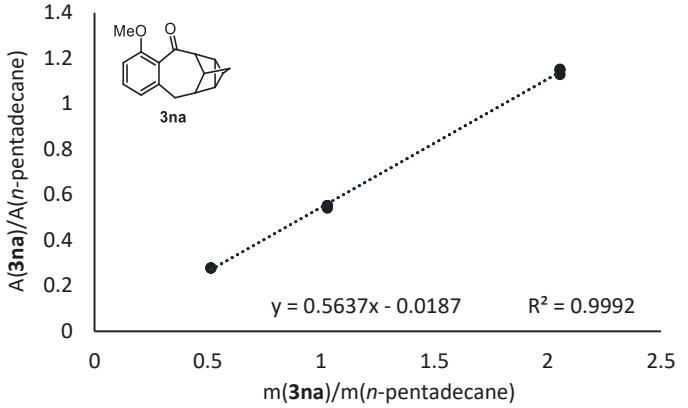

Figure S 263. GC-FID calibration of **3na** with *n*-pentadecane as an internal standard.

Table S 18. Values for the calibration of **3na** with *n*-pentadecane as an internal standard.

Entry	m(3na) (mg)	m(*n*-pentadecane) (mg)	A(3na)	A(*n*-pentadecane)
1	3.2	1.6	3722	3296
2	3.2	1.6	3723	3232
3	3.2	1.6	3751	3267
4	1.6	1.6	1839	3393
5	1.6	1.6	1854	3356
6	1.6	1.6	1837	3323
7	1.6	3.1	1889	6778
8	1.6	3.1	1865	6710
9	1.6	3.1	1862	6686

10 Literature

[1] J. A. Werra, K. Wurst, L. B. Wilm, P. Löwe, M. B. Röthel, F. Dielmann, *Organometallics* **2023**, *42*, 597-605.
[2] M. J. O'Neil, 14th ed., The Merck index : an encyclopedia of chemicals, drugs, and biologicals, Merck Whitehouse Station, N.J., **2006**.
[3] P.-h. Chen, J. Sieber, C. H. Senanayake, G. Dong, *Chem. Sci.* **2015**, *6*, 5440-5445.
[4] T.-S. Mei, D.-H. Wang, J.-Q. Yu, *Org. Lett.* **2010**, *12*, 3140-3143.
[5] J. A. Cadge, P. J. Gates, J. F. Bower, C. A. Russell, *J. Am. Chem. Soc.* **2022**, *144*, 19719-19725.
[6] R. Li, B. Li, H. Zhang, C.-W. Ju, Y. Qin, X.-S. Xue, D. Zhao, *Nat. Chem.* **2021**, *13*, 1006-1016.
[7] L. S. Liebeskind, L. J. Lescosky, C. M. McSwain, Jr., *J. Org. Chem.* **1989**, *54*, 1435-1439.
[8] P. R. Story, S. R. Fahrenholtz, *J. Org. Chem.* **1963**, *28*, 1716-1717.
[9] L. Liu, N. Ishida, M. Murakami, *Angew. Chem. Int. Ed.* **2012**, *51*, 2485-2488.
[10] M. Šámal, S. Chercheja, J. Rybáček, J. Vacek Chocholoušová, J. Vacek, L. Bednárová, D. Šaman, I. G. Stará, I. Starý, *J. Am. Chem. Soc.* **2015**, *137*, 8469-8474.
[11] H. Wang, C. Zhou, Z. Gao, S. Li, G. Li, *Angew. Chem. Int. Ed.* **2023**, *62*, e202300905.
[12] F. De Wael, G. G. Muccioli, D. M. Lambert, T. Sergent, Y.-J. Schneider, J.-F. Rees, J. Marchand-Brynaert, *European Journal of Medicinal Chemistry* **2010**, *45*, 3564-3574.
[13] A. Leclair, Q. Wang, J. Zhu, *ACS Catal.* **2022**, *12*, 1209-1215.
[14] T. Kobayashi, T. Hosoya, S. Yoshida, *J. Org. Chem.* **2020**, *85*, 4448-4462.
[15] K. Nishikawa, H. Fukuda, M. Abe, K. Nakanishi, Y. Tazawa, C. Yamaguchi, S. Hiradate, Y. Fujii, K. Okuda, M. Shindo, *Phytochemistry* **2013**, *96*, 223-234.
[16] T. Yano, T. Kawasaki, T. Yuhki, N. Ishida, M. Murakami, *Org. Lett.* **2018**, *20*, 1224-1227.
[17] R. V. Stevens, G. S. Bisacchi, *J. Org. Chem.* **1982**, *47*, 2393-2396.
[18] P. R. Story, *J. Org. Chem.* **1961**, *26*, 287-290.
[19] A. A. Nagarkar, M. Yasir, A. Crochet, K. M. Fromm, A. F. M. Kilbinger, *Angew. Chem. Int. Ed.* **2016**, *55*, 12343-12346.
[20] W. Maudez, C. Roy, P. D. Tran, C. Thurier, F. Karmous, P. Doppelt, *Chem. Vap. Deposition* **2014**, *20*, 59-68.
[21] H. D. Verkruijsse, L. Brandsma, *Recl. Trav. Chim. Pays-Bas* **1986**, *105*, 66-68.
[22] B. S. Pilgrim, D. A. Roberts, T. G. Lohr, T. K. Ronson, J. R. Nitschke, *Nat. Chem.* **2017**, *9*, 1276-1281.
[23] P. Liu, H. Dong, B. Gong, S. Gao, A. Lin, H. Yao, *Org. Lett.* **2024**, *26*, 8244-8248.
[24] J. A. Ciaccio, A. L. Drahus, R. M. Meis, C. T. Tingle, M. Smrtka, R. Geneste, *Synth. Commun.* **2003**, *33*, 2135-2143.
[25] J. Duan, Y.-F. Du, X. Pang, X.-Z. Shu, *Chem. Sci.* **2019**, *10*, 8706-8712.
[26] G. M. Sheldrick, *Acta Crystallogr., Sect. A* **2008**, *64*, 112-122.
[27] G. Sheldrick, *Acta Crystallogr., Sect. C* **2015**, *71*, 3-8.
[28] O. V. Dolomanov, L. J. Bourhis, R. J. Gildea, J. A. K. Howard, H. Puschmann, *J. Appl. Crystallogr.* **2009**, *42*, 339-341.
[29] C. F. Macrae, I. Sovago, S. J. Cottrell, P. T. A. Galek, P. McCabe, E. Pidcock, M. Platings, G. P. Shields, J. S. Stevens, M. Towler, P. A. Wood, *J. Appl. Crystallogr.* **2020**, *53*, 226-235.

11 IR-Spectra

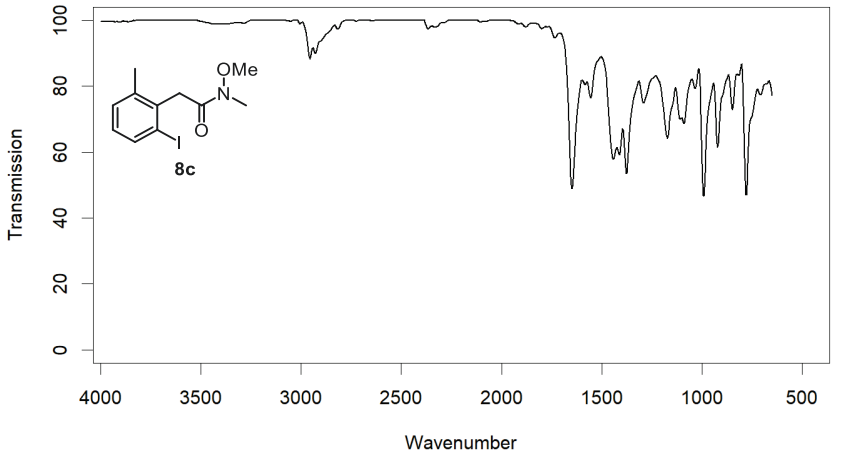

Figure S 264. IR spectrum of **8c**.

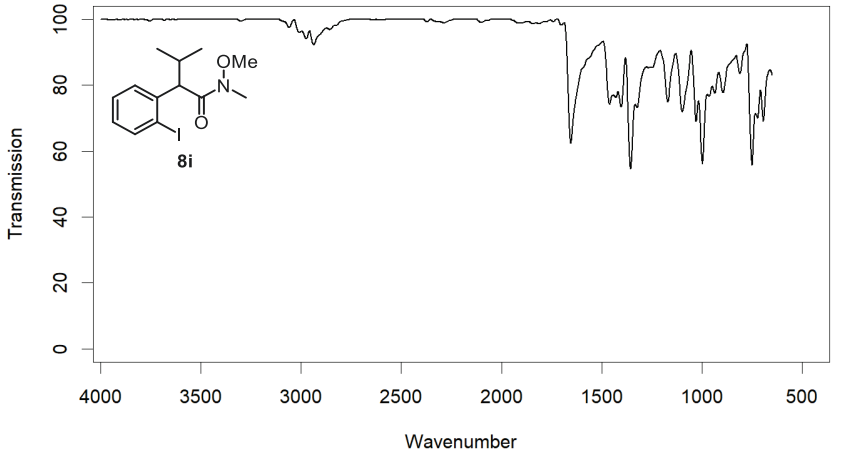

Figure S 265. IR spectrum of **8i**.

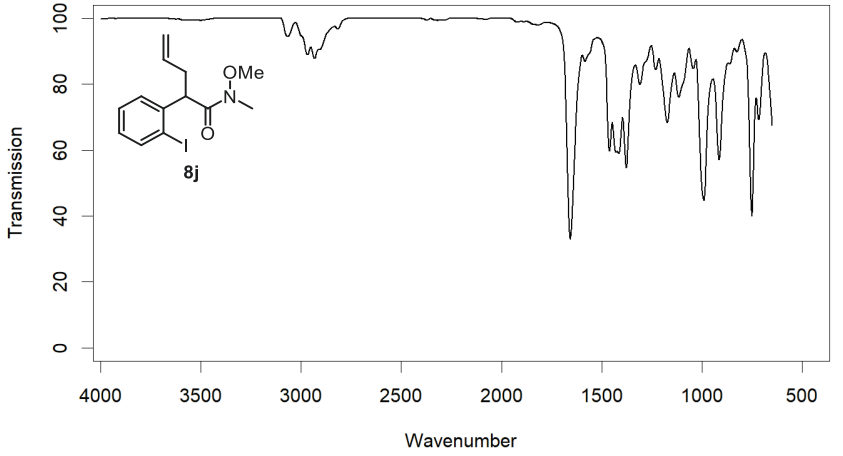

Figure S 266. IR spectrum of **8j**.

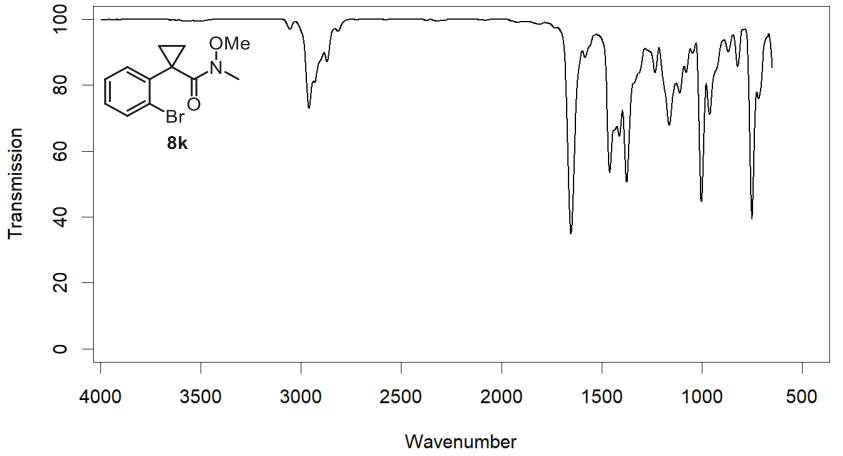

Figure S 267. IR spectrum of **8k**.

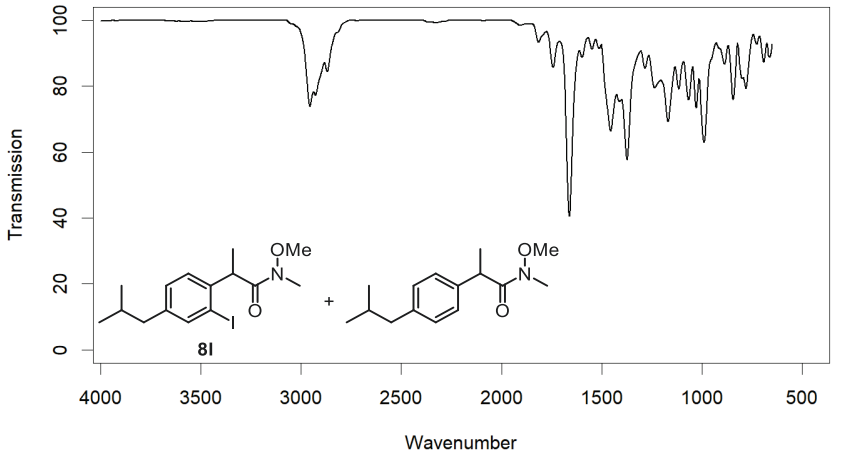

Figure S 268. IR spectrum of a mixture of **8l** and N-Methoxy-N-methyl-2-(4-isobutylphenyl)propenamide (78:22).

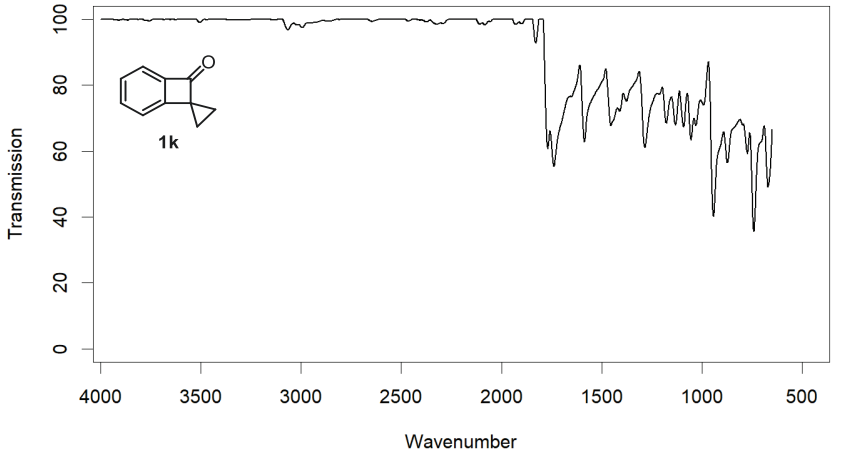

Figure S 269. IR spectrum of **1k**.

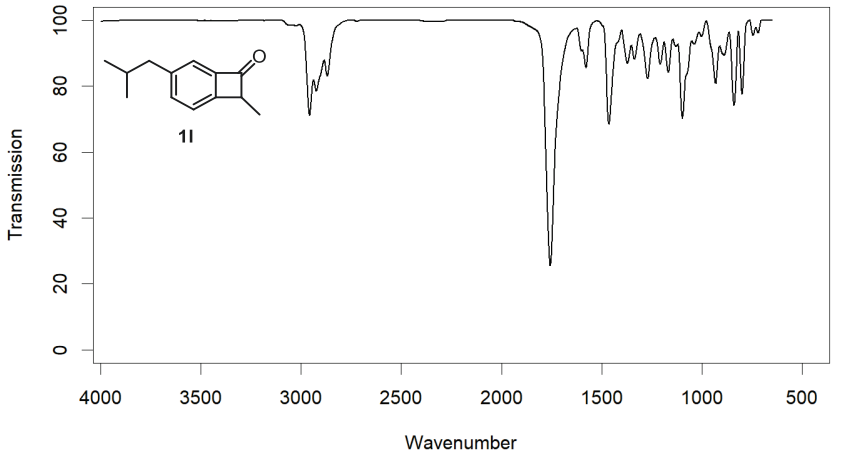

Figure S 270. IR spectrum of **1l**.

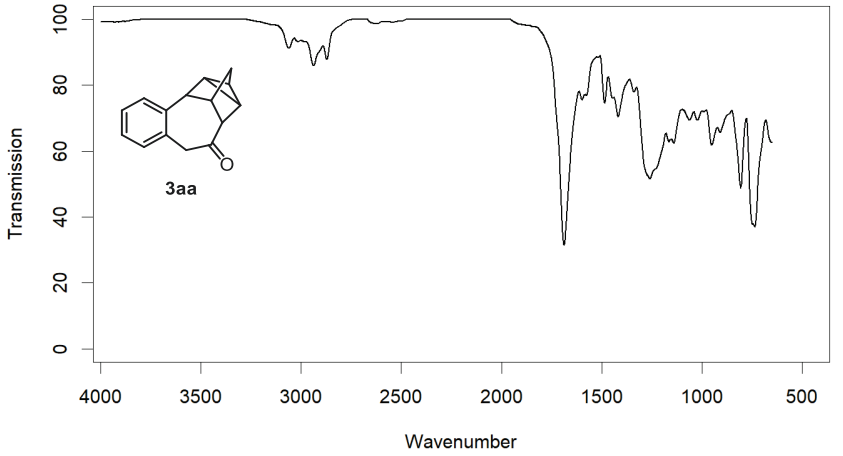

Figure S 271. IR spectrum of **3aa**.

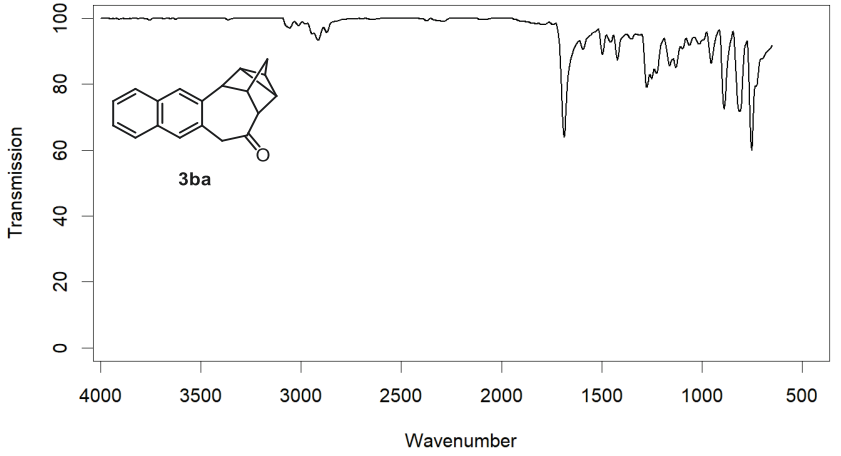

Figure S 272. IR spectrum of **3ba**.

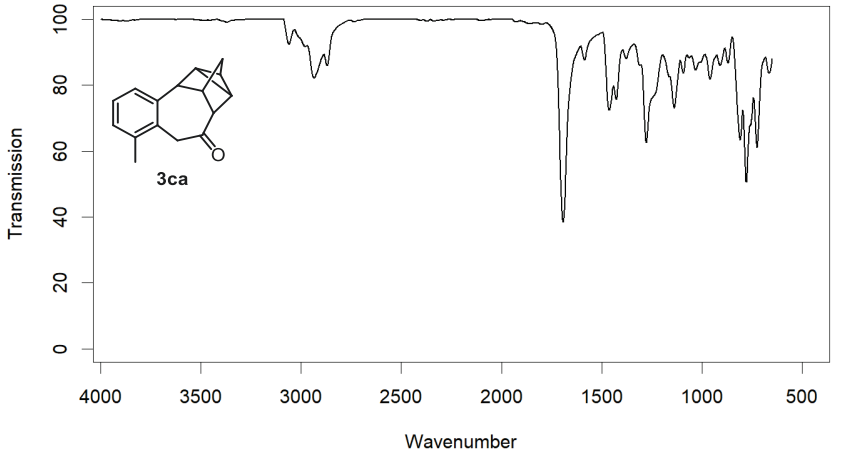

Figure S 273. IR spectrum of **3ca**.

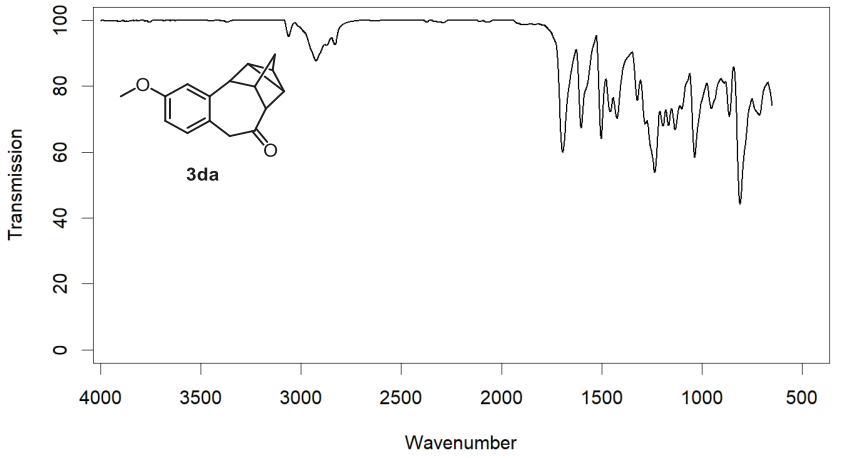

Figure S 274. IR spectrum of **3da**.

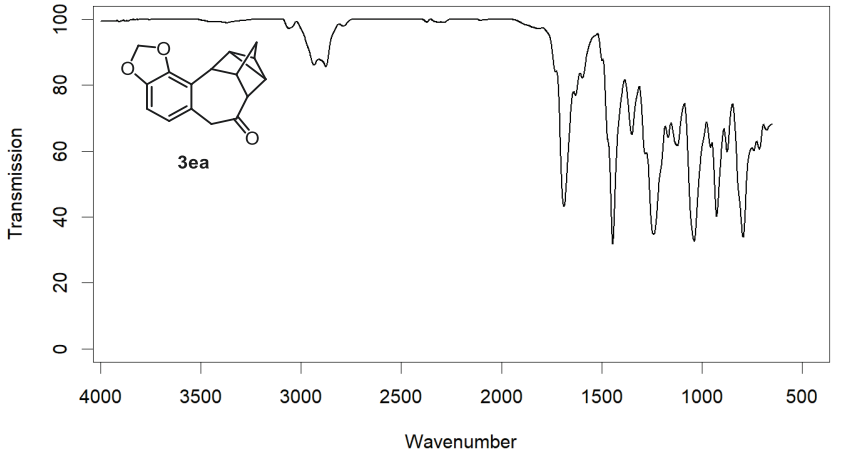

Figure S 275. IR spectrum of **3ea**.

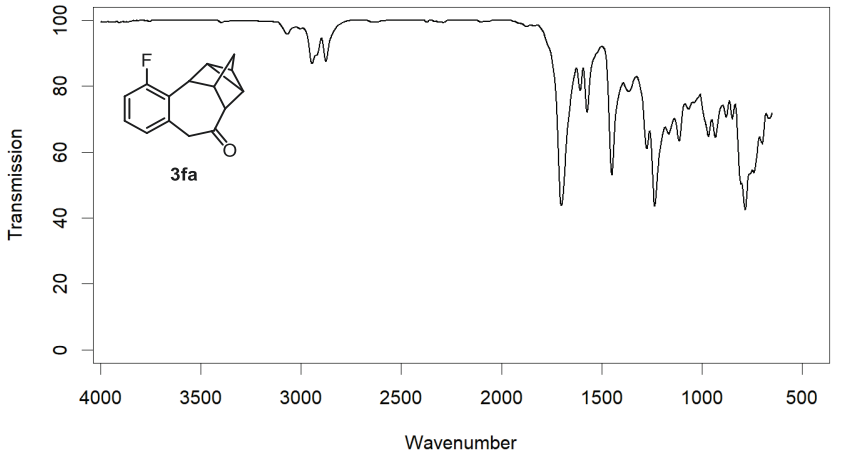

Figure S 276. IR spectrum of **3fa**.

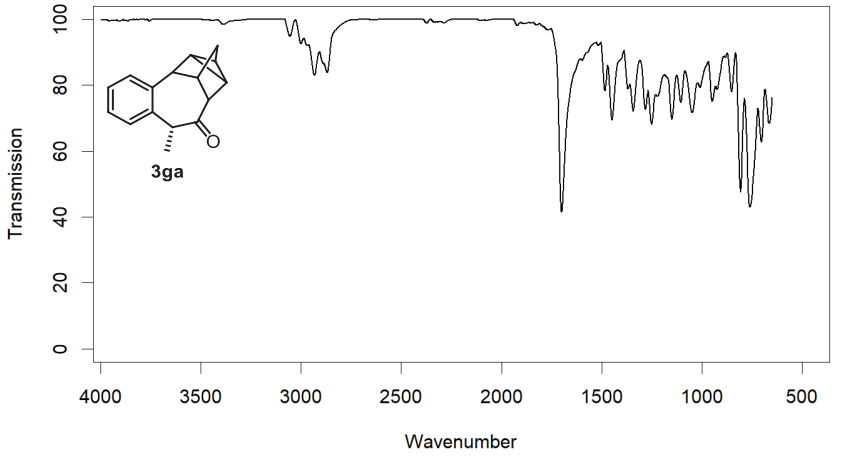

Figure S 277. IR spectrum of **3ga**.

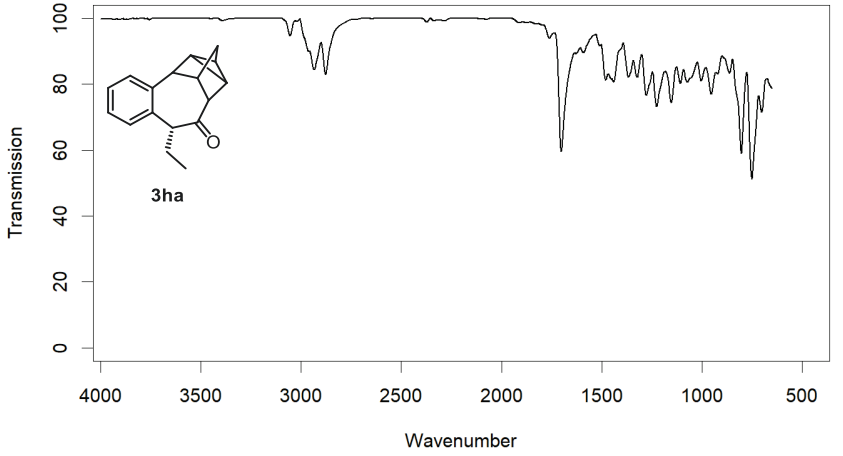

Figure S 278. IR spectrum of **3ha**.

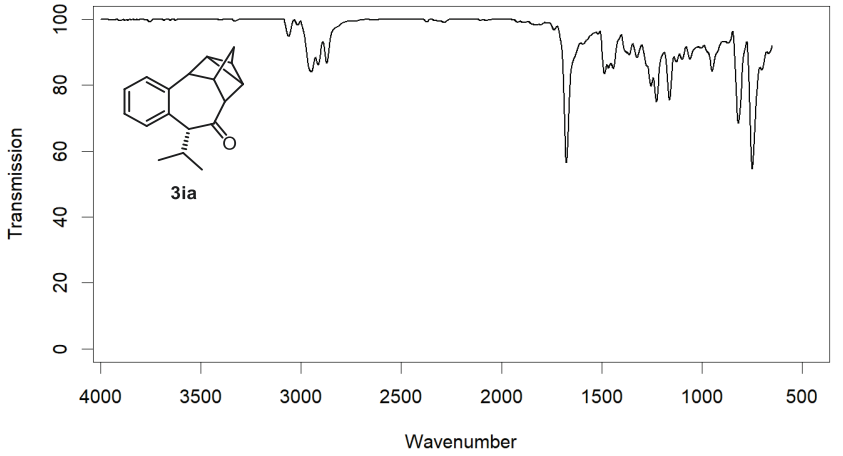

Figure S 279. IR spectrum of **3ia**.

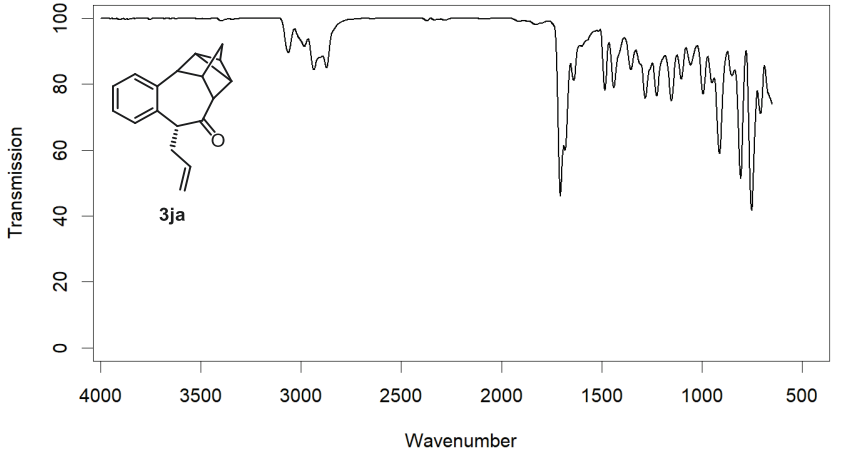

Figure S 280. IR spectrum of **3ja**.

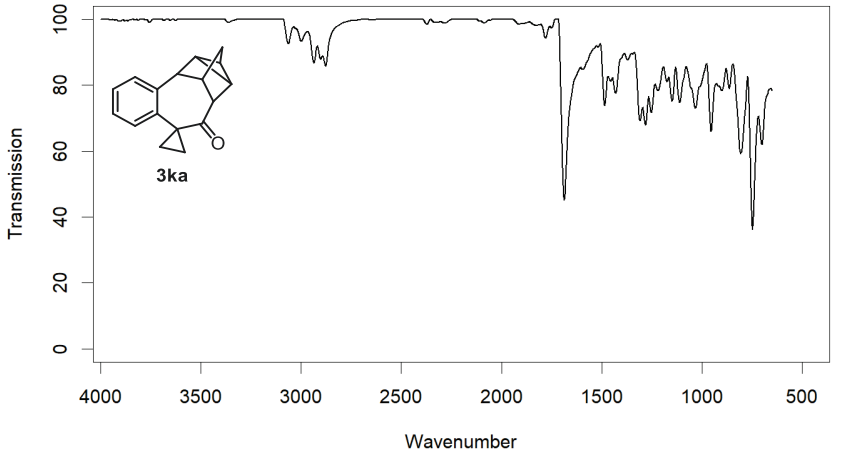

Figure S 281. IR spectrum of **3ka**.

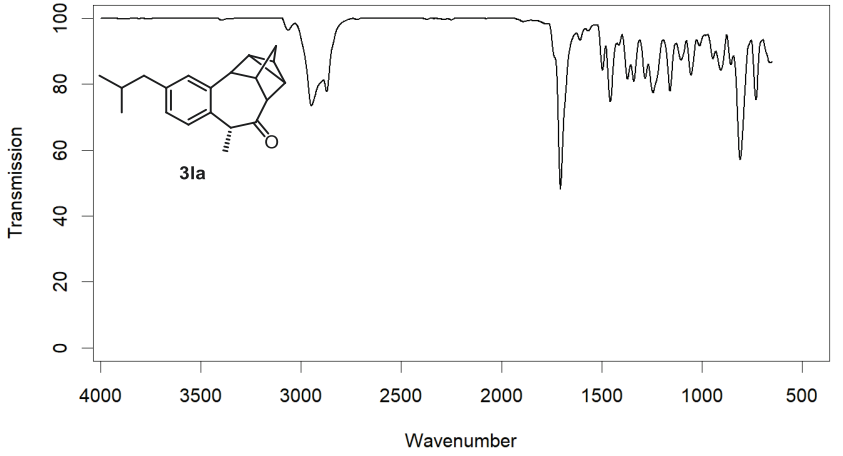

Figure S 282. IR spectrum of **3la**.

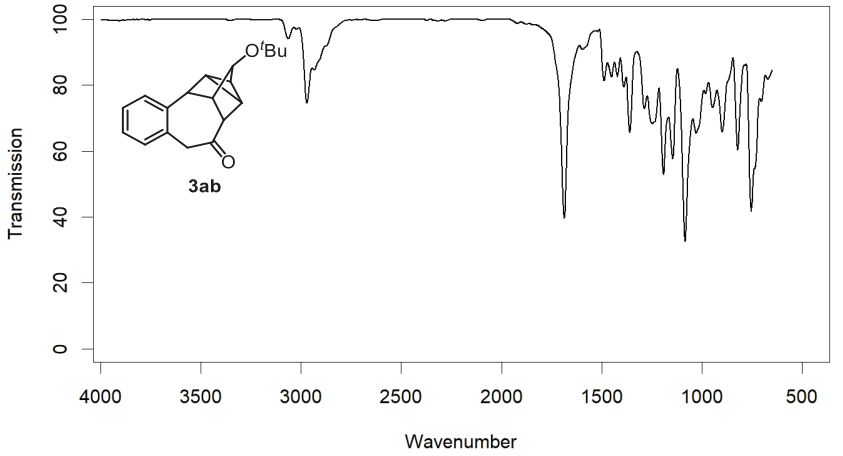

Figure S 283. IR spectrum of **3ab**.

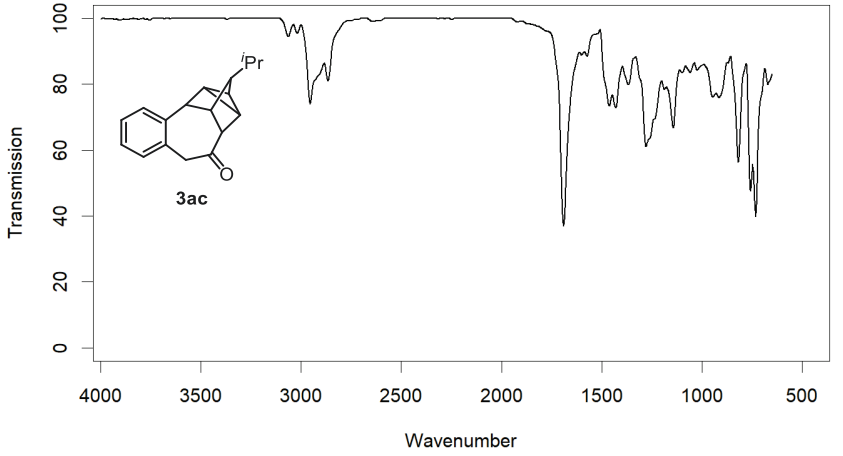

Figure S 284. IR spectrum of **3ac**.

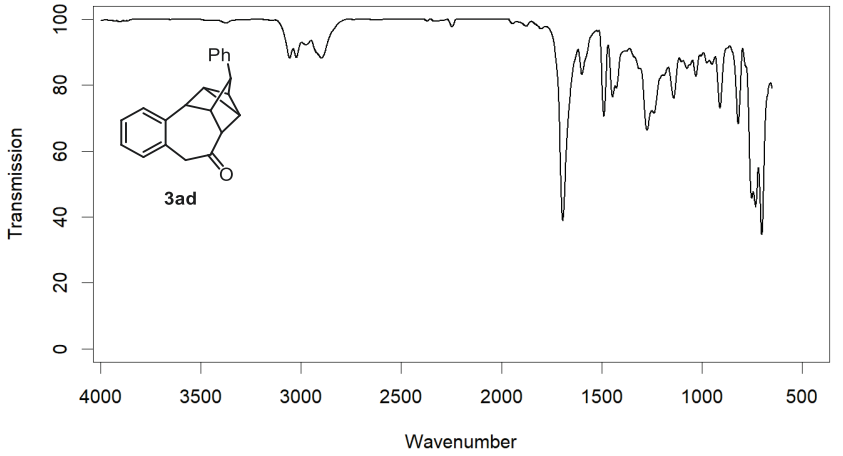

Figure S 285. IR spectrum of **3ad**.

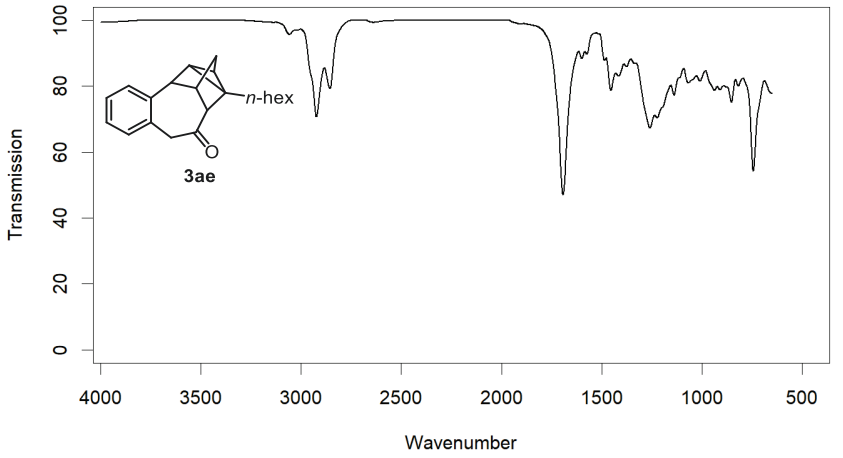

Figure S 286. IR spectrum of **3ae**.

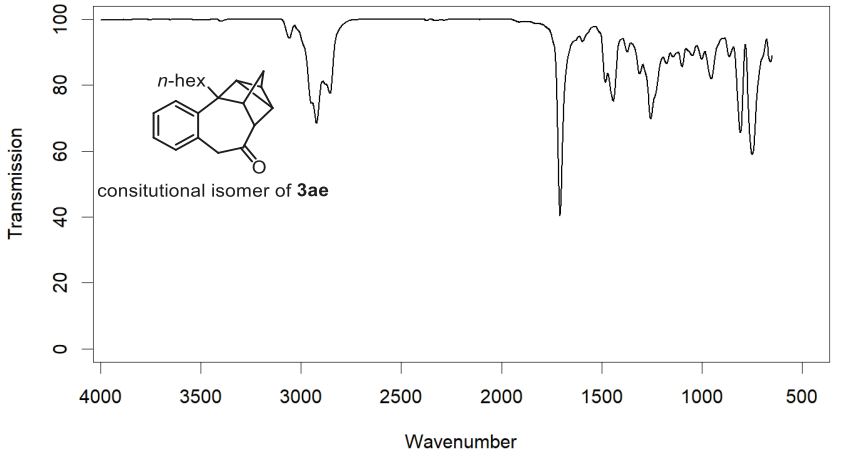

Figure S 287. IR spectrum of the constitutional isomer of **3ae**.

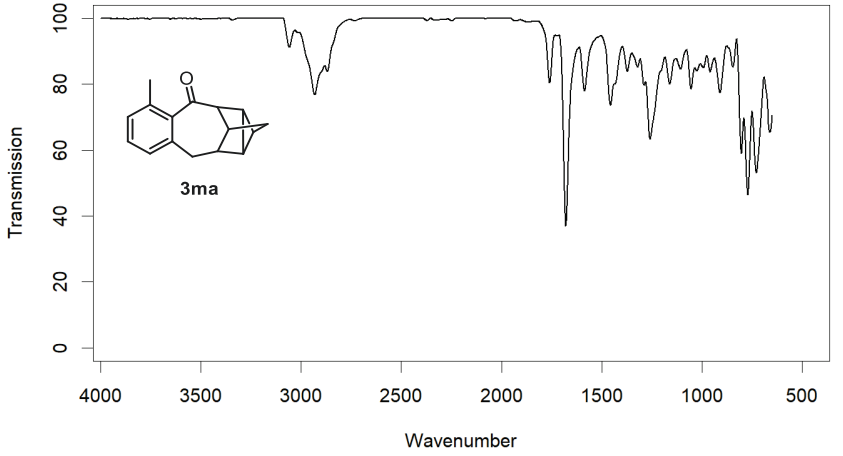

Figure S 288. IR spectrum of **3ma**.

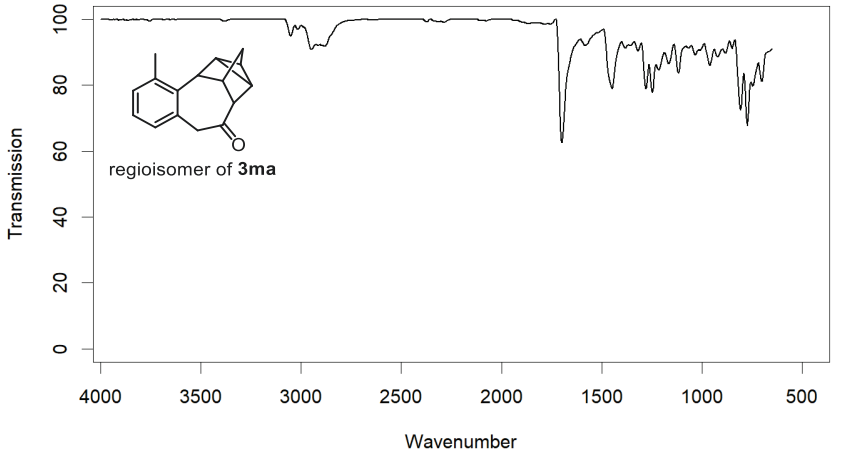

Figure S 289. IR spectrum of the regioisomer of **3ma**.

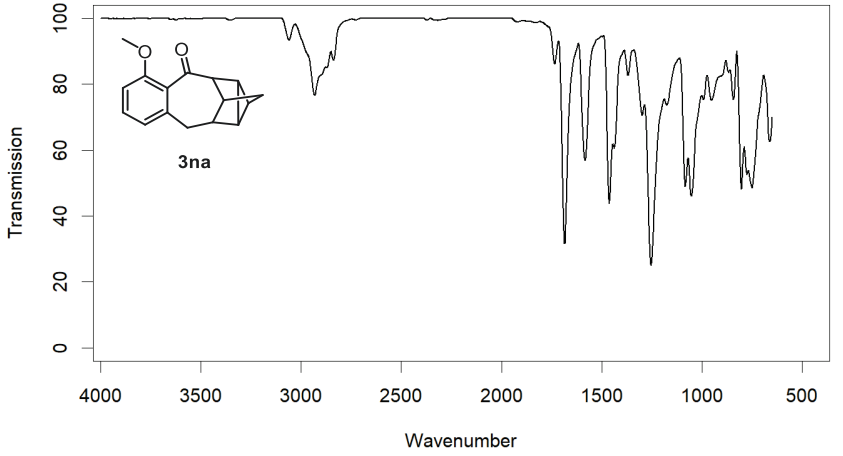

Figure S 290. IR spectrum of **3na**.

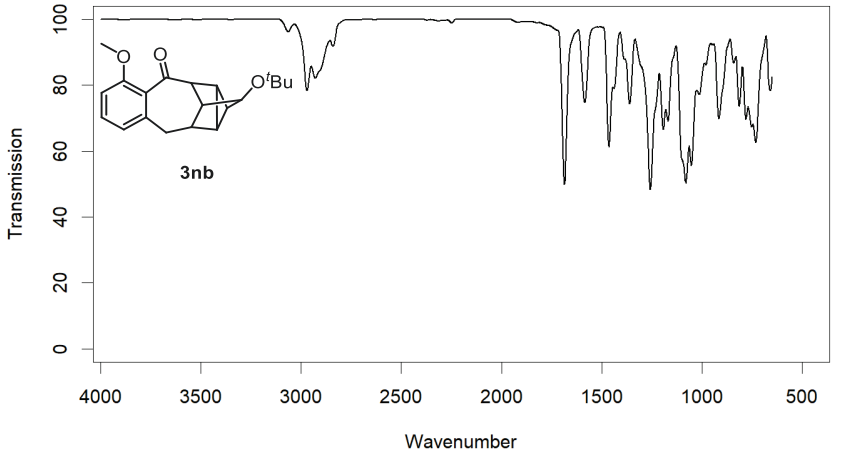

Figure S 291. IR spectrum of **3nb**.

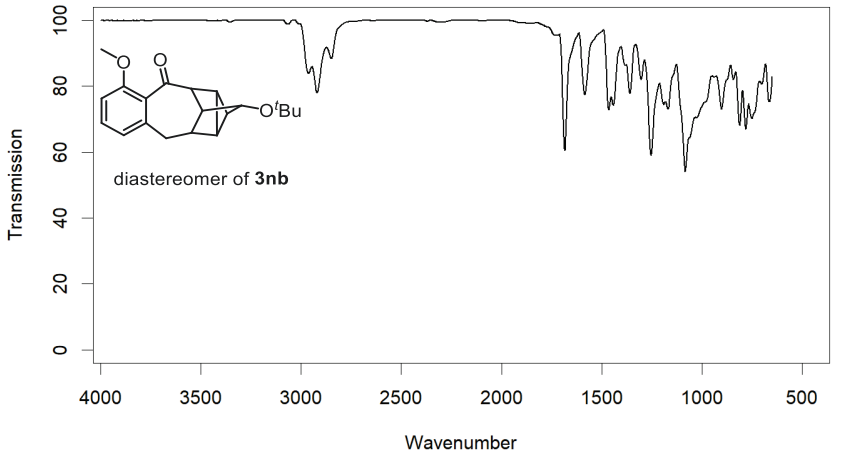

Figure S 292. IR spectrum of the diastereomer of **3nb**.

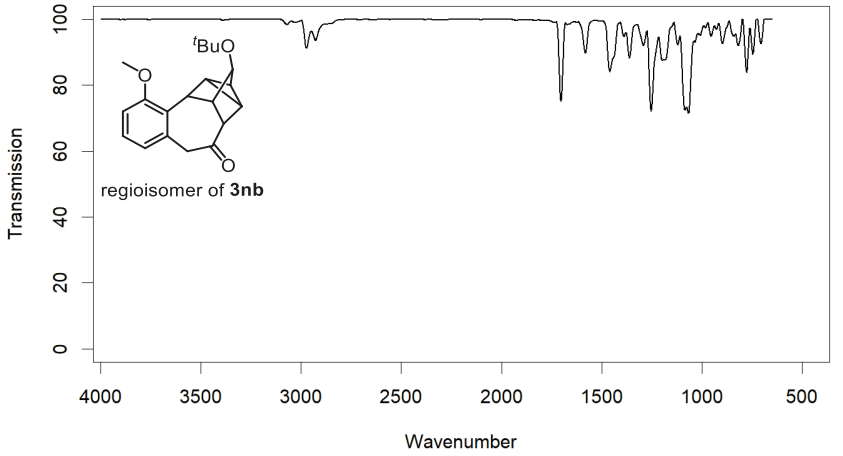

Figure S 293. IR spectrum of the regioisomer of **3nb**.

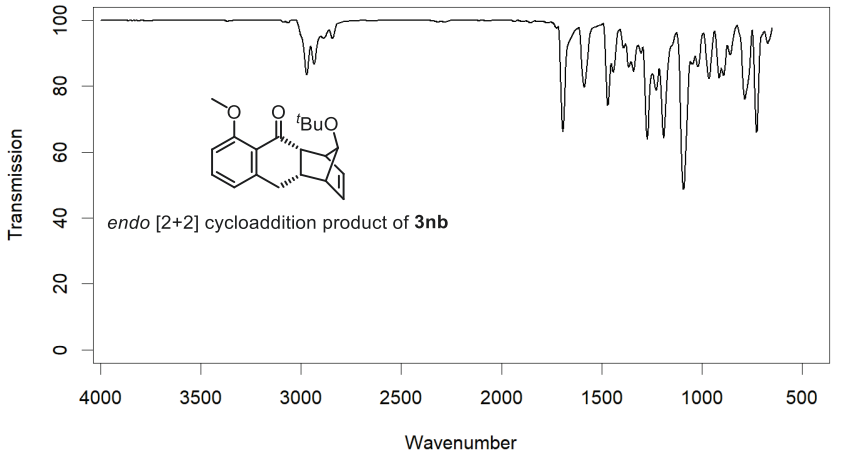

Figure S 294. IR spectrum of the endo [2+2] cycloaddition product of **3nb**.

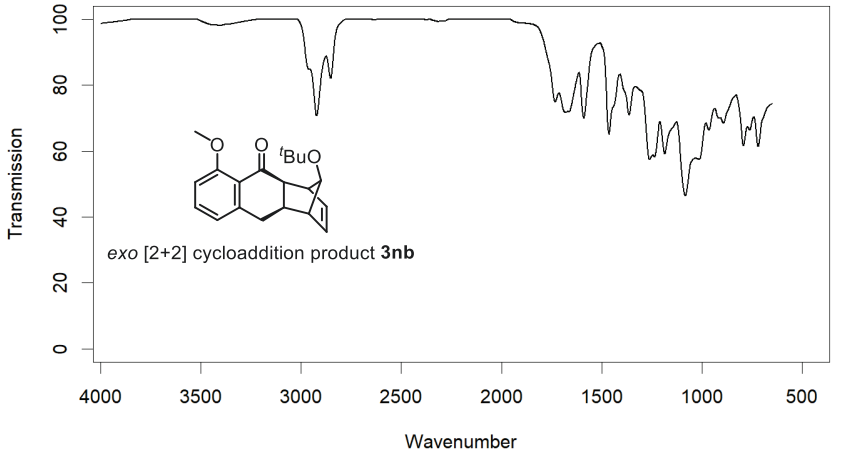

Figure S 295. IR spectrum of exo [2+2] cycloaddition product of **3nb**.

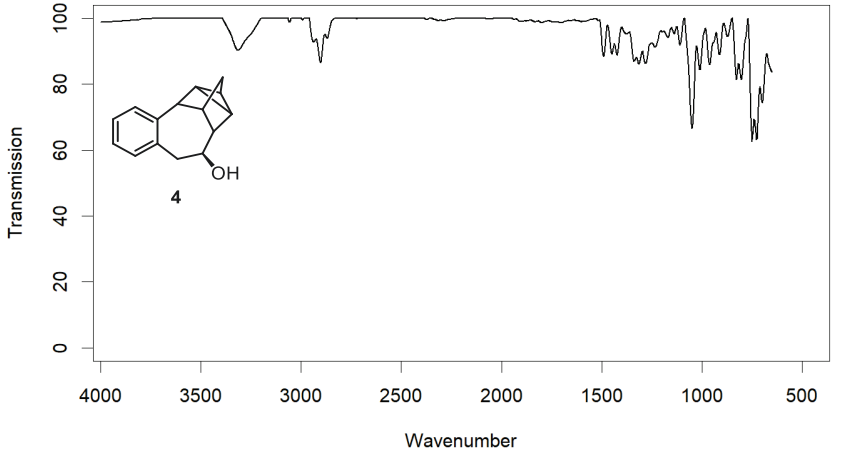

Figure S 296. IR spectrum of **4**.

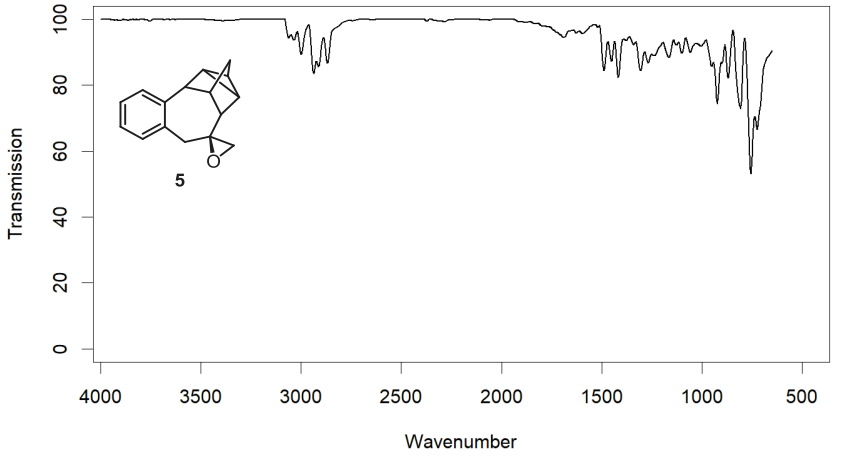

Figure S 297. IR spectrum of **5**.

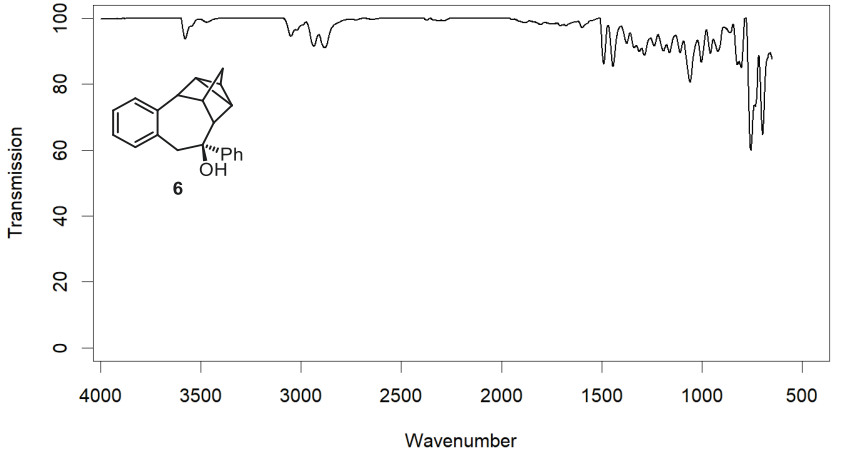

Figure S 298. IR spectrum of **6**.

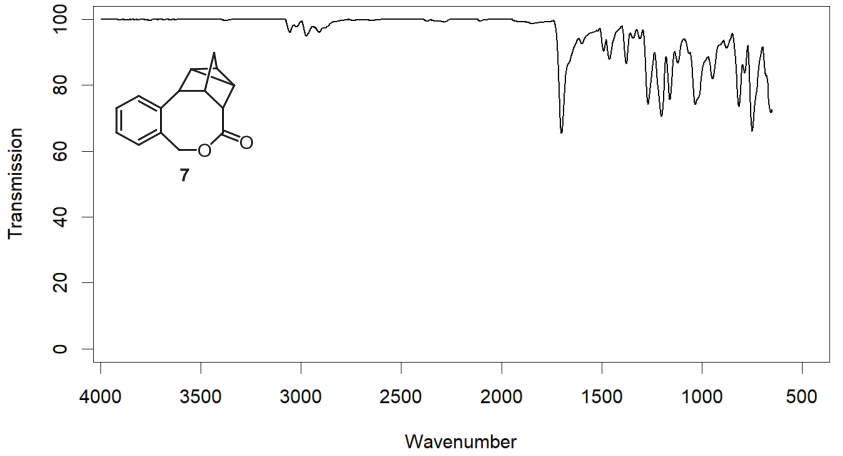

Figure S 299. IR spectrum of **7**.